PLOS ONE

RESEARCH ARTICLE

SOX10-Nano-Lantern Reporter Human iPS Cells; A Versatile Tool for Neural Crest Research

Tomoko Horikiri[1], Hiromi Ohi[2], Mitsuaki Shibata[3], Makoto Ikeya[3], Morio Ueno[1], Chie Sotozono[1], Shigeru Kinoshita[4], Takahiko Sato[1,5]*

1 Department of Ophthalmology, Kyoto Prefectural University of Medicine, Kyoto, Japan, **2** Department of Biomedical Engineering, Faculty of Life Sciences, Doshisha University, Kyotanabe, Japan, **3** Center for iPS Cell Research and Application, Kyoto University, Kyoto, Japan, **4** Department of Frontier Medical Science and Technology for Ophthalmology, Kyoto Prefectural University of Medicine, Kyoto, Japan, **5** Advanced Biomedical Engineering Research Center, Doshisha University, Kyotanabe, Japan

* takahiko@koto.kpu-m.ac.jp

Citation: Horikiri T, Ohi H, Shibata M, Ikeya M, Ueno M, Sotozono C, et al. (2017) SOX10-Nano-Lantern Reporter Human iPS Cells; A Versatile Tool for Neural Crest Research. PLoS ONE 12(1): e0170342. doi:10.1371/journal.pone.0170342

Editor: Irina Kerkis, Instituto Butantan, BRAZIL

Received: August 17, 2016

Accepted: January 3, 2017

Published: January 20, 2017

Data Availability Statement: All relevant data are within the paper and its Supporting Information files.

Funding: This work was supported by the Ministry of Education, Culture, Sports, Science, and Technology (26870285), the Japan Agency for Medical Research and Development (Projects for Technology Development, Development of Cell Transplantation Methods for Refractory Muscle Diseases and Centers for Clinical Application Research on Specific Disease/Organ), and the Nakatomi Foundation. The funders had no role in

Abstract

The neural crest is a source to produce multipotent neural crest stem cells that have a potential to differentiate into diverse cell types. The transcription factor SOX10 is expressed through early neural crest progenitors and stem cells in vertebrates. Here we report the generation of SOX10-Nano-lantern (NL) reporter human induced pluripotent stem cells (hiPS) by using CRISPR/Cas9 systems, that are beneficial to investigate the generation and maintenance of neural crest progenitor cells. SOX10-NL positive cells are produced transiently from hiPS cells by treatment with TGFβ inhibitor SB431542 and GSK3 inhibitor CHIR99021. We found that all SOX10-NL-positive cells expressed an early neural crest marker NGFR, however SOX10-NL-positive cells purified from differentiated hiPS cells progressively attenuate their NL-expression under proliferation. We therefore attempted to maintain SOX10-NL-positive cells with additional signaling on the plane and sphere culture conditions. These SOX10-NL cells provide us to investigate mass culture with neural crest cells for stem cell research.

Introduction

The neural crest cell is a unique, transient part of ectodermal derivatives in developing vertebrates and has multi-ability to migrate and differentiate into numerous cells including peripheral neurons, glia, craniofacial cartilage, cornea and so on [1]. Initial neural crest cells are raised at the edge of the neural plate and the non-neural ectoderm. According to the formation of the neural folds, neural crest cells subsequently occur epithelial mesenchymal transition to delaminate from dorsal neural tube and migrate through several pathways to reach target tissues and differentiate into various cell types as above [2–4].

It has been identified that a lot of genes, including FGF, WNT and retinoic acid signaling, are involving to neural crest specification and regulation, especially the transcription factor

study design, data collection and analysis, decision to publish, or preparation of the manuscript.

Competing Interests: The authors have declared that no competing interests exist.

SOX10 is a key regulator for the neural crest cells because it is specifically expressed in initial neural crest cells and defines the stemness of the neural crest cells [5–7]. *SOX10* mutations have been associated with Waardenburg syndrome and Hirschsprung disease. Their defects are recapitulated in *Sox10* heterozygous mice which are viable however display hypopigmentation and aganglionic megacolon [8].

In this study, we focused on the purification and the maintenance of neural crest cells differentiated from human induced pluripotent stem (hiPS) cells with Nano-lantern (NL) knock-in reporter, which is a chimeric fluorescent protein of enhanced Renilla luciferase and Venus [9]. In contrast to the previous SOX10-reporter lines as *SOX10* heterozygous or transgenic cells [8, 10–12], our construct achieved bicistronic expression of NL and targeted *SOX10* gene. We have identified additional proper signaling regulators to maintain SOX10-NL positive cells, although most of NL intensity are not detectable after *in vitro* culture for neural crest cells. SOX10-NL hiPS cells would be used for the research of human neural crest development and neural crest stem cell.

Materials and Methods

Ethical statement

This study was carried out according to the regulations of Kyoto Prefectural University of Medicine. The experimental protocols dealing with human subjects were approved by the Ethics committee and the Gene Recombination Experiment Safety Committee of Kyoto Prefectural University of Medicine (permit number: 26–5). Written informed consent was provided by each donor.

Gene targeting with human iPS cells

To construct a human *SOX10* targeting vector, we inserted 2A-Nano-lantern (NL) [9,13] and loxP-pGK-Neo-loxP (floxedNeo) cassette after the stop codon located on exon4 of *hSOX10* to cause bicistronic expressions of hSOX10 and NL (S1 Fig panel A). The sequence of 2A peptide was produced by synthesized oligos and NL fragments was amplified by PCR with KOD-Plus-Neo polymerase (TOYOBO) and pcDNA3-Nano-lantern (Addgene #51970) to construct pBS-2A-NL-pA. The fragment of floxedNeo was amplified by PCR from pBS-floxedNeo vector [14]. Both of 2A-NL-pA and floxedNeo fragments were ligated into pUC19 vector with In-Fusion HD Cloning Kit (Takara) by manufacture's protocol (S1 Fig panel B).

For 5' and 3' arm of *hSOX10* genomic sequences, they are amplified by PCR with genome DNA extracted from 201B7 hiPS cells [15]. These three fragments, 2A-NL-floxedNeo (2A-NL-fNeo), 5'of hSOX10, and 3' of hSOX10 were connected with In-Fusion HD Cloning Kit into pDT-A vector (pDT-A-hSOX10arm-2A-NL-fNeo, S1 Fig panel C) [16]. All PCR primers are listed in S1 Table.

To introduce into cultured cells with hSOX10-targeting plasmid vectors, pX330-hSOX10ex4, which was constructed with pX330 vector (Addgene #42230) [17] by ligating oligos into it, and linearized pDT-A-hSOX10arm-2A-NL-fNeo, the electroporator NEPA21 (NEPAGENE) was used for introducing plasmid DNAs into hiPS cells as described [18].

Cell culture and neural crest differentiation

hiPS cells were maintained on SNL feeder cells, treated with 10 mg/ml of mitomycin (Sigma) in DMEM supplemented with 10% of fetal bovine serum (GIBCO), in Primate ES cell medium (ReproCELL) supplemented with 4 ng/ml recombinant human FGF2 (WAKO) or 100 μg/ml G418 (Nacalai Tesque). Generated SOX10-NL iPS cells were maintained on iMatrix-511

(Nippi) coated plates with StemFit AK03N (Ajinomoto) as described under feeder-free culture system [19].

For neural crest induction, Fukuta *et al*. showed the detailed protocol to induce neural crest cells with hiPS cells [20]. In brief, single SOX10-NL iPS cell was expanded in mTeSR1 medium (STEMCELL Technology) for a few days, and induced into neural crest cells in IMDM and F-12 medium supplemented with chemically defined lipid concentrate (GIBCO), 1% of BSA (WAKO), Insulin-Transferrin-Selenium (GIBCO), and 1-thioglycerol (Sigma). Cultured plates were coated with Geltrex Matrix (GIBCO) or fibronectin (Millipore). SB431542 (Stemgent), CHIR99021 (Stemgent), EGF (WAKO), FGF2 (WAKO) were used for the induction and maintenance of neural crest cells. Embryoid bodies were formed as described to determine the differentiation ability of SOX10-NL hiPS cells [15].

Collected NL-positive neural crest cells were transferred onto fibronectin-coated dishes or Ultra-Low attachment 96well plates (Corning) for sphere formation with neural crest induction medium as describes in the result section.

Cell sorting

Cultured cells were dissociated with TrypLE select (GIBCO) at 37˚C for 5 min for detecting SOX10-NL expression. They were incubated sequentially with antibody against human CD271 (NGFR, p75NTR) conjugates with Alexa647 (BD; diluted 1/100) for 30 min on ice [21]. Dissociated cells were resuspended with 1% bovine serum albumin in PBS. Cell debris was eliminated with a cell strainer (BD; 35 μm) and suspensions were stained with SYTOX Red stain (Molecular Probes) to exclude dead cells. Cells were analyzed and collected by cell sorter using FACSJazz (BD).

Time-lapse imaging analyses

SOX10-NL positive (and NGFR-positive) and SOX10-NL negative (and NGFR-negative) cells were sorted and seeded onto fibronectin-coated tissue culture dishes for 24 hours. After cells were attached, time-lapse phase contrast images (magnification 10x, 5x5 tiles) were taken at 10 min intervals for 24 hours using BioStation CT (Nikon) at 37˚C with 5% CO_2. Cell migration rate was measured by tracking analysis using CL-Quant software (Nikon) for initial 12 hours with time-lapse images.

Quantitative PCR analyses

Total RNAs from sorted or cultured cells were extracted using RNeasy micro kit (QIAGEN) and genome DNAs were extracted by PureLink Genomic DNA kits (Invitrogen). For quantitative PCR analyses, single strand cDNA was prepared using SuperScript VILO kit (Invitrogen) as manufacture protocol. All RT-qPCR reactions were carried out in triplicate using THUNDERBIRD SYBR qPCR Mix (TOYOBO), normalized to mRNA level of ribosomal protein L13A (RPL13A) or genome DNA expression level of GAPDH as a control [22]. Primers sequences (5' to 3') are listed in S2 Table.

Immunofluorescence assay

Cultured cells were fixed in 4% paraformaldehyde for 10 min at 4˚C, permeabilized with 0.2% Triton and 50 mM NH_4Cl. Fixed samples were pre-treated with BlockingOne (Nacalai Tesque) for 30 min at RT, and incubated with anti-OCT3/4, anti-NANOG, anti-SSEA4, anti-TRA1-60 (Cell Signaling Technology; diluted 1/200), anti-GFP (Molecular Probes; diluted 1/500), anti-SOX10 (SantaCruz Biotechnology; diluted 1/100) antibodies in 5% of BlockingOne in PBST

for overnight at 4˚C. After three washes with 0.1% Tween20 in PBS, cells were incubated with Alexa488 or Alexa594-conjugated secondary antibodies (Molecular Probes; diluted 1/500). Cells were washed and mounted in SlowFade Diamond antifade mountant with DAPI (Molecular Probes). Fluorescent images were collected on the software of BZ-X700 (Keyence). For quantitation of cultured cells, numbers of dishes were analyzed from triplicate experiments.

Results

Human *SOX10* genomic DNA digestion with CRISPR/Cas9 system

To cause double strand break to the border between CDS and 3'UTR in *hSOX10* exon4 (Fig 1A), a Candidate sequence of the guide RNA (cactgtcccggccctaaagg-gGG, hSOX10ex4) to target by Cas9 was selected by CRISPRdirect website (http://crispr.dbcls.jp) [23], and inserted into pX330 vector to create pX330-hSOX10ex4 editing vector (Fig 1B). The effect of double strand break into *hSOX10* genomic sequence of hiPS cells was evaluated by the digestion of heteroduplex PCR products, involving the target region by pX330-hSOX10ex4 editing vector monitored with T7 endonuclease I (T7EI). Digested bands of 700 bp and 300 bp were found in T7EI-treated genome DNA samples, according to treated periods (Fig 1C). The data suggested that Cas9 and the guide-RNA expressing construct has an efficiency to target *hSOX10* genomic sequence.

Generation of SOX10-NL hiPS reporter line

In order to construct the targeting vector for human *SOX10* as designed in S1 Fig, the targeting sequences along with 5' and 3' homology arms (0.7 kbp and 1.0 kbp, respectively) were amplified by PCR and combined with 2A-NL-floxedNeo reporter sequence by In-Fusion technology efficiently into pDT-A-hSOX10arm-2A-NL-fNeo vector (Fig 2A, knock-in cassette).

hiPS cells were electroporated with pDT-A-hSOX10arm-2A-NL-fNeo targeting vector and pX330-hSOX10ex4 editing vector. The electroporated cells were plated on SNL feeder cells, and G418 selection was started two days later for a week. Single colonies were picked up, expanded and subsequently genomic DNA was used for screening the correct insertion of knock-in reporter cassette. PCR results showed that selected clone contained reporter cassette (Fig 2B, F1+R1, F2+R2). And this clone has been confirmed to obtain one copy of the targeted Neomycin resistance gene allele by comparing with known knock-in hiPS cell (Fig 2C, $hSOX10^{2A\text{-}NL\text{-}fNeo/+}$). To excise the Neomycin resistance gene cassette from $hSOX10^{2A\text{-}NL\text{-}fNeo/+}$ hiPS cells, pCAG-Cre vector was transiently transfected [24], and single hiPS colonies were picked up and confirmed the lack of floxed Neo sequence by PCR (Fig 2D, $hSOX10^{2A\text{-}NL/+}$).

The selected hiPS clone $hSOX10^{2A\text{-}NL/+}$ was confirmed to express pluripotency markers with OCT3/4, NANOG, SSEA4 and TRA-1-60, after gene targeting and antibiotic selection experiments (Fig 2E). This clone also had the multipotency to differentiate into ectodermal (*PAX6*), mesodermal (*T*), and endodermal (*FOXA2*) cells in embryoid bodies (Fig 2F). This clone was therefore chosen for the induction experiments to neural crest cells.

Confirmation of SOX10-NL activity during neural crest differentiation

hiPS $SOX10^{2A\text{-}NL/+}$ reporter cells were differentiated into the neural crest lineage using the protocol as described [20], with SB431542, a specific inhibitor of TGFß receptor kinase, and CHIR99021, an inhibitor of GSK3 to function as a WNT activator, for nine days (Fig 3A–3D), and NL activity and SOX10 expression were analyzed during the differentiated periods. Analyses of Fluorescence activated cell sorting (FACS) and luciferase activity showed NL reporter activity started to increase about day 5 of differentiation and around 20% of NL positive (NL+)

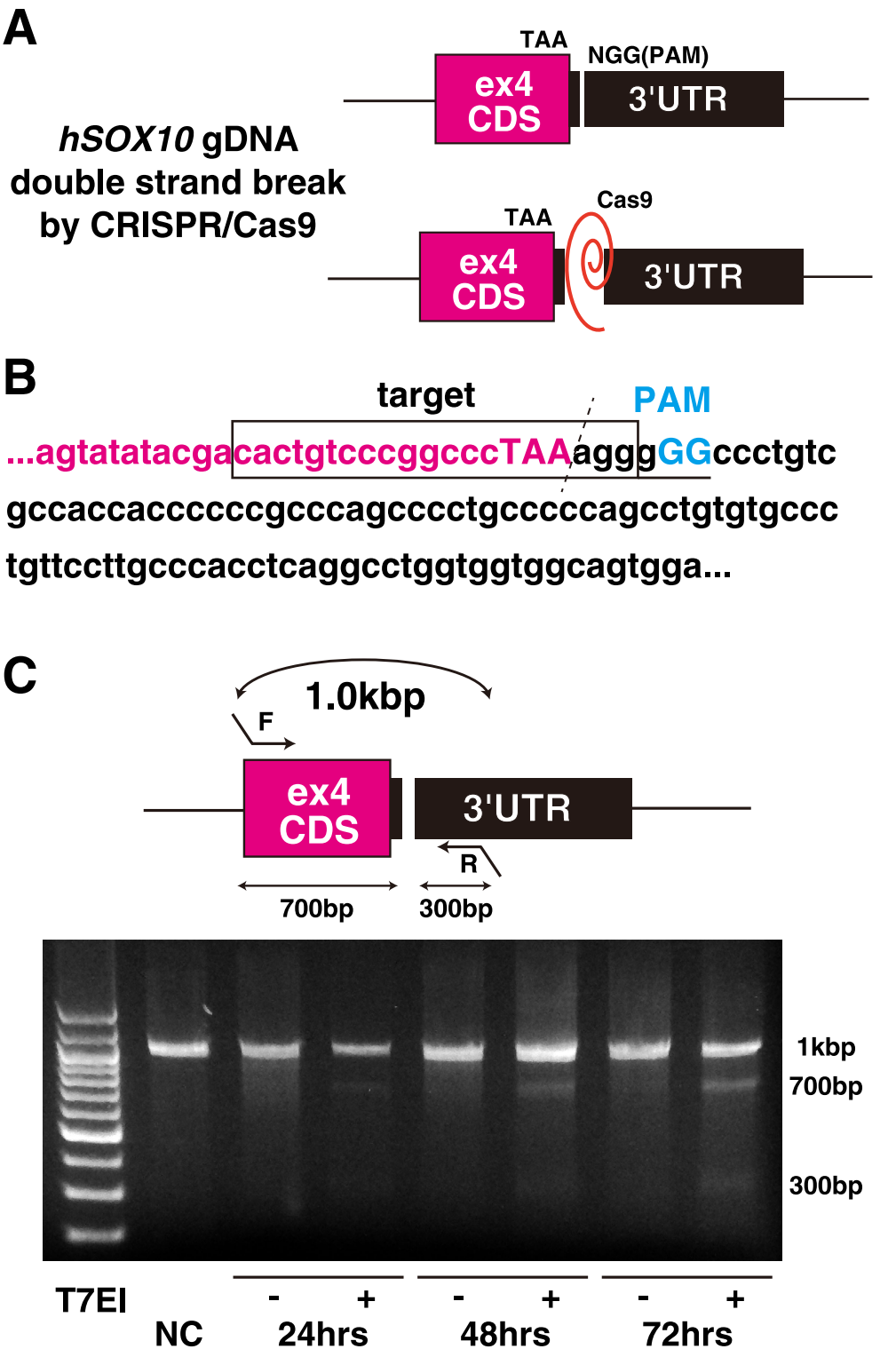

Fig 1. Effect of guide sequence to human *SOX10* on Cas9 activity. (A) A model of Cas9 activity to the human *SOX10* exon4 locus. (B) Cas9 with matching single guide RNA (sgRNA, red) and proto-spacer adaptor motif (PAM, blue) sequences adjacent to human *SOX10* stop codon. (C) T7 endonuclease 1 assay for Cas9-mediated cleavage (700bp and 300bp) on the gel showing comparable modification of targeted human *SOX10* genomic fragment in HEK293T cells according to transfected periods (24 hours, 48 hours, and 72 hours).

doi:10.1371/journal.pone.0170342.g001

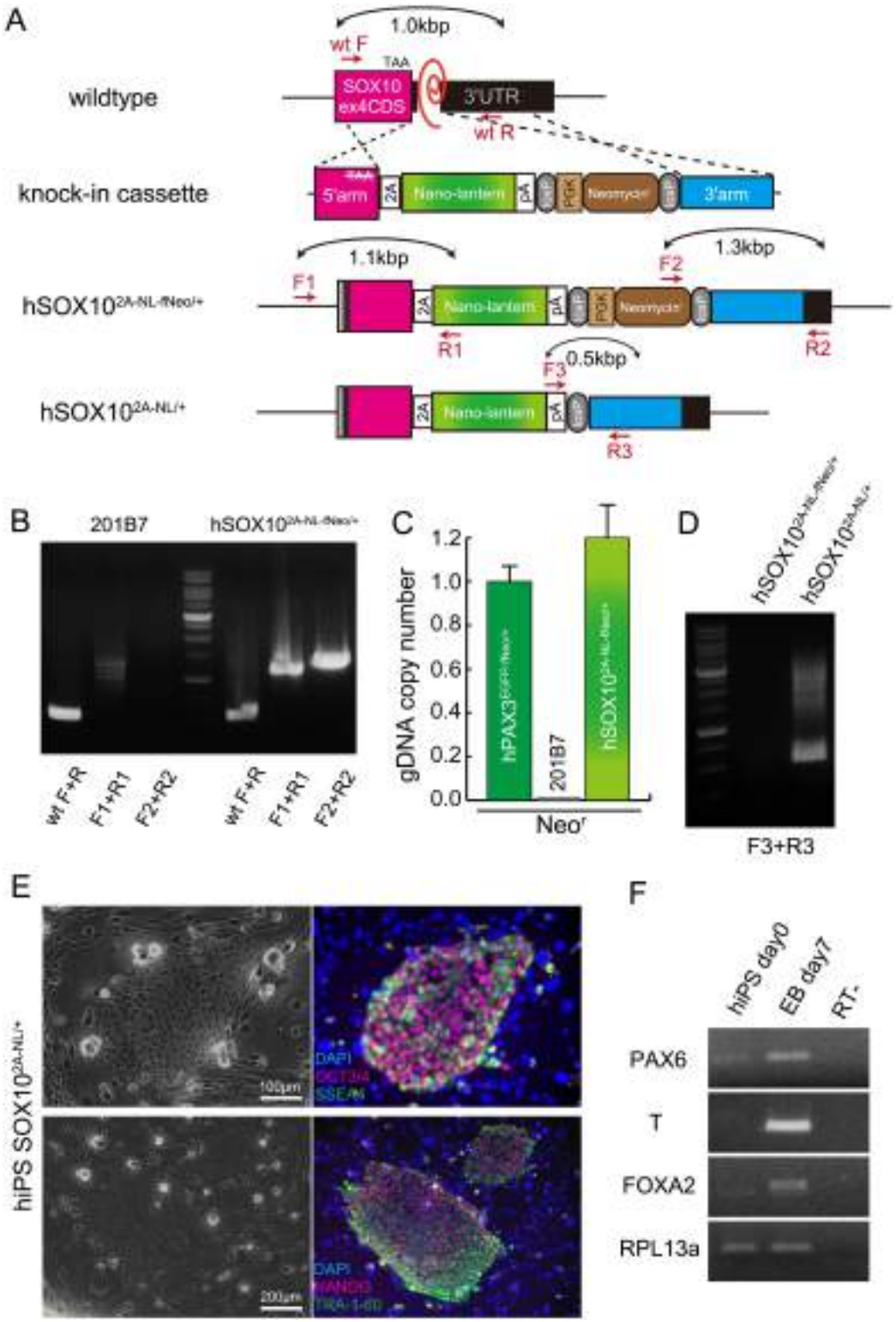

Fig 2. Generation of hSOX10-2A-Nano-lantern reporter hiPS cells. (A) A schematic representation of targeting cassette for *hSOX10*$^{2A\text{-}NL\text{-}fNeo/+}$ or *hSOX10*$^{2A\text{-}NL/+}$ knockin allele. (B) Genotyping PCR with genome DNA extracted from hiPS 201B7 and *hSOX10*$^{2A\text{-}NL\text{-}fNeo/+}$ hiPS cells. Genomic recombined 5'fragment of targeting cassette was detectable by F1 and R1 primers, and also 3' fragment by F2 and R2 primers. (C) DNA Copy number check by quantitative PCR with genome DNA extracted from hiPS 201B7, *Pax3*$^{EGFP\text{-}fNeo/+}$, and

hSOX10$^{2A\text{-}NL\text{-}fNeo/+}$ cells. All error bars indicate ±s.e.m. (n = 3) (D) The excision of loxP-Neo-loxP genomic fragment in *hSOX10*$^{2A\text{-}NL\text{-}fNeo/+}$ hiPS cells with Cre recombinase treatment to establish *hSOX10*$^{2A\text{-}NL/+}$ hiPS cells. (E) *hSOX10*$^{2A\text{-}NL\text{-}fNeo/+}$ cells were immunostained with indicated undifferentiated pluripotent cell markers, anti-OCT3/4 (red, upper panel) and anti-SSEA4 (green, upper panel), anti-NANOG (red, lower panel) and anti-TRA1-60 (green, lower panel) antibodies. Nuclei were stained with 4'6-diamidino-2-phenylindole (DAPI, blue). Scale bar, 100 μm. (F) Differentiation capacity into ectoderm (*PAX6*), mesoderm (*T*), endoderm (*FOXA2*) markers with embryonic bodies (EB day7) from *hSOX10*$^{2A\text{-}NL/+}$cells.

doi:10.1371/journal.pone.0170342.g002

cells were detected at day 9 of differentiation (Fig 3E, and S2 Fig). These differentiated cells at day 7 were fixed and stained with anti-SOX10 antibody to confirm co-expression of NL and SOX10. As expected, NL+ cells co-express SOX10, indicating that NL-reporter cassette mimics the activation of endogenous SOX10 expression (Fig 3F–3I). We also confirmed the co-expression by detecting enriched *SOX10* transcripts in NL+ sorted cells (Fig 3J). In order to expand NL+ sorted cells, NL+ cells were grown in described culture media supplemented with 10 ng/mL of FGF2 and 10 ng/mL of EGF on fibronectin-coated plates[16]. NL fluorescent expression could be detected in NL+ sorted cells cultured for 24 hours under microscopy, however their NL intensity was attenuated in cultured cells for 48 hours (Fig 3K–3N).

Characteristics of SOX10-NL+ neural crest cells

SOX10-NL+ cells were purified by FACS as neural crest cells differentiated from hiPS cells. The SOX10-NL+ population isolated from differentiated neural crest cells for day 6 to day 11 exhibited all co-expression with NGFR (Fig 4A), indicating that NL+ population was identified with neural crest marker NGFR. However the activity of NL was not detectable in all NGFR+ population (Fig 4A). To assess the identity of the NGFR+; NL+ or NGFR+; NL-negative (NGFR+NL-) cells, we investigated their differences. Same numbers of NGFR+NL+ or NGFR+NL- sorted cells were seeded on fibronectin-coated dishes and expanded for a week. Almost cultured cells were detected with NGFR+ in both conditions (Fig 4B–4E), however the percentage of NL+ was decreased in this culture condition as shown in Fig 3 (Fig 4E). And this NL+ proportion was declined according to passage numbers (Fig 4F). The cell numbers after expansion of NL+ cells showed much higher than those of NGFR+NL- cells, indicating that NL+ neural crest cells have a competent to be propagated than NGFR+ neural crest cells (Fig 4G).

Effects of pivotal exogenous factors to maintain SOX10-NL positive neural crest cells

SOX10-NL+ cells had a differentiation potential into cells of peripheral nervous system, and mesenchymal stem cells (S3 Fig), and an ability of cell migration (S4 Fig and S1 Movie), however these cells do not remain the activity of NL but rather spontaneously differentiate into NGFR+NL- cells in culture medium containing SB431542, FGF2 and EGF. We therefore sought the appropriated condition to expand cells keeping the NL activity. Subsequent screening of inhibitors and growth factors revealed that SB431542 was essential for the increase of the ratio of NL+ cells (Fig 5A). CHIR99021 also had the effect to NL+ cell positively, however high dose of this inhibitor (higher than 5 μM) conversely down-regulated the ratio of NL+ cells (Fig 5B). As shown in Fig 5A, we found that FGF2 might have the negative effect to NL+ activity although cultured cells supplemented with 10 ng/mL of FGF2 were grown well and healthy because of few dead cells, which were stained with SYTOX red (not shown). However high doses of FGF2, more than 500 pg/mL drastically reduced the NL activity, and the proportion of NL+ in NL+ cultured cells was gradually diminished by the amount of FGF2 (Fig 5C).

Kerosuo *et al.* recently indicated epithelial sphere culture of premigratory neural crest cells to maintain their self-renewing and multipotent state [25]. We tested to determine optimal

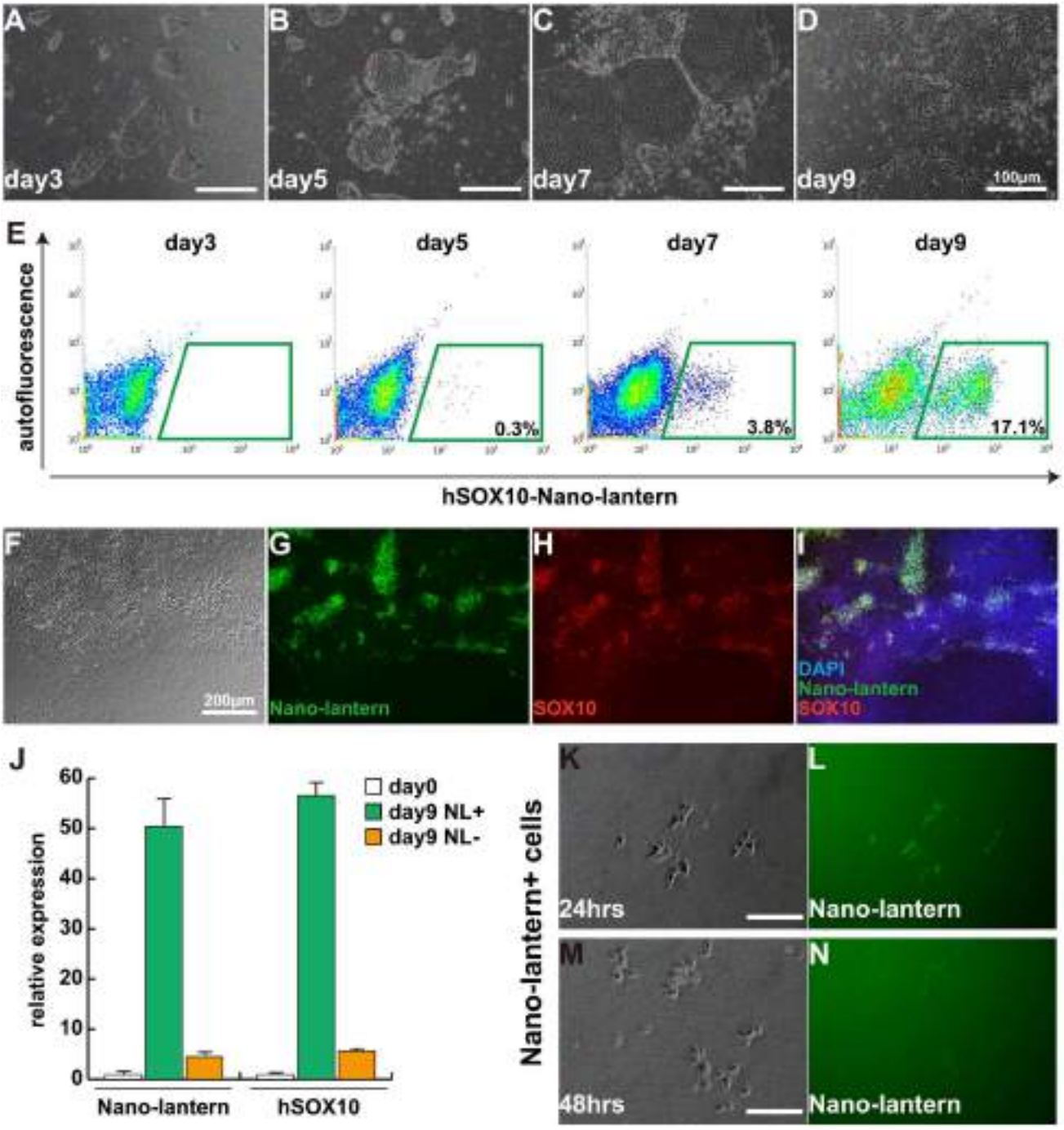

Fig 3. Induction of Nano-lantern-positive cells from *hSOX10*$^{2A\text{-}NL/+}$ hiPS cells. (A-D) Morphology of cultured cells from *hSOX10*$^{2A\text{-}NL/+}$ hiPS cells during 3 days (Day3) to 9 days (Day9). Scale bar, 100 μm. (E) FACs profiles for detecting Nano-lantern-positive cells from induced cells. (F-I) cultured cells for 7 days were immunostained with anti-GFP (Nano-lantern; G, green) and anti-SOX10 (H, red) antibodies. Nuclei were stained with 4'6-diamidino-2-phenylindole (DAPI, blue). Scale bar, 200 μm. (J) Relative expressions of *Nano-lantern* and *hSOX10* with Nano-lantern-positive (NL+) or negative (NL-) cells by FACs analyses. All error bars indicate ±s.e.m. (n = 3) (K-N) Cultured Nano-lantern-positive cells decrease the fluorescent intensity of Nano-lantern expression after 24 hours (K, L) to 48 hours (M, N). Scale bar, 50 μm.

doi:10.1371/journal.pone.0170342.g003

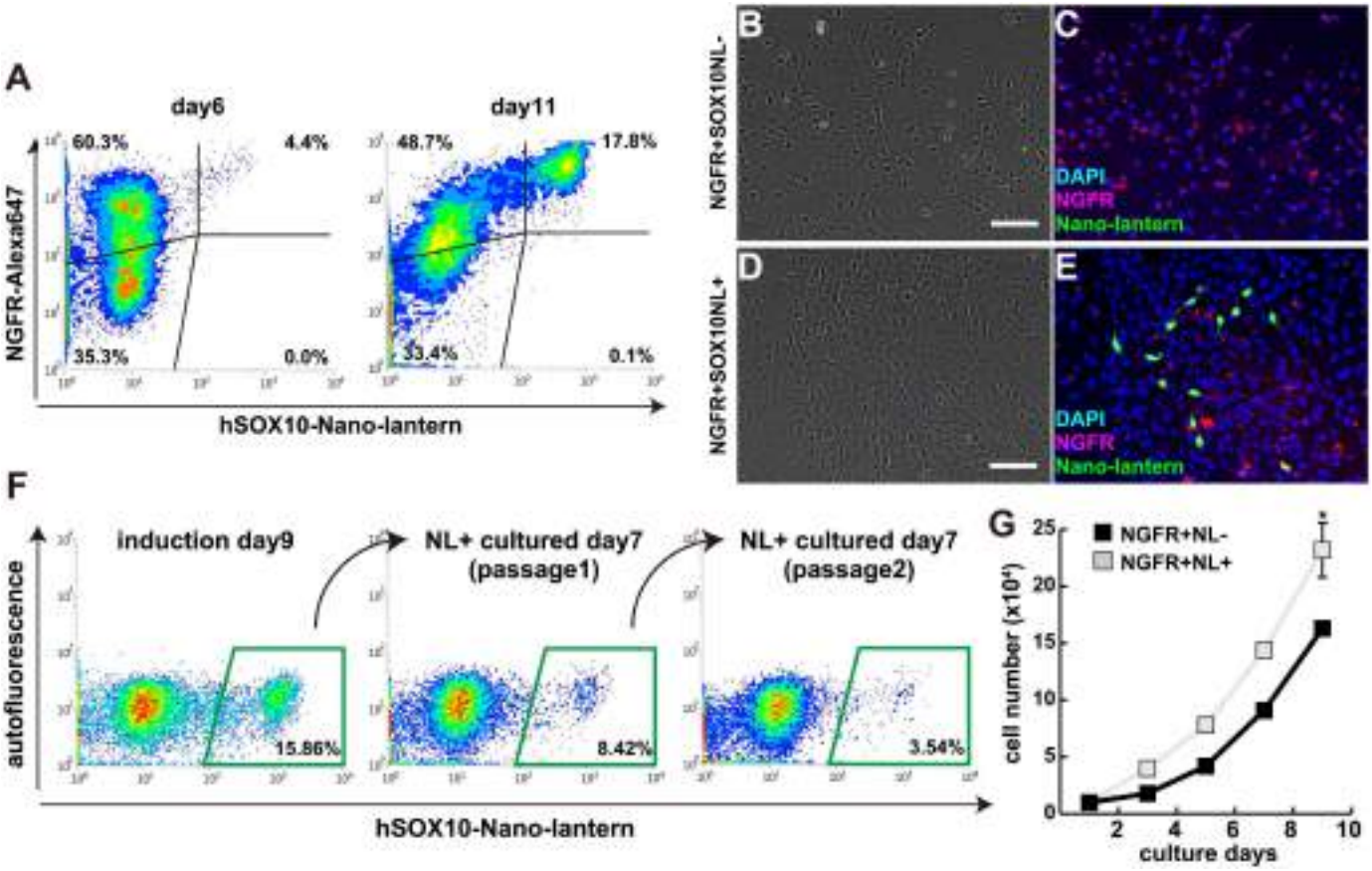

Fig 4. Characteristics of Nano-lantern-positive neural crest cells. (A) Flow cytometry plots of induced Nano-lantern-positive cells from *hSOX10*$^{2A\text{-}NL/+}$ hiPS cells for 6 days (day 6) or 11 days (day 11). All Nano-lantern-positive cells indicate in NGFR (p75)-positive fraction. (B-E) FACs-purified cells (NGFR+NL-; B, C or NGFR+NL+; D, E) were cultured for 7 days and immunostainted with anti-NGFR (red in C, E) and anti-GFP (Nano-lantern; green in C, E) antibodies. Nuclei were stained with 4'6-diamidino-2-phenylindole (DAPI, blue). Scale bar, 100 μm (F) Continuously decreased Nano-lantern-positive percentages in Nano-lantern-positively sorted and cultured cells. (G) Nano-lantern-positive cells (NGFR+NL+) grow faster than NGFR-positive; Nano-lantern-negative cells (NGFR+NL-). All error bars indicate ±s.e.m. (n = 3). *P* values are determined by t-test from a two-tailed distribution. *P<0.05.

doi:10.1371/journal.pone.0170342.g004

conditions for enabling SOX10-NL+ cells to aggregate. Spheres with NL+ cells were successively formed in the same condition of monolayer culture of NL+ cells, with 10 μM SB431542 and 1 μM CHIR99021 (Fig 5D). Furthermore, the proportion of NL+ cells in sphere culture condition was significantly reduced without SB431542 or CHIR99021, or with FGF2 (Fig 5E), compatible with the monolayer culture (Fig 5A). These data suggested that these pivotal factors in TGFß, WNT and FGF signaling are effective for the maintenance of NL positively regardless of cell-cell interaction.

Discussion

Here we present successful generation of SOX10-NL knock-in hiPS cells by the CRISPR/Cas9 and In-Fusion technologies, which are valuable to monitor SOX10 expression by both of fluorescent and luciferase activities. Nano-lantern enable us to perform not only real-time imaging in living cells as other fluorescent proteins, but also in vivo imaging by sensitive luminescent detection. This SOX10-NL hiPS cell lines can be also used for evaluation of directed differentiation toward neural crest lineage using chemical screening as well as to study temporal

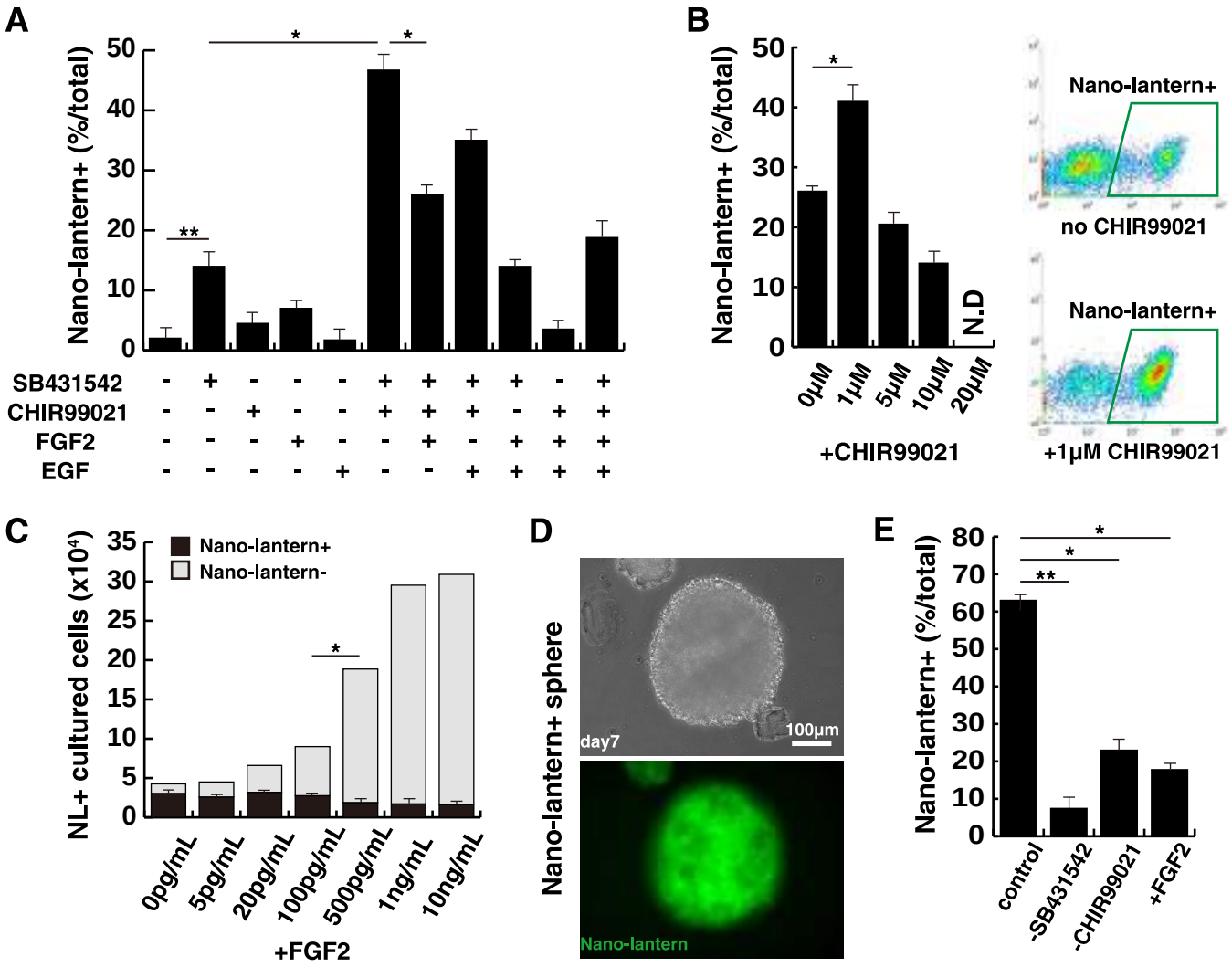

Fig 5. effects of exogenous factors to SOX10-Nano-lantern positive cells. (A) The combination effect of SB431542 and CHIR99021 inhibitors, FGF2, and EGF to cultured Nano-lantern-positive cells. (B) Different CHIR99021 concentrations for the expansion of Nano-lantern-positive cells. Cultured Nano-lantern-positive cells were analyzed by FACs with or without CHIR99021 (right panels). (C) Effects of FGF2 for the expansion of Nano-lantern-positive cells. total cultured cells were counted and the percentage of Nano-lantern-positive cells were analyzed. (D) 7 days cultured images of aggregated spheres derived from Nano-lantern+ cells (below; NL fluorescence image) (E) Effects to NL+ proportion in aggregated spheres without SB431542 and CHIR99021, or with FGF2. All error bars indicate ±s.e.m. (n = 3). *P* values are determined by t-test from a two-tailed distribution. *P<0.05; **P<0.01.

doi:10.1371/journal.pone.0170342.g005

emergence of neural crest stem cells during *in vitro* differentiation. Moreover, our approach shown here is simple, efficient and versatile to be applicable to generate other reporter knock-in cells, and ideal gene targeting for predominant genotype like *SOX10* because Haploinsufficiency of hetelozygous *SOX10* causes pigmentation and megacolon defect in Hirschsprung disease [8]. Therefore, we chose not to generate *SOX10* heterozygotes or BAC transgenic cells, which might affect to intact *SOX10* or other gene expression, but to target 3'UTR sequence of *SOX10* just with sequences of 2A signal peptide and Nano-lantern instead of *SOX10* stop codon to function intact *SOX10* coding sequence.

Although a variety of neural crest-derived cells, differentiated from the pluripotent stem cells have been used for each experiment, it has difficulty to maintain premigratory embryonic neural crest progenitors or neural crest stem cells marked by SOX10, without spontaneous

differentiation in vitro. We found that it was possible to induce SOX10-positive neural crest cells derived from hiPS cells as shown induction method before [20], although these cells were immediately differentiated into the NGFR-positive but SOX10-negative population because of additional FGF signaling, which support their growth. So we identified the necessity of the inhibition of TGFß, and the appropriate concentration of CHIR99021 and FGF2 for maintaining SOX10-NL activity in vitro culture. And this condition for SOX10-maintaining cell culture system also adapted to neural crest-sphere culture as well.

Taken together, these results demonstrate that SOX10-expressing cells have self-renewal capacity and a possibility to form neural crest derivatives under proper differentiated conditions, and provide mass culture method of neural crest cells and would promote the research to use derivatives from human neural crest cells for cell therapy or drug screenings.

Supporting Information

S1 Fig. General strategy of 2A-Nano-lantern (NL) targeting into the human *SOX10* allele. (A) Schematic diagram of the human *SOX10* locus on chromosome 22 and targeting cassette for SOX10-2A-NL-floxed Neo (*hSOX10*$^{2A\text{-}NL\text{-}fNeo/+}$) or SOX10-2A-NL (*hSOX10*$^{2A\text{-}NL/+}$) knockin allele with genomic double strand break caused by CRISPR/Cas9 system. (B) PCR-amplified 2A-NL and loxP-pGK-Neo-loxP fragments were recombined with In-fusion clonase into pUC19 vector (pUC19-2A-NLpA-floxedNeo). (C) Triple DNA fragments (*hSOX10* 5'arm, *hSOX*10 3'arm and 2A-NL-floxedNeo) were recombined with In-fusion clonase into pDT-A vector for targeting into the human *SOX10* allele.
(PDF)

S2 Fig. Luciferase activities of Nano-lantern with induced neural crest cells from *hSOX10*$^{2A\text{-}NL/+}$ hiPS cells. Collected cells were counted and analyzed with Renilla Luciferase Assay System (Promega) as manufacturing protocol.
(PDF)

S3 Fig. Induced cells of the peripheral nervous system (PNS) and mesenchymal stem cells differentiated from SOX10-Nano-lantern positive neural crest cells. (A) NL+ cells were differentiated for 14 days supplemented with N2 supplement (GIBCO), 10 ng/mL of BDNF, GDNF, NT-3 and NGF (WAKO). Differentiated cells were immunostained with anti-ß3-tubulin (right panel). Nuclei were stained with 40,6-diamidino-2-phenylindole (DAPI, middle panel). Scale bar, 100 μm. (B) Expression of cell surface markers in mesenchymal stem cells.
(PDF)

S4 Fig. SOX10-Nano-lantern positive cells migrate to appropriate chemoattractants. (A) Representative migrated images from the colony of confluent SOX10-NL+ cells after 36 hours with or without chemoattractants. (B) NL+ cells migrated to chemoattractants with BMP2, FGF8 and SDF1. (C) Sorted NL+NGFR+ cells displayed higher migration rate than NL-NGFR- cells as shown in S1 Movie. $^{*}P<0.05$, $^{**}P<0.01$.
(PDF)

S1 Movie. Movie data for tracking analysis of SOX10-Nano-lantern positive cells. SOX10-NL+NGFR+ cells (left panel) and SOX10-NL-NGFR- cells (right panel).
(WMV)

S1 Table. primer sequences for *SOX10-2A-Nanolantern* targeting vector.
(PDF)

S2 Table. Primer sequences for RT-PCR or genomic PCR used in this study.
(PDF)

Acknowledgments

We are grateful to Dr. Akira Takai (RIKEN QBiC) for detecting Nano-lantern expression, Nikon cooperation for movie data.

Author Contributions

Conceptualization: TS.

Formal analysis: TH HO TS.

Funding acquisition: MI MU TS.

Investigation: TH HO MS TS.

Methodology: TH HO TS.

Project administration: TS.

Supervision: CS SK TS.

Validation: TH TS.

Writing – original draft: MI TS.

Writing – review & editing: TH TS.

References

1. Le Douarin NM, Kalcheim C. *The Neural Crest*. Cambridge (Cambridge University Press) 1999.
2. Anderson DJ. Cellular and molecular biology of neural crest cell lineage determination. Trends Genet. 1997; 13: 276–280. PMID: 9242050
3. Sauka-Spengler T, Bronner-Fraser M. A gene regulatory network orchestrates neural crest formation. Nat Rev Mol Cell Biol. 2008; 9: 557–568. doi: 10.1038/nrm2428 PMID: 18523435
4. Mayor R, Theveneau E. The neural crest. Development 2013; 140: 2247–2251. doi: 10.1242/dev.091751 PMID: 23674598
5. Honoré SM, Aybar MJ, Mayor R. Sox10 is required for the early development of the prospective neural crest in Xenopus embryos. Dev. Biol. 2003; 260: 79–96. PMID: 12885557
6. Kim J, Lo L, Dormand E, Anderson DJ. SOX10 maintains multipotency and inhibits neuronal differentiation of neural crest stem cells. Neuron 2003; 38: 17–31. PMID: 12691661
7. Kelsh RN. Sorting out Sox10 functions in neural crest development. BioEssays 2006
8. Britsch S, Goerich DE, Riethmacher D, Peirano RI, Rossner M, Nave KA, et al. The transcription factor Sox10 is a key regulator of peripheral glial development. Genes Dev. 2001; 15: 66–78. doi: 10.1101/gad.186601 PMID: 11156606
9. Saito K, Chang YF, Horikawa K, Hatsugai N, Higuchi Y, Hashida M, et al. Luminescent proteins for high-speed single-cell and whole-body imaging. Nat Commun. 2012; 3: 1262. doi: 10.1038/ncomms2248 PMID: 23232392
10. Kawaguchi J, Nichols J, Gierl MS, Faial T, Smith A. Isolation and propagation of enteric neural crest progenitor cells from mouse embryonic stem cells and embryos. Development 2010; 137: 693–704. doi: 10.1242/dev.046896 PMID: 20147374
11. Corpening JC, Deal KK, Cantrell VA, Skelton SB, Buehler DP, Southard-Smith EM. Isolation and Live Imaging of Enteric Progenitors Based on Sox10-Histone2BVenus Transgene Expression. Genesis 2011; 49: 599–618. doi: 10.1002/dvg.20748 PMID: 21504042
12. Chambers SM, Qi Y, Mica Y, Lee G, Zhang XJ, Niu L, et al. Combined small-molecule inhibition accelerates developmental timing and converts human pluripotent stem cells into nociceptors. Nat Biotechnol. 2012; 30: 715–720. doi: 10.1038/nbt.2249 PMID: 22750882

13. Szymczak AL, Workman CJ, Wang Y, Vignali KM, Dilioglou S, Vanin EF, et al. Correction of multi-gene deficiency in vivo using a single 'self-cleaving' 2A peptide-based retroviral vector. Nat Biotechnol. 2004; 22: 589–594. doi: 10.1038/nbt957 PMID: 15064769

14. Hiramuki Y, Sato T, Furuta Y, Surani MA, Sehara-Fujisawa A. Mest but Not MiR-335 Affects Skeletal Muscle Growth and Regeneration. PLoS One 2015; 10: e0130436. doi: 10.1371/journal.pone.0130436 PMID: 26098312

15. Takahashi K. Tanabe K, Ohnuki M, Narita M, Ichisaka T, Tomoda K, et al. Induction of pluripotent stem cells from adult human fibroblasts by defined factors. Cell 2007; 131: 861–872. doi: 10.1016/j.cell.2007.11.019 PMID: 18035408

16. Ikeya M, Kawada M, Nakazawa Y, Sakuragi M, Sasai N, Ueno M, et al. Gene disruption/knock-in analysis of mONT3: vector construction by employing both *in vivo* and *in vitro* recombinations. Int J Dev Biol. 2005; 49: 807–823. doi: 10.1387/ijdb.051975mi PMID: 16172977

17. Ran FA, Hsu PD, Wright J, Agarwala V, Scott DA, Zhang F. Genome engineering using the CRISPR-Cas9 system. Nat Protoc. 2013; 8: 2281–2308. doi: 10.1038/nprot.2013.143 PMID: 24157548

18. Li HL. Fujimoto N, Sasakawa N, Shirai S, Ohkame T, Sakuma T, et al. Precise correction of the dystrophin gene in duchenne muscular dystrophy patient induced pluripotent stem cells by TALEN and CRISPR-Cas9. Stem Cell Rep. 2015; 4: 143–154.

19. Nakagawa M. Taniguchi Y, Senda S, Takizawa N, Ichisaka T, Asano K, et al. A novel efficient feeder-free culture system for the derivation of human induced pluripotent stem cells. Sci. Rep. 2014; 4: 3594. doi: 10.1038/srep03594 PMID: 24399248

20. Fukuta M, Nakai Y, Kirino K, Nakagawa M, Sekiguchi K, Nagata S, et al. Derivation of Mesenchymal Stromal Cells from Pluripotent Stem Cells through a Neural Crest Lineage using Small Molecule Compounds with Defined Media. PLoS One 2014; 9: e112291. doi: 10.1371/journal.pone.0112291 PMID: 25464501

21. Lee G, Kim H, Elkabetz Y, Al Shamy G, Panagiotakos G, Barberi T, et al. Isolation and directed differentiation of neural crest stem cells derived from human embryonic stem cells. Nat Biotechnol. 2007; 25: 1468–1475. doi: 10.1038/nbt1365 PMID: 18037878

22. Sato T, Yamamoto T, Sehara-Fujisawa A. miR-195/497 induce postnatal quiescence of skeletal muscle stem cells. Nat. Commun. 2014; 5: 4597. doi: 10.1038/ncomms5597 PMID: 25119651

23. Naito Y, Hino K, Bono H, Ui-Tei K. CRISPRdirect: software for designing CRISPR/Cas guide RNA with reduced off-target sites. Bioinformatics 2015; 31: 1120–1123. doi: 10.1093/bioinformatics/btu743 PMID: 25414360

24. Sakai K, Miyazaki J. A transgenic mouse line that retains Cre recombinase activity in mature oocytes irrespective of the *cre* transgene transmission. Biochem Biophys Res Commun. 1997; 237: 318–24. PMID: 9268708

25. Kerosuo L, Nie S, Bajpai R, Bronner ME. Crestospheres: Long-Term Maintenance of Multipotent, Premigratory Neural Crest Stem Cells. Stem Cell Rep. 2015; 5: 499–507.

Effect of Trabeculotomy on Corneal Endothelial Cell Loss in Cases of After Penetrating-Keratoplasty Glaucoma

Ayaka Kusakabe, BS, MS, Naoki Okumura, MD, PhD,* Koichi Wakimasu, MD,† Kanae Kayukawa, MD,† Masami Kondo, BS,* Noriko Koizumi, MD, PhD,* Chie Sotozono, MD, PhD,‡ Shigeru Kinoshita, MD, PhD,†‡§ and Kazuhiko Mori, MD, PhD‡*

Purpose: The aim of this study was to evaluate the effect of trabeculotomy (TLO) on glaucoma and endothelial cell loss after penetrating keratoplasty (PK).

Methods: A retrospective study was conducted on consecutive patients who underwent PK and in whom more than 24 months of follow-up was available. Patients were categorized into the PK+TLO group [ie, TLO for post-PK glaucoma (n = 10)] and the PK group [PK alone (n = 73)]. Intraocular pressure (IOP) was evaluated during each follow-up examination. Central corneal endothelium images were obtained and analyzed to determine corneal endothelial cell (CEC) density.

Results: The mean duration period from original PK to TLO for secondary glaucoma was 25.5 ± 34.9 months in the PK+TLO group. Mean preoperative IOP in the PK+TLO group was 35.8 mm Hg, and decreased to 17.5 mm Hg at 24 months postoperative ($P < 0.01$). CEC density decreased in the same manner in both groups. In the PK+TLO group, mean CEC density was 1838 cells per square millimeter before TLO and decreased to 1195 cells per square millimeter at 24 months after TLO. In the PK group, mean CEC density decreased from 1870 to 1209 cells per square millimeter at each corresponding time point.

Conclusions: TLO for post-PK glaucoma appeared to safely lower IOP, although repeated surgeries were required in some patients, and did not accelerate CEC loss.

Key Words: penetrating keratoplasty, trabeculotomy, corneal endothelial cell density

(*Cornea* 2017;36:317–321)

Received for publication September 11, 2016; revision received October 1, 2016; accepted October 4, 2016. Published online ahead of print November 16, 2016.

From the *Department of Biomedical Engineering, Faculty of Life and Medical Sciences, Doshisha University, Kyotanabe, Japan; †Department of Ophthalmology, Baptist Yamasaki Eye Clinic, Kyoto, Japan; ‡Departments of Ophthalmology; and §Frontier Medical Science and Technology for Ophthalmology, Kyoto Prefectural University of Medicine, Kyoto, Japan.

The authors have no funding or conflicts of interest to disclose.

Supplemental digital content is available for this article. Direct URL citations appear in the printed text and are provided in the HTML and PDF versions of this article on the journal's Web site (www.corneajrnl.com).

Reprints: Kazuhiko Mori, MD, PhD, Department of Ophthalmology, Kyoto Prefectural University of Medicine, 465 Kajii-cho, Hirokoji-agaru, Kawaramachi-dori, Kamigyo-ku, Kyoto 602-0841, Japan (e-mail: kmori@koto.kpu-m.ac.jp).

Glaucoma is recognized as one of the most devastating complications that can arise after corneal transplantation, as it can often lead to corneal graft failure and glaucomatous optic neuropathy resulting in visual field loss. In 1969, Irvine and Kaufman[1] reported a high incidence of intraocular pressure (IOP) elevation after penetrating keratoplasty (PK). Currently, it is widely accepted that the incidence of glaucoma after PK is high, ranging from 9% to 35% of all cases.[2–8]

Topical administration of antiglaucoma drugs is a first-line treatment for the control of IOP. However, as management of glaucoma after corneal transplantation is difficult, surgical treatments are often required.[8] Trabeculectomy (TLE), implantation of a glaucoma drainage device, and cyclophotocoagulation are the surgical procedures most commonly used for the treatment of glaucoma after corneal transplantation. However, they are reportedly associated with a high risk of corneal endothelial cell (CEC) loss and eventual graft failure.[8,9]

Trabeculotomy (TLO) reduces IOP by improving the outflow facility, and it is reportedly effective for the treatment of several types of glaucoma.[10–13] However, the effectiveness of TLO for the treatment of post-PK glaucoma has yet to be fully elucidated. Reportedly, one major advantage of TLO is that it is a very safe procedure without risk of bleb-related complications.[14] In this study, we investigated the effect of TLO for the treatment of post-PK glaucoma and its influence on CEC loss.

MATERIALS AND METHODS

This study was conducted in accordance with a protocol approved by the Institutional Review Board of Baptist Eye Clinic, Kyoto, Japan. Clinical trial registration was obtained at UMIN UMIN000021104 (http://www.umin.ac.jp/english/). In this retrospective study, we reviewed the medical records of consecutive patients who underwent PK at Baptist Eye Clinic between January 2001 and October 2011 and in whom more than 24-month follow-up data were available. Patients who underwent TLE, pars plana vitrectomy, or goniosynechialysis were excluded from the study. The included patients were categorized into those who underwent TLO for the treatment of glaucoma after PK and those who did not undergo TLO after PK (Fig. 1). Of the patients who underwent TLO after PK, 3 were excluded from the study because of discontinuation of follow-up as a result of poor

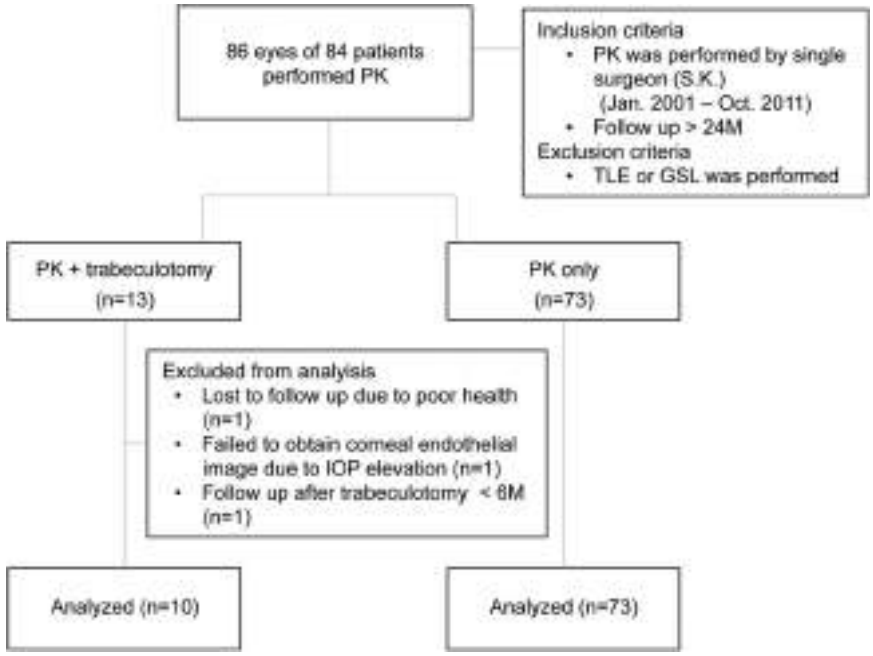

FIGURE 1. Flowchart of the patients included in the study. GSL, goniosynechialysis; PPV, pars plana vitrectomy.

health (n = 1), failure to obtain a corneal endothelial image as a result of elevated IOP (n = 1), or not being able to undergo follow-up for more than 6 months after TLO (n = 1). In the patients included in the study, anterior segments were evaluated by slit-lamp microscopy, corneal endothelium was observed by noncontact specular microscopy (EM-3000; Tomey Corporation, Nagoya, Japan), and IOP was evaluated by noncontact tonometry (RKT-7700 or TONOREF2; NIDEK CO, LTD, Aichi, Japan) at each follow-up visit.

In each patient, PK was performed by first administering general anesthesia or retrobulbar anesthesia in accordance with the patient's overall health status. Next, partial-thickness trephination of the host cornea was performed using a Barron radial vacuum trephine (Katena Products Inc, Denville, NJ), and the cornea was then excised using curved corneal scissors. Donor corneas were trephined using a Barron vacuum donor cornea punch (Katena Products). In each patient, the corneal graft was sutured with 4 to 8 interrupted and continuous-running 10-0 nylon sutures. After PK, topical antibiotics and corticosteroid eye drops were administered and then gradually tapered down. All PKs were performed by the same surgeon (S.K.).

In the patients of the TLO-group, sub-Tenon capsule anesthesia was first performed. Next, a fornix-based conjunctival flap and two 3- × 3-mm-square deep scleral flaps with 1/2 and 4/5 thickness were made. The outer wall of the Schlemm canal was then dissected, and TLO probes (HS-2155B2; Handaya Co, Ltd, Tokyo, Japan) were inserted into the canal. A double-mirror goniolens (OMUSG; Ocular Instruments Inc, Bellevue, WA) was placed on the surface of the cornea to confirm insertion of the TLO probes into the Schlemm canal, and the probes were then rotated into the anterior chamber. The scleral and conjunctival flaps were then sutured with interrupted 10-0 nylon sutures. All TLOs were performed by the same surgeon (K.M.).

The donor and recipient characteristic data are presented as mean ± SD. The mean CEC loss data are presented as mean ± SE. The Student *t*-test was used to determine statistical significance (*P* value) of the differences in the mean

TABLE 1. Characteristics of the Donor and Recipient Eyes

	PK+TLO (n = 10)	PK (n = 73)	*P*
Donor characteristics			
Age			0.47
Mean ± SD, yrs	62.9 ± 8.7	60.1 ± 11.7	
Range	49–75	19–75	
Size			0.5
Mean ± SD, mm	7.6 ± 0.3	7.6 ± 0.2	
Range	7–7.75	7–7.75	
CEC density			
Mean ± SD, cells/mm^2	2756 ± 338	2892 ± 329	0.23
Recipient characteristics			
Age			0.44
Mean ± SD, yrs	61.0 ± 16.8	64.5 ± 12.7	
Range	27–85	22–84	
Sex, n (%)			0.33
Male	6 (60.0)	29 (40.8)	
Female	4 (40.0)	42 (59.2)	
Regraft, n (%)	4 (40.0)	0 (0.0)	
Diagnosis, n (%)			
Bullous keratopathy*	5 (50.0)	28 (38.4)	
Corneal opacity	2 (20.0)	21 (28.8)	
Dystrophy (non-Fuchs)	1 (10.0)	13 (17.8)	
Keratoconus	1 (10.0)	6 (8.2)	
Fuchs dystrophy	1 (10.0)	3 (4.1)	
Others	1 (10.0)	2 (2.7)	

*Including edema after cataract surgery and argon-laser-iridectomy-induced edema.

TABLE 2. IOP-Lowering Effect of TLO

Time Post TLO, mo	No. Patients	No. Repeated TLO	Mean IOP ± SD, mm Hg	*P*
Preoperative	10	0	35.8 ± 11.3	
6	10	3	19.7 ± 7.8	0.0004
12	8	4	18.4 ± 5.6	0.0003
18	8	4	16.8 ± 4.9	0.0002
24	8	4	17.5 ± 5.7	0.0007

values of the 2-sample comparison. The Fisher exact test was used for analysis of the sex data.

RESULTS

Of the total number of PKs performed during the study period, 86 eyes of 84 patients (mean age: 62.9 ± 8.7 years, range: 49–75 years) met the inclusion criteria. Thirteen eyes underwent TLO after PK due to elevated IOP; 3 of those eyes were excluded from the study because of not meeting the inclusion criteria. Seventy-three eyes underwent only PK. Mean recipient age was 61.0 ± 16.8 years (range: 27–85 years) in the PK+TLO group and 64.5 ± 12.7 years (range: 22–84 years) in the PK group. The baseline characteristics were similar between both groups. However, IOP before performing TLO was significantly higher in the PK+TLO than in the PK group ($P < 0.01$). In the PK+TLO group, 10 eyes had twice undergone a repeat graft at the time of the patient being included in the study. In the PK group, no eyes had a history of a previously repeated graft. The indications for corneal transplantation were similar among the patients in each group. Bullous keratopathy (including edema after cataract surgery and argon laser iridectomy–induced edema), corneal opacity, and corneal dystrophies were the most common indications (Table 1). Survival of the graft was maintained in all eyes in the PK+TLO group, with no episodes of graft rejection being observed during the 72-month follow-up period.

The mean preoperative IOP in the PK+TLO group was 35.8 ± 11.3 mm Hg. After TLO, the mean IOP decreased to 19.7 ± 7.8 mm Hg at 6 months, 18.4 ± 5.6 mm Hg at 12 months, 16.8 ± 4.9 mm Hg at 18 months, and 17.5 ± 5.7 mm Hg at 24 months ($P < 0.01$). Repeated TLO was performed in 4 of the 10 patients during the 24-month follow-up period (Table 2). TLO was repeated once in 3 patients and twice in 1 patient.

The time course of CEC density after TLO for post-PK glaucoma is shown in Figure 2. The mean duration period from original PK to TLO for secondary glaucoma was 25.5 ± 34.9 months in the PK+TLO group. To compare CEC density at a similar follow-up time from PK, cell densities at 24, 30, 36, and 48 months after PK were plotted for 0, 6, 12, 18, and 24 months after TLO. CEC density decreased in the same manner in both PK+TLO group and PK group. In the PK+TLO group, the mean CEC density before TLO and at 6, 12, 18, and 24 months after TLO was 1838, 1635, 1402, 1306, and 1195 cells per square millimeter, respectively. In the PK group, mean CEC density was 1870, 1727, 1509, 1356, and 1209 cells per square millimeter, respectively, at each corresponding time point in which the time after PK was similar to that of the PK+TLO group ($P = 0.18$, $P = 0.56$, $P = 0.69$, $P = 0.58$, and $P = 0.05$).

Our findings show that TLO for post-PK glaucoma did not accelerate CEC loss (see Table, Supplemental Digital Content 1, http://links.lww.com/ICO/A469). In the PK+TLO group, the mean postoperative CEC loss was 23.0% [95% confidence interval (CI), 7.7%–38.2%] in 0 to 12 months, 30.2% (95% CI, 16.5%–43.9%) in 0 to 24 months, 36.4% (95% CI, 14.7%–58.2%) in 0 to 36 months, 36.4% (95% CI, 14.7%–58.2%) in 0 to 48 months, 40.7% (95% CI, 18.4%–63.0%) in 0 to 60 months, and 55.1% (95% CI, 38.1%–72.2%) in 0 to 72 months. In the PK group, the mean CEC

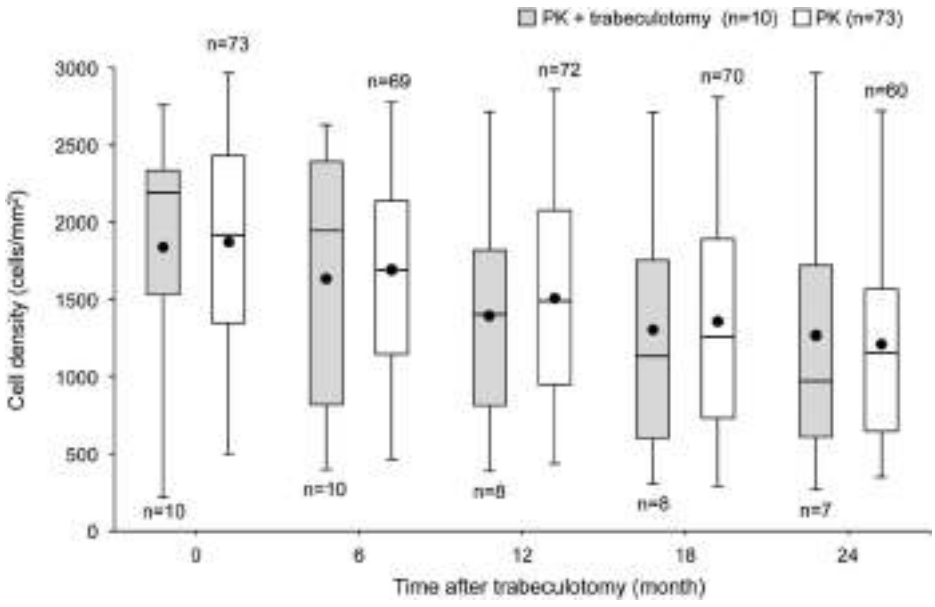

FIGURE 2. CEC loss after TLO after PK. PK+TLO indicates the CEC density of the patients who underwent TLO for post-PK glaucoma. PK indicates the CEC density of the patients who underwent PK alone. The black dots indicate the mean value, the horizontal lines in the boxes indicate medians, the bottom of each box indicates the 25th percentile, and the top of each box indicates the 75th percentile. The horizontal lines outside the boxes indicate the range of CEC density. The mean duration period from the original PK to TLO for secondary glaucoma was 25.5 ± 34.9 months in the PK+TLO group. To compare CEC density at a similar follow-up time from PK, cell density at 24, 30, 36, and 48 months after PK were plotted for 0, 6, 12, 18, and 24 months after TLO.

loss was 22.9% (95% CI, 19.3%–26.5%) in 0 to 12 months, 35.0% (95% CI, 30.0%–39.9%) in 0 to 24 months, 47.8% (95% CI, 42.6%–53.0%) in 0 to 36 months, 58.2% (95% CI, 52.8%–63.6%) in 0 to 48 months, 67.3% (95% CI, 62.4%–72.1%) in 0 to 60 months, and 70.2% (95% CI, 65.1%–75.3%) in 0 to 72 months. The time duration is shown from PK to the follow-up period in both groups.

DISCUSSION

It has been reported that in patients who undergo PK, there is a major risk of developing glaucoma after surgery, yet the mechanism remains unclear.[15–17] The Collaborative Corneal Transplantation Studies Research Group reported that the existence of glaucoma before PK increased the rate of graft failure from 29% to 48%.[15] The Cornea Donor Study also reported in a large, multicenter, prospective study that glaucoma treatment before PK increased the risk of graft failure over the 5-year postoperative period (medications and no surgery: 20%; no medications and surgery: 29%; and medications and surgery: 58%, respectively), yet it was only 11% in patients without preoperative glaucoma.[17]

It has been reported that after PK, glaucoma develops in 9% to 31% of the patients during the early postoperative period and in 18% to 35% of the patients during the late postoperative period.[2–8] Tandon et al[9] performed a meta-analysis and reported that TLE, glaucoma drainage device implantation, and cyclophotocoagulation reduced IOP by 13.6, 20.2, and 20.4 mm Hg, respectively. In their review, the rate of graft failure after those treatments was 24%, 35%, and 21%, respectively, suggesting a higher risk of surgical treatment for maintaining the transplanted graft.[9] In this study, we demonstrated that CEC density after TLO for post-PK glaucoma decreased in a fashion similar to that after PK alone, and that there was no episode of graft failure during 2 years postoperatively. The rate of graft rejection after post-PK TLE reportedly ranges from 24% to 30%[18–20]; however, another study reported that the risk of rejection was not increased.[21] The findings of this current study showing no episode of rejection during the 72 months after post-PK TLO indicates that TLO did not increase the risk of graft rejection. Although the number of patients treated with TLO, as well as the follow-up period, was limited in this study, our findings suggest that TLO is both safe and effective for treating post-PK glaucoma, with minimal damage to corneal endothelium.

Basic research using monkey and human enucleated eyes showed that TLO disrupts the trabecular meshwork and the inner layer of the Schlemm canal, and then reduces the resistance to aqueous humor outflow.[22,23] The IOP-lowering effect of TLO has been shown in relation to several forms of glaucoma, such as primary open-angle glaucoma,[10] developmental glaucoma,[13] steroid-induced glaucoma,[12] uveitis-induced glaucoma,[14] and exfoliative glaucoma.[11] In terms of post keratoplasty, Yuki et al reported preliminary results that TLO successfully lowered IOP in 4 glaucoma patients after Descemet stripping endothelial keratoplasty.[24] In this study, we found that TLO decreased post-PK-glaucoma-related IOP from 35.8 to 18.4 mm Hg at 1 year and 17.5 mm Hg at 2 years ($P < 0.01$). Although multiple TLOs were performed in some patients in this study, IOP was effectively reduced and CEC loss did not accelerate, thus suggesting that repeated TLO is a safe and effective therapeutic option. Although the mechanism by which glaucoma develops post-PK remains unclear, involvement of the use of steroids, inflammation, distortion of angle, and closed angle due to peripheral anterior synechiae have been reported.[8,25] Further study is needed to elucidate the types of post-PK glaucoma in which the associated elevated IOP is effectively reduced by TLO.

It should be noted that the limitations of this study include its retrospective design and the small sample size of patients who underwent post-PK TLO. A prospective study is needed to better evaluate the role of TLO in the treatment of post-PK glaucoma.

In conclusion, the findings of this study show that TLO for the treatment of post-PK glaucoma successfully lowered IOP and did not accelerate CEC loss, thus suggesting that TLO is an effective surgical procedure for the management of post-PK glaucoma. Although TLO is not currently considered a first-line surgical procedure for the treatment of post-PK glaucoma, we propose that it should be reconsidered as a safe and effective therapeutic option.

ACKNOWLEDGMENTS

The authors thank Dr Hiroko Nakagawa for her valuable assistance with the collection of patient data and Mr John Bush for editing the manuscript.

REFERENCES

1. Irvine AR, Kaufman HE. Intraolar pressure following penetrating keratoplasty. *Am J Ophthalmol.* 1969;68:835–844.
2. Goldberg DB, Schanzlin DJ, Brown SI. Incidence of increased intraocular pressure after keratoplasty. *Am J Ophthalmol.* 1981;92:372–377.
3. Karesh JW, Nirankari VS. Factors associated with glaucoma after penetrating keratoplasty. *Am J Ophthalmol.* 1983;96:160–164.
4. Foulks GN. Glaucoma associated with penetrating keratoplasty. *Ophthalmology.* 1987;94:871–874.
5. Kirkness CM, Moshegov C. Post-keratoplasty glaucoma. *Eye (Lond).* 1988;(suppl 2):S19–S26.
6. Wilson SE, Kaufman HE. Graft failure after penetrating keratoplasty. *Surv Ophthalmol.* 1990;34:325–356.
7. Chien AM, Schmidt CM, Cohen EJ, et al. Glaucoma in the immediate postoperative period after penetrating keratoplasty. *Am J Ophthalmol.* 1993;115:711–714.
8. Ayyala RS. Penetrating keratoplasty and glaucoma. *Surv Ophthalmol.* 2000;45:91–105.
9. Tandon A, Espandar L, Cupp D, et al. Surgical management for postkeratoplasty glaucoma: a meta-analysis. *J Glaucoma.* 2014;23:424–429.
10. Tanihara H, Negi A, Akimoto M, et al. Long-term results of non-filtering surgery for the treatment of primary angle-closure glaucoma. *Graefes Arch Clin Exp Ophthalmol.* 1995;233:563–567.
11. Honjo M, Tanihara H, Inatani M, et al. Phacoemulsification, intraocular lens implantation, and trabeculotomy to treat pseudoexfoliation syndrome. *J Cataract Refract Surg.* 1998;24:781–786.
12. Honjo M, Tanihara H, Inatani M, et al. External trabeculotomy for the treatment of steroid-induced glaucoma. *J Glaucoma.* 2000;9:483–485.

13. Ikeda H, Ishigooka H, Muto T, et al. Long-term outcome of trabeculotomy for the treatment of developmental glaucoma. *Arch Ophthalmol.* 2004;122:1122–1128.
14. Voykov B, Dimopoulos S, Leitritz MA, et al. Long-term results of ab externo trabeculotomy for glaucoma secondary to chronic uveitis. *Graefes Arch Clin Exp Ophthalmol.* 2016;254:355–360.
15. Maguire MG, Stark WJ, Gottsch JD, et al. Risk factors for corneal graft failure and rejection in the collaborative corneal transplantation studies. Collaborative Corneal Transplantation Studies Research Group. *Ophthalmology*. 1994;101:1536–1547.
16. Reinhard T, Kallmann C, Cepin A, et al. The influence of glaucoma history on graft survival after penetrating keratoplasty. *Graefes Arch Clin Exp Ophthalmol.* 1997;235:553–557.
17. Sugar A, Tanner JP, Dontchev M, et al. Recipient risk factors for graft failure in the cornea donor study. *Ophthalmology*. 2009;116:1023–1028.
18. Kirkness CM, Steele AD, Ficker LA, et al. Coexistent corneal disease and glaucoma managed by either drainage surgery and subsequent keratoplasty or combined drainage surgery and penetrating keratoplasty. *Br J Ophthalmol.* 1992;76:146–152.
19. Kirkness CM, Ling Y, Rice NS. The use of silicone drainage tubing to control post-keratoplasty glaucoma. *Eye (Lond).* 1988;2(pt 5):583–590.
20. WuDunn D, Alfonso E, Palmberg PF. Combined penetrating keratoplasty and trabeculectomy with mitomycin C. *Ophthalmology*. 1999;106:396–400.
21. Figueiredo RS, Araujo SV, Cohen EJ, et al. Management of coexisting corneal disease and glaucoma by combined penetrating keratoplasty and trabeculectomy with mitomycin-C. *Ophthalmic Surg Lasers.* 1996;27:903–909.
22. Ellingsen BA, Grant WM. Influence of intraocular pressure and trabeculotomy on aqueous outflow in enucleated monkey eyes. *Invest Ophthalmol.* 1971;10:705–709.
23. Ellingsen BA, Grant WM. Trabeculotomy and sinusotomy in enucleated human eyes. *Invest Ophthalmol.* 1972;11:21–28.
24. Yuki K, Shimmura S, Shiba D, et al. Trabeculotomy for the treatment of glaucoma after Descemet stripping endothelial keratoplasty. *Br J Ophthalmol.* 2008;92:1299–1300.
25. Ing JJ, Ing HH, Nelson LR, et al. Ten-year postoperative results of penetrating keratoplasty. *Ophthalmology*. 1998;105:1855–1865.

Effect of the Rho-Associated Kinase Inhibitor Eye Drop (Ripasudil) on Corneal Endothelial Wound Healing

Naoki Okumura,[1] Yugo Okazaki,[1] Ryota Inoue,[1] Kazuya Kakutani,[1] Shinichiro Nakano,[1] Shigeru Kinoshita,[2] and Noriko Koizumi[1]

[1]Department of Biomedical Engineering, Faculty of Life and Medical Sciences, Doshisha University, Kyotanabe, Japan
[2]Department of Frontier Medical Science and Technology for Ophthalmology, Kyoto Prefectural University of Medicine, Kyoto, Japan

Correspondence: Noriko Koizumi, Department of Biomedical Engineering, Faculty of Life and Medical Sciences, Doshisha University, Kyotanabe 610-0321, Japan; nkoizumi@mail.doshisha.ac.jp.

Submitted: November 5, 2015
Accepted: February 10, 2016

Citation: Okumura N, Okazaki Y, Inoue R, et al. Effect of the rho-associated kinase inhibitor eye drop (ripasudil) on corneal endothelial wound healing. *Invest Ophthalmol Vis Sci*. 2016;57:1284–1292. DOI:10.1167/iovs.15-18586

Purpose. Ripasudil (Glanatec), a selective rho-associated coiled coil-containing protein kinase (ROCK) inhibitor, was approved as a glaucoma and ocular hypertension treatment in Japan in 2014. The purpose of this study was to investigate the feasibility of using ripasudil eye drops to treat corneal endothelial injuries.

Methods. Cultured human corneal endothelial cells (HCECs) were treated with ripasudil, and 5-bromo-2′-deoxyuridine (BrdU) incorporation was evaluated by ELISA. A rabbit corneal endothelial damage model was also created by mechanically scraping the corneal endothelium, followed by topical ripasudil eye drop application for 2 weeks. The anterior segment was evaluated by slit-lamp microscopy, and central corneal thickness was measured by ultrasound pachymetry. Corneal specimens were evaluated by phalloidin staining and immunohistochemical analysis using antibodies against Ki67, N-cadherin, and Na^+/K^+-ATPase.

Results. Many more BrdU-positive cells were observed among the HCECs treated with ripasudil (0.3–30 μM) than among the control HCECs. Ripasudil-treated eyes in a rabbit model showed 91.5 ± 2.0% Ki67-positive cells after 48 hours, whereas control eyes showed 52.6 ± 1.3%. Five of six corneas became transparent in ripasudil-treated eyes, whereas zero of six corneas became transparent in the control eyes. Regenerated cell densities were higher in the eyes treated with ripasudil than in eyes treated with vehicle. Eyes treated with ripasudil expressed N-cadherin and Na^+/K^+-ATPase in almost all CECs, whereas this expression was decreased in control eyes.

Conclusions. Ripasudil promoted corneal endothelial wound healing, supporting its development as eye drops for treating acute corneal endothelial damage due to eye surgeries, especially cataract surgery.

Keywords: corneal endothelial cells, bullous keratopathy, Rho kinase inhibitor

The corneal endothelium regulates corneal transparency by balancing corneal hydration through pump and barrier functions. Hexagonal corneal endothelial cells (CECs) form a monolayer sheet at a cell density of approximately 2500 cells/mm^2 in late adulthood, but corneal endothelial damage—due to Fuchs' endothelial corneal dystrophy, cataract surgery, and corneal trauma—induces compensatory migration and spreading, which results in a cell density drop. When corneal endothelial cell density reaches a critical level, typically 500 cells/mm^2, the corneal endothelial function is not compensated, and the cornea then exhibits haziness, together with edema. The only therapy is corneal transplantation, as no pharmaceutical intervention has yet been introduced into clinical settings.[1]

In 2009, we reported that the rho-associated kinase (ROCK) inhibitor, Y-27632, promoted in vitro cell proliferation of cultured CECs.[2] Subsequently, we demonstrated that topical application of Y-27632 in the form of eye drops enhances in vivo corneal endothelial wound healing in rabbit and monkey models.[3,4] Following the animal experiments, we performed clinical research on corneal endothelial dysfunction patients who were treated with Y-27632 eye drops following a 2-mm-diameter transcorneal freezing procedure. Rho-associated kinase inhibitor eye drops showed effectiveness in reducing the central corneal thickness in patients with early stage Fuchs' endothelial corneal dystrophy (these patients still had residual healthy corneal endothelium at the peripheral cornea), whereas the ROCK inhibitor did not reduce central corneal thickness in patients with an advanced stage of corneal endothelial dysfunction with diffuse edema.[4,5] These results from our clinical research suggest that ROCK inhibitor eye drops enhance corneal endothelial wound healing by promoting residual CEC proliferation, as long as some relatively healthy CECs remain. However, despite accumulating evidence, no commercially available ROCK inhibitor has been developed for the treatment of corneal endothelial injury.

In the field of ophthalmology, ROCK inhibitors have attracted much interest among investigators as potent drugs for glaucoma treatment, because ROCK inhibitors reduce the intraocular pressure by increasing the outflow facility of the aqueous humor.[6–10] Ripasudil hydrochloride hydrate, a selective ROCK inhibitor, has been developed as a glaucoma drug and has been shown in phase 1 clinical trials to reduce IOP in healthy adult volunteers.[11] Randomized clinical studies have demonstrated that 0.4% ripasudil eye drops reduced intraocular

Investigative Ophthalmology & Visual Science

pressure in patients with primary open-angle glaucoma and ocular hypertension.[12,13] Subsequently, in 2014, a commercial preparation of ripasudil hydrochloride hydrate eye drops (Glanatec ophthalmic solution 0.4%, Kowa Company Ltd., Nagoya, Japan) was approved in Japan for the treatment of glaucoma and ocular hypertension.[14] The 50% inhibitory concentration (IC_{50}) of ripasudil is 0.051 μM for ROCK 1 and 0.019 μM for ROCK 2, whereas the IC_{50} for PKACα, PKC, and CaMKIIα are 2.1, 27, and 0.37 μM, respectively.[15] This high selectivity for ROCK is considered to contribute to the safety of ripasudil, which shows minimal off-target effects through inhibition or activation of other signaling pathways.

In the present study, we tested the feasibility of repositioning ripasudil as a treatment for corneal endothelial injuries. Drug repositioning (i.e., the repurposing of an existing drug for new indications[16–18]) is one possible strategy for drug development that could have a faster approval time and lower investment cost than traditional drug discovery. Here we showed that ripasudil treatment promotes in vitro CEC proliferation in cultured human CECs (HCECs) in a similar fashion to that shown by the conventional ROCK inhibitors Y-27632 and fasudil. We also demonstrated that ripasudil eye drops promoted wound healing and facilitated regeneration of the corneal endothelium in a rabbit wound model.

Methods

Animal Experiment Approval

In all experiments, animals were housed and treated in accordance with the ARVO Statement for the Use of Animals in Ophthalmic and Vision Research. The rabbit experiments were performed at Doshisha University (Kyoto, Japan) according to the protocol approved by the University's Animal Care and Use Committee (Approval A15012). Human donor corneas were obtained from SightLife (Seattle, WA, USA) for research purposes.

Cell Culture

A total of four human donor corneas (from persons >40 years of age) were used for cultivation of HCECs by the protocol described previously.[19] Briefly, Descemet's membranes containing the HCECs were stripped from donor corneas, and the membranes were digested with 1 mg/mL collagenase A (Roche Applied Science, Penzberg, Germany) at 37°C for 12 hours. The HCECs were seeded in 1 well of a 48-well plate coated with laminin E8 fragments (iMatrix-511; Nippi, Inc., Tokyo, Japan) (0.5 μg/cm^2). The culture medium was prepared according to published protocols.

First, bone marrow mesenchymal stem cells (BM-MSCs) were cultured according to previously reported protocols.[20] Briefly, basal medium for HCECs was prepared (OptiMEM-I [Life Technologies Corp., Carlsbad, CA, USA] containing 8% fetal bovine serum, 5 ng/mL epidermal growth factor [Sigma-Aldrich Corp., St. Louis, MO, USA], 20 μg/mL ascorbic acid [Sigma-Aldrich Corp.], 200 mg/L calcium chloride, 0.08% chondroitin sulfate [Wako Pure Chemical Industries, Ltd., Osaka, Japan], 50 μg/mL gentamicin, and 10 μM SB431542 [Merck Millipore, Billerica, MA, USA]) and conditioned by culturing BM-MSCs for 24 hours. The basal medium conditioned with BM-MSCs was then collected for use as the culture medium for HCECs. The HCECs were cultured with Y-27632 (Wako Pure Chemical Industries, Ltd.), fasudil (Wako Pure Chemical Industries, Ltd.), or ripasudil (Kowa Company, Ltd., Nagoya, Japan) to evaluate the effect of each ROCK inhibitor on HCEC proliferation.

Immunohistochemistry

Cultured HCECs or rabbit corneal specimens were fixed in 4% formaldehyde and incubated in 1% BSA to block nonspecific binding. The samples were investigated by conducting immunohistochemical analyses of Ki67 (Sigma-Aldrich Corp.), N-cadherin (1:300; BD Biosciences, San Jose, CA, USA), and Na^+/K^+-ATPase (1:300; Upstate Biotechnology, Lake Placid, NY, USA) antibodies. Alexa Fluor 488–conjugated goat anti-mouse (Life Technologies Corp.) was used as a secondary antibody at a 1:1000 dilution. Cell morphology was evaluated after actin staining with a 1:400 dilution of Alexa Fluor 594–conjugated phalloidin (Life Technologies Corp.). Proliferative cells were evaluated by 5-ethynyl-2 Click-iT 5-ethynyl-2′-deoxyuridine (EdU) imaging kits (Life Technologies Corp.) according to the manufacturer's instructions. Briefly, the HCECs (1×10^4 cells per well) were cultured in a 96-well plate and incubated with 10 μM EdU for 6 hours at 37°C. Following fixation with 4% paraformaldehyde and permeabilization with 0.3% Triton X-100 (Nacalai Tesque, Kyoto, Japan), the HCECs were incubated with a reaction cocktail. Nuclei were stained with 4′,6-diamidino-2-phenylindole (DAPI) (Vector Laboratories, Burlingame, CA, USA). The specimens were viewed with a fluorescence microscope (TCS SP2 AOBS; Leica Microsystems, Wetzlar, Germany).

Cell Proliferation Assay

Human CECs were cultured at a density of 5000 cells per well in a 96-well plate. Cell proliferation was determined by evaluating incorporation of 5-bromo-2′-deoxyuridine (BrdU) into DNA by use of the Cell Proliferation Biotrak ELISA system, version 2 (GE Healthcare Life Sciences, Buckinghamshire, United Kingdom) according to the manufacturer's instructions. Briefly, HCECs were incubated with 10 μM BrdU for 24 hours. Cultured cells were incubated with fixation solution and incubated with 100 μL monoclonal antibody against BrdU for 30 minutes. The BrdU absorbance was measured by a spectrophotometric microplate reader.

Rabbit Corneal Endothelial Damage Model by Corneal Freezing

As an in vivo wound model, the corneal endothelium of 48 eyes of 24 Japanese white rabbits was damaged in a modified protocol, as described previously.[3,21,22] Briefly, a stainless steel 7-mm-diameter probe was immersed in liquid nitrogen for 3 minutes, and the center of the rabbit cornea was cryofrozen with the probe for 15 seconds under general anesthesia. This procedure was carefully confirmed not to induce complete blindness or any severe general adverse effect. One 0.4% ripasudil eye drop (four times daily) or 0.8% ripasudil eye drop (two times daily) was topically instilled (50 μL) in one eye of each of six rabbits, whereas vehicle was instilled in the fellow eye of each rabbit as a control ($n = 6$). Ripasudil eye drops and vehicles were provided by the Kowa Company. After 48 hours of treatment, the rabbits were euthanized, and the corneal endothelium wound area was evaluated by Alizarin red staining and examined with a fluorescence microscope (BZ-9000; Keyence, Osaka, Japan). The Ki67-positive cells located at the leading edge (3.5 mm distant from the center of the cornea), middle area (4.5 mm distant from the center of the cornea), and periphery (5.5 mm distant from the center of the cornea) were also evaluated in the same specimens. These experiments were performed in duplicate.

Investigative Ophthalmology & Visual Science

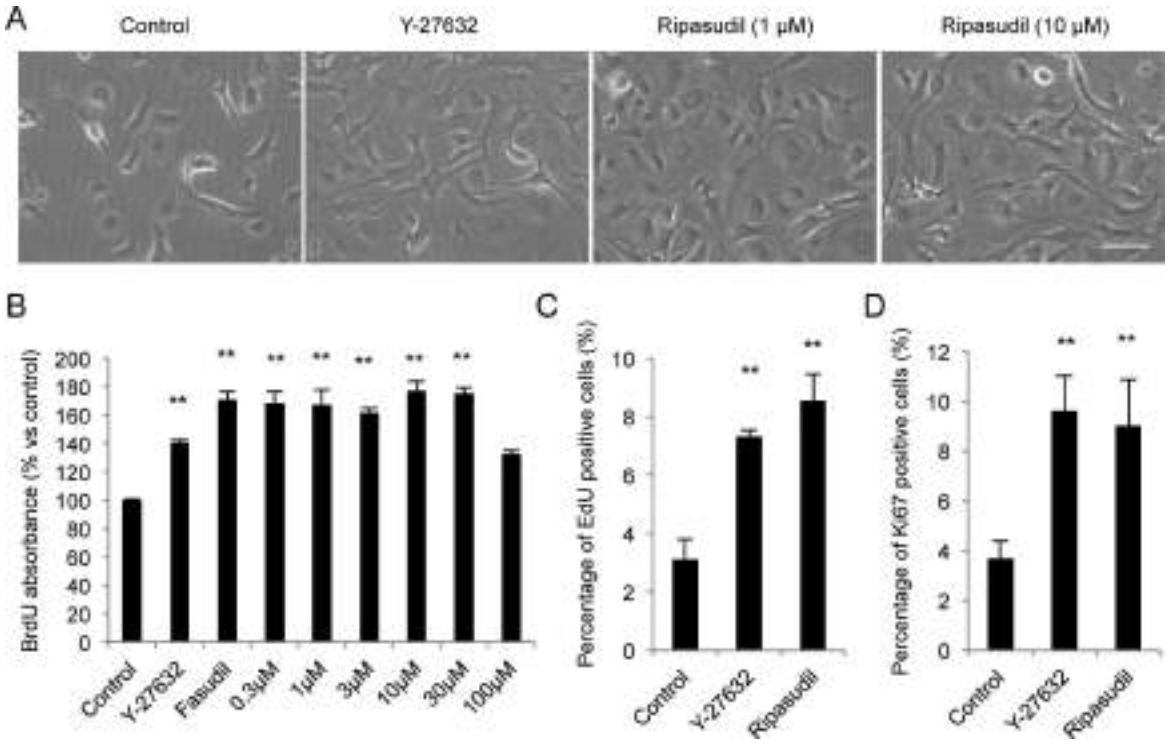

Figure 1. Effect of ripasudil on in vitro corneal endothelial cell proliferation. (**A**) Cultured HCECs were seeded onto the culture plate and incubated for 24 hours, followed by treatment with the ROCK inhibitors Y-27632 (10 μM), fasudil (10 μM), and ripasudil (0.3–100 μM) for 48 hours. Representative phase contrast images are shown. *Scale bar*: 50 μm. (**B**) The HCECs were cultured at the density of 5000 cells per well in a 96-well plate for 24 hours, and DNA synthesis was detected by ELISA as incorporation of BrdU into DNA. BrdU incorporation was significantly enhanced at the ripasudil concentrations from 0.3 to 30 μM. $^{**}P < 0.01$. (**C**, **D**) The effect of ripasudil on proliferation of corneal endothelium was evaluated by EdU and Ki67 staining after 48 hours of treatment. The numbers of EdU- and Ki67-positive cells were significantly higher following treatment of HCECs with ripasudil. $^{**}P < 0.01$.

Rabbit Corneal Endothelial Damage Model by Mechanical Scraping

A rabbit corneal endothelial damage model was created to mimic surgical trauma. Half the area of the corneal endothelium of 24 eyes of 12 Japanese white rabbits was mechanically scraped from the Descemet's membrane with a 20-gauge silicone needle (Soft Tapered Needle; Inami & Co., Ltd., Tokyo, Japan) while the animals were under general anesthesia. The scraped area was confirmed as damaged by 0.04% trypan blue staining. The experimenter who created the endothelial damage model was blinded to subsequent treatment with ripasudil or vehicle. Before this procedure, the lenses were removed with an Alcon Series 20000 Legacy Surgical System (Alcon, Inc., Fort Worth, TX, USA) to deepen the anterior chamber. One eye of each rabbit was used for 0.4% ripasudil treatment and the contralateral eye served as the control. The corneal endothelium of both eyes was used in the experiment to reduce the number of rabbits required for the study and to provide a correct evaluation of the effect, because wound healing varied with the individual rabbits. This procedure was confirmed not to induce complete blindness or any severe general adverse effects.

Rabbit Corneal Assessment

Anterior segments were evaluated by slit-lamp microscopy for 2 weeks. Scheimpflug images and a corneal thickness map were obtained with a Pentacam instrument (OCULUS; Optikgeräte GmbH, Wetzlar, Germany). Corneal endothelium was evaluated by contact specular microscopy (Konan scanning slit specular microscope; Konan Medical, Nishinomiya, Japan). Corneal thickness was determined with an ultrasound pachymeter (SP-2000; Tomey, Nagoya, Japan), and the mean of 10 measured values was then calculated (up to a maximum thickness of 1200 μm, the instrument's maximum reading).

Statistical Analysis

The statistical significance (*P* value) of differences in the mean values of the two-sample comparison was determined with the Student's *t*-test. Values shown on the graphs represent the mean ± SEM.

Results

Effect of Ripasudil on HCECs Proliferation In Vitro

Cultured HCECs were seeded on a culture plate and cultured for 24 hours, and then HCECs were treated with the following ROCK inhibitors for 48 hours: Y-27632 (10 μM), fasudil (10 μM), and ripasudil (0.3–100 μM). Representative phase contrast images showed that higher numbers of cells were observed when cells were treated with ROCK inhibitors (Fig. 1A). The proliferative potential was assessed by BrdU incorporation into the newly synthesized DNA. An ELISA showed that concentrations of ripasudil from 0.3 to 30 μM significantly enhanced BrdU incorporation (Fig. 1B). The numbers of cells staining for the proliferative EdU and Ki67 markers were greater for the ripasudil (10 μM) treatment than for the control treatment (Figs. 1C, 1D).

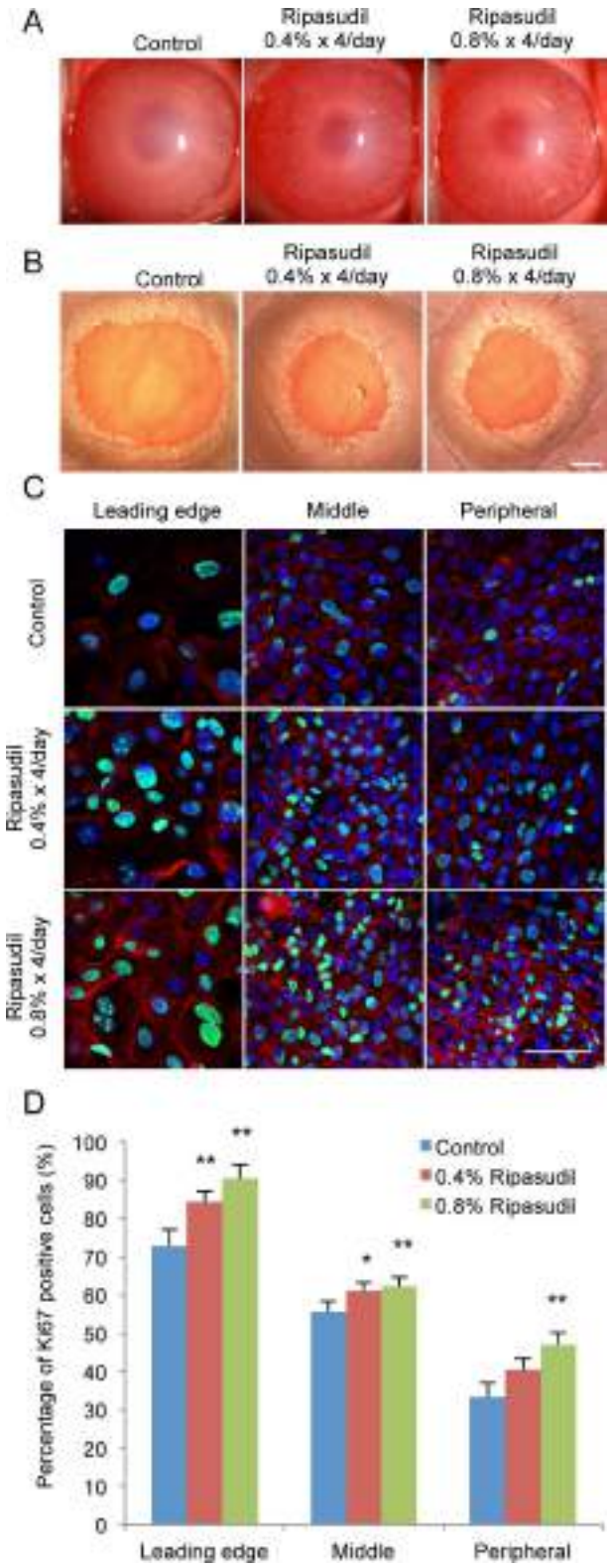

Figure 2. Effect of ripasudil eye drops on corneal endothelial proliferation in a rabbit corneal freezing model. (**A**) A stainless-steel 7-mm-diameter probe was immersed in liquid nitrogen for 3 minutes and then placed onto the rabbit cornea for 15 seconds with the animal under general anesthesia. Then, one 0.4% ripasudil (four times daily) or 0.8% ripasudil (two times daily) eye drop was topically instilled, whereas vehicle was instilled in the fellow eye of each rabbit as a control ($n = 6$). Slit-lamp microscopy showed that control eyes exhibited hazy corneas after 48 hours, but eyes treated with 0.4% or 0.8% ripasudil eye drops exhibit less hazy corneas. No other adverse effects, such as the delay of corneal epithelial wound healing, severe conjunctival injection, and corneal opacity were observed. (**B**) The wound area of the corneal endothelium was evaluated by Alizarin red staining after 48 hours of treatment. Alizarin red staining images showed that the wound area tended to be smaller in eyes treated with 0.4% or 0.8% ripasudil eye drops than in control eyes. *Scale bar*: 1 mm. (**C**, **D**) Ki67$^+$ cells located at the leading edge (3.5 mm distant from the center of the cornea), middle area (4.5 mm distant from the center of the cornea), and periphery (5.5 mm distant from the center of the cornea) were evaluated. Ki67 staining confirmed that 0.4% or 0.8% ripasudil eye drops promoted cell proliferation throughout the wound edge to the peripheral area. Administration of 0.8% ripasudil (two times per day) enhanced Ki67 expression to a higher level than was observed with 0.4% ripasudil eye drops (four times daily). Morphology was evaluated using actin staining performed with Alexa Fluor 594–conjugated phalloidin. Nuclei were stained with DAPI. Representative images of pupil centers are shown. *Scale bar*: 50 μm. These experiments were performed in duplicate.

Effect of Ripasudil Eye Drops on Corneal Endothelial Proliferation in a Transcorneal Freezing Rabbit Model

We tested the effect of 0.4% ripasudil eye drop (four times daily) and 0.8% ripasudil (two times daily) in the rabbit partial corneal endothelial wound model, because the topical and systemic safety of doses lower than these was already confirmed in commercially available ripasudil eye drops (Glanatec ophthalmic solution 0.4%; Kowa Company, Ltd.) in clinical trials.[11] Slit-lamp microscopy showed that control rabbits with 7-mm-diameter corneal endothelial wounds created by transcorneal freezing exhibited hazy corneas after 48 hours. On the other hand, rabbits treated with 0.4% or 0.8% ripasudil eye drops exhibited less haze in their corneas, and no other adverse effects, such as delay of corneal epithelial wound healing, severe conjunctival injection, and corneal opacity, were observed (Fig. 2A). Coincidently, representative Alizarin red staining images showed that the wound area tended to be smaller in eyes treated with 0.4% or 0.8% ripasudil eye drops than in control eyes (Fig. 2B). The Ki67 staining demonstrated that 0.4% or 0.8% ripasudil eye drops promoted cell proliferation throughout the wound edge to the peripheral area of the residual corneal endothelium (Fig. 2C). The percentage of Ki67-positive cells in the leading edge was 72.8 ± 4.3% in the control, but it was 84.4 ± 2.5% and 90.5 ± 1.7% in the eyes treated with 0.4% and 0.8% ripasudil, respectively. In the peripheral area, Ki67-positive cells accounted for 33.5 ± 3.7% of the cells in the control and 40.4 ± 2.7% and 47.1 ± 3.1% of the cells in the eyes treated with 0.4% and 0.8% ripasudil, respectively (Fig. 2D).

Effect of Ripasudil Eye Drops on Corneal Endothelial Wounds in a Mechanical Scraping Rabbit Model

Next, we evaluated whether ripasudil eye drops are an effective treatment for severe corneal endothelial damage; for example, the damage occurring during ocular surgeries such as cataract surgery, which is one of the leading causes of bullous keratopathy. We mechanically scraped half the area of the rabbit corneal endothelium and applied 0.4% ripasudil eye drops (three times daily). Slit-lamp microscopic images showed that eyes treated with vehicle as a control exhibited corneal edema, whereas eyes treated with ripasudil exhibited almost clear corneas (Fig. 3A). Five of six eyes treated with ripasudil recovered corneal transparency in the pupil center, whereas six of six control eyes did not. Scheimpflug images and corneal

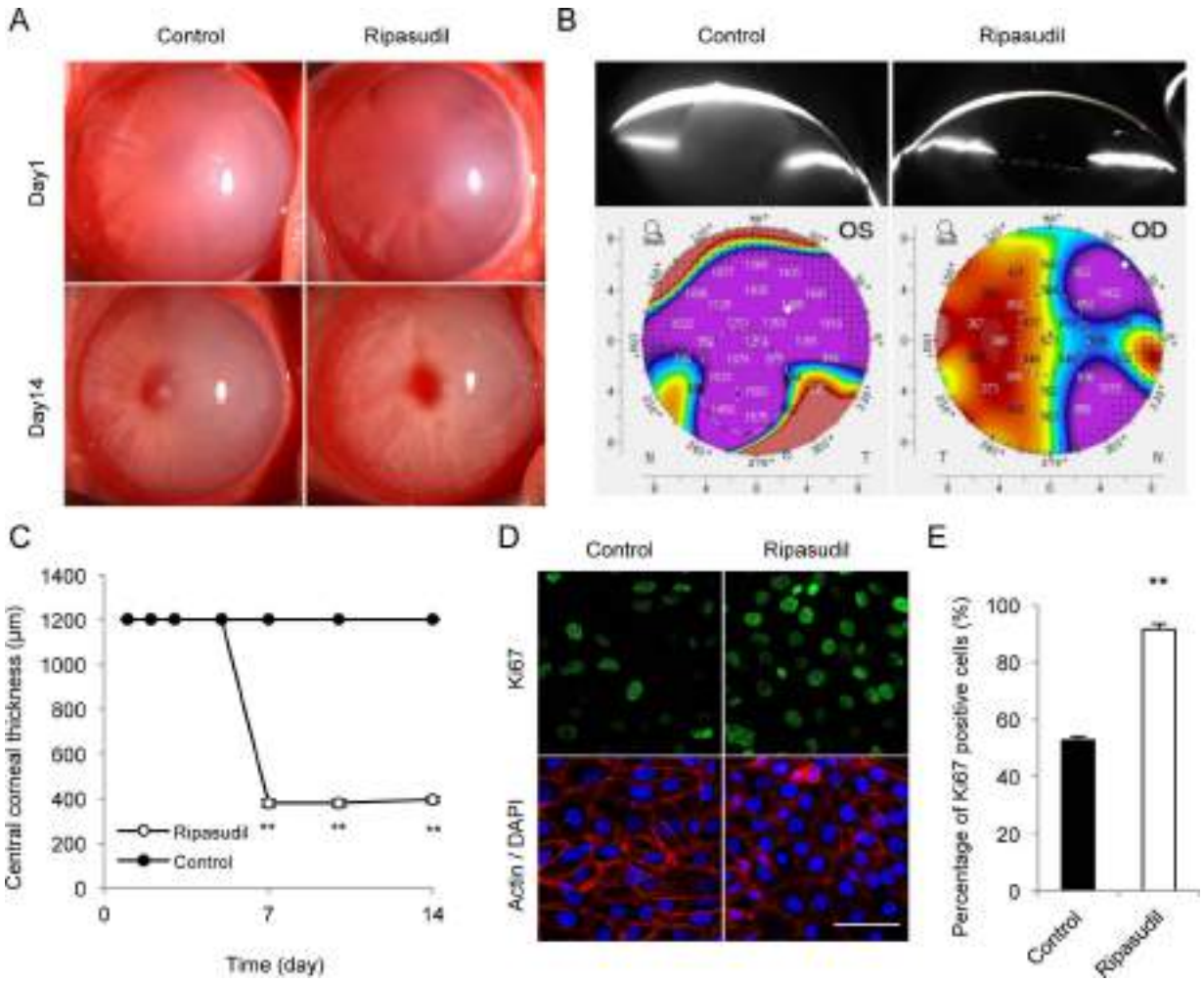

FIGURE 3. Effect of ripasudil eye drops on wound healing in a mechanical damage corneal endothelial rabbit model. (**A**) Half the area of the corneal endothelium was mechanically scraped in six rabbits, and 0.4% ripasudil eye drops were applied (three times daily) for 2 weeks. Vehicle was applied to the fellow eyes as a control. The damage to the scraped area was confirmed by 0.04% trypan blue staining, and the experimenter who created the endothelial damage model was blinded to the subsequent treatment with ripasudil or vehicle. Representative slit-lamp microscope images are shown. (**B**) Representative Scheimpflug images and corneal thickness maps obtained by Pentacam HR are shown. Values for the corneal thickness map are indicated in micrometers. (**C**) The central corneal thickness was evaluated by ultrasound pachymetry. The central corneal thickness of eyes treated with ripasudil was 392.8 ± 12.6 μm, but that of eyes treated with vehicle was 1200 μm. $^{**}P < 0.01$. (**D**, **E**) After 48 hours of ripasudil eye drops, Ki67-positive cells in the wounded area at the center of cornea were evaluated. The control eye showed 52.6 ± 1.32% of the cell population as Ki67 positive, whereas the ripasudil-treated eyes showed 91.5 ± 1.97% Ki67-positive cells. *Scale bar*: 50 μm. $^{**}P < 0.01$.

thickness maps obtained with a Pentacam HR instrument also demonstrated that control eyes exhibited corneal edema throughout the whole area. By contrast, ripasudil-treated eyes showed less edema in the cornea, including the pupillary area, although edema was still evident in the peripheral damaged area (Fig. 3B). The central corneal thickness of eyes treated with ripasudil was 392.8 ± 12.8 μm, but that of eyes treated with vehicle was 1200 μm (more than the maximum readings of ultrasound pachymetry in all eyes; Fig. 3C). The Ki67-positive cells in the wounded area at the center of cornea were evaluated after 48 hours of ripasudil eye drops. The control eye showed 52.6 ± 1.3% of the cell population as Ki67 positive, whereas the ripasudil-treated eyes showed 91.5 ± 2.0% Ki67-positive cells (Figs. 3D, 3E).

Effect of Ripasudil Eye Drops on Regenerated Corneal Endothelium

Contact specular microscopy showed that control eyes exhibited blurred corneal endothelial images from the border (center of the cornea) to the damaged area. On the other hand, regenerated corneal endothelium was observed throughout whole area of the cornea with hexagonal and monolayer morphology (Fig. 4A). Cell density was significantly higher in the eyes treated with ripasudil than in eyes treated with vehicle, although the corneal endothelial cell density tended to be lower in the damaged area than in nondamaged areas in both treated eyes and control eyes (Fig. 4B).

Regenerated corneal endothelium in the damaged area of the control eye exhibited a fibroblastic phenotype with the formation of stress fibers, but that of the treated eye exhibited a hexagonal monolayer phenotype and actin fibers were distributed at the cell cortex (Fig. 4C). Eyes treated with ripasudil expressed N-cadherin (a marker of adherence junctions) and Na^+/K^+-ATPase (a marker of pump function) in almost all the CECs, but this expression was lower in the control eyes (Figs. 4D, 4E). The Ki67 expression was not observed in either the control or the ripasudil-treated eyes (Fig. 4F). This indicates that corneal endothelial cell

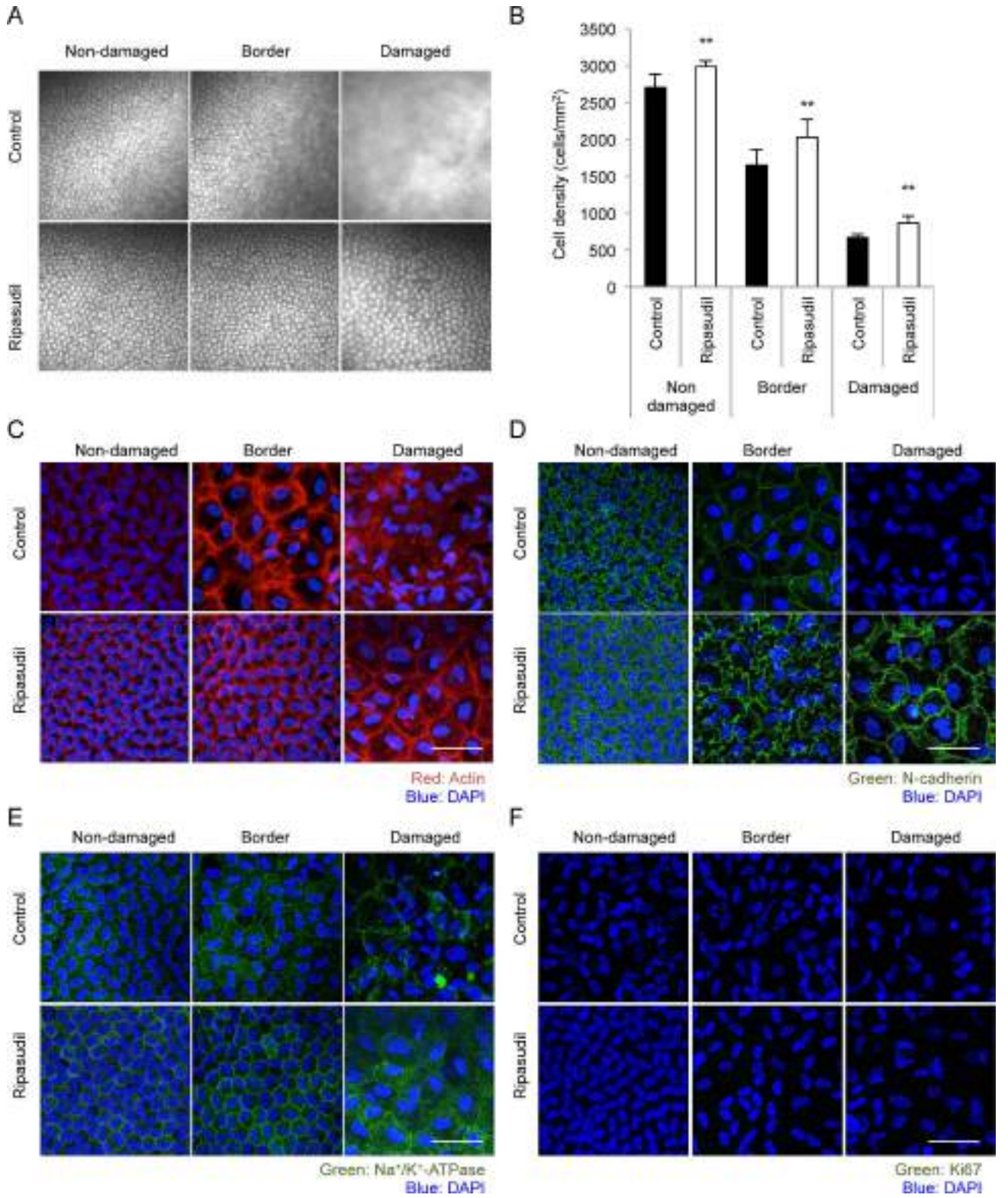

Figure 4. Effect of ripasudil eye drops on regenerated corneal endothelium in a mechanical damage corneal endothelial rabbit model. (**A**) Regenerated corneal endothelium was evaluated by contact specular microscopy after 14 days. Nondamaged areas, borders (pupil center), and damaged areas were evaluated. (**B**) The corneal endothelial cell density of the eyes treated with ripasudil was significantly higher in all areas (nondamaged areas, border, and damaged areas) than in the eyes treated with vehicle. (**C**) Regenerated corneal endothelium was evaluated histologically after 14 days. Morphology was evaluated using actin staining performed with Alexa Fluor 594–conjugated phalloidin. (**D**, **E**) Functional recovery was analyzed by immunostaining for N-cadherin (**D**) and Na^+/K^+-ATPase (**E**). (**F**) Cell proliferative status was analyzed by Ki67 immunostaining. No Ki67-positive cells were observed in either the ripasudil treated eyes or the control eyes after 14 days. Nuclei were stained with DAPI. Representative images of pupil centers are shown. *Scale bar*: 50 μm.

Investigative Ophthalmology & Visual Science

proliferation was no longer observed once the remaining CECs had covered the damaged area and cell–cell contact was reestablished, even following treatment with ripasudil eye drops.

Discussion

In many countries, bullous keratopathy caused by cataract surgery is one of the leading causes of corneal transplantation due to corneal endothelial dysfunction.[23–25] In the United States, 12.2% of the corneas are used for post–cataract surgery corneal edema.[26] As in western countries, 20–40% of corneal transplantation in Asian countries is performed to treat bullous keratopathy caused by cataract surgery.[27–29] The World Health Organization reported that 51% of blindness is caused by cataracts on a global basis[30]; therefore, it is reasonable to estimate that numerous patients will undergo cataract surgery in the near future, and a certain percentage of those patients will unfortunately experience severe corneal endothelial damage during their surgeries. The development of pharmaceutical treatments is urgently needed.

Wound healing is a combined effect of cell migration, spreading, and proliferation in various tissues. However, wound healing of the corneal endothelium is mainly caused by migration and spreading due to the severely limited proliferation ability of corneal cells.[31] Consequently, critical damage induces impairment of wound healing and loss of function.[32] For that reason, researchers, including our group, have devoted much effort in the search for pharmaceutical agents (e.g., epidermal growth factor,[33] platelet-derived growth factor (PDGF),[34] FGF-2,[35] and ROCK inhibitors[3]) that can promote proliferation of CECs for the treatment of corneal endothelial disease.

We recently reported a preliminary successful result for pilot clinical research of using the ROCK inhibitor, Y-27632, as a form of eye drops for treating corneal endothelial injury.[36] In that clinical research, patients had experienced severe corneal edema due to cataract surgery, and they recovered their corneal transparency following treatment with Y-27632 eye drops.[36] We proposed that the ROCK inhibitor promotes cell proliferation of residual undamaged healthy CECs and ultimately reduces the risk of development of bullous keratopathy; therefore, ROCK inhibitors might be developed as eye drops for treating corneal endothelial injury. However, Y-27632 is currently only available for research use, not for clinical use, so the development of ROCK inhibitors other than Y-27632 represents a bottleneck for treating corneal endothelial injury in the clinical setting.

Injury to the corneal endothelium decreases the corneal endothelial cell density, but severe damage due to various corneal endothelial diseases induces fibroblastic transformation[37,38] that is thought to represent an endothelial–mesenchymal transformation.[39] Fibroblastic transformation of CECs causes the cells to lose not only their morphologic character but also the activity of the corneal endothelial pump and barrier functions.[40] Similarly, we showed here that the CECs of a rabbit wound model exhibited a fibroblastic morphology with corneal edema. Although this current study showed that ROCK inhibitor treatment regenerated a higher density of CECs and also suppressed fibroblastic formation, further investigation is needed to determine whether suppression of fibroblastic changes is a consequence of faster wound healing or a direct anti fibroblastic effect of the ROCK inhibitor.[41,42]

The Ki67-positive proliferating cells were observed 48 hours after corneal endothelial damage in the current rabbit model, but were not observed when the damaged area was fully covered by CECs in both the control and ROCK inhibitor–treated eyes. This finding suggests that ROCK inhibitors do not induce cell proliferation once CECs form cell–cell contacts between adjacent cells. In other words, if a pharmaceutical agent that promotes cell proliferation is available in the clinical settings, the "golden time" begins immediately following the injury until just before the injured area is covered by compensatory migration and spreading of the remaining CECs.

ROCK has been researched as a potential therapeutic target for vascular disease, cancer, neuronal degenerative disease, asthma, and glaucoma, because ROCK signaling activation is involved in numerous diseases.[41,42] In contrast to the accumulation of evidence showing that ROCK inhibitors have potency against various diseases, only two drugs have been approved for clinical use: (1) fasudil for the treatment of cerebral vasospasm[43] and (2) ripasudil for the treatment of glaucoma and ocular hypertension.[14] Ripasudil clinical trials revealed slight to mild conjunctival hyperemia in more than half of the participants, whereas no other severe adverse effect was observed.[11,12] In terms of the corneal endothelium, we reported that ripasudil induces guttae-like findings in humans, but these are transient, and no corneal endothelial damage was observed.[44] We also reported that the guttae-like findings arise due to the formation of protrusions along cell–cell junctions as a consequence of the reduction in actomyosin contractility caused by inhibition of ROCK signaling.[45] In the present in vitro evaluation, ripasudil enhanced cell proliferation to almost the same level seen with Y-27632. In the rabbit wound model, ripasudil eye drops restored transparency in five of six corneas, and Y-27632 eye drops showed the same effect in a previous report.[36] The effects of long-term use of ripasudil eye drops on the corneal endothelium in clinical settings still remain in question. Therefore, further study to confirm its safety and efficacy is necessary for the development of ripasudil eye drops as a therapeutic modality for corneal endothelial diseases.

Here, we showed that ripasudil eye drops are potent enhancers of corneal endothelial wound healing in a rabbit model that mimics severe corneal endothelial injury. Thus, we propose that drug repositioning of ripasudil for treating corneal endothelial diseases would be a judicious strategy for delivering ROCK inhibitor eye drops in the clinical setting.

Acknowledgments

The authors thank Kowa Company for providing ripasudil eye drops.

Supported by Program for the Strategic Research Foundation at Private Universities from the Ministry of Education, Culture, Sports, Science and Technology (MEXT) (NK, NO).

SK holds patent no. 5657252, regarding the application of ROCK inhibitor for corneal endothelium. NO and NK are listed as inventors on the patent.

Disclosure: **N. Okumura**, P; **Y. Okazaki**, None; **R. Inoue**, None; **K. Kakutani**, None; **S. Nakano**, None; **S. Kinoshita**, P; **N. Koizumi**, P

References

1. Tan DT, Dart JK, Holland EJ, Kinoshita S. Corneal transplantation. *Lancet*. 2012;379:1749–1761.
2. Okumura N, Ueno M, Koizumi N, et al. Enhancement on primate corneal endothelial cell survival in vitro by a ROCK inhibitor. *Invest Ophthalmol Vis Sci*. 2009;50:3680–3687.

3. Okumura N, Koizumi N, Ueno M, et al. Enhancement of corneal endothelium wound healing by Rho-associated kinase (ROCK) inhibitor eye drops. *Br J Ophthalmol*. 2011;95:1006–1009.
4. Okumura N, Koizumi N, Kay EP, et al. The ROCK inhibitor eye drop accelerates corneal endothelium wound healing. *Invest Ophthalmol Vis Sci*. 2013;54:2493–2502.
5. Koizumi N, Okumura N, Ueno M, Nakagawa H, Hamuro J, Kinoshita S. Rho-associated kinase inhibitor eye drop treatment as a possible medical treatment for fuchs corneal dystrophy. *Cornea*. 2013;32:1167–1170.
6. Honjo M, Tanihara H, Inatani M, et al. Effects of rho-associated protein kinase inhibitor Y-27632 on intraocular pressure and outflow facility. *Invest Ophthalmol Vis Sci*. 2001;42:137–144.
7. Tokushige H, Inatani M, Nemoto S, et al. Effects of topical administration of y-39983, a selective rho-associated protein kinase inhibitor, on ocular tissues in rabbits and monkeys. *Invest Ophthalmol Vis Sci*. 2007;48:3216–3222.
8. Williams RD, Novack GD, van Haarlem T, Kopczynski C. Group ARPAS. Ocular hypotensive effect of the Rho kinase inhibitor AR-12286 in patients with glaucoma and ocular hypertension. *Am J Ophthalmol*. 2011;152:834–841.
9. Inoue T, Tanihara H. Rho-associated kinase inhibitors: a novel glaucoma therapy. *Prog Retin Eye Res*. 2013;37:1–12.
10. Van de Velde S, Van Bergen T, Sijnave D, et al. AMA0076, a novel, locally acting Rho kinase inhibitor, potently lowers intraocular pressure in New Zealand white rabbits with minimal hyperemia. *Invest Ophthalmol Vis Sci*. 2014;55:1006–1016.
11. Tanihara H, Inoue T, Yamamoto T, et al. Phase 1 clinical trials of a selective Rho kinase inhibitor, K-115. *JAMA Ophthalmol*. 2013;131:1288–1295.
12. Tanihara H, Inoue T, Yamamoto T, et al. Phase 2 randomized clinical study of a Rho kinase inhibitor, K-115, in primary open-angle glaucoma and ocular hypertension. *Am J Ophthalmol*. 2013;156:731–736.
13. Tanihara H, Inoue T, Yamamoto T, et al. Intra-ocular pressure-lowering effects of a Rho kinase inhibitor, ripasudil (K-115), over 24 hours in primary open-angle glaucoma and ocular hypertension: a randomized, open-label, crossover study. *Acta Ophthalmol*. 2015;93:e254–260.
14. Garnock-Jones KP. Ripasudil: first global approval. *Drugs*. 2014;74:2211–2215.
15. Isobe T, Mizuno K, Kaneko Y, Ohta M, Koide T, Tanabe S. Effects of K-115, a rho-kinase inhibitor, on aqueous humor dynamics in rabbits. *Curr Eye Res*. 2014;39:813–822.
16. Jin G, Wong ST. Toward better drug repositioning: prioritizing and integrating existing methods into efficient pipelines. *Drug Discov Today*. 2014;19:637–644.
17. Langedijk J, Mantel-Teeuwisse AK, Slijkerman DS, Schutjens MH. Drug repositioning and repurposing: terminology and definitions in literature. *Drug Discov Today*. 2015;20:1027–1034.
18. Wurth R, Thellung S, Bajetto A, Mazzanti M, Florio T, Barbieri F. Drug-repositioning opportunities for cancer therapy: novel molecular targets for known compounds. *Drug Discov Today*. 2016;21:190–199.
19. Okumura N, Kusakabe A, Hirano H, et al. Density-gradient centrifugation enables the purification of cultured corneal endothelial cells for cell therapy by eliminating senescent cells. *Sci Rep*. 2015;5:15005.
20. Nakahara M, Okumura N, Kay EP, et al. Corneal endothelial expansion promoted by human bone marrow mesenchymal stem cell-derived conditioned medium. *PLoS One*. 2013;8:e69009.
21. Matsubara M, Tanishima T. Wound-healing of the corneal endothelium in the monkey: a morphometric study. *Jpn J Ophthalmol*. 1982;26:264–273.
22. Matsubara M, Tanishima T. Wound-healing of corneal endothelium in monkey: an autoradiographic study. *Jpn J Ophthalmol*. 1983;27:444–450.
23. Al-Yousuf N, Mavrikakis I, Mavrikakis E, Daya SM. Penetrating keratoplasty: indications over a 10 year period. *Br J Ophthalmol*. 2004;88:998–1001.
24. Ghosheh FR, Cremona FA, Rapuano CJ, et al. Trends in penetrating keratoplasty in the United States 1980-2005. *Int Ophthalmol*. 2008;28:147–153.
25. Keenan TD, Jones MN, Rushton S, et al. Trends in the indications for corneal graft surgery in the United Kingdom: 1999 through 2009. *Arch Ophthalmol*. 2012;130:621–628.
26. Eye Bank Association of America. *Eye Banking Statistical Report*. Washington, DC; 2013.
27. Dandona L, Naduvilath TJ, Janarthanan M, Ragu K, Rao GN. Survival analysis and visual outcome in a large series of corneal transplants in India. *Br J Ophthalmol*. 1997;81:726–731.
28. Shimazaki J, Amano S, Uno T, Maeda N, Yokoi N. National survey on bullous keratopathy in Japan. *Cornea*. 2007;26:274–278.
29. Tan DT, Janardhanan P, Zhou H, et al. Penetrating keratoplasty in Asian eyes: the Singapore Corneal Transplant Study. *Ophthalmology*. 2008;115:975–982.
30. Pascolini D, Mariotti SP. Global estimates of visual impairment: 2010. *Br J Ophthalmol*. 2012;96:614–618.
31. Joyce NC. Proliferative capacity of the corneal endothelium. *Prog Retin Eye Res*. 2003;22:359–389.
32. Bourne WM. Clinical estimation of corneal endothelial pump function. *Trans Am Ophthalmol Soc*. 1998;96:229–239. discussion 239–242.
33. Hoppenreijs VP, Pels E, Vrensen GF, Oosting J, Treffers WF. Effects of human epidermal growth factor on endothelial wound healing of human corneas. *Invest Ophthalmol Vis Sci*. 1992;33:1946–1957.
34. Hoppenreijs VP, Pels E, Vrensen GF, Treffers WF. Effects of platelet-derived growth factor on endothelial wound healing of human corneas. *Invest Ophthalmol Vis Sci*. 1994;35:150–161.
35. Lu J, Lu Z, Reinach P, et al. TGF-beta2 inhibits AKT activation and FGF-2-induced corneal endothelial cell proliferation. *Exp Cell Res*. 2006;312:3631–3640.
36. Okumura N, Inoue R, Okazaki Y, et al. Effect of the Rho kinase inhibitor Y-27632 on corneal endothelial wound healing. *Invest Ophthalmol Vis Sci*. 2015;56:6067–6074.
37. Naumann GO, Schlotzer-Schrehardt U. Keratopathy in pseudoexfoliation syndrome as a cause of corneal endothelial decompensation: a clinicopathologic study. *Ophthalmology*. 2000;107:1111–1124.
38. Kawaguchi R, Saika S, Wakayama M, Ooshima A, Ohnishi Y, Yabe H. Extracellular matrix components in a case of retrocorneal membrane associated with syphilitic interstitial keratitis. *Cornea*. 2001;20:100–103.
39. Lee HT, Lee JG, Na M, Kay EP. FGF-2 induced by interleukin-1 beta through the action of phosphatidylinositol 3-kinase mediates endothelial mesenchymal transformation in corneal endothelial cells. *J Biol Chem*. 2004;279:32325–32332.
40. Okumura N, Kay EP, Nakahara M, Hamuro J, Kinoshita S, Koizumi N. Inhibition of TGF-beta signaling enables human corneal endothelial cell expansion in vitro for use in regenerative medicine. *PLoS One*. 2013;8:e58000.
41. Liao JK, Seto M, Noma K. Rho kinase (ROCK) inhibitors. *J Cardiovasc Pharmacol*. 2007;50:17–24.
42. Olson MF. Applications for ROCK kinase inhibition. *Curr Opin Cell Biol*. 2008;20:242–248.

Investigative Ophthalmology & Visual Science

43. Hu E, Lee D. Rho kinase as potential therapeutic target for cardiovascular diseases: opportunities and challenges. *Expert Opin Ther Targets*. 2005;9:715–736.
44. Nakagawa H, Koizumi N, Okumura N, Suganami H, Kinoshita S. Morphological changes of human corneal endothelial cells after rho-associated kinase inhibitor eye drop (ripasudil) administration: a prospective open-label clinical study. *PLoS One*. 2015;10:e0136802.
45. Okumura N, Okazaki Y, Inoue R, et al. Rho-associated kinase inhibitor eye drop (ripasudil) transiently alters the morphology of corneal endothelial cells. *Invest Ophthalmol Vis Sci*. 2015;56:7560–7567.

Investigative Ophthalmology & Visual Science

Current Pharmaceutical Design, 2017, *23*, 660-666

REVIEW ARTICLE

The Role of Rho Kinase Inhibitors in Corneal Endothelial Dysfunction

Naoki Okumura[1], Shigeru Kinoshita[2] and Noriko Koizumi[1,*]

[1]*Department of Biomedical Engineering, Faculty of Life and Medical Sciences, Doshisha University, Kyotanabe, Japan;* [2]*Department of Frontier Medical Science and Technology for Ophthalmology, Kyoto Prefectural University of Medicine, Kyoto, Japan*

ARTICLE HISTORY

Received: October 13, 2016
Accepted: November 24, 2016

DOI: 10.2174/1381612822666161205110027

Abstract: ***Background:*** The cornea is transparent tissue that serves as the window of the eye, allowing light to enter from the outer environment. The corneal endothelium maintains corneal transparency; thus, its dysfunction results in corneal haziness and causes severe vision loss. The only available therapeutic choice for treating corneal endothelial dysfunction has been transplantation using donor corneas; consequently, researchers have been pressed to develop new therapeutic options.

Methods: The goal of the review is to provide an overview of the research into Rho kinase (ROCK) inhibitors in the field of corneal endothelium therapy and the potential for clinical use of ROCK inhibitors.

Results: We reported that ROCK inhibitor enhances wound healing in the corneal endothelium. We further proposed the development of ROCK inhibitors as drugs that suppress the incidence of bullous keratopathy following severe corneal endothelial damage, especially that occurring during cataract surgery, one of the leading causes of corneal transplantation. We also proposed the use of ROCK inhibitors as adjunct drugs for cell-based therapeutic treatment of corneal endothelial dysfunction. ROCK inhibitors promote the engraftment of injected cultured corneal endothelial cells to the recipient cornea, thereby enabling the regeneration of corneal endothelium. Of note, we have initiated clinical research into cell injection therapy using a ROCK inhibitor as an adjunct drug.

Conclusion: This review documents the potency of ROCK inhibitors in clinical use, both as eye drops and as adjunct drugs for cell-based therapy for the treatment of corneal endothelial dysfunction.

Keywords: Cornea, Rho kinase, corneal endothelial dysfunction, fuchs endothelial corneal dystrophy.

INTRODUCTION

Rho is a small GTPase that is activated by guanine nucleotide exchange factors (GEFs). GTP-bound RhoA activates Rho kinase (ROCK), a serine/threonine kinase that phosphorylates a number of substrates. Two isoforms, ROCK I and ROCK II, were isolated as GTP-bound proteins that interact with RhoA proteins. These two isoforms share a 60% similarity in amino acid sequence and a 90% similarity in the kinase domain [1, 2]. The Rho/ROCK signaling pathways regulate a wide range of cell functions, including cell adhesion, motility, proliferation, differentiation, and apoptosis [2, 3].

The wide spectrum of fundamental biological events influenced by ROCK has led to its recognition as an important therapeutic target in a variety of pathophysiological conditions. Indeed, ROCK inhibitors have been intensively researched as treatments for a wide range of diseases, including vascular disease, cancer, asthma, insulin resistance, kidney failure, osteoporosis, neuronal degenerative disease, and glaucoma [2, 4-6]. Two ROCK inhibitors have been approved for clinical use [6]: Fasudil was approved for the treatment of cerebral vasospasm in 1995, while ripasudil was approved in eye drop form in Japan in 2014 for the treatment of glaucoma and ocular hypertension [7]. Recently, we have proposed ROCK inhibitors as having therapeutic potential for the treatment of corneal endothelial disease by promoting proliferation of corneal endothelial cells (CECs) and as adjunct drugs for cell-based therapy to enhance cultured CEC engraftment when treating corneal endothelial dysfunction. This review provides an overview of the research into ROCK inhibitors in the field of corneal endothelium therapy and the potential for clinical use of ROCK inhibitors.

*Address correspondence to this auhtor at the Department of Biomedical Engineering, Faculty of Life and Medical Sciences, Doshisha University, Kyotanabe 610-0321, Japan; Tel/Fax: +81-774-65-6125;
E-mail: nkoizumi@mail.doshisha.ac.jp

CORNEAL ENDOTHELIAL DISEASES

Corneal Endothelial Dysfunction

The cornea is transparent tissue that serves as the window of the eye, allowing the entry of light from the outer environment. The anterior corneal surface is covered by the tear film, while the posterior surface is bathed by aqueous humor. The corneal endothelium maintains the corneal transparency by the action of its pump and barrier function. Therefore, severe damage to the corneal endothelium due to pathological conditions, including corneal endothelial dystrophies, surgical trauma, and endotheliitis, can disrupt this function and adversely affect corneal transparency. This can lead ultimately to bullous keratopathy, characterized by irreversible corneal haziness and severe vision loss.

Corneal transplantation has been the only therapeutic choice for treating corneal endothelial dysfunction [8]. A statistical report by the Eye Bank Association of America indicated that among the 76,431 donor corneas provided by US eye banks in 2013, 28,961 were used for corneal endothelial keratoplasty. In the US, the number of donor corneas used for corneal endothelial keratoplasty has been increasing; *i.e.*, 25,965 corneas were provided for corneal endothelial keratoplasty, while 19,294 corneas were provided for penetrating keratoplasty [9]. Nevertheless, corneal transplantation has several problematic issues, such as a worldwide shortage of donor corneas (especially in non-US countries), the difficulty of the surgical procedure, and graft failure in both acute and chronic phases. These challenges have led researchers to seek out new therapeutic options.

ROCK INHIBITORS AS DRUGS FOR ENHANCING WOUND HEALING IN CORNEAL ENDOTHELIUM

In Vitro Experiments

In 2009, we reported that the selective ROCK inhibitor Y-27632 has unique effects in cultured monkey CECs, including 1)

1873-4286/17 $58.00+.00

promotion of proliferative ability, 2) enhancement of cell adhesion onto a substrate, and 3) suppression of apoptosis induced by cell dissociation during cell passaging [10]. These findings in monkey CECs were subsequently confirmed in human CECs by later researchers, including our group [11, 12]. On the other hand, Pipparelli and colleagues reported an opposite result, where a ROCK inhibitor did not induce CEC proliferation [13]. However, Peh and colleagues reported that same ROCK inhibitor, Y-27632, increased proliferation of human CECs by 1.96 to 3.36 fold, and suggested that human CECs derived from young donors are more responsive to ROCK inhibitor. They suggested that the opposing results of Pipparelli and colleagues could possibly be explained by a different status of the cornea, such as age [12]. In addition, the effect of ROCK inhibitors in promoting CEC proliferation was confirmed by other ROCK inhibitors, such as Y-39983 and ripasudil [11].

Early studies indicated that Rho inactivation blocks the G1-S cell phase progression in Swiss 3T3 fibroblasts, and that the microinjection of active RhoA into quiescent cells induces G1-S phase progression [14, 15]. Likewise, inhibition of ROCK signaling promotes cell-cycle progression in other cell types [16]. However, the general consensus is that the role of ROCK signaling is highly dependent on the cell type [17], which could explain the promotion of CEC proliferation. We demonstrated that the mechanism of action of a ROCK inhibitor to promote cell proliferation in the corneal endothelium involved both cyclin D (positive G1 regulator) and p27 (negative G1 regulator) activated by PI 3-kinase signaling [11]. In addition, the ongoing efforts to develop ROCK inhibitors as anticancer drugs could have led to some publication bias towards results that show suppression of cell proliferation in various cell types by ROCK inhibitors.

Animal Experiments Using ROCK Inhibitors in a Corneal Cryofreezing-Induced Corneal Endothelial Wound Model

One problematic feature of the corneal endothelium in the clinical setting is that it has a severely limited proliferative ability [18 19]. Therefore, if ROCK inhibitors can modulate proliferation *in vivo*, they could have applications as drugs targeting the corneal endothelium. We tested this possibility in rabbits in which a circular corneal endothelial wound was created by transcorneal cryogenic injury (average diameter; 6.4 mm). These rabbit models were then treated with the ROCK inhibitor Y-27632 in the form of eye drops. The ROCK inhibitor promoted the expression of Ki67 in the undamaged residual corneal endothelium in a dose-dependent manner. Wound healing was promoted by administration of Y-27632, so that the mean wound area was 0.23 fold smaller for the Y-27632 group than for the control group. Faster wound healing was also evident by the greater corneal transparency and the thinner corneal thickness in the Y-27632 eye-drop treated group than in the control group [20]. A different ROCK inhibitor, Y-39983, also promoted cell proliferation associated with faster wound healing [11].

The limitation of these *in vivo* experiments using rabbit models is that species-specific differences exist in regard to cell proliferation ability. Rabbit, mouse, and bovine CECs exhibit proliferative potency, whereas the CECs from cats, monkeys, and humans show severely limited proliferative potency [21-25]. We therefore employed a primate model, where a corneal endothelial wound was created in cynomolgus monkeys in a similar fashion to that in the rabbit model to evaluate the feasibility of ROCK inhibitor therapy in humans [26]. The administration of a ROCK inhibitor in eye drop form again promoted corneal endothelial wound healing in this primate model, with higher CEC density and normal expression of function-related markers. Collectively, these animal experiments confirmed that proliferation of the corneal endothelium is promoted by administration of a ROCK inhibitor in eye drop form.

Pilot Clinical Study of a ROCK Inhibitor Combined with Corneal Cryofreezing

A pilot clinical study of the use of ROCK inhibitor eye drops for corneal endothelial dysfunction was conducted from May to August 2010 at the Kyoto Prefectural University of Medicine [26]. Eight eyes of 8 patients scheduled for corneal transplantation were enrolled in this study. The patients were divided into 2 groups: 1) "diffuse corneal edema", with widespread corneal edema throughout the central and peripheral cornea and 2) "central corneal edema", with corneal edema in the center and relatively less edema in the peripheral region. In the clinical study, the central corneal endothelium was removed by transcorneal freezing using a 2-mm-diameter stainless-steel rod to create a space where the substrate was not covered by damaged corneal endothelium. This was followed by topical administration of 10 mM of Y-27632 in eye drop form 6 times daily for 7 days. The central corneal edema patients showed a reduction in central corneal thickness, an indicator of corneal endothelial health, following the treatment. By contrast, the eyes with diffuse corneal edema showed no reduction or worsening of central corneal thickness (Fig. **1**). None of the patients in either group showed irreversible corneal haze due to the transcorneal freezing. Notably, one patient in the central corneal edema group showed a dramatic response. The patient was a 52-year-old Japanese male diagnosed with late-onset Fuchs endothelial corneal dystrophy, who had a central corneal thickness of 703 μm and visual acuity of 20/63. After using the ROCK inhibitor eye drops, following transcorneal freezing, his corneal edema disappeared and the cornea became transparent, with a central corneal thickness of 568 μm and visual acuity of 20/20 [26, 27]. This patient eventually canceled a planned corneal transplantation, and his corneal transparency was maintained for more than 6 years.

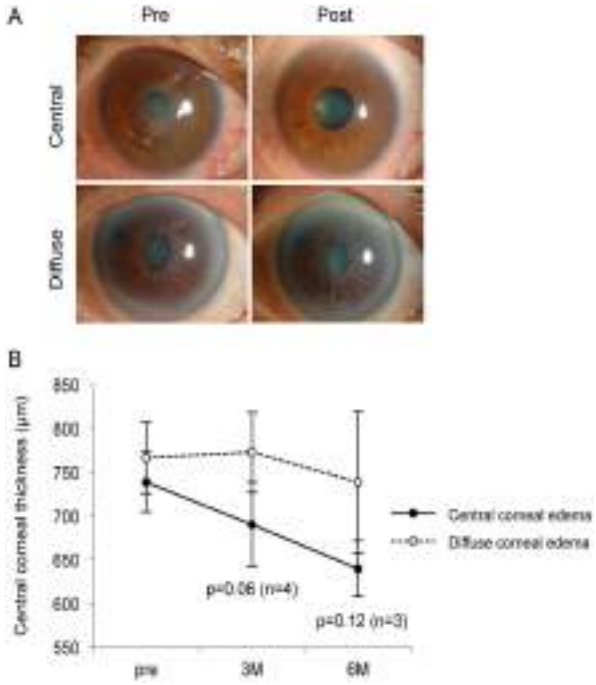

Fig. (1). Clinical trial of ROCK-inhibitor Y-27632 eye drops for central corneal edema or diffuse corneal edema due to corneal endothelial diseases. (A) Representative case of a central corneal edema patient is shown in the upper images. Before treatment, central corneal edema was observed. Six months after treatment, the corneal edema was significantly reduced and visual acuity recovered from logMAR 0.70 to -0.18. A representative case of a diffuse corneal edema patient is shown in the lower images. Before treatment, the patient showed diffuse corneal edema due to bullous keratopathy induced by argon laser iridotomy. Six months after treatment,

the corneal edema persisted and visual acuity was not recovered. (B) In the central corneal edema patients, central corneal thickness was reduced 6 months after treatment compared to pre-treatment levels. In contrast, the central corneal thickness did not reduce in eyes with diffuse corneal edema. Reproduced with permission from Okumura *et al*. [10]

This pilot study showed the possibility of a therapeutic effect in early stage patients with central corneal edema; however, it had several limitations. The cohort size was small, so further studies with larger numbers of earlier stage patients are needed. In addition, the study was a single hand study without a control group in which patients underwent transcorneal freezing but received no ROCK inhibitor eye drops. A randomized control study with a larger cohort is needed for generalization of the effect of ROCK inhibitor eye drops in the corneal endothelium. A recent study has examined the effect of surgical removal of the central corneal endothelium with Descemet's membrane, although this procedure remains controversial [28-30]. The effect of ROCK inhibitor eye drops in combination with this procedure may be worth investigating.

Animal Experiments Mimicking Severe Damage to the Corneal Endothelium Due to Cataract Surgery

The pilot clinical trial using Y-27632 following transcorneal freezing revealed that Y-27632 eye drops reduced corneal edema in patients with early stage Fuchs' endothelial corneal dystrophy who had central edema but relatively healthy corneal endothelium remaining at the peripheral area. We therefore postulated that ROCK inhibitor eye drops might be effective in the patients who have relatively healthy residual corneal endothelium and "space" for the remaining cells to proliferate and migrate. This idea led us to investigate the effect of ROCK inhibitors on the severe corneal endothelium damage observed following cataract surgery despite the presence of a certain amount of relatively healthy corneal endothelium.

A rabbit corneal endothelial damage model was created to mimic surgical trauma by mechanical removal of half the area of the corneal endothelium, rather than transcorneal freezing. Administration of Y-27632 eye drops increased the expression of Ki67 positive cells compared to control eyes. Five out of 6 corneas recovered transparency in the Y-27632-treated eyes, while 0 out of 6 corneas recovered transparency in the control eyes [33]. This effect of ROCK inhibitor eye drops in this animal model was further confirmed by using ripasudil, another ROCK inhibitor [34]. Ripasudil hydrochloride hydrate eye drops were approved as GLANATEC® ophthalmic solution 0.4% in Japan for the treatment of glaucoma and ocular hypertension [7]. The 50% inhibitory concentration (IC_{50}) of ripasudil is 0.051 μM for ROCK 1 and 0.019 μM for ROCK 2, whereas the IC_{50} for PKACα, PKC, and CaMKIIα are 2.1, 27, and 0.37μM, respectively [35]. Repurposing of an existing drug for new indications, or so-called "drug repositioning," is one possible strategy for drug development that gains faster approval and lowers the investment cost. The effect of ripasudil on corneal endothelial wound healing in animal models supports the development of ripasudil as a drug for corneal endothelial injury as one possible strategy for hastening the introduction of ROCK inhibitors into the clinical setting.

Pilot Clinical Study of a ROCK Inhibitor for Corneal Endothelial Injury Caused by Cataract Surgery

The safety and effectiveness of ROCK inhibitor eye drops was evaluated in patients whose corneal endothelium was severely damaged during cataract surgery [33]. Three eyes of 3 patients were enrolled in this preliminary pilot clinical study at the Kyoto Prefectural University of Medicine, which ran from October 2012. All 3 patients developed corneal edema due to corneal endothelial damage following cataract surgery. In two patients, more than half the area of the Descemet's membrane, with the corneal endothelium, was detached accidentally from the corneal stroma and removed during cataract surgery. The other patient developed an iris cyst following an old trauma, and the corneal endothelial cell density was low. That patient underwent cataract surgery and iris cyst removal, and then developed corneal edema immediate after the surgery. All patients received Y-27632 eye drops 6 times daily for 4 months, followed by 4 times daily for 2 further months. All three patients faced the possibility of developing irreversible corneal haziness, but they all eventually recovered corneal clarity and avoided the need for corneal transplantation (Fig. **2**). This study had a number of limitations, including the very preliminary nature of the cases, the lack of vehicle control cases, and a lack of follow up of patients without treatment to exclude the possibility that the patients would have recovered corneal transparency as a natural course. However, these three cases are sufficiently encouraging to conduct a randomized clinical trial and to develop ROCK inhibitor eye drops as a drug for acute corneal endothelial damage, especially that induced by cataract surgery.

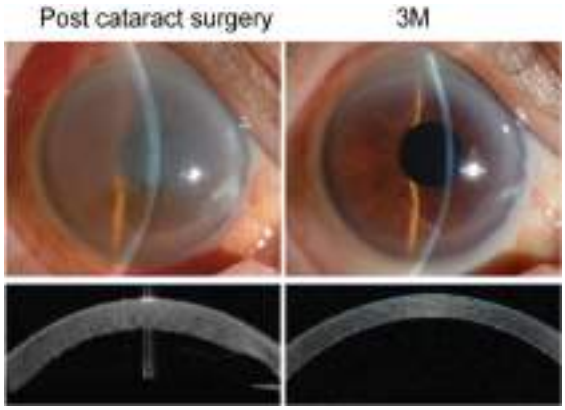

Fig. (2). Pilot clinical research into the use of ROCK inhibitor eye drops for the treatment of acute corneal endothelial damage due to cataract surgery.
An 84-year-old female diagnosed with cataract underwent cataract surgery. During the surgery, the Descemet's membrane spontaneously detached from the upper incision tunnel and over 2/3 was aspirated. The patient was referred to the cornea clinic of Kyoto Prefectural University of Medicine due to severe corneal edema (upper left: slitlamp microscope image, lower left: Scheimpflug image). The patient was treated with 1mM Y-27632 eye drops for 6 months (upper right: anterior segment image, lower right: Scheimpflug image).
Reproduced with permission from Okumura *et al*. [33].

In the United States, 12.2% of the corneal transplantations are performed for treating post-cataract surgery corneal edema. In Asian countries 20–40% of corneal transplantation is performed to treat bullous keratopathy caused by cataract surgery [8, 31, 32]. The incidence of bullous keratopathy caused by cataract surgery tends to decrease in developed courtiers [9], possibly because the surgeons have experienced a learning curve, and the surgical techniques and devices are more developed. However, the World Health Organization reported that cataract accounts for 51% of the global causes of blindness [36], indicating that numerous cataract patients are awaiting surgery. Thus, a reasonable prediction is that physicians should still remain aware of corneal endothelial damage, especially following cataract surgery, and especially in developing countries. If pharmaceutical agents such as ROCK inhibitors can be applied immediately after severe corneal endothelial damage, this should minimize the incidence of bullous keratopathy (Fig. **3**).

Effect of ROCK Inhibitors on the Morphology of the Corneal Endothelium

In cynomolgus monkeys, instillation of ripasudil induced morphological changes in the corneal endothelium [37], but the reasons for these changes remain unclear. The corneal endothelium is a

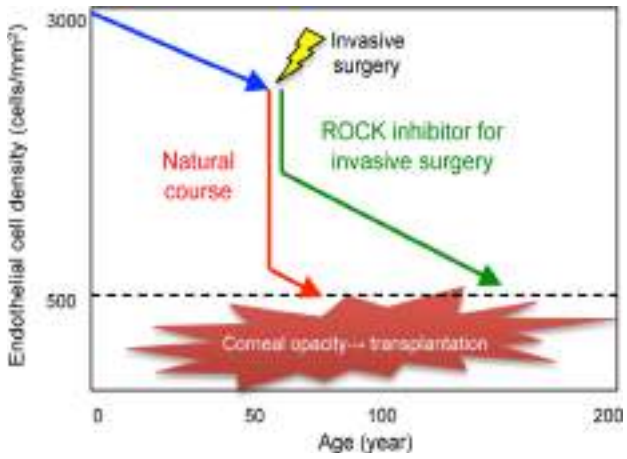

Fig. (3). Future treatment strategy for corneal endothelial damage induced by invasive surgery.
Schematic image shows possible therapeutic stagey by using ROCK inhibitor eye drop to reduce the incidence of bullous keratopathy due to cataract surgery.

non-regenerative tissue, so the possibility that morphological changes cause cell death should be investigated. We have evaluated these morphological changes in healthy human volunteers. Six healthy subjects were administered ripasudil 0.4% (GLANATEC®) twice daily for 1 week. Noncontact specular microscopy demonstrated that morphological changes of corneal endothelial cells, including indistinct cell borders and pseudo guttae, were transiently observed after ripasudil administration. These morphological changes were reversible and the corneas returned to normal after cessation of the treatment. No corneal edema was observed and corneal endothelial cell density did not decrease after 1 week of repetitive administration [38].

The morphological changes observed by noncontact specular microscopy were histologically investigated in rabbits [39]. Electron microscopy demonstrated the formation of protrusions along the cell borders; these recovered by 3–6 hours after ripasudil instillation. This formation of protrusions along the cell borders seems to be associated with the pseudo guttae-like morphological changes observed with specular microscopy in the clinical setting. Since ROCK inhibitors modulate the actin cytoskeleton, protrusion formation is a reasonable effect expected for ripasudil eye drops. This eye drop formulation has been approved in Japan and is widely used; therefore, clinicians should remain aware of potential effects of long-term use of ripasudil eye drops on the corneal endothelium.

AS ADJUNCTIVE DRUGS FOR CELL-BASED THERAPY

Cell-based Therapy for Treating Corneal Endothelial Dysfunction

Regenerative medicine has been anticipated to provide innovative therapeutic modalities for various diseases, including corneal endothelial dysfunction. Indeed, a number of researchers, including our group, have cultured corneal endothelial cells on scaffolds in the form of sheets, and have demonstrated that animal models of corneal endothelial dysfunction can be treated by transplantation with these cultured CEC sheets [40-43]. However, several obstacles remain that limit translation of cell sheet transplantation to the clinical setting, including the specifications (e.g., safety profile) of the artificial carrier used, the degree of transparency required for visual quality, and the ability to provide good adhesion to the recipient corneal stroma. Additionally, transplantation of a flexible monolayer endothelial cell sheet into the anterior chamber is technically difficult [44]. Therefore, we have developed a method for regenerating corneal endothelium by injection of CECs, rather than by sheet transplantation. The main disadvantage of injection is that the adhesion of the injected cells onto the corneal tissue is poor, resulting in no regeneration of corneal endothelium. Magnetic cell guidance, using iron powder incorporated into cultivated CECs, has been proposed as a way to promote cell adhesion [45, 46], but this method has yet to be applied in humans.

Animal Experiments

We hypothesized that the adhesion of injected CECs onto the recipient cornea could be enhanced by modification of the adhesive property using ROCK inhibitors (Fig. **4**). We evaluated the combined injection of cultivated CECs with a ROCK inhibitor by suspending cultured rabbit CECs in 200 µl of DMEM supplemented with 100 µM of Y-27632. This suspension was then injected into the anterior chamber of the eyes of corneal endothelial dysfunction rabbit model, where the entire corneal endothelium had been scraped off mechanically [47]. After the cell injection, the rabbits were kept in the face-down position for 3 hours under general anesthesia. Control rabbit eyes were injected with CECs without Y-27632; these eyes showed limited cell adhesion on the recipient corneas, as well as associated fibroblastic changes in the injected cells, with the end result being hazy corneas. By contrast, the eyes injected with the combination of CECs and Y-27632 recovered transparent corneas, and histological assessment showed the CECs to have assumed a monolayer and a normal hexagonal morphology of the regenerated corneal endothelium (Fig. **5A**).

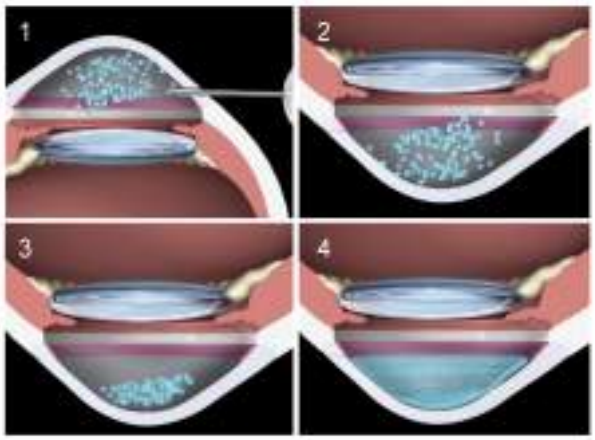

Fig. (4). Concept of cultured corneal endothelial cell (CEC) injection for corneal endothelial dysfunction.
Schematic images show the cultured CEC injection procedure. 1) co-injection of cultured CECs with ROCK inhibitor into the anterior chamber, 2) face-down position for the CECs to sink down to the anterior chamber side of the cornea, 3) maintenance of the face-down position for 3 hours, 4) regeneration of corneal endothelium by injected cultured CECs.
Reproduced from Okumura *et al*. [48].

A preclinical study was then conducted in a primate model to assess the safety and efficacy of cell-based therapy using ROCK inhibitors [48]. The entire corneal endothelium was removed mechanically to generate the corneal endothelial dysfunction model in cynomolgus monkeys. The injection of the combination of cultured monkey CECs and Y-27632 restored corneal transparency. The corneas of control monkeys, in which no cells were injected, and the corneas of monkeys in which cells alone were injected, without Y-27632, showed hazy corneas due to corneal endothelial dysfunction (Fig. **5B**). Regeneration of the corneal endothelium was further confirmed by the combined injection of cultured human CECs with ROCK inhibitor in this primate model. The injection of human CECs also regenerated corneal endothelium in primate eyes and restored a transparent cornea (Fig. **6**).

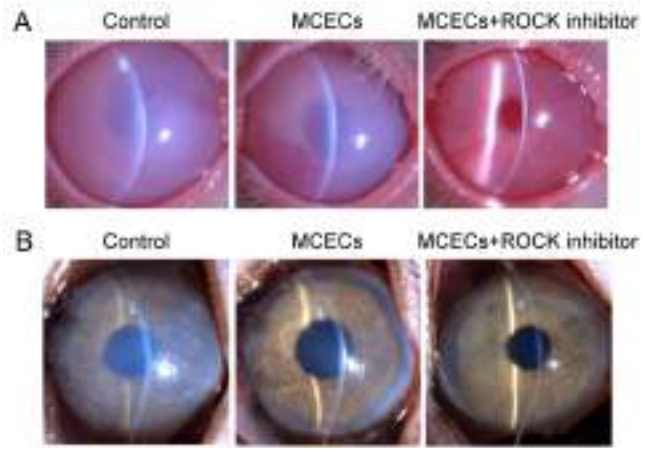

Fig. (5). Combined injection of cultured corneal endothelial cells (CECs) and a ROCK inhibitor in rabbit and monkey corneal endothelial dysfunction models.
(A) Slit-lamp photographs of rabbit eyes co-injected with cultivated rabbit CECs and Y-27632, injected with cultivated CECs only, and a control corneal endothelial dysfunction model after 48 hours. The rabbit eyes injected with the combination of cultivated CECs and Y-27632 recovered complete transparency of the cornea. By contrast, the eyes injected with cultivated CECs without Y-27632 and the control eyes exhibited a hazy cornea with severe edema.
Reproduced with permission from *Elsevier* from Okumura *et al.* [47]
(B) A representative slit-lamp image shows the monkey corneal endothelial dysfunction model (left). A representative slit-lamp image shows the corneal endothelial dysfunction model following injection of monkey CECs (5.0×10^5 cells) suspended in 200 µl of DMEM without (middle) or with (right) the ROCK inhibitor Y-27632. All images were obtained 14 days after treatment.
Reproduced from Okumura *et al.* [48].

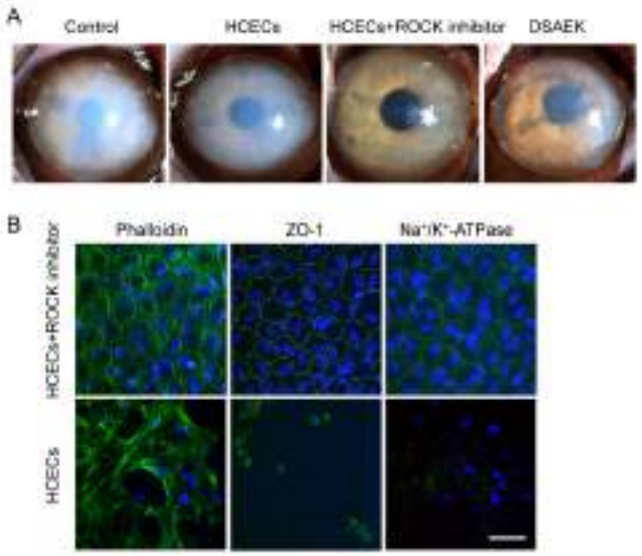

Fig. (6). Preclinical research into combined injection of cultured human corneal endothelial cells (HCECs) and a ROCK inhibitor in a monkey corneal endothelial dysfunction model.
(A) Representative slit-lamp images were obtained for the monkey corneal endothelial dysfunction model. Images shown are from a monkey injected with HCECs (5.0×10^5 cells) without the ROCK inhibitor Y-27632, a monkey injected with HCECs (5.0×10^5 cells) and Y-27632, and a monkey transplanted with a human donor cornea according to DSAEK procedure. All images were obtained 7 days after treatment.
(B) Cell morphology of regenerated corneal endothelium was evaluated by phalloidin staining. Function-related markers of CECs (Na^+/K^+-ATPase and ZO-1) showed immunostaining in the regenerated corneal endothelium. Nuclei were stained with DAPI. Scale bar: 100 µm.
Reproduced from Okumura *et al.* [48].

One possible adverse effect of cell injection is an aberration due to the delivery of transplanted cells to other organs [48]. In these primate experiments, no HCEC-derived cells were detected by PCR in any monkey organs other than the regenerated corneal endothelium, suggesting that the safety profile of cell-based therapy combined with ROCK inhibitor is very good.

The U.S. Food and Drug Administration (FDA) regulates regenerative medicine products through the Center for Biologics Evaluation and Research (CBER) in the United States, and other countries also have similar systems [49]. Based on the FDA requirements [50], we ran animal experiments to test the safety and efficacy of human CECs, produced using Good Manufacturing Practices (GMPs) in the same fashion as we intend to use in the transplantation of these cells into human patients in clinical trials. The GMP-grade human CECs were cultured in the cell-processing center at the Kyoto Prefectural University of Medicine according to the protocol required for clinical application [44], and then injected into the monkey corneal endothelial dysfunction model. We confirmed that the primate cornea became transparent and was associated with regeneration of the corneal endothelium by the injected GMP-grade human CECs.

Mechanism of Enhancement of Cell Adhesion on Substrates by ROCK Inhibitors

The mechanism underlying the promotion of cell adhesion of CECs to the substrate during cell culture [10] by ROCK inhibitors remains unclear. We recently reported that cell dissociation from the culture plate induced the activation of the RhoA/ROCK/MLC pathway, resulting in actin contraction that impairs cell adhesion [48] (Fig. **7**). Similar to our findings in CECs, human embryonic stem cells are vulnerable to apoptosis following dissociation due to ROCK-dependent activation of actomyosin [51]. Though the dissociation-induced cellular response depends on the cell type, the inhibition of ROCK signaling may be worth examining for improving cell engraftment efficiency in the settings of cell-based therapies in other organs.

Clinical Study of Cell-based Therapy Combined with ROCK Inhibitors

In 2013, we initiated a first-in-man clinical trial of cell-based therapy to treat corneal endothelial dysfunction at the Kyoto Prefectural University of Medicine, after obtaining the necessary approval from the Japanese Ministry of Health, Labour and Welfare (Clinical trial registration: UMIN000012534). Diligent feedback from clinical trials, by evaluating possible side effects, will be needed to ensure patient safety; therefore, we are currently collecting clinical data.

CONCLUSION

Evidence is accumulating that ROCK inhibitors enhance wound healing in the corneal endothelium by promoting cell proliferation. In addition to the findings in animal models, pilot clinical research has shown that ROCK inhibitors might be useful during the acute phase of corneal endothelial injury, especially injury induced by cataract surgery, where some healthy corneal endothelium remains, even if it is not effective for the treatment of the chronic phase of bullous keratopathy. Randomized clinical trials initiated by pharmaceutical companies are the only way to enable the introduction of ROCK inhibitors as standard treatment for acute corneal endo-

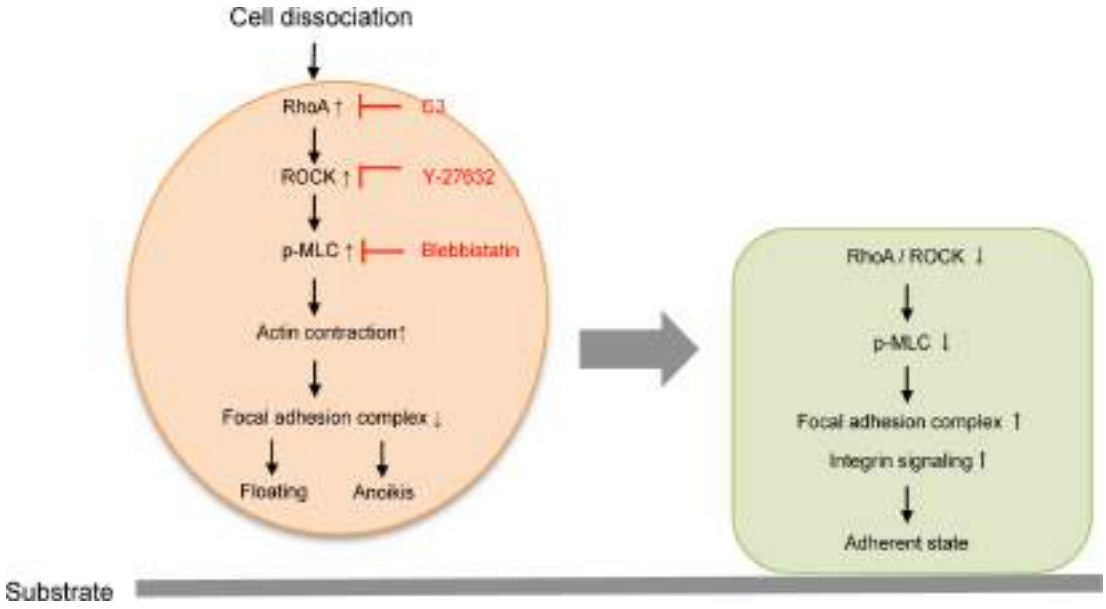

Fig. (7). The molecular pathway by which a ROCK inhibitor treatment improves cell engraftment of CECs.
(Right) Cell dissociation during the harvesting of CECs from culture plate activates RhoA/ROCK/ MLC pathways. Activation of this pathway suppresses activation of the focal adhesion complex, subsequently inhibiting cell adhesion while inducing anoikis. (Left) By contrast, inhibition of actomyosin activation by a ROCK inhibitor activates the focal adhesion complex and enhances cell/ECM adhesion.
Reproduced from Okumura *et al.* [48].

thelial damage. We hope that physicians will have access to ROCK inhibitors and eventually reduce the number of bullous keratopathy patients who need corneal transplantation. In addition, the use of ROCK inhibitors as adjunct drugs for enhancing injected CEC engraftment can regenerate corneal endothelium, but this also needs clinical trials initiated by pharmaceutical companies for adoption of this cell-based therapy as one of the standard procedures for treating bullous keratopathy. Conventional transplantations using donor corneas remain an option, but we believe that these new therapeutic modalities have a promising future that can provide less invasive and more effective therapy for the patients.

CONFLICT OF INTEREST

Shigeru Kinoshita obtained a patent regarding the application of ROCK inhibitor for corneal endothelium (registration number: 5657252). N.O. and N.K. are listed as inventors of the patent.

ACKNOWLEDGEMENTS

This study was supported by the Highway Program for realization of regenerative medicine (Kinoshita and Koizumi) and the Program for the Strategic Research Foundation at Private Universities from MEXT (Koizumi N and Okumura N). The authors thank Drs. Chie Sotozono, Morio Ueno, Junji Hamuro, Takahiro Nakamura, Hiroko Nakagawa, Michio Hagiya, EunDuck P. Kay, Makiko Nakahara, Junji Kitano, Keita Fujii, Shinichiro Nakano, Yuji Sakamoto, Hiroaki Takahashi, and Yoshiki Sasai for their invaluable advice and contributions, and Mr. Monty Montoya and Mr. Bernie Iliakis (SightLife™) for providing the donor corneas.

REFERENCES

[1] Nakagawa O, Fujisawa K, Ishizaki T, Saito Y, Nakao K, Narumiya S. ROCK-I and ROCK-II, two isoforms of Rho-associated coiled-coil forming protein serine/threonine kinase in mice. FEBS Lett 1996; 392: 189-93.

[2] Riento K, Ridley AJ. Rocks: multifunctional kinases in cell behaviour. Nat Rev Mol Cell Biol 2003; 4: 446-56.

[3] Narumiya S, Tanji M, Ishizaki T. Rho signaling, ROCK and mDia1, in transformation, metastasis and invasion. Cancer Metastasis Rev 2009; 28: 65-76.

[4] Shi J, Wei L. Rho kinase in the regulation of cell death and survival. Arch Immunol Ther Exp (Warsz) 2007; 55: 61-75.

[5] Olson MF. Applications for ROCK kinase inhibition. Curr Opin Cell Biol 2008; 20: 242-8.

[6] Feng Y, LoGrasso PV, Defert O, Li R. Rho kinase (ROCK) inhibitors and their therapeutic potential. J Med Chem 2016; 59: 2269-300.

[7] Garnock-Jones KP. Ripasudil: first global approval. Drugs 2014; 74: 2211-5.

[8] Tan DT, Dart JK, Holland EJ, Kinoshita S. Corneal transplantation. Lancet 2012; 379: 1749-61.

[9] Eye Bank Association of America. Eye banking statistical report. Washington, D.C. 2013.

[10] Okumura N, Ueno M, Koizumi N, *et al.* Enhancement on primate corneal endothelial cell survival *in vitro* by a ROCK inhibitor. Invest Ophthalmol Vis Sci 2009; 50: 3680-7.

[11] Okumura N, Nakano S, Kay EP, *et al*. Involvement of cyclin D and p27 in cell proliferation mediated by ROCK inhibitors Y-27632 and Y-39983 during corneal endothelium wound healing. Invest Ophthalmol Vis Sci 2014; 55: 318-29.

[12] Peh GS, Adnan K, George BL, *et al*. The effects of Rho-associated kinase inhibitor Y-27632 on primary human corneal endothelial cells propagated using a dual media approach. Sci Rep 2015; 5: 9167.

[13] Pipparelli A, Arsenijevic Y, Thuret G, Gain P, Nicolas M, Majo F. ROCK inhibitor enhances adhesion and wound healing of human corneal endothelial cells. PLoS One 2013; 8: e62095.

[14] Yamamoto M, Marui N, Sakai T, *et al*. ADP-ribosylation of the rhoA gene product by botulinum C3 exoenzyme causes Swiss 3T3 cells to accumulate in the G1 phase of the cell cycle. Oncogene 1993; 8: 1449-55.

[15] Olson MF, Ashworth A, Hall A. An essential role for Rho, Rac, and Cdc42 GTPases in cell cycle progression through G1. Science 1995; 269: 1270-2.

[16] Croft DR, Olson MF. The Rho GTPase effector ROCK regulates cyclin A, cyclin D1, and p27Kip1 levels by distinct mechanisms. Mol Cell Biol 2006; 26: 4612-27.

[17] Liao JK, Seto M, Noma K. Rho kinase (ROCK) inhibitors. J Cardiovasc Pharmacol 2007; 50: 17-24.

[18] Joyce NC. Proliferative capacity of the corneal endothelium. Prog Retin Eye Res 2003; 22: 359-89.

[19] Joyce NC. Cell cycle status in human corneal endothelium. Exp Eye Res 2005; 81: 629-38.

[20] Okumura N, Koizumi N, Ueno M, *et al*. Enhancement of corneal endothelium wound healing by Rho-associated kinase (ROCK) inhibitor eye drops. Br J Ophthalmol 2011; 95: 1006-9.

[21] Van Horn DL, Hyndiuk RA. Endothelial wound repair in primate cornea. Exp Eye Res 1975; 21: 113-24.

[22] Van Horn DL, Sendele DD, Seideman S, Buco PJ. Regenerative capacity of the corneal endothelium in rabbit and cat. Invest Ophthalmol Vis Sci 1977; 16: 597-613.

[23] Matsubara M, Tanishima T. Wound-healing of the corneal endothelium in the monkey: a morphometric study. Jpn J Ophthalmol 1982; 26: 264-73.

[24] Treffers WF. Human corneal endothelial wound repair. *In vitro* and *in vivo*. Ophthalmology 1982; 89: 605-13.

[25] Matsubara M, Tanishima T. Wound-healing of corneal endothelium in monkey: an autoradiographic study. Jpn J Ophthalmol 1983; 27: 444-50.

[26] Okumura N, Koizumi N, Kay EP, *et al.* The ROCK inhibitor eye drop accelerates corneal endothelium wound healing. Invest Ophthalmol Vis Sci 2013; 54(4): 2493-502.

[27] Koizumi N, Okumura N, Ueno M, Nakagawa H, Hamuro J, Kinoshita S. Rho-associated kinase inhibitor eye drop treatment as a possible medical treatment for Fuchs corneal dystrophy. Cornea 2013; 32: 1167-70.

[28] Shah RD, Randleman JB, Grossniklaus HE. Spontaneous corneal clearing after Descemet's stripping without endothelial replacement. Ophthalmology 2012; 119: 256-60.

[29] Galvis V, Tello A, Miotto G. Human corneal endothelium regeneration. Ophthalmology 2012; 119: 1714-5.

[30] Bleyen I, Saelens IE, van Dooren BT, van Rij G. Spontaneous corneal clearing after Descemet's stripping. Ophthalmology 2013; 120: 215.

[31] Dandona L, Naduvilath TJ, Janarthanan M, Ragu K, Rao GN. Survival analysis and visual outcome in a large series of corneal transplants in India. Br J Ophthalmol 1997; 81: 726-31.

[32] Shimazaki J, Amano S, Uno T, Maeda N, Yokoi N. National survey on bullous keratopathy in Japan. Cornea 2007; 26: 274-8.

[33] Okumura N, Inoue R, Okazaki Y, *et al*. Effect of the rho kinase inhibitor Y-27632 on corneal endothelial wound healing. Invest Ophthalmol Vis Sci 2015; 56: 6067-74.

[34] Okumura N, Okazaki Y, Inoue R, *et al.* Effect of the rho-associated kinase inhibitor eye drop (ripasudil) on corneal endothelial wound healing. Invest Ophthalmol Vis Sci 2016; 57: 1284-92.

[35] Isobe T, Mizuno K, Kaneko Y, Ohta M, Koide T, Tanabe S. Effects of K-115, a rho-kinase inhibitor, on aqueous humor dynamics in rabbits. Curr Eye Res 2014; 39: 813-22.

[36] World Health Organization. Global data on visual impairments. 2010.

[37] Wato E, Omichi K, Yoneyama S, Tanaka M, Kagawa M, Amano Y. Host and graft thickness after Descemet stripping endothelial keratoplasty for Fuchs endothelial dystrophy. Fundam Toxicol Sci 2010; 1: 39-47.

[38] Nakagawa H, Koizumi N, Okumura N, Suganami H, Kinoshita S. Morphological changes of human corneal endothelial cells after rho-associated kinase inhibitor eye drop (ripasudil) administration: A prospective open-label clinical study. PLoS One 2015; 10: e0136802.

[39] Okumura N, Okazaki Y, Inoue R, *et al.* Rho-associated kinase inhibitor eye drop (ripasudil) transiently alters the morphology of corneal endothelial cells. Invest Ophthalmol Vis Sci 2015; 56: 7560-7.

[40] Ishino Y, Sano Y, Nakamura T, *et al*. Amniotic membrane as a carrier for cultivated human corneal endothelial cell transplantation. Invest Ophthalmol Vis Sci 2004; 45: 800-6.

[41] Mimura T, Yamagami S, Yokoo S, *et al*. Cultured human corneal endothelial cell transplantation with a collagen sheet in a rabbit model. Invest Ophthalmol Vis Sci 2004; 45: 2992-7.

[42] Sumide T, Nishida K, Yamato M, *et al.* Functional human corneal endothelial cell sheets harvested from temperature-responsive culture surfaces. FASEB J 2006; 20: 392-4.

[43] Koizumi N, Sakamoto Y, Okumura N, *et al.* Cultivated corneal endothelial cell sheet transplantation in a primate model. Invest Ophthalmol Vis Sci 2007; 48: 4519-26.

[44] Okumura N, Kinoshita S, Koizumi N. Cell-based approach for treatment of corneal endothelial dysfunction. Cornea 2014; 33 Suppl 11: S37-41.

[45] Mimura T, Shimomura N, Usui T, *et al*. Magnetic attraction of iron-endocytosed corneal endothelial cells to Descemet's membrane. Exp Eye Res 2003; 76: 745-51.

[46] Patel SV, Bachman LA, Hann CR, Bahler CK, Fautsch MP. Human corneal endothelial cell transplantation in a human *ex vivo* model. Invest Ophthalmol Vis Sci 2009; 50: 2123-31.

[47] Okumura N, Koizumi N, Ueno M, *et al*. ROCK inhibitor converts corneal endothelial cells into a phenotype capable of regenerating *in vivo* endothelial tissue. Am J Pathol 2012; 181: 268-77.

[48] Okumura N, Sakamoto Y, Fujii K, *et al*. Rho kinase inhibitor enables cell-based therapy for corneal endothelial dysfunction. Sci Rep 2016; 6: 26113.

[49] Bailey AM. Balancing tissue and tumor formation in regenerative medicine. Sci Transl Med 2012; 4: 147fs28.

[50] Harding J, Mirochnitchenko O. Preclinical studies for induced pluripotent stem cell-based therapeutics. J Biol Chem 2014; 289: 4585-93.

[51] Ohgushi M, Matsumura M, Eiraku M, *et al.* Molecular pathway and cell state responsible for dissociation-induced apoptosis in human pluripotent stem cells. Cell Stem Cell 2010; 7: 225-39.

Activation of the Rho/Rho Kinase Signaling Pathway Is Involved in Cell Death of Corneal Endothelium

Naoki Okumura,[1] Keita Fujii,[1] Takato Kagami,[1] Nakahara Makiko,[1] Miu Kitahara,[1] Shigeru Kinoshita,[2] and Noriko Koizumi[1]

[1]Department of Biomedical Engineering, Faculty of Life and Medical Sciences, Doshisha University, Kyotanabe, Japan
[2]Department of Frontier Medical Science and Technology for Ophthalmology, Kyoto Prefectural University of Medicine, Kyoto, Japan

Correspondence: Noriko Koizumi, Department of Biomedical Engineering, Faculty of Life and Medical Sciences, Doshisha University, Kyotanabe 610-0394, Japan; nkoizumi@mail.doshisha.ac.jp.

Submitted: June 13, 2016
Accepted: November 28, 2016

Citation: Okumura N, Fujii K, Kagami T, et al. Activation of the Rho/Rho kinase signaling pathway is involved in cell death of corneal endothelium. *Invest Ophthalmol Vis Sci*. 2016;57:6843–6851. DOI:10.1167/iovs.16-20123

Purpose. Rho kinase (ROCK) pathways control fundamental cell functions, making ROCK an important therapeutic target in several pathophysiologic conditions. The purpose of this study was to investigate whether inhibition of ROCK can suppress apoptosis of the corneal endothelium and to determine the role of ROCK signaling in regulating apoptosis.

Methods. The effects of inhibitors of ROCK or myosin light chain (MLC) were evaluated in cultured monkey corneal endothelial cells (MCECs) irradiated with ultraviolet (UV) (100 J/m^2) to induce apoptosis. Annexin V and TUNEL staining and Western blot for apoptosis-related proteins and focal adhesion complexes were then performed. RhoA activation was further evaluated by pull-down assays. ROCK inhibitor and caspase inhibitor effects on apoptosis were also evaluated in MCECs treated with ethylene glycol tetraacetic acid (EGTA) to induce MLC phosphorylation.

Results. ROCK or MLC inhibition suppressed the caspase-3 cleavage and Annexin V and TUNEL expression typically seen during UV-mediated apoptosis of MCECs. The apoptotic stimulus activated RhoA and then induced phosphorylation of MLC via ROCK activation. EGTA-mediated phosphorylation of MLC was sufficient to induce the loss of cell contact with the substrate and subsequent apoptosis. Western blot showed that ROCK inhibition upregulated the expression of the focal adhesion complex in adhered cells, following UV stress.

Conclusions. Apoptotic stimuli activated Rho/ROCK/MLC phosphorylation in the corneal endothelium, and subsequent actomyosin contraction induced apoptosis by loss of cell adhesion. ROCK inhibition suppressed MLC phosphorylation and subsequent cell death, and it counteracted the loss of cell adhesion by activating the focal adhesion complex.

Keywords: corneal endothelium, Rho kinase, apoptosis

The corneal endothelium controls corneal hydration, thereby maintaining corneal transparency. The cell density of corneal endothelial cells (CECs) in healthy individuals ranges from 2000 to 3000 cells/mm^2, but can drop below a critical cell density (<1000 cells/mm^2) for various pathologic reasons, resulting in corneal haziness.

Fuchs endothelial corneal dystrophy (FECD) is the leading cause of corneal transplantation, with a prevalence as high as 4% of the population older than 40 years in the United States.[1] The corneal endothelium of FCED patients shows progressive damage, and several possible explanations have been proposed for the pathogenesis of FECD, including oxidative stress, mitochondrial abnormalities, microRNA, extracellular matrix, and unfolded protein response. However, histologic assessments and several basic research studies have demonstrated that apoptosis plays an important role in the cell loss associated with FECD.[2–7] The only treatment for loss of corneal transparency due to FECD is corneal transplantation,[8] but research continues for the identification of drug therapies to regulate corneal endothelium cell loss.[9,10]

Rho kinase (ROCK) is a serine/threonine kinase that undergoes activation by interaction with Rho GTPases. The Rho/ROCK signaling pathways control a wide range of fundamental cell functions, including cell adhesion, motility, proliferation, differentiation, and apoptosis. The wide spectrum of biological events influenced by ROCK has led to the recognition of ROCK as an important therapeutic target in a variety of pathophysiologic conditions.[11–13] Indeed, inhibition of ROCK has been intensively researched for treating various diseases ranging from vascular disease, cancer, and neuronal degenerative disease to asthma and glaucoma.[11–13] One ROCK inhibitor, fasudil, has been approved for the treatment of cerebral vasospasm in 1995, and another, ripasudil, has been approved in eye drop form in Japan in 2014 for the treatment of glaucoma and ocular hypertension.[12,14,15] Recently, we have proposed ROCK inhibitors as eye drops for promoting CEC proliferation[16–18] and as adjunct drugs for cell-based therapy to enhance engraftment when treating corneal endothelial dysfunction.[19,20]

We previously have reported that the ROCK inhibitor Y-27632 suppresses the apoptosis of cultured monkey CECs (MCECs) during cell passaging, but the underlying mechanisms remain unclear.[21] The possible involvement of an anti-apoptotic effect motivated us to investigate the feasibility of using a ROCK

inhibitor as a drug to regulate pathologic conditions, especially those associated with FECD. In the execution phase of apoptosis, ROCK is pivotal in regulating morphologic events such as membrane blebbing, nuclear disintegration, and formation of apoptotic bodies in various cell types.[11,22,23] However, the importance of ROCK in the early stages of apoptosis is highly dependent on the cell type and stimulus.[11] The aim of the current study was to investigate whether inhibition of ROCK suppresses apoptosis of the corneal endothelium and to determine the role of ROCK signaling in the regulation of apoptosis.

Methods

Cell Culture

Animals were housed and treated in accordance with the ARVO Statement for the Use of Animals in Ophthalmic and Vision Research. Six corneas from three cynomolgus monkeys (3–5 years of age; estimated equivalent human age: 5–20 years) housed at NISSEI BILIS Co., Ltd. (Osaka, Japan) were used for the experiments. The MCECs were cultivated as described previously.[19] Briefly, the Descemet's membrane, including the MCECs, was stripped from the cornea and digested with Dulbecco's modified Eagle's medium (DMEM; Life Technologies Corp., Carlsbad, CA, USA) supplemented with 1 mg/mL collagenase A (Roche Applied Science, Penzberg, Germany) at 37°C for 12 hours. The isolated MCECs were recovered in culture medium, seeded on culture plates coated with FNC Coating Mix (Athena Environmental Sciences, Inc., Baltimore, MD, USA), and cultured in DMEM supplemented with 10% fetal bovine serum, 50 U/mL penicillin, 50 μg/mL streptomycin, and 2 ng/mL fibroblast growth factor 2 (Life Technologies Corp.). Monkey corneal endothelial cells at passages 4 through 8 were used for these experiments. In some experiments, cells were treated with culture medium supplemented with ethylene glycol tetraacetic acid (EGTA) (3 mM; Wako Pure Chemical Industries, Ltd., Osaka, Japan), Z-VAD-FMK (10 μM, Wako Pure Chemical Industries, Ltd.), Y-27632 (10 μM, Wako Pure Chemical Industries, Ltd.), or blebbistatin (10 μM, Wako Pure Chemical Industries, Ltd.). Cells were examined with a phase contrast microscope (DMI4000 B; Leica Microsystems, Wetzlar, Germany) or a time-lapse phase contrast microscope (BZ-9000; KEYENCE, Osaka, Japan).

For UV stimulation, MCECs were washed gently with phosphate-buffered saline (PBS) and exposed to UV (100 J/m^2) by using a UV CrossLinker CX-2000 (UVP, Upland, CA, USA), and were further cultured with fresh culture medium. For hydrogen peroxide stimulation, MCECs were grown in culture medium supplemented with hydrogen peroxide (1000 μM) and cultured for a further 24 hours.

Ultraviolet or Hydrogen Peroxide Treatment of Corneal Specimens

Rabbit corneal specimens were placed corneal endothelial side up and exposed to UV (100 J/m^2) by using the UV CrossLinker CX-2000, followed by incubation in DMEM for 24 hours. Rabbit corneal specimens were stimulated with hydrogen peroxide by culturing in DMEM supplemented with hydrogen peroxide (1000 μM) for 24 hours.

Immunoblotting

The cultured MCECs were washed with ice-cold PBS and lysed with ice-cold RIPA buffer containing phosphatase inhibitor cocktail 2 (Sigma-Aldrich Corp., St. Louis, MO, USA) and protease inhibitor cocktail (Roche Applied Science). Following centrifugation, the supernatant containing the total proteins was fractionated by SDS-PAGE. The separated proteins were transferred to polyvinylidene difluoride (PVDF) membranes, blocked with 3% nonfat dry milk, and incubated overnight at 4°C with the following primary antibodies: caspase-3 (1:1000; Cell Signaling Technology, Inc., Danvers, MA, USA), ROCK1 (1:1000; Santa Cruz Biotechnology, Santa Cruz, CA, USA), phosphorylated myosin light chain (MLC, 1:1000; Merck Millipore, Billerica, MA, USA), phosphorylated focal adhesion kinase (FAK, 1:1000; Cell Signaling Technology), FAK (1:1000; Cell Signaling Technology), phosphorylated paxillin (1:1000; Cell Signaling Technology), poly (ADP-ribose) polymerase (PARP) (1:1000; Cell Signaling Technology), and glyceraldehyde-3-phosphate dehydrogenase (GAPDH) (1:3000; Medical & Biological Laboratories Co., Ltd., Aichi, Japan). The blots were probed with horseradish peroxidase–conjugated secondary antibodies (1:5000; GE Healthcare, Piscataway, NJ, USA), developed with luminal for enhanced chemiluminescence using the ECL Advanced Western Blotting Detection Kit (Nacalai Tesque, Kyoto, Japan), and documented with an LAS4000S (Fuji Film, Tokyo, Japan) cooled charge-coupled device camera gel documentation system. Molecular weight markers (Bio-Rad, Hercules, CA, USA) were run alongside all samples.

Immunohistochemistry

Cultured MCECs or corneal specimen samples were fixed for 20 minutes with 4% paraformaldehyde, and excess paraformaldehyde was removed by washing with Dulbecco's PBS. The samples were permeabilized with 0.5% Triton X-100 (Nacalai Tesque) and then incubated with 1% bovine serum albumin to block nonspecific binding. Specimens were incubated with primary antibodies against phosphorylated MLC (1:200; Merck Millipore). Alexa Fluor 488–conjugated goat anti-mouse (Life Technologies Corp.) antibodies were used as secondary antibodies at a 1:1000 dilution. Actin staining was performed by incubation with a 1:400 dilution of Alexa Fluor 546–conjugated phalloidin (Life Technologies Corp.). Nuclei were stained with 4′,6-diamidino-2-phenylindole (DAPI; Vector Laboratories, Burlingame, CA, USA).

The mitochondrial membrane potential was evaluated by 5,5′,6,6′-tetrachloro-1,1′,3,3′-tetraethylbenzimidazolylcarbocyanine iodide (JC-1) staining according to the manufacturer's protocol. Briefly, MCECs were exposed to UV (100 J/m^2) and further cultured for 10 hours with culture medium supplemented with 10 μM Y-27632 or 10 μM Z-VAD-FMK. The MCECs were then incubated with MitoScreen (10 μM; Merck Millipore) for 15 minutes and fixed with 4% formaldehyde for 10 minutes.

Cell apoptosis was evaluated by incubating the samples in medium supplemented with Annexin V (Medical & Biological Laboratories Co., Ltd.) for 15 minutes, followed by fixation with 4% paraformaldehyde for 10 minutes. Excess paraformaldehyde was removed and the samples were washed with PBS. TUNEL staining was also performed for the analysis of apoptosis according to the kit manufacturer's protocol. Briefly, MCECs were fixed with 4% formaldehyde for 10 minutes, permeabilized with 0.5% Triton X-100 solution for 5 minutes, and equilibrated by covering them with equilibration buffer for 10 minutes. The samples were then incubated with terminal deoxynucleotidyl transferase incubation buffer, which reacts with the 3′-OH ends of fragmented DNA. The slides were examined with a fluorescence microscope (DM 2500; Leica Microsystems).

Rho Pull-Down Assay

The Rho activation assay (Merck Millipore) was performed according to the manufacturer's protocol. Briefly, MCECs were

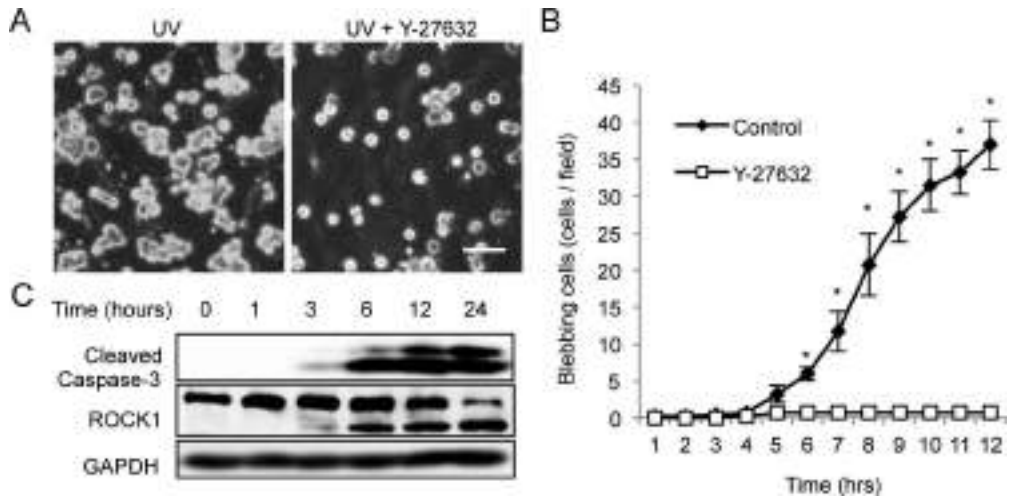

Figure 1. Effect of ROCK inhibition on membrane blebbing in MCECs. **(A)** Cultured MCECs were washed gently with PBS and irradiated with UV (100 J/m^2). Phase contrast images showed that UV stimulation induced a loss of cell adhesion from the culture plate and the surrounding cells, associated with plasma membrane blebbing. However, the selective ROCK inhibitor Y-27632 suppressed this loss of cell adhesion, as well as the membrane blebbing. Representative phase contrast images of MCECs stimulated by UV after 6 hours are shown. *Scale bar*: 50 μm. **(B)** Blebbing cells were evaluated by time-lapse phase contrast microscopy. $^*P < 0.01$. **(C)** Western blot was performed after UV stimulation to evaluate cleavage of caspase-3 and ROCK1. A slight amount of cleavage of caspase-3 was observed after 3 hours, and cleavage became more apparent after 6 hours of UV stimulation, accompanied by a coincident cleavage of ROCK1 in the MCECs.

cultured until confluency, irradiated with UV (100 mJ/m^2), and further incubated for 6 hours. The MCECs were washed with ice-cold Tris-buffered saline, lysed with ice-cold Mg^{2+} lysis/wash buffer (Merck Millipore) containing phosphatase inhibitor cocktail 2 (Sigma-Aldrich Corp.), and then agitated. The samples were reacted with Rho Assay Reagent (Merck Millipore) to bind GTP-Rho. The supernatant, representing total proteins, was analyzed by immunoblotting, as described as above. A primary antibody for anti-Rho, clone 55 (Merck Millipore), was used at 3:1000 dilution.

Flow Cytometry

Cell apoptosis was evaluated by using Annexin V Assay Kits (Medical & Biological Laboratories Co., Ltd.) according to the manufacturer's protocol. Briefly, cells were incubated with DMEM supplemented with Annexin V for 15 minutes and then harvested by digestion with Accumax (Innovative Cell Technologies, San Diego, CA, USA). Recovered cells were then analyzed by flow cytometry using a CellQuest Pro software (BD Biosciences, Franklin Lakes, NJ, USA).

Statistical Analysis

The statistical significance (*P* value) of differences between mean values of the two-sample comparison was determined with the Student's *t*-test. The comparison of multiple sample sets was analyzed by using Dunnett's multiple-comparison test. The data represent the mean ± SEM.

Results

Suppression of Plasma Membrane Blebbing by ROCK Inhibition

Phase contrast images showed that UV stimulation induced a loss of cell adhesion of MCECs to the culture plate and that the released cells showed plasma membrane blebbing, which is a phenotypic feature associated with the execution phase of apoptosis. However, the selective ROCK inhibitor Y-27632 suppressed this loss of cell adhesion as well as membrane blebbing of MCECs after stimulation with UV (Fig. 1A). Time-lapse phase contrast microscopy showed that the numbers of MCECs exhibiting membrane blebbing increased in a time-dependent manner after UV irradiation, but membrane blebbing was almost totally suppressed by Y-27632 treatment (Fig. 1B). Two isoforms, ROCK1 and ROCK2, were isolated as RhoA-interacting proteins. Membrane blebbing is induced by ROCK1 activation, which is caused by ROCK1 cleavage triggered by caspase-3 activation in other cell types. Western blot showed that slight cleavage of caspase-3 occurred after 3 hours and this cleavage became more apparent after 6 hours of UV stimulation, with a coincident cleavage of ROCK1 in the MCECs (Fig. 1C). Time-lapse phase contrast imaging showed that the blebbing became evident after 6 hours of UV stimulation and paralleled the cleavage of caspase-3 and ROCK1.

Effect of Inhibition of ROCK/MLC Pathway on Apoptosis of MCECs

We then evaluated the effect of ROCK signaling inhibition on UV-mediated apoptosis in MCECs. Phase contrast images showed that UV-induced cell detachment was suppressed by the pan-caspase inhibitor Z-VAD-FMK after 12 hours of UV irradiation (Fig. 2A). Western blot showed the presence of cleavage products of caspase-3 (19-kDa partially cleaved and 17-kDa cleaved products) in UV-stimulated cells. PARP helps cells to maintain viability, so cleavage of PARP, which is caused by cleaved caspase-3, is used as a marker of cells undergoing apoptosis. The UV treatment of the MCECs induced an identical PARP cleavage to that seen for caspase-3. By contrast, Z-VAD-FMK suppressed the formation of the 17-kDa cleavage products of caspase-3 and the 89-kDa cleavage products of PARP (Fig. 2B), indicating that the damage to MCECs caused by UV is mainly due to apoptosis associated with caspase-3 activation.

We also evaluated the effect of inhibition of MLC activity on apoptosis of MCECs, as MLC is downstream of ROCK. Blebbistatin (an inhibitor of MLC) suppressed the cleavage of

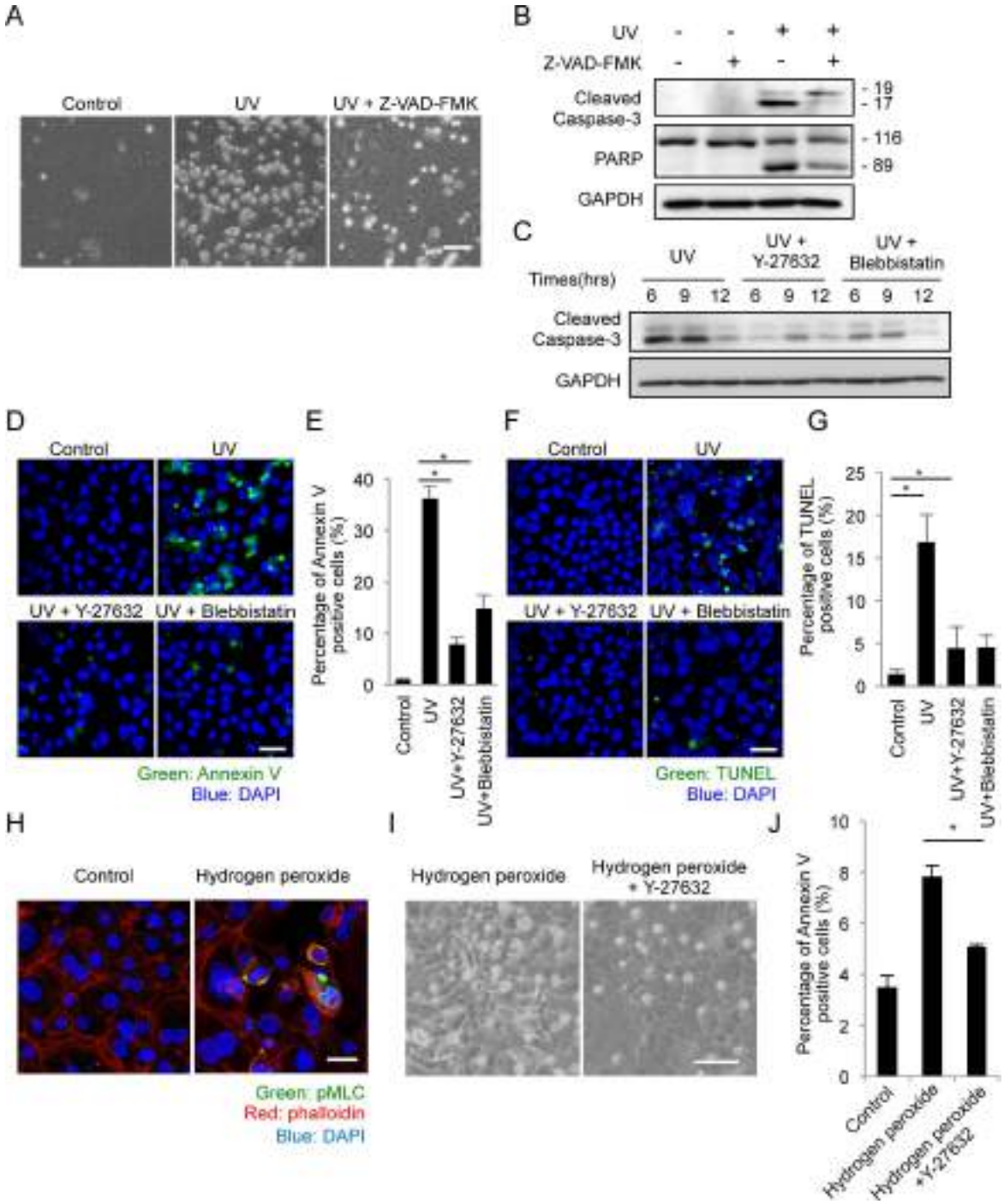

Figure 2. Effect of inhibition of ROCK/MLC pathway on apoptosis of MCECs. (**A**) Cultured MCECs were washed gently with PBS and exposed to UV (100 J/m^2), followed by further incubation for 12 hours in culture medium supplemented with the pan-caspase inhibitor Z-VAD-FMK. Representative phase contrast images show that UV-induced cell detachment was suppressed by caspase inhibition. *Scale bar*: 100 μm. (**B**) Activation of caspase-3 and PARP was evaluated by Western blot after 12 hours of UV stimulation. Ultraviolet exposure induced partially cleaved 19-kDa and fully cleaved 17-kDa products of caspase-3. The UV treatment also induced PARP cleavage in MCECs. By contrast, Z-VAD-FMK suppressed the appearance of the 17-kDa cleavage product of caspase-3 and the 89-kDa cleavage product of PARP, showing that damage to the MCECs caused by UV is mainly due to apoptosis. (**C**) Cleavage of caspase-3 was evaluated by Western blot after UV irradiation of MCECs. Y-27632 and blebbistatin (an inhibitor of MLC) treatment suppressed cleavage of caspase-3 in the UV-treated cells. (**D**, **E**) Monkey corneal endothelial cells were exposed to UV (100 J/m^2) and then cultured in Dulbecco's modified Eagle's medium supplemented with Y-27632/blebbistatin for 24 hours. The presence of apoptotic cells was evaluated by staining the MCECs with Annexin V. Evaluation of the numbers of Annexin V–positive apoptotic cells produced in response to UV irradiation revealed a significant suppression by Y-27632 or blebbistatin treatment. Values are the averages of four independent images. Experiments were performed in triplicate. Nuclei were stained with DAPI. *Scale bar*: 50 μm. *$P < 0.01$. (**F**, **G**) Apoptotic cells were evaluated by TUNEL staining. The numbers of TUNEL-positive apoptotic cells were evaluated. Values are the averages of four independent images. Experiments were performed in triplicate. Nuclei were stained with DAPI. *Scale bar*: 50 μm. *$P < 0.01$. (**H**) Monkey corneal endothelial cells were stimulated with hydrogen peroxide by culturing with Dulbecco's modified Eagle's medium supplemented with hydrogen peroxide (1000 μM) for 24 hours. Phosphorylation of MLC was evaluated by immunostaining. Actin was stained by phalloidin and nuclei were stained with DAPI. *Scale bar*: 50 μm. (**I**, **J**) After stimulation by hydrogen peroxide (1000 μM) for 24 hours, MCECs were evaluated by phase contrast microscopy. Annexin V–positive apoptotic cells were evaluated by flow cytometry. *Scale bar*: 50 μm. *$P < 0.01$.

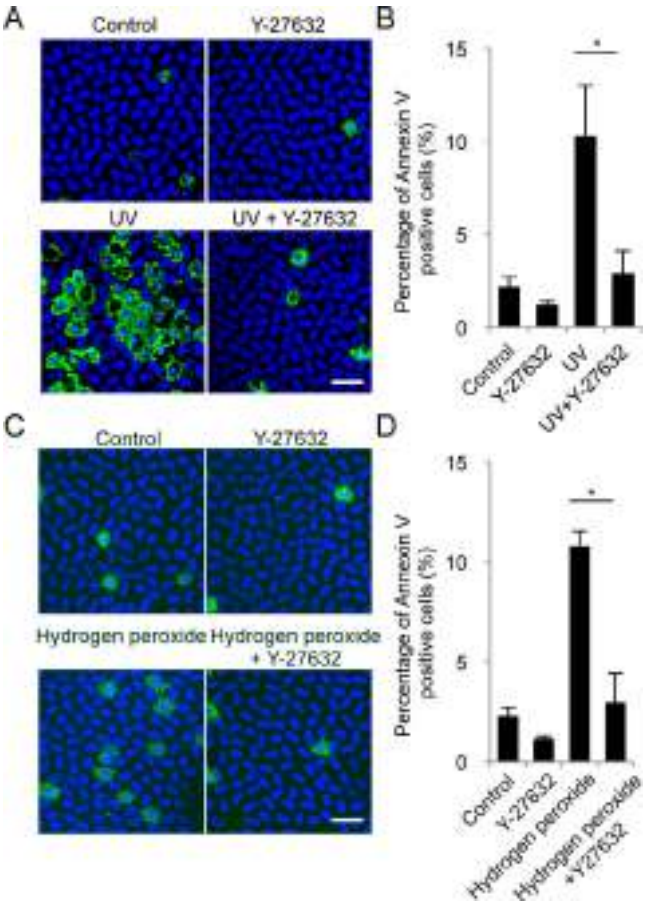

Figure 3. Effect of inhibition of ROCK on apoptosis of ex vivo rabbit corneal endothelium. (**A**, **B**) Rabbit corneal specimens were placed corneal endothelial side up and exposed to UV (100 J/m^2), followed by incubation in Dulbecco's modified Eagle's medium for 24 hours. Apoptotic cells were detected by staining the corneal specimens with Annexin V and counting the numbers of Annexin V–positive apoptotic cells. Values are the averages of data from four independent corneas. Experiments were performed at least in triplicate. *Scale bar*: 50 μm. *$P < 0.01$. (**C**, **D**) Hydrogen peroxide stimulation of rabbit corneal specimens incubated in Dulbecco's modified Eagle's medium supplemented with hydrogen peroxide (1000 μM) for 24 hours. Specimens were stained with Annexin V and the numbers of Annexin V–positive cells were evaluated. Values are averages of data from four independent corneas. Experiments were performed at least in triplicate. *Scale bar*: 50 μm. *$P < 0.01$.

caspase-3 in a similar fashion to that seen with the ROCK inhibitor (Fig. 2C). Annexin V staining showed that early apoptosis induced by UV was significantly suppressed by Y-27632 or blebbistatin after 24 hours of UV irradiation (Figs. 2D, 2E). TUNEL staining also showed that late apoptosis was significantly decreased in the MCECs treated with Y-27632 or blebbistatin (Figs. 2F, 2G). These data indicated that inhibition of the ROCK/MLC pathway counteracts UV-mediated apoptosis of MCECs. Apoptosis was induced by UV or by hydrogen peroxide, and effect of Y-27632 on corneal endothelial apoptosis was evaluated. Immunostaining showed that hydrogen peroxide induced phosphorylation of MLC (which is downstream from ROCK1), which is associated with cell contraction and membrane blebbing (Fig. 2H). Phase contrast images showed that hydrogen peroxide caused cell detachment after 24 hours, associated with membrane shrinkage and blebbing, but Y-27632 suppressed this cell detachment (Fig. 2I). Flow cytometry demonstrated that hydrogen peroxide induced Annexin V–positive apoptotic cells at 7.8%, but Y-27632 treatment significantly suppressed the apoptotic cell percentage to 5.0% ($P < 0.01$) (Fig. 2J).

Effect of Inhibition of ROCK on Apoptosis of Ex Vivo Corneal Endothelium

We next conducted ex vivo experiments with rabbit corneal specimens. Annexin V–positive apoptotic CECs were observed at a level of 10.3% in rabbit corneas after 24 hours of UV irradiation, but treatment with Y-27632 suppressed this percentage to 2.9% (Fig. 3A). A similar apoptotic response was seen with hydrogen peroxide treatment, where the appearance of Annexin V–positive cells was significantly suppressed by Y-27632 treatment (10.8% [control] versus 3.0% [Y-27632]) after 24 hours (Fig. 3B). In addition, we confirmed that Y-27632 caused a similar suppression of UV-induced corneal endothelial apoptosis in human corneal specimens as was observed in the rabbit specimens (Supplementary Figs. S1A, S1B).

Phosphorylation of MLC by RhoA Activation During the Initiation Phase of Apoptosis in MCECs

RhoA is recognized as a central modulator for ROCK activation; therefore, we examined the activation of Rho in UV-stimulated MCECs. Exposure of MCECs to UV irradiation resulted in substantial recognition of GTP-bound RhoA in pull-down assays, suggesting that cellular stress induced the activation of RhoA (Fig. 4A). Consistent with RhoA activation, immunofluorescent images showed UV-induced phosphorylation of MLC after 3 hours of UV irradiation. However, Y-27632 counteracted the MLC phosphorylation in a similar fashion to blebbistatin, indicating that MLC phosphorylation is a result of ROCK activation (Fig. 4B). Monkey corneal endothelial cells were phosphorylated beginning approximately 30 minutes after UV irradiation, and 33.3% of the MCECs were phosphorylated at 6 hours (Fig. 4C). This MLC phosphorylation was observed earlier than ROCK1 cleavage and the subsequent membrane blebbing is shown in Figure 1, suggesting that ROCK was activated by RhoA activation during the early phase of apoptosis. ROCK1, in turn, was activated by ROCK1 cleavage by casplase-3 activation during the execution phase of apoptosis. Immunostaining and Western blot performed 3 hours after UV irradiation demonstrated that ROCK inhibitor treatment suppressed the MLC phosphorylation during the initiation phase (Figs. 4B, 4D).

Effect of MLC Phosphorylation on Apoptosis of MCECs

We recently have reported that cell dissociation results in phosphorylation of MLC in MCECs.[20] In the present study, we used EGTA to induce MLC phosphorylation to assess its effects on apoptosis. As found previously, EGTA treatment resulted in MLC phosphorylation and subsequent actin contraction, followed by cell detachment from the substrate and surrounding cells (Figs. 5A, 5B). By contrast, both Y-27632 and blebbistatin counteracted this induction of MLC phosphorylation and actin contraction, and the cells maintained a monolayer confluent sheet rather than assuming the round morphology associated with actomyosin contraction. Phase contrast images showed that Y-27632 and blebbistatin suppressed cell detachment (Figs. 5A, 5B). However, MCECs exhibited MLC phosphorylation associated with actin contraction even when treated with Z-VAD-FMK, showing that cell

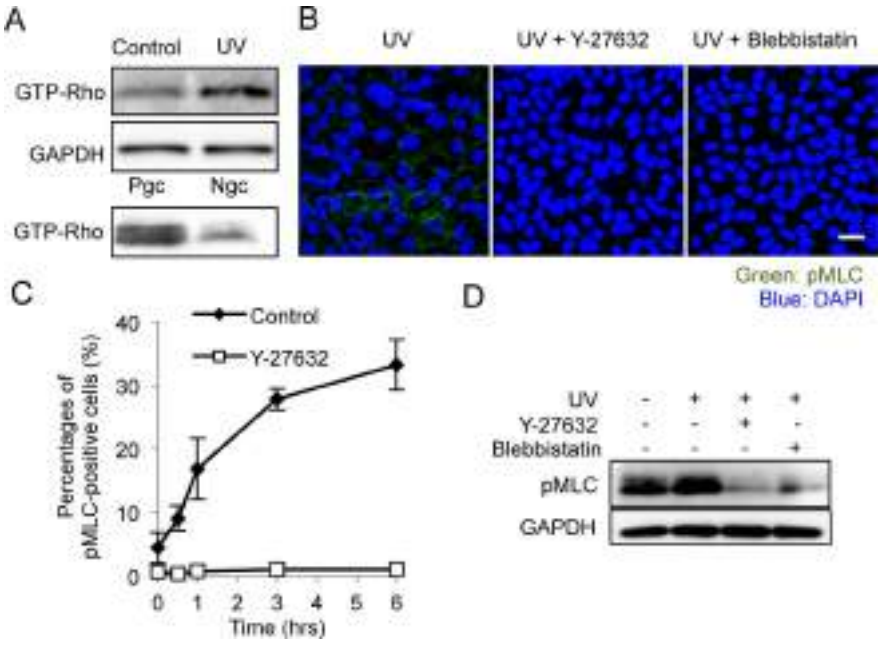

Figure 4. RhoA activation and subsequent phosphorylation of MLC during the initiation phase of apoptosis. (**A**) Monkey corneal endothelial cells were cultured until confluency, irradiated with UV (100 mJ/m^2), and incubated. Activation of Rho was then evaluated by a pull-down assay. (**B**, **C**) Myosin light chain phosphorylation was assessed by immunostaining. Ultraviolet induced the phosphorylation of MLC after 3 hours of UV irradiation, while Y-27632 and blebbistatin counteracted this MLC phosphorylation. The percentages of MCECs showing MLC phosphorylation were evaluated. Nuclei were stained with DAPI. *Scale bar*: 50 μm. (**D**) Monkey corneal endothelial cells were stimulated by exposure to UV and then incubated with or without Y-27632/blebbistatin. Phosphorylation of MLC was evaluated by Western blot 3 hours after UV treatment. Experiments were performed in triplicate.

detachment was not a consequence of apoptosis, whereas actin contraction was due to MLC phosphorylation. Western blot also showed that the MLC phosphorylation due to EGTA treatment induced the cleavage of caspase-3 and PARP, whereas Y-27632 and blebbistatin treatment suppressed these cleavages (Fig. 5C).

We also evaluated the effect of ROCK inhibition on the focal adhesion complex, as it may also be involved in modulation of cell detachment. Focal adhesion kinase and paxillin are important components of focal adhesion and transmit downstream signaling of integrins. Western blot showed that Y-27632 treatment promoted the phosphorylation of FAK and paxillin in adhered cells exposed to UV irradiation stress (Fig. 5D). Taken together, the data support the possibility that perception of apoptotic stimuli by the corneal endothelium induced the activation of the RhoA/ROCK/MLC pathway, promoted actomyosin contraction, and finally caused apoptosis or anoikis. Treatment with a ROCK inhibitor suppressed apoptosis by counteracting the RhoA/ROCK/MLC signaling as well as by activation of the focal adhesion complex (Fig. 6).

Discussion

The execution phase of apoptosis is characterized by morphologic events, and ROCK activation is recognized as its major regulator.[11,22,23] Loss of contact with the extracellular matrix and surrounding cells leads to a transient membrane blebbing by apoptotic cells, which is regulated by actomyosin contraction via MLC phosphorylation. In 2001, caspase-3–mediated cleavage and activation of ROCK1 was demonstrated as pivotal in inducing MLC phosphorylation and subsequent membrane blebbing in NIH3T3 cells treated with TNF-α and in Jurkat cells treated with agonistic anti-Fas antibodies.[22,23] Subsequent research has confirmed the same mechanism in various cell types and with different kinds of apoptotic stimuli.[24–27]

Our current data agree with previous findings with other cell types, as the corneal endothelium shared the same system for regulating membrane blebbing involving caspase-3 and ROCK1 cleavage during the execution phase. However, the contribution of ROCK signaling to the initiation of the apoptotic phase varies widely, depending on the cell type and apoptotic stimulus. The first reports showing a role for caspase-3–mediated cleavage of ROCK1 in membrane blebbing have indicated that inhibition of ROCK does not suppress caspase-3 activation and subsequent apoptosis in TNF-α–treated NIH3T3 and anti-Fas antibody–treated Jurkat cells.[22,23] Likewise, in lung epithelial cells, ROCK activation is required for membrane blebbing but is not required for other apoptosis-related events.[24] These reports suggest that activation of ROCK signaling is indispensable for the morphologic events occurring during the execution phase but not for earlier apoptosis processes.

However, several lines of evidence indicate that ROCK activation contributes to the initiation phase as well as the execution phase. For example, MLC phosphorylation plays a central role in the TNF-α–mediated apoptosis of vascular endothelial cells.[28] ROCK-dependent rearrangement of actin cytoskeleton is also a critical event in early apoptosis, possibly due to assembly of the death-inducing signaling complex, and inhibition of ROCK attenuates TNF-α–mediated apoptosis.[29] Similarly, ROCK signaling is activated by inhibition of ERK-MAPK signaling in vascular endothelial cells and causes cell death, while inhibition of ROCK rescues the cells from the effects of ERK-MAPK inhibition.[30] Apoptosis of erythroblast cells mediated by phorbol-12-myristate-13-acetate is also triggered by upregulation of the Rho/ROCK pathway and is mediated by caspase-8 and caspase-10 associated with myosin contraction.[31] Human embryonic stem cells show poor

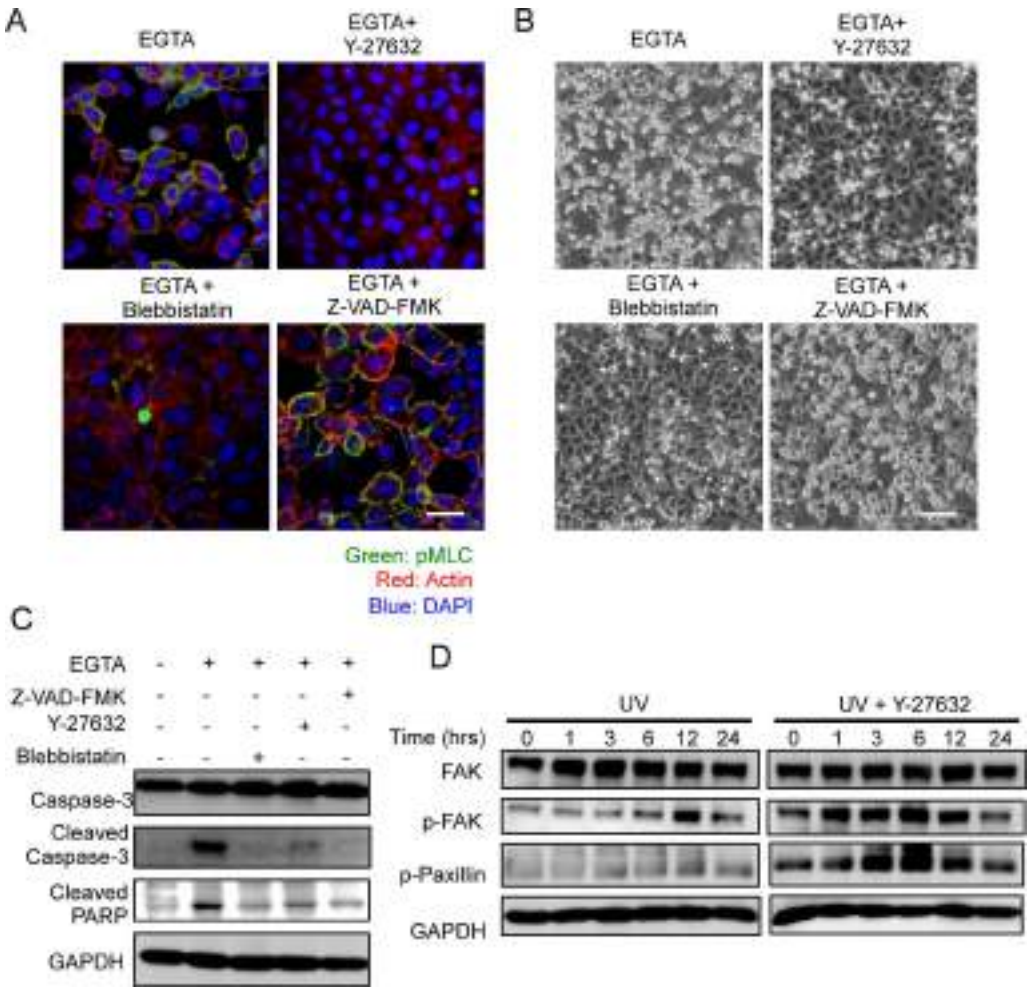

Figure 5. RhoA activation and subsequent phosphorylation of MLC during the initiation phase of apoptosis. (**A**) Confluent MCECs were incubated in culture medium supplemented with EGTA (3 mM) to induce MLC phosphorylation, which was assessed by immunostaining. Representative images after 6 hours of incubation with EGTA supplemented with Y-27632, blebbistatin, or Z-VAD-FMK. *Scale bar*: 50 μm. (**B**) Representative phase contrast images of MCECs after 6 hours of incubation with EGTA. *Scale bar*: 100 μm. (**C**) Western blot to evaluate cleavage of caspase-3 and PARP performed after 24 hours of EGTA treatment. Ethylene glycol tetraacetic acid mediated MLC phosphorylation, which induced cleavage of caspase-3 and PARP, but Y-27632 and blebbistatin suppressed these cleavages. Experiments were performed in triplicate. (**D**) Ultraviolet-mediated apoptosis was induced by UV irradiation, and activation of focal adhesion complexes were evaluated by Western blot. Expression of focal adhesion complexes in adhered cells under stress of UV irradiation was promoted by Y-27632. Experiments were performed in triplicate.

survival after cell dissociation, but this is attenuated by a ROCK inhibitor.[32] Other research has demonstrated that dissociation-induced apoptosis is caused by a ROCK-dependent hyperactivation of actomyosin, and that Rho-GEF (guanine nucleotide exchange factor) is an indispensable regulator of Rho/ROCK/actomyosin activation.[33]

Our data agree with these previous reports, as we demonstrated that activation of the Rho/ROCK pathway contributes to the initiation phase of apoptosis in the corneal endothelium. We showed that UV stimulation activated Rho and was followed by induction of actin cytoskeletal contraction by MLC phosphorylation via ROCK activation. We also showed that EGTA-mediated MLC phosphorylation was sufficient to cause apoptosis associated with caspase-3 activation, and that MLC phosphorylation was sufficient for inducing the loss of cell adhesion even in the absence of apoptosis. These data suggest that the loss of contact with the substrate or with the surrounding cells due to MLC phosphorylation regulates apoptosis of the corneal endothelium.

The Rho subfamily members function as molecular switches that cycle between GDP-bound inactive and GTP-bound active forms. This transition is controlled by the cooperation of positive regulators (GEFs) and negative regulators (GTPase activating proteins [GAPs]).[34] Further research is required on the types of proapoptotic signals that activate Rho and the involvement of GEF and GAPs in the activation. Another important question awaiting further study is whether the activation of Rho/ROCK/MLC contributes to cell loss in the diseased condition of the corneal endothelium, especially the FECD condition, in order to determine the usefulness of ROCK signaling as a target for treating disease in the clinical setting.

In summary, we showed that cellular stresses to the corneal endothelium activated Rho/ROCK/MLC phosphorylation. Subsequently, phosphorylated MLC induced the loss of cell adhesion, which then promoted cell death due to apoptosis or anoikis. We demonstrated that ROCK inhibition suppressed MLC phosphorylation and subsequent cell death and counteracted the loss of cell adhesion by activating the focal adhesion complex. These findings suggest that regulation of apoptosis in

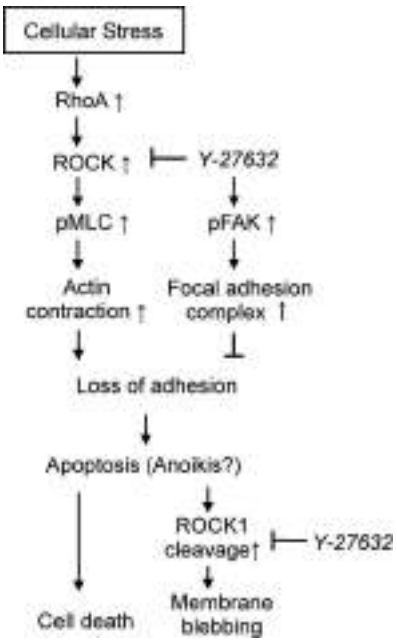

Figure 6. The molecular pathway for a role for ROCK signaling in apoptosis and mechanisms to explain how ROCK inhibitor suppresses apoptosis of the corneal endothelium. Apoptotic stimuli perceived by the corneal endothelium induce the activation of the RhoA/ROCK/MLC pathway. Actomyosin contraction, induced by MLC phosphorylation, causes a loss of adhesion, followed by apoptosis or anoikis. ROCK inhibitor treatment suppresses apoptosis by counteracting RhoA/ROCK/MLC signaling, as well as by activating expression of the focal adhesion complex.

a pathologic status such as FECD might be achieved by targeting the Rho/ROCK signaling pathway.

Acknowledgments

The authors thank Yuji Sakamoto for technical assistance for handling the monkey corneas.

Supported by the Program for the Strategic Research Foundation at Private Universities from MEXT (NK and NO).

Disclosure: **N. Okumura**, None; **K. Fujii**, None; **T. Kagami**, None; **N. Makiko**, None; **M. Kitahara**, None; **S. Kinoshita**, P; **N. Koizumi**, P

References

1. Lorenzetti DW, Uotila MH, Parikh N, Kaufman HE. Central cornea guttata: incidence in the general population. *Am J Ophthalmol*. 1967;64:1155–1158.
2. Albon J, Tullo AB, Aktar S, Boulton ME. Apoptosis in the endothelium of human corneas for transplantation. *Invest Ophthalmol Vis Sci*. 2000;41:2887–2893.
3. Jurkunas UV, Bitar MS, Funaki T, Azizi B. Evidence of oxidative stress in the pathogenesis of Fuchs endothelial corneal dystrophy. *Am J Pathol*. 2010;177:2278–2289.
4. Jun AS, Meng H, Ramanan N, et al. An alpha 2 collagen VIII transgenic knock-in mouse model of Fuchs endothelial corneal dystrophy shows early endothelial cell unfolded protein response and apoptosis. *Hum Mol Genet*. 2012;21:384–393.
5. Matthaei M, Hu J, Kallay L, et al. Endothelial cell microRNA expression in human late-onset Fuchs' dystrophy. *Invest Ophthalmol Vis Sci*. 2014;55:216–225.
6. Okumura N, Minamiyama R, Ho LT, et al. Involvement of ZEB1 and Snail1 in excessive production of extracellular matrix in Fuchs endothelial corneal dystrophy. *Lab Invest*. 2015;95:1291–1304.
7. Vedana G, Villarreal G Jr, Jun AS. Fuchs endothelial corneal dystrophy: current perspectives. *Clin Ophthalmol*. 2016;10:321–330.
8. Tan DT, Dart JK, Holland EJ, Kinoshita S. Corneal transplantation. *Lancet*. 2012;379:1749–1761.
9. Ziaei A, Schmedt T, Chen Y, Jurkunas UV. Sulforaphane decreases endothelial cell apoptosis in Fuchs endothelial corneal dystrophy: a novel treatment. *Invest Ophthalmol Vis Sci*. 2013;54:6724–6734.
10. Kim EC, Meng H, Jun AS. N-Acetylcysteine increases corneal endothelial cell survival in a mouse model of Fuchs endothelial corneal dystrophy. *Exp Eye Res*. 2014;127:20–25.
11. Shi J, Wei L. Rho kinase in the regulation of cell death and survival. *Arch Immunol Ther Exp (Warsz)*. 2007;55:61–75.
12. Olson MF. Applications for ROCK kinase inhibition. *Curr Opin Cell Biol*. 2008;20:242–248.
13. Feng Y, LoGrasso PV, Defert O, Li R. Rho kinase (ROCK) inhibitors and their therapeutic potential. *J Med Chem*. 2016;59:2269–2300.
14. Tanihara H, Inoue T, Yamamoto T, et al. Additive intraocular pressure-lowering effects of the Rho kinase inhibitor ripasudil (K-115) combined with timolol or latanoprost: a report of 2 randomized clinical trials. *JAMA Ophthalmol*. 2015;133:755–761.
15. Tanihara H, Inoue T, Yamamoto T, et al. Intra-ocular pressure-lowering effects of a Rho kinase inhibitor, ripasudil (K-115), over 24 hours in primary open-angle glaucoma and ocular hypertension: a randomized, open-label, crossover study. *Acta Ophthalmol*. 2015;93:e254–e260.
16. Koizumi N, Okumura N, Ueno M, Nakagawa H, Hamuro J, Kinoshita S. Rho-associated kinase inhibitor eye drop treatment as a possible medical treatment for fuchs corneal dystrophy. *Cornea*. 2013;32:1167–1170.
17. Okumura N, Koizumi N, Kay EP, et al. The ROCK inhibitor eye drop accelerates corneal endothelium wound healing. *Invest Ophthalmol Vis Sci*. 2013;54:2439–2502.
18. Okumura N, Okazaki Y, Inoue R, et al. Effect of the Rho-associated kinase inhibitor eye drop (ripasudil) on corneal endothelial wound healing. *Invest Ophthalmol Vis Sci*. 2016;57:1284–1292.
19. Okumura N, Koizumi N, Ueno M, et al. ROCK inhibitor converts corneal endothelial cells into a phenotype capable of regenerating in vivo endothelial tissue. *Am J Pathol*. 2012;181:268–277.
20. Okumura N, Sakamoto Y, Fujii K, et al. Rho kinase inhibitor enables cell-based therapy for corneal endothelial dysfunction. *Sci Rep*. 2016;6:26113.
21. Okumura N, Ueno M, Koizumi N, et al. Enhancement on primate corneal endothelial cell survival in vitro by a ROCK inhibitor. *Invest Ophthalmol Vis Sci*. 2009;50:3680–3687.
22. Coleman ML, Sahai EA, Yeo M, Bosch M, Dewar A, Olson MF. Membrane blebbing during apoptosis results from caspase-mediated activation of ROCK I. *Nat Cell Biol*. 2001;3:339–345.
23. Sebbagh M, Renvoize C, Hamelin J, Riche N, Bertoglio J, Breard J. Caspase-3-mediated cleavage of ROCK I induces MLC phosphorylation and apoptotic membrane blebbing. *Nat Cell Biol*. 2001;3:346–352.
24. McElhinney B, Poynter ME, Shrivastava P, Hazen SL, Janssen-Heininger YM. Eosinophil peroxidase catalyzes JNK-mediated membrane blebbing in a Rho kinase-dependent manner. *J Leukoc Biol*. 2003;74:897–907.

25. Domnina LV, Ivanova OY, Pletjushkina OY, et al. Marginal blebbing during the early stages of TNF-induced apoptosis indicates alteration in actomyosin contractility. *Cell Biol Int*. 2004;28:471–475.
26. Lane JD, Allan VJ, Woodman PG. Active relocation of chromatin and endoplasmic reticulum into blebs in late apoptotic cells. *J Cell Sci*. 2005;118:4059–4071.
27. Zihni C, Mitsopoulos C, Tavares IA, Ridley AJ, Morris JD. Prostate-derived sterile 20-like kinase 2 (PSK2) regulates apoptotic morphology via C-Jun N-terminal kinase and Rho kinase-1. *J Biol Chem*. 2006;281:7317–7323.
28. Petrache I, Verin AD, Crow MT, Birukova A, Liu F, Garcia JG. Differential effect of MLC kinase in TNF-alpha-induced endothelial cell apoptosis and barrier dysfunction. *Am J Physiol Lung Cell Mol Physiol*. 2001;280:L1168–L1178.
29. Petrache I, Crow MT, Neuss M, Garcia JG. Central involvement of Rho family GTPases in TNF-alpha-mediated bovine pulmonary endothelial cell apoptosis. *Biochem Biophys Res Commun*. 2003;306:244–249.
30. Mavria G, Vercoulen Y, Yeo M, et al. ERK-MAPK signaling opposes Rho-kinase to promote endothelial cell survival and sprouting during angiogenesis. *Cancer Cell*. 2006;9:33–44.
31. Lai JM, Hsieh CL, Chang ZF. Caspase activation during phorbol ester-induced apoptosis requires ROCK-dependent myosin-mediated contraction. *J Cell Sci*. 2003;116:3491–3501.
32. Watanabe K, Ueno M, Kamiya D, et al. A ROCK inhibitor permits survival of dissociated human embryonic stem cells. *Nat Biotechnol*. 2007;25:681–686.
33. Ohgushi M, Matsumura M, Eiraku M, et al. Molecular pathway and cell state responsible for dissociation-induced apoptosis in human pluripotent stem cells. *Cell Stem Cell*. 2010;7:225–239.
34. Burridge K, Wennerberg K. Rho and Rac take center stage. *Cell*. 2004;116:167–179.

Investigative Ophthalmology & Visual Science

Hindawi
Journal of Ophthalmology
Volume 2017, Article ID 5614089, 11 pages
https://doi.org/10.1155/2017/5614089

Research Article

A Surgical Cryoprobe for Targeted Transcorneal Freezing and Endothelial Cell Removal

Alina Akhbanbetova,[1] Shinichiro Nakano,[2] Stacy L. Littlechild,[1] Robert D. Young,[1] Madara Zvirgzdina,[1] Nigel J. Fullwood,[3] Ian Weston,[4] Philip Weston,[4] Shigeru Kinoshita,[5] Naoki Okumura,[2] Noriko Koizumi,[2] and Andrew J. Quantock[1]

[1]*Structural Biophysics Research Group, School of Optometry and Vision Sciences, Cardiff University, Maindy Road, Cardiff CF24 4HQ, UK*
[2]*Department of Biomedical Engineering, Faculty of Life and Medical Sciences, Doshisha University, 1-3 Miyakodami-Tatara, Kyoto 610-0321, Japan*
[3]*Division of Biomedical and Life Sciences, Faculty of Health and Medicine, Lancaster University, Lancaster LA1 4YQ, UK*
[4]*Network Medical Products Ltd. Coronet House, Kearsley Road, Ripon, North Yorkshire HG4 2SG, UK*
[5]*Department of Frontier Medical Science and Technology for Ophthalmology, Kyoto Prefectural University of Medicine, Hirokoji-Kawaramachi, Kyoto 602-0841, Japan*

Correspondence should be addressed to Andrew J. Quantock; quantockaj@cardiff.ac.uk

Received 13 December 2016; Accepted 13 February 2017; Published 16 May 2017

Academic Editor: Neil Lagali

Purpose. To examine the effects of transcorneal freezing using a new cryoprobe designed for corneal endothelial surgery. *Methods*. A freezing console employing nitrous oxide as a cryogen was used to cool a series of different cryoprobe tip designs made of silver for high thermal conductivity. In vitro studies were conducted on 426 porcine corneas, followed by preliminary in vivo investigations on three rabbit corneas. *Results*. The corneal epithelium was destroyed by transcorneal freezing, as expected; however, the epithelial basement membrane remained intact. Reproducible endothelial damage was optimally achieved using a 3.4 mm diameter cryoprobe with a concave tip profile. Stromal edema was seen in the pre-Descemet's area 24 hrs postfreeze injury, but this had been resolved by 10 days postfreeze. A normal collagen fibril structure was seen 1 month postfreeze, concurrent with endothelial cell repopulation. *Conclusions*. Transcorneal freezing induces transient posterior stromal edema and some residual deep stromal haze but leaves the epithelial basement membrane intact, which is likely to be important for corneal re-epithelialization. Localized destruction of the endothelial monolayer was achieved in a consistent manner with a 3.4 mm diameter/concave profile cryoprobe and represents a potentially useful approach to remove dysfunctional corneal endothelial cells from corneas with endothelial dysfunction.

1. Introduction

Corneal transparency is maintained in the healthy eye by a monolayer of endothelial cells on the inner surface of the cornea. Even though human corneal endothelial cells do not possess the capacity for proliferation in vivo, the endothelium as a whole has a functional reserve to cope with cell loss via the spreading and enlargement of cells adjacent to those lost [1, 2]. Excessive endothelial loss and deterioration caused by eye pathologies such as Fuchs' endothelial corneal dystrophy (FECD), however, lead to corneal edema, clouding, and eventually loss of vision. FECD is a progressive degenerative disorder that is a major indication for corneal transplant surgery. Surgical intervention in the form of a full-thickness-penetrating keratoplasty—or more commonly nowadays a posterior lamellar graft—is the main treatment option. But, despite the success of corneal graft surgery, some questions about the long-term survival of the donor tissue [3]

and the recurring problem of sufficient tissue availability remains. These limitations have led researchers to seek potential alternatives to corneal transplantation to treat corneal endothelial dysfunction.

One promising route involves the use of selective inhibitors of the Rho kinase pathway. The so-called ROCK inhibitors regulate the actin cytoskeleton and influence vital cell activities such as motility, proliferation, and apoptosis [4]. Owing to their demonstrable value, numerous studies have been conducted in recent years which focus on the effect of ROCK inhibitors on corneal endothelial cells both in vivo and ex vivo [5–9]. One approach involves transcorneal freezing to damage corneal endothelial cells in the central portion of the cornea in patients with FECD followed by the topical delivery of a ROCK inhibitor, Y27632, in the form of eye drops to encourage peripheral endothelial cells that had been unaffected by the freeze injury to repopulate the central zone of the corneal endothelium [10–12]. Freeze damage is achieved by application of a cold probe to the corneal surface. Another approach involves cell injection therapy whereby cultivated human corneal endothelial cells are injected into the anterior chamber of the eyes with FECD in a suspension that includes Y27632 ROCK inhibitor [13]. This agent has also been tested in the form of eye drops as a long-term pharmacological treatment for bullous keratopathy [14].

A small series of first-in-man surgeries to test the concept of transcorneal freezing followed by short-term ROCK inhibitor eye drop application for the treatment of FECD was conducted a few years ago and showed promise [10–12]. In this approach, the tip of a stainless steel rod, 2 mm in diameter, was immersed in liquid nitrogen at −196°C before being applied to the surface of the central cornea for an arbitrarily chosen time of 15 sec. The assumption was that central corneal endothelial cells located underneath the cold-rod applicator would be destroyed by freeze injury, although this could not be directly confirmed in the human subjects because the cloudy FECD corneas did not allow a view of the endothelium by specular microscopy. The freezing of corneal tissue has also been used as a modality to induce an injury to facilitate basic research into corneal wound healing [15–28]. If corneal freezing is to be used in a clinical setting, however, (either for the destruction of diseased cells in the central endothelium prior to ROCK inhibitor eye drop application for FECD as described above or to pretreat the cornea prior to targeted drug delivery to combat conditions such as fungal keratitis) we contend that it needs to be achieved in a more sophisticated, reliable, and reproducible manner than that achieved with an immersion-cooled steel rod. Here, we report the development and validation of a new cryoprobe based on the expansion of nitrous oxide as a cryogen and its effect, in vitro and in vivo, on the corneal epithelium, stroma, and endothelium.

2. Materials and Methods

2.1. Cryoprobe Development. A console that uses nitrous oxide as a cryogen was manufactured in conjunction with a series of cryoprobes with newly designed tips, some of which matched the cornea's curvature (Figure 1). This prototype project was carried out by Coronet Medical Technologies Ltd., the ophthalmic arm of Network Medical Products Ltd. Enclosed gas expanded within the tip and was recycled therein, achieving a low temperature based on the Joule/Thomson effect. The tip of the cryoprobe, used to contact the corneal surface, was circular around the probe's main axis and a number of designs were tested. Probe tips were 1.8 mm, 2.4 mm, or 3.4 mm in diameter and were manufactured from silver for high thermal conductivity. Larger diameter probe tips were not considered because of the option of multiple surface freeze placements should a wider area of the cornea need to be treated. Probes had either a flat surface profile or a concave one with a radius of curvature of 8 mm. For ease of use, a foot switch was incorporated into the design, which initiates cooling at the cryoprobe tip and maintains the reduced temperature throughout the whole time it is depressed. The foot switch is linked to a timer on the main console that provides a visual output of freezing time plus an audible signal (with a mute option) at 1 sec intervals when the foot switch is depressed. Freezing temperature at the probe tip (−50°C) is reached within 2 sec of depressing of the foot switch; after release, ambient room temperature is achieved within seconds. The hand-held cryoprobe has an ergonomic-angled design to allow easy application to the corneal surface (Figure 1). Probes should be thoroughly cleaned, inspected, and autoclaved prior to use.

2.2. Transcorneal Freezing In Vitro. The porcine cornea is comparable to that of the human cornea in terms of its structure and its overall dimensions and the pig eye is thus often used for practice by trainee corneal surgeons. The central corneal thickness in adult pigs is usually around 660 μm [29, 30], which approximates a representative measurement of edematous corneal thickness in individuals with FECD [31, 32]. The porcine eyes, therefore, were well suited for our investigations, and the intact eyeballs, including extraocular muscles, were obtained soon after slaughter at a local abattoir (W. T. Maddock, Kembery Meats, Maesteg, Wales, UK). These were brought to the laboratory on ice and experiments were begun within 2-3 h of death. When the eyes arrived at the home laboratory, ultrasound measurements of central corneal thickness were made with a Tomey SP-100 pachymeter (Erlangen, Germany), which revealed that the corneas had thickened (~1000 μm) postmortem compared to those of published values [31, 32]. Consequently, the eyes were placed in a humidified incubator (Brinsea Octagon 100, Egg Incubator, Sandford, UK) at 45°C for 30–45 min to reverse the postmortem swelling and attain a thickness similar to what might be expected in humans with FECD. In total, 426 porcine eyes were used for the in vitro experiments in which the corneal thickness ranged from 483 μm to 831 μm owing to differences in eye size and likely differential postmortem swelling and deswelling.

Immediately after an eye was removed from the humidified incubator, its central corneal thickness was recorded as an average of eight measurements. The cryoprobe tip was then applied to the corneal surface and cooling was activated by pressing the foot switch to control the flow of nitrous

Figure 1: The transcorneal freezing machine attached to a cylinder of medical grade nitrous oxide (the cryogen), which comprises a main console with a monitor screen that illustrates freeze time, cryogen levels, and readiness for freeze plus interchangeable probe tips and a footswitch (not shown). Inset: the 3.4 mm diameter concave probe tip manufactured from silver for high thermal conductivity.

oxide gas. Freezing times of 3, 5, 9, and 13 sec were tested, allowing an additional 2 sec for the freezing temperature to be reached in all cases (thus, a 3 sec freeze required for a 5 sec application and foot-switch depression). The cornea was then carefully excised at the limbus after which staining solutions of 0.2% alizarin red (~1 ml) and 0.25% trypan blue were applied sequentially to the endothelial surface for 60–90 sec each to identify dead cells. The stains were then gently washed off using approximately 5 ml of 0.9% sodium chloride buffer solution, after which digital images of the corneal endothelial surface were captured on a Zeiss Stemi 1000 light microscope (Carl Zeiss, Jena, Germany). A successful freeze injury was deemed to have occurred when a clear circular wound area was seen. The endothelial wound area in each corneal image was manually traced and calculated using Image J software (http://imagej.nih.gov/ij/). Magnification was calibrated for each set of experiments using the image of an eyepiece graticule. Averages of three measurements were calculated and data were further collated using Microsoft Excel software (Microsoft Corp., Redmond, WA, USA).

2.3. Statistical Analysis. Statistical analyses were carried out operating IBM SPSS Statistics software (Version 23.0, IBM Corporation, New York, USA). Spearman's rank order correlation test was run to determine the relationship between central corneal thickness and endothelial wound areas induced by the freezing.

2.4. Scanning Electron Microscopy. To investigate the endothelial damage morphologically, four treated corneas were examined by scanning electron microscopy (SEM). Immediately after excision, the corneas were fixed in 2.5% glutaraldehyde and 2% paraformaldehyde in 0.1 M sodium cacodylate buffer, pH 7.3, for at least 2 h. Samples were then washed in PBS followed by the gradual dehydration through a graded ethanol series (from 50% to 100% in 30 min steps), after which the ethanol was replaced by hexamethyldisilazane for 20 min to minimize the shrinkage of the specimens. After drying, the corneas were placed on stubs (Agar Scientific, Stansted, UK) and sputter coated with gold (Edwards S150 sputter coater, Edwards High Vacuum Co. International, Wilmington, USA) to allow imaging in a JEOL JSM 5600 scanning electron microscope (JEOL Company, Tokyo, Japan) operating with a beam acceleration voltage of 15.0 kV.

2.5. Transcorneal Freezing In Vivo. Three adult New Zealand White rabbits were used to investigate corneal recovery after transcorneal freezing. At all stages, animals were treated in accordance with the ARVO Statement for the Use of Animals in Ophthalmic and Vision Research, and the research was approved by the IRB of Doshisha University. As reported later, the 3.4 mm concave cryoprobe was found to be the most effective in inducing endothelial damage in the porcine eye in vitro, but owing to the thinner cornea of the rabbit, the 2.4 mm concave cryoprobe was chosen for the in vivo transcorneal freezing experiments.

Under general anesthesia, a 2.4 mm probe was applied to the corneal surface of the rabbit eyes for a total of 5 sec. The contralateral eye was used as a control. Transcorneal freezing did not induce any severe general adverse effects. After 24 h, 10 days, and 1 month of treatment, the anterior segment of each eye was assessed by the use of a slit-lamp microscope and the rabbits were then euthanized. Corneal thickness was determined by the use of an ultrasound pachymeter (SP-2000; Tomey, Nagoya, Japan), and the mean of eight measured values was calculated. Intraocular pressure was measured by the use of a Tonovet tonometer (292000; KRUUSE, Langeskov, Denmark). Transmission electron microscopy (TEM) was conducted, as described below, on the corneas of the rabbits that were euthanized at 24 h- and 1-month time points after transcorneal freezing.

2.6. Transmission Electron Microscopy. The rabbit corneas were examined by TEM 24 h and 1 month postfreeze was conducted in Doshisha University, Japan. Briefly, after animals were euthanized, corneas were excised at the limbus and fixed in 2.5% glutaraldehyde and 2% paraformaldehyde in 0.1 M Sörensen buffer (pH 7.2–7.4) overnight at 4°C. Samples in fresh fixative were then express shipped to the UK. Full-thickness-dissected portions of the corneas were then subjected to alcohol dehydration and resin infiltration, after which they were embedded in epoxy resin (Araldyte CY212 resin, TAAB Laboratories, England, UK). Ultrathin sections were stained with uranyl acetate and lead citrate and examined on a JEOL 1010 microscope operating at 80 kV (JEOL Company, Tokyo, Japan).

3. Results

3.1. In Vitro Transcorneal Freezing. Initial experiments into the degree of endothelial damage caused by transcorneal freezing induced by four different types of cryoprobe tip—that is, 1.8 mm diameter/flat profile, 2.4 mm diameter/flat profile, 2.4 mm diameter/concave profile, and 3.4 mm diameter/concave profile—revealed that the time of contact with the corneal surface did not affect the area of endothelial damage, with freezing times of 3, 5, 9, and 13 sec tested (data not shown). Based on this outcome, a freezing time of 3 sec was chosen for all the in vitro experiments described herein. It also became apparent during the initial investigations that the probe tip had to be in contact with the corneal surface before the foot switch was depressed to initiate cooling. If the probe tip was cooled in air prior to being brought into contact with the cornea, no appreciable endothelial damage was seen; no matter how long, up to 15 sec, the probe remained in contact with the cornea.

Light microscopy of the endothelial surfaces of the postfreeze, trypan blue-stained corneas indicated the area of cell damage caused by the four different probes used in these experiments. Representative images of 426 technical replicates denoting the typical extent of endothelial damage are shown in Figure 2, with examples of what were considered to be successful or unsuccessful freeze injuries. A successful freeze injury was defined as one that resulted in a well-delineated circular area of cell damage. An unsuccessful freeze injury, on the other hand, was considered to have occurred either when there was no evidence of any cell damage or when the area of damage was irregular. Based on these criteria, only 14 of 102 eyes (14%) treated with the 1.8 mm diameter/flat profile probe were judged to have been successfully wounded, whereas 78 of 108 (72%) treated with the larger (i.e., 2.4 mm diameter) flat profile probe contained successful endothelial injuries. A similar number of the eyes exhibited corneal endothelial freeze damage—that is, 76 eyes of 108 (70%)—when the 2.4 mm diameter cryoprobe with a concave profile was used. Our data clearly indicated, however, that the 3.4 mm diameter/concave profile cryoprobe induced the most consistent endothelial damage with 90 eyes of 108 (83%) being successfully wounded in a reproducible manner (Table 1).

To quantify the extent of endothelial cell damage, we used Image J to manually trace around each wound deemed to have been successfully created (i.e., $n = 258$ of 426 technical replicates). The area of each wound was calculated, which, unsurprisingly, disclosed that larger probe tips led to more extensive endothelial damage (Table 1). All of the 426 corneas examined were subjected to multiple pachymetry measurements immediately prior to transcorneal freezing. This revealed that the average corneal thickness was 649 μm ($\pm$61 μm SD), which is a fair representative value for corneal edema in humans with endothelial dysfunction [31, 32]. Moreover, when the corneal thickness of the individual corneas was taken into account, a statistical Spearman's rank order correlation test identified that there was a weak relationship between central corneal thickness and endothelial damage when treated with the smallest and largest probes

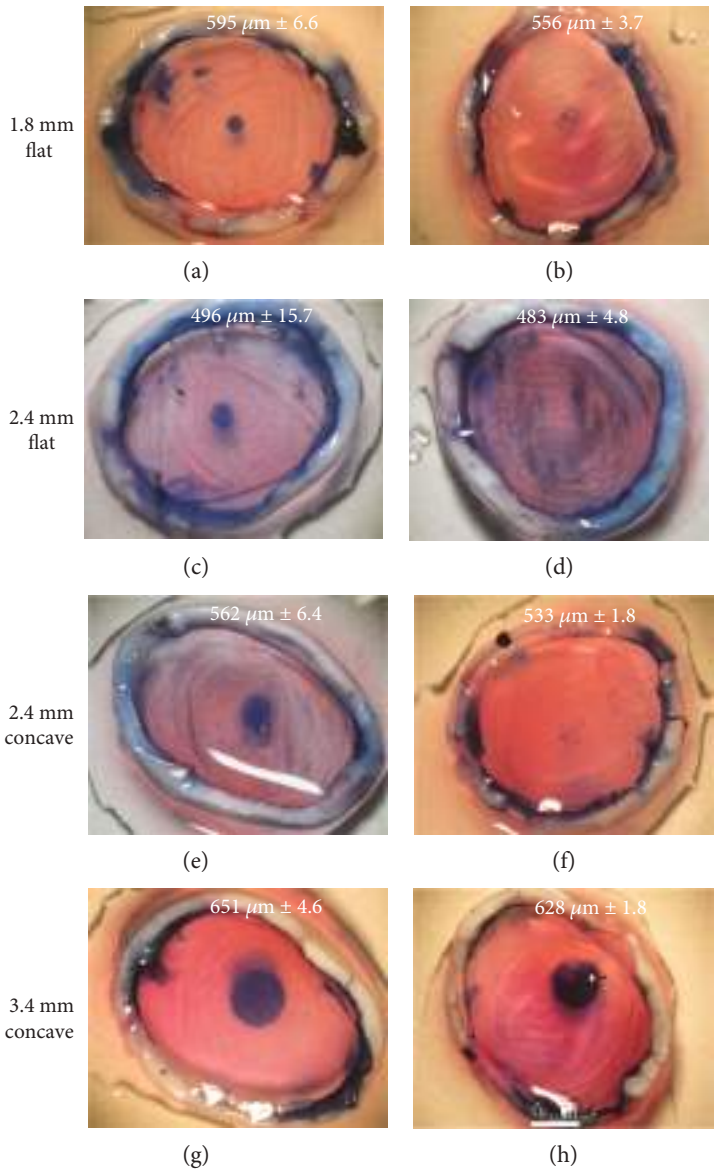

Figure 2: Representative images of corneal endothelial freeze injury on the pig eyes ex vivo induced by 3 sec freeze with four different cryoprobe tips and assessed by trypan blue staining. The thickness of each cornea is indicated on each panel (±SD) based on eight pachymetry readings. The area of cell damage is seen via the blue stain, and successful and non/less successful freeze injuries are shown in the left and right columns, respectively. Freezing with the 1.8 mm diameter/flat profile probe only rarely resulted in a reproducible wound (a and b). Endothelial freeze injury was more reliably achieved with 2.4 mm diameter probe tips with flat or concave profiles (c–f), but the optimal result and best consistency was achieved using the 3.4 mm diameter/concave profile cryoprobe (g and h). Scale bar, 3 mm. See Table 1 also.

Table 1: Data summary of transcorneal freezing for 3 sec on porcine eyes.

Probe tip (mm)/profile	Number of eyes	Number of eyes with successful freeze (%)	Mean/SD damaged area (mm^2)	Mean diameter (mm)	Mean/SD corneal thickness (nm)
1.8/flat	102	14 (14)	0.79/0.4	1.0	642/64
2.4/flat	108	78 (72)	2.12/1.0	1.6	650/71
2.4/concave	108	76 (70)	2.29/1.0	1.6	645/87
3.4/concave	108	90 (83)	6.91/1.9	2.9	654/59

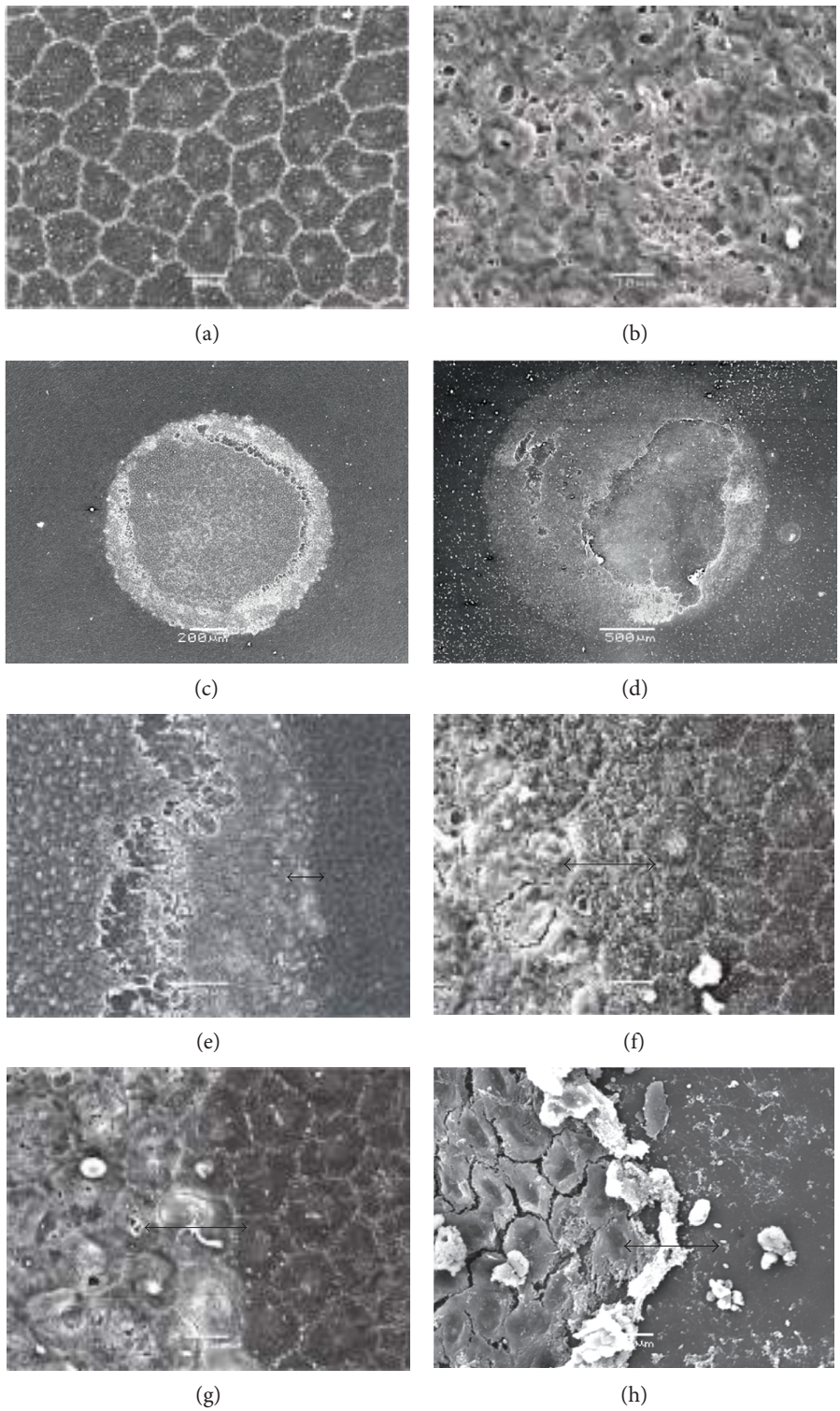

Figure 3: SEM of the endothelium of transcorneally frozen pig corneas. (a) An untreated pig cornea with cell boarders in white showing a characteristic hexagonal mosaic. The outline if the cell nucleus is evident as a slightly lighter area within each cell. Scale bar, 10 μm. (b) A representative image taken at the same magnification of the freeze-damaged area after treatment with a 2.4 mm diameter/concave profile tip, illustrating severe damage to endothelial cells by freezing. Scale bar, 10 μm. (c and d) Lower magnification images of endothelial freeze-injured wounds showing circular areas of endothelial cell damage including some endothelial debridement, exposing Descemet's membrane (c): 2.4 mm diameter/concave profile cryoprobe (scale bar, 200 μm); (d): 3.4 mm diameter/concave profile cryoprobe (scale bar, 500 μm). As expected, the larger probe induces more widespread damage (see Table 1 also). (e–h) Transition zones between unfrozen endothelial cells and those that were destroyed by freeze injury are often sharp (e) and (g); same area but different magnification (scale bars,10 μm, apart from (g) which is 50 μm).

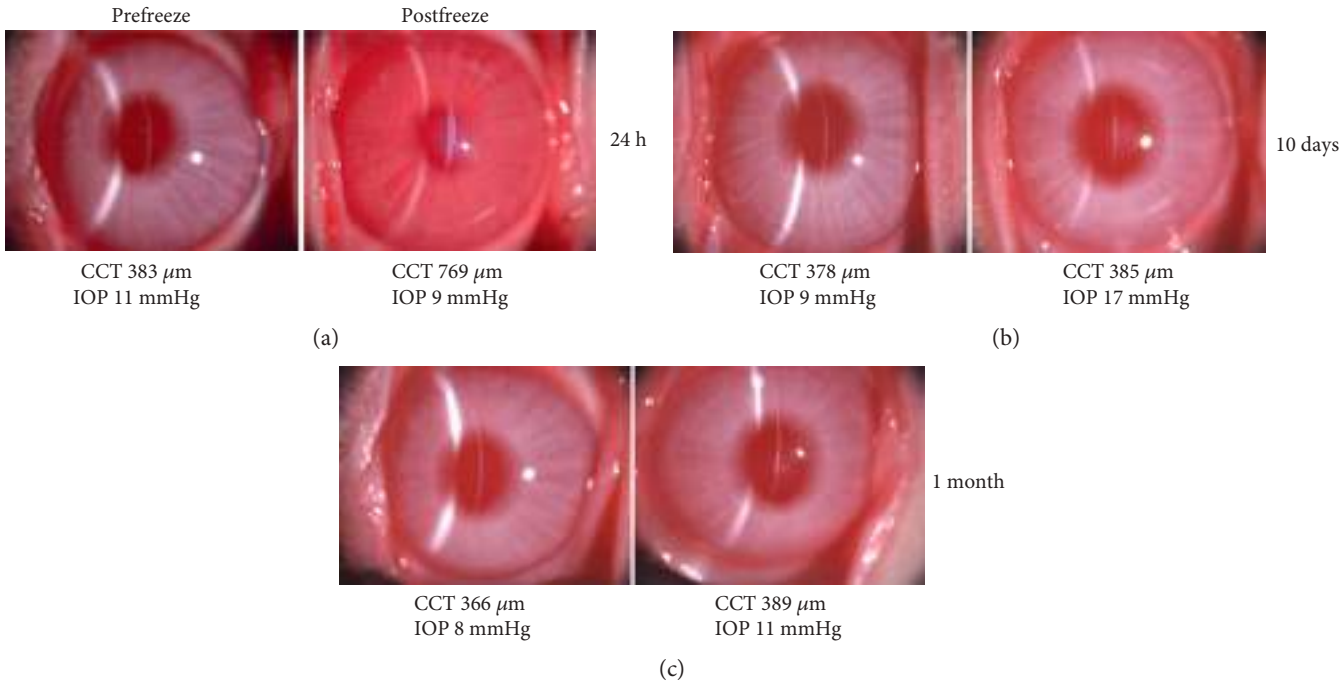

Figure 4: Effects of a 3 sec freeze on the rabbit cornea in vivo using the 2.4 mm diameter/concave profile cryoprobe tip. (a) 24 hrs after freeze, central corneal thickness (CCT) is increased considerably (769 μm) compared to that before freeze (383 μm), and the cornea is hazy, indicative of corneal endothelial damage, as well as epithelial and stromal cell damage. (b) 10 days after a freeze injury (in a different animal), CCT was at normal levels. (c) This was the case also, 1 month after treatment. (b and c) Some corneal haziness at the level of the posterior stroma or Descemet's membrane is evident at 10 days and 1 month.

(1.8 mm diameter ($r = -0.208$, $n = 102$, $p = 0.408$) and 3.4 mm diameter ($r = -0.258$, $n = 108$, $p = 0.007$) but a stronger relationship using the 2.4 mm diameter probe tips with concave and flat profiles ($r = -0.433$, $n = 108$, $p < 0.001$; 2.4 mm ($r = -0.466$, $n = 108$, $p < 0.001$, respectively) (Table 1).

To provide higher resolution information as to the status of the cells after freeze injury in the in vitro pig eye model, we conducted a series of SEM studies (Figure 3). This indicated that the corneal endothelial monolayer was severely disrupted in the central portion of the cornea beneath the site of the cryoprobe injury. Injured cells tended to become damaged and/or disassociated from each other, whereas noninjured cells adjacent to the area of damage exhibited classic hexagonal endothelial cell morphology. Interestingly, there appeared to be two transition zones between healthy nonfrozen cells and the more centrally damaged ones. The immediate transition at the inner edge of the morphologically normal cells was fairly abrupt; and in some cases, this was on a μm scale (Figures 3(e), 3(f), and 3(g)). More centrally, there was evidence of cellular dissociation (Figure 3(e)) and also total removal of large areas of frozen endothelial cells, exposing a bare Descemet's membrane (Figures 3(d) and 3(h)).

To investigate endothelial healing after transcorneal freeze, a small number of rabbit corneas were studied. For these investigations, a 2.4 mm diameter/concave profile cryoprobe was used rather than the 3.4 mm concave one owing to the relative thinness (approximately 350–400 μm) of the rabbit cornea compared to that of the pig (approximately 660 μm [29, 30]). This revealed that one day after a 3 sec surface freeze, the rabbit cornea had become significantly edematous, with its thickness approximately twice the normal value (Figure 4(a)). The central corneal thickness returned to normal values by day 7, and this was maintained up to one month post-freeze (Figure 4(c)). Slit-lamp images showed some evidence of corneal haze at the level of the posterior stroma or Descemet's membrane at 10 days and 1 month (Figures 4(b) and 4(c), resp.).

TEM examinations of rabbit corneas 24 hrs after freeze indicated that the corneal epithelium peripheral to the wound area was structurally normal, with typical epithelial stratification, cell-cell contact and surface microvilli (Figure 5(a)). As expected, the corneal epithelium was severely damaged in the central freeze-injured region of the cornea, with considerable cellular vacuolation and membrane destruction (Figure 5(b)). However, it was clear that the epithelial basement membrane remained intact, which presumably is important to aid subsequent epithelial resurfacing of the wound area. In the deep stroma, increased collagen fibril spacing accompanied by disorder in the fibril arrangement was sometimes observed focally 24 hrs post-freeze (Figure 5(c)), but this had been resolved by the 1-month timepoint at which time the stromal architecture appeared normal throughout the cornea (Figure 5(d)). These structural matrix changes likely contribute to the increased corneal thickness and opacity seen at 24 hrs (Figure 4(a)).

Just as with the corneal epithelium, the corneal endothelium in the periphery of the cornea away from the region of the tissue under the surface wound zone remained unaffected

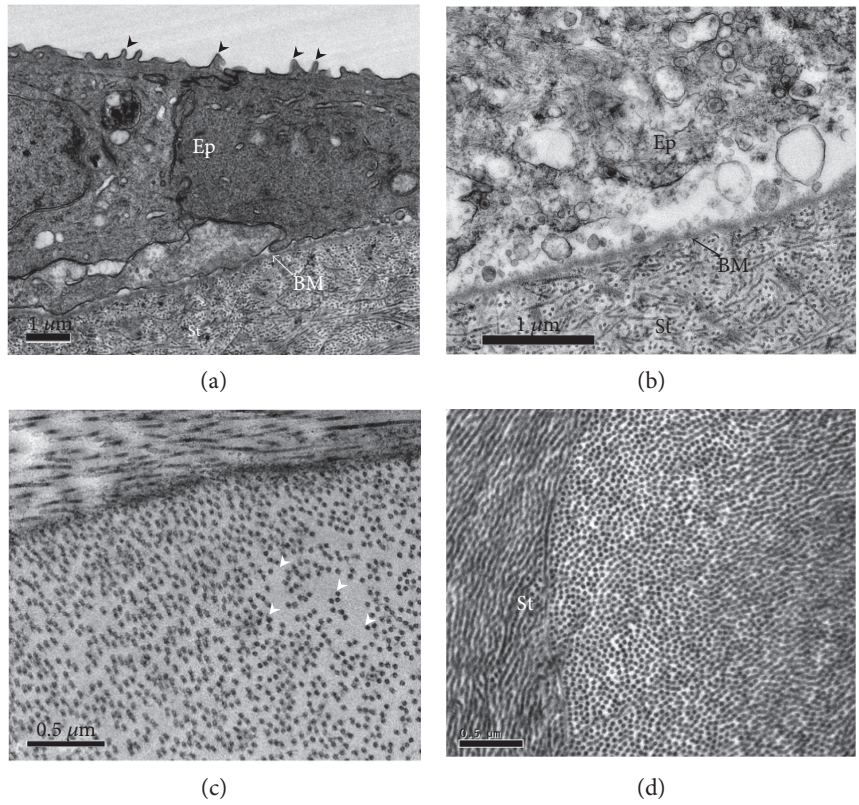

Figure 5: TEM of the corneal epithelium (Ep), epithelial basement membrane (BM), and stroma (St) following a 3 sec transcorneal freeze injury using a 2.4 mm diameter/concave profile cryoprobe on rabbit cornea in vivo. (a) The peripheral epithelium away from the wound zone, 24 hrs after the cryoprobe was applied and appeared morphologically normal. Arrowheads indicate microvilli on apical surface of epithelial cells. (b) Intact basement membrane is observed in the central freeze-injured area 24 hrs postfreeze. (c) After 24 hrs freeze injury, occasional focal regions of stromal matrix disruption were evident in the cornea, manifesting as tissue regions with increased spacing between collagen fibrils. (d) One month after the freezing, throughout the cornea, the spacing between collagen fibril appeared normal. Scale bars, 1 μm (a and b) and 0.5 μm (c and d).

24 hrs after transcorneal freeze of the central rabbit cornea (Figure 6(a)). The endothelium more centrally, however, began to exhibit clear signs of damage (Figure 6(b)). The central endothelium was often fully debrided with a bare Descemet's membrane that showed no apparent structural changes (Figure 6(c)). One month after freeze, the central corneal endothelium had reattained its normal character, although occasionally fibrous tissue deposition between Descemet's membrane and the recovered endothelium was observed (Figure 6(d)), which perhaps contributes to the deep stromal haze seen at this time (Figure 4(c)).

4. Discussion

A number of investigative surgical procedures, which utilize the selective ROCK inhibitor, Y27632, to combat FECD and bullous keratopathy are under investigation, including cell-injection therapy [10–14]. However, one alternative approach for FECD, especially in its early stage, involves freezing the central cornea using a cold probe to damage corneal endothelial cells beneath the surface contact area; this is then followed by the short-term delivery, for one week, of Y27632 in eye drop formulation [10–12]. In these surgeries, freezing was achieved by touching the corneal surface with a stainless steel rod, which had been immersed in liquid nitrogen. An arbitrary freezing time of 15 sec was chosen for these experiments, along with a 2 mm diameter for the steel rod. Encouragingly, the outcomes of these surgeries showed some promise, especially if the extent of the corneal endothelial dysfunction was not widespread, but if the approach is to be adopted more widely by the ophthalmic community, the corneal freeze would probably need to be achieved in a more reliable manner and with more knowledge of the nature and extent of the freeze damage.

Historically, and up to the present day, corneal freezing has been carried out by a variety of methods, most of which use it to induce an experimental injury for research into corneal wound healing [15–17, 28]. Freezing studies tend to employ either a brass rod or dowel, which had been immersed in liquid nitrogen [17–21] or similarly cooled steel ones [22, 23]. Retinal cryoprobes have also been used in investigational studies of transcorneal freezing [24, 33]. Here, we report the design and manufacture of a corneal cryoprobe that uses circulating nitrous oxide as a cryogen and report the type of freeze damage it induces.

Typically, the tips of cryoprobes that use high-pressure gas as a cryogen are made of stainless steel owing to the need to contain high-pressure gas safely. In our design, however,

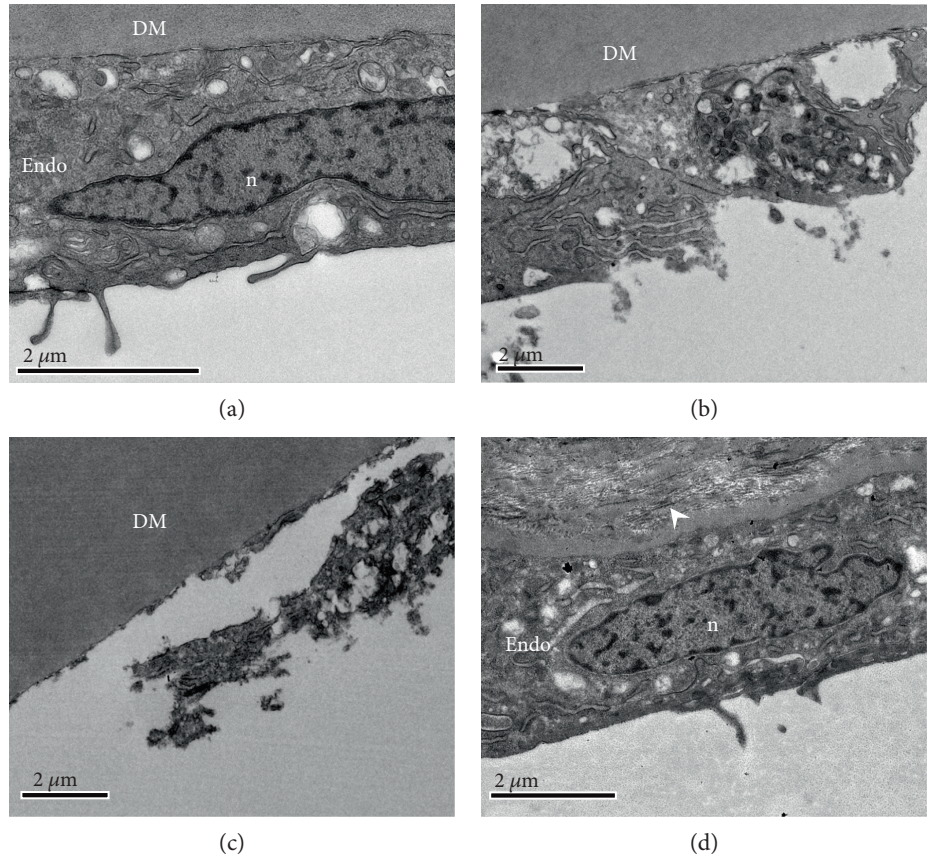

Figure 6: TEM of corneal epithelium following a 3 sec transcorneal freeze injury using a 2.4 mm diameter/concave profile cryoprobe on the rabbit cornea in vivo. (a) An endothelial cell (Endo) at 24 hrs postfreeze in a region peripheral to the freeze-injured area appeared morphologically normal, with normal organelles and nucleus (n). It adhered to Descemet's membrane (DM). (b) Closer to the region below the cryoprobe surface application, there were clear signs of cell damage including the destruction of the cell membrane, while even more centrally, (c) the cell damage was more extreme revealing a bare Descemet's membrane, consistent with the SEM analysis (Figure 3). (d) One month after the transcorneal freezing was performed, the central region of the inner cornea contained fairly normal endothelial cells that were sometimes accompanied by extracellular matrix material (white arrowheads) in the area posterior to Descemet's membrane. Scale bars, 2 μm.

the use of stainless steel would have resulted in a freeze that started in the center of the tip and thereafter spread, albeit quickly, to its outer circumference at a speed which relies on the thermal conductivity of the metal. To achieve a more uniform cooling across the probe tip, we manufactured a cryoprobe tip out of silver, which has a higher thermal conductivity than that of steel. The benefit of this design feature is that the diameter of the freeze in the cornea is decoupled from the depth of the freeze. Cooling in this design is based on the expansion and internal recycling of nitrous oxide inside the cryoprobe tip. At the point of its transition from liquid to gas, nitrous oxide exists at a temperature of −88.5°C, and this transition, which occurs inside our probe tip, of course, rapidly cools it. Owing to thermal conductivity within the whole probe and thermal loss at ambient room temperature, an equilibrium is reached, which in our design means that the temperature at the outer surface of the probe tip reaches −50°C.

The response of a cell to freezing is explained by Fraunfelder in his comprehensive review of corneal cryotherapy, the main mechanisms of cell damage being a piercing of the cell membrane by ice crystals or the creation of a sizeable osmotic imbalance between the inside and outside of the cell because of the removal of liquid water into the ice crystals [34]. Armitage also describes, from the other side of the coin, how careful freezing using time-mediated freeze-thaw protocols accompanied by the use of cryoprotectants can lead to cell survival [35]. The freezing we achieve here can probably be thought of as being fairly conservative in terms of the rate of endothelial cooling, but our current observations clearly indicate that sufficient levels of endothelial damage are achieved after a single freeze treatment. Experiments that applied additional treatments to the same surface location did not enhance the extent of the freeze injury (data not shown). We also found that if the foot switch was depressed to initiate cooling of the probe tip before it was brought into contact with the corneal surface, then no appreciable endothelial freeze damage was seen, even if the cryoprobe was kept in contact with the cornea for periods up to 15 sec. It is not immediately clear why this is the case, but perhaps, frosting of the probe tip when it is cooled in the moist air could contribute to this. This likely lack of frosting also might help facilitate the easy

release of the probe tip from the corneal surface after the foot switch is released, which we found to happen within a second or two of the cryogen circulation being suspended.

In the experiments described here, the central corneal epithelium was destroyed by the application of the cryoprobe, as we would expect. But, it is of potential importance that the corneal epithelial basement membrane remains intact as seen by TEM. The lack of epithelial basement membrane damage will presumably aid the epithelial resurfacing of the debrided epithelial area. Fibril arrangement changes are also apparent focally in the stromal matrix after the in vivo rabbit freeze injury, but these are transient, and the increased collagen fibril separation and disorganization which are seen 24 hrs after the treatment subsequently decrease as corneal thickness reduces. The obvious conclusion is that the recovering endothelium is mostly responsible. Of course, the in vivo healing studies reported here do not reflect the situation in the human cornea because of the different behavior of the endothelial cells and their limited replicative ability in humans. TEM also discloses the presence of fibrotic extracellular matrix tissue in the region of Descemet's membrane one month after freeze injury (Figure 6(d)). This might contribute to the deep stromal haze seen at this time, although a potential contribution to light scatter by freeze-damaged keratocytes cannot be discounted.

As mentioned, the use of ROCK inhibitors has aided the recovery of the corneal endothelium in situations where diseased corneal endothelial cells have been scraped away surgically [13] or frozen with a cooled steel rod applied to the corneal surface [10–12]. A report by Balachandran et al. [36] and Shah and associates also suggests that corneal endothelial cells can repopulate in FECD patients after damage alone [37–39]. The data presented here show that endothelial cells can be functionally damaged and/or removed by the application of a cryogenic cold probe and that this can be done in a targeted and reproducible manner with cell damage restricted to the area below the surface contact. Of course, the transcorneal freezing technique is unlikely to induce any significant change to the guttae which exist in FECD and their continued presence will conceivably hinder the reformation of a normal endothelial layer. Nevertheless, cell damage can be achieved through use of a silver 3.4 mm diameter cryoprobe with a concave profile, which was discovered to be the optimal design of the cryoprobes tested in the experiments described here. It thus has the potential to rapidly and reliably induce damage to the human corneal endothelium via transcorneal freezing, leaving the epithelial basement membrane intact. This has the potential to be used prior to the application of ROCK inhibitors to the eye in the form of eye drops [10–12] or as slow-release chemicals from thin films [40] to aid the recovery of corneal endothelial function.

Disclosure

The technology, the use of our freezing device coupled with the application of a Rho-kinase inhibitor for the nonevasive treatment of endothelial dysfunction, is the subject of patent (WO2013034907) currently under examination in Europe, Japan, and the United States of America. Preliminary results of this study were presented at the ARVO Annual Meeting, Seattle, USA, 1–5 May 2016.

Conflicts of Interest

The authors declare that there is no conflict of interest regarding the publication of this paper.

Acknowledgments

This research was supported by a Wellcome Trust Health Innovation Challenge Fund grant (HICF-T4-277 to Andrew J. Quantock, Noriko Koizumi, and Shigeru Kinoshita) and a Ph.D. Studentship to Alina Akhbanbetova and Andrew J. Quantock funded by the Life Science Research Network Wales, an initiative funded through the Welsh Government's Ser Cymru programme. The corneal programme at Cardiff University is funded by the BBSRC and MRC.

References

[1] W. M. Bourne, "Biology of the corneal endothelium in health and disease," *Eye*, vol. 17, no. 8, pp. 912–918, 2003.

[2] H. E. Kaufman and J. I. Katz, "Pathology of the corneal endothelium," *Investigative Ophthalmology & Visual Science*, vol. 16, no. 4, pp. 265–268, 1977.

[3] V. M. Borderie, P. Y. Boëlle, O. Touzeau, C. Allouch, S. Boutboul, and L. Laroche, "Predicted long-term outcome of corneal transplantation," *Ophthalmology*, vol. 116, no. 12, pp. 2354–2360, 2009.

[4] C. D. Nobes and A. Hall, "Rho, rac, and cdc42 GTPases regulate the assembly of multimolecular focal complexes associated with actin stress fibers, lamellipodia, and filopodia," *Cell*, vol. 81, no. 1, pp. 53–62, 1995.

[5] S. Li, C. Wang, Y. Dai et al., "The stimulatory effect of ROCK inhibitor on bovine corneal endothelial cells," *Tissue & Cell*, vol. 45, no. 6, pp. 387–396, 2013.

[6] N. Okumura, M. Ueno, N. Koizumi et al., "Enhancement on primate corneal endothelial cell survival in vitro by a ROCK inhibitor," *Investigative Ophthalmology & Visual Science*, vol. 50, no. 8, pp. 3680–3687, 2009.

[7] N. Okumura, N. Koizumi, M. Ueno et al., "ROCK inhibitor converts corneal endothelial cells into a phenotype capable of regenerating in vivo endothelial tissue," *The American Journal of Pathology*, vol. 181, no. 1, pp. 268–277, 2012.

[8] G. S. L. Peh, K. Adnan, B. L. George et al., "The effects of Rho-associated kinase inhibitor Y-27632 on primary human corneal endothelial cells propagated using a dual media approach," *Scientific Reports*, vol. 5, p. 9167, 2015.

[9] A. Pipparelli, Y. Arsenijevic, G. Thuret, P. Gain, M. Nicolas, and F. Majo, "ROCK inhibitor enhances adhesion and wound healing of human corneal endothelial cells," *PLoS One*, vol. 8, no. 4, articlsse e62095, 2013.

[10] N. Okumura, N. Koizumi, E. P. Kay et al., "The ROCK inhibitor eye drop accelerates corneal endothelium wound healing," *Investigative Ophthalmology & Visual Science*, vol. 54, no. 4, pp. 2493–2502, 2013.

[11] N. Koizumi, N. Okumura, M. Ueno, H. Nakagawa, J. Hamuro, and S. Kinoshita, "Rho-associated kinase inhibitor

eye drop treatment as a possible medical treatment for Fuchs corneal dystrophy," *Cornea*, vol. 32, no. 8, pp. 1167–1170, 2013.

[12] N. Koizumi, N. Okumura, M. Ueno, and S. Kinoshita, "New therapeutic modality for corneal endothelial disease using Rho-associated kinase inhibitor eye drops," *Cornea*, vol. 33, Supplement 11, pp. S25–S31, 2014.

[13] N. Okumura, S. Kinoshita, and N. Koizumi, "Cell-based approach for treatment of corneal endothelial dysfunction," *Cornea*, vol. 33, Supplement 11, pp. S37–S41, 2014.

[14] N. Okumura, R. Inoue, Y. Okazaki et al., "Effect of the Rho kinase inhibitor Y-27632 on corneal endothelial wound healing," *Investigative Ophthalmology & Visual Science*, vol. 56, no. 10, pp. 6067–6074, 2015.

[15] A. E. Maumenee and W. Kornblueth, "Regeneration of corneal stromal cells: I. Technique for destruction of corneal corpuscles by application of solidified (frozen) carbon dioxide," *American Journal of Ophthalmology*, vol. 31, no. 6, pp. 699–702, 1948.

[16] J. P. Faure, Y. Z. Kim, and B. Graf, "Formation of giant cells in the corneal endothelium during its regeneration after destruction by freezing," *Experimental eye Research*, vol. 12, no. 1, pp. 6–12, 1971.

[17] D. L. Van Horn, D. D. Sendele, S. Seideman, and P. J. Buco, "Regenerative capacity of the corneal endothelium in rabbit and cat," *Investigative Ophthalmology & Visual Science*, vol. 16, no. 7, pp. 597–613, 1977.

[18] J. S. Minkowski, S. P. Bartels, F. C. Delori, S. R. Lee, K. R. Kenyon, and A. H. Neufeld, "Corneal endothelial function and structure following cryo-injury in the rabbit," *Investigative Ophthalmology & Visual Science*, vol. 25, no. 12, pp. 1416–1425, 1984.

[19] P. Buco, D. L. Van Horn, W. H. Schutten, and K. Cohen, "Effects of transcorneal freezing on protein content of aqueous humor and intraocular temperature in rabbit and cat," *Investigative Ophthalmology & Visual Science*, vol. 17, no. 12, pp. 1199–1202, 1973.

[20] T. Mimura, S. Yokoo, M. Araie, S. Amano, and S. Yamagami, "Treatment of rabbit bullous keratopathy with precursors derived from cultured human corneal endothelium," *Investigative Ophthalmology & Visual Science*, vol. 46, no. 10, pp. 3637–3644, 2005.

[21] T. Mimura, S. Yamagami, S. Yokoo et al., "Sphere therapy for corneal endothelium deficiency in a rabbit model," *Investigative Ophthalmology & Visual Science*, vol. 46, no. 9, pp. 3128–3135, 2005.

[22] H. Ichijima, W. M. Petroll, P. A. Barry et al., "Actin filament organization during endothelial wound healing in the rabbit cornea: comparison between transcorneal freeze and mechanical scrape injuries," *Investigative Ophthalmology & Visual Science*, vol. 34, no. 9, pp. 2803–2812, 1993.

[23] W. M. Petroll, P. A. Barry-Lane, H. D. Cavanagh, and J. V. Jester, "ZO-1 reorganization and myofibroblast transformation of corneal endothelial cells after freeze injury in the cat," *Experimental eye Research*, vol. 64, no. 2, pp. 257–267, 1997.

[24] S. J. Tuft, K. A. Williams, and D. J. Coster, "Endothelial repair in the rat cornea," *Investigative Ophthalmology & Visual Science*, vol. 27, no. 8, pp. 1199–1204, 1986.

[25] S. B. Han, H. Ang, D. Balehosur et al., "A mouse model of corneal endothelial decompensation using cryoinjury," *Molecular Vision*, vol. 19, pp. 1222–1230, 2013.

[26] H. H. Chi and C. D. Kelman, "Effects of freezing on ocular tissues. I. Clinical and histologic study of corneal endothelium," *American Journal of Ophthalmology*, vol. 61, no. 4, pp. 630–641, 1966.

[27] N. J. Fullwood, Y. Davies, I. A. Nieduszynski, B. Marcyniuk, A. E. A. Ridgway, and A. J. Quantock, "Cell surface-associated keratan sulfate on normal and migrating corneal endothelium," *Investigative Ophthalmology & Visual Science*, vol. 37, no. 7, pp. 1256–1270, 1996.

[28] D. L. Van Horn and R. A. Hyndiuk, "Endothelial wound repair in primate cornea," *Experimental eye Research*, vol. 21, no. 2, pp. 113–124, 1975.

[29] C. Faber, E. Scherfig, J. U. Prause, and K. E. Sørensen, "Corneal thickness in pigs measured by ultrasound pachymetry in vivo," *Scandinavian Journal of Laboratory Animal Science*, vol. 35, no. 1, pp. 39–43, 2008.

[30] I. Sanchez, R. Martin, F. Ussa, and I. Fernandez-Bueno, "The parameters of the porcine eyeball," *Graefe's Archive for Clinical and Experimental Ophthalmology*, vol. 249, no. 4, pp. 475–482, 2011.

[31] L. J. Kopplin, K. Przepyszny, B. Schmotzer et al., "Relationship of Fuchs endothelial corneal dystrophy severity to central corneal thickness," *Archives of Ophthalmology (Chicago, Ill. 1960)*, vol. 130, no. 4, pp. 433–439, 2012.

[32] D. J. Repp, D. O. Hodge, K. H. Baratz, J. W. McLaren, and S. V. Patel, "Fuchs' endothelial corneal dystrophy: subjective grading versus objective grading based on the central-to-peripheral thickness ratio," *Ophthalmology*, vol. 120, no. 4, pp. 687–694, 2013.

[33] E. G. Olsen and M. Davanger, "The healing of human corneal endothelium. An in vitro study," *Acta Ophthalmologica*, vol. 62, no. 6, pp. 885–892, 1984.

[34] F. W. Fraunfelder, "Liquid nitrogen cryotherapy for surface eye disease (an AOS thesis)," *Transactions of the American Ophthalmological Society*, vol. 106, no. 1, pp. 301–324, 2008.

[35] W. J. Armitage, "Cryopreservation for corneal storage," *Developments in Ophthalmology*, vol. 43, pp. 63–69, 2009.

[36] C. Balachandran, L. Ham, C. A. Verschoor, T. S. Ong, J. van der Wees, and G. R. J. Melles, "Spontaneous corneal clearance despite graft detachment in Descemet membrane endothelial keratoplasty," *American Journal of Ophthalmology*, vol. 148, no. 2, pp. 227–234, 2009, e1.

[37] R. D. Shah, J. B. Randleman, and H. E. Grossniklaus, "Spontaneous corneal clearing after Descemet's stripping without endothelial replacement," *Ophthalmology*, vol. 119, no. 2, pp. 256–260, 2012.

[38] V. Galvis, A. Tello, and G. Miotto, "Human corneal endothelium regeneration," *Ophthalmology*, vol. 119, no. 8, pp. 1714–1715, 2012.

[39] E. Manche and A. Chan, "Preoperative pupil size and LASIK," *Ophthalmology*, vol. 118, no. 12, pp. 2526–2526, 2011, author reply 2526-7.

[40] W. Chan, A. Akhbanbetova, A. J. Quantock, and C. M. Heard, "Topical delivery of a Rho-kinase inhibitor to the cornea via mucoadhesive film," *European Journal of Pharmaceutical Sciences*, vol. 91, pp. 256–264, 2016.

BJO Online First, published on October 5, 2017 as 10.1136/bjophthalmol-2017-310913

The existence of dead cells in donor corneal endothelium preserved with storage media

Koji Kitazawa,[1,2] Tsutomu Inatomi,[3] Hidetoshi Tanioka,[3] Satoshi Kawasaki,[4] Hiroko Nakagawa,[3] Osamu Hieda,[3] Hideki Fukuoka,[3] Naoki Okumura,[5] Noriko Koizumi,[5] Bernie Iliakis,[6] Chie Sotozono,[3] Shigeru Kinoshita[1]

[1]Department of Frontier Medical Science and Technology for Ophthalmology, Kyoto Prefectural University of Medicine, Kyoto, Japan
[2]Baptist Eye Institute, Kyoto, Japan
[3]Department of Ophthalmology, Kyoto Prefectural University of Medicine, Kyoto, Japan
[4]Department of Ophthalmology, Osaka University, Suita, Japan
[5]Department of Biomedical Engineering, Faculty of Life and Medical Sciences, Doshisha University, Kyotanabe, Japan
[6]SightLife, Seattle, Washington, DC, USA

Correspondence to
Professor Shigeru Kinoshita, Department of Frontier Medical Science and Technology for Ophthalmology, Kyoto Prefectural University of Medicine, 465 Kajii-cho, Hirokoji-agaru, Kawaramachi-dori, Kamigyo-ku, Kyoto 602-0842, Japan; shigeruk@koto.kpu-m.ac.jp

Received 20 June 2017
Revised 17 July 2017
Accepted 13 August 2017

ABSTRACT

Aim To investigate the viability of donor corneal endothelial cells (CECs) preserved in storage media by histological examination.

Methods Twenty-eight donor corneas were obtained from SightLife Eye Bank (Seattle, Washington), and redundant peripheral portions of those corneas were used for histological examination after removal of the centre corneal graft for transplantation. To assess cell viability in the corneal endothelium, biostaining experiments were performed using propidium iodide, calcein-AM, Hoechst 33 342, annexin V, anti-vimentin antibody and toluidine blue.

Results Histological analysis of the endothelium showed that the cytoplasm of dead cells had low-intensity fluorescence and that their nuclei stained red, while almost all living cells had green cytoplasm and blue-stained nuclei. The mean dead cell rate in the 28 donor corneas was 4.9%±3.3% (mean ±SD) (range: 0.6%–10.5%). The propidium iodide-positive cells stained positive for annexin V, negative for vimentin and pale for toluidine blue. After the specimens were incubated in a culture medium, the red nucleus dead cells dropped off from the level of the blue nucleus living cells.

Conclusion Our findings showed the existence of dead cells in storage-media-preserved donor corneal endothelium and that they dropped off after incubation, thus suggesting that the decrease of CECs following keratoplasty may be related to the presence of dead cells.

INTRODUCTION

It has been reported that endothelial cell density (ECD) is approximately 6000 cells/mm^2 at birth, yet gradually decreases with age.[1–3] In fact, in normal human corneas without a past history of surgical intervention or a traumatic event, ECD reportedly decreases at a rate of 0.6% per year.[4] The rate of endothelial cell loss post penetrating keratoplasty (PK) or Descemet's stripping automated endothelial keratoplasty (DSAEK) is relatively rapid, with the yearly postoperative rate of decrease reportedly being 4%–8% post PK[5 6] and 1%–4% post DSAEK.[7–10] However, the underlying mechanism of endothelial cell loss post corneal transplantation has yet to be fully elucidated.

In the USA and Japan, donor corneas are currently preserved with Optisol-GS (Bausch & Lomb, Irvine, California) corneal storage media, a hybrid of K-sol and DexSol medium containing chondroitin sulfate and dextran,[11] and stored at the temperature of between 2°C and 8°C. However, in Europe, the preferred method for the long-term preservation of donor corneas is in organ culture media at temperatures ranging between 31°C and 37°C.[12] To evaluate whether or not donor corneal endothelium is suitable for use in corneal transplantation, it is usually tested by specular microscopy and/or trypan blue staining. However, these examinations only detect the cell-to-cell junction of endothelial cells, including the focal tight junctions, and do not detect the viability of these cells. Thus, we speculate that not only ECD, coefficient of variation and percentage of hexagonality, but also the viability of endothelial cells should be considered to be a possible cause of endothelial cell loss at early phase after keratoplasty.

In this study, we used a detailed histological technique to examine the viability of the corneal endothelium and to elucidate the decrease of ECD after keratoplasty using donor corneas preserved in Optisol-GS.

MATERIALS AND METHODS

Samples

This study was approved by the Committee for Ethical Issues in Human Research of Kyoto Prefectural University of Medicine and was performed in accordance with the tenets set forth in the Declaration of Helsinki. Twenty-eight donor corneas were obtained from SightLife Eye Bank (Seattle, Washington) for keratoplasty. After removal of the centre corneal graft for transplantation, the redundant peripheral portions of all 28 donor corneas were used for histological examination. These peripheral portions were cut to a width of 5 mm, and these tissue fragments were then used for the histological examinations. Four additional donor corneas for research that adhered to the same criteria as those used for corneal transplantation were obtained from SightLife Eye Bank. These four whole donor corneas were then cut from the centre to the peripheral area to produce specimen strips measuring 5 mm in width, and these tissue fragments were then used for the endothelial cell viability test.

Histological examination

To assess cell viability in the corneal endothelium samples, biostaining experiments were performed using 10 mM propidium iodide (PI), 1 mM calcein-AM and 10 mM Hoechst 33 342 (Dojindo Molecular Technologies Inc, Kumamoto, Japan) at

To cite: Kitazawa K, Inatomi T, Tanioka H, *et al*. *Br J Ophthalmol* Published Online First: [*please include* Day Month Year]. doi:10.1136/bjophthalmol-2017-310913

37°C for 15 min.[13] After washing one time in phosphate buffered saline (PBS), the specimens were then covered with a cover glass and observed with a microscope (AX70; Olympus Corporation, Tokyo, Japan) or with a confocal laser microscope (TCS-SP2; Leica Microsystems K.K., Tokyo, Japan).

Quadruple staining was performed as follows: first, the endothelium samples were stained with 20 mM PI and fluorescein isothiocyanate (FITC)-labelled annexin V (Medical & Biological Laboratories Co, Ltd, Nagoya, Japan). Next, after washing one time in PBS and fixation with 4% paraformaldehyde, the specimens were reacted with 0.5% Triton-X100 in PBS and anti-vimentin (DAKO), and then reacted with secondary antibody cy5-labelled anti-mouse IgG (Abcam Plc., Tokyo, Japan) and 10 mM Hoechst 33 342. The specimens were then covered with a cover glass and observed with a confocal laser microscope (TCS-SP2; Leica Microsystems). Fluorescent images of the corneal endothelium were observed by fluorescent microscopy and taken with a chilled charge-coupled device digital camera. The ECD was determined by counting the number of blue nuclei cells (Hoechst 33 342-positive), and dead cell rate (DCR, percentage) was calculated by counting average dead cells (PI-positive and calcein-AM-negative) in three randomly selected areas. The ECD was determined by counting the number of blue nuclei cells (Hoechst 33 342-positive), and DCR (percentage) was calculated by counting average dead cells (PI-positive and calcein-AM-negative) in randomly selected three areas

Some specimens were fixed in 2.5% glutaraldehyde (Electron Microscopy Sciences, Hatfield, Pennsylvania) in 0.1 M phosphate buffer (PB), washed three times in PB and post-fixed for 1 hour with 2% aqueous osmium tetroxide. The samples were then passed through a graded ethanol series, transferred to propylene oxide and embedded in Epon 812 (TAAB Laboratories Equipment Ltd, Aldermaston, UK). Horizontal semi-thin sections (250 nm) were then cut from resin-embedded blocks using a glass knife, stained with toluidine blue solution and examined under light microscopy.

In addition, the endothelium of one tissue fragment was stained with PI and Hoechst 33 342 and was incubated in a culture medium comprising Dulbecco's modified Eagle medium (DMEM; Life Technologies Corporation, Carlsbad, California) supplemented with 10% fetal bovine serum, 50 U/mL penicillin, 50 µg/mL streptomycin at 37°C in a 5% CO_2 incubator as we previously reported[14] and the time-dependent change of the dead cells was investigated by the use of time-lapse cinemicrography techniques with a microscope (BIOREVO BZ-9000 and CO_2 Incubator Unit 971884; KEYENCE Corporation, Itasca, Illinois).

The correlation of the DCR of endothelium and each donor's information were calculated by Pearson and Spearman correlation coefficients.

RESULTS

Usually, the ECD rates of the donor corneas are determined by specular microscopy examination of the corneoscleral disc by the SightLife Eye Bank prior to shipment via air transport, and that tissue information is included with the corneas (figure 1A). In addition, we stained the endothelium with Alizarin red S at the peripheral area of each donor cornea at the time of corneal transplant and measured the ECD (figure 1B).

Staining by PI (figure 2A), calcein-AM (figure 2B) and Hoechst 33 342 (figure 2C) allowed for the discrimination between living cells and dead cells. PI specifically stained the nuclei of the dead cells and showed an increase of membrane permeability, followed by a decrease of cell viability. There was calcein-AM dye uptake in the cells, and the dye was hydrolysed to FITC to generate fluorescence by the enzyme in viable cells. In contrast, the enzyme was decreased in low viability cells, and the cytoplasm of the cells showed a low green fluorescence level. Hoechst 33 342 was able to penetrate easily into all cells, and it stained all of the nuclei of the endothelial cells blue. A merging of the microscopy images of all three fluorescein dyes showed that living cells appeared as green cytoplasm with a blue nucleus, and also showed that the cells with deceased viability that were determined to be dead cells appeared as low green fluorescent cytoplasm with a red nucleus (figure 2D). The cells of low green fluorescent cytoplasm with a red nucleus were thought to be dead cells and were examined by quadruple staining in more detail. Dead cells that stained positive for annexin V indicated the cell membrane of an apoptosis cell, and those that stained negative for vimentin indicated that they were part of the cytoskeleton of the corneal endothelium (figure 2E). In addition, in the semi-thin sections of the endothelium from the Epon 812-embedded specimens, the dead cells had pale staining for toluidine blue. Therefore, we theorised that the cytoplasm component of those cells was decreased (figure 2F).

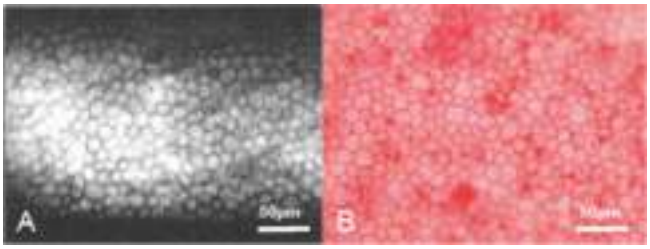

Figure 1 Endothelial examinations of the donor cornea obtained from a US eye bank. (A)Tissue information provided by SightLife Eye Bank shows a corneal endothelium image obtained by specular microscopy. (B) The endothelium was stained with Alizarin red S at the unused peripheral area of the donor cornea after the trephination, the time of corneal transplantation. The hexagonal array of endothelium can be seen in both A and B.

We theorised that if the red nucleus cells were dead, then they would drop off from the Descemet's membrane. The specimens were then incubated in a culture medium for the short time, and dead cells were observed at the same level around living cells on the Descemet's membrane (figure 3A). After a one night incubation, no red nucleus cells were observed on the Descemet's membrane, yet red nucleus cells were found to exist on the upper-side of the endothelial layer (figure 3B). In addition, use of the time-lapse cinemicrography technique showed that the PI-positive dead cells (red nucleus) were at the same level as the living cells (blue nucleus) initially. However, after 7 hours (figure 3J), the red nucleus cells dropped off from the level of the blue nucleus cells (figure 3C-M).

Staining by PI, calcein-AM and Hoechst 33 342 showed that the number of dead cells varied per specimen (figure 4). We defined the dead cell as PI-positive and calcein-AM-negative and Hoechst 33 342-positive cell. The DCR of the 28 donor corneas varied from 0.6% to 10.5%, 4.9±3.3% (mean±SD) (table 1). In table 1, the DCR is shown in a descending order from highest DCR percentage to lowest DCR percentage, and we found no significant correlation between the DCR and specific factors related to the 28 donor corneas including age and sex of the donor, elapsed time from death to preservation, total preservation time or cause of death. No significant correlations between

the DCR of endothelium and each donor's information were observed.

The DCR of the whole donor corneas was determined by dividing the red-nuclei cell count by the blue-nuclei cell count, the same as with the residual portions of the 28 donor corneas. The DCR of the whole donor corneas ranged from 1.3% to 2.4%, 1.9±0.39% (mean±SD) at the centre of corneas and from 1.3% to 3.0%, 1.9%±0.7% (mean±SD) at the periphery of the corneas.

DISCUSSION

It has generally been thought that donor corneas are suitable for corneal transplantation by testing with specular microscopy and/or trypan blue, yet these examinations only detect the junctions of the endothelial cells. We have now found through the examination of donor corneas that these corneal endothelia contain dead cells, and we theorise that these dead cells remain attached through the focal tight junction when at a low temperature and that they subsequently drop off when they warm to body temperature following corneal transplantation. We speculate that the increases of dead cells in the donor cornea endothelia were caused by some type of stress, for example, stress related to oxidisation. Previous studies have reported that a rewarming process which returned to physiological conditions produced reactive oxygen or nitrogen species (ie, ROS, RNS) and increased intracellular free radicals, thus leading to induced apoptosis.[15–17] In fact, previous studies have reported that cold-rewarming injury endothelial stress led to the change of cell morphology and induced apoptosis.[18 19] Thus, and similar to what a rewarming process has been described, it may happen to

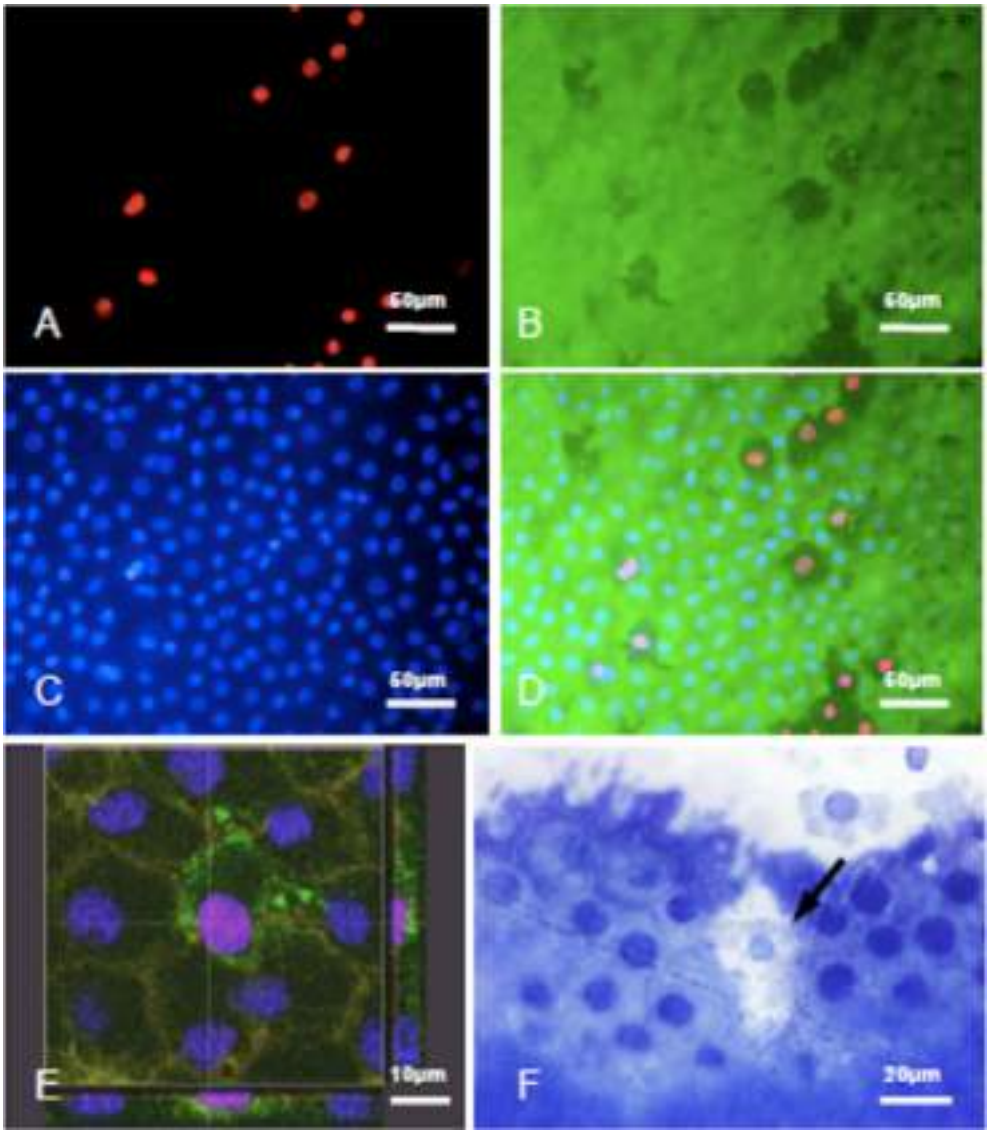

Figure 2 Identification staining of viable cells and dead cells in donor cornea endothelium. (A) PI specifically stained the nuclei of the dead cells red and showed an increase of membrane permeability, followed by a decrease of cell viability. (B) Calcein-AM dye was hydrolysed to FITC to generate fluorescence by the enzyme in viable cells, and decreased enzyme in the cells showed a low fluorescence level. (C) Hoechst 33 342 stained all of the nuclei of the endothelial cells blue. (D) A merging of these three images shows the cells with dead cells appearing as pale cytoplasm with a red nucleus. (E) A confocal microscope image showing quadruple staining with annexin V; the cell membrane of the apoptosis cell (green), vimentin; one of the cytoskeletons of corneal endothelium (yellow), PI (red) and Hoechst 33 342 (blue). (F) An image of toluidine blue staining of a semi-thin section of the endothelium from the Epon 812-embedded specimens; the centre cell is assumed to be dead due to the pale (arrow) staining. FITC, fluorescein isothiocyanate; PI, propidium iodide.

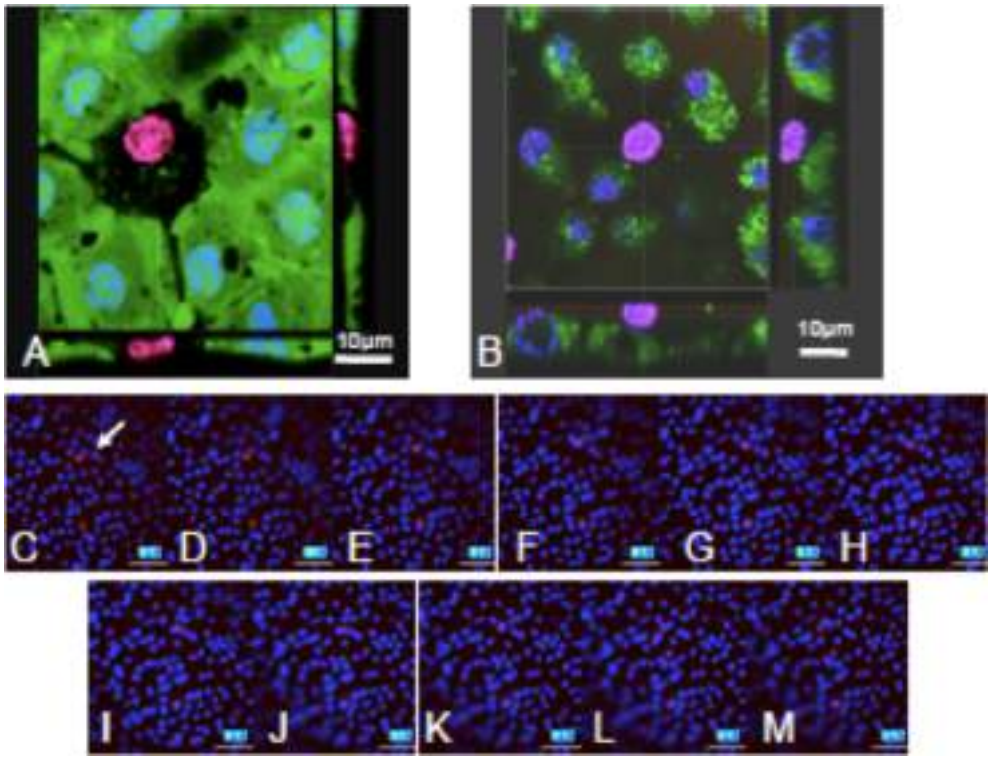

Figure 3 The locomotion of a dead cell after incubation in the culture medium. (A) The corneal specimen was incubated for 30 min in medium at under 37°C, then stained with PI, calcein-AM, and Hoechst 33 342. A dead cell (red nuclei) existed between living cells and they were found on the Descemet's membrane. (B) The corneal specimen was incubated overnight in a medium at under 37°C, then stained with PI, calcein-AM and Hoechst 33 342. A dead cell (red nuclei) existed near these living cells. (C–M) Observation of dead cells via the time-lapse cinemicrography technique. Endothelium of a tissue fragment was stained with PI and Hoechst 33 342 and was incubated in the culture medium. Initially, the PI-positive dead cells (red nucleus) were found at the same level as the living cells (blue nucleus). (J) After 7 hours, the red nucleus cells dropped off from the level of the blue nucleus cells. Time-lapse cinemicrography revealed that the dead cells were eliminated by the movement of the surrounding living cells. PI, propidium iodide.

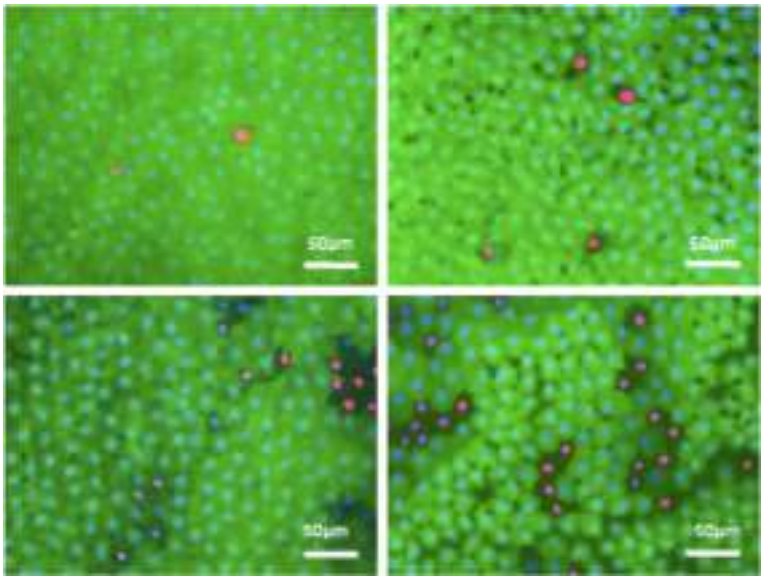

Figure 4 Images of the PI, calcein-AM and Hoechst 33 342 staining of various numbers of dead cells in the endothelium. The donor cornea endothelium consisted of various rates (table 1) of dead cells that appeared as a low fluorescence of the green and red nuclei. PI, propidium iodide.

corneal endothelial cells (CECs) in the donor cornea. It suggest that the endothelia in the donor cornea may contain cells that are in the process of dying, and it could somewhat affect a graft survival time due to CEC loss following keratoplasty.

The Cornea Donor Study Group study showed that donor age has little effect on ECD in donor corneas.[17] In this present study, no significant correlation was found between the DCR and specific factors related to the 28 donor corneas; factors such

Table 1 Donor cornea dead cell rate and associated data

No.	DCR(%)	Cell density 1) (cells/mm^2)	Cell density 2) (cells/mm^2)	Age (year)	Death to preservtion time (h:mm)	Preservation time (day)	Sex	Cause of death
1	10.5	2143	ND	72	3:55	6	F	Colon cancer
2	10.5	2613	2000	50	11:05	5	M	Blunt force trauma
3	10.4	2994	2533	72	6:25	6	M	Lung cancer
4	10.1	2616	2500	64	5:40	6	M	Closed head injury 27 ATV
5	10.1	2924	2275	56	5:53	7	F	Pulmonary HTN
6	9.8	2724	2567	53	17:16	3	M	Cerebral vascular accident
7	8.3	2510	1667	66	5:31	7	M	MI
8	6.5	2646	2700	73	21:20	6	F	Acute MI
9	6.1	2848	3500	62	14:03	7	M	Intestinal haemorrhage
10	6.0	2645	2567	49	7:22	5	M	MI
11	5.8	2788	2300	70	7:11	4	F	Ovarian cancer
12	5.7	2728	2167	74	7:56	4	F	Dissecting aortic aneurysm
13	4.8	3069	2333	51	6:23	4	M	End-stage liver desease
14	4.5	3548	ND	64	5:13	4	F	Aspiration
15	4.3	3003	ND	26	12:45	6	M	Cystic fibrosis
16	4.1	3251	2600	37	17:58	5	F	Blunt force head trauma
17	3.6	2647	2067	41	3:59	7	M	Acute cardiac dysrhythmia
18	3.0	2507	2367	43	21:11	6	F	MI
19	2.5	3106	ND	64	5:45	6	F	Oesophagus cancer
20	2.0	2884	ND	51	5:55	7	M	Anoxic encephalopathy
21	1.9	2588	2200	66	8:30	6	M	Colon cancer
22	1.5	2805	2700	39	3:59	5	M	Anoxic encephalopathy
23	1.2	2813	2367	62	7:09	5	M	Ruptured spleen
24	1.1	2571	2367	66	5:15	7	M	Acute MI
25	1.0	2511	1900	48	7:05	7	M	Dilated cardiomyopathy
26	0.8	2684	1933	38	4:54	7	F	Cystic fibrosis
27	0.6	2629	1667	52	13:35	5	M	Gunshot wound to head

The DCRs (percentage) are shown in descending order (from highest to lowest), along with the following donor-specific associated data: (1) measurements obtained by specular microscopy from the data sheet of the donor cornea, and (2) measurements obtained by Alizarin red S staining at our institution.
ATV, all-terrain vehicle; DCR, dead cell rate; HTN, hypertension; MI, myocardial infarction; ND, not detected.

as age and sex of the donor, death to preservation time, total preservation time or cause of death. Therefore, as the preservation was performed by the eye bank under normal conditions and time periods, it was thought that the DCRs were not influenced by the range of factors contained in the donor-specific tissue information provided by the eye bank. The toxicity of the antibiotic, other existing materials or the condition of the oxygen in the preservation medium may all be factors related to the existence of the dead cells. It has been reported that the postoperative ECD after keratoplasty is generally decreased from the ECD of the donor cornea prior to surgery.[20–22] We previously reported that a higher number of CECs as considering graft size might need for reconstruction of the corneal endothelium.[23] Thus, the existence of dead cells on the endothelium of donor cornea suggests the association with rapid loss of CECs at least early phase after keratoplasty.

In the previous reports, the results of examinations of endothelium by transmission and scanning electron microscopy,[24–26] trypan blue and Alizarin red S double-staining,[27] and calcein-AM and ethidium homodimer-1 staining that identified dead cells[27 28] were presented to indicate the superiority of the new preservation medium or method during the investigation of the preservation of the cornea. In this present study, our experiment used calcein-AM and PI that identified both living and dead cells, and moreover, we used Hoechst 33 342 that stained all of the cell nuclei.[13] Therefore, it proved easy to identify all of the cell nuclei in the endothelium. In addition, these PI-positive cells stained positive for annexin V (an apoptosis marker), negative for vimentin (one of the cytoskeleton cells of endothelium) and pale for toluidine blue. These results strongly suggest that these cells were dead cells. The dead cells were identified in the preserved donor cornea, the same type of donor cornea that is used for keratoplasty, and the mean DCR was 4.9%. We feel that in addition to examination by specular microscopy and Alizarin red staining, examination of the viability of the endothelium is important for maintenance of the ECD rate after keratoplasty. The latest paper regarding to investigation of donor corneal endothelium revealed that ECD did not influence the graft survival after DSAEK.[29] Therefore, we think that the viability test, not just cell density proved to be one of the important examinations when the preservation medium was reconsidered, and it could lead to improve the graft survival rate.

In this study, we were unable to use a large number of intact donor corneas for the examinations due to the fact that the supply of these corneas is limited and generally reserved for transplantations. Therefore, in a large number of our cases, our examinations were restricted to the use of the residual portions of donor corneas obtained after corneal transplantations. The four whole donor corneas for research that did not include any trephination-related artefact were provided by SightLife Eye Bank, and the existence of dead cells in the preserved donor cornea was confirmed by the use of these four intact corneas. In the USA and Japan, donor corneas are currently preserved in Optisol-GS stored to the temperature between 4°C and 8°C.[30]

It has been reported that dead cells in corneal endothelium may derive from the fold created by the distortion when isolating the eye or preparing the corneoscleral rim.[27 31] In this present study, we sometimes found linear dead cells. Even though that decentralised or diffused endothelial cell death was not caused by any type of physical impact, we theorise that it was caused by preservation conditions or the biological status of the donor cornea.

In conclusion, the findings of this present study showed the existence of low viability cells in the endothelium of preserved donor corneas, thus suggesting that these cells fall off soon or that the decrease of CECs following keratoplasty may be related to the presence of dead cells. We hope that the development of preservation medium, as considering the cell viability, will lead to more successful graft survival.

Contributors ShK: conception and design of the study and obtaining of funding. KK and HT: collection, management, analysis and interpretation of data; and searching the literature. KK, HT and ShK: writing of the article. KK, HT, SaK, TI, HN, OH, HF, NO, NK, BI and ShK: approval of the manuscript. HT: statistical expertise.

Funding This study was supported in part by a Grant-in-Aid for scientific research from the Ministry of Education, Science, Culture, and Sports of Japan.

Competing interests None declared.

Patient consent Tissue used were anonymous.

Ethics approval the Committee for Ethical Issues in Human Research of Kyoto Prefectural University of Medicine.

Provenance and peer review Not commissioned; externally peer reviewed.

REFERENCES

1 Bourne WM, Kaufman HE. Specular microscopy of human corneal endothelium in vivo. *Am J Ophthalmol* 1976;81:319–23.
2 Sturrock GD, Sherrard ES, Rice NS. Specular microscopy of the corneal endothelium. *Br J Ophthalmol* 1978;62:809–14.
3 Sherrard ES, Novakovic P, Speedwell L. Age-related changes of the corneal endothelium and stroma as seen in vivo by specular microscopy. *Eye* 1987;1:197–203.
4 Bourne WM, Nelson LR, Hodge DO. Central corneal endothelial cell changes over a ten-year period. *Invest Ophthalmol Vis Sci* 1997;38:779–82.
5 Bourne WM, Hodge DO, Nelson LR. Corneal endothelium five years after transplantation. *Am J Ophthalmol* 1994;118:185–96.
6 Ing JJ, Ing HH, Nelson LR, *et al*. Ten-year postoperative results of penetrating keratoplasty. *Ophthalmology* 1998;105:1855–65.
7 Price MO, Calhoun P, Kollman C, *et al*. Descemet stripping endothelial keratoplasty: ten-year endothelial cell loss compared with penetrating keratoplasty. *Ophthalmology* 2016;123:1421–7.
8 Price MO, Price FW. Endothelial keratoplasty - a review. *Clin Exp Ophthalmol* 2010;38:128–40.
9 Busin M, Bhatt PR, Scorcia V. A modified technique for descemet membrane stripping automated endothelial keratoplasty to minimize endothelial cell loss. *Arch Ophthalmol* 2008;126:1133–7.
10 Price MO, Price FW. Endothelial cell loss after descemet stripping with endothelial keratoplasty influencing factors and 2-year trend. *Ophthalmology* 2008;115:857–65.
11 Kaufman HE, Beuerman RW, Steinemann TL, *et al*. Optisol corneal storage medium. *Arch Ophthalmol* 1991;109:864–8.
12 Jeng BH. Preserving the cornea: corneal storage media. *Curr Opin Ophthalmol* 2006;17:332–7.
13 Tanioka H, Hieda O, Kawasaki S, *et al*. Assessment of epithelial integrity and cell viability in epithelial flaps prepared with the epi-LASIK procedure. *J Cataract Refract Surg* 2007;33:1195–200.
14 Koizumi N, Sakamoto Y, Okumura N, *et al*. Cultivated corneal endothelial cell sheet transplantation in a primate model. *Invest Ophthalmol Vis Sci* 2007;48:4519–26.
15 Alva N, Palomeque J, Carbonell T. Oxidative stress and antioxidant activity in hypothermia and rewarming: can RONS modulate the beneficial effects of therapeutic hypothermia? *Oxid Med Cell Longev* 2013;2013:1–10.
16 Bhaumik G, Srivastava KK, Selvamurthy W, *et al*. The role of free radicals in cold injuries. *Int J Biometeorol* 1995;38:171–5.
17 Talaei F, Bouma HR, Van der Graaf AC, *et al*. Serotonin and dopamine protect from hypothermia/rewarming damage through the CBS/H2S pathway. *PLoS One* 2011;6:e22568.
18 Rauen U, Kerkweg U, Wusteman MC, *et al*. Cold-induced injury to porcine corneal endothelial cells and its mediation by chelatable iron: implications for corneal preservation. *Cornea* 2006;25:68–77.
19 Rootman DS, Hasany SM, Basu PK. A morphometric study of endothelial cells of human corneas stored in MK media and warmed at 37 degrees C. *Br J Ophthalmol* 1988;72:545–9.
20 Bourne WM, Nelson LR, Maguire LJ, *et al*. Comparison of Chen Medium and Optisol-GS for human corneal preservation at 4 degrees C: results of transplantation. *Cornea* 2001;20:683–6.
21 Frueh BE, Böhnke M, Prospective BM. Prospective, randomized clinical evaluation of Optisol vs organ culture corneal storage media. *Arch Ophthalmol* 2000;118:757–60.
22 Naor J, Slomovic AR, Chipman M, *et al*. A randomized, double-masked clinical trial of Optisol-GS vs Chen Medium for human corneal storage. *Arch Ophthalmol* 2002;120:1280–5.
23 Kitazawa K, Yokota I, Sotozono C, *et al*. Measurement of corneal endothelial surface area using anterior segment optical coherence tomography in normal subjects. *Cornea* 2016;35:1229–33.
24 Ritterband DC, Shah MK, Meskin SW, *et al*. Efficacy and safety of moxifloxacin as an additive in Optisol-GS a preservation medium for corneal donor tissue. *Cornea* 2006;25:1084–9.
25 Nelson LR, Hodge DO, Bourne WM. In vitro comparison of Chen medium and Optisol-GS medium for human corneal storage. *Cornea* 2000;19:782–7.
26 Lindstrom RL, Kaufman HE, Skelnik DL, *et al*. Optisol corneal storage medium. *Am J Ophthalmol* 1992;114:345–56.
27 Means TL, Geroski DH, Hadley A, *et al*. Viability of human corneal endothelium following Optisol-GS storage. *Arch Ophthalmol* 1995;113:805–9.
28 Imbert D, Cullander C. Assessment of cornea viability by confocal laser scanning microscopy and MTT assay. *Cornea* 1997;16:666–74.
29 Potapenko IO, Samolov B, Armitage MC, *et al*. Donor endothelial cell count does not correlate with descemet stripping automated endothelial keratoplasty transplant survival after 2 years of follow-up. *Cornea* 2017;36:649–54.
30 Nakagawa H, Inatomi T, Hieda O, *et al*. Clinical outcomes in descemet stripping automated endothelial keratoplasty with internationally shipped precut donor corneas. *Am J Ophthalmol* 2014;157:50–5.
31 Albon J, Tullo AB, Aktar S, *et al*. Apoptosis in the endothelium of human corneas for transplantation. *Invest Ophthalmol Vis Sci* 2000;41:2887–93.

The existence of dead cells in donor corneal endothelium preserved with storage media

Koji Kitazawa, Tsutomu Inatomi, Hidetoshi Tanioka, Satoshi Kawasaki, Hiroko Nakagawa, Osamu Hieda, Hideki Fukuoka, Naoki Okumura, Noriko Koizumi, Bernie Iliakis, Chie Sotozono and Shigeru Kinoshita

Br J Ophthalmol published online October 5, 2017

BJO Online First, published on August 29, 2016 as 10.1136/bjophthalmol-2016-308893

Panoramic view of human corneal endothelial cell layer observed by a prototype slit-scanning wide-field contact specular microscope

Hiroshi Tanaka,[1] Naoki Okumura,[2] Noriko Koizumi,[2] Chie Sotozono,[1] Yasuhiro Sumii,[3] Shigeru Kinoshita[4]

[1]Department of Ophthalmology, Kyoto Prefectural University of Medicine, Graduate School of Medicine, Kyoto, Japan
[2]Department of Biomedical Engineering, Faculty of Life and Medical Sciences, Doshisha University, Kyotanabe, Japan
[3]Konan Medical, Inc, Nishinomiya, Japan
[4]Department of Frontier Medical Science and Technology for Ophthalmology, Kyoto Prefectural University of Medicine, Kyoto, Japan

Correspondence to
Professor Shigeru Kinoshita, Department of Frontier Medical Science and Technology for Ophthalmology, Kyoto Prefectural University of Medicine, 465 Kajii-cho, Hirokoji-agaru, Kawaramachi-dori, Kamigyo-ku, Kyoto 602-0841, Japan; shigeruk@koto.kpu-m.ac.jp

Received 22 April 2016
Revised 11 July 2016
Accepted 6 August 2016

To cite: Tanaka H, Okumura N, Koizumi N, *et al*. *Br J Ophthalmol* Published Online First: [*please include* Day Month Year] doi:10.1136/bjophthalmol-2016-308893

ABSTRACT

Purpose To observe the most peripheral region of the corneal endothelial cell (CEC) layer as long as optically recordable by use of a prototype slit-scanning wide-field contact specular microscope and produce a panoramic image to evaluate the variation of CEC density with ageing.

Design Observational case series study.

Methods This study involved 15 eyes of 15 normal healthy subjects divided into three groups according to age: A (20–40 years), B (41–60 years) and C (>60 years). The corneal endothelial layer of each eye was recorded in a horizontal direction, from nasal to temporal, with a slit-scanning wide-field contact specular microscope (Konan) and endothelial cell density (ECD) in three specific regions (central, mid-peripheral, and peripheral) was automatically calculated via built-in analysis software.

Results Corneal endothelial images from near the surgical limbus to limbus in all eyes were clearly recorded and panoramic images were made by combining still images. ECD in groups A, B and C were 2809±186, 2717±91 and 2580±129 cells/mm^2 at the centre, 2902±242, 2772±97 and 2604±187 cells/mm^2 at the mid-periphery and 2893±308, 2691±99 and 2533±112 cells/mm^2 at the periphery. Significance differences in ECD was found between groups A and C in all regions and groups between B and C at mid-peripheral region.

Conclusions A prototype slit-scanning wide-field contact specular microscope enabled us to record the endothelial layer from the surgical limbus to limbus of the cornea and compare specific areas among subjects, and showed that ECD in each region of the cornea decreases with ageing.

Trial registration number UMIN000021264, Results.

INTRODUCTION

It is well known that corneal endothelial morphometric analysis in vivo plays an important role in understanding the condition and dynamics of corneal endothelial cells (CECs).[1 2] Although that analysis can be calculated via contact specular microscopy, non-contact specular microscopy and confocal microscopy, the area of analysis is much more limited; that is, an area approximately 3 mm from the centre of the cornea. Hence, analysis of a wider area of CEC layer in vivo allows for a deeper understanding of the cell dynamics.

Since 1968, several contact and non-contact clinical specular microscopes have been developed to observe and obtain images of human CEC layer at high magnification in vivo.[3 4] Qualitative and quantitative analyses of CECs have provided information regarding changes in cell density, cell size, coefficient of variation (CV) of area and cell morphology (ie, the rate of hexagonal shape cells (6A) with ageing). Although a number of reports have investigated the difference of endothelial cell density (ECD) between the centre and peripheral regions of the cornea using a contact and non-contact specular microscope in vivo[5–8] and histology in vitro,[9–11] to the best of our knowledge, this is the first report to evaluate corneal ECD near the surgical limbus by comparing with in vivo wide-field CEC layer images.

In this study, investigation of the most peripheral CECs in vivo was performed via the use of a prototype slit-scanning wide-field contact specular microscope that is able to provide live imaging of CEC layer and location data. The purpose of this study was to elucidate the CEC dynamics over a wide area in vivo by comparing the ECD, 6A and CV with ageing via slit-scanning wide-field contact specular microscopy.

METHODS

Subjects

Approval for this study was obtained from the Ethics Committee of Kyoto Prefectural University of Medicine, Kyoto, Japan, and the study protocol followed the tenets set forth in the Declaration of Helsinki. Written informed consent was obtained from all subjects prior to their involvement in the study.

Volunteers from the local community were recruited from July 2015 to October 2015. In order to insure that normal healthy subjects were selected, each volunteer received a complete ophthalmologic evaluation via slit-lamp biomicroscopy, as well as intraocular pressure, refraction, best spectacle-corrected visual acuity examination. Exclusion criteria included a history of contact lens wear, prior ocular trauma or surgery, or ocular or systemic diseases that may affect the cornea.

In total, this study included 15 normal subjects (six males and nine females; age range 25–77 years) who were divided into the following three groups according to age: group A (20–40 years old), group B (41–60 years old) and group C (>60 years old).

Instrumentation used for examination

In this study, examination of each subject was performed using a prototype KSSP slit-scanning wide-

field contact specular microscope (Konan Medical, Nishinomiya, Hyogo, Japan) with a 1/2-inch camera including a 400 000-pixel charge-coupled-device sensor with 9.9× magnification, and a 40× magnification contact cone lens made from fluorite with numerous slits on both sides (figure 1A). To record the corneal endothelial layer, the layer is illuminated through the slits on one side of the device and the endothelial cell images are reflected back through the slits on the opposite side. Briefly, oxybuprocaine 0.4% eye drops were used to anaesthetise the right eye of each subject. The subjects were then asked to concentrate on the fixed light with their left eye, and manually focused on the CEC layer images at the rate of 60-frames per second were recorded with the slit-scan technique while the right eye was swept in the horizontal direction from the nasal to temporal side with the cornea being flattened by the contact lens. Focused still images were then extracted from the MPEG-2 file and manually connected together to produce a panoramic image. Overlapping portions of the images, judged from the morphology of CECs or dark band from the Descemet fold, are combined to form the panorama image (figure 1B). The centre and peripheral points were detected from the panoramic images, and the mid-point between the centre and periphery was defined as the 'mid-peripheral' point. Then, the ECD, 6A and CV of each point in a 0.3 mm×0.3 mm area were calculated via the computer algorithm (Konan Medical).

Statistical analysis

Statistical analysis of the data was performed and basic descriptive statistics were calculated on all of the gathered data, with the values reported as mean±SD. Differences in each parameter across age groups were tested by Friedman test. Comparisons between groups were conducted via the Steel-Dwass test. A p value of <0.05 was considered statistically significant.

RESULTS

Continuous CEC layer images, from end-to-end, in the cornea in all subjects were able to be clearly recorded by use of the slit-scanning wide-field contact specular microscope and were able to be connected into panoramic images (figure 2). Six specific areas of the cornea were identified from the panoramic images and calculated by the computer algorithm (figure 3). The slit-scanning wide-field contact specular microscopy results are summarised in the table 1. Our results showed a mean±SD corneal ECD as follows: group A: 2809±186 cells/mm^2 at the centre of the cornea, 2902±248 cells/mm^2 at the mid-peripheral region (the mid-point between the centre and peripheral region) and 2893±308 cells/mm^2 at the peripheral region; group B: 2717±91 cells/mm^2 at the centre of the cornea, 2772±92 cells/mm^2 at the mid-peripheral region and 2691±99 cells/mm^2 at the peripheral region; and group C: 2580±129 cells/mm^2 at the centre of the cornea, 2604±184 cells/mm^2 at the mid-peripheral region, and 2533±112 cells/mm^2 at the peripheral region. The correlation between ECDs versus age is represented by scatter plots (figure 4).

In each group, ECD at the mid peripheral region had a tendency to be higher than that at the centre and peripheral regions, however, there was no significance ($p>0.05$). The age comparison results showed significance in ECD between groups A and C at the centre ($p<0.05$), the mid-peripheral region ($p<0.05$), and the peripheral region ($p<0.05$) and groups B and C at the mid-peripheral region ($p<0.05$). Significance was found in CV between groups A and C ($p<0.01$) and group B

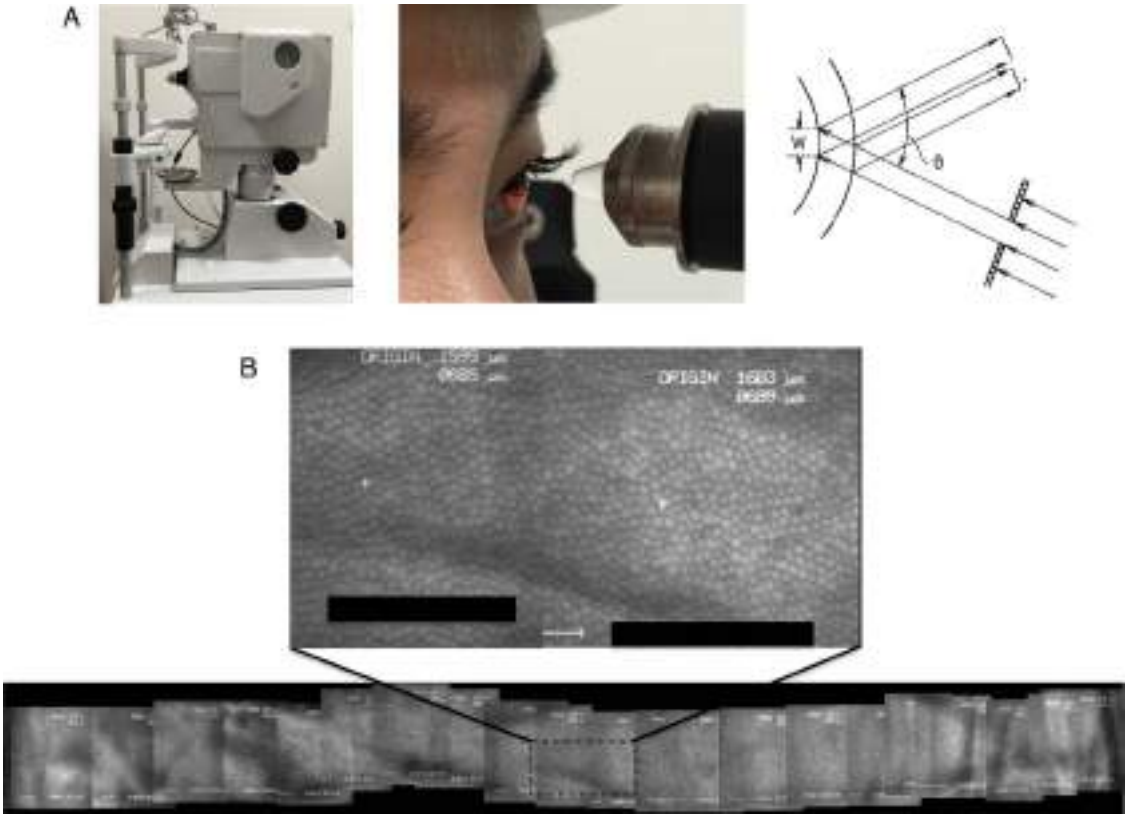

Figure 1 Images showing the prototype slit-scanning wide-field contact specular microscope (left) and proper measurement method (right) (A). A panoramic image produced by combining still images (0.5 mm×0.7 mm) from the recorded endothelial cell layer (B).

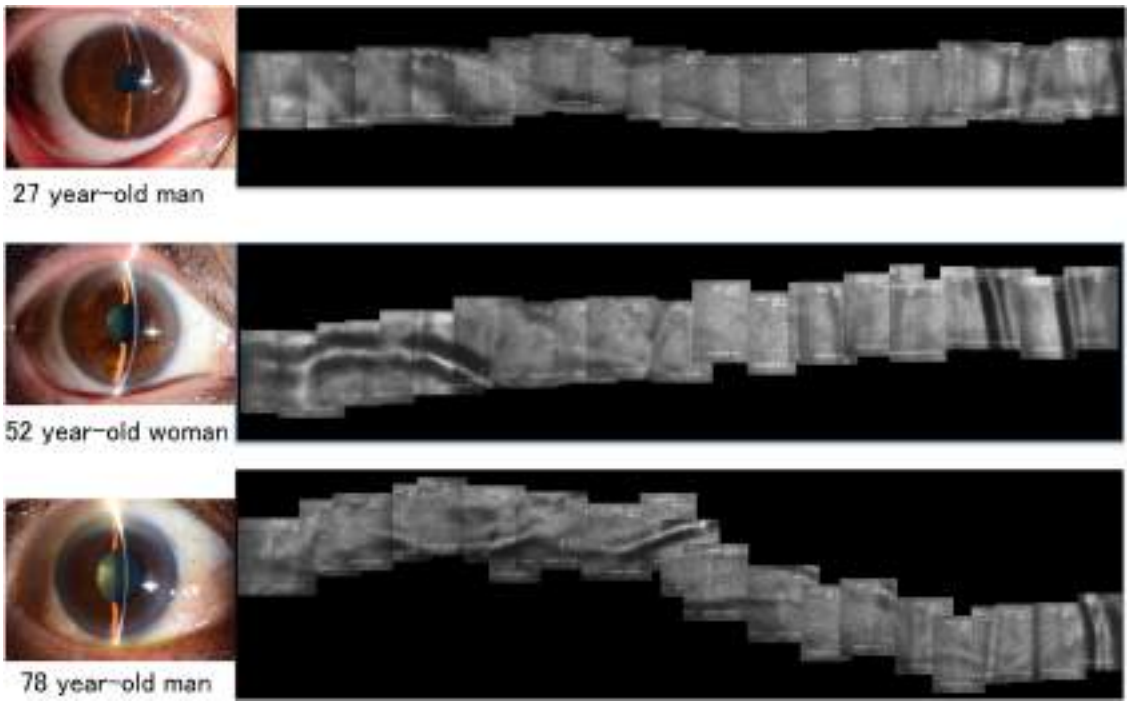

Figure 2 Typical example images including the anterior segment of the eye (left) and endothelial cell layer images (right) of the subjects in the three age groups.

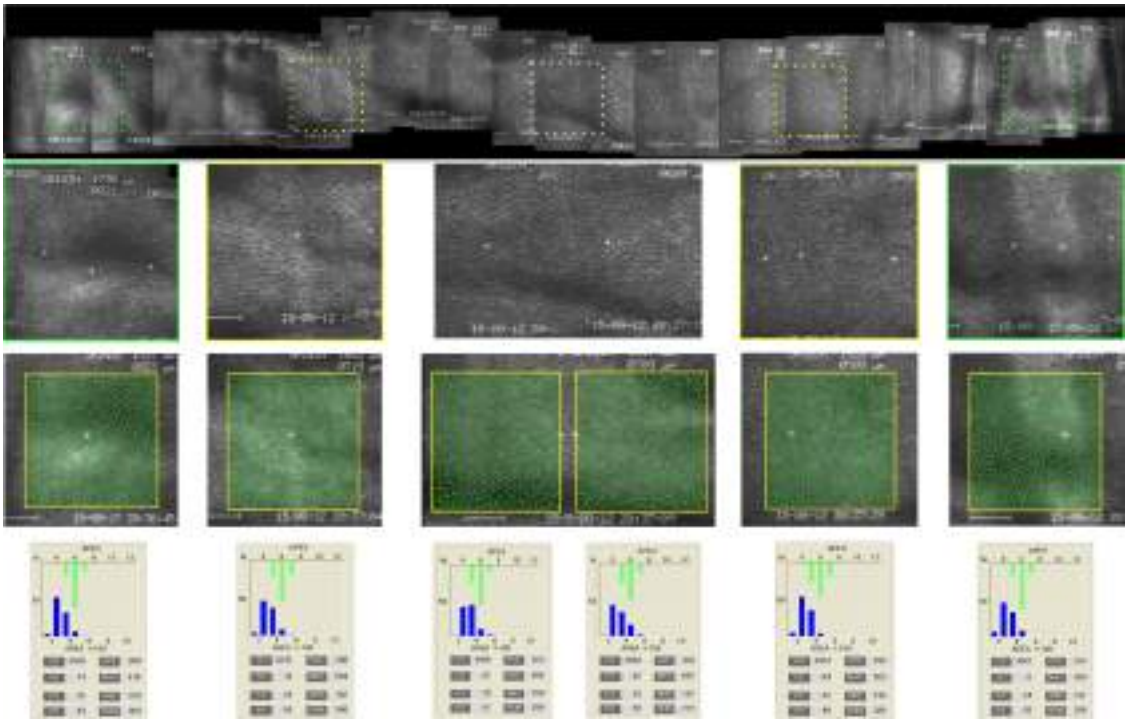

Figure 3 Images showing the measurement method of corneal endothelial cell density in the centre, mid-peripheral and peripheral regions.

and C ($p<0.05$) at the centre. There was no significant difference in the rate of hexagonal shape (6A) was found between the regions in comparison with age.

DISCUSSION

In this study, a new slit-scanning wide-field contact specular microscope was used to successfully obtain a panoramic image of the optically recordable area of the corneal endothelium cell layer from near the surgical limbus to limbus in vivo in healthy subjects over a broad range of ages. Using the obtained results, we were able to identify specific areas of analysis and compare ECD between generations. The results showed a difference of ECD in each region of the cornea in relation to age in normal healthy subjects.

Table 1 Mean endothelial cell density (ECD, cells/mm^2), the rate of hexagonal shape cells (6A) and coefficient of variation (CV) of area in each region in the examined groups

	No. of eyes	Region	ECD (cells/mm^2)	Increased rate in ECD from centre (%)	Hexagonal shape cells (%)	CV
Group A (20–40 years old)	5	Centre	2809±186 (n=10)		54±7	26±3
		Mid-peripheral	2902±248 (n=10)	3.3	55±10	26±6
		Peripheral	2893±308 (n=10)	2.9	57±10	27±4
Group B (41–60 years old)	5	Centre	2717±91 (n=10)		49±5	30±3
		Mid-peripheral	2772±92 (n=10)	2.0	52±6	30±4
		Peripheral	2691±99 (n=10)	−1.0	52±5	31±4
Group C (>60 years old)	5	Centre	2580±129 (n=10)		50±6	32±3
		Mid-peripheral	2604±184 (n=10)	0.9	49±5	32±3
		Peripheral	2533±112 (n=10)	−1.8	42±7	32±3

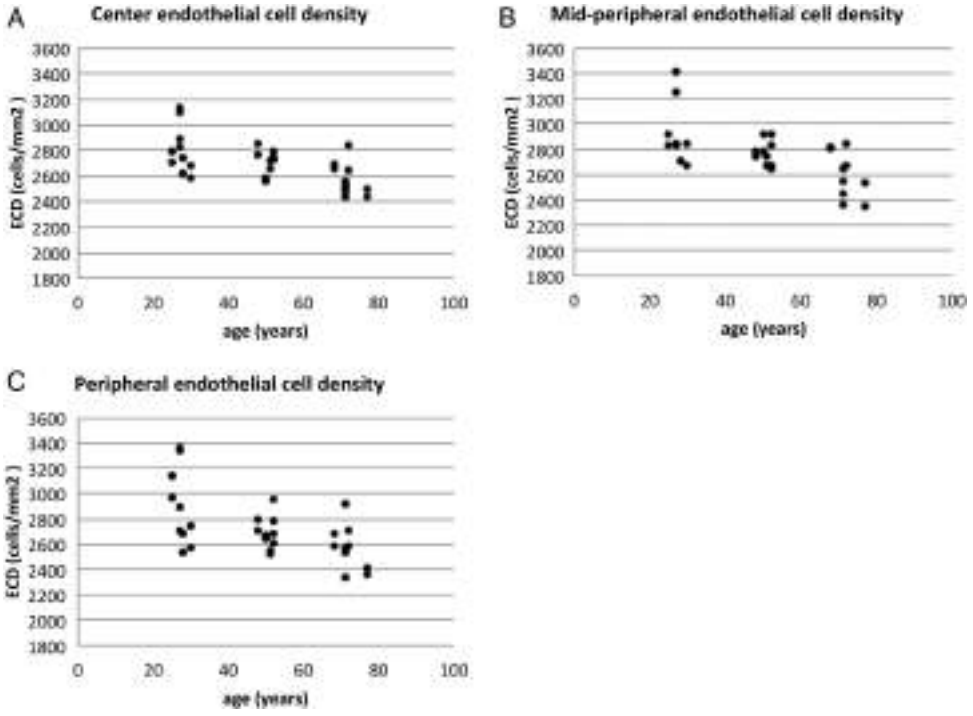

Figure 4 Scatter plot of the centre (A), mid-peripheral (B) and peripheral (C) region corneal endothelial cell density versus age.

Use of the new wide-field contact specular microscope enabled us to observe corneal endothelium, from end-to-end, with ease, as the unique functions of this new instrument allow clinicians to do the following: (1) to record and observe wide-field (0.7 mm×0.5 mm) pictures of CEC layer in real time, thus preventing clinicians from overlooking a local abnormality, (2) to record continuous images of a CEC layer, even in thick corneas, at the edge by manually focusing on the layer of corneal endothelium and by only fixating on one point without depending on patient eye movement, (3) to record sharper images than can be obtained via the use of conventional contact or non-contact specular microscopes, because slit-scanning decrease the corneal scattering. With conventional specular microscopes, the condition of corneal endothelium across the entire cornea cannot be calculated, but only predicted, from the information of several regions depending on the target location. In fact, conventional non-contact specular microscopy allows a clinician to evaluate only the mid-peripheral region, whereas in vitro studies allow for examination of the cell-dense peripheral region close to the Schwalbe's line.[5 11] In contrast to the conventional instruments, the new wide-field contact specular microscopy allows for observation of the corneal endothelium in the more peripheral region in real time, as long as the cornea is transparent. Moreover, a focal change and anomaly of corneal endothelium can be detected on the monitor. In terms of reproducibility when using this device, we previously checked the intra-observer and inter-observer variability (data not shown).

It is vital to be able to monitor corneal endothelial conditions over an extensive area of the cornea post intraocular surgery. For example, the primary postoperative complication seen in patients post angle-supported or iris-fixated phakic intraocular lens (IOL) implantation is endothelial cell loss,[12–14] and a primary concern post corneal transplantations such as Descemet's stripping automated endothelial keratoplasty (DSAEK)[15] and Descemet's membrane endothelial keratoplasty (DMEK)[16 17] is being able to know the dynamics of the transplanted corneal endothelium. As the findings of this study show, as long as the cornea is transparent, wide-field contact specular microscopy allows for the corneal endothelial layer to be observed post these treatments in both wide and specific areas.

One of the greatest improvements that this instrument offers is the ability to identify the area being measured. Although still images at several points on the cornea can be obtained by non-contact specular microscopy, those images lack specific reproducible locations. Using slit-scanning wide-field contact microscope, clinicians can detect the relative location to compare the adjacent cells and Descemet's membrane folds.

It should be noted that one of the limitations of this study was the small number of subjects examined. In this study, the difference of ECD at the centre of the cornea per year of age was 0.21%, similar to that in previous reports.[18 19] No significant difference of ECD in relation to ageing was found at the mid-peripheral area, yet a significant difference was found at the centre and peripheral regions. Anna and associates reported that ECD in the central and peripheral regions has difference with ageing, and that ECD in only older adults showed a significant difference between the central and peripheral areas.[6] Taken together, these results suggest that compared with the central and mid-peripheral areas, endothelial cell loss in the peripheral area is most affected by ageing. All of the subjects involved in this study had no corneal epithelial damage, and it should be noted that when using a contact specular microscope, it is important to be careful to not inflict any ocular surface damage to the patient. Moreover, care should be taken with patients in whom the corneal epithelial layer can easily be detached due to endothelial dysfunction. In such cases, it might be better for the patient to wear a contact lens while undergoing examination by wide-field contact specular microscopy.

In conclusion, the prototype slit-scanning wide-field specular microscope used in this study allowed for a successful topographical distribution analysis of CECs in normal healthy subjects and for a comparison via a panoramic image. Furthermore, slit-scanning wide-field contact specular microscopy allows for observation of CECs post intraocular surgery such as phakic IOL implantation and CEC transplantation (eg, DSAEK or DMEK) to reveal the dynamics of CECs in vivo.

Acknowledgements The authors wish to thank Mr John Bush of Kyoto Prefectural University of Medicine for his excellent and thorough review of the manuscript.

Contributors Design of the study (HT, NO, NK, CS, YS and SK), Acquisition, analysis or interpretation of data (HT), Drafting of the work (HT), and Revising the work (NO, NK, CS, YS and SK), Approval of the final version (HT, NO, NK, CS, YS and SK), Agreement for all aspects of the work (HT, NO, NK, CS, YS and SK).

Competing interests YS is an employee of Konan Medical, Inc.

Patient consent Obtained.

Ethics approval Kyoto Prefectural University of Medicine.

Provenance and peer review Not commissioned; externally peer reviewed.

REFERENCES

1 Matsuda M, Shiozaki Y, Suda T, *et al*. Chronological change of human corneal endothelial cell shape and its arrangement. *Nippon Ganka Gakkai Zasshi* 1982;86:1944–51.
2 Ohara K, Tsuru T. Morphometric parameters of the corneal endothelial cells. *Nippon Ganka Gakkai Zasshi* 1987;91:1073–8.
3 Maurice DM. Cellular membrane activity in the corneal endothelium of the intact eye. *Experientia* 1968;24:1094–5.
4 McCarey BE. Noncontact specular microscopy: a macrophotography technique and some endothelial cell findings. *Ophthalmology* 1979;86:1848–60.
5 Amann J, Holley GP, Lee SB, *et al*. Increased endothelial cell density in the paracentral and peripheral regions of the human cornea. *Am J Ophthalmol* 2003;135:584–90.
6 Roszkowska AM, Colosi P, D'Angelo P, *et al*. Age-related modifications of the corneal endothelium in adults. *Int Ophthalmol* 2004;25:163–6.
7 Blackwell WL, Gravenstein N, Kaufman HE. Comparison of central corneal endothelial cell numbers with peripheral areas. *Am J Ophthalmol* 1977;84:473–6.
8 Wiffen SJ, Hodge DO, Bourne WM. The effect of contact lens wear on the central and peripheral corneal endothelium. *Cornea* 2000;19:47–51.
9 Daus W, Völcker HE, Meysen H. Clinical significance of age-related regional differences in distribution of human corneal endothelium. *Klin Monbl Augenheilkd* 1990;196:449–55.
10 Schimmelpfennig BH. Direct and indirect determination of nonuniform cell density distribution in human corneal endothelium. *Invest Ophthalmol Vis Sci* 1984;1:223–9.
11 He Z, Campolmi N, Gain P, *et al*. Revisited microanatomy of the corneal endothelial periphery: new evidence for continuous centripetal migration of endothelial cells in humans. *Stem Cells* 2012;30:2523–34.
12 Alió JL, Abdelrahman AM, Javaloy J, *et al*. Angle-supported anterior chamber phakic intraocular lens explantation. Causes and outcome. *Ophthalmology* 2006;113:2213–20.
13 Javaloy J, Alió JL, Iradier MT, *et al*. Outcomes of ZB5M angle-supported anterior chamber phakic intraocular lenses at 12 years. *J Refract Surg* 2007;23:147–58.
14 Aerts AAS, Jonker SMR, Wielders LHP, *et al*. Phakic intraocular lens: two-year results and comparison of endothelial cell loss with iris-fixated intraocular lenses. *J Cataract Refract Surg* 2015;41:2258–65.
15 Nakagawa H, Inatomi T, Hieda O, *et al*. Clinical outcomes in Descemet stripping automated endothelial keratoplasty with internationally shipped precut donor corneas. *Am J Ophthalmol* 2014;157:50–5.
16 Jacobi C, Zhivov A, Korbmacher J, *et al*. Evidence of endothelial cell migration after Descemet membrane endothelial keratoplasty. *Am J Ophthalmol* 2011;152:537–42.
17 Hos D, Heindl LM, Bucher F, *et al*. Evidence of donor corneal endothelial cell migration from immune reactions occurring after Descemet membrane endothelial keratoplasty. *Cornea* 2014;33:331–4.
18 Bourne WM, Nelson LR, Hodge DO. Central corneal endothelial cell changes over a ten-year period. *Invest Ophthalmol Vis Sci* 1997;38:779–82.
19 Higa A, Sakai H, Sawaguchi S, *et al*. Corneal endothelial cell density and associated factors in a population-based study in Japan: the Kumejima study. *Am J Ophthalmol* 2010;149:794–9.

Corneal Endothelial Cells Have an Absolute Requirement for Cysteine for Survival

Naoki Okumura, MD, PhD, Ryota Inoue, BS, MS,* Kazuya Kakutani, BS, MS,* Makiko Nakahara, PhD,* Shigeru Kinoshita, MD, PhD,† Junji Hamuro, PhD,‡ and Noriko Koizumi, MD, PhD**

Purpose: The aim of this study was to evaluate which amino acid (s) among the 20 standard protein amino acids is indispensable for the survival of cultured human corneal endothelial cells (HCECs).

Methods: HCECs were cultured in amino acid screening media that were missing 1 specific amino acid, and cell growth was evaluated. After this first selection, we conducted a further evaluation of cell growth in response to the addition of 4 amino acids (cysteine, methionine, valine, and arginine) to amino acid-free culture media. We then evaluated the antioxidant effect of cysteine compared with other antioxidants in terms of apoptosis of HCECs, rabbit corneal endothelial cell (CECs), monkey CECs, and ex vivo human donor corneas.

Results: Culture in an amino acid-free Dulbecco Modified Eagle Medium (DMEM) decreased the cell numbers to 11.0% when compared with culture in normal DMEM. Removal of cysteine, methionine, valine, or arginine from DMEM significantly suppressed cell numbers (27.7%, 61.4%, 75.5%, and 60.6%, respectively) ($P < 0.01$), whereas removal of other amino acids did not significantly decrease cell numbers. A lack of cysteine induced apoptosis, but addition of antioxidants reversed this. Removal of cysteine induced in vitro apoptosis in HCECs, rabbit CECs, monkey CECs, and ex vivo human donor corneas, whereas the presence of cysteine almost completely suppressed this apoptosis.

Conclusions: Cysteine seems to be an indispensable amino acid for HCEC growth and survival. Its necessity might reflect a high requirement for antioxidants to protect HCECs from oxidative stress, as HCECs have high aerobic metabolic activity.

Key Words: amino acid, corneal endothelial cells, antioxidant

(*Cornea* 2017;0:1–7)

Corneal transplantation is presently the only therapy for treating corneal endothelial dysfunction, but new therapeutic options using tissue-engineering techniques are now attracting the attention of a number of researchers.[1–5] For instance, we have shown that the use of a Rho kinase inhibitor promotes efficient engraftment of cultured corneal endothelial cells (CECs) and that injection of CECs in the form of a cell suspension can regenerate the corneal endothelium in rabbit and monkey corneal endothelial dysfunction models.[6,7] Moreover, in 2013, we started a clinical trial involving cell injection therapy at Kyoto Prefectural University of Medicine (Clinical trial registration: UMIN000012534). This clinical trial involves isolation and culture of CECs from human donor corneas. These cultured cells are then injected, together with a Rho kinase inhibitor, into the anterior chamber of the eye (unpublished data). Further clinical data are still required from this ongoing trial, but evidence is accumulating that confirms the safety and efficacy of this novel cell-based therapy as a treatment for corneal endothelial dysfunction.

Cultured CECs for clinical use undergo multiple preparation steps before they are injected by physicians into a patient's eye in the operating room: 1) in vitro expansion (isolation from donor corneas, primary culture on a culture plate, and passage culture),[8–10] 2) preparation and transportation of CECs in the form of a cell suspension (recovery from the culture plate and suspension in the injection vehicle),[11] and 3) injection into the anterior chamber of the eye. Hence, CECs are unavoidably kept under nonphysiological conditions from the time they are isolated from the donor corneas to the time they are injected in the clinical setting. Therefore, the media and vehicles used for these CEC preparation steps should be optimized to minimize exposure to stress by the cells destined for clinical use.

In this study, we conducted experiments to examine which amino acid(s) among the 20 standard protein amino acids is indispensable for survival of isolated human corneal endothelial cells (HCECs). Our aim was to identify amino acids that were absolutely required in the media and vehicles used for cell preparation to minimize damage to HCECs being cultured for use in cell-based therapy.

MATERIALS AND METHODS

Ethics Statement

Human corneas were handled in accordance with the tenets set forth in the Declaration of Helsinki. Informed written consent regarding eye donation for research was obtained from the next of kin of deceased donors. Donor corneas were obtained from SightLife (Seattle, WA). All

Received for publication January 11, 2017; revision received March 28, 2017; accepted April 1, 2017.

From the *Department of Biomedical Engineering, Faculty of Life and Medical Sciences, Doshisha University, Kyotanabe, Japan; Departments of †Frontier Medical Science and Technology for Ophthalmology; and ‡Ophthalmology, Kyoto Prefectural University of Medicine, Kyoto, Japan.

The authors have no funding or conflicts of interest to disclose.

Reprints: Noriko Koizumi, MD, PhD, Department of Biomedical Engineering, Faculty of Life and Medical Sciences, Doshisha University, Kyotanabe 610-0394, Japan (e-mail: nkoizumi@mail.doshisha.ac.jp).

tissue was recovered under the tenets of the Uniform Anatomical Gift Act (UAGA) of the particular state in which the donor consent was obtained and in which the tissue was recovered. Cynomolgus monkey corneas were provided by Nissei Bilis Co, Ltd (Otsu, Japan) after they were killed by an overdose of intravenous pentobarbital sodium for other research purposes. The protocols for the general welfare of the monkeys and the procedures for isolation of the corneas were approved by the institutional animal care and use committee of Nissei Bilis Co, Ltd

Preparation of HCEC Culture Medium

The culture medium for HCECs was prepared as described previously.[9,12] Briefly, confluent NIH-3T3 fibroblasts were incubated for 2 hours with 4 μg/mL mitomycin C (Kyowa Hakkko Kirin Co, Ltd, Tokyo, Japan), and then seeded onto plastic dishes at a cell density of 2×10^4 cells/cm^2. The attached cells were then washed 3 times with Ca^{2+}- and Mg^{2+}-free phosphate-buffered saline (PBS), and the medium was replaced with a basal culture medium containing OptiMEM-I (Life Technologies, Carlsbad, CA), 8% fetal bovine serum (FBS), 5 ng/mL epidermal growth factor (Sigma-Aldrich, St. Louis, MO), 20 μg/mL ascorbic acid (Sigma-Aldrich), 200 mg/L calcium chloride, 0.08% chondroitin sulfate (Sigma-Aldrich), and 50 μg/mL of gentamicin (Life Technologies). The NIH-3T3 cells were maintained for an additional 24 hours, and then the medium was collected and centrifuged at 2000*g* for 10 minutes. The supernatant was filtered through a 0.22-μm filtration unit (EMD Millipore Corporation, Billerica, MA) and used as an HCEC culture medium.

Cultivation of HCECs

Four human donor corneas (from persons older than 40 yrs) were used for HCEC cultivation, as described previously.[9,12] Briefly, the Descemet membrane–corneal endothelium complex was stripped and digested with 1 mg/mL collagenase A (Roche Applied Science, Penzberg, Germany) at 37°C for 2 hours, followed by washing with OptiMEM-I. The HCECs obtained from the individual donor corneas were resuspended in the human CEC culture medium prepared as described above and plated into 2 wells of a 12-well plate coated with FNC Coating Mix (Athena Environmental Sciences, Inc, Baltimore, MD). The HCECs were maintained in a humidified atmosphere at 37°C in 5% CO_2, and the culture medium was replaced with a fresh medium every 2 days. When the cells reached confluency (in 14–28 d), they were rinsed with PBS, trypsinized with 0.05% trypsin–ethylenediaminetetraacetic acid (EDTA) (Life Technologies) for 5 minutes at 37°C, and passaged at 1:2 ratio.

Rabbit and Monkey CEC Culture

Four rabbit eyes and 2 monkey eyes were used for the rabbit corneal endothelial cell (RCEC) culture and monkey corneal endothelial cell (MCEC) culture, respectively. The culture protocol was described previously.[4,6] Briefly, Descemet membrane with RCECs or MCECs was stripped and incubated in 0.6 U/mL of Dispase II (Roche Applied Science) to release the CECs. The isolated CECs were resuspended in the culture medium and seeded on a culture plate coated with FNC Coating Mix (Athena Environmental Sciences, Inc). All primary cell cultures and serial passages were performed in a growth medium composed of Dulbecco Modified Eagle Medium (DMEM; Nacalai Tesque, Kyoto, Japan) supplemented with 10% FBS, 50 U/mL penicillin, 50 μg/mL streptomycin, and 2 ng/mL fibroblast growth factor 2 (Life Technologies).

Screening of Indispensable Amino Acid for HCECs

As the first selection, the effect of removal of individual amino acids was evaluated using amino acid-free DMEM (hereafter referred to as Zero medium; gifted from Ajinomoto

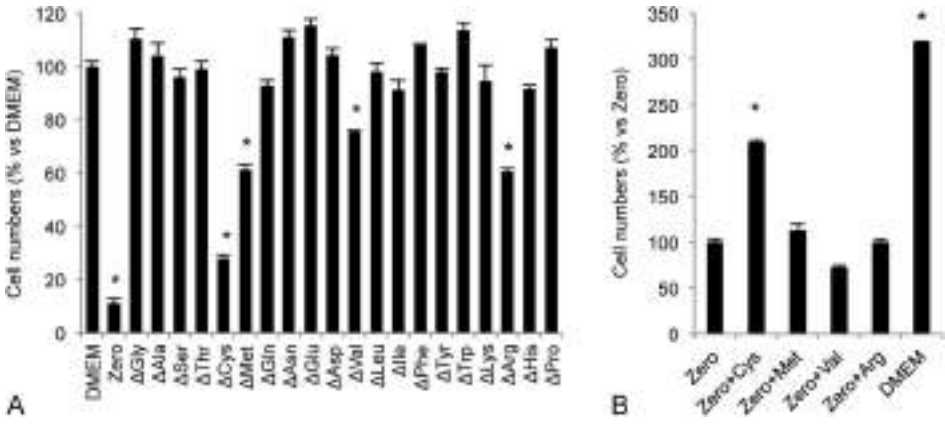

FIGURE 1. Screening of the indispensable amino acid for HCECs. A, HCECs were seeded at a cell density of 5.0×10^3 cells/cm^2 per well in a 96-well plate and were further cultured for 48 hours. The effect of removal of an individual amino acid was evaluated by replacing the culture medium with DMEM from which 1 of 20 amino acids was removed: [glycine (gly), alanine (ala), serine (ser), threonine (thr), cysteine (cys), methionine (met), glutamine (gln), asparagine (asn), glutamic acid (glu), aspartic acid (asp), valine (val), leucine (leu), isoleucine (ile), phenylalanine (phe), tyrosine (tyr), tryptophan (trp), lysine (lys), arginine (arg), histidine (his), and proline (pro)]. DMEM and Zero medium (amino acid-free DMEM culture medium) were used as controls. The number of viable cells was determined after 72 hours of cultivation. $*P < 0.01$. B, Four amino acids (cysteine, methionine, valine, and arginine) were added to Zero medium, and the effect of each amino acid was evaluated on cell numbers. $*P < 0.01$. Experiments were performed in triplicate.

Co, Inc, Tokyo, Japan), and DMEM from which only 1 of each of the 20 protein amino acids was removed (gifted from Ajinomoto Co, Inc). HCECs were seeded at a cell density of 5.0×10^3 cells/cm^2 per well on a 96-well plate with DMEM and were further cultured for 48 hours. The culture medium was then replaced with fresh DMEM, Zero medium, or DMEM from which 1 amino acid was removed, and the cells were further cultured for 72 hours. After this first selection, HCECs were cultured in culture media containing only 1 of the 4 most effective amino acids and cell survival was reevaluated. Namely, the effect of supplementation of cysteine (0.5 mM), methionine (0.5 mM), valine (0.5 mM), arginine (0.5 mM), or their combinations with Zero medium was evaluated. The effects of N-acetylcysteine (NAC; Sigma-Aldrich) (0.05 mM) and ascorbic acid (Wako Pure Chemical Industries, Ltd, Osaka, Japan) (0.1 mM) were also evaluated. The number of viable cells was determined by a CellTiter-Glo Luminescent Cell Viability Assay using a Veritas Microplate Luminometer (Promega, Fitchburg, WI) according to the manufacturer's protocol. Six samples were prepared for each group. Cell morphology was determined by phase contrast microscopy, and cell density was measured using ImageJ software (US National Institutes of Health, Bethesda, MD).

Effect of Amino Acid on Apoptosis

HCECs, RCECs, and MCECs were cultured until confluency, and then further cultured at 37°C for 72 hours

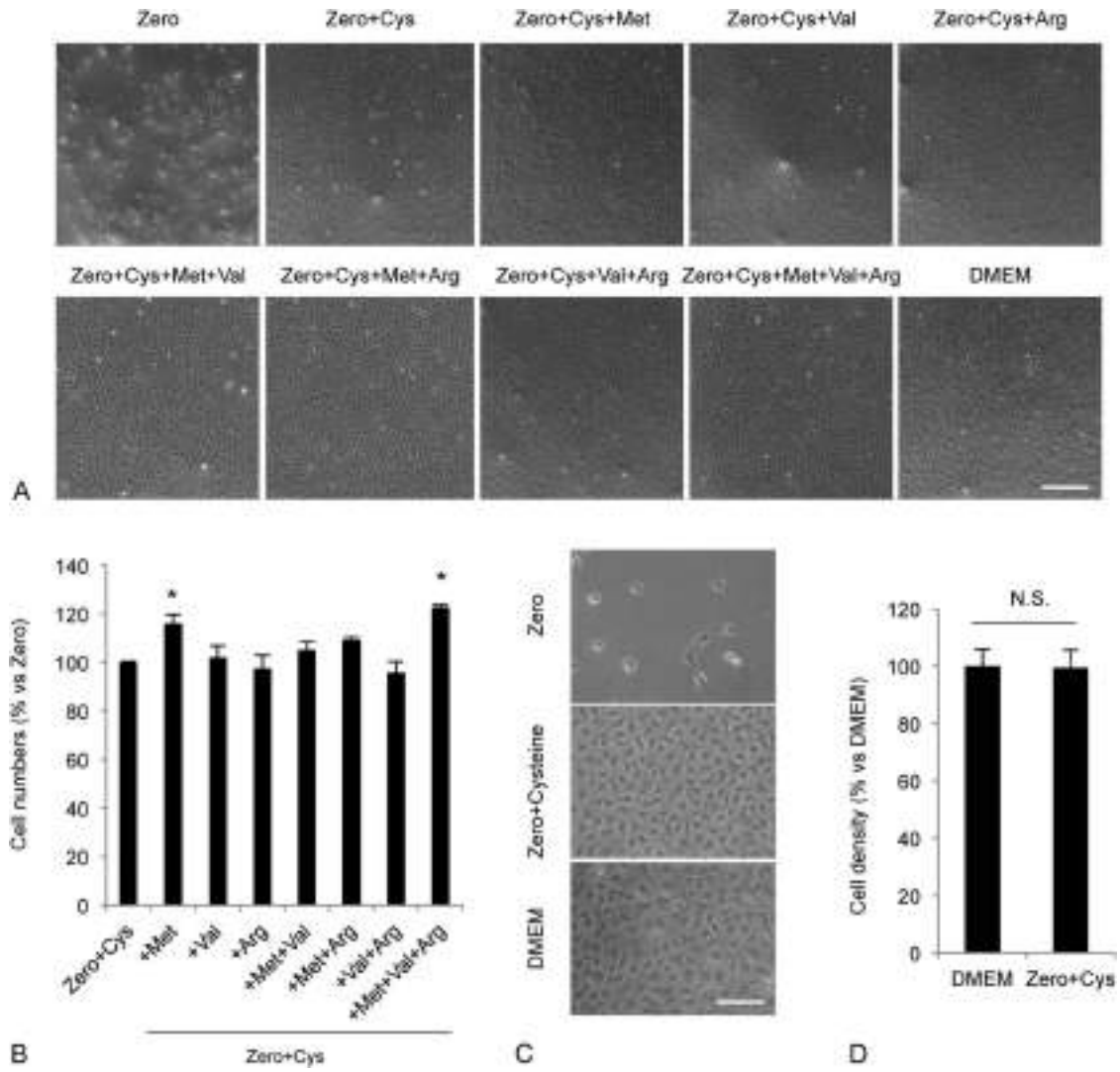

FIGURE 2. Effect of a combination of 4 screened amino acids on HCEC viability. A and B, HCECs were seeded at a cell density of 5.0×10^3 cells/cm^2 per well in a 96-well plate and were further cultured for 48 hours. The culture medium was replaced with a fresh medium consisting of Zero medium (amino acid-free DMEM culture medium) supplemented with cysteine, methionine, valine, or arginine. After 72 hours, cells were observed by phase contrast microscopy. The number of viable cells was determined after 72 hours of cultivation. *$P < 0.01$. C and D, HCECs were cultured in Zero medium or Zero medium supplemented with cysteine until they formed a contact-inhibited sheet-like structure. Cell morphology and density were evaluated by phase contrast microscopy. Scale bar: 50 μm. *$P < 0.01$. Experiments were performed in triplicate.

in Zero medium, Zero medium supplemented with cysteine (0.05 mM), or Zero medium supplemented with cystine (the oxidized dimer form of cysteine; Sigma-Aldrich) (0.05 mM). For ex vivo analysis, 4 human corneas were cut into 4 pieces and cultured at 37°C for 72 hours in Zero medium, or Zero medium supplemented with cysteine (0.05 mM) or ascorbic acid (0.1 mM). After cultivation, the culture medium was replaced with fresh DMEM supplemented with Annexin V and propidium iodide (PI) (Medical & Biological Laboratories Co, Ltd, Aichi, Japan) for 5 minutes. The cells were then fixed for 20 minutes with 4% paraformaldehyde, and excess paraformaldehyde was removed by washing with PBS. Nuclei were stained with DAPI (Vector Laboratories, Burlingame, CA). The slides were examined with a fluorescence microscope (TCS SP2 AOBS; Leica Microsystems, Wetzlar, Germany).

Statistical Analysis

Statistical significance (P value) in mean values of the 2-sample comparison was determined with the Student t test. Statistical significance in the comparison of multiple sample sets was analyzed with the Dunnett multiple-comparisons test. $P < 0.05$ was considered as statistically significant. Results were expressed as mean ± SEM.

RESULTS

Screening of the Indispensable Amino Acid for Corneal Endothelium

We screened for amino acids indispensable to corneal endothelium survival by culturing HCECs in amino acid-free DMEM culture medium (Zero medium) or in media in which 1 amino acid (glycine, alanine, serine, threonine, cysteine, methionine, glutamine, asparagine, glutamic acid, aspartic acid, valine, leucine, isoleucine, phenylalanine, tyrosine, tryptophan, lysine, arginine, histidine, or proline) was removed. Cell numbers were decreased to 11.0% by Zero medium after 72 hours of cultivation when compared with culture in DMEM. Removal of cysteine, methionine, valine, or arginine significantly suppressed cell numbers (27.7%, 61.4%, 75.5%, and 60.6%, respectively) ($P < 0.01$), whereas removal of any of the other amino acid did not significantly alter cell numbers (Fig. 1A). We next added cysteine, methionine, valine, or arginine to Zero medium and evaluated the effect of each amino acid on cell numbers. Only supplementation with cysteine to Zero medium significantly increased cell numbers ($P < 0.01$) (Fig. 1B). Next, we evaluated the combination of all 4 amino acids. Phase contrast images showed that HCECs cultured with medium supplemented with cysteine showed similar cell morphology and confluency to cells cultured in DMEM (Fig. 2A). Cell numbers were similar when the other amino acids were added in addition to cysteine, although cell numbers were slightly increased when HCECs were cultured with medium supplemented with cysteine and methionine or with cysteine, methionine, valine, and arginine, when compared with cysteine alone ($P < 0.01$) (Fig. 2B).

Cell density is accepted as one of the most important indicators of corneal endothelium health. Therefore, we cultured HCECs until they formed contact-inhibited sheet-like structures, and then we evaluated cell morphology and density. Phase contrast images showed that supplementation with cysteine alone enabled formation of the sheet-like structure with hexagonal morphology seen after DMEM culture and resulted in a cell density similar to that seen with DMEM culture (Figs. 2C, D).

Effect of Cysteine and Antioxidants on the Survival of Corneal Endothelial Cells

We examined the effect of cysteine concentration on corneal endothelium survival by culturing HCECs in Zero medium supplemented with various concentrations of cysteine for 72 hours. Cell numbers were significantly increased by cysteine, when added at 0.00195 to 0.5 mM (especially

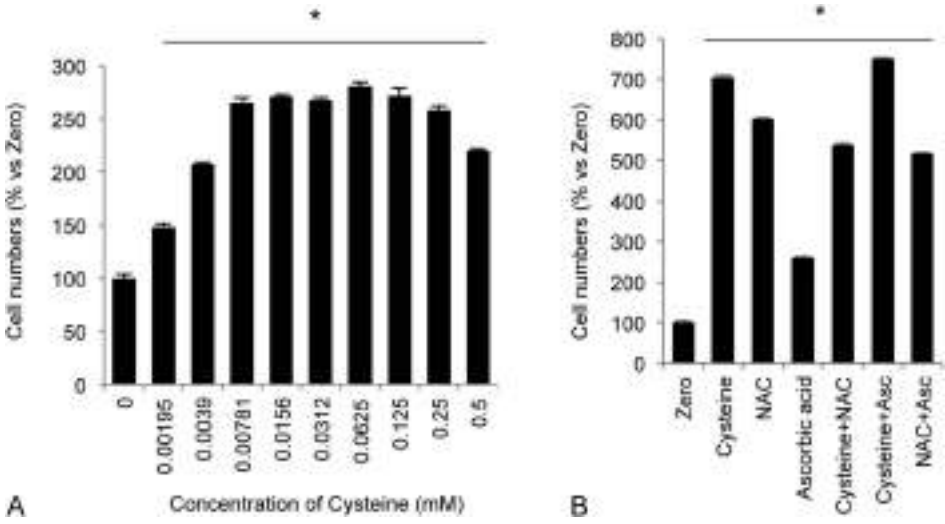

FIGURE 3. Effect of cysteine and antioxidants on the survival of HCECs. A, HCECs were seeded at a cell density of 5.0×10^3 cells/cm^2 per well in a 96-well plate and were further cultured for 48 hours. The medium was replaced with a fresh medium consisting of Zero medium (amino acid-free DMEM culture medium) supplemented with cysteine at various concentrations. The number of viable cells was determined after 72 hours of cultivation. *$P < 0.01$. B, HCECs were seeded in Zero medium supplemented with cysteine (0.5 mM), N-acetylcysteine (NAC, 0.05 mM), and ascorbic acid (0.1 mM), and the number of viable cells was determined after 72 hours of cultivation. *$P < 0.01$. Experiments were performed in duplicate.

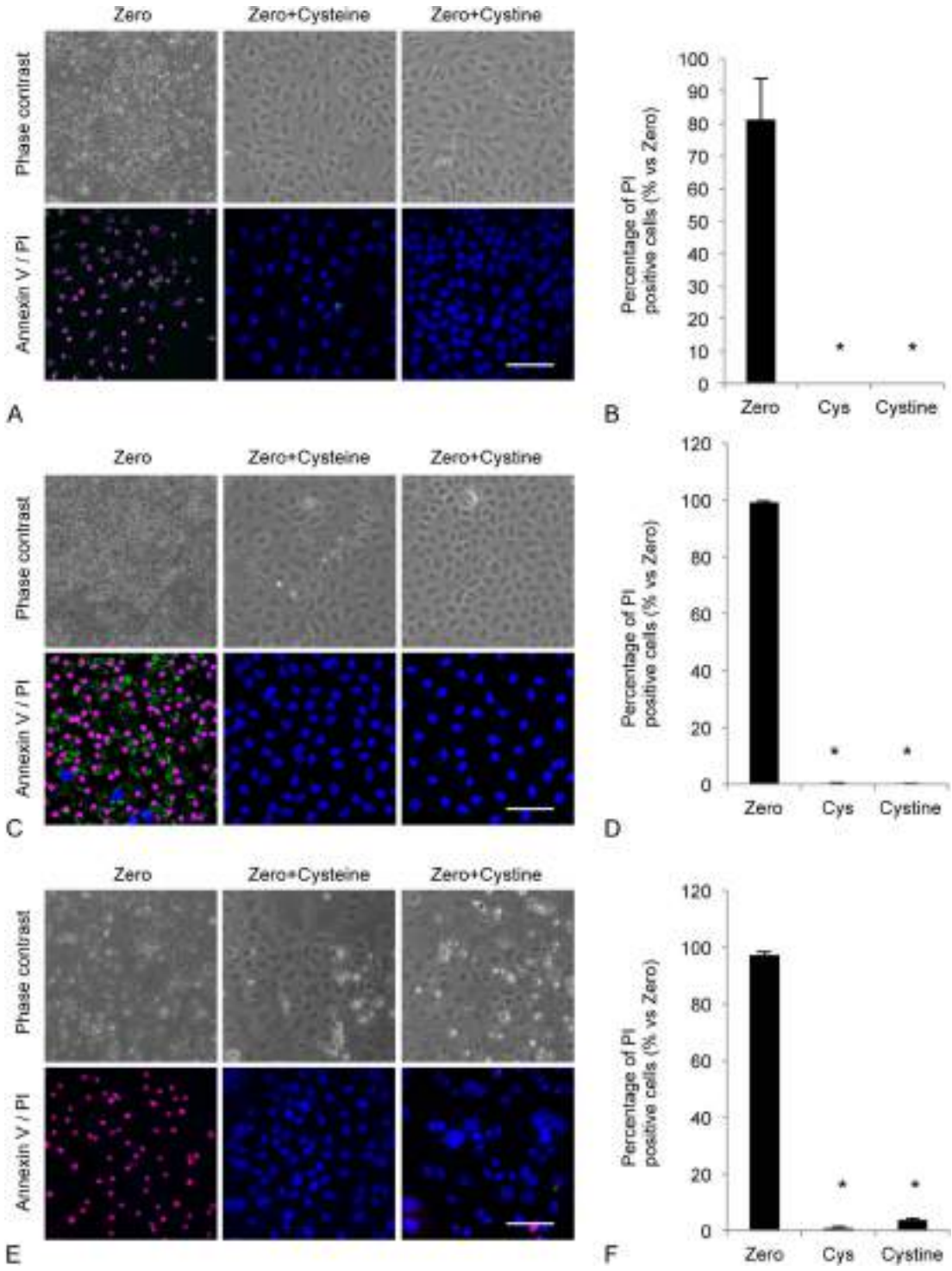

FIGURE 4. Effect of cysteine on apoptosis. A and B, HCECs were seeded and cultured until confluent. The culture medium was then replaced with Zero medium (amino acid-free DMEM culture medium), Zero medium supplemented with cysteine, or Zero medium supplemented with cystine, which is the oxidized dimer form of cysteine and is a more stable form of cysteine. After 72 hours of cultivation, the antiapoptotic effects of cysteine and cystine were evaluated by Annexin V and PI staining. Nuclei were stained with DAPI. The percentage of PI-positive cells was plotted in a graph. Scale bar: 50 μm. *$P < 0.01$. C and D, The antiapoptotic effect of cysteine and cystine was evaluated in cultured RCECs. Scale bar: 50 μm. *$P < 0.01$. E and F, The antiapoptotic effect of cysteine and cystine was evaluated in cultured MCECs. All experiments were performed at least in triplicate. Scale bar: 50 μm. *$P < 0.01$.

0.00781–0.25 mM) (Fig. 3A). Cysteine plays various important roles in the regulation of biological functions, and its strong antioxidant property is one of its characteristic features.[13–16] We evaluated the effect of other antioxidants on HCECs and demonstrated that NAC and ascorbic acid also prevented the decrease in the cell number induced by a lack of cysteine (Fig. 3B).

We next evaluated the protective role of cysteine and its more stable dimer form, cystine, on cell survival. Annexin V and PI staining showed that almost all HCECs, after 72 hours of cultivation in Zero medium, were Annexin V-positive, early apoptotic cells or were PI-positive, late apoptotic cells. By contrast, HCECs cultured in Zero medium supplemented with cystine or cysteine showed little apoptosis ($P < 0.01$) (Figs. 4A, B). Likewise, cystine and cysteine significantly suppressed cell death of cultured RCECs (Figs. 4C, D) and MCECs (Figs. 4E, F) ($P < 0.01$).

We conducted ex vivo experiments using human donor corneas. After 72 hours of organ culture in Zero medium, Annexin V-positive early apoptotic cells or PI-positive late apoptotic cells were evident, whereas very few positive cells were observed after culture in Zero medium supplemented with cystine or ascorbic acid (Fig. 5A). The percentage of PI-positive, late apoptotic cells was 89.2% in Zero medium, but almost no PI-positive cells were observed after culture in Zero medium supplemented with cystine or ascorbic acid ($P < 0.01$) (Fig. 5B).

DISCUSSION

Amino acid metabolism is a central part of cellular metabolic homeostasis. The 20 protein amino acids make fundamental contributions to cellular functions, such as biosynthesis of proteins, nucleotides, lipids, glutathiones, and polyamines.[17] Amino acid metabolism is flexible and highly dependent on the type of tissues and environment.[17] However, the effects of amino acids on corneal endothelium function remain unclear. In this study, we screened the 20 protein amino acids using specially designed media lacking 1 specific amino acid and showed that cysteine, methionine, valine, and arginine play important roles in the survival of CECs. We demonstrated that CEC survival and growth were severely impaired in the absence of cysteine in the culture medium, but the CECs showed surprising survival when cultured in media deficient in other amino acids.

Cysteine is required for general protein biosynthesis, but it is unique because it is also required for the biosynthesis of glutathione, in which it is a rate-limiting precursor.[13–16] Glutathione is a tripeptide thiol consisting of glutamate, cysteine, and glycine and is essential for the prevention of damage induced by reactive oxygen species (ROS), which generate free radical peroxides and lipid peroxides.[15,18,19] ROS are produced as a consequence of cellular activity, including the activity of mitochondria and NADPH oxidases. When ROS production exceeds the capacity of the cell to reduce them, ROS can damage DNA, lipids, and proteins.[18,19] One role of glutathione is to reduce ROS, but intracellular glutathione has a short half-life. Consequently, a lack of cysteine results in rapid glutathione depletion.[20] In this study, the presence of cysteine, but not other amino acids, was found to be crucial for CEC survival. The short half-life of glutathione could be a reasonable explanation for the finding that CECs require cysteine from the environment (from the culture medium in the current experiments).

One phenotypic feature of CECs is their metabolic pump function, by which transporters for sodium (Na^+) and bicarbonate (HCO_3^-) maintain an osmotic gradient. This pump function requires metabolic energy, and the numerous mitochondria in CECs give these cells the second highest aerobic metabolic rate among cells in the eye (the retinal photoreceptors have the highest rate).[21] Much research has indicated that CECs are sensitive to ROS, probably because of their high aerobic metabolic activity.[22–27] The corneal endothelium always contains high levels of antioxidants under physiological conditions in the form of glutathione and ascorbic acid, which are highly regulated in the aqueous humor.[21] We showed that antioxidants such as NAC and ascorbic acid attenuated the cell death attributed to the lack of cysteine. Likewise, Kim et al[28] reported that addition of NAC to cultured bovine CECs counteracted cell death mediated by oxidative stress or endoplasmic reticulum stress. These results support an important antioxidant role of cysteine in counteracting the ROS arising from the high aerobic metabolic activity of the CECs.

ROS are often discussed in the context of oxidative stress, but ROS are not only a toxic byproduct of mitochondrial respiration, they are also involved in physiological cell

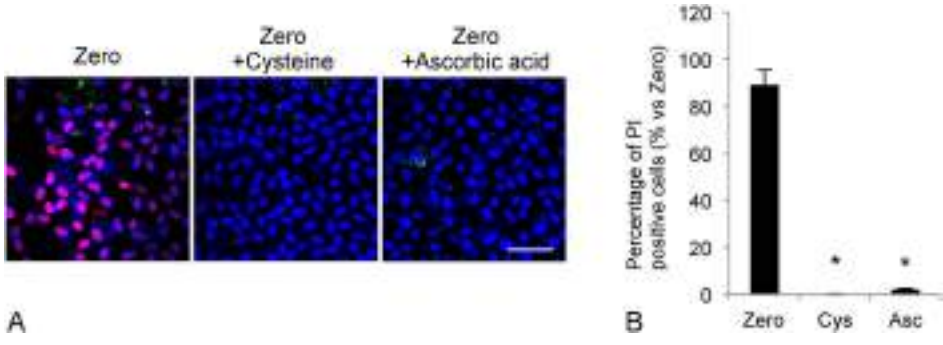

FIGURE 5. Ex vivo evaluation of the antiapoptotic effect of cysteine. A, Human donor corneas were cultured in Zero medium (amino acid-free DMEM culture medium), or in Zero medium supplemented with cysteine (0.05 mM) or ascorbic acid (0.1 mM) at 37°C. After cultivation for 72 hours, samples were stained with Annexin V and PI. Nuclei were stained with DAPI. Scale bar: 50 μm. B, The percentages of PI-positive cells were plotted in a graph. *$P <$ 0.01. Experiments were performed with 4 independent donor corneas.

signaling processes regulated by oxidative conditions.[29] ROS-dependent posttranslational modifications often involve the thiol side chain of cysteine (the most sensitive redox transformation), which suggests an important role of cysteine in redox regulation.[16] Indeed, abnormal levels of cysteine cause various disease conditions, including slow growth in children, liver damage, edema, lethargy, impaired survival in HIV-infected individuals, metabolic disorders, and tumor progression.[13,30] Further research is needed to elucidate the role of cysteine in oxidative posttranslational modifications in CECs.

We originally intended to conduct this study to optimize the amino acid formula for the culture medium and transportation and injection vehicles required to sustain CECs used in the settings of cell-based therapy. The finding that an absolute requirement was evident only for cysteine was unexpected. However, the finding that CECs can survive without supplementation with other amino acids suggests that the roles of other amino acids, apart from cysteine, can be maintained by intracellular production. This finding may also reflect the flexibility and redundancy of the other amino acids in terms of their biological roles. One limitation of our study is that cysteine, which we found indispensable for CECs, is included in many of the commonly used culture media, and then we could not offer a new culture medium or vehicle including appropriate combination of amino acids. However, our data are still important, as we provide evidence that the culture medium usually used for CEC cultivation includes sufficient quantities of all amino acids. In addition, our results indicate that CECs are easily impaired by oxidative stress and require sufficient antioxidants in their surrounding environment.

In conclusion, amino acid screening demonstrated that cysteine is an indispensable amino acid for the growth and survival of CECs. This necessity might reflect the high requirement for antioxidants to protect CECs from ROS, as CECs have high aerobic mitochondrial activity because of their vital pump functions in the eye. Precautions should therefore be taken to protect CECs from oxidative stress throughout the whole procedure used to prepare these cells for cell-based therapy.

ACKNOWLEDGMENTS

The authors thank Drs Akira Okano and Kenji Takehana for valuable discussion regarding amino acids and thank Ajinomoto Co, Inc for providing culture media.

REFERENCES

1. Ishino Y, Sano Y, Nakamura T, et al. Amniotic membrane as a carrier for cultivated human corneal endothelial cell transplantation. *Invest Ophthalmol Vis Sci.* 2004;45:800–806.
2. Mimura T, Yamagami S, Yokoo S, et al. Cultured human corneal endothelial cell transplantation with a collagen sheet in a rabbit model. *Invest Ophthalmol Vis Sci.* 2004;45:2992–2997.
3. Mimura T, Yamagami S, Yokoo S, et al. Sphere therapy for corneal endothelium deficiency in a rabbit model. *Invest Ophthalmol Vis Sci.* 2005;46:3128–3135.
4. Koizumi N, Sakamoto Y, Okumura N, et al. Cultivated corneal endothelial cell sheet transplantation in a primate model. *Invest Ophthalmol Vis Sci.* 2007;48:4519–4526.
5. Hatou S, Yoshida S, Higa K, et al. Functional corneal endothelium derived from corneal stroma stem cells of neural crest origin by retinoic acid and Wnt/β-catenin signaling. *Stem Cells Dev.* 2013;22:828–839.
6. Okumura N, Koizumi N, Ueno M, et al. ROCK inhibitor converts corneal endothelial cells into a phenotype capable of regenerating in vivo endothelial tissue. *Am J Pathol.* 2012;181:268–277.
7. Okumura N, Sakamoto Y, Fujii K, et al. Rho kinase inhibitor enables cell-based therapy for corneal endothelial dysfunction. *Sci Rep.* 2016;6:26113.
8. Okumura N, Ueno M, Koizumi N, et al. Enhancement on primate corneal endothelial cell survival in vitro by a ROCK inhibitor. *Invest Ophthalmol Vis Sci.* 2009;50:3680–3687.
9. Nakahara M, Okumura N, Kay EP, et al. Corneal endothelial expansion promoted by human bone marrow mesenchymal stem cell-derived conditioned medium. *PLoS One*. 2013;8:e69009.
10. Okumura N, Kay EP, Nakahara M, et al. Inhibition of TGF-beta signaling enables human corneal endothelial cell expansion in vitro for use in regenerative medicine. *PLoS One*. 2013;8:e58000.
11. Okumura N, Kakutani K, Inoue R, et al. Generation and feasibility assessment of a new vehicle for cell-based therapy for treating corneal endothelial dysfunction. *PLoS One*. 2016;11:e0158427.
12. Okumura N, Kusakabe A, Hirano H, et al. Density-gradient centrifugation enables the purification of cultured corneal endothelial cells for cell therapy by eliminating senescent cells. *Sci Rep.* 2015;5:15005.
13. Herzenberg LA, De Rosa SC, Dubs JG, et al. Glutathione deficiency is associated with impaired survival in HIV disease. *Proc Natl Acad Sci U S A.* 1997;94:1967–1972.
14. Griffith OW. Biologic and pharmacologic regulation of mammalian glutathione synthesis. *Free Radic Biol Med.* 1999;27:922–935.
15. Townsend DM, Tew KD, Tapiero H. The importance of glutathione in human disease. *Biomed Pharmacother.* 2003;57:145–155.
16. Weerapana E, Wang C, Simon GM, et al. Quantitative reactivity profiling predicts functional cysteines in proteomes. *Nature*. 2010;468:790–795.
17. Lukey MJ, Katt WP, Cerione RA. Targeting amino acid metabolism for cancer therapy. *Drug Discov Today.* 2016;16:30480–30489.
18. Reddie KG, Carroll KS. Expanding the functional diversity of proteins through cysteine oxidation. *Curr Opin Chem Biol.* 2008;12:746–754.
19. Izquierdo-Alvarez A, Ramos E, Villanueva J, et al. Differential redox proteomics allows identification of proteins reversibly oxidized at cysteine residues in endothelial cells in response to acute hypoxia. *J Proteomics.* 2012;75:5449–5462.
20. Lo M, Wang YZ, Gout PW. The x(c)- cystine/glutamate antiporter: a potential target for therapy of cancer and other diseases. *J Cell Physiol.* 2008;215:593–602.
21. Dawson GD, Ubels LJ, Edelhauser FH. *Chapter 4 Cornea and Sclera*. 11th ed. Amsterdam, The Netherlands: Elsevier Inc; 2011.
22. Koh SW, Waschek JA. Corneal endothelial cell survival in organ cultures under acute oxidative stress: effect of VIP. *Invest Ophthalmol Vis Sci.* 2000;41:4085–4092.
23. Behndig A, Karlsson K, Brannstrom T, et al. Corneal endothelial integrity in mice lacking extracellular superoxide dismutase. *Invest Ophthalmol Vis Sci.* 2001;42:2784–2788.
24. Serbecic N, Beutelspacher SC. Anti-oxidative vitamins prevent lipid-peroxidation and apoptosis in corneal endothelial cells. *Cell Tissue Res.* 2005;320:465–475.
25. Murano N, Ishizaki M, Sato S, et al. Corneal endothelial cell damage by free radicals associated with ultrasound oscillation. *Arch Ophthalmol.* 2008;126:816–821.
26. Shin YJ, Kim JH, Seo JM, et al. Protective effect of clusterin on oxidative stress-induced cell death of human corneal endothelial cells. *Mol Vis.* 2009;15:2789–2795.
27. Joyce NC, Zhu CC, Harris DL. Relationship among oxidative stress, DNA damage, and proliferative capacity in human corneal endothelium. *Invest Ophthalmol Vis Sci.* 2009;50:2116–2122.
28. Kim EC, Meng H, Jun AS. N-Acetylcysteine increases corneal endothelial cell survival in a mouse model of Fuchs endothelial corneal dystrophy. *Exp Eye Res.* 2014;127:20–25.
29. Li P, Wu M, Wang J, et al. NAC selectively inhibit cancer telomerase activity: a higher redox homeostasis threshold exists in cancer cells. *Redox Biol.* 2016;8:91–97.
30. Shahrokhian S. Lead phthalocyanine as a selective carrier for preparation of a cysteine-selective electrode. *Anal Chem.* 2001;73:5972–5978.

Hindawi
Journal of Ophthalmology
Volume 2017, Article ID 2646904, 8 pages
https://doi.org/10.1155/2017/2646904

Review Article

Application of Rho Kinase Inhibitors for the Treatment of Corneal Endothelial Diseases

Naoki Okumura,[1] Shigeru Kinoshita,[2] and Noriko Koizumi[1]

[1]*Department of Biomedical Engineering, Faculty of Life and Medical Sciences, Doshisha University, Kyotanabe, Japan*
[2]*Department of Frontier Medical Science and Technology for Ophthalmology, Kyoto Prefectural University of Medicine, Kyoto, Japan*

Correspondence should be addressed to Noriko Koizumi; nkoizumi@mail.doshisha.ac.jp

Received 2 March 2017; Accepted 5 June 2017; Published 2 July 2017

Academic Editor: Neil Lagali

ROCK (Rho kinase) signaling regulates a wide spectrum of fundamental cellular events and is involved in a variety of pathological conditions. It has therefore attracted research interest as a potential therapeutic target for combating various diseases. We showed that inhibition of ROCK enhances cell proliferation, promotes cell adhesion onto a substrate, and suppresses apoptosis of corneal endothelial cells (CECs). In addition, we reported that a ROCK inhibitor enhances wound healing in the corneal endothelium in animal models and in pilot clinical research. We also demonstrated the usefulness of a ROCK inhibitor as an adjunct drug in tissue engineering therapy as it enhances the engraftment of CECs onto recipient corneas. In 2013, we initiated a clinical trial to test the effectiveness of injection of cultured human CECs into the anterior chamber of patients with corneal endothelial decompensation. This paper reviews the accumulating evidence supporting the potency of ROCK inhibitors in clinical use, both as eye drops and as adjunct drugs in cell-based therapies, for the treatment of corneal endothelial decompensation.

1. Introduction

The corneal endothelium, through its pump-and-leak barrier functions, maintains corneal transparency by regulating the amount of water inside the corneal stroma. One clinical feature of the corneal endothelial cell (CEC) phenotype is poor regenerative ability, as CECs have severely limited proliferative capacity [1]. Consequently, any damage to the corneal endothelium is repaired by compensatory migration and spreading of the residual CECs to cover the wounded area, with a resulting drop in the CEC density. This density is typically 2000–2500 cells/mm^2 in a normal subject, and a drop below a critical level, usually less than 500–1000 cells/mm^2, can result in a hazy cornea due to decompensation of the corneal epithelium.

The only current therapeutic choice for treating corneal endothelial decompensation is corneal transplantation using donor corneas [2]. Penetrating keratoplasty, in which a whole-thickness cornea is replaced with a donor cornea, has been performed since 1906 [3]. Descemet's stripping endothelial keratoplasty (DSEK) was introduced in the clinical setting in the last decade to reduce the invasiveness of penetrating keratoplasty and to improve clinical outcomes and is now performed routinely worldwide, largely replacing penetrating keratoplasty. The further introduction and gradual adoption of Descemet's membrane endothelial keratoplasty (DMEK) is now resulting in higher recovery of visual quality even in comparison to DSEK [4].

The evolution of surgical procedures has enabled less invasive treatment of corneal endothelial decompensation with better clinical outcomes. However, these surgeries still have associated issues, such as the difficulty of the actual surgical technique, graft rejection, acute and chronic cell loss, and the shortage of donor corneas. Therefore, new and innovative therapies are still in great demand. One research direction focuses on tissue engineering therapy, and another is pharmaceutical treatment (Figure 1). We have proposed the use of Rho kinase (ROCK) inhibitors for both pharmaceutical and tissue engineering treatments, and our preliminary results in clinical research indicate success for both

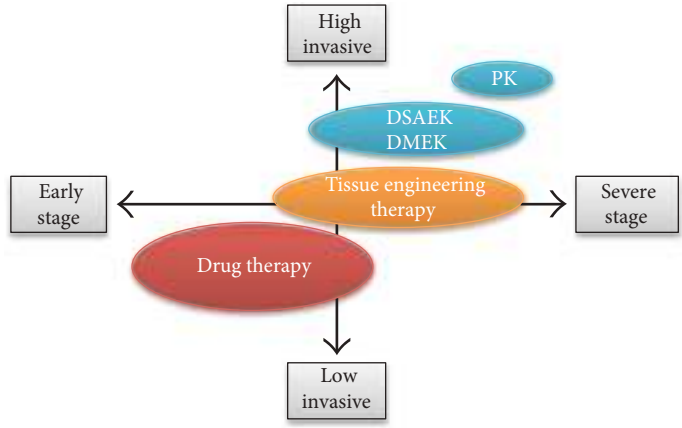

Figure 1: Future treatment strategies for corneal endothelial decompensation. Pharmaceutical treatments and tissue engineering therapies are possible innovative therapeutic modalities. Reproduced from Okumura [49].

applications. This review provides an overview of the research into ROCK inhibitors and their potential for the clinical treatment of corneal endothelial decompensation.

2. ROCK Signaling as a Potent Therapeutic Target for Various Diseases

Rho is a small GTPase that is activated by guanine nucleotide exchange factors (GEFs). Upon binding to GTP, RhoA activates ROCK, a serine/threonine kinase that phosphorylates various substrates. ROCK, initially isolated as a GTP-bound protein, has two isoforms, ROCK I and ROCK II, which share a 60% similarity in amino acid sequence and a 90% similarity in the kinase domain [5, 6]. ROCK signaling regulates a wide spectrum of fundamental cellular events, such as cell adhesion, motility, proliferation, differentiation, and apoptosis [6, 7]. ROCK signaling is involved in variety of diseases, including vascular disease, cancer, asthma, insulin resistance, kidney failure, osteoporosis, neuronal degenerative disease, and glaucoma [8–10]. ROCK signaling has therefore attracted interest as a potential therapeutic target for these diseases.

Two ROCK inhibitors have been approved for use in the clinical setting. Fasudil was approved in 1995 in Japan, where it is used to suppress cerebral vasospasm by inhibition of actomyosin contraction [9]. Ripasudil was approved in Japan in 2014 in an eye drop form to increase the outflow of the aqueous humor as a treatment for glaucoma and ocular hypertension [11].

The importance of ROCK signaling is generally accepted in a wide spectrum of cellular events and pathological conditions; however, its role varies depending on cell type and cell status [12]. In 2009, we found that the use of a selective ROCK inhibitor, Y-27632, enhanced CEC proliferation, promoted CEC adhesion onto a substrate, and suppressed CEC apoptosis [13]. These findings confirmed that the use of a ROCK inhibitor could greatly improve our ability to culture CECs for subsequent application in tissue engineering therapies. However, we quickly discovered that the benefits of ROCK inhibitor use were not limited only to efficient cell cultivation.

3. ROCK Inhibitors Can Promote Wound Healing in the Corneal Endothelium

Early studies showed that inactivation of Rho blocks serum-stimulated DNA synthesis, whereas activation of RhoA induces G_1/S progression in 3T3 fibroblasts [14, 15]. A majority of subsequent studies confirmed that inhibition of the Rho/ROCK signaling pathway suppresses cell cycle progression in various types of cells, including lung carcinoma, melanoma, and kidney tumor cells [16–18]. However, our analysis showed that treatment of CECs with a ROCK inhibitor increased cyclin D levels and suppressed phosphorylation of $p27^{kip1}$ by activation of phosphatidylinositol 3-kinase signaling [19]. Cyclin D and p27 are regulators of the G_1/S progression, so this explained how ROCK inhibition promoted the proliferation of CECs [19]. Subsequent researchers also demonstrated that the use of the ROCK inhibitor Y-27632 increased cell proliferation [20], although one study found no enhanced CEC proliferation following Y-27632 treatment [21]. Peh and colleagues explained this discrepancy by suggesting that CECs derived from young donors are more responsive to Y-27632 and the effect of ROCK inhibition can vary depending on the status of the cornea [20]. More studies are needed to clarify the role of corneal status on the response to ROCK inhibitors and promotion of CEC proliferation.

4. ROCK Inhibitor Eye Drops Promote Wound Healing in the Corneal Endothelium of Animal Models

The administration of a ROCK inhibitor in an eye drop form promoted corneal endothelial wound healing in a rabbit model in which the central corneal endothelium was damaged with a stainless steel cryoprobe (6 mm diameter) [19, 22]. Two ROCK inhibitors, Y-27632 and Y-39983, enhanced the rate of wound healing and accelerated the recovery of corneal transparency. The numbers of Ki67-positive proliferating cells were also increased by administration of the eye drops, suggesting that ROCK inhibition

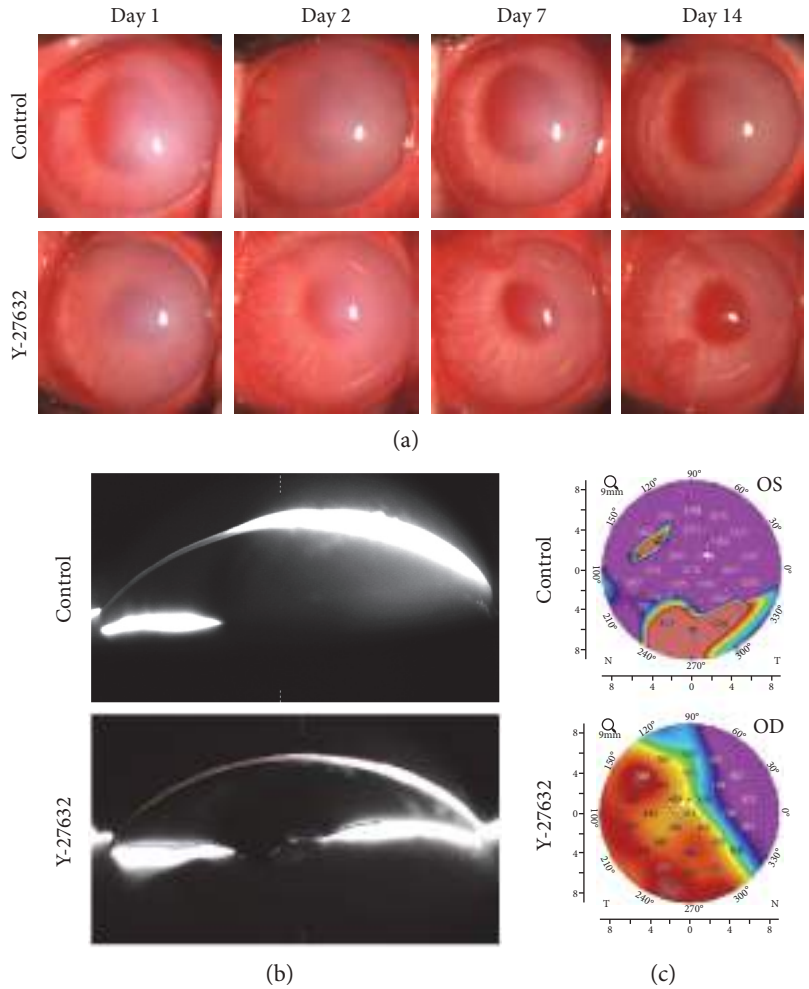

Figure 2: Effect of Y-27632 on wound healing in a corneal endothelial damage rabbit model. (a) Half of the corneal endothelium area was mechanically scraped. Y-27632 (10 mM) diluted in phosphate-buffered saline (PBS) was applied topically 6 times daily, and PBS was applied 6 times daily as a control. Corneal transparency was assessed by slit-lamp microscopy for 14 days ($n = 6$). Representative anterior segment images are shown. (b, c) Anterior segments were also evaluated with a Pentacam®. Representative Scheimpflug images and corneal thickness maps obtained with the Pentacam HR are shown. Values in the corneal thickness map are indicated in μm. Reproduced from Okumura et al. [27].

promoted CEC proliferation both in vitro and in vivo. However, the rabbit corneal endothelium has proliferative ability, whereas this ability is limited in the primate model and in humans [23–25]. We confirmed that ROCK inhibitor eye drops promoted similar corneal endothelial wound healing in the primate animal model to that observed in the rabbit model [26].

The cryoprobe damaged both the corneal epithelium and the corneal endothelium, so we used a different rabbit model, in which a semicircular area accounting for 50% of the corneal endothelium was scraped from the Descemet's membrane with a 20-gauge silicone needle [27, 28]. The use of ROCK inhibitor eye drops in this surgical model also resulted in enhanced wound healing and a significant increase in Ki67-positive proliferating cells when compared with the use of the vehicle in control eyes. Five out of 6 control eyes exhibited hazy corneas due to corneal endothelial decompensation after 2 weeks, but 6 out of 6 eyes treated with Y-27632 drops exhibited transparent corneas (Figure 2).

5. Are ROCK Inhibitor Eye Drops Clinically Useful for the Treatment of Fuchs Endothelial Corneal Dystrophy?

We obtained approval from the institutional review board of the Kyoto Prefectural University of Medicine in 2010 to test ROCK inhibitor eye drops as a treatment for corneal endothelial dysfunction (approval number C-626-2) [26, 29]. Eight patients with corneal endothelial dysfunction who were scheduled for DSEK were enrolled in our clinical research study. Patients were categorized into 2 groups: (1) a central edema group, whose corneal edema was evident in the corneal center and who had a relatively transparent area remaining in the peripheral area (all 4 patients in this

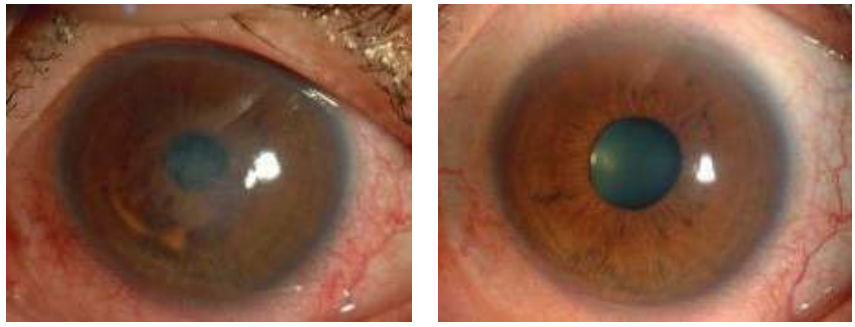

(a) Pre-treatment (b) Post-treatment

Figure 3: Clinical research on the use of ROCK-inhibitor Y-27632 eye drops for treatment of corneal decompensation. A representative case of a patient with central corneal edema due to Fuchs endothelial corneal dystrophy is shown. Before treatment, central corneal edema was observed (a), but the corneal edema was eliminated and visual acuity recovered from logMAR 0.70 to −0.18 after 6 months of treatment (b). Reproduced from Okumura et al. [26].

group had diagnoses of early- to intermediate-stage Fuchs endothelial corneal dystrophy), and (2) a diffuse edema group, whose corneal edema was observed throughout the cornea, from the center to the periphery. The central corneal endothelium was removed with a 2 mm diameter stainless cryoprobe, and the eyes were then treated with Y-27632 eye drops (10 mM) applied 6 times daily for 7 days. The limited number of patients precluded obtaining statistically significant differences, but a clear trend was observed for a reduction in central corneal thickness in the central edema group, but not in the diffuse edema group, in response to the eye drop treatment. Notably, one patient in the central edema group, a 52-year-old Japanese male diagnosed with late-onset Fuchs endothelial corneal dystrophy, showed a dramatic recovery. His pretreatment central corneal thickness of 703 μm and visual acuity of 20/63 recovered to 568 μm and 20/20, respectively, after the ROCK inhibitor treatment (Figure 3). Contact specular microscopy showed that the average corneal endothelial densities in the central and peripheral cornea were 1549 ± 90 and 705 ± 61 cells/mm^2, respectively, after 18 months. We were unable to perform specular microscopy in the central cornea because of the edema that existed before the treatment, but mild guttae were detected, mainly from the central to the paracentral area, after treatment [26, 29]. The limitation of this pilot clinical research was the small number of the patients and the absence of control cases who underwent the same central corneal endothelial removal with the cryoprobe but not with the ROCK inhibitor treatment. In addition, transcorneal freezing with a cryoprobe probably removes only corneal endothelial cells but not Descemet's membrane with guttae. A further study is necessary to determine whether corneal endothelial cells repopulate on the guttae and retain a functional status or whether the cryoprobe affects the guttae. The inflammatory response due to damaged epithelial cells and keratocytes can affect the corneal endothelial wound healing process. Accordingly, several other research groups have recently tested the effect of ROCK inhibitor eye drops for the treatment of early-stage Fuchs endothelial corneal dystrophy following Descemet's membrane removal instead of cryoprobe removal of the central corneal endothelium, but the clinical response seems to be controversial [30–32]. Further randomized clinical trials in larger cohorts are necessary to validate the effectiveness of ROCK inhibitor eye drops as a treatment for Fuchs endothelial corneal dystrophy.

6. Are ROCK Inhibitor Eye Drops Effective at Preventing Postcataract Surgery Corneal Decompensation?

Another possible indication for ROCK inhibitor administration is acute corneal endothelial damage, especially that occurring during cataract surgery. Corneal decompensation following cataract surgery is one of the leading causes of corneal transplantation in many countries, accounting for 12.2% and 20–40% of the corneal transplantations performed in the United States and in Asian countries, respectively [33–35]. The factor that determines whether the cornea becomes transparent or undergoes corneal decompensation is the density of CECs available for redistribution. Corneal haze will occur if the CEC density is insufficient. We hypothesized that ROCK inhibitor eye drops could in fact promote the proliferation of the residual CECs following corneal endothelial damage and increase the numbers of CECs available for coverage, thereby reducing the risk of corneal decompensation [36].

Our findings are preliminary, but our evaluation of the safety and effectiveness of ROCK inhibitor eye drops supports their use as a treatment for corneal endothelial damage [27]. Two patients were referred to the cornea clinic in Kyoto Prefectural University of Medicine after more than half of the area of the Descemet's membrane was accidentally removed during cataract surgery. One additional patient had undergone cataract surgery and removal of an iris cyst that had formed following a previous eye trauma, and almost half of the area of the cornea was exposed where the iris cyst was removed. All three patients showed severe corneal edema after surgery and were at high risk for subsequent corneal decompensation. However, the administration of ROCK inhibitor eye drops led to the recovery of corneal transparency within 1-2

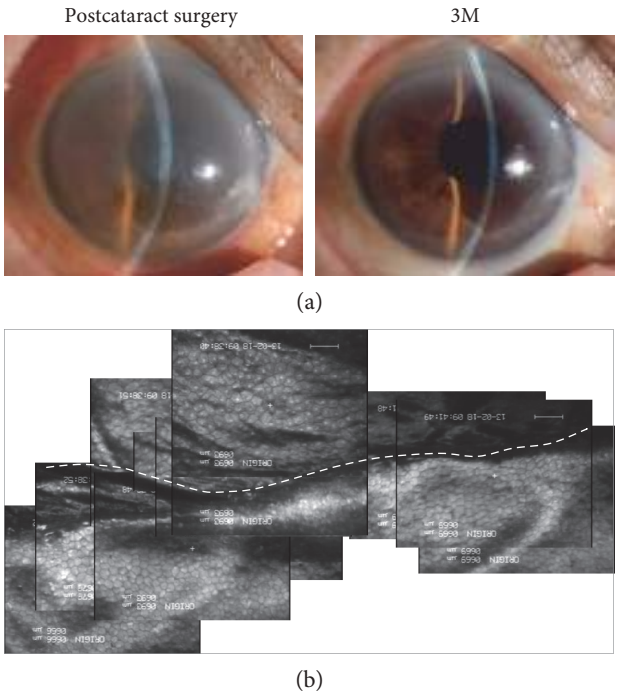

Figure 4: Pilot clinical research on the use of ROCK inhibitor eye drops for the treatment of acute corneal endothelial damage due to cataract surgery. (a) An 84-year-old female diagnosed with cataract underwent phacoemulsification. During the surgery, the Descemet's membrane was spontaneously detached from the upper incision tunnel and over 2/3 was aspirated. The patient was referred to the cornea clinic of Kyoto Prefectural University of Medicine due to severe corneal edema. The patient was treated with the 1 mM Y-27632 eye drops for 6 months. At 2 weeks, the cornea had recovered its clarity, and the patient's visual acuity had improved to 20/20 at 3 months. (b) Panoramic image of the corneal endothelium, evaluated by contact specular microscopy after 3 months. The Descemet's removal line is indicated as a white dotted line. Reproduced from Okumura et al. [27].

months in all three eyes (Figure 4). Recovery time tends to be faster than previously reported, where patients with iatrogenic Descemet's membrane removal during cataract surgery spontaneously recovered corneal clarity within 1–6 months [37–39]. However, further randomized clinical trials are needed to validate these findings and to confirm the effectiveness of ROCK inhibitors as a treatment for corneal endothelial damage. However, the positive findings from these preliminary clinical cases have motivated us to develop ROCK inhibitors as drugs for the treatment of corneal endothelial damage due to cataract surgery.

Ripasudil eye drops were approved in Japan as GLANATEC® ophthalmic solution 0.4% for the treatment of glaucoma and ocular hypertension [11]. In rabbit experiments, we demonstrated that ripasudil shows similar effects on corneal endothelial wound healing as other ROCK inhibitors [28]. Hence, repositioning of ripasudil as a drug for corneal endothelial diseases seems to be one possible strategy to bring ROCK inhibitors quickly into clinical settings.

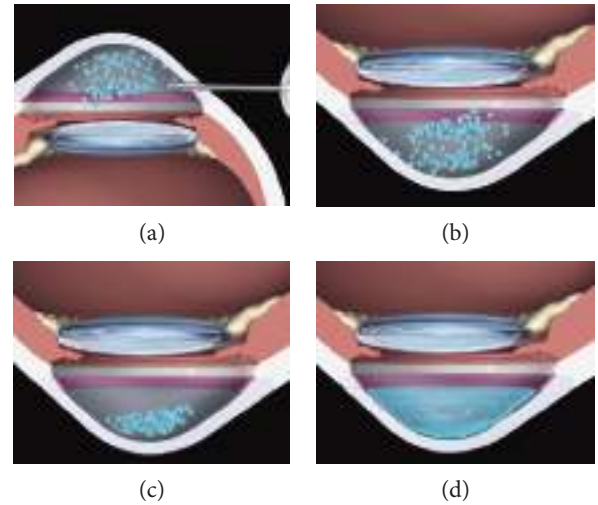

Figure 5: Schematic images of the cultured corneal endothelial cell (CEC) injection therapy. (a) Coinjection of cultured CECs with a ROCK inhibitor into the anterior chamber; (b) patient in the facedown position, to allow the CECs to sink down to the anterior chamber side of the cornea; (c) maintenance of the facedown position for 3 hours; (d) regeneration of the corneal endothelium by the injected cultured CECs. Reproduced from Okumura et al. [48].

7. ROCK Inhibitor Treatment Enables Cell-Based Therapy

Tissue engineering has been anticipated as new therapy that can replace conventional corneal transplantation using donor corneas. At least two possible strategies are available for transplanting cultured CECs to recipient corneas [40]. One strategy is to make a cultured corneal endothelial sheet and transplant it in a procedure much like DSEK or DMEK. We and several other researchers have cultured CECs on a substrate and transplanted the resulting CEC sheet into animal models [41–43]. The transplanted CEC sheet regenerated a transparent cornea in animal models, but the transplantation of the fragile monolayer sheet into the anterior chamber and attachment onto the back side of the cornea involve difficult surgical techniques.

The second strategy is to inject cultured CECs in the form of a cell suspension into the anterior chamber. The CECs injected into the anterior chamber will not spontaneously attach to the recipient corneal epithelial layer, so magnetic guidance or injection of CEC spheres was proposed to enhance the CEC engraftment [44–46]. We considered cell injection to have several advantages over sheet transplantation, including a simplified transplantation procedure, less invasiveness to patients, easier preparation of cell stock, and avoidance of artificial substrate use. Our finding that ROCK inhibitor treatment enhances adhesion of CECs onto a substrate [13] prompted us to initiate animal experiments in which cultured CECs were injected into the anterior chamber in combination with a ROCK inhibitor. We used two animal models of corneal endothelial dysfunction (rabbit and cynomolgus monkey), injected cultured CECs in the form of a cell suspension combined with a ROCK inhibitor, and

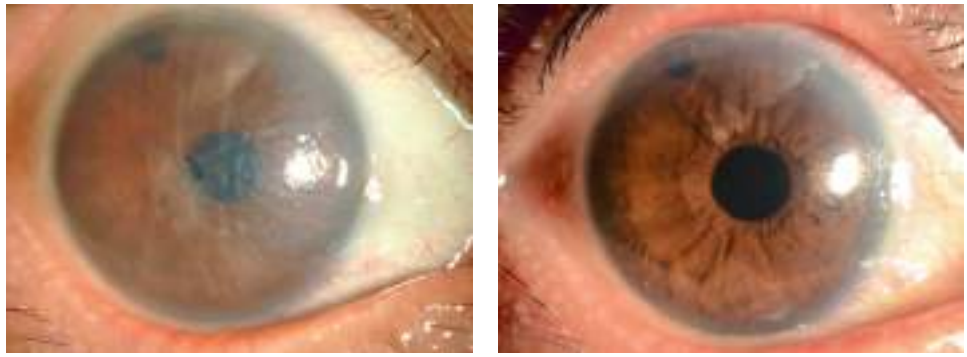

(a) Pre-treatment (b) Post-treatment

Figure 6: Representative images of the effectiveness of cultured corneal endothelial cell (CEC) injection therapy in clinical research. Representative slit-lamp microscopy images of the first patient, a Japanese female with corneal endothelial decompensation induced by argon laser iridotomy (a). After mechanical removal of an 8 mm diameter section of the corneal endothelium, cultured human CECs together with a ROCK inhibitor were injected into the anterior chamber. Preoperative visual acuity was 0.04 due to the edema in the corneal epithelium and stroma. The postoperative visual acuity recovered to 1.0, together with the associated recovery of corneal transparency (b).

demonstrated regeneration of the corneal endothelium and restoration of a transparent cornea [47, 48]. We have since accumulated evidence that confirms the safety and effectiveness of cultured CEC injections in combination with a ROCK inhibitor in animal models. The safety and functional profiles of cultured human CECs for clinical use have also been carefully evaluated [48].

8. Clinical Study of Cell-Based Therapy Using ROCK Inhibitors

In 2013, we obtained the approval from the Japanese Ministry of Health, Labour, and Welfare to initiate a first-in-man clinical trial of cell-based therapy to treat corneal endothelial dysfunction at the Kyoto Prefectural University of Medicine (Clinical trial registration: UMIN000012534) (Figure 5). Clinical data are still under analysis, but our initial clinical results seem to indicate that this treatment is both safe and effective. Further clinical data are anticipated that will determine the effectiveness in terms of clinical outcomes, such as visual acuity, CEC density, and rejection rate, when compared to conventional corneal transplantations.

Representative slit-lamp microscopy images from our first patient, a Japanese female with corneal endothelial decompensation induced by argon laser iridotomy, are shown in Figure 6. We mechanically removed an area approximately 8 mm diameter from the corneal endothelium, without removing Descemet's membrane, and injected cultured human CECs in combination with a ROCK inhibitor into the anterior chamber. The patient was kept in a facedown position overnight to enable the injected CECs to settle onto the Descemet's membrane. The patient's preoperative visual acuity was 0.04 and she had corneal epithelial and stromal edema, whereas her postoperative visual acuity recovered to 1.0 and was associated with the recovery of corneal transparency (Figure 6).

9. Conclusions

We have demonstrated that ROCK inhibitors, supplied in the form of eye drops, promote cell proliferation in animal models and most likely in humans. However, the development of these drugs to target corneal endothelium damage will require randomized clinical trials of (1) ROCK inhibitor eye drop administration following central corneal endothelial removal, either by Descemet's membrane removal or cryoprobe treatment, for the treatment of Fuchs endothelial corneal dystrophy and (2) ROCK inhibitor eye drop administration for the treatment of acute corneal endothelial damage due to cataract surgery. The use of ROCK inhibitors in tissue engineering therapy is also very promising, as indicated by the enhanced engraftment of CECs onto recipient tissues. We have treated 31 patients with cell injection therapy at the time of this review article. The collected data are currently undergoing an independent review to ensure diligent assessment of our clinical results for evaluation of the safety and effectiveness of this treatment.

For decades, the only therapy for the corneal endothelium has been corneal transplantation. Therefore, the promising responses to ROCK inhibitors would appear to open up new therapeutic possibilities.

Conflicts of Interest

Shigeru Kinoshita obtained a patent regarding the application of a ROCK inhibitor for corneal endothelium treatment (registration number: 5657252). Noriko Koizumi is listed as one of the inventors of the patent.

Acknowledgments

This study was supported by grants from the Program for the Strategic Research Foundation at Private Universities from MEXT (Noriko Koizumi and Naoki Okumura) and the

Program for Realization of Regenerative Medicine (Shigeru Kinoshita and Noriko Koizumi).

References

[1] N. C. Joyce, "Proliferative capacity of the corneal endothelium," *Progress in Retinal and eye Research*, vol. 22, no. 3, pp. 359–389, 2003.

[2] D. T. Tan, J. K. Dart, E. J. Holland, and S. Kinoshita, "Corneal transplantation," *Lancet*, vol. 379, no. 9827, pp. 1749–1761, 2012.

[3] L. M. Nijm, M. J. Mannis, and E. J. Holland, "The evolution of contemporary keratoplasty," *Cornea Third Edition*, vol. 2, pp. 1321–1325, 2011.

[4] M. O. Price and F. W. Price Jr., "Endothelial keratoplasty - a review," *Clinical & Experimental Ophthalmology*, vol. 38, no. 2, pp. 128–140, 2010.

[5] O. Nakagawa, K. Fujisawa, T. Ishizaki, Y. Saito, K. Nakao, and S. Narumiya, "ROCK-I and ROCK-II, two isoforms of Rho-associated coiled-coil forming protein serine/threonine kinase in mice," *FEBS Letters*, vol. 392, no. 2, pp. 189–193, 1996.

[6] K. Riento and A. J. Ridley, "Rocks: multifunctional kinases in cell behaviour," *Nature Reviews. Molecular Cell Biology*, vol. 4, no. 6, pp. 446–456, 2003.

[7] S. Narumiya, M. Tanji, and T. Ishizaki, "Rho signaling, ROCK and mDia1, in transformation, metastasis and invasion," *Cancer Metastasis Reviews*, vol. 28, no. 1-2, pp. 65–76, 2009.

[8] J. Shi and L. Wei, "Rho kinase in the regulation of cell death and survival," *Archivum Immunologiae et Therapiae Experimentalis (Warsz)*, vol. 55, no. 2, pp. 61–75, 2007.

[9] M. F. Olson, "Applications for ROCK kinase inhibition," *Current Opinion in Cell Biology*, vol. 20, no. 2, pp. 242–248, 2008.

[10] Y. Feng, P. V. LoGrasso, O. Defert, and R. Li, "Rho kinase (ROCK) inhibitors and their therapeutic potential," *Journal of Medicinal Chemistry*, vol. 59, no. 6, pp. 2269–2300, 2016.

[11] K. P. Garnock-Jones, "Ripasudil: first global approval," *Drugs*, vol. 74, no. 18, pp. 2211–2215, 2014.

[12] J. K. Liao, M. Seto, and K. Noma, "Rho kinase (ROCK) inhibitors," *Journal of Cardiovascular Pharmacology*, vol. 50, no. 1, pp. 17–24, 2007.

[13] N. Okumura, M. Ueno, N. Koizumi et al., "Enhancement on primate corneal endothelial cell survival in vitro by a ROCK inhibitor," *Investigative Ophthalmology & Visual Science*, vol. 50, no. 8, pp. 3680–3687, 2009.

[14] M. Yamamoto, N. Marui, T. Sakai et al., "ADP-ribosylation of the RhoA gene product by botulinum C3 exoenzyme causes Swiss 3T3 cells to accumulate in the G1 phase of the cell cycle," *Oncogene*, vol. 8, no. 6, pp. 1449–1455, 1993.

[15] M. F. Olson, A. Ashworth, and A. Hall, "An essential role for Rho, Rac, and Cdc42 GTPases in cell cycle progression through G1," *Science*, vol. 269, no. 5228, pp. 1270–1272, 1995.

[16] X. Yang, Y. Zhang, S. Wang, and W. Shi, "Effect of fasudil on growth, adhesion, invasion, and migration of 95D lung carcinoma cells in vitro," *Canadian Journal of Physiology and Pharmacology*, vol. 88, no. 9, pp. 874–879, 2010.

[17] C. Spencer, J. Montalvo, S. R. McLaughlin, and B. A. Bryan, "Small molecule inhibition of cytoskeletal dynamics in melanoma tumors results in altered transcriptional expression patterns of key genes involved in tumor initiation and progression," *Cancer Genomics Proteomics*, vol. 8, no. 2, pp. 77–85, 2011.

[18] L. M. Knowles, L. A. Gurski, J. K. Maranchie, and J. Pilch, "Fibronectin matrix formation is a prerequisite for colonization of kidney tumor cells in fibrin," *Journal of Cancer*, vol. 6, no. 2, pp. 98–104, 2015.

[19] N. Okumura, S. Nakano, E. P. Kay et al., "Involvement of cyclin D and p27 in cell proliferation mediated by ROCK inhibitors Y-27632 and Y-39983 during corneal endothelium wound healing," *Investigative Ophthalmology & Visual Science*, vol. 55, no. 1, pp. 318–329, 2014.

[20] G. S. Peh, K. Adnan, B. L. George et al., "The effects of Rho-associated kinase inhibitor Y-27632 on primary human corneal endothelial cells propagated using a dual media approach," *Scientific Reports*, vol. 5, p. 9167, 2015.

[21] A. Pipparelli, Y. Arsenijevic, G. Thuret, P. Gain, M. Nicolas, and F. Majo, "ROCK inhibitor enhances adhesion and wound healing of human corneal endothelial cells," *PloS One*, vol. 8, no. 4, article e62095, 2013.

[22] N. Okumura, N. Koizumi, M. Ueno et al., "Enhancement of corneal endothelium wound healing by Rho-associated kinase (ROCK) inhibitor eye drops," *The British Journal of Ophthalmology*, vol. 95, no. 7, pp. 1006–1009, 2011.

[23] D. L. Van Horn and R. A. Hyndiuk, "Endothelial wound repair in primate cornea," *Experimental Eye Research*, vol. 21, no. 2, pp. 113–124, 1975.

[24] D. L. Van Horn, D. D. Sendele, S. Seideman, and P. J. Buco, "Regenerative capacity of the corneal endothelium in rabbit and cat," *Investigative Ophthalmology & Visual Science*, vol. 16, no. 7, pp. 597–613, 1977.

[25] M. Matsubara and T. Tanishima, "Wound-healing of the corneal endothelium in the monkey: a morphometric study," *Japanese Journal of Ophthalmology*, vol. 26, no. 3, pp. 264–273, 1982.

[26] N. Okumura, N. Koizumi, E. P. Kay et al., "The ROCK inhibitor eye drop accelerates corneal endothelium wound healing," *Investigative Ophthalmology & Visual Science*, vol. 54, no. 4, pp. 2493–2502, 2013.

[27] N. Okumura, R. Inoue, Y. Okazaki et al., "Effect of the Rho kinase inhibitor Y-27632 on corneal endothelial wound healing," *Investigative Ophthalmology & Visual Science*, vol. 56, no. 10, pp. 6067–6074, 2015.

[28] N. Okumura, Y. Okazaki, R. Inoue et al., "Effect of the Rho-associated kinase inhibitor eye drop (ripasudil) on corneal endothelial wound healing," *Investigative Ophthalmology & Visual Science*, vol. 57, no. 3, pp. 1284–1292, 2016.

[29] N. Koizumi, N. Okumura, M. Ueno, H. Nakagawa, J. Hamuro, and S. Kinoshita, "Rho-associated kinase inhibitor eye drop treatment as a possible medical treatment for Fuchs corneal dystrophy," *Cornea*, vol. 32, no. 8, pp. 1167–1170, 2013.

[30] R. D. Shah, J. B. Randleman, and H. E. Grossniklaus, "Spontaneous corneal clearing after Descemet's stripping without endothelial replacement," *Ophthalmology*, vol. 119, no. 2, pp. 256–260, 2012.

[31] V. Galvis, A. Tello, and G. Miotto, "Human corneal endothelium regeneration," *Ophthalmology*, vol. 119, no. 8, pp. 1714-1715, 2012.

[32] I. Bleyen, I. E. Saelens, B. T. van Dooren, and G. van Rij, "Spontaneous corneal clearing after Descemet's stripping," *Ophthalmology*, vol. 120, no. 1, p. 215, 2013.

[33] L. Dandona, T. J. Naduvilath, M. Janarthanan, K. Ragu, and G. N. Rao, "Survival analysis and visual outcome in a large

series of corneal transplants in India," *The British Journal of Ophthalmology*, vol. 81, no. 9, pp. 726–731, 1997.

[34] J. Shimazaki, S. Amano, T. Uno, N. Maeda, N. Yokoi, and Japan Bullous Keratopathy Study Group, "National survey on bullous keratopathy in Japan," *Cornea*, vol. 26, no. 3, pp. 274–278, 2007.

[35] Eye Bank Association of America, *Eye Banking Statistical Report*, Eye Bank Association of America, Washington, D.C., 2015, http://restoresight.org/what-we-do/publications/statistical-report.

[36] N. Okumura, S. Kinoshita, and N. Koizumi, "The role of Rho kinase inhibitors in corneal endothelial dysfunction," *Current Pharmaceutical Design*, vol. 23, no. 4, pp. 660–666, 2016.

[37] R. E. Braunstein, S. Airiani, M. A. Chang, and M. G. Odrich, "Corneal edema resolution after "descemetorhexis"," *Journal of Cataract and Refractive Surgery*, vol. 29, no. 7, pp. 1436–1439, 2003.

[38] A. Agarwal, S. Jacob, A. Agarwal, and M. A. Kumar, "Iatrogenic descemetorhexis as a complication of phacoemulsification," *Journal of Cataract and Refractive Surgery*, vol. 32, no. 5, pp. 895–897, 2006.

[39] R. Jullienne, P. Manoli, T. Tiffet et al., "Corneal endothelium self-healing mathematical model after inadvertent descemetorhexis," *Journal of Cataract and Refractive Surgery*, vol. 41, no. 10, pp. 2313–2318, 2015.

[40] N. Okumura, S. Kinoshita, and N. Koizumi, "Cell-based approach for treatment of corneal endothelial dysfunction," *Cornea*, vol. 33, Supplement 11, pp. S37–S41, 2014.

[41] Y. Ishino, Y. Sano, T. Nakamura et al., "Amniotic membrane as a carrier for cultivated human corneal endothelial cell transplantation," *Investigative Ophthalmology & Visual Science*, vol. 45, no. 3, pp. 800–806, 2004.

[42] T. Mimura, S. Yamagami, S. Yokoo et al., "Cultured human corneal endothelial cell transplantation with a collagen sheet in a rabbit model," *Investigative Ophthalmology & Visual Science*, vol. 45, no. 9, pp. 2992–2997, 2004.

[43] N. Koizumi, Y. Sakamoto, N. Okumura et al., "Cultivated corneal endothelial cell sheet transplantation in a primate model," *Investigative Ophthalmology & Visual Science*, vol. 48, no. 10, pp. 4519–4526, 2007.

[44] T. Mimura, N. Shimomura, T. Usui et al., "Magnetic attraction of iron-endocytosed corneal endothelial cells to Descemet's membrane," *Experimental Eye Research*, vol. 76, no. 6, pp. 745–751, 2003.

[45] T. Mimura, S. Yamagami, T. Usui et al., "Long-term outcome of iron-endocytosing cultured corneal endothelial cell transplantation with magnetic attraction," *Experimental Eye Research*, vol. 80, no. 2, pp. 149–157, 2005.

[46] S. V. Patel, L. A. Bachman, C. R. Hann, C. K. Bahler, and M. P. Fautsch, "Human corneal endothelial cell transplantation in a human ex vivo model," *Investigative Ophthalmology & Visual Science*, vol. 50, no. 5, pp. 2123–2131, 2009.

[47] N. Okumura, N. Koizumi, M. Ueno et al., "ROCK inhibitor converts corneal endothelial cells into a phenotype capable of regenerating in vivo endothelial tissue," *The American Journal of Pathology*, vol. 181, no. 1, pp. 268–277, 2012.

[48] N. Okumura, Y. Sakamoto, K. Fujii et al., "Rho kinase inhibitor enables cell-based therapy for corneal endothelial dysfunction," *Scientific Reports*, vol. 6, p. 26113, 2016.

[49] N. Okumura, "Treatment of corneal endothelial diseases," *IOL & RS (Japanese)*, vol. 30, no. 1, pp. 53–58, 2016.

The Effect of a p38 Mitogen-Activated Protein Kinase Inhibitor on Cellular Senescence of Cultivated Human Corneal Endothelial Cells

Akane Hongo, Naoki Okumura, Makiko Nakahara, EunDuck P. Kay, and Noriko Koizumi

Department of Biomedical Engineering, Faculty of Life and Medical Sciences, Doshisha University, Kyotanabe, Japan

Correspondence: Noriko Koizumi, Department of Biomedical Engineering, Faculty of Life and Medical Sciences, Doshisha University, Kyotanabe 610-0321, Japan; nkoizumi@mail.doshisha.ac.jp.

Submitted: November 23, 2016
Accepted: June 6, 2017

Citation: Hongo A, Okumura N, Nakahara M, Kay EP, Koizumi N. The effect of a p38 mitogen-activated protein kinase inhibitor on cellular senescence of cultivated human corneal endothelial cells. *Invest Ophthalmol Vis Sci*. 2017;58:3325–3334. DOI:10.1167/iovs.16-21170

Purpose. We have begun a clinical trial of a cell-based therapy for corneal endothelial dysfunction in Japan. The purpose of this study was to investigate the usefulness of a p38 MAPK inhibitor for prevention cellular senescence in cultivated human corneal endothelial cells (HCECs).

Methods. HCECs of 10 donor corneas were divided and cultured with or without SB203580 (a p38 MAPK inhibitor). Cell density and morphology were evaluated by phase-contrast microscopy. Expression of function-related proteins was examined by immunofluorescent staining. Cellular senescence was evaluated by SA-β-gal staining and Western blotting for p16 and p21. Senescence-associated factors were evaluated by membrane blotting array, quantitative PCR, and ELISA.

Results. Phase-contrast microscopy showed a significantly higher cell density for HCECs cultured with SB203580 than without SB203580 (2623 ± 657 cells/mm^2 and 1752 ± 628 cells/mm^2, respectively). The HCECs cultured with SB203580 maintained a hexagonal morphology and expressed ZO-1, N-cadherin, and Na^+/K^+-ATPase in the plasma membrane, whereas the control HCECs showed an altered staining pattern for these marker proteins. HCECs cultured without SB203580 showed high positive SA-β-gal staining, a low nuclear/cytoplasm ratio, and expression of p16 and p21. IL-6, IL-8, CCL2, and CXCL1 were observed at high levels in low cell density HCECs cultured without SB203580.

Conclusions. Activation of p38 MAPK signaling due to culture stress might be a causative factor that induces cellular senescence; therefore, the use of p38 MAPK inhibitor to counteract senescence may achieve sufficient numbers of HCECs for tissue engineering therapy for corneal endothelial dysfunction.

Keywords: corneal endothelial cells, p38 MAPK, tissue engineering therapy

The corneal endothelium plays an essential role in maintaining corneal transparency via its pump and barrier functions.[1,2] Damage to the corneal endothelium causes a concurrent compensatory migration and enlargement of the remaining cells to cover the damaged area due to the very limited proliferative ability of the corneal endothelial cells (CECs).[3,4] Healthy human CECs (HCECs), with cell densities of 2500 to 3000 cells/mm^2, perform the characteristic endothelial functions, but HCECs with cell densities less than 500 to 1000 cells/mm^2 are unable to regulate the water flow into stroma, which results in stromal swelling.[1,2,5] Various causes, such as Fuchs' endothelial corneal dystrophy, surgical trauma, transplanted cornea failure, and cytomegalovirus, can induce a cell density drop and subsequently induce severe vision loss.[6]

The only therapy for corneal endothelial dysfunction has been transplantation with donor corneas.[7] Recently, endothelial keratoplasties, such as Descemet's stripping endothelial keratoplasty[8] and Descemet's membrane endothelial keratoplasty,[9] have been performed instead of full-thickness penetrating keratoplasty, and these procedures successfully provide a less invasive and more efficient therapy. However, problems still exist, such as a shortage of donor corneas, the learning curve of the surgeries, and graft failure at both acute and chronic phases.[7] Several research groups, including ours, have endeavored to develop tissue engineering–based approaches that will provide a more efficient therapeutic modality than the conventional transplantation of donor corneas.[10–14] For instance, we demonstrated that corneal endothelium can be regenerated by injecting a suspension consisting of a combination of cultured CECs and a Rho-associated kinase (ROCK) inhibitor into rabbit and monkey corneal endothelial dysfunction models.[14,15] In addition, we recently started a human clinical trial at Kyoto Prefectural University of Medicine after obtaining the necessary approval (Clinical trial registration: UMIN000012534).

Several groups have reported the successful culture of HCECs,[3,16] but maintaining the cultured HCECs with the desired morphology and function has proven difficult.[17] Moreover, HCECs show a cell density drop when cultured, especially when passaging the cells.[18] Hence, the establishment of culture protocols for HCECs has been recognized as a bottleneck in tissue engineering therapy for the corneal endothelium.

Cell senescence is typically triggered by activation of signaling pathways. One likely candidate in this case is the mitogen-activated protein kinase (MAPK) signal transduction

pathways, which are among the most widespread mechanisms of eukaryotic cell regulation. MAPK has four main signaling modules: extracellular-signal-regulated kinase (ERK), ERK5, Jun-NH2-terminal kinases (JNK), and p38 MAPK. The JNK, ERK5, and p38 MAPK signaling pathways are activated in response to physical stress signals, whereas the ERK pathway is activated by mitotic stimuli. Signaling by p38 MAPK is associated with various cellular activities, such as cell proliferation, differentiation, migration, and apoptosis.[19] In addition, p38 MAPK plays an important role in cellular senescence.[20]

In this study, we determined whether cell density drop of HCECs under culture condition is a phenotypic feature associated with cellular senescence. In addition, we evaluated whether inhibition of p38 MAPK could suppress cellular senescence.

Materials and Methods

Ethics Statement

The human donor corneas used in this study were handled in accordance with the tenets of the Declaration of Helsinki. Informed written consent was obtained from the next of kin of all deceased donors with regard to eye donation for research. Donor corneas were obtained from SightLife (Seattle, WA, USA). All tissue specimens were recovered under the tenets of the Uniform Anatomical Gift Act of the particular state in which the donor consent had been obtained and the tissue recovered.

Cell Culture

The 10 human donor corneas were used for culturing HCECs. The mean donor age was 52.9 ± 17.1 years. All corneas were stored at 4°C in storage medium (Optisol-GS; Chiron Vision, Irvine, CA, USA) for less than 14 days before use. The HCECs were cultured according to published protocols, with some modifications.[21] Briefly, Descemet's membranes containing the HCECs were stripped from the donor corneas and the membranes were digested with 1 mg/mL collagenase A (Roche Applied Science, Penzberg, Germany) at 37°C for 12 hours. The resulting HCECs were suspended in Opti-MEM I (Life Technologies, Carlsbad, CA, USA) and divided equally into two tubes. The HCECs in one tube were then seeded in culture medium with p38 MAPK inhibitor (10 μM SB203580; Cayman Chemical, Ann Arbor, MI, USA) in a well of a 48-well plate, and cells in another tube were seeded with culture medium without p38 MAPK inhibitor, as a control. The plates were coated with laminin E8 fragments (iMatrix-511; Nippi, Incorporated, Tokyo, Japan).[22] The culture medium used for this study was Opti-MEM I supplemented with 8% fetal bovine serum, 5 ng/mL epidermal growth factor, 20 μg/mL ascorbic acid (Sigma-Aldrich Corp., St. Louis, MO, USA), 200 mg/L calcium chloride, 0.08% chondroitin sulfate (Wako Pure Chemical Industries, Ltd., Osaka, Japan), and 50 μg/mL gentamicin (Life Technologies). The HCECs were cultured at 37°C in a humidified atmosphere containing 5% CO_2, and the culture medium was changed every 2 days. When HCECs were passaged, they were rinsed in Ca^{2+}- and Mg^{2+}-free PBS, trypsinized with 0.05% Trypsin-EDTA (Life Technologies) for 5 minutes at 37°C, and seeded at a 1:2 ratio. Cell morphology was evaluated by phase-contrast microscopy and cell density was evaluated after the cultures reached confluence using the KSS-400EB software (Konan Medical, Inc., Hyogo, Japan).

Immunofluorescent Staining

The HCECs were seeded on a 24-well cell culture plate coated with laminin E8 fragments, and further cultured for 6 weeks after reaching confluence. HCECs were fixed in 4% paraformaldehyde for 10 minutes at room temperature and then incubated for an hour with 1% BSA. Cells were incubated overnight at 4°C with antibodies against ZO-1 (1:200; Thermo Fisher Scientific, Inc., Waltham, MA, USA), N-cadherin (1:200; BD Biosciences, San Jose, CA, USA), and Na^+/K^+-ATPase (1:200; Merck Millipore, Darmstadt, Germany). After washing with PBS, either Alexa Fluor 488-conjugated goat anti-mouse (Life Technologies) or Alexa Fluor 594-conjugated donkey anti-rabbit IgG (Life Technologies) was used as the secondary antibody at a 1:1000 dilution. F-actin were stained with a 1:400 dilution of Alexa Fluor 546 conjugated phalloidin (Life Technologies). Nuclei were stained with 4′,6-diamidino-2-phenylindole (DAPI) (Dojindo Laboratories, Kumamoto, Japan). The samples were examined by fluorescence microscopy (BZ-9000; Keyence, Osaka, Japan). More information about the antibodies is presented in Supplementary Table S1.

The nuclear/cytoplasmic area ratio was determined using the ImageJ (http://imagej.nih.gov/ij/; provided in the public domain by the National Institutes of Health, Bethesda, MD, USA) software and images of F-actin and DAPI staining. The cell borders determined by F-actin staining were manually traced using ImageJ, and the cytoplasmic area was measured. Likewise, the nuclear area determined by DAPI staining was manually traced using ImageJ and measured. The average of the nuclear area/cytoplasmic area for 10 cells was used as the nuclear/cytoplasmic area ratio.

β-Galactosidase Senescence Staining

HCECs were seeded at a density of 1×10^4 cells per well in 48-well cell culture plates coated with laminin E8 fragments. The cells were cultured for 24 hours, using the Senescence Detection Kit (Merck Millipore), according to the manufacturer's instructions. Briefly, cultured HCECs were washed with PBS once and fixed with the fixative solution for 10 minutes. The samples were then washed twice with PBS and stained for SA-β-gal with a staining solution mix at 37°C. Cells (both SA-β-gal–positive cells and all cells) that showed the whole area of the nucleus in the images were counted manually in triplicate images for each passage (passages 3 to 5) using ImageJ software. The average from three images was used to calculate the percentage of SA-β-gal–positive cells.

Immunoblotting

Cultured HCECs were washed with ice-cold PBS and lysed with ice-cold RIPA buffer containing phosphatase inhibitor cocktail 2 (Sigma-Aldrich Corp.) and protease inhibitor cocktail (Roche Applied Science). Samples were centrifuged and the supernatant containing the proteins was fractionated by SDS-PAGE. The separated proteins were transferred to polyvinylidene difluoride membranes and blocked with 5% nonfat dry milk. The samples were incubated overnight at 4°C with the primary antibodies: p16 (1:1000; BD Biosciences), p21 (C-19) (1:1000; Santa Cruz Biotechnology, Santa Cruz, CA, USA), phospho-p38 MAPK (Thr180/Tyr182) (1:1000; Cell Signaling Technology, Inc., Danvers, MA, USA), p38 MAPK (1:1000; Cell Signaling Technology), phospho-ATF-2 (Thr71) (1:1000; Cell Signaling Technology), ATF-2 (1:1000; Merck Millipore), and glyceraldehyde-3-phosphate dehydrogenase (GAPDH) (1:1000; Medical & Biological Laboratories Co., Ltd., Aichi, Japan). The blots were probed with horseradish peroxidase (HRP)-conjugated secondary antibodies (1:5000;

GE Healthcare, Piscataway, NJ, USA), developed with luminal for enhanced chemiluminescence using the highly sensitive luminol-based chemiluminescence assay kits for Western blotting (Chemi-Lumi One Ultra; Nacalai tesque, Kyoto, Japan), and documented with an Amersham Imager 600 (GE Healthcare) for high-resolution digital imaging of protein in membranes. Molecular weight markers (Bio-Rad, Hercules, CA, USA) were used alongside all samples. More information about the antibodies is presented in Supplementary Table S1. The relative density of the immunoblot bands was determined using Image J software. Relative fold differences were compared with the control values.

Membrane Blotting Array

The release of cytokines and chemokines was measured using the Proteome Profiler Array (Human cytokine arrays Panel A; R&D Systems, Inc., Minneapolis, MN, USA), according to manufacturer's protocol. Briefly, after culturing HCECs with or without SB203580 for 6 weeks, the culture medium was replaced with a fresh medium and further cultured for 72 hours. The culture medium was then recovered and centrifuged. Human cytokine array detection antibody cocktail was added to the recovered culture medium and incubated at room temperature for 1 hour. Membranes were blocked with blocking regents, and incubated with sample overnight at 4°C. The membrane was washed and streptavidin-HRP and chemiluminescent detection reagents were added. The data were analyzed by measuring the pixel density in each spot of the array using the LAS4000S (GE Healthcare) cooled charge-coupled-device camera gel documentation system.

Quantitative Real-Time PCR

Gene expression levels were analyzed using TaqMan real-time PCR. Total RNA was extracted from the corneal endothelium from cultured HCECs using the RNeasy Mini Kit (250) (QIAGEN, Hilden, Germany), and cDNA was synthesized with ReverTra Ace (Toyobo Co., Ltd., Osaka, Japan). TaqMan probes for *IL-6*, Hs00985639_m1; *IL-8*, Hs00174103_m1; *CCL2*, Hs00234140_m1; *CXCL1*, Hs00236937_m1; *CXCL10*, Hs01124252_g1; *MIF*, Hs00236988_g1; and *GAPDH*, Hs00266705_g1 were used. The PCR was performed using the StepOne (Thermo Fisher Scientific, Inc.) real-time PCR system. GAPDH was used as an internal standard.

Enzyme-Linked Immunosorbent Assay

The amount of IL-6 and IL-8 in the supernatants of HCECs was determined by Human DuoSet ELISA kit (R&D Systems), according to the instructions of the manufacturer. Briefly, samples were collected using the same protocol as described for the membrane blotting array. A 96-well plate, precoated with a monoclonal antibody specific for human IL-6 or IL-8, was covered with the diluted capture antibody overnight at room temperature. The plate was washed with wash buffer three times and blocked with 1% BSA for 1 hour. After BSA removal, samples and standards were pipetted into the wells and incubated for 2 hours at room temperature. After washing the well, an enzyme-linked polyclonal antibody specific for human IL-6 or IL-8 was added to the wells and incubated for 2 hours at room temperature. The reagent was removed from the well and a substrate solution added. The absorbance was measured at 450 nm and the concentrations were determined by interpolation from a standard calibration curve.

Table. Donor Information of HCECs

No.	Donor Age	Sex	Cell Density of Donor Cornea, cells/mm^2	Preservation Time, d
1	53	Male	2642	14.2
2	54	Male	2674	12.3
3	62	Male	2875	7.2
4	61	Female	3294	5.8
5	73	Male	2701	7.4
6	28	Male	2824	7.4
7	14	Female	3301	8.8
8	63	Female	2806	7.2
9	62	Female	2574	7.1
10	59	Female	2906	5.9

Statistical Analysis

The statistical significance (*P* value) of the mean values for two-sample comparisons was determined with the Student's *t*-test. The statistical significance for the comparison of multiple sample sets was determined with the Dunnett's multiple-comparisons test. All data represent the mean ± SE.

Results

Effect of a p38 MAPK Inhibitor on Cell Density and Functional Phenotype of HCECs

We investigated the effect of p38 MAPK inhibitor on endothelial phenotypes using 10 human donor corneas to establish 10 respective HCECs cultures (Table). Phase-contrast microscopy showed a contact-inhibited monolayer of hexagonal endothelial cells both in control and SB203580-treated cells (Fig. 1A; Supplementary Fig. S1). Of interest, HCECs were smaller in size when cultured with SB203580 than without SB203580. The mean cell density was significantly higher for HCECs treated with SB203580 than without SB203580 (2623 ± 657 cells/mm^2 and 1752 ± 628 cells/mm^2, respectively) (Fig. 1B). The HCECs cultured with SB203580 expressed ZO-1, N-cadherin, and Na^+/K^+-ATPase in the plasma membrane, along with F-actin in the cytoskeleton of the polygonal cells, whereas the control HCECs cultured without SB203580 showed a greatly altered staining pattern for these marker proteins. F-actin was observed in the cortex of the cells cultured with SB203580, whereas cortical F-actin distribution was irregular in the control HCECs (Fig. 1C). In addition, long-term cultivation of HCECs showed that cells maintained a higher cell density when cultured with SB203580 than without SB203580 throughout the 18 months (Fig. 2).

Effect of a p38 MAPK Inhibitor on Senescence of HCECs

A decrease in cell density typically accompanies senescence in clinical settings. Therefore, we examined if culture stress might induce cellular senescence in HCECs and we further tested if the p38 MAPK signaling pathway is involved in this cellular senescence. The percentage of SA-β-gal–positive cells was significantly lower in HCECs treated with SB203580 than in control cells (25.2% and 64.9% [passage 3], 25.5% and 71.3% [passage 4], and 35.2% and 63.1% [passage 5], respectively) (Figs. 3A, 3B). The ratio of nuclear/cytoplasmic areas was significantly higher in HCECs cultured with SB203580

Investigative Ophthalmology & Visual Science

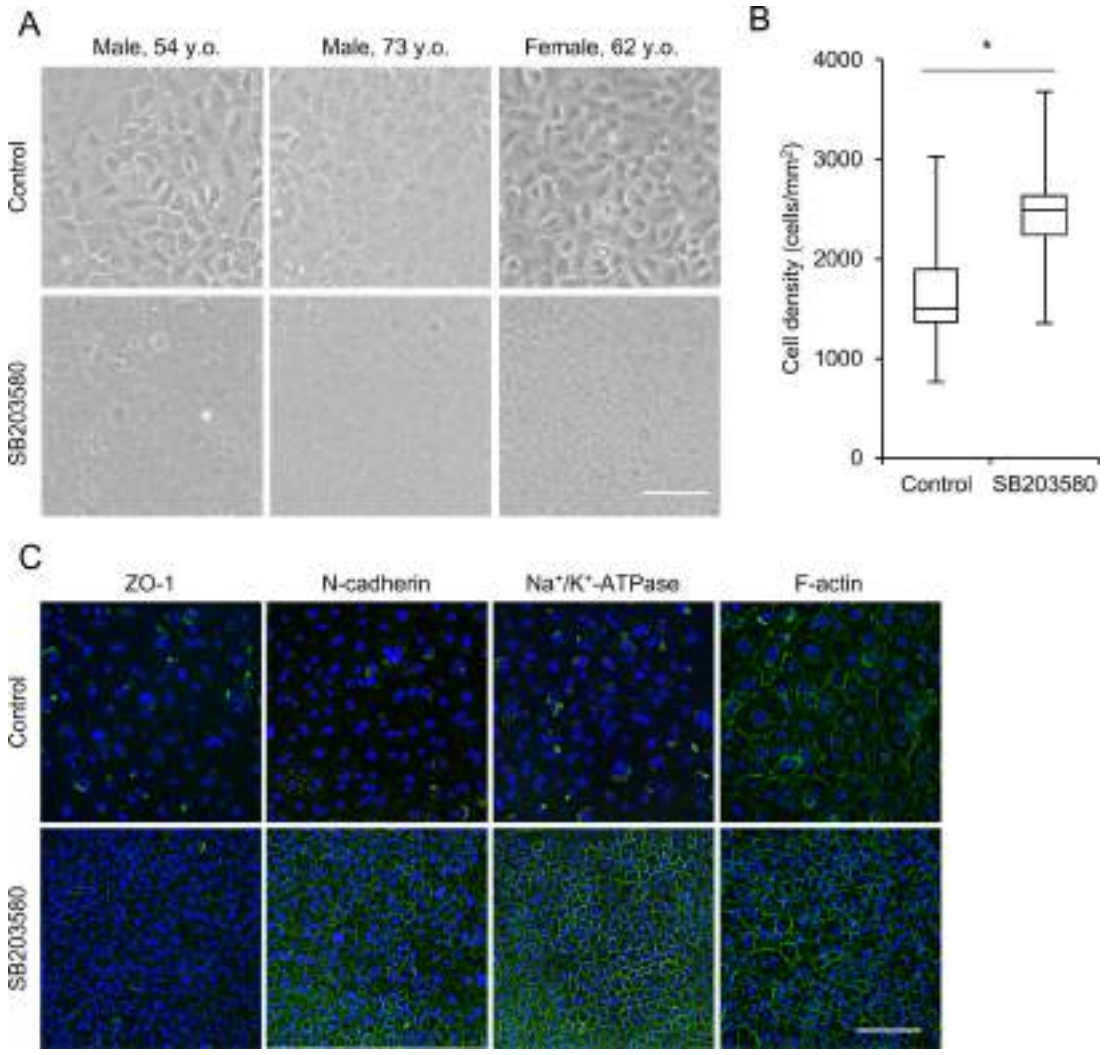

FIGURE 1. Cell density and functional phenotype of HCECs cultured with or without SB203580. (**A**) Phase-contrast images of primary cultured HCECs (passage 0) with or without SB203580. *Scale bar*: 100 μm. (**B**) The cell density of HCECs (passage 0) cultured with or without SB203580. Ten HCEC cultures from 10 independent donor corneas were used for the analysis. $^*P < 0.05$. The *horizontal lines* in the *boxes* indicate medians, the *bottom* of each *box* indicates the 25th percentile, and the *top* of each *box* indicates the 75th percentile. The *horizontal lines* outside the boxes indicate the ranges of cell density. (**C**) Expression of the function-related markers, ZO-1, N-cadherin, Na^+/K^+-ATPase was assessed by immunofluorescence staining. Actin cytoskeleton was assessed by F-actin staining. An HCEC culture established from a single donor cornea at passage 1 were used for the experiment. Nuclei were stained with DAPI. *Scale bar*: 100 μm.

than in control cells (0.22 and 0.10 [passage 3], respectively) (Fig. 3C). We evaluated the expression level of p16 and p21, as these inhibitory proteins are associated with senescence. Western blotting analysis demonstrated that the expression of p16 and p21 was reduced in the cells cultured with SB203580, whereas HCECs expressed high levels of p16 and p21 in the absence of SB203580 (Figs. 3D, 3E). Taken together, HCECs exhibit a senescent phenotype under culture conditions and inhibition of p38 MAPK signaling counteracts cellular senescence.

Suppression of the Senescence and Senescence-Associated Secretory Phenotype (SASP) by a p38 MAPK Inhibitor

Acquisition of an SASP, which includes secretion of inflammatory, growth-regulating, and tissue-remodeling factors, is one of the typical phenotypes of various senescent cell types. We evaluated the expression of 36 cytokines and chemokines related to SASP in culture medium cultured with or without SB203580 for 72 hours. The expression of six cytokines and chemokines (CXCL10, CCL5, CXCL1, IL-8, CCL2, and IL-6) was lower in HCECs treated with SB203580 than in control cells, whereas the expression of MIF was higher than in the control cells (Fig. 4A; Supplementary Fig. S2).

We further examined the expression levels of these cytokines by quantitative PCR (Figs. 4B–G). The expression levels of *IL-6*, *IL-8*, *CCL2*, and *CXCL1* were significantly downregulated in HCECs treated with SB203580 when compared with the control cells. The expression of CXCL10 at the protein level was suppressed, as shown in Figure 4A; however, the expression level of the *CXCL10* transcript was not statistically reliable (Fig. 4F). In addition, ELISA showed that the expression of IL-6 and IL-8 in culture medium was significantly downregulated by SB203580 (Figs. 4H, 4I). Thus, inhibition of p38 MAPK signaling pathway in HCECs counteracts the acquisition of SASP due to the culture conditions.

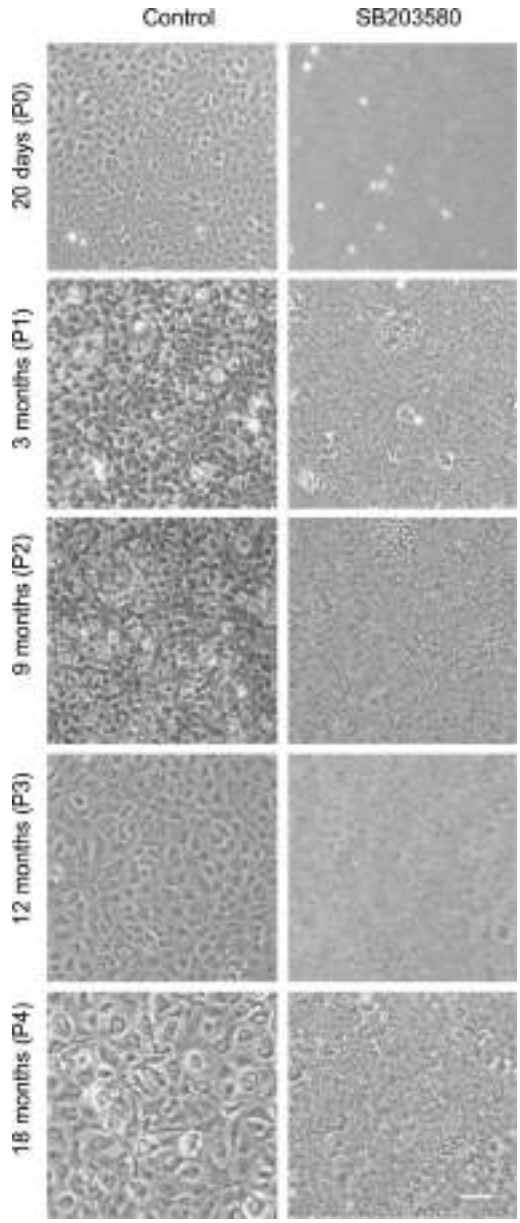

FIGURE 2. Phase-contrast images of long-term culture of HCECs with or without SB203580. HCECs were passaged and cultured with or without SB203580 for 18 months. Representative phase-contrast images show that a higher cell density of HCECs was maintained by culture with SB203580 than without SB203580 throughout the 18 months. Representative images of two HCEC cultures derived from two independent donor corneas are shown. *Scale bar*: 100 μm.

The Role of the p38 MAPK Signaling Pathway in HCECs

The p38 MAPK inhibitor blocked cellular senescence; therefore, we tested whether activation of the p38 MAPK signaling pathway was associated with cellular senescence in HCECs. Western blotting showed that anisomycin upregulated the phosphorylation of p38 MAPK and ATF-2, suggesting that anisomycin activated the p38 MAPK signaling pathway (Figs. 5A, B). HCECs treated with anisomycin exhibited a hexagonal and monolayer morphology, but the cell size was larger than the control cell size (data not shown). The cell density was significantly lower for the HCECs treated with anisomycin than for the control cells (Fig. 5C). Expression of p16 and p21 was greatly upregulated by anisomycin, whereas SB203580 was able to block this effect of anisomycin (Figs. 5D–F). Taken together, the p38 MAPK inhibitor, as shown in the schematic presentation in Figure 5G, is able to block the culture stress and the induction of p38 MAPK signaling-mediated senescent phenotypes.

DISCUSSION

Since 2013, we have been performing a clinical trial of injection of a combination of cultured HCECs and a ROCK inhibitor as a treatment for corneal endothelial dysfunction. However, the in vitro expansion of HCECs proved surprisingly difficult and we often had an insufficient number of cells with adequate cell quality for clinical use.[18] HCECs are difficult to maintain under culture conditions, and even if they survive, they show limited proliferative ability and undergo massive fibroblastic transformation with loss of functional phenotypes. Consequently, our research group and others have continuously strived to develop a successful culture method. For instance, we reported the effect of a ROCK inhibitor[23] and conditioned medium obtained from good manufacturing practice (GMP)-grade human bone marrow-derived mesenchymal stem cells[21] that enhanced HCEC proliferation. We also showed that activation of TGF-β signaling causes the fibroblastic transformation in HCECs, and that a TGF-β signaling inhibitor enables HCECs to avoid fibroblastic changes and maintain the HCEC phenotype.[24]

One remaining challenge is that HCECs tend to decrease their cell density, especially after several cell passages, leading to failure to obtain sufficient quantities of cells.[18] The CEC density is the most important indicator for corneal endothelial health in clinical settings,[25] so low cell density has become a concern with respect to transplanting cultured HCECs in humans. Recently, we have demonstrated that transplanted CECs of low cell density could regenerate corneal endothelium, but the cell density of the regenerated corneal endothelium was lower than that of the eye transplanted with high cell density CECs in a rabbit corneal endothelial dysfunction model.[18] These results suggested that obtaining high cell density CECs is essential for good prognosis after tissue engineering therapy.

Senescence, as defined by Hayflick,[26] is a loss of replicative ability due to the shortening of telomeres. A later study showed that senescence is induced by exhaustion of replicative capacity as well as by stress and oncogenes.[27–29] As cellular senescence is heterogeneous and cell-type dependent, no single biomarker can identify cellular senescence.[30] We used several biomarkers in the present study to show that the cell density drop in HCECs is a phenotypic feature of cellular senescence. We demonstrated that low cell density HCECs, which were cultured without a p38 MAPK inhibitor, showed high positive SA-β-gal staining, a low nuclear-cytoplasm ratio, and high expression of p16 and p21. SA-β-gal is the biomarker most frequently used to show upregulation of the lysosome mass induced by the loss of capabilities to respond to cellular damage and stress.[31,32] However, the sole use of SA-β-gal as marker often yields false-positive results, necessitating the use of a combination of several markers.[30] We evaluated cell size, because membrane lipid composition and membrane biophysical properties are altered by cellular senescence, resulting in an alteration of cell size.[33,34] In addition, cyclin dependent kinase inhibitors (CKIs), such as p16 and p21, have been used as biomarkers, because cell cycle arrest is recognized as a hallmark of cellular senescence.[30] Indeed, overexpression of p21 promotes cellular senescence,[35] and downregulation of

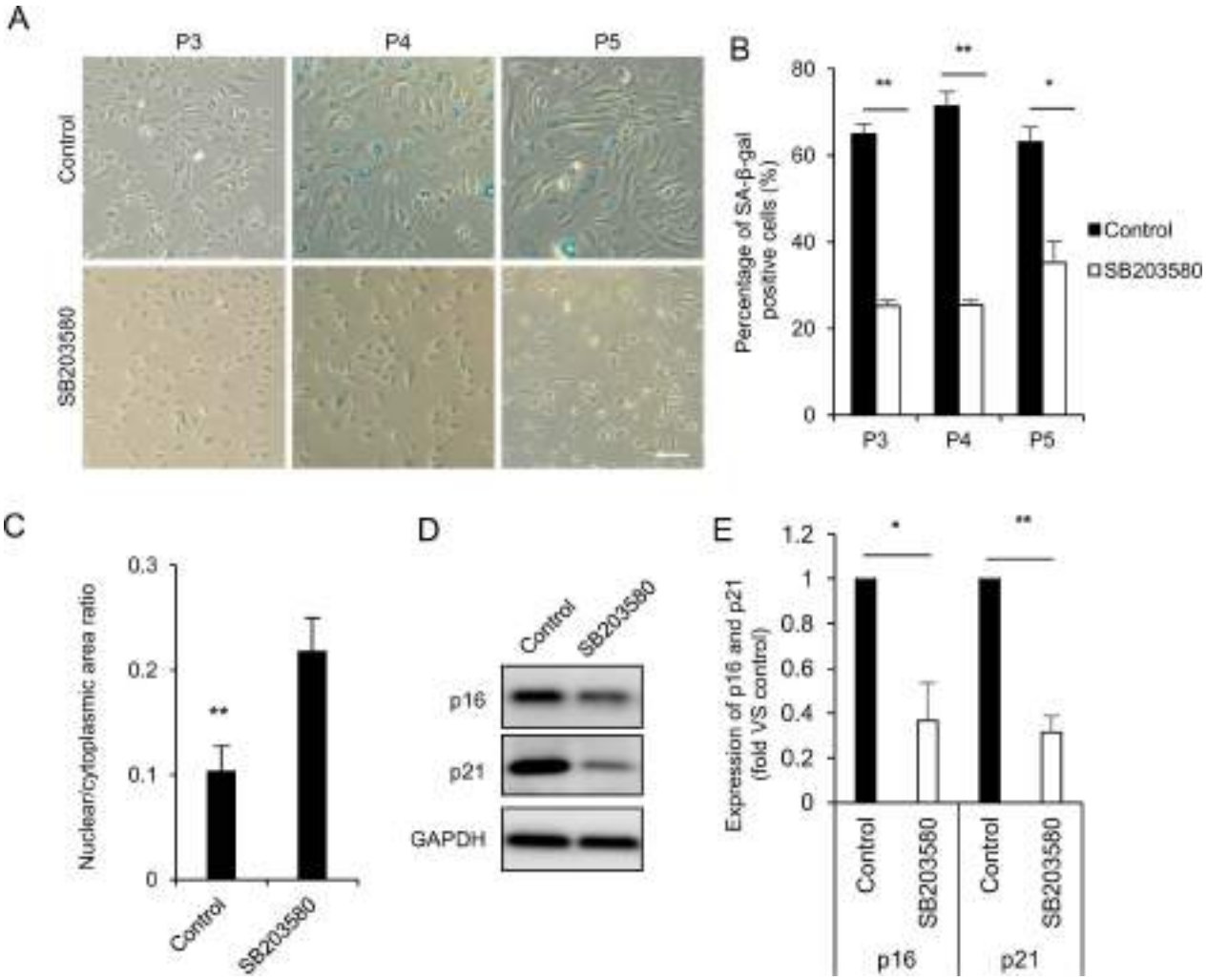

Figure 3. Suppression of senescent phenotypes by a p38 MAPK inhibitor. (**A**, **B**) The senescing cells were assessed by staining for SA-β-gal. The representative phase-contrast images depict HCECs treated with or without SB203580. The graph shows the percentage of SA-β-gal–positive cells (passages 3 to 5). The experiment was performed in triplicate and representative data from one of three independent experiments using an HCEC culture established from a single donor cornea are shown. *Scale bar*: 100 μm. $^{*}P < 0.05$, $^{**}P < 0.01$. (**C**) Nuclear/cytoplasmic area ratio in HCECs (passage 1) with or without SB203580 was determined by immunofluorescent staining images of F-actin and DAPI. Representative images analyzed are shown in Figure 1C. The cell borders determined by F-actin staining were manually traced using ImageJ and the cytoplasmic area was measured. Likewise, nuclear areas determined by DAPI staining were manually traced using ImageJ and measured. The average of 10 cells was plotted as a graph. The experiments were performed in triplicate and representative data from one of three independent experiments are shown. $^{**}P < 0.01$. (**D**) Expression of p16 and p21, the two major senescent-related G1 proteins, in HCECs (passage 3) cultured with or without SB203580 was evaluated by Western blotting. The experiments were performed in three HCEC cultures derived from three independent donor corneas. (**E**) Expression levels of p16 and p21 evaluated by Western blotting were assessed by densitometry. $^{*}P < 0.05$, $^{**}P < 0.01$.

p21 in senescent cells restores replicative capacity.[36] The expression levels of p16 and p21 in the corneal endothelium were higher in older donors than in young donors, suggesting that these CKIs might be suitable biomarkers.[3,37] Collectively, the results showing that low cell density HCECs exhibited multiple biomarkers of senescence indicated that the cell density drop during cell culture is induced by cellular senescence.

Consistently, we also showed that the low cell density HCECs exhibited SASP. The SASP phenomenon has been observed in various cell types, such as aged human fibroblasts and epithelial cells, and it is recognized as a robust marker of senescence.[38–40] The secreted factors include inflammatory mediators, growth factors, and detached cell surface molecules, but SASP is cell-type and senescence-stage dependent.[41,42] Here, we demonstrated that IL-6, IL-8, CCL2, and CXCL1 were expressed at high levels in low cell density HCECs. This finding suggests that these molecules are markers of SASP in HCECs and that they could be useful quality control markers in regenerative medicine, as they provide a contact-free and nondestructive evaluation.

In the current study, we showed that inhibition of the p38 MAPK signaling pathway counteracted the cell density drop observed during cell culture by suppressing senescence. In addition, activation of p38 MAPK signaling mediated by anisomycin induced the senescence associated with the cell density drop. Iwasa and his colleagues[20] induced four different types of senescence: Ras-induced, replicative, oxidative stress–induced, and culture shock–induced senescence, and they demonstrated that p38 MAPK is a senescence-executing molecule. In addition, inhibition of p38 MAPK signaling counteracted the senescence programs. Recently, other researchers have shown that inhibition of p38 MAPK decreased p16 levels and restored replicative capacity in aged

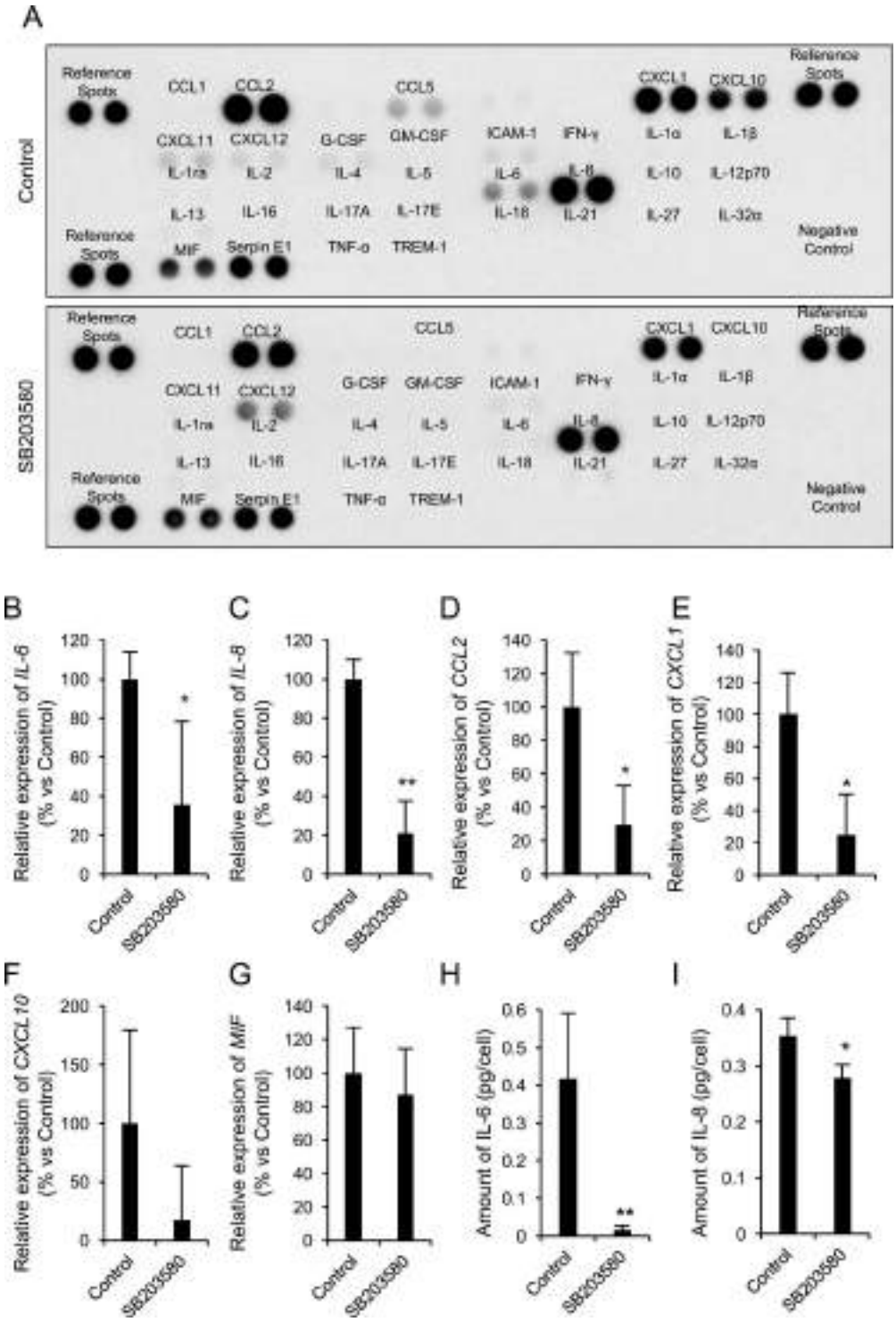

Figure 4. Suppression of the senescence and the SASP by a p38 MAPK inhibitor. (**A**) Expression of 36 cytokines and chemokines in HCECs (passage 0) cultured with or without SB203580. Representative data from experiments using three HCEC cultures derived from three independent donor corneas are shown. (**B**–**G**) Expression of the cytokines and chemokines that differ in HCECs (passage 1) cultured with and without SB203580, evaluated by quantitative PCR. The experiments were performed in duplicate using six HCEC cultures established from six independent donor corneas. $^{*}P < 0.05$, $^{**}P < 0.01$. (**H**, **I**) ELISA evaluation of IL-6 and IL-8 in the culture medium derived from HCEC cultures established from four independent donor corneas (passage 0) cultured with or without SB203580. $^{*}P < 0.05$, $^{**}P < 0.01$.

muscle stem cells.[43] We showed that these antisenescent effects of inhibition of p38 MAPK signaling are consistently shown in HCECs, and could be applicable in tissue engineering therapy.

In conclusion, activation of p38 MAPK signaling due to culture stress may be a causative factor that induces cellular senescence, whereas the use of a p38 MAPK inhibitor can counteract this senescence and allow the generation of

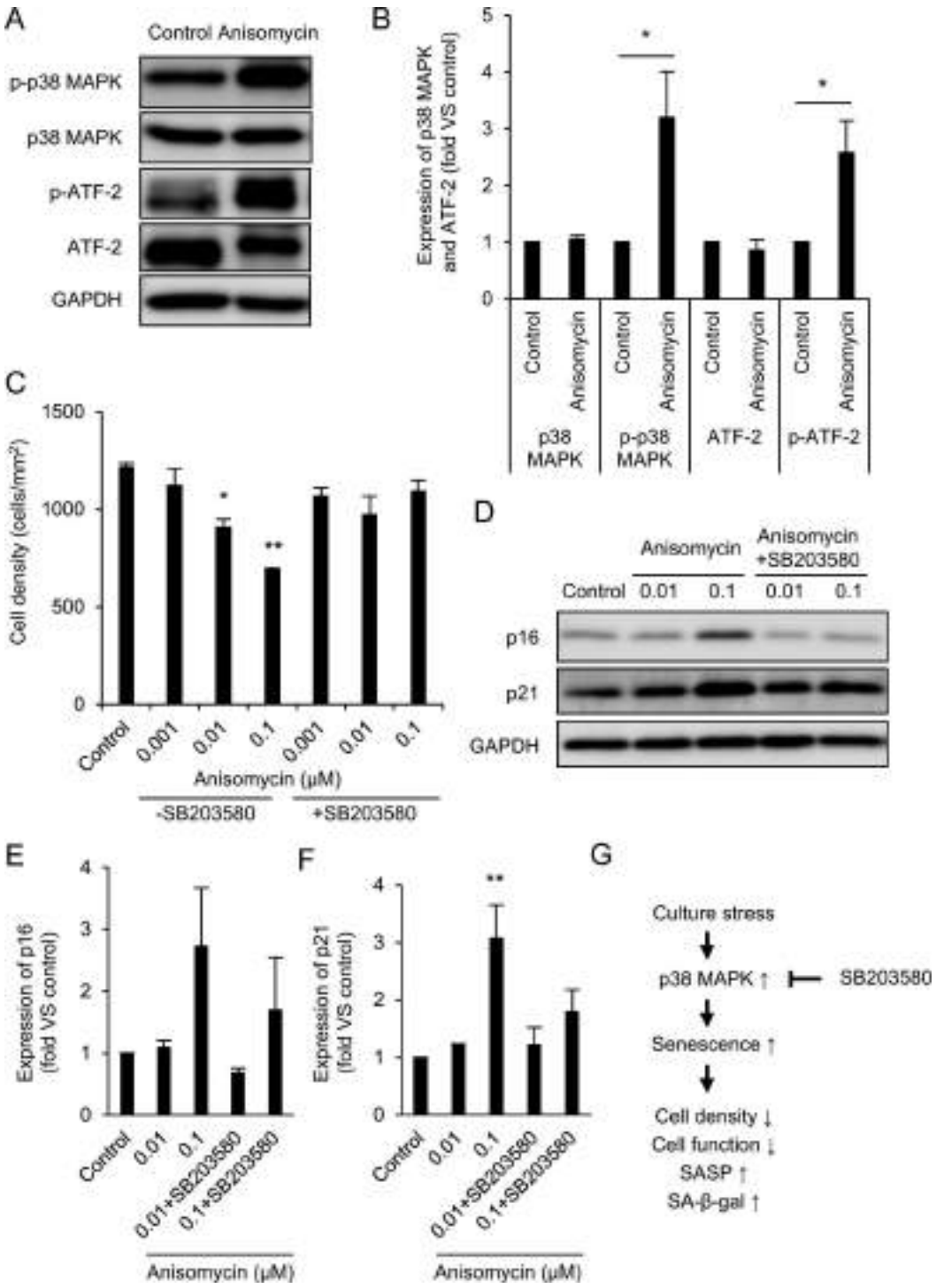

Figure 5. The role of p38 MAPK signaling pathway on HCECs. (**A**) Western blot analysis of the expression of phosphorylated p38 MAPK, p38 MAPK, phosphorylated ATF-2 and ATF-2 in HCECs (passage 15) treated with or without 10 μM anisomycin. Representative data from triplicate experiments using three HCEC cultures established from three independent donor corneas are shown. (**B**) Expression levels of phosphorylated p38 MAPK, p38 MAPK, phosphorylated ATF-2, and ATF-2 were evaluated by Western blotting and assessed by densitometry. $^{*}P < 0.05$. (**C**) Cell density of HCECs (passage 15) treated with or without anisomycin (0.001 μM, 0.01 μM, 0.1 μM) with or without SB203580 (10 μM). Representative data from triplicate experiments using three HCEC cultures established from three independent donor corneas are shown. $^{*}P < 0.05$, $^{**}P < 0.01$. (**D**) Western blot analysis of the expression of p16 and p21 in HCECs (passage 11) treated with or without anisomycin (0.01 μM, 0.1 μM) with or without SB203580 (10 μM). Representative data from triplicate experiments using four HCEC cultures established from four independent donor corneas are shown. (**E**, **F**) Expression levels of p16 and p21 were evaluated by Western blotting and assessed by densitometry. $^{**}P < 0.01$. (**G**) A model of the involvement of p38 MAPK signaling pathway in cellular senescence of HCECs under culture conditions, showing how SB203580 maintains a nonsenescent phenotype.

sufficient numbers of HCECs for tissue engineering therapy for treatment of corneal endothelial dysfunction. Furthermore, the antisenescence effects of p38 MAPK inhibitors may be worth evaluating in different cell types in other settings of regenerative medicine.

Acknowledgments

The authors thank Fuyuki Ishikawa for valuable advice for experiments presented in the article and Monty Montoya and Bernie Iliakis (SightLife) for providing donor corneas.

Supported by the Program for the Strategic Research Foundation at Private Universities from MEXT (NK, NO).

Disclosure: **A. Hongo**, None; **N. Okumura**, P; **M. Nakahara**, None; **E.P. Kay**, None; **N. Koizumi**, P

References

1. Bonanno JA. Molecular mechanisms underlying the corneal endothelial pump. *Exp Eye Res*. 2012;95:2–7.
2. Bourne WM. Clinical estimation of corneal endothelial pump function. *Trans Am Ophthalmol Soc*. 1998;96:229–239; discussion 239–242.
3. Joyce NC. Proliferative capacity of the corneal endothelium. *Prog Retin Eye Res*. 2003;22:359–389.
4. Joyce NC. Cell cycle status in human corneal endothelium. *Exp Eye Res*. 2005;81:629–638.
5. Geroski DH, Matsuda M, Yee RW, Edelhauser HF. Pump function of the human corneal endothelium. Effects of age and cornea guttata. *Ophthalmology*. 1985;92:759–763.
6. Eye Bank Association of America. 2015 Eye Banking Statistical Report. Available at: http://restoresight.org/wp-content/uploads/2016/03/2015-Statistical-Report.pdf.
7. Tan DT, Dart JK, Holland EJ, Kinoshita S. Corneal transplantation. *Lancet*. 2012;379:1749–1761.
8. Gorovoy MS. Descemet-stripping automated endothelial keratoplasty. *Cornea*. 2006;25:886–889.
9. Melles GR, Lander F, Rietveld FJ. Transplantation of Descemet's membrane carrying viable endothelium through a small scleral incision. *Cornea*. 2002;21:415–418.
10. Ishino Y, Sano Y, Nakamura T, et al. Amniotic membrane as a carrier for cultivated human corneal endothelial cell transplantation. *Invest Ophthalmol Vis Sci*. 2004;45:800–806.
11. Mimura T, Yamagami S, Yokoo S, et al. Cultured human corneal endothelial cell transplantation with a collagen sheet in a rabbit model. *Invest Ophthalmol Vis Sci*. 2004;45:2992–2997.
12. Sumide T, Nishida K, Yamato M, et al. Functional human corneal endothelial cell sheets harvested from temperature-responsive culture surfaces. *FASEB J*. 2006;20:392–394.
13. Koizumi N, Sakamoto Y, Okumura N, et al. Cultivated corneal endothelial cell sheet transplantation in a primate model. *Invest Ophthalmol Vis Sci*. 2007;48:4519–4526.
14. Okumura N, Koizumi N, Ueno M, et al. ROCK inhibitor converts corneal endothelial cells into a phenotype capable of regenerating in vivo endothelial tissue. *Am J Pathol*. 2012;181:268–277.
15. Okumura N, Sakamoto Y, Fujii K, et al. Rho kinase inhibitor enables cell-based therapy for corneal endothelial dysfunction. *Sci Rep*. 2016;6:26113.
16. Miyata K, Drake J, Osakabe Y, et al. Effect of donor age on morphologic variation of cultured human corneal endothelial cells. *Cornea*. 2001;20:59–63.
17. Okumura N, Hirano H, Numata R, et al. Cell surface markers of functional phenotypic corneal endothelial cells. *Invest Ophthalmol Vis Sci*. 2014;55:7610–7618.
18. Okumura N, Kusakabe A, Hirano H, et al. Density-gradient centrifugation enables the purification of cultured corneal endothelial cells for cell therapy by eliminating senescent cells. *Sci Rep*. 2015;5:15005.
19. Roberts PJ, Der CJ. Targeting the Raf-MEK-ERK mitogen-activated protein kinase cascade for the treatment of cancer. *Oncogene*. 2007;26:3291–3310.
20. Iwasa H, Han J, Ishikawa F. Mitogen-activated protein kinase p38 defines the common senescence-signalling pathway. *Genes Cells*. 2003;8:131–144.
21. Nakahara M, Okumura N, Kay EP, et al. Corneal endothelial expansion promoted by human bone marrow mesenchymal stem cell-derived conditioned medium. *PLoS One*. 2013;8:e69009.
22. Okumura N, Kakutani K, Numata R, et al. Laminin-511 and -521 enable efficient in vitro expansion of human corneal endothelial cells. *Invest Ophthalmol Vis Sci*. 2015;56:2933–2942.
23. Okumura N, Ueno M, Koizumi N, et al. Enhancement on primate corneal endothelial cell survival in vitro by a ROCK inhibitor. *Invest Ophthalmol Vis Sci*. 2009;50:3680–3687.
24. Okumura N, Kay EP, Nakahara M, Hamuro J, Kinoshita S, Koizumi N. Inhibition of TGF-beta signaling enables human corneal endothelial cell expansion in vitro for use in regenerative medicine. *PLoS One*. 2013;8:e58000.
25. Bourne WM, Nelson LR, Hodge DO. Central corneal endothelial cell changes over a ten-year period. *Invest Ophthalmol Vis Sci*. 1997;38:779–782.
26. Hayflick L. The limited in vitro lifetime of human diploid cell strains. *Exp Cell Res*. 1965;37:614–636.
27. Campisi J. The biology of replicative senescence. *Eur J Cancer*. 1997;33:703–709.
28. Toussaint O, Medrano EE, von Zglinicki T. Cellular and molecular mechanisms of stress-induced premature senescence (SIPS) of human diploid fibroblasts and melanocytes. *Exp Gerontol*. 2000;35:927–945.
29. Bartkova J, Rezaei N, Liontos M, et al. Oncogene-induced senescence is part of the tumorigenesis barrier imposed by DNA damage checkpoints. *Nature*. 2006;444:633–637.
30. Matjusaitis M, Chin G, Sarnoski EA, Stolzing A. Biomarkers to identify and isolate senescent cells. *Ageing Res Rev*. 2016;29:1–12.
31. Dimri GP, Lee X, Basile G, et al. A biomarker that identifies senescent human cells in culture and in aging skin in vivo. *Proc Natl Acad Sci U S A*. 1995;92:9363–9367.
32. Bassaneze V, Miyakawa AA, Krieger JE. A quantitative chemiluminescent method for studying replicative and stress-induced premature senescence in cell cultures. *Anal Biochem*. 2008;372:198–203.
33. Fulop T, Le Page A, Garneau H, et al. Aging, immunosenescence and membrane rafts: the lipid connection. *Longev Healthspan*. 2012;1:6.
34. Kim MS, Jo S, Park JT, et al. Method to purify and analyze heterogeneous senescent cell populations using a microfluidic filter with uniform fluidic profile. *Anal Chem*. 2015;87:9584–9588.
35. Huang Y, Corbley MJ, Tang Z, et al. Down-regulation of p21WAF1 promotes apoptosis in senescent human fibroblasts: involvement of retinoblastoma protein phosphorylation and delay of cellular aging. *J Cell Physiol*. 2004;201:483–491.
36. Schnabl B, Purbeck CA, Choi YH, Hagedorn CH, Brenner D. Replicative senescence of activated human hepatic stellate cells is accompanied by a pronounced inflammatory but less fibrogenic phenotype. *Hepatology*. 2003;37:653–664.
37. Joyce NC. Proliferative capacity of corneal endothelial cells. *Exp Eye Res*. 2012;95:16–23.

Investigative Ophthalmology & Visual Science

38. Acosta JC, O'Loghlen A, Banito A, et al. Chemokine signaling via the CXCR2 receptor reinforces senescence. *Cell*. 2008; 133:1006–1018.

39. Campisi J, Andersen JK, Kapahi P, Melov S. Cellular senescence: a link between cancer and age-related degenerative disease? *Semin Cancer Biol*. 2011;21:354–359.

40. Acosta JC, Banito A, Wuestefeld T, et al. A complex secretory program orchestrated by the inflammasome controls paracrine senescence. *Nat Cell Biol*. 2013;15:978–990.

41. Coppe JP, Desprez PY, Krtolica A, Campisi J. The senescence-associated secretory phenotype: the dark side of tumor suppression. *Annu Rev Pathol*. 2010;5:99–118.

42. Maciel-Baron LA, Morales-Rosales SL, Aquino-Cruz AA, et al. Senescence associated secretory phenotype profile from primary lung mice fibroblasts depends on the senescence induction stimuli. *Age (Dordr)*. 2016;38:26.

43. Cosgrove BD, Gilbert PM, Porpiglia E, et al. Rejuvenation of the muscle stem cell population restores strength to injured aged muscles. *Nat Med*. 2014;20:255–264.

Investigative Ophthalmology & Visual Science

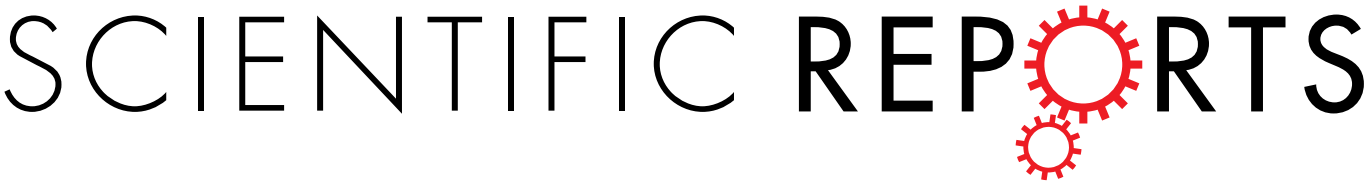

OPEN

Laminin-511 and -521-based matrices for efficient *ex vivo*-expansion of human limbal epithelial progenitor cells

Received: 23 February 2017
Accepted: 22 May 2017
Published: [illegible] 2017

Naresh Polisetti[1], Lydia Sorokin[2], Naoki Okumura[3], Noriko Koizumi[3], Shigeru Kinoshita[4], Friedrich E. Kruse[1] & Ursula Schlötzer-Schrehardt[1]

Optimization of culture conditions for human limbal epithelial stem/progenitor cells (LEPC) that incorporate the *in vivo* cell-matrix interactions are essential to enhance LEPC *ex vivo*-expansion and transplantation efficiency. Here, we investigate the efficacy of laminin (LN) isoforms preferentially expressed in the limbal niche as culture matrices for epithelial tissue engineering. Analyses of expression patterns of LN chains in the human limbal niche provided evidence for enrichment of LN-α2, -α3, -α5, -β1, -β2, -β3, -γ1, -γ2 and -γ3 chains in the limbal basement membrane, with LN-α5 representing a signature component specifically produced by epithelial progenitor cells. Recombinant human LN-521 and LN-511 significantly enhanced *in vitro* LEPC adhesion, migration and proliferation compared to other isoforms, and maintained phenotype stability. The bioactive LN-511-E8 fragment carrying only C-terminal domains showed similar efficacy as full-length LN-511. Functional blocking of α3β1 and α6β1 integrins suppressed adhesion of LEPC to LN-511/521-coated surfaces. Cultivation of LEPC on fibrin-based hydrogels incorporating LN-511-E8 resulted in firm integrin-mediated adhesion to the scaffold and well-stratified epithelial constructs, with maintenance of a progenitor cell phenotype in their (supra)basal layers. Thus, the incorporation of chemically defined LN-511-E8 into biosynthetic scaffolds represents a promising approach for xeno-free corneal epithelial tissue engineering for ocular surface reconstruction.

Limbal epithelial stem/progenitor cells (LEPC) are located in the basal layer of the epithelium at the corneoscleral limbus and are responsible for homeostasis of the corneal epithelium, which is an important prerequisite for corneal transparency and visual function[1,2]. Any damage or injury to this stem/progenitor cell reservoir and/or destruction of its niche microenvironment can lead to corneal neovascularization, chronic inflammation, and stromal scarring associated with corneal opacity and loss of vision[3–5]. Transplantation of *ex vivo*- expanded LEPC on amniotic membrane or fibrin gels is an established therapeutic strategy to regenerate the damaged corneal surface in patients with limbal stem cell deficiency (LSCD)[6–9]. Since its introduction in 1997[10], cultured limbal epithelial transplantation (CLET) has been applied in various clinical centres with follow-up periods of more than 15 years[8,11–14]. Despite many variables between studies (regarding inclusion/exclusion criteria, culture methods, transplantation techniques, and clinical outcome measures), long-term engraftment of autologous cultivated limbal epithelial cells has been shown to be good and the overall success rates of autologous CLET for unilateral LSCD with a follow-up period of at least 24 months were reported to amount to 72–76%[8,15,16]. In spite of these good clinical outcomes confirming CLET as an adequate therapy to successfully reconstruct the corneal surface in the majority of patients, long-term corneal regeneration in other series often proved less satisfactory due to recurrent mild neovascularisation of the corneal surface in many patients[17]. These complications might be caused by low quality of the graft or inadequate properties of transplanted progenitor cells[8,11,18]. A major hurdle in

[1]Department of Ophthalmology, Universitätsklinikum Erlangen, Friedrich-Alexander-Universität Erlangen-Nürnberg, Erlangen, Germany. [2]Institute of Physiological Chemistry and Pathobiochemistry and Cells-in-Motion Cluster of Excellence, University of Muenster, Muenster, Germany. [3]Department of Biomedical Engineering, Faculty of Life and Medical Sciences, Doshisha University, Kyotanabe, Japan. [4]Department of Frontier Medical Science and Technology for Ophthalmology, Kyoto Prefectural University of Medicine, Kyoto, Japan. Correspondence and requests for materials should be addressed to U.S.-S. (email: ursula.schloetzer-schrehardt@uk-erlangen.de)

in vitro culturing of LEPC is that they readily differentiate, hampering their use for therapeutic applications[19,20]. These limitations underscore the need for developing novel standardized LEPC culture techniques that ensure preservation of the stem/progenitor cell phenotype and function during cultivation and after transplantation.

In vivo, LEPC reside in a highly specialized and complex microenvironment that is known as the limbal niche, where stem cell quiescence, proliferation and differentiation are maintained in balance[21]. Besides several types of supporting niche cells that include melanocytes and mesenchymal stromal cells, the limbal niche comprises a specific extracellular matrix (ECM) composition[22]. Indeed, the ECM has been recognized as a crucial part of many stem cell niches mediating biophysical, mechanical and biochemical signals that regulate stem cell survival, proliferation and differentiation[23–26]. Laminins (LNs) are the best-described ECM constituents present in basement membranes (BM) of adult stem cell niches, where they influence cell behaviors, such as cell adhesion, differentiation, and phenotype stability. To date, five alpha (α1-5), four beta (β1-4), and three gamma (γ1-3) chains have been identified that can combine to form up to 16 heterotrimeric isoforms in mammalian tissues, showing tissue-specific distribution patterns[27–30]. We have previously shown that LN chains α1, α2, α5, β1, β2, γ1 and γ3 are preferentially localized to the BM of the limbal epithelium compared to that of the corneal epithelium, where LN chains α3, β3 and γ2 predominate[31]. Our work has further suggested that LEPC are anchored to LN-α2 and -α5 in their niche by expression of LN receptors α3β1 and α6β4 integrins[32]. The heterogeneity of LN isoform expression in BMs of ocular surface epithelia, which has been also reported by other groups[33–35], suggests a functional role for LN-α2 and -α5 containing isoforms in the limbal stem cell niche.

Stem cell-based tissue engineering aims to mimic the native stem cell niche and to present the appropriate microenvironmental cues, including ECM components, in a controlled and reproducible fashion in order to maintain stem cell function within the graft[36,37]. We have previously reported that the LN-332 isoform can serve as a suitable substrate to induce transdifferentiation of hair follicle stem cells into corneal epithelial-like cells in the presence of limbal fibroblast conditioned medium[38]. It has also been suggested that proteolytic fragments of LN-332 γ2 chain potentiate the outgrowth of limbal epithelial cells on intact amniotic membrane[39], and that vitronectin adsorbed to therapeutic contact lenses support LEPC expansion[40]. Otherwise, little attention has been paid to the role of the ECM in LEPC *ex vivo*-expansion, and the effect of limbus-specific LNs on LEPC phenotype and function *in vitro* has not been investigated. We hypothesize that the LN isoforms that are specifically expressed in the limbal stem cell niche may be used as exogenous cues to promote *ex vivo*-expansion and maintenance of LEPC. In this study, we systematically analyze expression patterns of LN chains in LEPC clusters isolated by laser capture microdissection (LCM), in tissue sections and in cultured LEPC by quantitative RT-PCR (qPCR) and confocal microscopy, and test the effects of niche-specific recombinant LN isoforms on LEPC adhesion, migration, proliferation and differentiation *in vitro*. We also examine the efficacy of a recombinant human LN-511-E8 fragment[41,42] for epithelial tissue engineering using fibrin-based hydrogels as carrier. Our findings demonstrate that LN-α5 constitutes a signature BM component of the limbal niche and that LN-511 or -521 promote *ex vivo*-expansion and maintenance of LEPC. The C-terminal fragment of LN-511 (LN-511-E8 fragment) shows comparable efficacy as full-length LN-511 and supports the formation of well stratified epithelial constructs with maintenance of a progenitor cell phenotype. Thus, LN-511-E8 represents a chemically defined, xeno-free substrate for improved corneal epithelial tissue engineering and future clinical application.

Results

Expression of laminin chains in the limbal stem cell niche *in situ*. Expression patterns of different LN chains were analyzed in LCM-dissected LEPC clusters, containing both epithelial stem/progenitor cells and associated niche cells[32], and basal corneal epithelial cell (BCEC) populations by qPCR (n = 5). Quality control of amplified RNA and purity of dissected cell populations were as described previously[32]. All LN chains were expressed in both LEPC and BCEC populations except LN-γ3 (*LAMC3*). Expression levels of LN-α2 (*LAMA2*: 3.1 ± 0.6-fold; p = 0.02), LN-α4 (*LAMA4*: 98.3 ± 50.0-fold; p = 0.02), LN-α5 (*LAMA5:* 7.2 ± 4.6-fold; p = 0.01), LN-β2 (*LAMB2*: 3.0 ± 0.4-fold; p = 0.04), LN-β3 (*LAMB3*: 3.0 ± 0.8-fold; p = 0.02) and LN-γ2 (*LAMC2*: 3.0 ± 0.8-fold; p = 0.04) were significantly higher in LEPC compared with BCEC, whereas no differential expression patterns were observed for LN-α1 (*LAMA1*), -α3 (*LAMA3*), -β1 (*LAMB1*), -β4 (*LAMB4*), and -γ1 (*LAMC1*) (Fig. 1A). Of note, corneal epithelial expression levels of LN-α4 and –α5 were hardly above the detection threshold.

By immunohistochemistry using chain-specific antibodies (Table 1; n = 10), the LN-α2, -α3, -α5, -ß1, -ß2, -ß3, -γ1, and -γ2 chains were shown to be strongly expressed in the limbal BM, whereas LN-α1 and -γ3 chains were only weakly expressed (Fig. 1B). The LN-α4 chain was not detected in epithelial but only in vascular basement membranes (Fig. 1B). Antibodies against LN-ß4 were not available. The most pronounced *differential* expression patterns between limbal and corneal regions were observed for LN-α2, -α5, -ß2, and -γ3 chains, which could be hardly detected in the corneal BM (Fig. 1B).

Concurrent with the qPCR data, the immunohistochemical findings suggest that the human limbal niche is specifically enriched for LN-α2 and -α5 chains.These were found to co-localize with the progenitor cell markers cytokeratin (CK)15, N-cadherin, and p63α as well as with integrins α3, α6 and ß1 expressed by LEPC clusters in the basal epithelium at the limbus (data for LN-α5 is shown in Fig. 1C).

Expression of laminin chains in limbal stem/progenitor and associated niche cells *in vitro*. To determine the relative contribution of LEPC and their associated stromal niche cells to expression of LN chains in the limbal niche, we established cultures of both LEPC and limbal mesenchymal stromal cells (LMSC) from collagenase-digested LEPC clusters (n = 5) as described previously (Fig. 2A)[32]. To verify the purity of cell populations, we analyzed the expression profiles of established corneal epithelial (progenitor) markers,

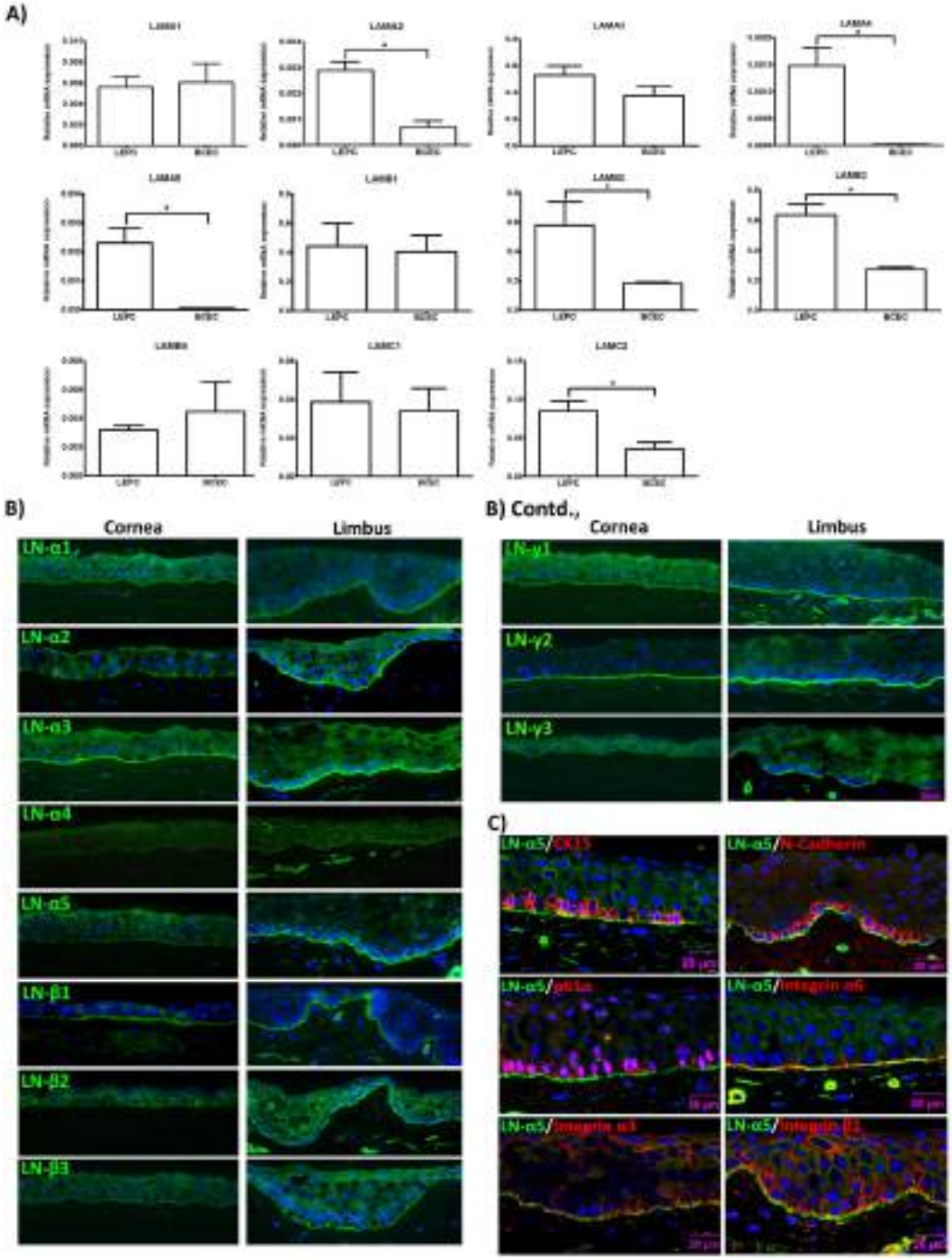

Figure 1. Expression of laminin chains in the limbal stem cell niche *in situ*. (**A**) Quantitative real-time polymerase chain reaction (qRT-PCR) primer assays showing higher expression levels of laminin α2 (LAMA2), α4 (LAMA4), α5 (LAMA5), β2 (LAMB2), β3 (LAMB3), and γ2 (LAMC2) in microdissected limbal epithelial stem/progenitor cell (LEPC) clusters compared with basal corneal epithelial cell (BCEC) populations; laminin α1 (LAMA1), α3 (LAMA3), β1 (LAMB1), β4 (LAMB4), γ1 (LAMC1) showed no differential expression patterns. Data are expressed as means ($2^{-\Delta CT} \times 1{,}000$) ± SEM ($n = 5$); *$p < 0.05$; Mann-Whitney *U* test. (**B**) Immunofluorescence analyses of corneoscleral tissue sections showing differential staining patterns of laminin α2, α5, β2, β3, γ2, and γ3, but similar staining patterns of laminin α1, α3, β1, and γ1 in the basement membranes of corneal and limbal epithelia; laminin α4 was largely negative in epithelial basement membranes. Nuclei are counterstained with DAPI (blue); scale bar = 60 μm. (**C**) Immunofluorescence double labeling of laminin (LN) α5 (green) and cytokeration (CK)15, N-Cadherin, p63α, integrin α6, integrin α3, and integrin β1 (red); nuclear counterstaining with DAPI (blue); scale bar = 20 μm.

Antibody (clone), Host species	Antibody concentration	Application	Antibody source [Ref.]
CD31 (WM59), mouse	15 µg/ml	Flow Cytometry	BD
CD34 (563), mouse	50 µg/ml	Flow Cytometry	BD
CD44 (G44-26), mouse	25 µg/ml	Flow Cytometry	BD
CD45 (HI30), mouse	50 µg/ml	Flow Cytometry	BD
CD73 (AD2), mouse	50 µg/ml	Flow Cytometry	BD
CD90 (5E10), mouse	100 µg/ml	Flow Cytometry	BD
CD105 (266), mouse	50 µg/ml	Flow Cytometry	BD
Mouse IgG1k	100 µg/ml	Flow Cytometry	BD
CD49c (Integrin α3) APC (P1B5), mouse	1.25 µg/ml	Flow Cytometry	eBioscience
CD49f (Integrin α6) APC (GoH3), rat	1.25 µg/ml	Flow Cytometry	eBioscience
CD29 (Integrin β1) FITC (TS2/16), mouse	2.5 µg/ml	Flow Cytometry	eBioscience
CD104 (Integrin β4) eFluor 660 (439-9B), rat	10 µg/ml	Flow Cytometry	eBioscience
IgG1 isotype FITC (IS5-21F5), mouse	2.5 µg/ml	Flow Cytometry	Miltenyi Biotec
IgG1 isotype APC (IS5-21F5), mouse	1.25–2.5 µg/ml	Flow Cytometry	Miltenyi Biotec
IgG2b isotype APC (141945), rat	1.25–10 µg/ml	Flow Cytometry	R&D Systems
Integrin α3 (ASC-1), mouse	20 µg/ml	Blocking	Millipore
Integrin α6 (NKI-GoH3), rat	20 µg/ml	Blocking	Millipore
Integrin β1 (P5D2), mouse	2.5 µg/ml	Blocking	R&D Systems
Cytokeratin 3 (AE5), mouse	1:100	Immunohistochemistry	Chemicon/Millipore
Cytokeratin 15 (LHK15), mouse	1:500	Immunohistochemistry	Abcam
Integrin α3 (P1B5), mouse	1:200	Immunohistochemistry	Dako
Integrin α6 (GoH3), rat	1:100	Immunohistochemistry	Chemicon/Millipore
Integrin β1 (HB1.1), mouse	1:500	Immunohistochemistry	Chemicon/Millipore
Ki-67 (SP6), rabbit	1:1000	Immunohistochemistry	Abcam
Laminin α1 (317), rabbit	1:500	Immunohistochemistry	L. Sorokin[63]
Laminin α2 (401), rabbit	1:500	Immunohistochemistry	L. Sorokin[63]
Laminin α3, rabbit	1:6000	Immunohistochemistry	R. Timpl/T. Sasaki
Laminin α4 (377), rabbit	1:2000	Immunohistochemistry	L. Sorokin[63]
Laminin α5 (405), rabbit	1:4000	Immunohistochemistry	L. Sorokin[63]
Laminin β1 (IIID9), mouse	undiluted	Immunohistochemistry	L. Sorokin[63]
Laminin β2 (409), rabbit	1:200	Immunohistochemistry	L. Sorokin[63]
Laminin β3, rabbit	1:6000	Immunohistochemistry	R. Timpl/T. Sasaki
Laminin γ1 (3E10), rat	undiluted	Immunohistochemistry	L. Sorokin[63]
Laminin γ2 (LE4-6), rabbit	1:4000	Immunohistochemistry	R. Timpl/T. Sasaki
Laminin γ3, rabbit	1:2000	Immunohistochemistry	R. Timpl/T. Sasaki
N-Cadherin (6G11), mouse	1:25	Immunohistochemistry	Dako
p63α, rabbit	1:100	Immunohistochemistry	Cell Signaling

Table 1. List of antibodies used.

such as cytokeratin 3 (KRT3) and 15 (KRT15) and carcinoembryonic antigen-related cell adhesion molecule 1 (CEACAM1), as well as mesenchymal (stem cell) markers, such as intercellular cell adhesion molecule 1 (ICAM1), sex determining region Y –box 2 (SOX2), and stem cell factor receptor (KIT) by qPCR primer assays ($n = 5$). As expected, LEPC populations showed significantly higher expression levels of KRT3 (10.3 ± 6.3-fold), KRT15 (5.6 ± 2.1-fold) and CEACAM (11.6 ± 4.5-fold), while LMSC populations showed higher expression levels of ICAM1 (5.4 ± 2.9-fold), SOX2 (5.0 ± 2.1-fold) and KIT (19.6 ± 10.2-fold) ($p = 0.02$) (Fig. 2B). LMSC were further characterized by flow cytometry ($n = 3$) with more than 90% of the cells expressing the mesenchymal stem cell markers CD73, CD90, CD105, and CD44 (Fig. 2C).

Differential gene expression analyses ($n = 5$) showed that LN-α3 (27.1 ± 17.3-fold; $p = 0.02$), -α5 (15.6 ± 10.4-fold; $p = 0.02$), -β3 (32.1 ± 27.3-fold; $p = 0.02$), and -γ2 (23.4 ± 11.9-fold; $p = 0.03$) chains were predominantly expressed in the LEPC population compared to LMSC, whereas LN-α2 (5.2 ± 2.6-fold; $p = 0.02$), -α4 (30.9 ± 21.5-fold; $p = 0.02$), -β2 (4.4 ± 0.8-fold; n.s.), -γ1 (2.7 ± 0.6-fold; $p = 0.02$), and -γ3 (8.4 ± 1.5-fold; $p = 0.02$) chains were predominantly expressed in LMSC compared to LEPC (Fig. 2D).

Together, these expression data obtained *in vivo* and *in vitro* suggest that LN-α5 constitutes a signature BM component of the limbal niche, which is endogenously produced by LEPC and becomes strongly enriched in the BM of the limbal niche.

Effect of laminin isoforms on LEPC adhesion, migration, proliferation and differentiation. The cell-binding activities of LN isoforms are largely determined by α chains[27,43]. As the availability of purified LN

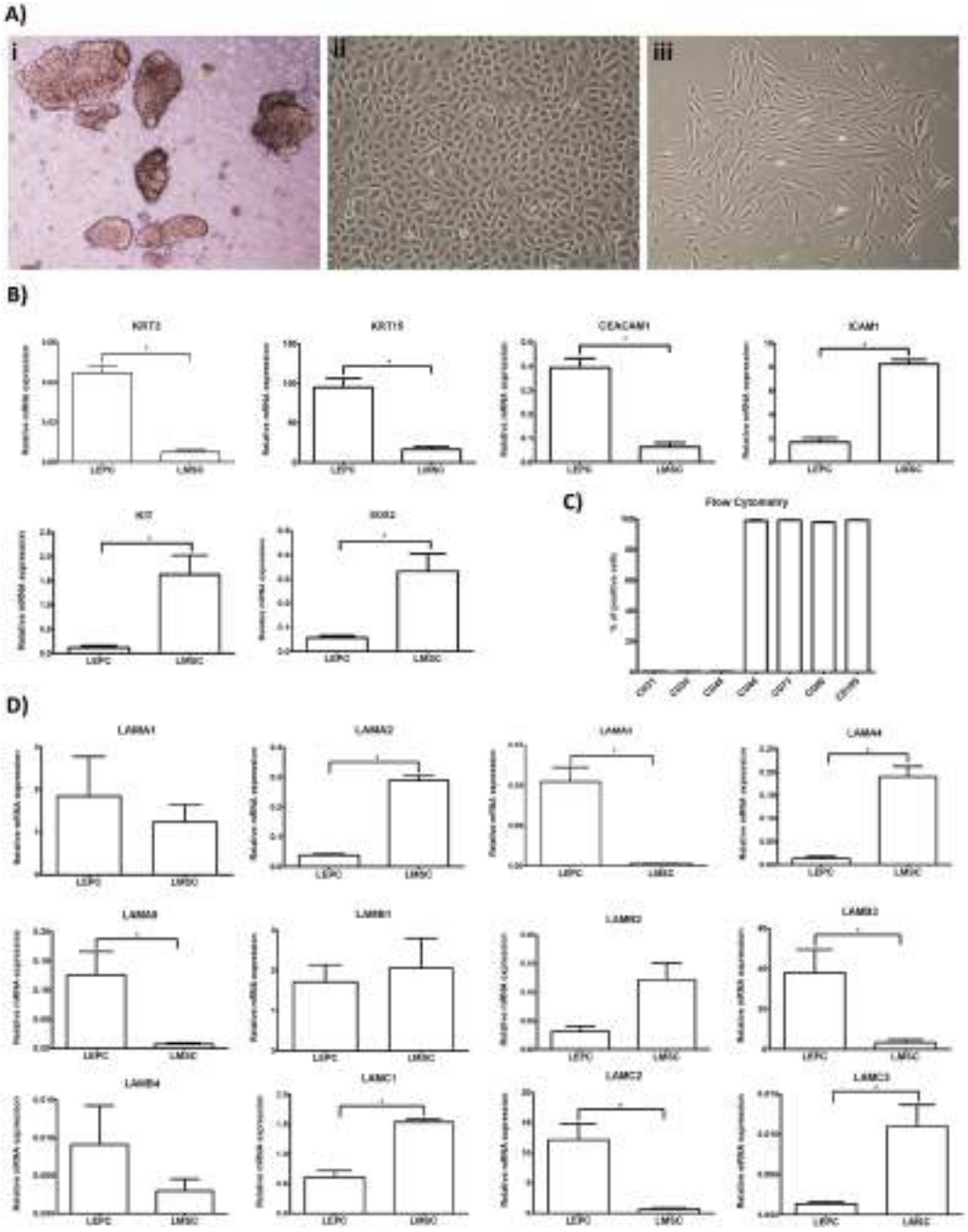

Figure 2. Expression of laminin chains in limbal stem/progenitor and associated niche cells *in vitro*. (**A**) Phase contrast images of (i) limbal epithelial cell clusters after collagenase digestion, (ii) cultured limbal epithelial progenitor cells, and (iii) associated mesenchymal stromal cells. (**B**) Quantitative real-time polymerase chain reaction (qRT-PCR) primer assays confirming differential expression of established epithelial *(KRT3*, *KRT15*, *CEACAM1*) and mesenchymal *(ICAM1*, *KIT*, *SOX2)* markers in cultured limbal epithelial progenitor cells (LEPC) compared with cultured limbal mesenchymal stromal cells (LMSC). Data are expressed as means $(2^{-\Delta CT} \times 1{,}000) \pm$ SEM ($n = 5$). (**C**) Flow cytometry analyses of cultured LMSC showing positive expression of CD44, CD73, CD90, and CD105, but negative expression of CD31, CD34, and CD45. Percentages (%) of positive cells are expressed as means ± SEM ($n = 3$). (**D**) qRT-PCR primer assays showing higher expression levels of laminin α3 (LAMA3), α5 (LAMA5), β3 (LAMB3), γ2 (LAMC2) in cultured LEPC, and higher expression levels of laminin α2 (LAMA2), α4 (LAMA4), β2 (LAMB2), γ1 (LAMC1), γ3 (LAMC3) in cultured LMSC; laminin α1 (LAMA1), β1 (LAMB1), and β4 (LAMB4) showed no differential expression patterns. Data are expressed as means $(2^{-\Delta CT} \times 1{,}000) \pm$ SEM ($n = 5$); *$p < 0.05$; Mann-Whitney *U* test. (Abbreviations: KRT, Keratin; CEACAM1, carcinoembryonic antigen-related cell adhesion molecule 1; ICAM1, intercellular cell adhesion molecule 1; Sox2, sex determining region Y-box 2; CD, cluster of differentiation).

isoforms is limited, we performed *in vitro* tests of LEPC function using the two main LN-α5 chain containing isoforms, i.e. recombinant LN-511 and -521, as substrates, compared to isoforms containing LN-α1, -α2, -α3 or -α4 chains, i.e. recombinant LN-111, -211, -332, -411, and -421. Recombinant LN-511-E8 fragment which carries only C-terminal domains, where the main β1-integrin binding sites occur[41], was tested in addition.

The effect of the different LNs on cell adhesion was evaluated by determining the number of adherent LEPC on LN-coated (1.0 µg/cm^2) culture wells at 30 and 60 min after seeding compared to uncoated tissue culture plates (n = 4). Coating with LN-521, LN-511, LN-511-E8 and LN-332 increased cell adhesion significantly over the uncoated control both after 30 and 60 min of incubation (Fig. 3A). Differences were significant ($p = 0.02$) for LN-521 (2.6-fold at 30 min and 1.9-fold at 60 min), LN-511 (2.0- and 1.5-fold), LN-511-E8 (2.5- and 1.6-fold) and LN-332 (2.1- and 1.4-fold). LN-421, LN-411, LN-221, and LN-111 did not support adhesion better than uncoated tissue culture plastic. Phase contrast microscopy showed a dense monolayer of epithelial cells on LN-521, -511, and 511-E8, but rather sparser layers on the other LN isoforms 24 hours after seeding (Fig. 3B).

LN-511/521 has been reported to bind to integrin α3β1 and α6β1, while LN-332 binds to integrin α6β4 on the cell membrane[44]. Because integrins α3β1and α6β4 have been previously reported to mediate anchorage of LEPC to their niche[32], we analyzed the expression of these integrin subunits on the cell surface of cultured LEPC (n = 3) and evaluated the effect of integrin blocking on LEPC adhesion to LN-521, -511, -511-E8 and -332 (n = 4). As demonstrated by flow cytometry, almost 100% of LEPC expressed α3, α6, β1 and β4 integrins on their surface (Fig. 3C) and both neutralizing antibodies against α3β1 and α6β1 integrins significantly reduced adhesion of LEPC to LN-521 (α6β1: 39.1% (−1.6-fold); α3β1: 54.0% (−2.2-fold)), LN-511 (α6β1: 42.6% (−1.7-fold); α3β1: 52.5% (−2.1-fold)), LN-511-E8 (α6β1: 25.7% (−1.3-fold; α3β1: 20.4% (−1.2-fold)), and LN-332 (α6β1: 28.2% (−1.4-fold); α3β1: 32.2%(−1.5-fold)) as early as 1 hour after seeding ($p = 0.02$) (Fig. 3D). These findings indicate that LN-α5 and –α3 mediate LEPC adhesion through integrins α3β1 and α6β1 integrin binding.

To evaluate the effect of LN isoforms on LEPC migration, cells were plated on the different LN isoforms and gap closure following removal of a culture insert was analyzed 3 and 6 hours afterwards (n = 3). All LN isoforms, except LN-211 and LN-411, induced a significant increase in cell migration compared to uncoated controls at both time points (LN-521: 2.1- and 1.5-fold; LN-511: 1.7- and 1.4-fold; LN-511-E8: 2.5- and 1.6-fold; LN-421: 2.9- and 1.6-fold; LN-332: 1.8- and 1.4-fold; LN-111: 2.3- and 1.5-fold) ($p = 0.02$) (Fig. 3E).

The effect of LN isoforms on cell proliferation was assessed by BrdU incorporation assay 48 and 72 hours after seeding of LEPC on LN-coated culture wells (n = 5). Compared with uncoated controls, proliferation rates were significantly increased only in LEPC plated on LN-521 (1.7- and 1.4-fold), LN-511 (1.5- and 1.4-fold), and LN-511-E8 (1.5- and 1.4-fold) and were reduced in cells plated on LN-332 (−1.4- and −1.6-fold) ($p = 0.02$) (Fig. 4A). These findings were confirmed by cell counting (n = 3; $p = 0.02$) (Fig. 4B) and immunocytochemical staining for the proliferation marker Ki-67 (n = 3), which showed an increased percentage of positive cells on LN-521 (41.7 ± 2.5%; 1.4-fold; $p = 0.001$), LN-511 (36.4 ± 3.6%; 1.2-fold; $p = 0.004$), and LN-511-E8 (41.5 ± 2.5%; 1.4-fold; $p = 0.009$) but a decreased percentage of positive cells on LN-332 (16.7 ± 3.1%; −1.8-fold; $p = 0.0007$) compared to uncoated control (28.7 ± 2.8%) (Fig. 4C, right). Accordingly, mRNA expression levels of Ki-67 were also increased in LEPC cultured on LN-521 (2.6 ± 0.3-fold), LN-511 (3.1 ± 0.4-fold), and LN-511-E8 (2.8 ± 0.3-fold) and decreased in LEPC cultured in LN-332 (−4.1 ± 0.4-fold) compared to control (n = 5; $p = 0.02$) (Fig. 4C, left).

To assess a potential effect of LN isoforms on the differentiation state of LEPC, mRNA expression levels of KRT3, a cornea-specific differentiation marker, and KRT15, an established progenitor cell marker, were analyzed by qRT-PCR in LEPC passages 1 to 3 (n = 5). Although there was a trend towards suppression of KRT3 expression in LEPC cultivated on LN-521, -511, -511-E8, and -421 compared to control (Fig. 4D), differences were not statistically significant. Expression levels of KRT15 were also not significantly different from controls, except for LN-332, which supported maintenance of high KRT15 expression levels for up to 3 passages ($p = 0.02$).

These observations suggest that LN-332 supports an undifferentiated phenotype but inhibits proliferation, whereas LN-521, -511, and 511-E8 support cell proliferation without affecting differentiation, rendering LN-α5 containing isoforms as suitable candidates for tissue engineering purposes.

Tissue engineering of corneal epithelial constructs. Since recombinant LN-E8 fragments have been shown to promote efficient and scalable culture of human stem cells under defined xeno-free conditions[41,45], we tested the applicability of LN-511-E8 for tissue engineering of corneal epithelial constructs (n = 5). To generate multilayered epithelial cell sheets on 3D-scaffolds suitable for clinical application, LEPC were seeded and cultivated for 12 to 14 days on fibrin gels prepared with or without incorporation of LN-511-E8 (10 µg/ml). LEPC expansion was markedly increased on LN-containing gels compared with untreated gels resulting in a confluent monolayer on LN-511-E8 by 5 days after seeding (Fig. 5A). Light microscopic analyses of tissue constructs showed a stratified epithelial cell sheet consisting of a cuboidal basal layer and 5 to 6 layers of flattened suprabasal cells on LN-511-E8 containing gels, but only 3 to 4 cell layers on LN-free gels (Fig. 5B). Transmission electron microscopy confirmed formation of well-organized multi-layered epithelial cell sheets consisting of a basal layer of cuboid cells covered by several layers of flattened elongated cells (Fig. 5C,i). Suprabasal cells showed typical ultrastructural signs of epithelial differentiation, such as desmosomes, cytoplasmic filaments, and apical microvilli. Basal cells appeared to be firmly attached to the LN-511-E8 containing fibrin gels by formation of hemidesmosomes and newly produced BM, whereas they appeared to only loosely adhere to LN-free fibrin gels where no BM deposition was evident (Fig. 5C,ii).

Immunofluorescence analysis of epithelial constructs showed expression of corneal epithelial differentiation marker CK3 in superficial layers and expression of progenitor cell markers CK15 and p63α in (supra) basal layers (Fig. 5D). The cell-matrix receptors α3, α6 and ß1 integrin could be mainly immunolocalized to the basal aspects of epithelial sheets, which also provided evidence of endogenous expression of LN-α5 and -α3. Protein expression was found to be generally more pronounced in epithelial constructs established on

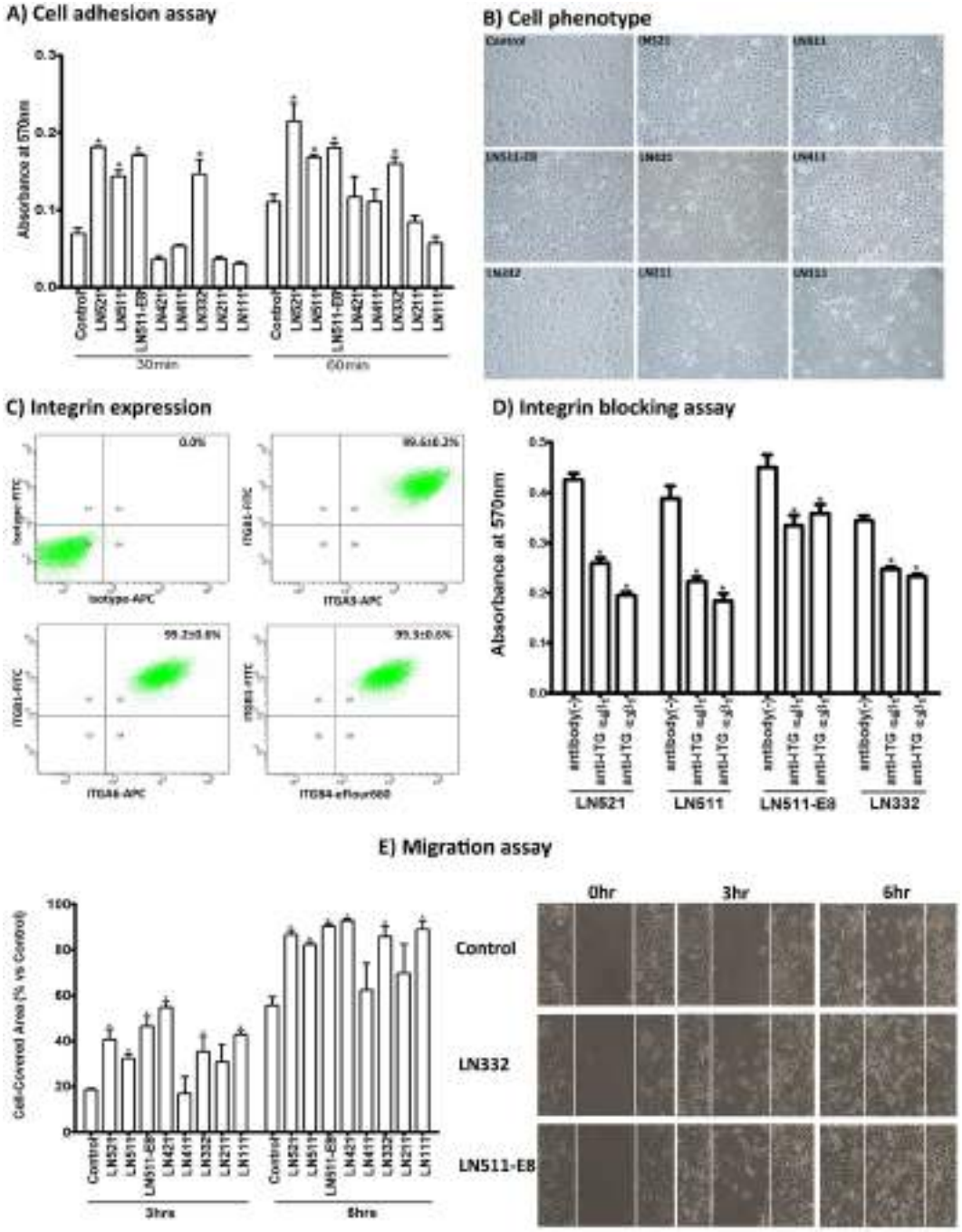

Figure 3. Effect of laminin isoforms on limbal progenitor cell adhesion and migration. (**A**) The effect of laminin (LN) isoforms on cell adhesion was tested by seeding limbal epithelial progenitor cells (LEPC) at a density of 50,000 cells/cm^2 and spectrophotometric measurement of adherent cells 30 and 60 minutes after seeding. Data are expressed as means ± SEM (n = 4). (**B**) Phase contrast images of LEPC cultured on LN isoforms; magnification ×100. (**C**) Flow cytometry analyses of cultured LEPC showing expression of integrin α3 (ITGA3), integrin α6 (ITGA6), integrin β1 (ITGB1), and integrin β4 (ITGB4) on their surface. Percentages (%) of positive cells are expressed as means ± SEM percentage (%) (n = 3). (**D**) Functional blocking of integrin-mediated LEPC adhesion to LN-521, -511, -511-E8 and -332 was tested using neutralizing antibodies against integrin α3β1 and α6β1 60 minutes seeding. Data are expressed as means ± SEM (n = 4). (**E**) The effect of LN isoforms on LEPC migration was analyzed in two well-culture inserts with a defined cell-free gap and measurement of gap closure 3 and 6 hours after removal of the culture inserts. Data are expressed as means ± SEM (n = 3); *$p < 0.05$; Mann-Whitney *U* test.

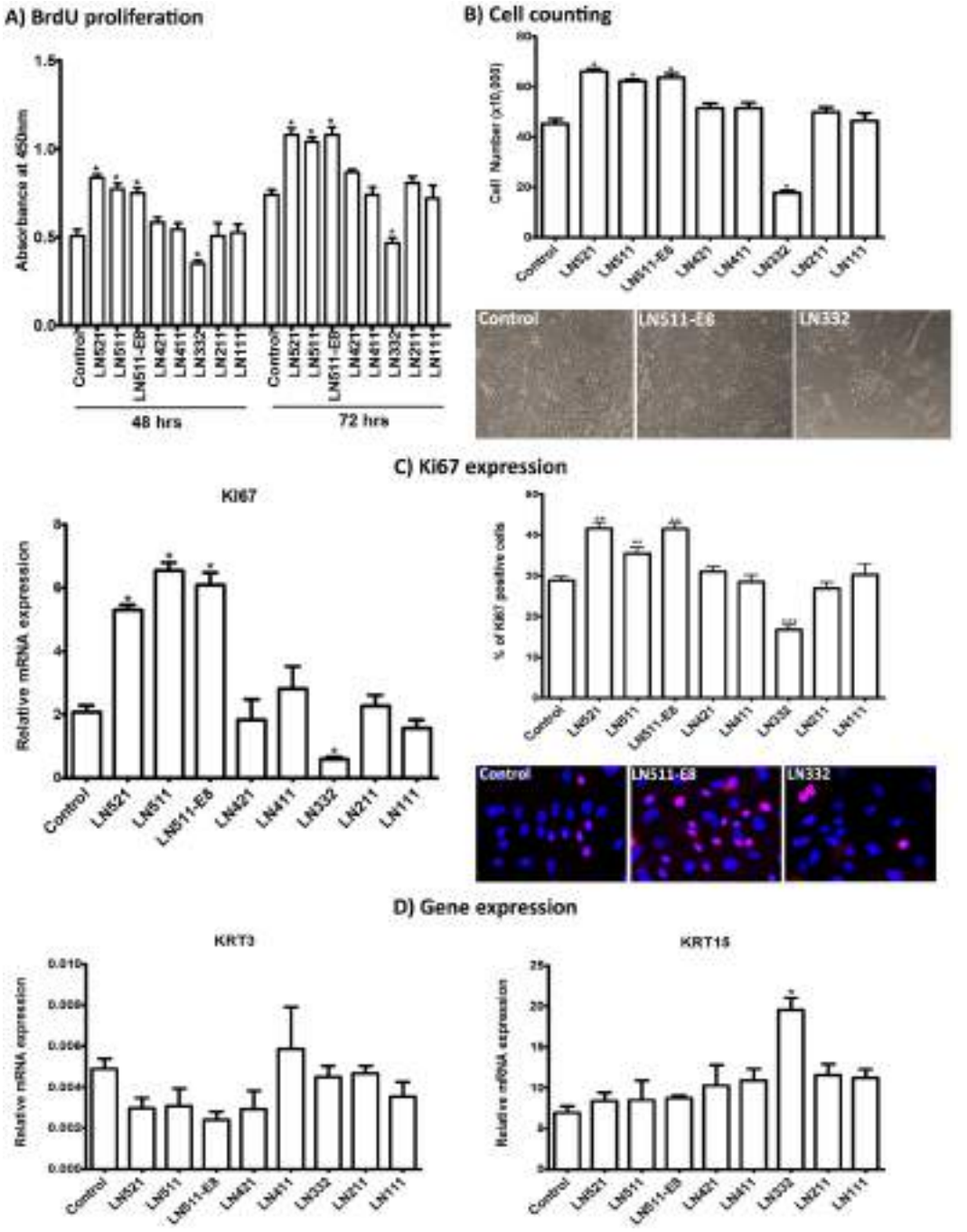

Figure 4. Effect of laminin isoforms on limbal progenitor cell proliferation and differentiation. (**A**) The effect of laminin (LN) isoforms on cell proliferation was tested by seeding limbal epithelial progenitor cells (LEPC) at a density of 15,000 cells/cm^2 and spectrophotometric measurement of BrdU incorporation 48 and 72 hours after incubation. Data are expressed as means ± SEM (n = 5). (**B**) The effect of LN isoforms on LEPC proliferation was also analyzed by cell counting using CASY technology 7 days after seeding (15,000 cells/cm^2); phase contrast images show LEPC cultured on tissue culture-treated plastic (control), LN-511-E8 and LN-332 before trypsinization for counting. Data are expressed as means ± SEM (n = 3). (**C**) The effect of LN isoforms on LEPC proliferation was additionally analyzed by Ki-67 expression on the mRNA level (left) and on the protein level (right). Ki-67 (KI67) mRNA levels were assessed by quantitative real-time polymerase chain reaction (qRT-PCR) primer assays, and data are expressed as means ($2^{-\Delta CT} \times 1{,}000$) ± SEM ($n = 5$). Ki-67 protein levels were monitored by counting the number of Ki-67-positive cell nuclei (magenta) and nuclei counterstained with DAPI (blue) using Cell F program (magnification ×200). Percentages (%) of positive cells are expressed as means ± SEM (n = 3). (**D**) The effect of LN isoforms on LEPC differentiation was analyzed by qRT-PCR primer assays of KRT3 and KRT15 expression levels. Data are expressed as means ($2^{-\Delta CT} \times 1{,}000$) ± SEM ($n = 5$); *p < 0.05; **p < 0.01; ***p < 0.001; Mann-Whitney *U* test.

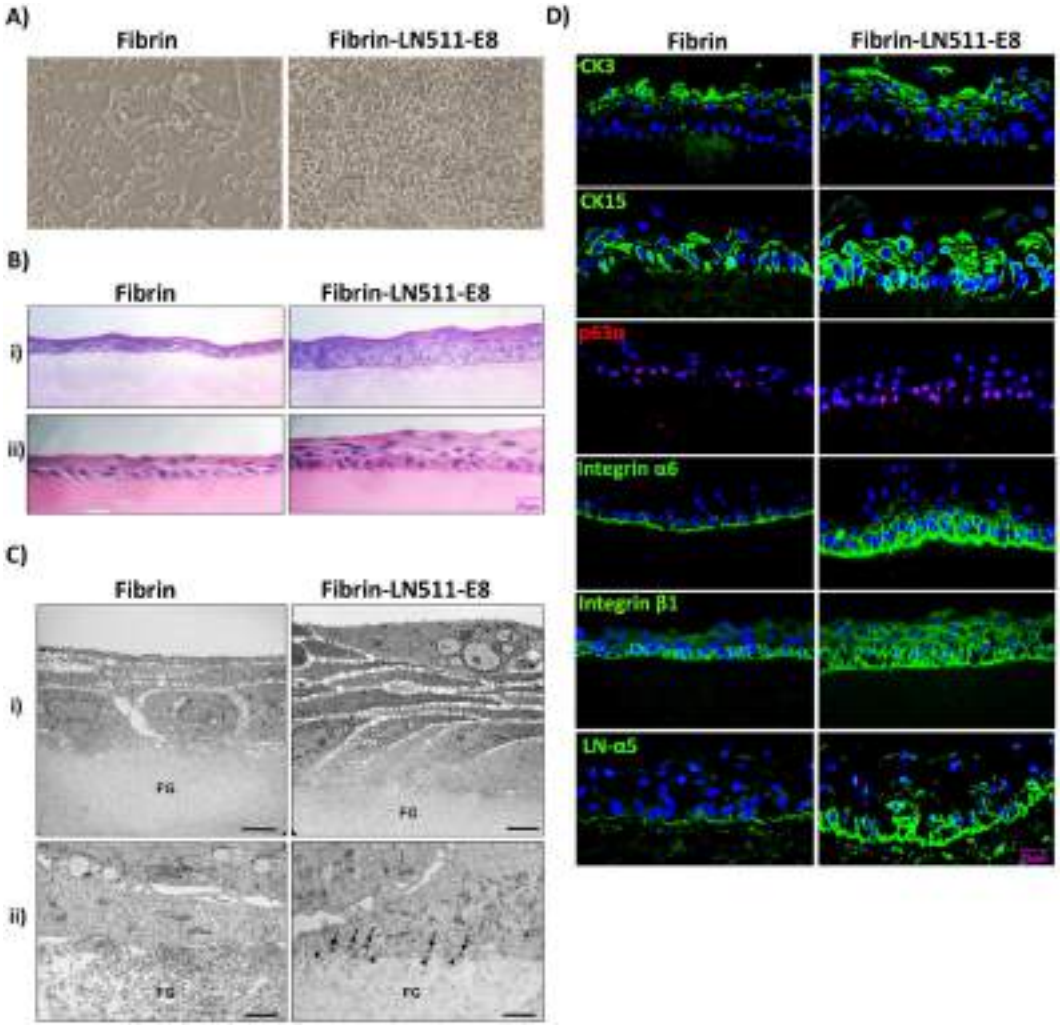

Figure 5. Tissue engineering of corneal epithelial constructs. (**A**) Phase contrast images of limbal epithelial progenitor cells (LEPC) growing on fibrin gels without or with incorporated recombinant laminin (LN)-511-E8 for 5 days (magnification ×100). (**B**) Light micrographs of epithelial cell sheets after two weeks of LEPC culture on fibrin gels without or with incorporated LN-511-E8 (i, periodic acid-Schiff staining; ii, hematoxylin-eosin staining; scale bar = 25 µm). (**C**) Transmission electron micrographs of epithelial cell sheets after two weeks of LEPC culture on fibrin gels (FG) without or with incorporated LN-511-E8; formation of hemidesmosomes (arrows) and basement membrane (arrowheads) can be seen on LN-511-E8 containing gels (scale bar = 5 µm in i, and 1 µm in ii). (**D**) Immunofluorescence analysis of epithelial constructs showing expression patterns of cytokeratin (CK)3, CK15, p63α, integrin α6, integrin ß1, and LN-α5 in epithelial constructs established on LN-511-E8 containing gels and bare fibrin gels (nuclear counterstaining with DAPI (blue); scale bar = 25 µm).

LN-511-E8 containing gels than on pure fibrin gels. These data suggest that LN-511-E8-coated fibrin gels promote *ex vivo*-expansion of LEPC and the generation of a stratified, firmly adherent, corneal epithelial-like cell sheet containing both differentiated and undifferentiated cells, which appears amenable for transplantation onto the corneal surface.

Discussion

Using qPCR on microdissected LEPC clusters and confocal microscopy on tissue sections, we show that the BM of the limbal niche is enriched for LN chains α2, α3, α5, β1, β2, β3, γ1, and γ2, co-localizing with integrins α3, α6 and ß1 on the LEPC surface. Of note, mRNA expression of LN-γ3 could not be detected in LEPC, although LN-γ3 protein was clearly identified in the limbal zone by immunohistochemistry in this and previous studies[31,46,47]. In order to determine the role of LEPC in LN deposition within the limbal niche, we performed differential mRNA expression analyses in cultivated LEPC and supporting LMSC populations, both derived from LEPC clusters within the niche[32]. Our results clearly show the predominant expression of LN-α3 and –α5 by LEPC together with LN-β1, -β3, and -γ2 chains, suggesting the probable secretion of LN-332 and LN-511 by epithelial cells. By contrast, the LMSC preferentially expressed LN-α2 and -α4 chains together with -β2, -γ1 and -γ3 chains, and thus probably secrete and deposit LN-211/221 and LN-411/421/423 into the limbal BM. This differential expression pattern of laminin chains by epithelial and stromal fibroblast-like cells is consistent with findings in

the epidermal BM, containing both epidermally derived LN-α3 and -α5 and mesenchymally derived LN-α2 and -α4, and suggests that, as in the skin, interaction between epithelial and mesenchymal cells is required to establish the limbal niche[48,49]. The differential expression of LN-α5, but not LN-α3, by LEPC compared to BCEC further suggests that the LN-α5 chain may be an endogenous signature component of progenitor cells and may also present an appropriate exogenous cue for *ex vivo*-expansion of LEPC.

As a major component of BMs, LN isoforms are also enriched in other adult stem cell niches, where they regulate stem/progenitor cell function through interaction with cell surface receptors transducing molecular signals to the intracellular compartment[23–26,50]. Consistent with the data presented here, interactions are predominantly mediated by one of the four LN-binding integrins, α3β1, α6β1, α6β4[43,44], and in the case of myogenic cells also α7β1, which activate specific signaling networks to modulate diverse cellular functions, such as adhesion, migration, proliferation, differentiation, stability of phenotype, and resistance towards apoptosis. The epidermal stem cell niche, for instance, contains LN-332 and LN-511, which interact with α6β4 and α3β1 integrins, respectively, and are hypothesized to maintain stem cell homeostasis through a precise ratio of LN-332 to LN-511[51–53]. Deposition of LN-332 and LN-511 gradients within the epidermal BM is regulated by integrin-linked kinase (ILK), which plays a crucial role in linking the ECM to the actin cytoskeleton of skin and hair follicle stem cells[52]. Detachment from LN-511/521-containing BMs has been considered a key factor in promoting epithelial differentiation. LN-332 and LN-511/521 have been also reported to be synthesized and secreted by human corneal epithelial cells *in vivo*, and to play a crucial role in the adhesion and migration of corneal epithelial *in vitro*[54,55]. Together with the data presented here, there is convincing evidence that both LN-332 and LN-511/521 through interaction with integrins α6β4 and α3β1/α6β1, respectively, form part of the limbal niche. However, whether the ratio between the two LN isoforms and their gradient of expression in the limbal BM determine LEPC function, requires further investigation. It also remains to be determined, whether ILK, which has been reported to transfer β1 integrin-mediated signals from the ECM to the Wnt/ß-catenin pathway in LEPC cultivated on amniotic membrane[56], is a key regulator of the limbal niche ECM microenvironment.

Here, we further show that the different LN isoforms have different functions on LEPC *in vitro*. Whereas LN-511/521 supported integrin α3β1/α6β1-mediated LEPC adhesion, migration and proliferation without major effects on cellular differentiation, LN-332 promoted LEPC adhesion and migration, but suppressed proliferation, and maintained an undifferentiated phenotype, as reflected by high expression of the progenitor marker KRT15. All other LN isoforms tested, i.e. LN-421, -411, -211 and -111, showed no superior effects on adhesion and proliferation of LEPC compared to tissue culture control wells. These observations are different to the skin, where LN-α3 has been shown to promote and LN-α5 to inhibit keratinocyte proliferation[48]. However, in accordance with our observations, LN-511 and -521, which are also expressed in Descemet's membrane and corneal endothelium, strongly supported *in vitro* adhesion and proliferation of human corneal endothelial cells[42]. Thus, the particular characteristics of LN-511/521, i.e. support of adhesion, proliferation and phenotype stability of corneal cells, render these isoforms best qualified for tissue engineering of LEPC-derived epithelial cell sheets without abandoning the progenitor phenotype. Indeed, recombinant LN-511 and -521 have been frequently used as substrates for efficient stem/progenitor cell expansion *in vitro* and have been shown to protect against apoptosis, to stimulate proliferation, and to maintain pluripotency and long-term self-renewal of both pluripotent and adult stem cells including human keratinocyte stem cells[57–60].

Short recombinant E8 fragments derived from the long arm of LN have been reported as a viable and safe alternative to intact LN proteins in tissue engineering applications, because they do not involve the risk of contamination with xenogenic pathogens and immunogens[41].These fragments have been shown to represent the minimum fraction conferring β1 integrin-binding activity and supporting efficient adhesion and proliferation of pluripotent stem cells in defined xeno-free media[45,61,62]. E8 fragments of LN-511 have also been used as a substrate for cultivation of human corneal endothelial cells with a similar efficacy to that obtained with full-length LN[42]. This could be confirmed by the present study, showing that LN-511-E8 fragments had similar potency in stimulating LEPC adhesion, migration, proliferation, and phenotype stability as intact LN-511. We further show that recombinant LN-511-E8 fragments incorporated into and on top of fibrin-based hydrogels improve *ex vivo*-expansion of LEPC and generation of a stratified epithelial cell sheet. The epithelial constructs generated on LN-511-E8 pre-functionalized scaffolds proved to be superior to those on bare scaffolds, displaying a well-organized stratified structure and firm attachment by α3β1 and α6β1 integrin-mediated anchorage to LN-α5 as well as preservation of a progenitor cell phenotype in (supra)basal layers and a differentiated phenotype in superficial layers.

In conclusion, *in vitro* presentation of appropriate ECM cues influencing stem cell function *in vivo* may represent a useful strategy to improve LEPC expansion and to maintain stem/progenitor cell function within the graft. The incorporation of chemically defined, bioactive, recombinant human E8 fragments of the limbal niche constituent LN-511 into clinically approved biosynthetic scaffolds like fibrin gels represents a promising avenue for safe, xeno-free corneal epithelial tissue engineering for ocular surface reconstruction. This defined culture technique may provide a significant improvement over current protocols for *ex vivo*-expansion of LEPC on undefined matrices, such as amniotic membrane or murine feeder cells, suffering from an intrinsic biologic variability, but this proposition has to be evaluated in preclinical *in vivo* studies. Future studies are also required to elucidate the nature of signaling pathways that are activated by LN-integrin interactions to determine LEPC function *in vivo* and *in vitro*.

Methods

Human tissues and study approval. Human donor corneas (n = 5 for LCM, n = 10 for immunohistochemistry) not suitable for transplantation with appropriate research consent were procured by the Erlangen Cornea Bank. In addition, organ-cultured corneoscleral tissue (n = 42) with appropriate research consent was

provided by the Erlangen Cornea Bank after corneal endothelial transplantation. Informed consent to corneal tissue donation was obtained from the donors or their relatives. Experiments using human tissue samples were approved by the Institutional Review Board of the Medical Faculty of the University of Erlangen-Nürnberg (No. 4218-CH) and adhered to the tenets of the Declaration of Helsinki.

Laser capture microdissection (LCM) and amplification of RNA. LCM and amplification of RNA was performed as previously described[32]. Briefly, corneal specimens destined for LCM were obtained from five donors (mean age, 69.6 ± 10.4 years) within 15 hours after death. After labeling of the superior, inferior, nasal, and temporal quadrants of donor globes, tissue sectors were embedded in optimal cutting temperature (OCT) compound (Tissue-Tek, Sakura Finetek Europe) and snap frozen in liquid nitrogen. Serial cryosections of 12 µm thickness were obtained under RNAse-free conditions from the superior or inferior quadrants, placed onto UV-irradiated (3000 mJ/cm^2) PEN (polyethylene naphtalate) Membrane Slides (Carl Zeiss Microscopy, Göttingen, Germany), and stained with 0.01% cresyl violet. The PALM MicroBeam IV system (Carl Zeiss Microscopy) was used to isolate clusters of basal limbal epithelial cells (LEPC) and basal epithelial cells from central cornea (BCEC). From each donor eye, 100 cryosections were dissected (50 from the superior and 50 from the inferior quadrants, respectively) yielding a total of 500 cryosections used for sample collection.

RNA isolation from these specimens was achieved using the RNeasy Micro Kit (Qiagen, Hilden, Germany) including an on-column DNase digestion step according to the manufacturer's instructions. Quality control was performed on a 2100 Agilent Bioanalyzer using the RNA 6000 Pico Kit (Agilent Technologies, Santa Clara, CA). Samples with an RNA concentration of 650–2,000 pg/µl and a RIN (RNA integrity number) of ≥7.0 were used for further analysis. Following RNA-amplification using the MessageAmp II aRNA Amplification Kit (Life Technologies GmbH, Darmstadt, Germany) according to the manufacturer's protocol, aRNA (amplified RNA) concentration was measured on a Nanodrop ND1000 spectrophotometer (Thermo Scientific, Wilmington, DE) and quality control was again performed using Agilent technology.

Real time RT-PCR. First-strand cDNA synthesis was performed using 5 µg of aRNA from tissue samples or RNA from cultured cells and Superscript II reverse transcriptase (Invitrogen, Karlsruhe, Germany) as previously described[32]. PCR reactions were run in triplicate in 1× TaqMan Probe Mastermix (Roche Diagnostics, Mannheim, Germany) or 1× SsoFast EvaGreen Supermix (Bio-Rad Laboratories, München, Germany), respectively, according to the manufacturers' recommendations. Primer sequences (Eurofins, Anzing, Germany) are given in Table 2. For normalization of gene expression levels, ratios relative to the housekeeping gene GAPDH were calculated by the comparative C_T method ($\Delta\Delta C_T$). Genes were considered as differentially expressed when their expression levels exceeded a two-fold difference in all specimens analyzed.

Immunohisto- and immunocytochemistry. Corneoscleral tissue samples obtained from 10 normal human donor eyes (mean age, 72.3 ± 11.6 years) and 3D-cultures were embedded in optimal cutting temperature (OCT) compound and frozen in isopentane-cooled liquid nitrogen. Cryosections of 4 µm thickness were cut from the superior or inferior quadrants, fixed in cold acetone for 10 minutes, blocked with 10% normal goat serum, and incubated in primary antibodies (Table 1) diluted in PBS overnight at 4 °C. Antibody binding was detected by Alexa 488-conjugated secondary antibodies (Molecular Probes, Eugene, OR) and nuclear counterstaining was performed with DAPI (Sigma-Aldrich, St. Louis, Missouri). Immunolabelled cryosections and cultured LEPC were examined with a fluorescence microscope (Olympus BX51; Olympus, Hamburg, Germany) or a laser scanning confocal microscope (LSM 780; Carl Zeiss Microscopy). In negative control experiments, the primary antibodies were replaced by PBS or equimolar concentrations of an irrelevant isotypic primary antibody.

Cell culture. LEPC clusters were isolated from 42 corneoscleral buttons (mean age, 69.2 ± 7.1 years) as previously described[32]. Briefly, organ-cultured corneoscleral tissue with appropriate research consent was provided by the Erlangen Cornea Bank after corneal endothelial transplantation. After rinsing in Hanks' balanced salt solution, the tissues were cut into 12 one-clock-hour sectors, from which limbal segments were obtained by incisions made at 1 mm before and beyond the anatomical limbus. Each limbal segment was enzymatically digested with 2 mg/mL collagenase A at 37 °C for 18 hours to generate epithelial-mesenchymal stem/progenitor cell clusters. Cell clusters were isolated from single cells by using reversible cell strainers with a pore size of 37 µm (Stem Cell Technologies, Köln, Germany). Isolated cell clusters were further dissociated into single cells by digestion with 0.25% trypsin and 0.02% EDTA (Pan Biotech, Aidenbach, Germany) at 37 °C for 10–15 min. Single cell suspensions were seeded into T75 flasks (Corning, Tewksbury, MA) in Keratinocyte serum free medium (KSFM) supplemented with bovine pituitary extract, epidermal growth factor (Life Technologies) and 1× penicillin-streptomycin-amphotericin B mix (Pan Biotech) to enrich epithelial cell population (LEPC) and the flasks were incubated at 37 °C under 5% CO_2 and 95% humidity. To enrich the associated mesenchymal stromal cells (LMSC), single cell suspensions were seeded into T75 flasks in Mesencult media (Stem Cell Technologies) and incubated at 37 °C under 5% CO_2 and 95% humidity. The media was changed every second day. Cultivated cells were used for real time PCR (n = 10), flow cytometry (n = 3), functional assays (adhesion: n = 4, integrin blocking: n = 4, migration: n = 3, proliferation: n = 13) and tissue engineering (n = 5).

Flow cytometry. LEPC cluster derived and enriched mesenchymal cells (LMSC, P1) were isolated from 3 organ-cultured corneoscleral buttons (mean age, 66.5 ± 4.6 years) and characterized by flow cytometry using anti-CD90, -CD73, -CD105, -CD44, -CD34, -CD45, -CD31 and isotype control antibodies (BD Biosciences, Heidelberg, Germany). LEPC were characterized using anti-α3 integrin-APC, anti-α6 integrin-APC, anti-β1 integrin-FITC and anti-β4 integrin-eFluor660 antibodies (eBioscience, Frankfurt, Germany). Single cell

Gene Symbol	Accession No.	Product Length	Probe No./SYBR	Sequence 5′–3′
CEACAM1	NM_001024912.2	113	P79	TCTTTGGGGCTAAGAGAAAGG
				GAGGTACCTGAGTATAGAGAACTCCAA
GAPDH	NM_002046.3	72	P3	CAGCAAGAGCACAAGAGGAA
				GTGGTGGGGGACTGAGTGT
ICAM1	NM_000201.2	73	P30	TTGACCTTTTGGGCTCAAGT
				TGGTGTTGTGAGCCTATGGT
Ki-67	NM_002417.4	78	P50	TTACAAGACTCGGTCCCTGAA
				TTGCTGTTCTGCCTCAGTCTT
KIT	NM_000222.2	61	P6	GAGTAGCTTACCAGAAGCTTCCATAG
				CATAGGGACTGATGCCTTCC
KRT3	NM_057088.2	92	P74	CCTGTGATTGTCCAGGTGTG
				ATACATCAGAGCTGTAGTGAGCATC
KRT15	NM_002275.3	60	P10	CATTGGCATCAGGGAAGC
				TTGATGTGGAAATTGCTGCT
LAMA1	NM_005559.3	149	SYBR	CTGGGACCGAGTCCTGAAC
				ACACAACATCTCTCCCCAGAA
LAMA1	NM_005559.3	60	P38	AGGATGACCTCCATTCTGACTT
				CCTTACATGGGCACTGACCT
LAMA2	NM_000426.3	68	P81	GCAAGCCACTGGAGGTTAAT
				TGGGCATGATACAGGTTGAA
LAMA3	NM_198129.1	72	SYBR	GCACTGATTACCCAATGCACC
				ACCTGTCTGGTTTGTGTCCTG
LAMA3	NM_198129.1	65	P29	CCAGGAATATGGGTTGCTTG
				GGGAGCAGCACCAGGTAAT
LAMA4	NM_001105209.1	68	P55	GCCACACTCGTCCTTCTCTC
				CCCAGGTGAAACTCTCAAGG
LAMA5	NM_005560.3	75	P44	ATGACTCGCTCTGTGGAGGT
				GGGGTTGGCTGTGTCCTA
LAMB1	NM_002291.2	72	P82	AAGCCAGAAAGTTGCTGTGTATAG
				CCTTGTTCACCTCAGCCATT
LAMB2	NM_002292.3	100	P43	AAGGCCTACCCCAGTTCCTA
				GGGTTCACACTGGTTTATTGG
LAMB3	NM_001127641.1	72	P23	GGCATGCCATTGAAACTAAGA
				AGAACTAAAGGCGGGGGATA
LAMB4	NM_007356.2	67	P5	CCCCACACCCTGTCCTTATT
				ATTTTCCTGGTGGCATTTCA
LAMC1	NM_002293.3	92	P66	GCCATTATTTTATTGTCTAGCTCCA
				ATCCCTGTGTCAACCAGCAT
LAMC2	NM_005562.2	96	P65	CACTCTGTGCCTTTCTACAACTG
				CCAAGGTGGAAGTGCCTCT
LAMC3	NM_006059.3	67	P14	CAGGACTCCTCAGCATTTCC
				TTGCCATCTGCTGGAAGAG
SOX2	NM_003106.3	85	P65	GGGGGAATGGACCTTGTATAG
				GCAAAGCTCCTACCGTACCA

Table 2. Primers used in qRT-PCR primer assays. Primers were used for Probe based (Universal Probe Library) or SYBR Green based qRT-PCR assays with an annealing temperature of 60 °C.

suspensions ($0.5–1 \times 10^6$ cells) were incubated with saturating concentrations of respective primary antibodies or conjugated antibodies in 100 µl PBS, 0.1% sodium azide and 2% fetal calf serum for 40 min. After three washes, the cells were centrifuged at $200 \times g$ for 5 min. Primary antibody reactions were incubated with Alexa Fluor 488-conjugated goat anti-mouse IgG for 30 min. Cells were then washed and re-suspended in ice-cold PBS. After addition of 5 µl of 7-amino-actinomycin D (7-AAD) to exclude dead cells, cytometry was performed on a FACSCanto II (BD Biosciences) by using FACS Diva Software. A total of 10,000 events were acquired to determine the positivity of cell surface markers.

Cell adhesion assay. LEPC isolated from 4 organ-cultured corneoscleral buttons (mean age, 74.2 ± 5.8 years) were seeded onto 96 well-plates coated with recombinant LN-111, -211, -332, -411, -421, -511, -521 (1.0 µg/cm^2; BioLamina, Sundbyberg, Sweden) and recombinant LN-511-E8 (0.5 µg/cm^2; Nippi, Tokyo,

Japan) as per manufacturers' recommendations. Coating solutions were prepared in 1x DPBS (Dulbecco's phosphate-buffered saline) with calcium and magnesium and incubated in culture wells either for two hours at 37 °C (fast coating) or overnight at 4 °C (slow coating) as per manufacturer's instructions. Cells (P1-P2) were seeded at a density of 50,000 cells/cm^2 and left to adhere for 30 and 60 min at 37 °C. Standard tissue culture treated plates were used as control. After incubation, plates were washed with DPBS using a Static Cell Adhesion Wash Chamber (Glycotec, Maryland, USA) to remove non-adherent cells, and the adherent cells were fixed with 4% paraformaldehyde/PBS for 15 min and stained with 0.1% crystal violet for 20 min. After three washes with water, stained cells were extracted with 1% sodium dodecyl sulfate and quantified by measuring optical density (OD) at 570 nm using a spectrophotometer (Multiskan Spectrum; Thermo Scientific, Waltham, USA). All experiments (n = 4) were performed in quadruplicates. The fold change values were calculated as OD of the LN/OD of control.

The effect of an interaction between cellular integrins and extracellular LNs on cell adhesion was evaluated by seeding LEPC (50,000 cells/cm^2) in 96-well plates coated with recombinant LN-332, -511, -521, and LN-511-E8 in the presence or absence of integrin-neutralizing antibodies, i.e., anti-α3 integrin (20 µg/ml) (Merck Millipore, Darmstadt, Germany), anti-α6 integrin (20 µg/ml) (Merck Millipore) and anti-β1 integrin (2.5 µg/ml) (R&D Systems Inc., Minneapolis, MN, USA). 60 minutes after seeding, the numbers of adherent cells were determined as described above. LEPC used for integrin blocking assays were isolated from 4 organ-cultured corneoscleral buttons (mean age, 67.7 ± 6.1 years) and all experiments were performed in quadruplicates.

Cell migration assay. To exactly measure the change in the cell-covered area over time, 2 well-culture inserts with a defined cell-free gap were used (ibidi GmbH, Planegg, Germany). Briefly, the wells were coated with LN isoforms as described above and seeded with 70 µl of a LEPC suspension containing 5×10^5 cells/ml. LEPC were isolated from 3 organ-cultured corneoscleral buttons (mean age, 71.3 ± 6.1 years). After formation of a cellular monolayer (24 hours), the silicone inserts were removed and the culture medium was supplemented with 2.5 µg/ml of soluble LNs. Images of each well were acquired immediately following insert removal (0 hours) and after 3 and 6 hours by using an inverted microscope (CKX41, Olympus). Image analysis software Cell F (Olympus) was used to measure areas that were free of migrating cells. All experiments (n = 3) were performed in triplicates.

Cell proliferation assays. LEPC used for cell proliferation assays were isolated from a total of 13 corneoscleral buttons after corneal endothelial transplantation (mean age, 70.0 ± 8.0 years).The effect of LNs on LEPC proliferation was quantified using the Cell Proliferation ELISA BrdU Colorimetric Assay Kit (Roche Diagnostics). Cells (P1-P2) were seeded into 96-well plates, coated with LN isoforms as described above, at a density of 5000 cells/well, cultured for 48 and 72 hours, and labeled with BrdU according to the manufacturer's instructions. Absorbance was measured at 450 nm using a spectrophotometer (Multiskan Spectrum), and fold change values were calculated as described above. Experiments (n = 5) were performed in quadruplicates.

For immunocytochemical analysis of cell proliferation, LEPC (n = 3) were seeded at a density of 10,000 cells/well into 4 well- glass chamber slides (LabTek; Nunc, Wiesbaden, Germany), cultured for 72 hours, and stained with antibodies against Ki-67 (Abcam; Cambridge, UK). Ki-67 positive cells were counted in the 4 wells using Cell^F image analysis software (Olympus). Ki-67 expression was also analyzed by real time PCR as described above (n = 5).

In addition, cell numbers were counted after trypsinization of LEPC 7 days after seeding (5×10^4 cells/well) in 6-well culture plates using CASY technology (Schärfe System GmbH, Reutlingen, Germany) (n = 3).

Tissue engineering of epithelial constructs. Scaffolds for tissue engineering and 3D-cell culture were prepared from fibrin as previously described[38]. Briefly, the gels were prepared by dissolving fibrinogen and thrombin stock solutions (Tisseel; Baxter Deutschland GmbH, Unterschleißheim, Germany) in 1.1% NaCl and 1 mM $CaCl_2$ to a final concentration of 10 mg/ml fibrinogen and 3 IU/ml thrombin. Recombinant LN-511-E8 (10 µg/ml) was incorporated into the gels, which were placed into 24 well-culture inserts and allowed to polymerize at 37 °C. After washing with PBS, gels were additionally coated with LN-511-E8 (5 µg/ml) overnight. LN-511-E8 free gels served as controls. LEPC (P1) were isolated from 5 organ-cultured corneoscleral buttons (mean age, 65.0 ± 7.5 years) and seeded onto coated and uncoated control gels at a density of 1×10^5 cells/cm^2 and cultivated in KSFM media under low calcium concentrations (0.09 mM Ca^{2+}) for 5 to 6 days. Culture conditions were switched to DMEM/Ham's F12 (Hyclone; GE Health Care Life Sciences, Freiburg, Germany) supplemented with Human Corneal Growth Supplement (Life Technologies), 10% FCS (GE Health Care Life Sciences), and high calcium concentrations (1.2 mM Ca^{2+}) in order to promote cell differentiation. After another 6 to 8 days of cultivation, gels were fixed for immunohistochemistry as described above and for light and electron microscopy.

For light and electron microscopy, gels were fixed in 2.5% glutaraldehyde in 0.1 M phosphate buffer, dehydrated, and embedded in paraffin or epoxy resin, respectively, according to standard protocols. Paraffin sections were stained with hematoxylin and eosin, and ultrathin sections were stained with uranyl acetate-lead citrate and examined with an electron microscope (EM 906E; Carl Zeiss Microscopy).

Statistical analysis. Statistical analyses were performed using the GraphPad InStat statistical package for Windows (Version 5.04; Graphpad Software Inc., La Jolla, CA). Data are expressed as mean ± standard error of the mean from individual experiments. The Mann-Whitney *U* test was performed to assess statistical significance. A p value of <0.05 was considered statistically significant.

Data availability. Any additional data beyond those included in the main text that support the findings of this study are also available from the corresponding author upon request.

References

1. Schermer, A., Galvin, S. & Sun, T. T. Differentiation-related expression of a major 64K corneal keratin *in vivo* and in culture suggests limbal location of corneal epithelial stem cells. *J Cell Biol.* **103**(1), 49–62 (1986).
2. Cotsarelis, G., Cheng, S. Z., Dong, G., Sun, T. T. & Lavker, R. M. Existence of slow-cycling limbal epithelial basal cells that can be preferentially stimulated to proliferate: implications on epithelial stem cells. *Cell.* **57**(2), 201–209 (1989).
3. Dua, H. S., Miri, A. & Said, D. G. Contemporary limbal stem cell transplantation – a review. *Clin Exp Ophthalmol.* **38**(2), 104–117 (2010).
4. Kenyon, K. R. & Tseng, S. C. Limbal autograft transplantation for ocular surface disorders. *Ophthalmology* **96**(5), 709–722 (1989).
5. Sangwan, V. S. & Tseng, S. C. New perspectives in ocular surface disorders. An integrated approach for diagnosis and management. *Indian J Ophthalmol.* **49**(3), 153–168 (2001).
6. Tsai, R. J., Li, L. M. & Chen, J. K. Reconstruction of damaged corneas by transplantation of autologous limbal epithelial cells. *N Engl J Med.* **343**(2), 86–93 (2000).
7. Shortt, A. J. *et al*. Transplantation of *ex vivo* cultured limbal epithelial stem cells: a review of techniques and clinical results. *Surv Ophthalmol.* **52**(5), 483–502 (2007).
8. Rama, P. *et al*. Limbal stem-cell therapy and long-term corneal regeneration. *N Engl J Med.* **363**(2), 147–155 (2010).
9. Utheim, T. P. Limbal epithelial cell therapy: past, present, and future. *Methods Mol. Biol.* **1014**, 3–43 (2013).
10. Pellegrini, G. *et al*. Long-term restoration of damaged corneal surfaces with autologous cultivated corneal epithelium. *Lancet* **349**(9057), 990–993 (1997).
11. Pellegrini, G. *et al*. Biological parameters determining the clinical outcome of autologous cultures of limbal stem cells. *Regen Med.* **8**(5), 553–567 (2013).
12. Sejpal, K. *et al*. Cultivated limbal epithelial transplantation in children with ocular surface burns. *JAMA Ophthalmol.* **131**(6), 731–736 (2013).
13. Ganger, A., Vanathi, M., Mohanty, S. & Tandon, R. Long-term outcomes of cultivated limbal epithelial transplantation: evaluation and comparison of results in children and adults. *Biomed Res Int*. 480983, doi:10.1155/2015/480983 (2015).
14. Scholz, S. L. *et al*. Long-term results of autologous transplantation of limbal epithelium cultivated *ex vivo* for limbal stem cell deficiency. *Ophthalmologe.* **113**(4), 321–329 (2016).
15. Baylis, O., Figueiredo, F., Henein, C., Lako, M. & Ahmad, S. 13 years of cultured limbal epithelial cell therapy: a review of the outcomes. *J Cell Biochem.* **112**(4), 993–1002 (2011).
16. Holland, E. J. Management of limbal stem cell deficiency: a historical perspective, past, present, and future. *Cornea.* **34**(Suppl 10), S9–S15 (2015).
17. Nakamura, T., Inatomi, T., Sotozono, C., Koizumi, N. & Kinoshita, S. Ocular surface reconstruction using stem cell and tissue engineering. *Prog Retin Eye Res.* **51**, 187–207 (2016).
18. Daya, S. M. *et al*. Outcomes and DNA analysis of *ex vivo* expanded stem cell allograft for ocular surfacereconstruction. *Ophthalmology* **112**(3), 470–477 (2005).
19. Li, W., Hayashida, Y., He, H., Kuo, C. L. & Tseng, S. C. The fate of limbal epithelial progenitor cells during explant culture on intact amniotic membrane. *Invest Ophthalmol Vis Sci.* **48**(2), 605–613 (2007).
20. Pellegrini, G., Rama, P., Di Rocco, A., Panaras, A. & De Luca, M. Concise review: hurdles in a successful example of limbal stem cell-based regenerative medicine. *Stem Cells.* **32**(1), 26–34 (2014).
21. Ordonez, P. & Di Girolamo, N. Limbal epithelial stem cells: role of the niche microenvironment. *Stem Cells* **30**(2), 100–107 (2012).
22. Mei, H., Gonzalez, S. & Deng, S. X. Extracellular matrix is an important component of limbal stem cell niche. *J Funct Biomater.* **3**(4), 879–894 (2012).
23. Brizzi, M. F., Tarone, G. & Defilippi, P. Extracellular matrix, integrins, and growth factors as tailors of the stem cell niche. *Curr Opin Cell Biol.* **24**(5), 645–651 (2012).
24. Gattazzo, F., Urciuolo, A. & Bonaldo, P. Extracellular matrix: a dynamic microenvironment for stem cell niche. *Biochim Biophys Acta.* **1840**(8), 2506–2519 (2014).
25. Ahmed, M. & Ffrench-Constant, C. Extracellular matrix regulation of stem cell behavior. *Curr Stem Cell Rep.* **2**, 197–206 (2016).
26. Watt, F. M. & Huck, W. T. Role of the extracellular matrix in regulating stem cell fate. *Nat Rev Mol Cell Biol.* **14**(8), 467–473 (2013).
27. Miner, J. H. & Yurchenco, P. D. Laminin functions in tissue morphogenesis. *Annu Rev Cell Dev Biol.* **20**, 255–284 (2004).
28. Aumailley, M. *et al*. A simplified laminin nomenclature. *Matrix Biol.* **24**(5), 326–332 (2005).
29. Durbeej, M. Laminins. *Cell Tissue Res.* **339**(1), 259–268 (2010).
30. Aumailley, M. The laminin family. *Cell Adh Migr.* **7**(1), 48–55 (2013).
31. Schlötzer-Schrehardt, U. *et al*. Characterization of extracellular matrix components in the limbal epithelial stem cell compartment. *Exp Eye Res.* **85**(6), 845–860 (2007).
32. Polisetti, N., Zenkel, M., Menzel-Severing, J., Kruse, F. E. & Schlötzer-Schrehardt, U. Cell adhesion molecules and stem cell-niche-interactions in the limbal stem cell niche. *Stem Cells* **34**(1), 203–219 (2016).
33. Ljubimov, A. V. *et al*. Human corneal basement membrane heterogeneity: topographical differences in the expression of type IV collagen and laminin isoforms. *Lab Invest.* **72**(4), 461–473 (1995).
34. Tuori, A., Uusitalo, H., Burgeson, R. E., Terttunen, J. & Virtanen, I. The immunohistochemical composition of the human corneal basement membrane. *Cornea* **15**(3), 286–294 (1996).
35. Kabosova, A. *et al*. Compositional differences between infant and adult human corneal basement membranes. *Invest Ophthalmol Vis Sci.* **48**(11), 4989–4999 (2007).
36. Kim, Y., Ko, H., Kwon, I. K. & Shin, K. Extracellular matrix revisited: roles in tissue engineering. *Int Neurourol J.* **20**(Suppl 1), S23–29 (2016).
37. Tsai, R. J. & Tsai, R. Y. From stem cell niche environments to engineering of corneal epithelium tissue. *Jpn J Ophthalmol.* **58**(2), 111–119 (2014).
38. Blazejewska, E. A. *et al*. Corneal limbal microenvironment can induce transdifferentiation of hair follicle stem cells into corneal epithelial-like cells. *Stem Cells* **27**(3), 642–652 (2009).
39. Cheng, C. Y. *et al*. Novel laminin 5 gamma 2-chain fragments potentiating the limbal epithelial cell outgrowth on amniotic membrane. *Invest Ophthalmol Vis Sci.* **50**(10), 4631–4639 (2009).
40. Echevarria, T. J., Chow, S., Watson, S., Wakefield, D. & Di Girolamo, N. Vitronectin: a matrix support factor for human limbal epithelial progenitor cells. *Invest Ophthalmol Vis Sci.* **52**(11), 8138–8147 (2011).
41. Miyazaki, T. *et al*. Laminin E8 fragments support efficient adhesion and expansion of dissociated human pluripotent stem cells. *Nat Commun.* **3**, 1236, doi:10.1038/ncomms2231 (2012).
42. Okumura, N. *et al*. Laminin-511 and -521 enable efficient *in vitro* expansion of human corneal endothelial cells. *Invest Ophthalmol Vis Sci.* **56**(5), 2933–2942 (2015).
43. Yamada, M. & Sekiguchi, K. Molecular basis of laminin-integrin interactions. *Curr Top Membr.* **76**, 197–229 (2015).
44. Nishiuchi, R. *et al*. Ligand-binding specificities of laminin-binding integrins: a comprehensive survey of laminin-integrin interactions using recombinant alpha3beta1, alpha6beta1, alpha7beta1 and alpha6beta4 integrins. *Matrix Biol.* **25**(3), 189–197 (2006).
45. Miyazaki, T. & Kawase, E. Efficient and scalable culture of single dissociated human pluripotent stem cells using recombinant E8 fragments of human laminin isoforms. *Curr Protoc Stem Cell Biol.* **32**, 1C.18.1-8 (2015).
46. Levis, H. J. & Daniels, J. T. Recreating the human limbal epithelial stem cell niche with bioengineered limbal crypts. *Curr Eye Res.* **41**(9), 1153–1160 (2016).

47. Saghizadeh, M. *et al*. Alterations of epithelial stem cell marker patterns in human diabetic corneas and effects of c-met gene therapy. *Mol Vis.* **17**, 2177–2190 (2011).
48. Wegner, J. *et al*. Laminin α5 in the keratinocyte basement membrane is required for epidermal-dermal intercommunication. *Matrix Biol.* **56**, 24–41 (2016).
49. Fleger-Weckmann, A. *et al*. Deletion of the epidermis derived laminin γ1 chain leads to defects in the regulation of late hair morphogenesis. *Matrix Biol.* **56**, 42–56 (2016).
50. Faissner, A. & Reinhard, J. The extracellular matrix compartment of neural stem and glial progenitor cells. *Glia* **63**(8), 1330–1349 (2015).
51. Watt, F. M. & Fujiwara, H. Cell-extracellular matrix interactions in normal and diseased skin. *Cold Spring Harb Perspect Biol.* **3**(4), a005124, doi:10.1101/cshperspect.a005124 (2011).
52. Morgner, J. *et al*. Integrin-linked kinase regulates the niche of quiescent epidermal stem cells. *Nat Commun.* **6**, 8198, doi:10.1038/ncomms9198 (2015).
53. Sugawara, K., Tsuruta, D., Ishii, M., Jones, J. C. & Kobayashi, H. Laminin-332 and -511 in skin. *Exp Dermatol.* **17**(6), 473–480 (2008).
54. Lu, W., Ebihara, N., Miyazaki, K. & Murakami, A. Reduced expression of laminin-5 in corneal epithelial cells under high glucose condition. *Cornea* **25**(1), 61–67 (2006).
55. Ebihara, N. *et al*. The functions of exogenous and endogenous laminin-5 on corneal epithelial cells. *Exp Eye Res.* **71**(1), 69–79 (2000).
56. Ma, D. H. *et al*. Preservation of human limbal epithelial progenitor cells on carbodiimide cross-linked amniotic membrane via integrin-linked kinase-mediated Wnt activation. *Acta Biomater.* **31**, 144–155 (2016).
57. Domogatskaya, A., Rodin, S., Boutaud, A. & Tryggvason, K. Laminin-511 but not -332,-111, or -411 enables mouse embryonic stem cell self-renewal *in vitro*. *Stem Cells* **26**(11), 2800–2809 (2008).
58. Rodin, S., Antonsson, L., Hovatta, O. & Tryggvason, K. Monolayer culturing and cloning of human pluripotent stem cells on laminin-521-based matrices under xeno-free and chemically defined conditions. *Nat Protoc.* **9**(10), 2354–2368 (2014).
59. Laperle, A. *et al*. α-5 Laminin synthesized by human pluripotent stem cells promotes self-renewal. *Stem Cell Reports* **5**(2), 195–206 (2015).
60. Li, A., Pouliot, N., Redvers, R. & Kaur, P. Extensive tissue-regenerative capacity of neonatal human keratinocyte stem cells and their progeny. *J Clin Invest.* **113**(3), 390–400 (2004).
61. Sonnenberg, A. *et al*. Integrin recognition of different cell-binding fragments of laminin (P1, E3, E8) and evidence that alpha 6 beta 1 but not alpha 6 beta 4 functions as a major receptor for fragment E8. *J Cell Biol.* **110**(6), 2145–2155 (1990).
62. Nakagawa, M. *et al*. A novel efficient feeder-free culture system for the derivation of human induced pluripotent stem cells. *Sci Rep.* **4**, 3594, doi:10.1038/srep03594 (2014).
63. Sixt, M. *et al*. Cell adhesion and migration properties of beta 2-integrin negative polymorphonuclear granulocytes on defined extracellular matrix molecules. Relevance for leukocyte extravasation. *J Biol Chem.* **276**, 18878–18887 (2001).

Acknowledgements

We thank Dr. Takako Sasaki (University of Erlangen-Nürnberg) for providing anti-laminin α3, β3, γ2 and γ3 antibodies and Carmen Rummelt, Elke Meyer and Angelika Mößner for excellent technical assistance. DFG grant No. INST 410/45-1 FUGG.

Author Contributions

N.P.: Study design, collection, assembly, analysis of data, interpretation of data, and manuscript writing. L.S.: Study design and final approval of manuscript. N.O.: Study design and final approval of manuscript. N.K.: Study design and final approval of manuscript. S.K.: Study design and final approval of manuscript. K.F.E.: Study design and final approval of manuscript. U.S.-S.: Study design, collection, assembly, analysis and interpretation of data, manuscript writing.

Additional Information

Competing Interests: The authors declare that they have no competing interests.

Publisher's note: Springer Nature remains neutral with regard to jurisdictional claims in published maps and institutional affiliations.

Hindawi
Journal of Ophthalmology
Volume 2017, Article ID 1598218, 9 pages
https://doi.org/10.1155/2017/1598218

Research Article

Development of Poly Lactic/Glycolic Acid (PLGA) Microspheres for Controlled Release of Rho-Associated Kinase Inhibitor

Sho Koda,[1,2] Naoki Okumura,[1] Junji Kitano,[1] Noriko Koizumi,[1] and Yasuhiko Tabata[2]

[1]*Department of Biomedical Engineering, Faculty of Life and Medical Sciences, Doshisha University, Kyotanabe 610-0321, Japan*
[2]*Laboratory of Biomaterials, Department of Regeneration Science and Engineering, Institute for Frontier Life and Medical Sciences, Kyoto University, 53 Kawara-cho Shogoin, Sakyo-ku, Kyoto 606-8507, Japan*

Correspondence should be addressed to Yasuhiko Tabata; yasuhiko@frontier.kyoto-u.ac.jp

Received 7 February 2017; Revised 21 June 2017; Accepted 9 July 2017; Published 27 July 2017

Academic Editor: Vishal Jhanji

Purpose. The purpose of this study was to investigate the feasibility of poly lactic/glycolic acid (PLGA) as a drug delivery carrier of Rho kinase (ROCK) inhibitor for the treatment of corneal endothelial disease. *Method*. ROCK inhibitor Y-27632 and PLGA were dissolved in water with or without gelatin (W1), and a double emulsion [(W1/O)/W2] was formed with dichloromethane (O) and polyvinyl alcohol (W2). Drug release curve was obtained by evaluating the released Y-27632 by using high performance liquid chromatography. PLGA was injected into the anterior chamber or subconjunctiva in rabbit eyes, and ocular complication was evaluated by slitlamp microscope and histological analysis. *Results*. Y-27632 incorporated PLGA microspheres with different molecular weights, and different composition ratios of lactic acid and glycolic acid were fabricated. A high molecular weight and low content of glycolic acid produced a slower and longer release. The Y-27632 released from PLGA microspheres significantly promoted the cell proliferation of cultured corneal endothelial cells. The injection of PLGA did not induce any evident eye complication. *Conclusions*. ROCK inhibitor-incorporated PLGA microspheres were fabricated, and the microspheres achieved the sustained release of ROCK inhibitor over 7–10 days in vitro. Our data should encourage researchers to use PLGA microspheres for treating corneal endothelial diseases.

1. Introduction

The corneal endothelium maintains corneal transparency by pump and leaky barrier functions [1]. The corneal endothelium is located at the anterior chamber side of the posterior cornea at a cell density of 2000–3000 cells/mm^2 in a healthy subject. A phenotypical feature of corneal endothelial cells (CECs) is a severely limited proliferative ability [2]. When the corneal endothelium is impaired by any pathological conditions, trauma, or aging, the residual remaining CECs migrate and spread out to cover the impaired area, resulting in a cell density drop and increased polymorphism. The remaining CECs compensate the function to maintain corneal transparency, but once cell density drops to critical level, which is usually less than 500–1000 mm^2/cells, the cornea loses its transparency [1].

Corneal transplantation using a donor cornea is the only therapeutic choice for treating corneal endothelial decompensation [3]. Researchers, including our group, have searched pharmaceutical agents such as EGF [4], PDGF [5], FGF-2 [6], lithium [7], and Rho kinase (ROCK) inhibitor [8], which can promote the proliferation of CECs, for the treatment of corneal endothelial diseases. Indeed, we performed pilot clinical research and showed that ROCK inhibitor eye drops have a potency for treating early stages of Fuchs endothelial corneal dystrophy and severe corneal endothelial damage induced by cataract surgery by enhancing the proliferation of residual CECs [9–11].

Poly lactic/glycolic acid (PLGA), a copolymer of poly lactic acid (PLA) and poly glycolic acid (PGA), has been intensively researched as a drug delivery carrier [12, 13]. During the degradation of PLGA for drug release, lactic acid and glycolic acid are coreleased and are both biologically removed by the surrounding cells through normal metabolic pathways [14]. The biocompatibility, low toxicity, and drug encapsulation capabilities of PLGA-based drug delivery

Table 1: Summary of poly lactic/glycolic acid (PLGA) or poly lactic acid (PLA) microspheres.

Type	Molecular weight	Composition ratio Lactic acid : glycolic acid	Drug incorporation rate (%)	Particle size (μm)
5005	5000	50 : 50	12.5	12.63 ± 5.76
5010	10000	50 : 50	1.38	11.83 ± 6.85
7505	5000	75 : 15	1.17	14.30 ± 5.13
0005	5000	100 : 0	9.33	16.44 ± 6.09
0020	20000	100 : 0	2.11	13.94 ± 7.32
5005 + gelatin	5000	50 : 50	18.1	11.80 ± 7.74

systems have attracted the attention of researchers [12, 13]. Indeed, several therapies using PLGA have recently entered preclinical development [13, 15].

In the current study, we designed the PLGA microspheres, which incorporate ROCK inhibitor Y-27632, to enable efficient drug delivery for targeting corneal endothelium. We also evaluated the safety and stability of ROCK inhibitor released from PLGA microspheres through in vitro experiments. In addition, the safety of PLGA microsphere injection into the anterior chamber or subconjunctiva was evaluated in a rabbit model.

2. Materials and Methods

2.1. Microsphere Preparation. A selective ROCK inhibitor, Y-27632 (1 mg, Wako Pure Chemical Industries Ltd., Osaka, Japan), was dissolved in double-distilled water (200 μL) with or without gelatin (20 μg, Nitta Gelatin, Osaka, Japan) (W1) and poured into dichloromethane (2 mL, DCM, Nacalai Tesque, Kyoto, Japan) in which PLGA or poly (L-lactic acid) (PLA) (90 mg) was dissolved (O). The first inner W1/O emulsion was prepared by agitating for 60 secs using a vortex mixer at room temperature, followed by sonication for 300 secs using a UD-21P ultrasonic generator (Tomy Seiko Co. Ltd., Tokyo, Japan). The first emulsion was then poured into 1% polyvinyl alcohol (2 mL, PVA, Japan Vam & Poval Co. Ltd., Osaka, Japan) solution (W2), followed by vigorous mixing using a vortex mixer for 60 sec. This procedure permitted the formation of the double emulsion [(W1/O)/W2], in which the W1 phase was homogeneously dispersed in the O phase. The resulting double emulsion was poured into 1 wt% PVA solution (300 mL) and continuously stirred for 3 hours at 4°C until DCM was completely evaporated. The microspheres were washed several times with double-distilled water by centrifugation and freeze-dried into powdered microspheres. The microspheres with different composition ratios of lactic acid/glycolic acid were prepared similarly (Table 1).

The shape and size of the microspheres was evaluated using light microscopy (CKX41, Olympus Corp., Tokyo, Japan) and a micro scale (OB1, 1 mm scale length, 100 divisions, 0.01 mm pitch, MeCan Imaging Inc., Saitama, Japan). For scanning electron microscopy analysis, microspheres were fixed on an aluminum support with carbon-adhesive glue and coated with a 10 nm thick coating of gold-palladium (30 mA, 40 sec) (JSM 6701F; JEOL, Tokyo, Japan). The samples were observed using a scanning electron microscope (S-2380N, Hitachi Ltd., Tokyo, Japan).

2.2. Release Study. The Y-27632 release profiles from the PLGA microspheres were determined in vitro. PLGA microspheres in which Y-27632 (10 mg) was incorporated were incubated in a tube containing 1.0 mL phosphate-buffered saline solution (PBS; Nissui Pharmaceutical Co. Ltd., Tokyo, Japan) (pH: 7.4) at 37°C in a heat block (ALB-221, Scinics Co., Tokyo, Japan). PBS including released Y-27632 was evaluated at 1, 3, and 6 hour(s) and 1 to 30 day(s) after incubation. The concentration of Y-27632 in the samples was determined by high performance liquid chromatography (HPLC; Prominence, Shimazu Corp., Kyoto, Japan) equipped with one pump, an auto sampler, and an ultra violet (UV) detector. Calibration curves were prepared for Y-27632 based on the UV absorbance peak area at 269 nm. These calibration curves were used for the estimation of in vitro drug release. The Y-27632 release profile was calculated as follows: (cumulative amount of Y-27632 released)/(total incorporated Y-27632) × 100.

2.3. Cell Cultures. Eight corneas from four cynomolgus monkeys (3–5 years of age; estimated equivalent human age, 5–20 years) housed at Nissei Bilis Co. Ltd. (Otsu, Japan) were used for the study. The corneas were harvested at the time of the euthanization of the monkeys for other research purposes. CECs were cultured according to a modified protocol reported previously [16]. Briefly, Descemet's membrane including CECs was stripped from the cornea and incubated with 0.6 U/mL of Dispase II (Roche Applied Science, Penzberg, Germany) for 60 minutes at 37°C. CECs were then seeded onto a culture plate (CECs from one cornea to one well of a 12-well culture plate) with a culture medium composed of Dulbecco's modified Eagle's medium (DMEM, Life Technologies Corp., Carlsbad, CA) supplemented with 10% fetal bovine serum 50 U/mL penicillin, 50 μg/mL streptomycin, and 2 ng/mL basic fibroblast growth factor (bFGF; Life Technologies Corp.). ROCK inhibitor was not added to the culture medium when preparing CECs for experiments. When the cells reached confluence in 10 to 14 days, they were trypsinized with 0.05% trypsin-EDTA (Life Technologies Corp.) for 5 minutes at 37°C and passaged at ratios of 1 : 2 to 4. CECs obtained after the 4–7th passage that still maintained a hexagonal and monolayer sheet-like structure were used for the experiments.

2.4. In Vitro Assessment of Y-27632 Released from Microspheres. To evaluate the stability and safety of Y-27632

released from the PLGA/PLA microspheres, the effect of released Y-27632 on cell growth of CECs was evaluated. Y-27632 incorporating PLGA microspheres (0020) were incubated in PBS, and PBS was recovered at 3 and 7 days after incubation. The concentration of Y-27632 was then evaluated by HPLC, and the recovered PBS including the released Y-27632 was added to the culture medium at a final concentration of Y-27632 of 10 μM. Cultured monkey CECs were seeded at a density of 5.0×10^3 cells/cm^2 per well on a 96-well plate for 24 hours and then subjected to serum starvation for an additional 24 hours in the presence or absence of fresh Y-27632 (10 μM) or Y-27632 released from PLGA microspheres after 3 or 7 days (10 μM). The number of viable cells was determined by use of the CellTiter-Glo® Luminescent Cell Viability Assay (Promega, Fitchburg, Wisconsin) performed in accordance with the manufacturer's protocol. The number of CECs at 24 hours after treatment with Y-27632 was measured using the Veritas™ Microplate Luminometer (Promega, Fitchburg, Wisconsin).

2.5. Safety Assessment of Microspheres in Rabbit. To evaluate the safety of PLGA/PLA microspheres, 1 or 10 mg PLGA microspheres (0020) suspended in 200 μL PBS were injected into the anterior chamber and 1 mg PLGA microspheres suspended in 200 μL PBS were injected into the subconjunctiva of the 9 right eyes of 9 rabbits ($n = 3$). The left eyes were used as a control. The corneal appearance of the 9 rabbits was examined at 1, 2, 3, 5, 7, 10, and 14 days using a slitlamp microscope, and corneal opacification and conjunctival hyperemia were evaluated according to the grading system (Supplemental Table 1 available online at https://doi.org/10.1155/2017/1598218) modified from the previous report [17]. Intraocular pressure was determined with a Tonovet® (Icare Finland, Vantaa, Finland) instrument. Corneal thickness was determined through the use of an ultrasound pachymeter (SP-2000; Tomey, Nagoya, Japan).

2.6. Histological Examination of Rabbit Eyes after Poly Lactic/Glycolic Acid (PLGA) Microsphere Injection. After 14 days of PLGA microsphere injection, rabbits were euthanized, the eye balls were enucleated, and sclerocorneal specimens were prepared using ophthalmic surgical scissors. Samples were fixed in 4% formaldehyde and incubated for 30 minutes in 1% bovine serum albumin to block nonspecific binding. The samples were then incubated overnight at 4°C with antibodies against Na^+/K^+-ATPase (1 : 300, Upstate Biotechnology, Lake Placid, NY), ZO-1 (1 : 300, Life Technologies Corp.), and connexin 43 (1 : 300, Life Technologies Corp.). Alexa Fluor® 488-conjugated goat anti-mouse (Life Technologies Corp.) was used as a secondary antibody at a 1 : 1000 dilution. Cell morphology was evaluated after actin staining with a 1 : 400 dilution of Alexa Fluor 594-conjugated phalloidin (Life Technologies Corp.). Nuclei were stained with 4′,6-diamidino-2-phenylindole (DAPI, Dojindo Laboratories, Kumamoto, Japan). The samples were examined with a fluorescence microscope (TCS SP2 AOBS; Leica Microsystems, Wetzlar, Germany).

2.7. Statistical Analysis. The statistical significance (p value) of differences in the mean values of the two-sample comparison was determined with the Student's t-test. The statistical significance of comparisons of multiple sample sets was analyzed with Dunnett's multiple-comparisons test. $p < 0.05$ was considered as statistically significant. Results were expressed as mean ± standard error of the mean.

3. Results

3.1. Characteristics of Poly Lactic/Glycolic Acid (PLGA) or Poly Lactic Acid (PLA) Microspheres for Y-27632 Release. Y-27632-incorporated PLGA or PLA microspheres with different molecular weights and different composition ratios of lactic acid and glycolic acid were prepared (Table 1). All PLGA or PLA microspheres exhibited similar morphology and size. SEM showed that representative images of PLGA microspheres were spherical with a smooth surface (Figure 1(a), upper panel). The inside of the microspheres was porous core due to double emulsion, which is designed to incorporate Y-27632 (Figure 1(a), lower panel). We first evaluated the effect of molecular weight on the release profile in PLGA or PLA microspheres. PLGA5005 had released 65.5 ± 0.9% (approximately 8.22 μg) of the Y-27632 by 1 day and 98.7 ± 0.6% (approximately 12.4 μg) by 14 days, while PLGA5010, which has a higher molecular size than PLGA5005, released 40.8 ± 1.0% (approximately 0.56 μg) of Y-27632 by 1 day and 99.1 ± 1.7% (approximately 1.37 μg) by 14 days ($p < 0.01$ at 1 day). PLA0005 released 62.8 ± 0.8% (approximately 5.86 μg) of Y-27632 by 1 day and 77.7 ± 0.5% (approximately 7.25 μg) by 14 days, while PLA0020, which has a higher molecular size than PLA0005, released 30.2 ± 0.9% (approximately 0.64 μg) of Y-27632 by 1 day and 55.3 ± 0.6% (approximately 1.16 μg) by 14 days ($p < 0.01$ at both 1 day and 14 days) (Figure 1(b)). These data showed that a lower molecular weight increased the rate of drug release at a fixed composition ratio of lactic acid and glycolic acid. We next evaluated the effect of the composition of lactic acid and glycolic acid on the release profile. PLGA7505 released 58.9% of Y-27632 at 1 day and 97.4% at 14 days, and PLA0005 released 62.4% of Y-27632 at 1 day and 77.5% at 14 days. This data showed that a smaller amount of glycolic acid made the release slower and a smaller amount of lactic acid made the release of Y-27632 faster (Figure 1(c)).

The mean incorporation rate of Y-27632 was 8.74% in PLGA microspheres, though PLGA microspheres prepared with gelatin enabled a significantly higher incorporation of Y-27632 at 18.1%, showing that gelatin reduced the loss of ROCK inhibitor during preparation of the PLGA microspheres (Figure 1(d)). Characteristic release curves showed that both PLGA with or without gelatin have the potency to release Y-27632 and that the initial burst release of Y-27632 tended to decrease for microspheres with gelatin (Figure 1(e)).

3.2. In Vitro Evaluation of Y-27632 Released from Microspheres. The effect of Y-27632 released from PLGA microspheres on CEC proliferation was evaluated. Phase contrast images showed that CECs cultured with a culture medium supplemented with fresh Y-27632 (10 μM) showed

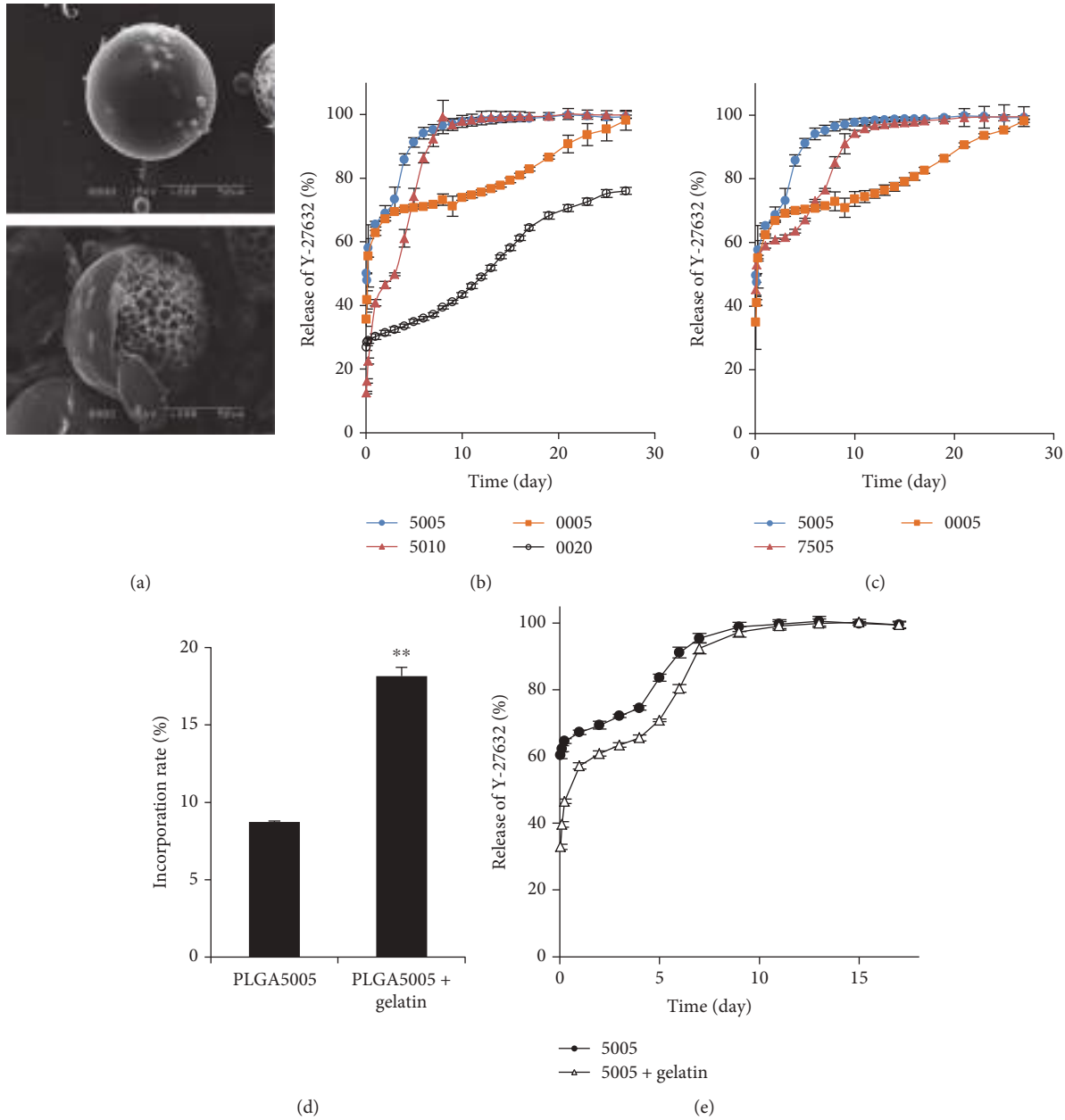

Figure 1: Characteristics of poly lactic/glycolic acid (PLGA) or poly lactic acid (PLA) microspheres for Y-27632 release. (a) PLGA microspheres were examined with a scanning electron microscope. The upper panel shows the surface of the microsphere, and the lower panel shows the internal structure of the microsphere. (b) PLGA or PLA microspheres were incubated in a PBS at 37°C for 14 days, and the amount of Y-27632 released was determined by HPLC. The effect of the molecular weight on the release profile for PLGA or PLA microspheres was evaluated. The cumulative amount of released Y-27632 was plotted in the graph ($n = 3$). (c) PLGA or PLA microspheres were incubated in PBS at 37°C, and the amount of Y-27632 released was determined by HPLC. The effect of the composition of lactic acid and glycolic acid on the release profile was evaluated ($n = 3$). The PLGA5005 release curve plotted is the same as that shown in Figure 1(b). (d) Y-27632 was dissolved in ultrapure water with or without gelatin, and PLGA5005 microspheres were prepared ($n = 3$). The incorporation rate was evaluated by HPLC. $^{**}p < 0.01$. (e) PLGA5005 with or without gelatin that incorporated Y-27632 was incubated at PBS at 37°C for 14 days, and the amount of Y-27632 released was determined by HPLC. Three independent experiments were performed.

higher numbers of cells than the control. The Y-27632 released from the PLGA microspheres was recovered after incubation and was added to a growth medium at a final concentration of 10 μM. Higher numbers of CECs were observed than those in the control after 24 hours of cultivation with those growth media that were supplemented with Y-27632 released from PLGA microspheres (Figure 2(a)). The cell numbers of CECs were significantly increased by the supplementation of fresh Y-27632 or the Y-27632 recovered from PLGA microspheres after an incubation of 3 and 7 days (118.8%, 110.6%, and 111.4%, resp.) (Figure 2(b)). These results showed that Y-27632 incorporated in PLGA

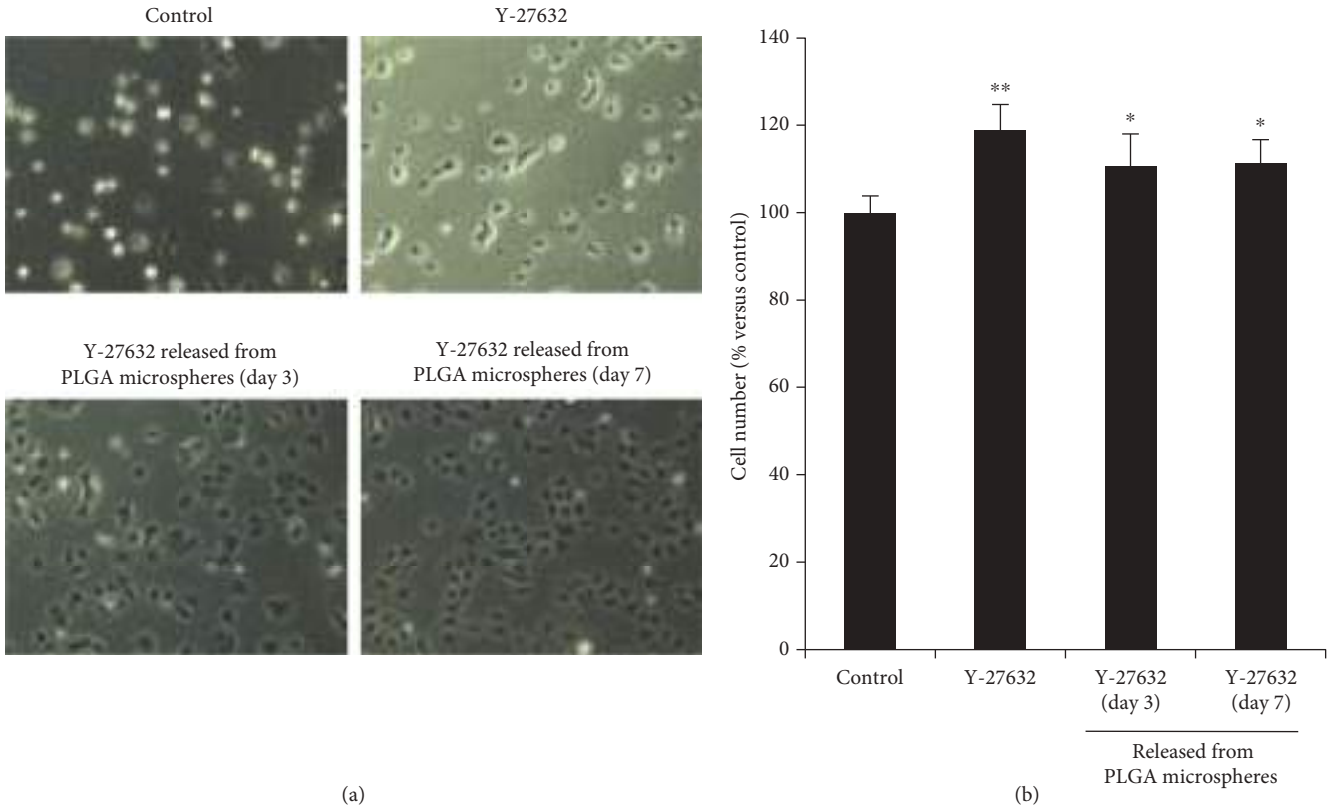

Figure 2: Stability and safety assessment of Y-27632 released from PLGA microspheres. (a) Y-27632 incorporating poly lactic/glycolic acid (PLGA) microspheres was incubated in PBS, and PBS was recovered after 3 and 7 days. The amount of Y-27632 released in the PBS was added to a culture medium as final concentration of Y-27632 as 10 μM. Phase contrast images of corneal endothelial cells (CECs) cultured for 24 hours are shown. (b) CECs were seeded at a density of 5.0×10^3 cells/cm^2 per well on a 96-well plate for 24 hours and subjected to serum starvation for an additional 24 hours supplemented with fresh Y-27632 (10 μM) or Y-27632 released from PLGA microspheres after 3 or 7 days (10 μM). Control cells were CECs cultured for an additional 24 hours without supplementation with Y-27632. The data represent average ± SE ($n = 5$). $^{**}p < 0.01$, $^{*}p < 0.05$. These experiments were performed in triplicate.

microspheres was released and its biological features were maintained.

3.3. In Vivo Safety Evaluation of Microspheres. We evaluated the feasibility of using PLGA microspheres in the eye by conducting a study using healthy rabbit eyes. Slitlamp microscopy showed that no eye complications, such as conjunctival injection, corneal opacity, cataract formation, or severe inflammation, occurred in any of the groups (Figure 3(a)). Corneal opacification and conjunctival hyperemia scores were zero in all of the eyes for all of the groups in which PLGA microspheres were injected into the anterior chamber (1 mg or 10 mg) and into the subconjunctiva (1 mg) (data not shown). Some PLGA microspheres were visible by slitlamp microscopy examination, especially in the iris, but no aggregation of microspheres was observed in the anterior chamber. Corneal thickness and intraocular pressure were not altered to abnormal levels during the 14-day observation period (Figures 3(b) and 3(c)).

Corneal endothelium of eyes in which PLGA microspheres were injected into the anterior chamber and the subconjunctiva expressed Na^+/K^+-ATPase (a marker of pump function), ZO-1 (a marker of tight junction), and connexin 43 (a marker of gap junctions) as did the control. Phalloidin staining showed that the cell morphology was hexagonal and monolayer in PLGA microsphere-treated eyes as with the control, and no morphological change was observed (Figure 4).

4. Discussion

Bullous keratopathy caused by cataract surgery is one of the leading causes of corneal transplantation due to corneal endothelial decompensation [3]. The Eye Bank Association of America reported that of the 28,394 corneal transplantations performed in 2015, 15,707 (55.3%) were for corneal endothelial decompensation [18]. In terms of bullous keratopathy due to severe corneal endothelial damage by cataract surgery, 8290 (29.2%) corneal transplantations were performed in the United States [18]. Likewise, 20–40% of corneal transplantations are performed to treat bullous keratopathy caused by cataract surgery in Asian countries [19–21].

In 2009, we reported that the ROCK inhibitor Y-27632 promoted cell proliferation of cultured CECs [8]. We subsequently demonstrated that the topical application of ROCK inhibitor such as Y-26732 and ripasudil as a form of eye drops enhances wound healing of the cornea endothelium by promoting cell proliferation of CECs in rabbit and monkey models [10, 11, 22, 23]. Based on these findings,

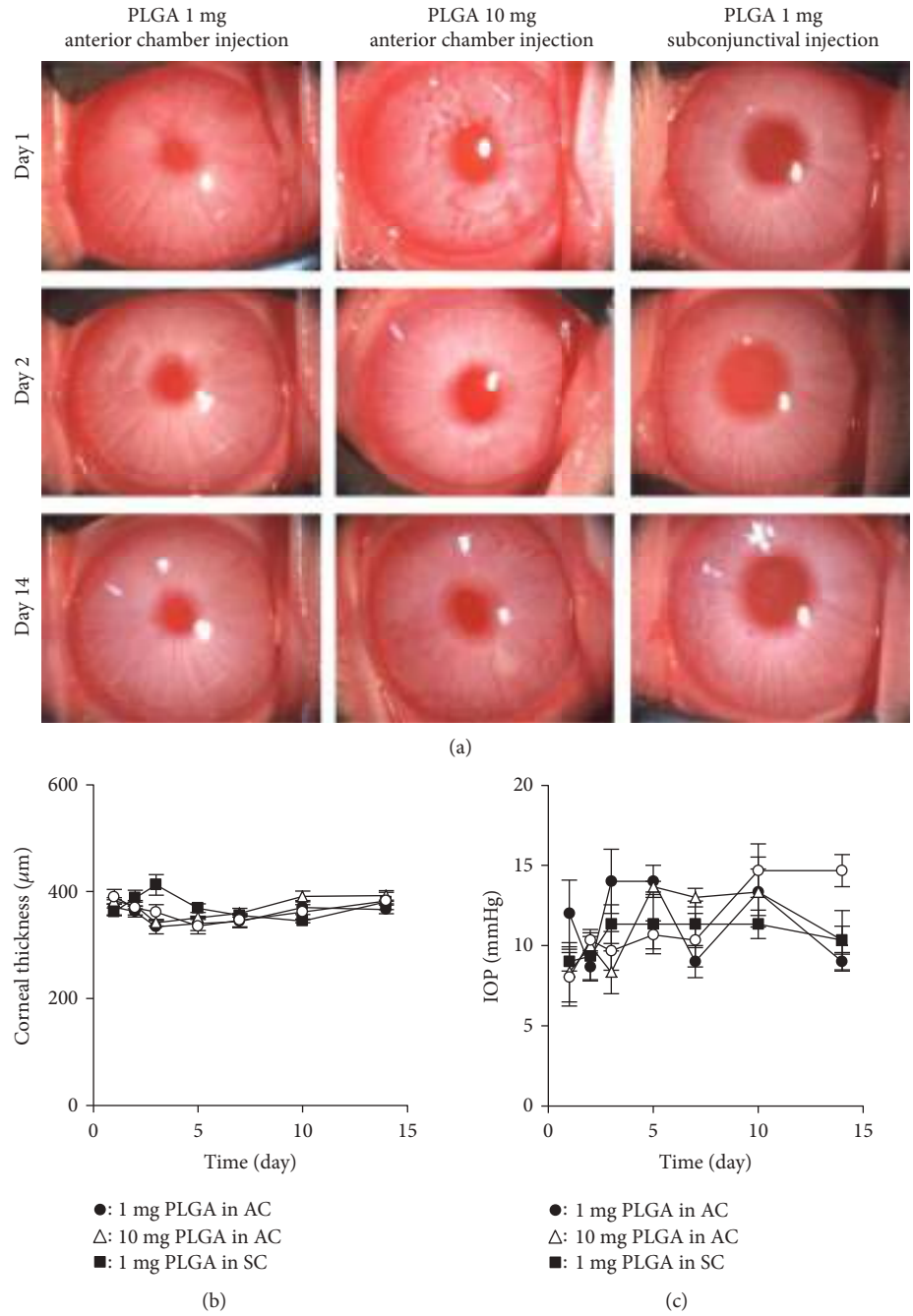

Figure 3: Safety assessment of poly lactic/glycolic acid (PLGA) microspheres in a rabbit eye. (a) One or 10 mg PLGA microspheres suspended in 200 μL phosphate buffer solution (PBS) was injected into the anterior chamber, and 1 mg PLGA microspheres suspended in 200 μL PBS was injected into the subconjunctiva. Nine right eyes of 9 rabbits were used for the experiments ($n = 3$). Anterior segments were evaluated by slitlamp microscopy for 14 days. (b, c) Corneal thickness and intraocular pressure were evaluated for 14 days and are shown in the graph. The central corneal thickness was evaluated by ultrasound pachymetry. Intraocular pressure was determined with a Tonovet.

we performed pilot clinical research in which patients with corneal decompensation were treated with Y-27632 eye drops following to a transcorneal freezing procedure to partially remove the damaged cornea endothelium. Y-27632 eye drops showed effectiveness in reducing the central corneal thickness in patients with early stage Fuchs endothelial corneal dystrophy [9, 10]. In addition, we demonstrated that ROCK inhibitor eye drops can enhance the wound healing of damaged corneal endothelium caused by cataract surgery, thus successfully avoiding the need for corneal transplantation [11]. Although further randomized clinical trials are necessary, ROCK inhibitor currently might be one of the most promising pharmaceutical agents that can be applied for corneal decompensation.

Possible complications of the injection of PLGA into the anterior chamber are direct mechanical damage to the

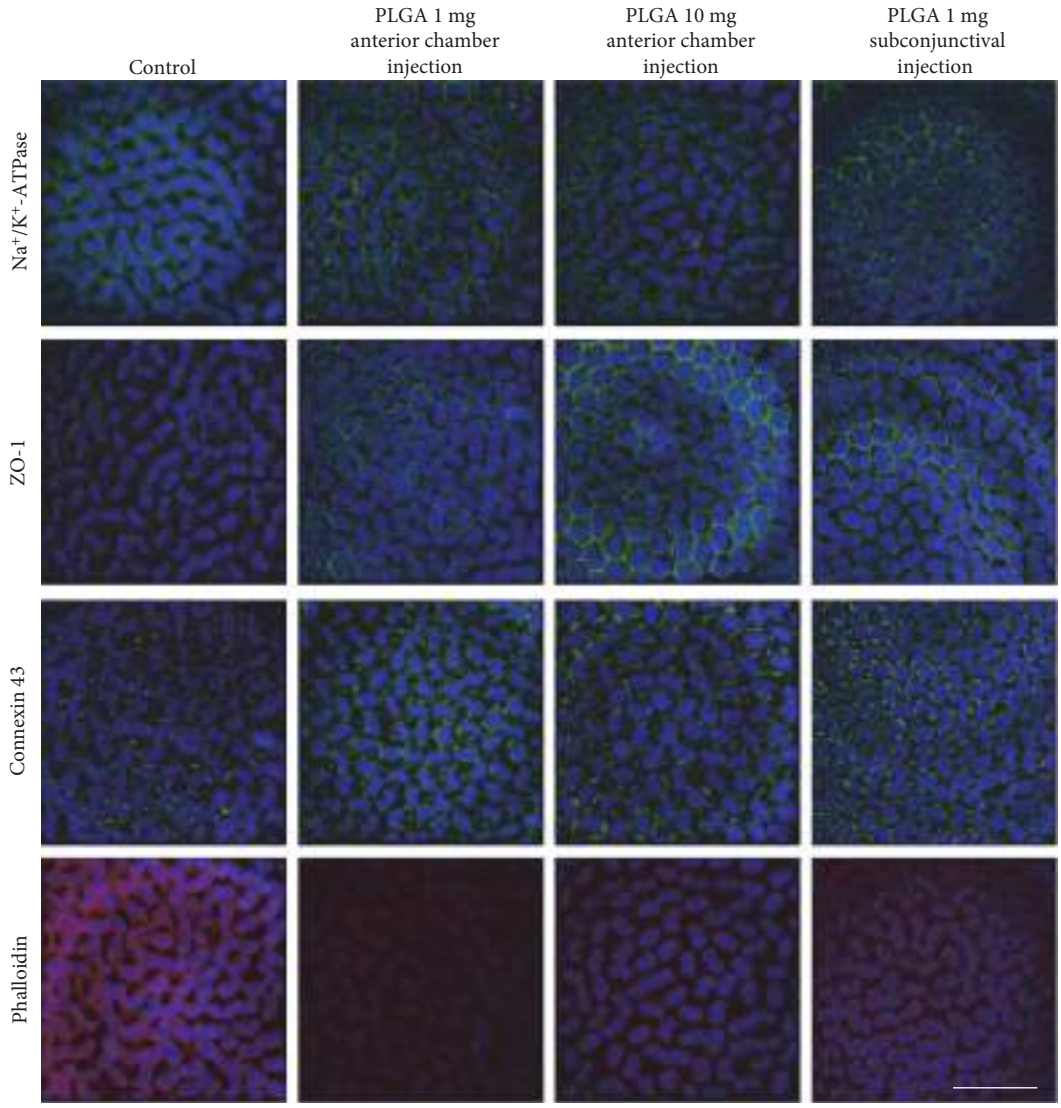

Figure 4: Histological evaluation of corneal endothelium in rabbit eyes injected with poly lactic/glycolic acid (PLGA) microspheres. One or 10 mg PLGA microspheres was injected into the anterior chamber, and 1 mg PLGA microspheres was injected into the subconjunctiva. After 14 days, corneal endothelium was evaluated by immunofluorescence staining and phalloidin staining. Na^+/K^+-ATPase (a marker of pump function), ZO-1 (a marker of tight junction), and connexin 43 (a marker of gap junctions) were used to evaluate the functional property of corneal endothelium. Phalloidin staining was used for morphological analysis. Nuclei were stained with DAPI. Scale bar: 50 μm.

corneal endothelium or lens, indirect damage to the corneal endothelium by biodegradation products from PLGA, and intraocular pressure elevation by inhibiting aqueous humor outflow. We therefore conducted a safety assessment using healthy rabbit eyes to evaluate the feasibility of applying PLGA microspheres for intracameral injection. Here, we showed that the injection of PLGA into the anterior chamber or the subconjunctiva did not induce any evident complications. No inflammatory response was observed, in agreement with the reported biocompatibility safety profile of PLGA. PLGA is capable of encapsulating a wide range of drugs of almost any molecular size [12]. Our in vitro study consistently showed that ROCK inhibitor released from PLGA promoted the proliferation of CECs in the same manner as unencapsulated ROCK inhibitor, suggesting that ROCK inhibitor was incorporated into and released from PLGA without damage to the molecular properties of the inhibitor. Further study is needed, but it is suggested that PLGA might be applicable as a drug carrier that is injected into the anterior chamber.

In our clinical research, we suggested that a ROCK inhibitor has the potency to promote the cell proliferation of residual relatively healthy CECs [9–11] and that there is a "golden time" for a ROCK inhibitor, when the wounded space has not yet been covered by the migration and spreading of residual CECs associated with a cell density drop [24]. We showed that ROCK inhibitor eye drops restored corneal clarity within one week in patients with Fuchs endothelial corneal dystrophy following a transcorneal freezing procedure and within 1-2 months in patients with severe corneal endothelial damage due to cataract surgery. Therefore, in this study, we aimed to fabricate a PLGA system that would

release Y-27632 for 7 to 10 days to improve the therapeutic efficacy during this window of opportunity; however, the release time should be optimized by further studies. The drug release from PLGA with degradation is influenced by various factors such as the initial molecular weight, the monomer composition rate of PLA and PGA, the drug type, and the pH of the surrounding circumstances [12, 25]. Among these factors, the molecular weight and the composition rate of PLA and PGA are recognized as important and are also easily controlled during fabrication [12]. Here, we showed that PLGA5010 exhibited a slower release than PLGA5005 and that PLA0020 exhibited slower release than PLA 0005, showing that PLGA or PLA microspheres with a high molecular weight produce slower and more prolonged Y-27632 release. This may be because polymers with lower molecular weights are less hydrophobic, which increases the rate of water absorption, consequent hydrolysis, and erosion [26]. The composition of PLA and PGA in PLGA is also an important factor influencing polymer degradation. In this study, PLGA7505 showed a slower release of Y-27632 than PLGA5005, and PLA0005 showed the slowest and longest release, although it exhibited an initial burst in release. This suggests that a lower content of GA in PLGA results in a slower and longer-term drug release from the PLGA microspheres. It has been demonstrated that the PGA : PLA ratio of 50 : 50 make PLGA the most hydrophilic and amorphous when compared to other ratios, resulting in faster degradation and drug release [12].

Although the further optimization of the release profile of the ROCK inhibitor is needed before clinical application, our results offers fundamental information for modifying the molecular weights and composition rates of PLA and PGA. Various mathematical, computational, and theoretical models may be applicable for the optimization of the release profile [27–29]. However, drug release from microspheres differs in the in vitro versus in vivo conditions, in part due to immunological responses and the plasticizing effects of biological substances [12]. For instance, the release of thymosin alpha 1 from PLGA was slightly faster in an in vivo assay than in an in vitro assay [30]. Conversely, other researchers have shown that PLGA degradation was slower in vivo than in vitro [31]. Therefore, pharmacokinetics studies are needed on the release of ROCK inhibitor in the anterior chamber. The drawback of this study is the lack of in vivo experiments that show an enhancement of corneal endothelial wound healing by ROCK inhibitor incorporated into PLGA. The fate of the PLGA injected into the anterior chamber is also not well characterized, and further in vivo experiments are needed prior to initiating clinical applications. In the clinical setting, however, the treatment of corneal endothelial damage induced by cataract surgery would seem to be an important target for this PLGA therapy.

In conclusion, we fabricated ROCK inhibitor-incorporated PLGA microspheres, and those microspheres act as carrier for the sustained release of the ROCK inhibitor over 7–10 days. In addition, the PLGA microspheres did not exhibit any evident complication in the eyes of a rabbit model. Although further optimization of the release profile of PLGA and in vivo experiments for safety and effectiveness assessment are required, PLGA microspheres would appear to represent a promising drug delivery carrier for ROCK inhibitor.

Ethical Approval

In all experiments, animals were housed and treated in accordance with the ARVO Statement for the Use of Animals in Ophthalmic and Vision Research. The rabbit experiments were performed at Doshisha University (Kyoto, Japan) according to the protocol approved by the University's Animal Care and Use Committee (Approval no. 1315).

Conflicts of Interest

Noriko Koizumi is listed as inventor of the patent regarding the application of the ROCK inhibitor for corneal endothelium (Registration no. 5657252).

Acknowledgments

The authors would like to acknowledge the grant from the Program for the Strategic Research Foundation at Private Universities from MEXT (Noriko Koizumi and Naoki Okumura). The authors are grateful to Dr. Takashi Saito for the valuable advice for the PLGA experiments.

References

[1] T. Nishida and S. Saika, "Cornea and sclera: anatomy and physiology," *Cornea Third Edition*, vol. 1, pp. 3–24, 2011.

[2] N. C. Joyce, "Proliferative capacity of corneal endothelial cells," *Experimental Eye Research*, vol. 95, no. 1, pp. 16–23, 2012.

[3] D. T. Tan, J. K. Dart, E. J. Holland, and S. Kinoshita, "Corneal transplantation," *Lancet*, vol. 379, no. 9827, pp. 1749–1761, 2012.

[4] V. P. Hoppenreijs, E. Pels, G. F. Vrensen, J. Oosting, and W. F. Treffers, "Effects of human epidermal growth factor on endothelial wound healing of human corneas," *Investigative Ophthalmology & Visual Science*, vol. 33, no. 6, pp. 1946–1957, 1992.

[5] V. P. Hoppenreijs, E. Pels, G. F. Vrensen, and W. F. Treffers, "Effects of platelet-derived growth factor on endothelial wound healing of human corneas," *Investigative Ophthalmology & Visual Science*, vol. 35, no. 1, pp. 150–161, 1994.

[6] J. Lu, Z. Lu, P. Reinach et al., "TGF-beta2 inhibits AKT activation and FGF-2-induced corneal endothelial cell proliferation," *Experimental Cell Research*, vol. 312, no. 18, pp. 3631–3640, 2006.

[7] E. C. Kim, H. Meng, and A. S. Jun, "Lithium treatment increases endothelial cell survival and autophagy in a mouse model of Fuchs endothelial corneal dystrophy," *The British Journal of Ophthalmology*, vol. 97, no. 8, pp. 1068–1073, 2013.

[8] N. Okumura, M. Ueno, N. Koizumi et al., "Enhancement on primate corneal endothelial cell survival in vitro by a ROCK inhibitor," *Investigative Ophthalmology & Visual Science*, vol. 50, no. 8, pp. 3680–3687, 2009.

[9] N. Koizumi, N. Okumura, M. Ueno, H. Nakagawa, J. Hamuro, and S. Kinoshita, "Rho-associated kinase inhibitor eye drop treatment as a possible medical treatment for fuchs corneal dystrophy," *Cornea*, vol. 32, no. 8, pp. 1167–1170, 2013.

[10] N. Okumura, N. Koizumi, E. P. Kay et al., "The ROCK inhibitor eye drop accelerates corneal endothelium wound healing," *Investigative Ophthalmology & Visual Science*, vol. 54, no. 4, pp. 2493–2502, 2013.

[11] N. Okumura, R. Inoue, Y. Okazaki et al., "Effect of the Rho kinase inhibitor Y-27632 on corneal endothelial wound healing," *Investigative Ophthalmology & Visual Science*, vol. 56, no. 10, pp. 6067–6074, 2015.

[12] Y. Xu, C. S. Kim, D. M. Saylor, and D. Koo, "Polymer degradation and drug delivery in PLGA-based drug-polymer applications: a review of experiments and theories," *Journal of Biomedical Materials Research Part B: Applied Biomaterials*, vol. 105, no. 6, pp. 1692–1716, 2016.

[13] R. J. Bose, S. H. Lee, and H. Park, "Lipid-based surface engineering of PLGA nanoparticles for drug and gene delivery applications," *Biomaterials Research*, vol. 20, p. 34, 2016.

[14] A. Gopferich, "Mechanisms of polymer degradation and erosion," *Biomaterials*, vol. 17, no. 2, pp. 103–114, 1996.

[15] F. Danhier, E. Ansorena, J. M. Silva, R. Coco, A. Le Breton, and V. Préat, "PLGA-based nanoparticles: an overview of biomedical applications," *Journal of Controlled Release*, vol. 161, no. 2, pp. 505–522, 2012.

[16] N. Koizumi, Y. Sakamoto, N. Okumura et al., "Cultivated corneal endothelial cell sheet transplantation in a primate model," *Investigative Ophthalmology & Visual Science*, vol. 48, no. 10, pp. 4519–4526, 2007.

[17] C. Sotozono, L. P. Ang, N. Koizumi et al., "New grading system for the evaluation of chronic ocular manifestations in patients with Stevens-Johnson syndrome," *Ophthalmology*, vol. 114, no. 7, pp. 1294–1302, 2007.

[18] Eye Bank Association of America, *Eye Banking Statistical Report*, Washington, D.C., 2015.

[19] L. Dandona, T. J. Naduvilath, M. Janarthanan, K. Ragu, and G. Rao, "Survival analysis and visual outcome in a large series of corneal transplants in India," *The British Journal of Ophthalmology*, vol. 81, no. 9, pp. 726–731, 1997.

[20] J. Shimazaki, S. Amano, T. Uno, N. Maeda, N. Yokoi, and Japan Bullous Keratopathy Study Group, "National survey on bullous keratopathy in Japan," *Cornea*, vol. 26, no. 3, pp. 274–278, 2007.

[21] D. T. Tan, P. Janardhanan, H. Zhou et al., "Penetrating keratoplasty in Asian eyes: the Singapore corneal transplant study," *Ophthalmology*, vol. 115, no. 6, pp. 975–982, 2008, e1.

[22] N. Okumura, N. Koizumi, M. Ueno et al., "Enhancement of corneal endothelium wound healing by Rho-associated kinase (ROCK) inhibitor eye drops," *The British Journal of Ophthalmology*, vol. 95, no. 7, pp. 1006–1009, 2011.

[23] N. Okumura, Y. Okazaki, R. Inoue et al., "Effect of the Rho-associated kinase inhibitor eye drop (Ripasudil) on corneal endothelial wound healing," *Investigative Ophthalmology & Visual Science*, vol. 57, no. 3, pp. 1284–1292, 2016.

[24] N. Okumura, S. Kinoshita, and N. Koizumi, "The role of Rho kinase inhibitors in corneal endothelial dysfunction," *Current Pharmaceutical Design*, vol. 23, no. 4, pp. 660–666, 2017.

[25] H. K. Makadia and S. J. Siegel, "Poly lactic-co-glycolic acid (PLGA) as biodegradable controlled drug delivery carrier," *Polymers (Basel)*, vol. 3, no. 3, pp. 1377–1397, 2011.

[26] S. Fredenberg, M. Wahlgren, M. Reslow, and A. Axelsson, "The mechanisms of drug release in poly(lactic-co-glycolic acid)-based drug delivery systems—a review," *International Journal of Pharmaceutics*, vol. 415, no. 1-2, pp. 34–52, 2011.

[27] D. Y. Arifin, L. Y. Lee, and C. H. Wang, "Mathematical modeling and simulation of drug release from microspheres: implications to drug delivery systems," *Advanced Drug Delivery Reviews*, vol. 58, no. 12-13, pp. 1274–1325, 2006.

[28] C. K. Sackett and B. Narasimhan, "Mathematical modeling of polymer erosion: consequences for drug delivery," *International Journal of Pharmaceutics*, vol. 418, no. 1, pp. 104–114, 2011.

[29] M. A. Lauzon, E. Bergeron, B. Marcos, and N. Faucheux, "Bone repair: new developments in growth factor delivery systems and their mathematical modeling," *Journal of Controlled Release*, vol. 162, no. 3, pp. 502–520, 2012.

[30] Q. Liu, H. Zhang, G. Zhou et al., "In vitro and in vivo study of thymosin alpha1 biodegradable in situ forming poly(lactide-co-glycolide) implants," *International Journal of Pharmaceutics*, vol. 397, no. 1-2, pp. 122–129, 2010.

[31] A. K. Mohammad and J. J. Reineke, "Quantitative detection of PLGA nanoparticle degradation in tissues following intravenous administration," *Molecular Pharmaceutics*, vol. 10, no. 6, pp. 2183–2189, 2013.

Development of Cell Analysis Software for Cultivated Corneal Endothelial Cells

Naoki Okumura, MD, PhD, Naoya Ishida, BS,† Kazuya Kakutani, BS, MS,* Akane Hongo, BS, MS,* Satoru Hiwa, PhD,† Tomoyuki Hiroyasu, PhD,† and Noriko Koizumi, MD, PhD**

Purpose: To develop analysis software for cultured human corneal endothelial cells (HCECs).

Methods: Software was designed to recognize cell borders and to provide parameters such as cell density, coefficient of variation, and polygonality of cultured HCECs based on phase contrast images. Cultured HCECs with high or low cell density were incubated with Ca^{2+}-free and Mg^{2+}-free phosphate-buffered saline for 10 minutes to reveal the cell borders and were then analyzed with software (n = 50).

Results: Phase contrast images showed that cell borders were not distinctly outlined, but these borders became more distinctly outlined after phosphate-buffered saline treatment and were recognized by cell analysis software. The cell density value provided by software was similar to that obtained using manual cell counting by an experienced researcher. Morphometric parameters, such as the coefficient of variation and polygonality, were also produced by software, and these values were significantly correlated with cell density (Pearson correlation coefficients −0.62 and 0.63, respectively).

Conclusions: The software described here provides morphometric information from phase contrast images, and it enables subjective and noninvasive quality assessment for tissue engineering therapy of the corneal endothelium.

Key Words: corneal endothelium, cell density, software

(*Cornea* 2017;36:1387–1394)

The corneal endothelium counteracts water imbibition into stroma by the functioning of an ion transport system. Consequently, dysfunction of the corneal endothelium induces corneal edema due to excessive influx of water, which results in vision loss. Corneal transplantation is typically the only therapeutic choice for treatment of corneal endothelial dysfunction. However, associated problems, such as shortage of donor corneas, surgical difficulty and invasiveness, and transplant rejection, have prompted researchers to seek new therapeutic modalities using tissue engineering technology.[1] For instance, several research groups, including ours, have successfully cultured corneal endothelial cells (CECs) on substrates such as amniotic membrane,[2] collagen sheets,[3,4] and sliced human corneal stroma,[5] and have successfully regenerated transparent corneas in animal models by transplanting these cultured CECs. Mimura et al also reported that injection of cultured CECs in the form of a sphere into the anterior chamber results in regeneration of the corneal endothelium in a rabbit model.[6] We also demonstrated that injection of CECs in combination with a Rho kinase inhibitor into the anterior chamber regenerates the corneal endothelium in rabbit and monkey corneal endothelial dysfunction models.[7,8] We have since initiated clinical research into CEC injection therapy in humans at the Kyoto Prefectural University of Medicine (Clinical trial registration: UMIN000012534).

Several reports of successful human corneal endothelial cell (HCEC) cultivation have been published,[9–12] but providing sufficient numbers of cells with guaranteed quality for clinical application has proven surprisingly difficult.[13] During cell cultivation, HCECs tend to undergo cell death, and even if they survive, they transform into a fibroblastic phenotype, in which the vital pump and barrier functions are lost; these cells also exhibit a senescent phenotype.[13,14] Consequently, establishment of cell cultivation protocols has been recognized as a pivotal issue for tissue engineering of the corneal endothelium for therapeutic purposes. Several reports have aimed at improving cultivation protocols by optimizing the culture medium,[15,16] enhancing cell proliferation,[17–19] suppressing fibroblast transformation,[14] and coating the culture plates with specific substrates.[20] These recent developments in culture techniques have allowed culture of cells in sufficient quantities for clinical use, and we have initiated culturing of HCECs of Good Manufacturing Practice grade at the Kyoto Prefectural University of Medicine for clinical purposes.

One remaining limitation of our culture protocol is the lack of a quality control protocol for these cells to ensure patient safety and a good prognosis after therapy. In this article, we describe software that we have designed for the

Received for publication November 27, 2016; revision received June 16, 2017; accepted June 22, 2017. Published online ahead of print August 22, 2017.
From the Departments of *Biomedical Engineering; and †Biomedical Information, Faculty of Life and Medical Sciences, Doshisha University, Kyotanabe, Japan.
The authors have no conflicts of interest to disclose.
Supplemental digital content is available for this article. Direct URL citations appear in the printed text and are provided in the HTML and PDF versions of this article on the journal's Web site (www.corneajrnl.com).
Reprints: Noriko Koizumi, MD, PhD, Department of Biomedical Engineering, Faculty of Life and Medical Sciences, Doshisha University, Kyotanabe 610-0321, Japan (e-mail: nkoizumi@mail.doshisha.ac.jp).

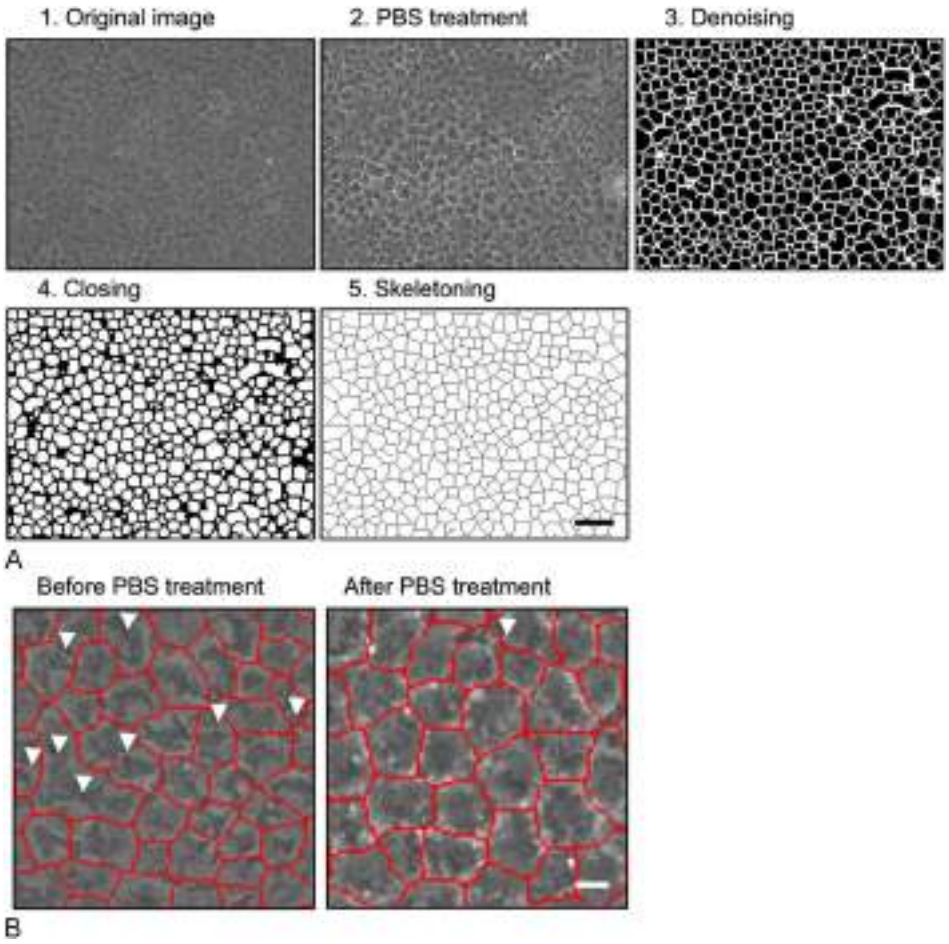

FIGURE 1. Cell analysis software for cultured HCECs. A, Cultured HCECs were incubated with PBS for 10 minutes and then imaged using a phase contrast microscope. The phase contrast image obtained after PBS treatment was analyzed with CECA. Images obtained by analyzing the phase contrast image after PBS treatment were shown by each step; that is, denoising, closing, and skeletonizing. Scale bar: 100 μm. B, The cell borders of HCECs before and after PBS cultivation were analyzed with CECA. The red line was recognized as a cell border by cell analysis software. The analyzed image of HCECs before PBS treatment showed that cell borders were not properly recognized (arrowhead), whereas the border of the HCECs treated with PBS were more likely to be recognized. Scale bar: 10 μm.

evaluation of cell density, polymegathism, and polymorphism of cultured HCECs, and we provide an evaluation of the feasibility of its use for the analysis of HCECs.

MATERIALS AND METHODS

Human donor corneas were obtained from SightLife (Seattle, WA) for research purposes. Sixteen human donor corneas (from persons older than 40 years) were used for cultivation of HCECs using the protocol described previously.[20] Briefly, Descemet membranes containing HCECs were stripped from donor corneas, and the membranes were digested with 1 mg/mL collagenase A (Roche Applied Science, Penzberg, Germany) at 37°C for 12 hours. The HCECs were seeded in 1 well of a 48-well plate coated with laminin E8 fragments (iMatrix-511; Nippi, Inc, Tokyo, Japan).[20] The culture medium was prepared according to published protocols.[16] First, bone marrow mesenchymal stem cells were plated at a density of 1.3×10^4 cells/cm^2 and cultured for 24 hours in Dulbecco's Modified Eagle's Medium (Life Technologies Corp, Carlsbad, CA) supplemented with 10% fetal bovine serum (FBS), 100 U/mL penicillin, and 100 μg/mL streptomycin. The culture medium was then replaced with OptiMEM-I (Life Technologies Corp) containing 8% FBS, 5 ng/mL epidermal growth factor (Sigma-Aldrich Co, St. Louis, MO), 20 μg/mL ascorbic acid (Sigma-Aldrich Co), 200 mg/L calcium chloride, 0.08% chondroitin sulfate (Wako Pure Chemical Industries, Ltd, Osaka, Japan), 50 μg/mL gentamicin, and 10 μM SB431542 (Merck Millipore, Billerica, MA),[14] and bone marrow mesenchymal stem cells were cultured for an additional 24 hours to condition this medium. The conditioned medium was then collected for use as the culture medium for HCECs. The HCECs were cultured at 37°C in a humidified atmosphere containing 5% CO_2, and the culture medium was changed every 2 days. Cells were examined with a phase contrast microscope (DMI4000 B; Leica Microsystems, Wetzlar, Germany). Phase contrast images of confluent cultured HCECs (2–8 passages) were prepared and separated by a single experimenter (K.K.) into the following 2 groups: a high cell density group, in which the cell density was maintained high during cultivation, and a low cell density group, in which the cell density was spontaneously reduced under the culture conditions. Fifty phase contrast images of HCECs treated with phosphate-buffered saline (PBS) were randomly selected from each group.

Cell analysis software for analyzing cultured HCECs [hereafter referred to as the corneal endothelial cell analyzer (CECA)] was developed at Doshisha University with programming by Python (Python Software Foundation, https://

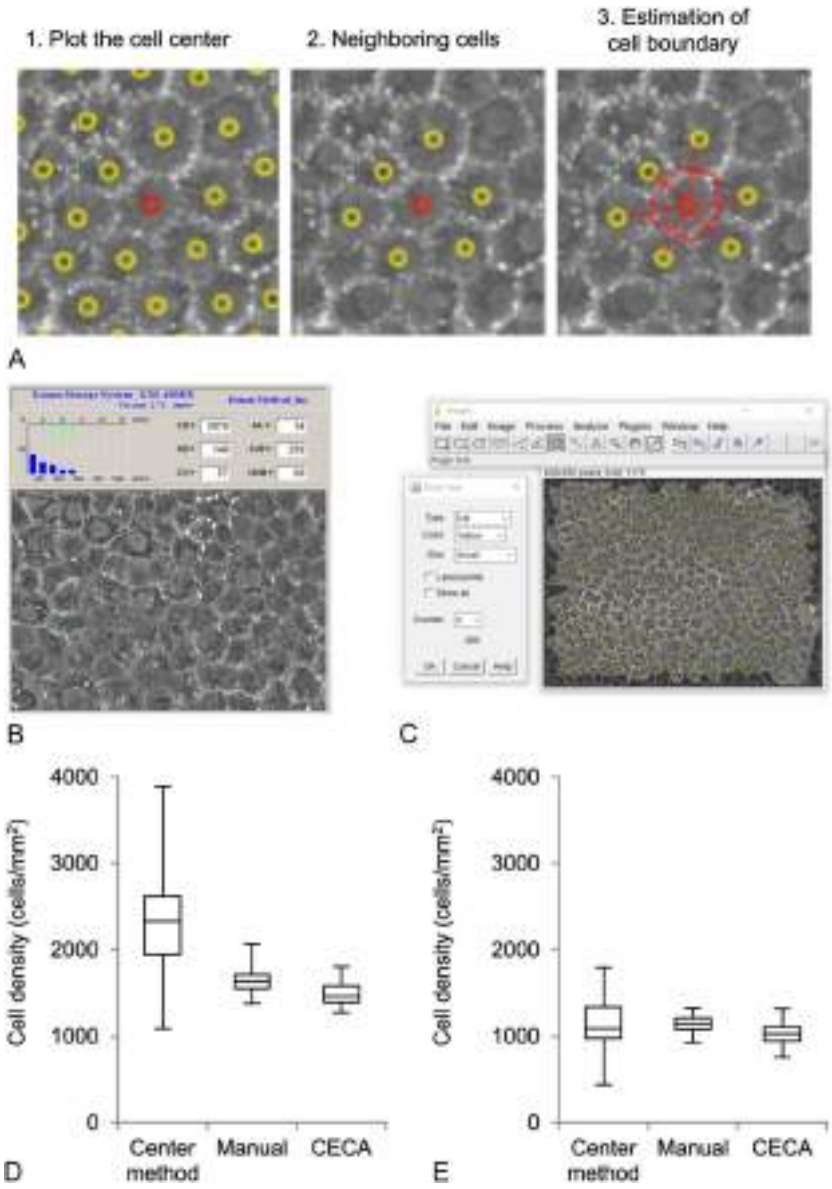

FIGURE 2. Analysis of the cultured corneal endothelial cell density using CECA. A, The algorithm of the center method using KSS-400EB software is shown. 1) The researcher plots the cell center manually, 2) the cell centers of surrounding cells are defined, and 3) the cell boundary is estimated as a perpendicular line that crosses the midpoint of the cell center and the cell centers of the surrounding cells. B, A representative analysis image obtained using KSS-400EB software is shown. C, For ImageJ analysis, the external borders were defined by CECA (the outside of the external border is shown in black, the inside of the external border is shown in gray). Manual cell counting was then conducted by plotting the centers of the cells manually, and the cell density was obtained by calculating the cell numbers/area using ImageJ software. A representative analysis image by ImageJ software is shown. The same phase contrast image was analyzed and is shown in (B and C). ImageJ software analyzed the whole area of the phase contrast image, whereas KSS-400EB software magnified a specific area and analyzed a smaller number of cells. D and E, Phase contrast images of HCECs with high and low cell density were analyzed by the following 3 methods. First, the centers of the cells were plotted manually, and cell density was analyzed by the center method using KSS-400EB software. Second, the centers of the cells were plotted manually, and cell density was obtained by calculating the cell numbers/area using ImageJ software. Third, the cell density was automatically analyzed by CECA. The cell centers were plotted by 2 independent researchers for the center method using KSS-400EB software and for manual analysis by ImageJ software. Representative data obtained by a single researcher are shown. The horizontal lines in the boxes indicate medians, the bottom of each box indicates the 25th percentile, and the top of each box indicates the 75th percentile. The horizontal lines outside the boxes indicate the range of CEC density.

www.python.org/, Beaverton, OR). Python was used in Eclipse (Eclipse Foundation, http://www.eclipse.org/, Ontario, Canada) with a PyDev (PyDev, http://www.pydev.org/) plug-in. First, HCECs were incubated in Ca^{2+}-free and Mg^{2+}-free PBS, and phase contrast images were obtained. These images were converted to a binary image that represented the cell boundary and the cell regions. The number of cells, cell areas, and numbers of surrounding neighbor cells were then obtained based on the binary images. The external borders of the cells used for the analysis were defined to eliminate cells that were on the edge of the phase contrast images. In addition, CECA was programmed to provide clinical parameters for the corneal endothelium; that is, the coefficient of variation (CV) and numbers of surrounding neighbor cells. As a control, the cell density was also evaluated by the center method using KSS-400EB software (Konan Medical, Inc, Hyogo, Japan) or by ImageJ software after manual counting by experienced researchers. For ImageJ analysis, the external borders were defined by CECA (ie, precisely the same area was evaluated by both ImageJ and CECA), and the cell density was then calculated as cell number/area. The algorithm of the center method includes the following steps: 1) the researcher plots the cell center manually using KSS-400EB software; 2) the cell center of the surrounding cells is defined [ie, the length between the cell center and the cell center of surrounding cells is selected to be 2.5 to 3.5 times the D_{min} (where D_{min} is the minimum length between plotted cell centers)]; and 3) the cell boundary is estimated as the perpendicular line that crosses the midpoint of the cell center and the cell centers of the surrounding cells. For the ImageJ

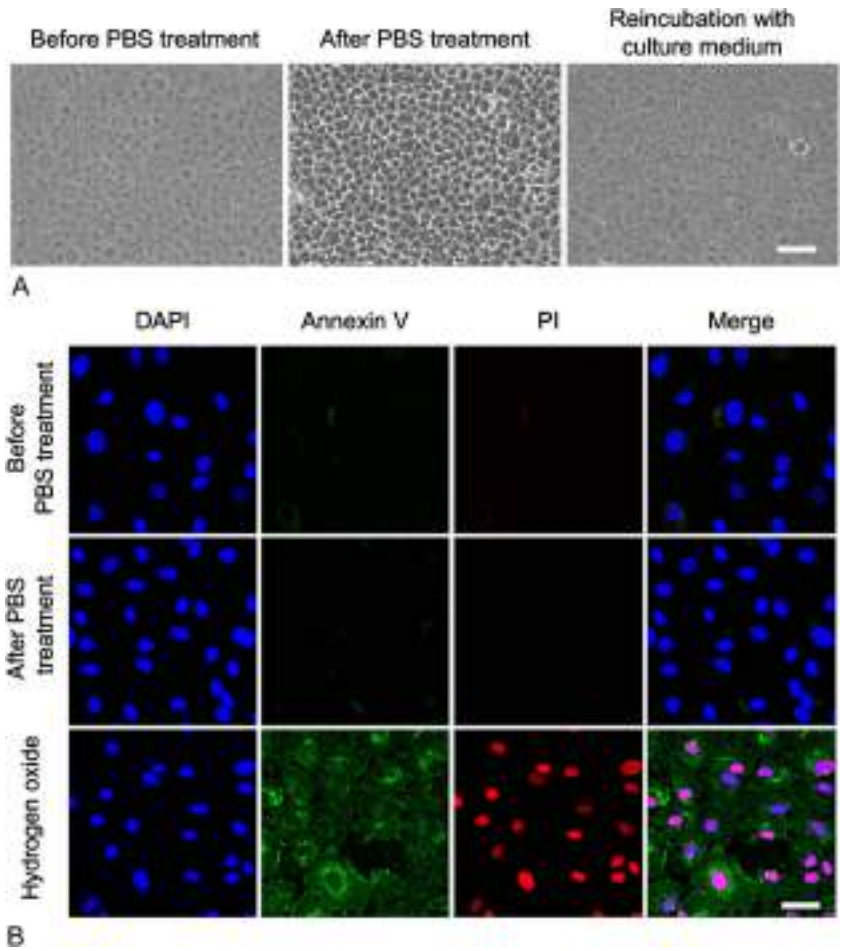

FIGURE 3. Effect of temporal treatment of HCECs with PBS. A, Images were obtained by phase contrast microscopy before PBS treatment, after incubation with PBS for 10 minutes, and after reincubation with the culture medium for 30 minutes. Scale bar: 100 μm. B, HCECs, obtained before and after PBS treatment, were stained with Annexin V and propidium iodide to evaluate apoptosis or cell death. Nuclei were stained with DAPI. Scale bar: 100 μm.

software analysis, cell centers were plotted manually using ImageJ software, and the cell density was then acquired (ie, the area divided by the number of cells).

Cell apoptosis was evaluated by incubating HCECs in a medium supplemented with Annexin V (Medical & Biological Laboratories Co, Ltd, Aichi, Japan) and propidium iodide (Medical & Biological Laboratories Co, Ltd) for 15 minutes, followed by fixation with 4% paraformaldehyde for 10 minutes. Excess paraformaldehyde was removed, and samples were washed with PBS. Nuclei were stained with 4′,6-diamidino-2-phenylindole (DAPI) (Vector Laboratories, Burlingame, CA). As a positive control for apoptosis, HCECs were stimulated in a culture medium supplemented with hydrogen peroxide (1000 μM) for 24 hours. Cells on slides were examined with a fluorescence microscope (DM 2500; Leica Microsystems).

The Pearson χ^2 test was performed for the study of the association between cell density and polymegathism, and cell density and polymorphism. $P < 0.05$ indicated statistical significance.

RESULTS

Phase contrast images showed indistinct cell border outlines for HCECs that had reached confluency (Fig. 1A). By contrast, distinct cell borders were observed after cultivation of HCECs in PBS for 10 minutes (Figs. 1A, 2). The images obtained by CECA designed for the HCECs analysis were processed through several steps; that is, denoising, closing, and skeletonizing. The denoising image was obtained by extreme emphasis of the cell boundaries of the PBS-treated HCEC image (Figs. 1A, 3). Unnecessary lines that appeared after the denoising process were removed by the closing process, and the cell boundaries represented as black lines were left (Figs. 1A, 4). A skeletonized image was then obtained by thinning the black line through the skeletonizing process (Figs. 1A, 5). Figure 1B shows representative images for software recognition of the cell border of HCECs before and after PBS cultivation. The red line was recognized as a cell border by CECA. The analyzed image of HCECs before PBS treatment showed poor recognition of the cell borders (arrowhead), whereas the image of HCECs treated with PBS showed greater numbers of correctly recognized cell borders (Fig. 1B).

We then evaluated the feasibility of CECA as a clinical instrument. Phase contrast images of the high cell density group and the low cell density group of HCECs (n = 50) treated with PBS were analyzed by the following 3 methods. First, the centers of the cells were plotted manually, and cell density was analyzed by the center method by using KSS-400EB software; the center method is a standard method for

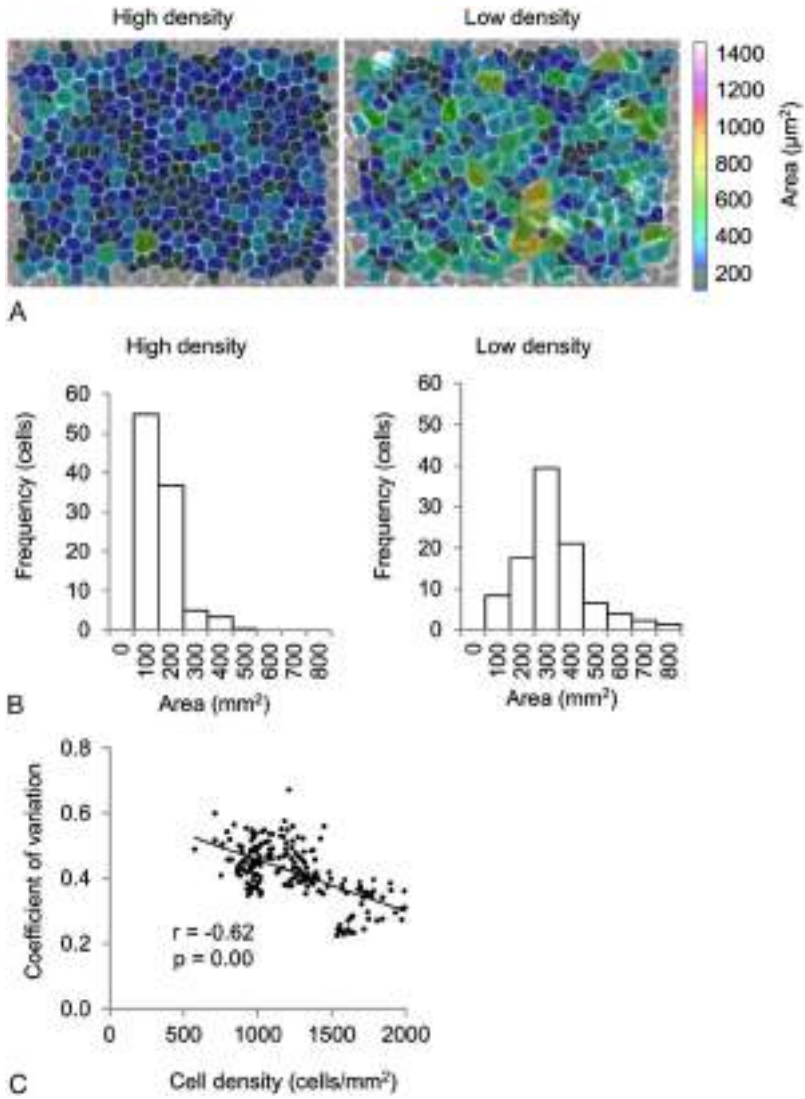

FIGURE 4. Color map and histogram of the cell area of HCECs. A and B, Representative color map and histogram of the cell areas of HCECs with high and low cell density, as provided by CECA, are shown. C, Correlation between the CV, which is clinically used as an indicator of polymegathism, and the cell density was plotted and analyzed by the Pearson χ^2 test (n = 200).

evaluating corneal endothelial cell density in the clinic using specular microscopy (Figs. 2A, B). Second, the centers of the cells were plotted manually, and the cell density was obtained by calculating the cell numbers/area using ImageJ software (Fig. 2C). Third, the cell density was automatically analyzed by CECA. In the high cell density group, the mean cell density analyzed by the center method was 2318 ± 585 cells/mm^2. ImageJ software gave a mean cell density of 1648 ± 148 cells/mm^2, which suggests that the center method is not accurate for cultured HCECs. By contrast, cell analysis software developed for this study showed a value (1489 ± 130 cells/mm^2) almost identical to that obtained by the experienced researcher's manual plotting and calculation with ImageJ (Fig. 2D). In the low cell density group, all 3 methods showed similar values for mean cell density, but the values for the center method had a larger deviation when compared with those obtained with ImageJ and CECA methods (Fig. 2E). KSS-400EB software was originally developed for evaluating the patient corneal endothelium in clinical settings, and the software design allows for analysis of smaller numbers of cells from a magnified image than is possible with ImageJ software and CECA. We then analyzed the same magnified phase contrast images used for KSS-400EB software by ImageJ to evaluate the effect of magnification of the original images. The cell density was higher when analyzed by the center method than by ImageJ (see Figure, Supplemental Digital Content, http://links.lww.com/ICO/A544), similar to the results shown in Figure 2D. The cell centers, determined by the center method and KSS-400EB software and by manual analysis using ImageJ software, were plotted by 2 independent researchers and similar results were obtained.

We conducted a study to evaluate the effect of temporal treatment of HCECs with PBS. Phase contrast images showed that incubation with PBS resulted in a more distinctive cell border outline, and the cells recovered their original morphology within 20 to 30 minutes after reincubation with the culture medium (Fig. 3A). HCECs incubated in PBS did not show positive staining for either Annexin V or propidium iodide, whereas positive control cells treated with hydrogen peroxide showed positive staining, which

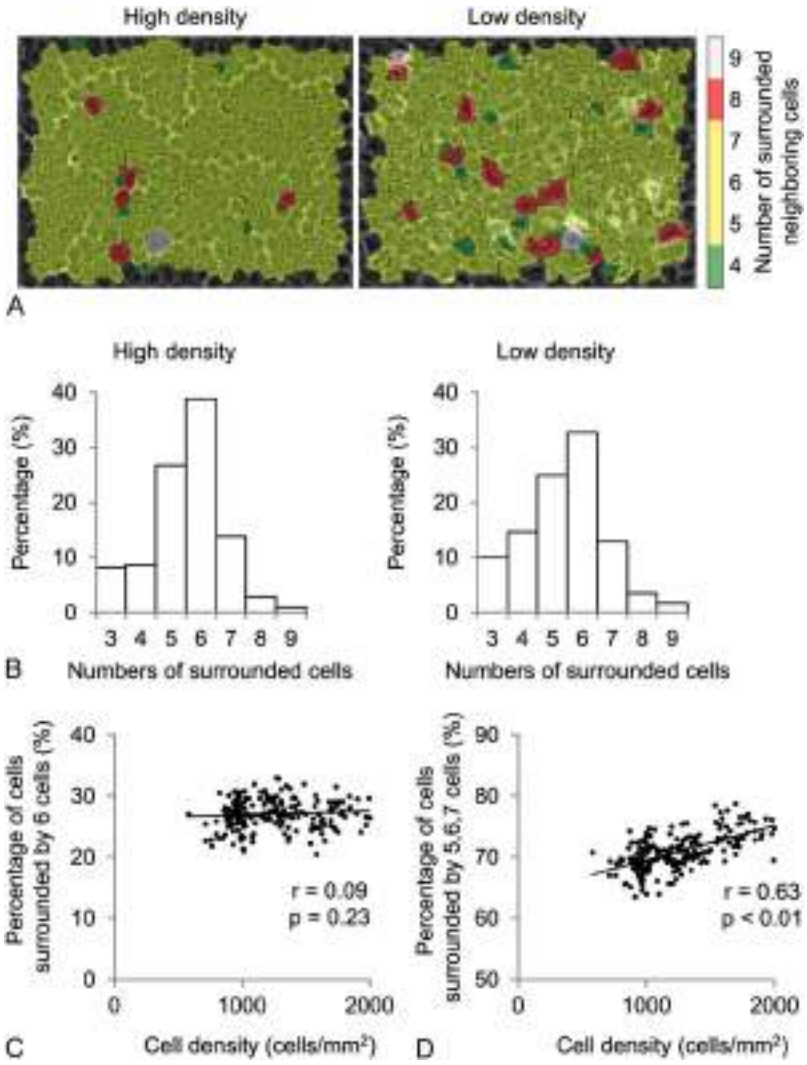

FIGURE 5. Color map and histogram of the number of surrounded HCECs. A and B, Representative color map and histogram of the number of surrounded HCECs with high and low cell density provided by CECA are shown. C, Correlation between percentage of cells surrounded by 6 neighboring cells and cell density was plotted and analyzed by the Pearson χ^2 test. D, Correlation between the percentage of cells surrounded by 5, 6, or 7 neighboring cells and cell density was plotted and analyzed by the Pearson χ^2 test (n = 200).

suggests that PBS incubation did not induce apoptosis and cell death (Fig. 3B).

CECA was programmed to provide color maps and histograms of the cell areas. Representative color maps and histograms visually demonstrated a smaller and less variable cell area for the high cell density cells than for the low cell density cells (Figs. 4A, B). The CV, which is clinically used as an indicator of polymegathism, highly correlated with cell density (Pearson correlation coefficient −0.62, $P < 0.01$, n = 200) (Fig. 4C). Polygonality was also provided as a color map and histogram by the software to evaluate polymorphism. Representative color maps and histograms showed that cells surrounded by 3 or 4 neighboring cells were more frequently observed in low cell density cell cultures than in high cell density cell cultures (Figs. 5A, B). The percentage of cells surrounded by 6 neighboring cells that were recognized as hexagonal cells by the software is clinically used as an indicator of polymorphism, but this feature was not correlated with the cell density. By contrast, the percentage of cells surrounded by 5, 6, or 7 neighboring cells was correlated with the cell density (Pearson correlation coefficient 0.63, $P < 0.01$, n = 200) (Figs. 5C, D).

DISCUSSION

In 2013, we initiated clinical research in Japan to explore tissue engineering therapy for corneal endothelial dysfunction. In this clinical research, we isolated HCECs from human donor corneas, expanded HCECs in vitro, and injected them, in combination with a Rho kinase inhibitor, into the anterior chamber (unpublished data). Cells for clinical use need to be manufactured to meet governmental requirements, and they need to go through a variety of safety and functional examinations to guarantee patient safety. This requires the ability to examine and evaluate cell cultures to determine the suitability for use in human therapies. Images of the human corneal endothelium are usually obtained clinically by specular microscopy. However, software used clinically with specular microscopy to examine parameters of the corneal endothelium cannot detect the outlines of cultured cells. Therefore,

we initiated this study to improve the imaging of cultured HCECs.

Cultured CECs in the confluent state form a single layer sheet, with cells in continuous contact with their neighboring adjacent cells. Cell–cell junctions form from the apical junction, which consists of adherence junctions and tight junctions.[21–24] The adherence junction forms from an adhesion molecule, N-cadherin binding to an anchoring protein, and catenin binding to itself. Likewise, adhesion molecules, such as claudins and occludin, bind to anchoring proteins, such as zonula occludens and catenins, to form tight junctions. Cadherin, claudin, and occludin require calcium for apical junction formation; therefore, treatment of HCECs with calcium-free PBS weakens the apical junction.[22–24] In this study, we demonstrated that the distinctive outline of HCECs was obtained after treatment with calcium-free PBS, and that this phenomenon can be reversed without damage to the cells. Treatment with calcium-free PBS after the analysis of cell morphological parameters using CECA is not destructive, so our data indicate that HCECs for which morphological data were analyzed by this current method can have clinical uses in cell-based therapy.

A single layer of CECs exhibiting polygonal shape forms the corneal endothelium. The cell density is approximately 3000 cells/mm^2 in humans aged 10 to 20 years, and it decreases at 0.3% to 0.6% per year throughout the lifetime.[25,26] The proliferative ability is severely limited,[27] so any damage to the corneal endothelium requires that neighboring cells cover the defect area, which in turn results in a decrease in cell density of the corneal endothelium. If the cell density drops below a critical level, the cornea exhibits edema due to endothelial dysfunction. Hence, cell density is widely used as an indicator of corneal endothelial health in clinical settings.

The cell density of cultured HCECs tended to decline, probably because of cellular senescence triggered by culture stress, especially during serial passage culture.[13] We recently demonstrated that the corneal endothelium was regenerated in the rabbit model after injection of either high or low cell density rabbit CECs, but the cell density of the regenerated corneal endothelium was higher in the eyes injected with high cell density CECs than with low cell density CECs. This suggested that the cell density of cultured CECs is a critical indicator for the prognosis of corneal endothelial tissue engineering therapy.[13] In our early stage clinical research, we assessed cell density manually using both KSS-400EB software and ImageJ software. In this study, we showed that CECA provided almost the same value as manual counting, whereas larger values (especially for high cell density cells) with larger variations were obtained with the center method than with manual counting. This suggests that the center method, which is the standard procedure used in current clinical settings, does not always provide an accurate value for cultured CECs. Therefore, CECA might be more suitable for providing a subjective evaluation, as a quality control for HCECs.

Similar to cell density, the uniformity of the cells is an indicator of corneal endothelial health.[28] The CV for the mean cell area (SD of mean cell area/mean cell area) is often used clinically, and its increase is termed polymegathism.[28] In the current study, the CV for HCECs with a cell density of approximately 2000 cells/mm^2 was 0.2 to 0.4, which is similar to or slightly higher than that of healthy young individuals (0.25) and healthy older subjects (0.3). Hexagonality is another parameter of uniformity, and it is 70% to 80% in healthy young individuals and 60% in healthy older subjects. Here, we showed that the percentage of cells surrounded by 6 neighboring cells, which we referred to as hexagonal cells, was 20% to 35% in culture, and it was not correlated with cell density. By contrast, the percentage of cells surrounded by 5, 6, or 7 cells was 70% to 80% for HCECs with a cell density of approximately 2000 cells/mm^2, and it correlated with cell density. Therefore, the percentage of pentagonal, hexagonal, or heptagonal cells might be an applicable parameter for determining the polygonality of cultured HCECs.

One drawback of this study is the lack of exact values for the cell density, CV, and hexagonality needed for HCECs for clinical use. Feedback is needed from clinical data to show which parameters are relevant to the prognosis of patients to determine the exact criteria that should be assessed for quality control purposes.

In conclusion, our designed software, CECA, provided morphometric information from phase contrast images. We showed that several parameters related to cell density, polymegathism, and polymorphism of cultured HCECs were obtained by the software with values similar to those obtained by experienced researchers. This software could therefore enable subjective and noninvasive quality assessment for tissue engineering therapy for treatment of corneal endothelium disorders.

ACKNOWLEDGMENTS

This study was supported by the Program for the Strategic Research Foundation at Private Universities from MEXT (N. Koizumi and N. Okumura). The authors thank Mr. Monty Montoya and Mr. Bernie Iliakis (SightLife) for providing donor corneas.

REFERENCES

1. Tan DT, Dart JK, Holland EJ, et al. Corneal transplantation. *Lancet*. 2012;379:1749–1761.
2. Ishino Y, Sano Y, Nakamura T, et al. Amniotic membrane as a carrier for cultivated human corneal endothelial cell transplantation. *Invest Ophthalmol Vis Sci.* 2004;45:800–806.
3. Mimura T, Yamagami S, Yokoo S, et al. Cultured human corneal endothelial cell transplantation with a collagen sheet in a rabbit model. *Invest Ophthalmol Vis Sci.* 2004;45:2992–2997.
4. Koizumi N, Sakamoto Y, Okumura N, et al. Cultivated corneal endothelial cell sheet transplantation in a primate model. *Invest Ophthalmol Vis Sci.* 2007;48:4519–4526.
5. Koizumi N, Okumura N, Kinoshita S. Development of new therapeutic modalities for corneal endothelial disease focused on the proliferation of corneal endothelial cells using animal models. *Exp Eye Res.* 2012; 95:60–67.
6. Mimura T, Yamagami S, Yokoo S, et al. Sphere therapy for corneal endothelium deficiency in a rabbit model. *Invest Ophthalmol Vis Sci.* 2005;46:3128–3135.
7. Okumura N, Koizumi N, Ueno M, et al. ROCK inhibitor converts corneal endothelial cells into a phenotype capable of regenerating in vivo endothelial tissue. *Am J Pathol.* 2012;181:268–277.

8. Okumura N, Sakamoto Y, Fujii K, et al. Rho kinase inhibitor enables cell-based therapy for corneal endothelial dysfunction. *Sci Rep.* 2016;6: 26113.
9. Miyata K, Drake J, Osakabe Y, et al. Effect of donor age on morphologic variation of cultured human corneal endothelial cells. *Cornea*. 2001;20: 59–63.
10. Joyce NC, Zhu CC. Human corneal endothelial cell proliferation: potential for use in regenerative medicine. *Cornea*. 2004;23:S8–S19.
11. Zhu C, Joyce NC. Proliferative response of corneal endothelial cells from young and older donors. *Invest Ophthalmol Vis Sci.* 2004;45:1743–1751.
12. Zhu YT, Chen HC, Chen SY, et al. Nuclear p120 catenin unlocks mitotic block of contact-inhibited human corneal endothelial monolayers without disrupting adherent junctions. *J Cell Sci.* 2012;125:3636–3648.
13. Okumura N, Kusakabe A, Hirano H, et al. Density-gradient centrifugation enables the purification of cultured corneal endothelial cells for cell therapy by eliminating senescent cells. *Sci Rep.* 2015;5:15005.
14. Okumura N, Kay EP, Nakahara M, et al. Inhibition of TGF-beta signaling enables human corneal endothelial cell expansion in vitro for use in regenerative medicine. *PLoS One.* 2013;8:e58000.
15. Peh GS, Beuerman RW, Colman A, et al. Human corneal endothelial cell expansion for corneal endothelium transplantation: an overview. *Transplantation*. 2011;91:811–819.
16. Nakahara M, Okumura N, Kay EP, et al. Corneal endothelial expansion promoted by human bone marrow mesenchymal stem cell-derived conditioned medium. *PLoS One.* 2013;8:e69009.
17. Okumura N, Ueno M, Koizumi N, et al. Enhancement on primate corneal endothelial cell survival in vitro by a ROCK inhibitor. *Invest Ophthalmol Vis Sci.* 2009;50:3680–3687.
18. Shima N, Kimoto M, Yamaguchi M, et al. Increased proliferation and replicative lifespan of isolated human corneal endothelial cells with L-ascorbic acid 2-phosphate. *Invest Ophthalmol Vis Sci.* 2011;52:8711–8717.
19. Peh GS, Adnan K, George BL, et al. The effects of Rho-associated kinase inhibitor Y-27632 on primary human corneal endothelial cells propagated using a dual media approach. *Sci Rep.* 2015;5:9167.
20. Okumura N, Kakutani K, Numata R, et al. Laminin-511 and -521 enable efficient in vitro expansion of human corneal endothelial cells. *Invest Ophthalmol Vis Sci.* 2015;56:2933–2942.
21. Farquhar MG, Palade GE. Junctional complexes in various epithelia. *J Cell Biol.* 1963;17:375–412.
22. Tsukita S, Furuse M, Itoh M. Structural and signalling molecules come together at tight junctions. *Curr Opin Cell Biol.* 1999;11:628–633.
23. Tsukita S, Furuse M. Occludin and claudins in tight-junction strands: leading or supporting players? *Trends Cell Biol.* 1999;9:268–273.
24. Tsukita S, Furuse M, Itoh M. Multifunctional strands in tight junctions. *Nat Rev Mol Cell Biol.* 2001;2:285–293.
25. Murphy C, Alvarado J, Juster R, et al. Prenatal and postnatal cellularity of the human corneal endothelium. A quantitative histologic study. *Invest Ophthalmol Vis Sci.* 1984;25:312–322.
26. Bourne WM, Nelson LR, Hodge DO. Central corneal endothelial cell changes over a ten-year period. *Invest Ophthalmol Vis Sci.* 1997;38:779–782.
27. Joyce NC. Proliferative capacity of corneal endothelial cells. *Exp Eye Res.* 2012;95:16–23.
28. Nishida T, Saika S. Cornea and sclera: anatomy and physiology. *Cornea*. 2011;1:3–24.

Safety of anterior chamber paracentesis using a 30-gauge needle integrated with a specially designed disposable pipette

Koji Kitazawa,[1,2,3] Chie Sotozono,[2] Noriko Koizumi,[4] Kenji Nagata,[2] Tsutomu Inatomi,[2] Hiroshi Sasaki,[5] Shigeru Kinoshita[1,3]

[1]Department of Frontier Medical Science and Technology for Ophthalmology, Kyoto Prefectural University of Medicine, Kyoto, Japan
[2]Department of Ophthalmology, Kyoto Prefectural University of Medicine, Kyoto, Japan
[3]Department of Ophthalmology, Baptist Eye Institute, Kyoto, Japan
[4]Faculty of Life and Medical Sciences, Department of Biomedical Engineering, Doshisha University, Kyotanabe, Japan
[5]Department of Ophthalmology, Kanazawa Medical University, Ishikawa, Japan

Correspondence to
Professor Shigeru Kinoshita, Department of Frontier Medical Science and Technology for Ophthalmology, Kyoto Prefectural University of Medicine, 465 Kajii-cho, Hirokoji-agaru, Kawaramachi-dori, Kamigyo-ku, Kyoto 602-0841, Japan; shigeruk@koto.kpu-m.ac.jp

Received 11 September 2016
Revised 8 December 2016
Accepted 25 December 2016
Published Online First 18 January 2017

ABSTRACT

Aims To investigate the safety of anterior chamber (AC) paracentesis using a 30-gauge needle integrated with a specially designed disposable pipette.

Methods In this retrospective observational case-series study, AC paracentesis was performed on 301 eyes of 301 patients between September 2009 and August 2016 at the Department of Ophthalmology, Kyoto Prefectural University of Medicine and the Baptist Eye Institute, Kyoto, Japan. AC paracentesis was performed with the patient placed in the supine position using a 30-gauge needle integrated with a disposable pipette with one hand, and the safety post procedure was then evaluated.

Results The indications for AC paracentesis were virus detection (ie, corneal endotheliitis, anterior infectious uveitis, cytomegalovirus retinitis and acute retinal necrosis) in 264 eyes, bacterial detection (ie, endophthalmitis) in 8 eyes and malignancy (ie, primary intraocular lymphoma, leukaemia and retinoblastoma) in 29 eyes. No serious complications such as infection, hyphema, lens trauma or severe inflammation including hypopyon and AC fibrin formation were observed.

Conclusions Our findings show that AC paracentesis with a disposable pipette is safe with no severe complications.

INTRODUCTION

Anterior chamber (AC) paracentesis is widely performed for the diagnosis of infectious uveitis[1 2] and involves a comprehensive PCR being performed on an aqueous humour sample obtained to detect infectious antigen DNA and to assist with the diagnosis of infectious ocular diseases.[3 4]

AC paracentesis using a 27 gauge (G) or 30 G needle on a tuberculin syringe is commonly performed. However, it requires that strict attention be paid to the length of the needle and the insertion angle in order to avoid touching the iris or lens. Various AC paracentesis-related complications have been reported, including trauma to the cornea, iris and lens, as well as hyphema,[1] corneal abscess[5] and endophthalmitis.[6]

In this study, we investigated the safety of AC paracentesis using a 30 G needle integrated with a specially designed disposable pipette.

METHODS

Subjects

This retrospective, observational case series was conducted at the Department of Ophthalmology, Kyoto Prefectural University of Medicine and the Baptist Eye Institute, Kyoto, Japan, and was approved by the Institutional Review Board of Kyoto Prefectural University of Medicine. All study procedures were conducted in accordance with the tenets of the Declaration of Helsinki, and informed consent was obtained from all patients post detailed explanation of the study protocols. Clinical trial registration was obtained from UMIN (UMIN000021877; http://www.umin.ac.jp/english/).

This study involved patients who visited the Kyoto Prefectural University of Medicine or Baptist Eye Institute between September 2009 and August 2016. The recorded patient-related characteristics, including gender, age, pupil status, lens status and indications for AC paracentesis, were examined (table 1).

AC paracentesis procedure

All procedures were performed under a microscope in an outpatient clinic and involved the use of a commercially available 30 G needle integrated with a specially designed disposable pipette (Nipro, Osaka, Japan) (figure 1A). The length of the exposed part of the needle is 4 mm. After topical anaesthesia, each patient was placed in a supine position on the bed in the outpatient clinic and the ocular surface was rinsed with povidone-iodine and sterile saline solution. All of the procedures were carefully undertaken using aseptic techniques to avoid any contamination. The paracentesis was inserted into the AC through the corneal limbus at a horizontal angle on the temporal side, paying attention to avoid contact with the patient's eyelashes, lens or iris when squeezing the bulb under a microscope. A 50–150 μL volume of aqueous humour was then spontaneously and slowly aspirated into the pipette when pressure was released from the bulb. The maximum of bulb volume to be aspirated was appropriately designed to be <300 μL to avoid the AC collapse (figure 1B). At the end of the procedure, the povidone-iodine was rinsed out with sterile saline solution. Complications secondary to paracentesis were evaluated within 3 months postoperative.

RESULTS

A total of 301 eyes of 301 patients (169 males, 132 females; mean age: 61.4±16.7 years) were enrolled. At AC paracentesis, 173 of the 301 patients had dilated pupils. Indications for AC paracentesis were virus detection for anterior or posterior uveitis (264 eyes), bacteria detection for endophthalmitis (8 eyes) and malignancy (29 eyes)

To cite: Kitazawa K, Sotozono C, Koizumi N, *et al*. *Br J Ophthalmol* 2017;**101**:548–550.

Table 1 Demographic characteristics of the patients

Gender, n (%)	
Male	169 (56.1)
Female	132 (43.9)
Mean age (SD)	61.4±16.7
Pupil status, n (%)	
Dilated pupil	173 (57.5)
Constricted pupil	128 (42.5)
Lens status, n (%)	
Phakia	188 (62.7)
Pseudophakia	113 (37.3)
Indication for paracentesis, n (%)	
Virus detection	264 (87.7)
Bacteria detection	8 (2.7)
Malignancy	29 (9.6)
Complication, n (%)	
Endophthalmitis	0 (0)
Corneal abscess	0 (0)
Lens trauma	0 (0)
Hyphema	0 (0)
AC fibrin formation	0 (0)
Hypopyon	0 (0)

AC, anterior chamber.

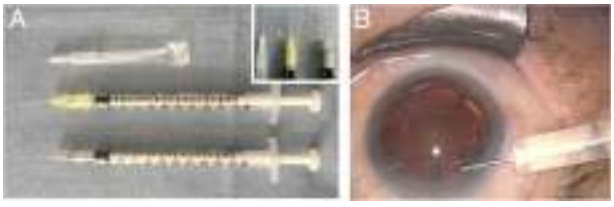

Figure 1 Image showing the anterior chamber (AC) paracentesis procedure. (A) Comparison of needle length and pipette design. The length of 30-gauge (G) needle with the disposable pipette (4 mm) is shorter than that of the 27 G and 30 G needles (19 mm), and the total length of the disposable pipette is less than half of that of a tuberculin syringe (top). The 30 G needle integrated with the disposable pipette (middle). A 30 G needle attached to a tuberculin syringe (bottom). A 27 G needle attached to a tuberculin syringe. (B) The AC paracentesis was inserted into the AC through the corneal limbus at a horizontal angle, paying strict attention to avoid contact with the patient's eyelashes, lens and iris while squeezing the bulb at the head of the device.

(table 1). Anterior or posterior uveitis included corneal endotheliitis (122 eyes) and iridocyclitis (108 eyes) due to human simplex virus (HSV), varicella zoster virus (VZV), cytomegalovirus retinitis (25 eyes) and acute retinal necrosis (9 eyes). Malignancy included primary intraocular lymphoma (27 eyes), leukaemia (1 eye) and retinoblastoma (1 eye).

Analysis of safety post AC paracentesis

No serious postoperative complications such as endophthalmitis, corneal abscess, hyphema, lens trauma and severe inflammation including AC fibrin formation and hypopyon were noted (table 1).

DISCUSSION

In most AC paracentesis cases, a 27 G or 30 G needle on a tuberculin syringe is used, which requires to pull a plunger. However, we used a short 30 G needle combined with a disposable pipette with a squeeze bulb located at its head, thus allowing the aqueous humour sample to be drawn from the patient using one hand. Potential risks after AC paracentesis include infection, hyphema, cataract formation and severe intraocular inflammation including AC fibrin formation and hypopyon; however, none of the 301 patients had serious postoperative complications. O'Rourke developed an aqueous pipette consisting of a short 30 G needle mounted inside plastic tubing,[7] and Wertheim also reported the 'minim' technique for diagnosing AC paracentesis.[8] Compared with a conventional syringe, the O'Rourke pipette and the minim technique, our pipette is designed with a shorter needle and is easier to control, and this modification decreases the risks of lens trauma and hyphema. Our pipette integrated with a needle offers the advantage of producing no dead space, which allows for the aqueous humour to be obtained efficiently, even in cases with a shallow AC. In fact, in the case of a tumour biopsy, although it could increase the risk of metastases due to the potential for tumour-cell transference to other tissues, AC paracentesis using this pipette was performed safely and was able to detect non-metastatic retinoblastoma tumour cells, thus leading to the judgement of enucleation.[9]

Recent developments in imaging technologies, such as optical coherence tomography, have enabled ophthalmologists to make more precise disease diagnoses.[10 11] However, the diagnosis of tumour and uveitis often require an AC paracentesis to be performed to detect the causative pathogen. For patients with uveitis of unknown origin, multiplex PCR is known to be useful for obtaining a correct diagnosis, as it can detect a small amount of virus and bacteria from the aqueous humour via DNA amplification.[4 12 13] Using PCR analysis of aqueous humour samples, we previously discovered that cytomegalovirus was the causative pathogen in patients with repeated corneal endotheliitis.[14 15] Thus, those findings indicate that AC paracentesis is a useful diagnostic tool.

In conclusion, our findings show that a short 30 G needle integrated with a disposable pipette is a safe device for obtaining aqueous humour without complications.

We hope that aqueous humour examinations will become widely performed in the future to improve the diagnosis and the understanding of pathophysiology in patients according to the detection virus/bacteria DNA or tumour cells and also the prognostic and predictive biomarkers of diseases.

Acknowledgements The authors wish to thank John Bush for editing the manuscript.

Contributors Conception and design of the study (KK, SK), collection of data (KK, NK, KN TI, CS, SK), management of data (KK), analysis of data (KK), interpretation of data (KK), writing of the article (KK, SK), approval of the manuscript (KK, CS, NK, KN, TI, HS, SK) and searching the literature (KK).

Funding This research was partially supported in part by Research Funds from the Kyoto Foundation for the Promotion of Medical Science.

Competing interests None declared.

Patient consent Obtained.

Ethics approval Kyoto Prefectural University of Medicine.

Provenance and peer review Not commissioned; externally peer reviewed.

REFERENCES

1 Van der Lelij A, Rothova A. Diagnostic anterior chamber paracentesis in uveitis: a safe procedure? *Br J Ophthalmol* 1997;81:976–9.
2 Trivedi D, Denniston AK, Murray PI. Safety profile of anterior chamber paracentesis performed at the slit lamp. *Clin Experiment Ophthalmol* 2011;39:725–8.
3 Shoughy SS, Alkatan HM, Al-Abdullah AA, *et al*. Polymerase chain reaction in unilateral cases of presumed viral anterior uveitis. *Clin Ophthalmol* 2015;9:2325–8.

4 Sugita S, Ogawa M, Shimizu N, *et al*. Use of a comprehensive polymerase chain reaction system for diagnosis of ocular infectious diseases. *Ophthalmology* 2013;120:1761–8.
5 Azuara-Blanco A, Katz LJ. Infectious keratitis in a paracentesis tract. *Ophthalmic Surg Lasers* 1997;28:332–3.
6 Helbig H, Noske W, Kleineidam M, *et al*. Bacterial endophthalmitis after anterior chamber paracentesis. *Br J Ophthalmol* 1995;79:866.
7 O'Rourke J, Taylor DM, Wang Y. Compact bulb pipette simplifies paracentesis. *Ophthalmic Surg Lasers Imaging* 2004;35:172–3.
8 Wertheim MS, Connell PP, Majid MA, *et al*. The minim technique for diagnostic anterior chamber paracentesis. *Eye (Lond)* 2009;23:1491.
9 Kitazawa K, Nagata K, Yamanaka Y, *et al*. Diffuse anterior retinoblastoma with sarcoidosis-like nodule. *Case Rep Ophthalmol* 2015;6:443–7.
10 Adhi M, Duker JS. Optical coherence tomography—current and future applications. *Curr Opin Ophthalmol* 2013;24:213–21.
11 Kitazawa K, Yokota I, Sotozono C, *et al*. Measurement of corneal endothelial surface area using anterior segment optical coherence tomography in normal subjects. *Cornea* 2016;35:1229–33.
12 Sugita S, Ogawa M, Inoue S, *et al*. Diagnosis of ocular toxoplasmosis by two polymerase chain reaction (PCR) examinations: qualitative multiplex and quantitative real-time. *Jpn J Ophthalmol* 2011;55:495–501.
13 Sugita S, Shimizu N, Watanabe K, *et al*. Use of multiplex PCR and real-time PCR to detect human herpes virus genome in ocular fluids of patients with uveitis. *Br J Ophthalmol* 2008;92:928–32.
14 Koizumi N, Yamasaki K, Kawasaki S, *et al*. Cytomegalovirus in aqueous humor from an eye with corneal endotheliitis. *Am J Ophthalmol* 2006;141:564–5.
15 Koizumi N, Inatomi T, Suzuki T, *et al*. Clinical features and management of cytomegalovirus corneal endotheliitis: analysis of 106 cases from the Japan corneal endotheliitis study. *Br J Ophthalmol* 2015;99:54–8.

PLOS ONE

RESEARCH ARTICLE

Feasibility of cell-based therapy combined with descemetorhexis for treating Fuchs endothelial corneal dystrophy in rabbit model

Naoki Okumura[1], Daiki Matsumoto[1], Yuya Fukui[1], Masataka Teramoto[1], Hirofumi Imai[1], Tetta Kurosawa[1], Tomoki Shimada[1], Friedrich Kruse[2], Ursula Schlötzer-Schrehardt[2], Shigeru Kinoshita[3], Noriko Koizumi[1]*

1 Department of Biomedical Engineering, Faculty of Life and Medical Sciences, Doshisha University, Kyotanabe, Japan, **2** Department of Ophthalmology, University of Erlangen-Nürnberg, Erlangen, Germany, **3** Department of Frontier Medical Science and Technology for Ophthalmology, Kyoto Prefectural University of Medicine, Kyoto, Japan

* nkoizumi@mail.doshisha.ac.jp

OPEN ACCESS

Citation: Okumura N, Matsumoto D, Fukui Y, Teramoto M, Imai H, Kurosawa T, et al. (2018) Feasibility of cell-based therapy combined with descemetorhexis for treating Fuchs endothelial corneal dystrophy in rabbit model. PLoS ONE 13 (1): e0191306. https://doi.org/10.1371/journal.pone.0191306

Editor: Alexander V. Ljubimov, Cedars-Sinai Medical Center, UNITED STATES

Received: August 27, 2017

Accepted: January 1, 2018

Published: January 16, 2018

Data Availability Statement: All relevant data are within the paper and its Supporting Information files.

Funding: This study was supported by the Program for the Strategic Research Foundation at Private Universities from MEXT (Koizumi, N. and Okumura, N.) (http://www.mext.go.jp/a_menu/koutou/shinkou/07021403/002/002/1218299.htm).

Competing interests: Shigeru Kinoshita and Noriko Koizumi are listed as the inventors of the patent

Abstract

Corneal transparency is maintained by the corneal endothelium through its pump and barrier function. Severe corneal endothelial damage results in dysregulation of water flow and eventually causes corneal haziness and deterioration of visual function. In 2013, we initiated clinical research of cell-based therapy for treating corneal decompensation. In that study, we removed an 8-mm diameter section of damaged corneal endothelium without removing Descemet's membrane (the basement membrane of the corneal endothelium) and then injected cultured human corneal endothelial cells (CECs) into the anterior chamber. However, Descemet's membrane exhibits clinically abnormal structural features [i.e., multiple collagenous excrescences (guttae) and thickening] in patients with Fuchs endothelial corneal dystrophy (FECD) and the advanced cornea guttae adversely affects the quality of vision, even in patients without corneal edema. The turnover time of cornea guttae is also not certain. Therefore, we used a rabbit model to evaluate the feasibility of Descemet's membrane removal in the optical zone only, by performing a small 4-mm diameter descemetorhexis prior to CEC injection. We showed that the corneal endothelium is regenerated both on the corneal stroma (the area of Descemet's membrane removal) and on the intact peripheral Descemet's membrane, based on the expression of function-related markers and the restoration of corneal transparency. Recovery of the corneal transparency and central corneal thickness was delayed in areas of Descemet's membrane removal, but the cell density of the regenerated corneal endothelium and the thickness of the central corneal did not differ between the areas with and without residual Descemet's membrane at 14 days after CEC injection. Here, we demonstrate that removal of a pathological Descemet's membrane by a small descemetorhexis is a feasible procedure for use in combination with cell-based therapy. The current strategy might be beneficial for improving visual quality after CEC injection as a treatment for FECD.

regarding the application of the ROCK inhibitor for corneal endothelium (registration number: 5657252). All authors have no ethical conflicts of interest.

Introduction

The cornea, a transparent tissue located at the front of the eye, allows light to enter the eye. Corneal transparency is maintained by the corneal endothelium through a pump and barrier function. The corneal endothelium, which is a monolayer cell sheet located at the anterior chamber aspect of the cornea, regulates the amount of water in the corneal stroma [1]. Therefore, severe corneal endothelial damage results in dysregulation of water flow and eventually leads to corneal haziness.

The only therapeutic option for treating this corneal endothelial decompensation is corneal transplantation using donor corneas [2]. The use of penetrating keratoplasty, in which a full thickness cornea is replaced by a donor cornea, was first documented in 1906, and this procedure has been widely performed [3]. Strategies for the replacement of damaged corneal endothelium that do not involve a full-thickness corneal transplantation, such as Descemet's stripping endothelial keratoplasty (DSEK) and Descemet's membrane endothelial keratoplasty (DMEK), were introduced in 2000s, and these two have gained worldwide prevalence [4–8]. However, surgical challenges, long-term cell loss after transplantation, and a shortage of donor cornea tissue still represent major problems associated with corneal transplantation [2, 9].

Accordingly, many researchers have devoted their efforts to the development of alternative techniques of regenerative medicine to overcome those problems [10–14]. Our group has found that inhibition of Rho kinase (ROCK) signaling enhances corneal endothelial cell (CEC) adhesion to a substrate [15], and we reported the usefulness of ROCK inhibitor in cell-based therapy with CECs [16, 17]. In rabbit and monkey corneal endothelial dysfunction models, injection of cultured CECs in combination with a ROCK inhibitor resulted in corneal endothelium regeneration [16, 17]. In 2013, we initiated clinical research into cell-based therapy at the Kyoto Prefectural University of Medicine (Clinical trial registration: UMIN000012534) [18]. In that clinical study, we removed an 8-mm diameter portion of the damaged corneal endothelium without removing Descemet's membrane (the basement membrane of the corneal endothelium), and then injected cultured human CECs, in combination with a ROCK inhibitor, into the anterior chamber. Our assumption was that the remaining basement membrane would provide ideal conditions for CEC adhesion and survival.

Corneal endothelial cell ablation without removal of Descemet's membrane has, however, both advantages and disadvantages in the clinical setting. Although the presence of a basement membrane may support efficient adhesion of injected cultured CECs and may provide ideal conditions for cell fate and viability, Descemet's membrane of patients with Fuchs endothelial corneal dystrophy (FECD) exhibits a clinically abnormal structure, including multiple collagenous excrescences (guttae) and thickening [19, 20]. Recent clinical studies have showed that guttae affect the quality of vision, even in patients without corneal edema, although guttae have been previously assumed not to affect visual quality [21]. Wacker and colleagues reported that anterior and posterior corneal high-order aberrations (HOAs) and backscatter are higher even in early stages of FECD than in non-FECD subjects [22]. They suggested that increased posterior HOAs due to guttae are responsible for decreased vision, even in the absence of clinically detectable corneal edema [22]. Watanabe and colleagues also showed that the presence of guttae negatively correlates with clinical parameters for quality of vision, such as corrected distance visual acuity, letter contrast sensitivity, and stray light [23]. They assumed that guttae induce irregularity and posterior corneal opacity, resulting in an increase in forward light scatter [23].

Thus, we were motivated to modify our surgical protocol for cultured CEC injection by removing the pathological Descemet's membrane in patients with FECD during surgery. In this study, we used a rabbit model to evaluate the feasibility of Descemet's membrane removal in the optical zone prior to CEC injection.

Materials and methods

Ethics statement

Human corneas were handled in accordance with the tenets set forth in the Declaration of Helsinki. Experiments using human tissue samples were approved by the Institutional Review Board of the Medical Faculty of the University of Erlangen-Nürnberg (No. 4218-CH). Informed verbal consent was acquired from the donors or their relatives. The rabbit experiments were performed at Doshisha University (Kyoto, Japan), according to the protocol approved by Doshisha University Animal Experiment Committee (Approval No. A17066).

Human corneal specimens

Corneal specimens for histopathologic examination were obtained during penetrating keratoplasty, performed in 1995, from patients with FECD with aquiring verval informed consent (n = 5, mean age 73.3 ± 7.9 years). Corneal specimens from normal donor eyes (n = 5, mean age 74.5 ± 5.7 years) with no history of ocular disease but deemed unsuitable for transplantation, were procured from the Erlangen Cornea Bank. Donor corneas were fixed within 15 hours after death in 4% paraformaldehyde/1% glutaraldehyde in 0.1M phosphate buffer (pH 7.4) and processed for light and transmission electron microscopy according to standard protocols.

Rabbit Corneal Endothelial Cell (RCEC) culture

Ten rabbit eyes were purchased from the Funakoshi Co., Ltd. (Tokyo, Japan). The rabbit corneal endothelial cells (RCECs) were cultivated as described previously [16, 24]. Briefly, Descemet's membrane with RCECs was stripped and incubated in 0.6 U/mL of Dispase II (Roche Applied Science, Penzberg, Germany). The RCECs isolated from the Descemet's membrane were seeded in one well of a 6-well plate coated with FNC Coating Mix® (Athena Environmental Sciences, Inc., Baltimore, MD). The RCECs were cultured in a growth medium composed of Dulbecco's modified Eagle's medium (DMEM, Life Technologies Corp., Carlsbad, CA) supplemented with 10% fetal bovine serum (FBS), 50 U/mL penicillin, 50 μg/mL streptomycin, and 2 ng/mL fibroblast growth factor 2 (Life Technologies Corp.). Cultivated RCECs were used at passages 2 through 3 for all experiments.

Injection of RCECs into a corneal endothelial dysfunction model with or without descemetorhexis

Eighteen rabbits were used in this experiment. One eye of each rabbit was used for the experiments to avoid blindness in both eyes. The rabbit corneal endothelial dysfunction model was created as described previously [16, 24]. Briefly, the lens was removed to deepen the anterior chamber. One week after this lens removal, the corneal endothelium was mechanically scraped from Descemet's membrane with a 20-gauge silicone needle (Soft Tapered Needle; Inami & Co., Ltd., Tokyo, Japan). Total removal of corneal endothelium was confirmed by 0.2% trypan blue (Sigma-Aldrich, St. Louis, MO, USA) staining. A 4 mm diameter continuous circular descemetorhexis (CCD) was performed in 6 eyes (CCD (+) group). A total of 5.0×10^5 RCECs, suspended in 200 μl DMEM supplemented with 100 μM Y-27632 ROCK inhibitor (Wako Pure Chemical Industries, Ltd.), was injected into the anterior chamber of the corneal endothelial dysfunction model and the animals were kept in the face-down position for 3 hours under general anesthesia. RCECs were injected into 6 eyes of the CCD (+) group (the corneal endothelium was totally removed and a 4 mm CCD was performed) and 6 eyes of the CCD (-) group (corneal endothelium was totally removed and CCD was not performed). As a control for the

corneal endothelial dysfunction model, 6 eyes had the corneal endothelium was totally removed, but CCD was not performed and no RCECs were injected.

The anterior segments of the eyes were evaluated by slit-lamp microscopy and with a Pentacam® (OCULUS Optikgeräte GmbH, Wetzlar, Germany) instrument for 2 weeks. Central corneal thickness was determined with an ultrasound pachymeter (SP-2000; Tomey, Nagoya, Japan), and the mean of 10 measured values was calculated (up to a maximum thickness of 1200 μm, the instrument's maximum reading). The corneal endothelium was evaluated by contact specular microscopy (Konan scanning slit specular microscope, Konan Medical, Nishinomiya, Japan). Intraocular pressure was determined with a Tonovet® (icare Finland, Vantaa, Finland) instrument.

Periodic acid-Schiff (PAS) staining and immunocytochemistry

Corneas were fixed in 4% buffered paraformaldehyde and processed for paraffin embedding. Sections cut 5 μm thick were stained with PAS according to standard protocols. Rabbit corneal specimens were fixed in 4% formaldehyde and incubated for 30 minutes in 1% bovine serum albumin (BSA) to block nonspecific binding. Corneas were examined by actin staining performed with a 1:400 dilution of Alexa Fluor® 546-conjugated phalloidin (Life Technologies Corp.). For immunohistochemical analyses, specimens were incubated overnight at 4˚C with primary antibodies against Na^+/K^+-ATPase (1:300, Upstate Biotechnology, Lake Placid, NY), ZO-1 (1:300, Life Technologies Corp.), and N-cadherin (1:300, BD Biosciences, San Jose, CA). The specimens were then incubated for 2 hours at 4˚C with secondary antibody, Alexa Fluor® 488-conjugated goat anti-mouse (1:1000, Life Technologies Corp.). Nuclei were stained with DAPI (Vector Laboratories, Burlingame, CA). The slides were examined with a fluorescence microscope (TCS SP2 AOBS; Leica Microsystems, Wetzlar, Germany).

Transmission electron microscopy

For transmission electron microscopy, cornea specimens were fixed in 4% paraformaldehyde/1% glutaraldehyde in 0.1M phosphate buffer, postfixed in 2% buffered osmium tetroxide, dehydrated in graded alcohol concentrations, and embedded in epoxy resin according to standard protocols. Ultrathin sections were stained with uranyl acetate and lead citrate and examined with a transmission electron microscope (EM 906E; Carl Zeiss NTS GmbH, Oberkochen, Germany).

Alternatively, corneal buttons were washed in 0.1M Sorensen phosphate buffer, processed through 0.5% uranyl acetate en bloc staining, and then dehydrated using an ascending ethanol series. Samples were transferred to propylene oxide and were embedded in Araldite CY212 resin. Ultrathin sections were collected on uncoated G300 copper grids and stained with 1% aqueous phosphotungstic acid and uranyl acetate. Sections were examined with a transmission electron microscope (JEOL 1010; JEOL, Tokyo, Japan) equipped with a charge-coupled device camera (Orius SC1000; Gatan, Pleasanton, CA).

Statistical analysis

The statistical significance (*P*-value) for mean values in two-sample comparisons was determined with the Student's t-test. The statistical significance of comparisons of multiple sample sets was analyzed with the Dunnett's multiple-comparisons test. Results were expressed as mean ± SEM.

Results

Histology of Descemet's membrane of FECD patients

PAS staining showed the presence of abnormal excrescences, which are clinically called guttae, on the posterior aspect of Descemet's membrane in patients with FECD (Fig 1A, right). No

similar excrescences were observed in non-FECD donor corneas (Fig 1A, left). Descemet's membrane was also thicker in corneas from patients with FECD in non-FECD donor corneas, which is consistent with previous reports on abnormal extracellular matrix accumulation by pathological CECs [25, 26]. TEM further showed that attenuated CECs adhered to the outer aspect of the excrescences on Descemet's membrane in FECD eyes (Fig 1B, right), while CECs formed a sheet-like monolayer on a smooth surface of Descemet's membrane in non-FECD eyes (Fig 1B, left).

RCEC injection in the rabbit corneal endothelial dysfunction model with removal of Descemet's membrane

In our previous rabbit corneal endothelial dysfunction model, we removed the entire corneal endothelium by mechanical scraping, leaving Descemet's membrane intact (the CCD- model in the present study) (Fig 2A, left). In the current study, our intention was to use a rabbit model to evaluate the feasibility of removing Descemet's membrane in the central cornea only and to couple this with cell-based therapy as a treatment for FECD. For this purpose, we removed a 4-mm diameter of Descemet's membrane in the optical zone by CCD following

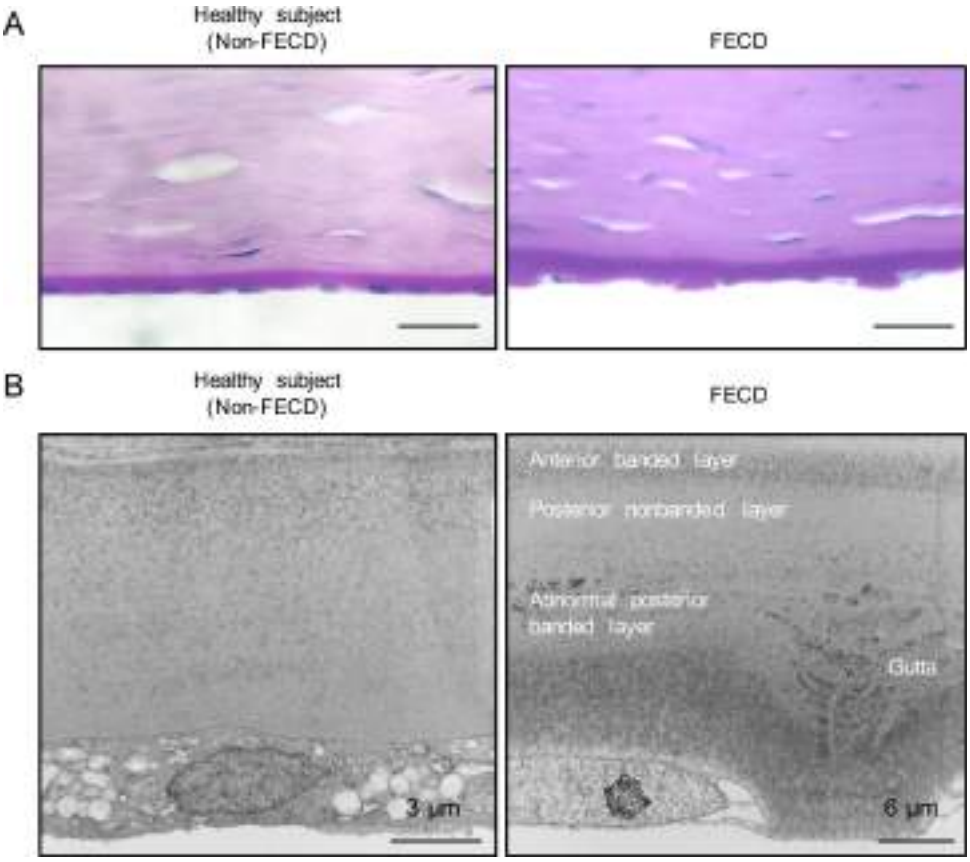

Fig 1. Histology of excrescences of Descemet's membrane in patients with FECD. (A) Representative PAS staining images of a healthy donor cornea (left).Representative PAS staining images of a cornea obtained from a patient with FECD. Excrescences, which are clinically called guttae", were observed on Descemet's membrane of the patient with FECD. Scale bar: 50 μm (right). (B) Ultra structural analysis of Descemet's membrane of non-FECD donor cornea was observed using TEM. Scale bar: 3 μm (left). Ultrastructural TEM analysis of Descemet's membrane of a cornea obtained from a patient with FECD. Flattened CECs adhered to the excrescences on Descemet's membrane. Scale bar: 6 μm (right).

https://doi.org/10.1371/journal.pone.0191306.g001

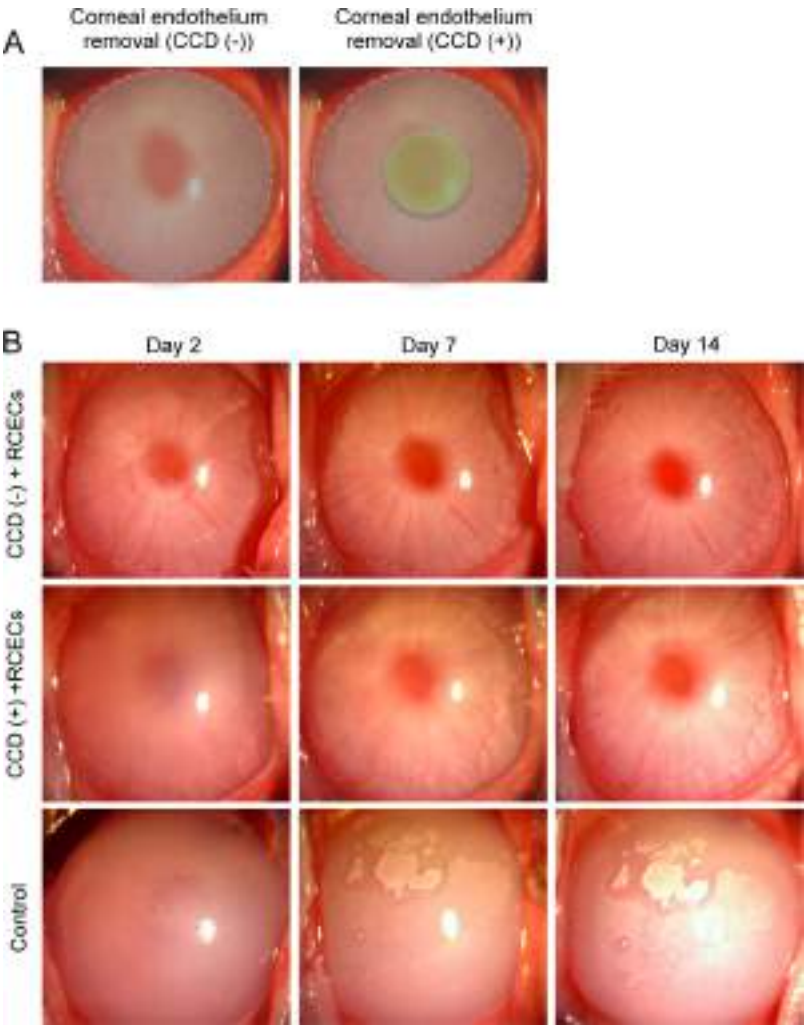

Fig 2. Rabbit corneal endothelium cell (RCEC) injection in the rabbit corneal endothelial dysfunction model with removal of a small central part of Descemet's membrane. (A) The corneal endothelium was totally scraped from the Descemet's membrane with a 20-gauge silicone needle, leaving the remaining Descemet's membrane intact. These eyes were used as the circular descemetorhexis (CCD) (-) group (left). As the CCD (+) group, a 4-mm diameter of Descemet's membrane was removed by CCD following total corneal endothelium removal. The gray area indicates the area where the corneal endothelium was removed. The green area indicates the area where Descemet's membrane was removed. (B) A total of 5.0×10^5 RCECs, suspended in 200 μl of medium supplemented with 100 μM Y-27632 ROCK inhibitor, was injected into the anterior chamber of the (CCD (-) and CCD (+) groups) (n = 6). Six eyes from which the corneal endothelium was totally removed and Descemet's membrane remained intact were used as controls. Corneal transparency was restored by intracameral injection of RCECs both in CCD (-) and CCD (+) groups, while control eyes exhibited hazy corneas due to corneal endothelial dysfunction.

https://doi.org/10.1371/journal.pone.0191306.g002

total corneal endothelium ablation (the CCD+ model) (Fig 2A, right). Slitlamp microscopy showed that corneal transparency was restored two days after injection of cultured RCECs in the CCD (-) model and the cornea was completely transparent after 7 days (Fig 2B, upper panel). In the CCD (+) model, corneal transparency recovered equally well as in the CCD (-) model 14 days after cultured RCEC injection. However, the time to restore corneal clarity was longer in the CCD (+) model than in the CCD (-) model (Fig 2B, middle panel). By contrast, control eyes without injection of cultured RCECs showed corneal haze due to corneal endothelial dysfunction throughout the entire 14-day experimental period (Fig 2B, lower panel).

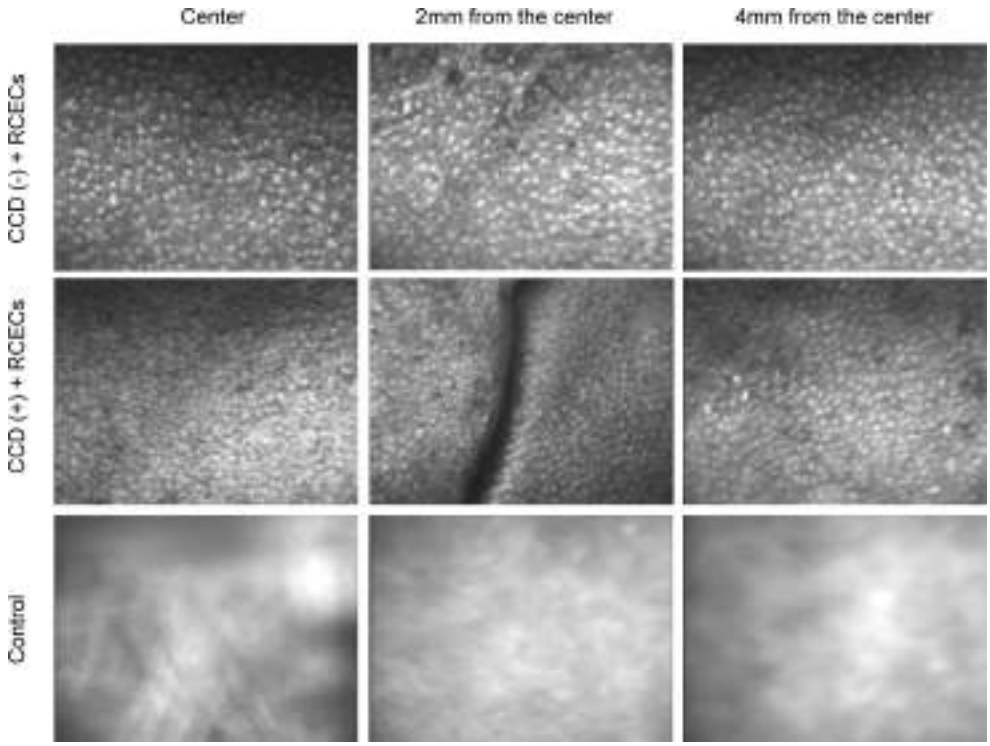

Fig 3. Evaluation of restored corneal endothelium by contact specular microscopy. Restored corneal endothelium was evaluated using contact specular microscopy 14 days after rabbit corneal endothelium cells (RCECs) injection. A representative image showed that monolayer corneal endothelium was restored in the eyes without circular descemetorhexis (CCD) (-) model) (upper panel). In the eyes with circular descemetorhexis (CCD (+) model), hexagonal monolayer corneal endothelium was observed throughout the center to the periphery. The edge of the CCD was observed, and cell density and morphology were similar for the regenerated RCECs directly on the corneal stroma and on Descemet's membrane. Cell density is likely to be similar regardless the area (middle panel). No corneal endothelial image was observed in the control eyes, which were not injected RCECs (Fig 3, lower panel).

https://doi.org/10.1371/journal.pone.0191306.g003

We next examined the restored corneal endothelium using contact specular microscopy 14 days after RCEC injection. Representative specular microscopic images of the CCD (-) model showed a regular monolayer of corneal endothelium with a homogenous cell density (Fig 3, upper panel). The CCD (+) model showed a monolayer of hexagonal corneal endothelial cells extending from the center to periphery, across the edge of the CCD. The cell density and morphology of the regenerated RCECs were similar in the central corneal stroma and on the peripheral Descemet's membrane (Fig 3, middle panel). No corneal endothelial image could be obtained in control eyes that had not undergone RCEC injection (Fig 3, lower panel).

Histological analysis of restored corneal endothelium

Immunofluorescence staining demonstrated the presence of the barrier function-related markers (N-cadherin and ZO-1) and pump function-related marker Na^+/K^+-ATPase along the cell-cell borders in the CCD (-) model. The expression patterns of these markers were similar in both the central and peripheral areas. Actin staining showed that the restored corneal endothelium exhibited a polygonal, contact-inhibited phenotype in both the central and peripheral areas (Fig 4, 1st to 2nd lines). In the CCD (+) model, N-cadherin, ZO-1, and Na^+/K^+-ATPase were also expressed along the cell-cell borders. Notably, the expression patterns of these markers were comparable in the central regions lacking Descemet's membrane and in

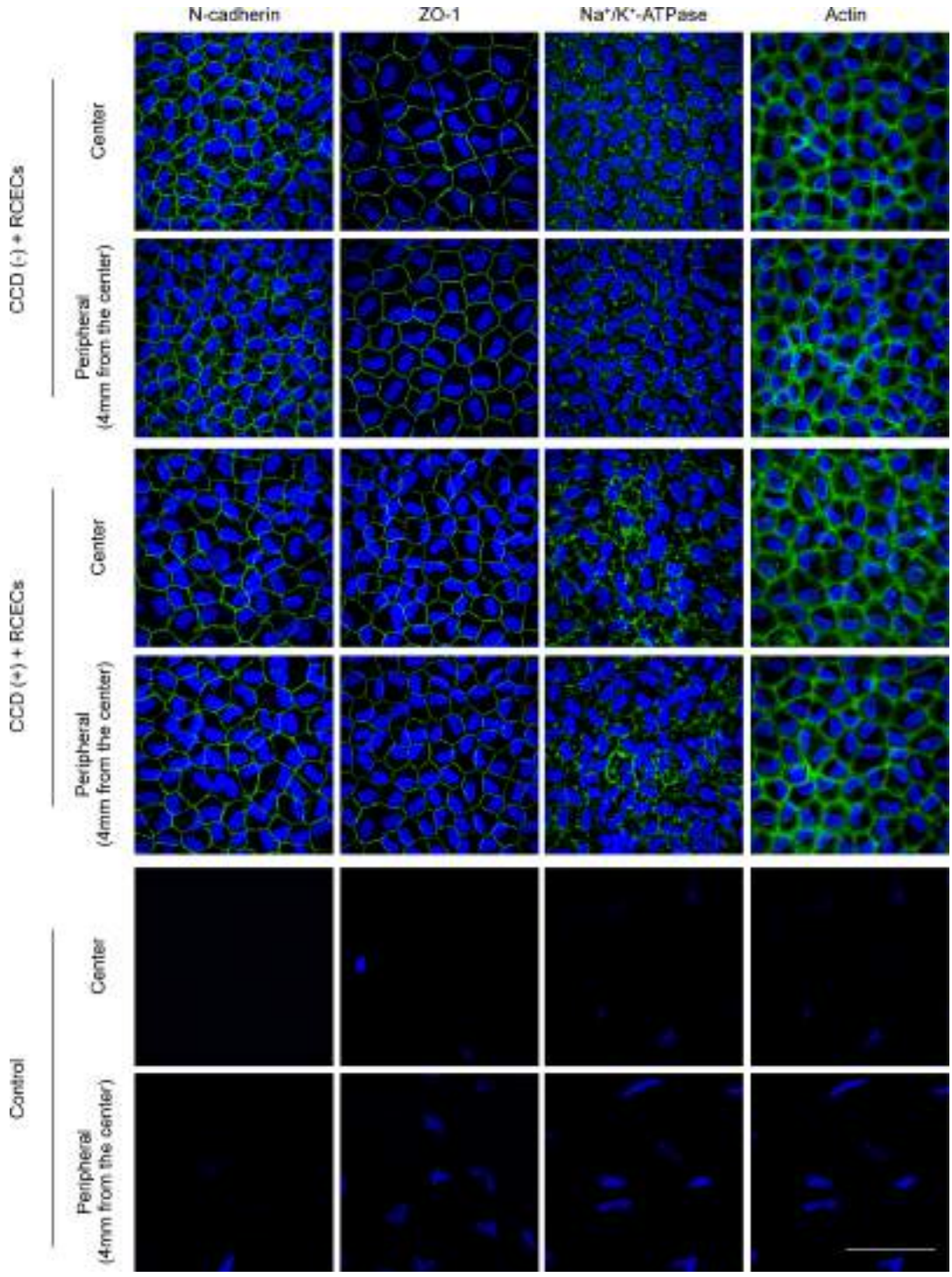

Fig 4. Histological assessment of corneal endothelium regenerated by injection of rabbit corneal endothelium cells (RCECs). Regenerated corneal endothelium was evaluated by immunofluorescent staining 2 weeks after RCECs injection. The eyes without circular descemetorhexis ((CCD) (-) model) showed barrier function-related markers (N-cadherin and ZO-1) and the pump function-related marker Na^+/K^+-ATPase at the cell-cell border. Expression patterns of those markers were similar in both the central and the peripheral areas. Actin staining showed that restored corneal endothelium had a polygonal contact-inhibited phenotypic pattern in both the central and peripheral areas (1st to 2nd lines). In the eyes with circular descemetorhexis (CCD (+) group), N-cadherin, ZO-1, and Na^+/K^+-ATPase were expressed at the cell-cell border. The expression patterns of these markers in the center, where Descemet's membrane was removed, was almost the same as in the peripheral area where Descemet's membrane

was not removed. Actin staining showed that the restored corneal endothelium was morphologically similar in both the central and peripheral areas (3rd to 4th lines). In the control eyes, which were not injected with RCECs, almost no cells were observed on Descemet's membrane (5th to 6th lines). Scale bar: 50 μm.

https://doi.org/10.1371/journal.pone.0191306.g004

the peripheral regions that retained intact Descemet's membrane. Actin staining demonstrated that the restored corneal endothelium was morphologically similar in both the center and the periphery (Fig 4, 3rd to 4th lines). In the control eyes without RCEC injection, almost no cells were observed on the Descemet's membrane without inflammatory cells (Fig 4, 5th to 6th lines).

Evaluation of the effect of CCD on clinical parameters

Scheimpflug images obtained with a Pentacam^{TM} instrument demonstrated anatomically normal corneas both in CCD (-) and CCD (+) models. Control eyes showed corneal edema due to corneal endothelial dysfunction (Fig 5A). A color map of corneal thickness showed that corneal thickness was obviously thinner in both the CCD (-) and CCD (+) models compared to the controls. The corneal volume for 3, 5, 7, and 10 mm diameters was similar for both the CCD (-) and CCD (+) models (Fig 5B). The central corneal thickness, evaluated with an ultrasound pachymeter, was significantly reduced in both the CCD (-) and CCD (+) models, when compared to controls, at 7, 10, and 14 days. The CCD (-) and CCD (+) models also showed recovery of the central corneal thickness to almost the normal range, whereas no recovery was observed in the controls. However, this recovery of corneal thickness was slower in the CCD (+) model than in the CCD (-) model (Fig 5C). The average cell density of restored corneal endothelium in the central area was 1602±241 cells/mm^2 in the CCD (-) model and 1435±202 cells/mm^2 in the CCD (+) model 14 days after surgery. In the peripheral area, the average cell density was 1625±302 cells/mm^2 in the CCD (-) model and 1718±114 cells/mm^2 in the CCD (+) model 14 days after surgery. These differences in cell density were not statistically significant (Fig 5D). Furthermore, no IOP elevation was observed in any of the groups (Fig 5E).

Discussion

The prevalence of FECD in the United States is thought to be 4% of the population aged over 40 years [27], and this high prevalence makes FECD a leading cause of corneal transplantation. Indeed, the Eye Bank Association of America reported that FECD was the most common indication for corneal transplantation (49.2% the of corneal endothelial keratoplasty and 3.0% of penetrating keratoplasty procedures) utilizing corneas provided by U.S. eye banks [28]. Likewise, Gain et al., who performed a global survey of corneal transplantation by a systematic review of published literature, reported that the top indication of corneal transplantation was FECD (39% of all corneal transplantations) [29]. Given that FECD is a leading cause of corneal transplantation, it will be the most common cause for use of cell-based therapy when cultured human CECs are approved by the authorities in various countries in the future.

We obtained approval from the Japanese Ministry of Health, Labour, and Welfare to initiate clinical research into cell-based therapy for treating corneal endothelial decompensation. The inclusion criteria for this clinical research were: 1) the patient is diagnosed with corneal endothelial decompensation, 2) the best spectacle-corrected visual acuity is under 20/40, 3) the central corneal thickness is greater than 630 μm with corneal epithelial edema, and 4) corneal endothelial cell density is unmeasurable or lower than 500 cells/mm^2 (Clinical trial registration: UMIN000012534, https://upload.umin.ac.jp/cgi-open-bin/ctr/ctr.cgi?function=brows&action=brows&type=summary&recptno=R000014592&language=E) [18]. Any types of original diagnoses resulting in corneal decompensation, such as FECD, corneal endothelial

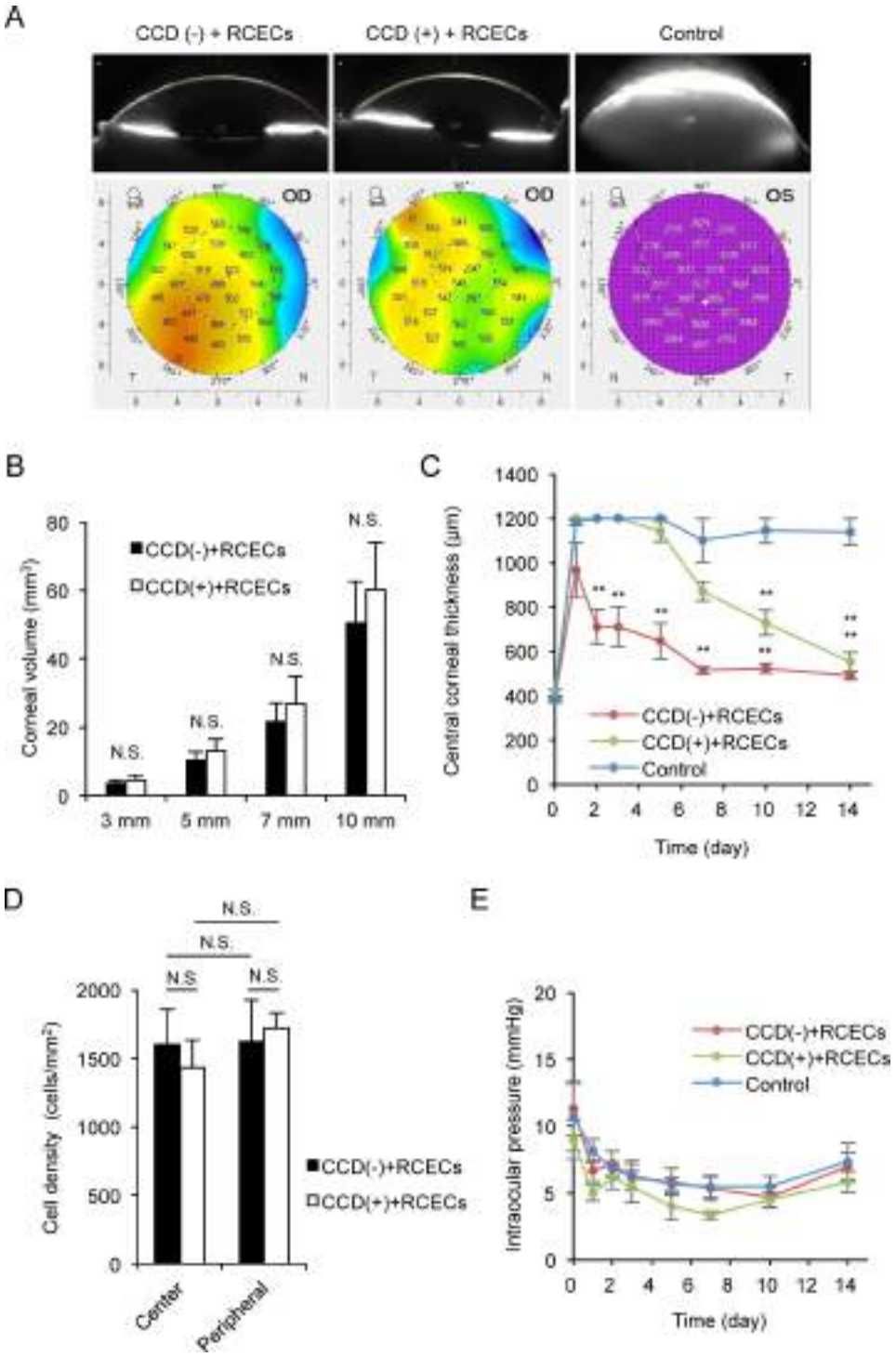

Fig 5. Assessment of the effect of circular descemetorhexis (CCD) on clinical parameters. (A) Scheimpflug images showed the restoration of an anatomically normal cornea in both the CCD (-) and CCD (+) models at 14 days after surgery. Control eyes showed corneal edema due to corneal endothelial dysfunction. A color map of corneal thickness showed that corneal thickness was thinner in both the CCD (-) and CCD (+) models when compared to the control. (B) The corneal volume was similar, when measured with a Pentacam^{TM} instrument at 3, 5, 7, and 10 mm diameters, in both the CCD (-) and CCD (+) models (n = 6). The corneal volume of the control group is not shown, as it was not evaluated with the Pentacam^{TM} instrument due to severe corneal edema. N.S. indicates no statistical significance. (C) The central corneal thickness was evaluated with an ultrasound pachymeter for 2 weeks after rabbit corneal endothelium cell (RCEC) injection.

The eyes of the CCD (-) and CCD (+) models showed recovery of the central corneal thickness to an almost normal range, whereas this thickness did not recover in the controls. However, recovery of corneal thickness was slower in the CCD (+) model than in the CCD (-) model (n = 6). $^{**}P < 0.01$, $^{*}P < 0.05$. (D) Cell density of the regenerated corneal endothelium was determined by analyzing immunofluorescence staining images using ImageJ software. The average cell density of the restored corneal endothelium was similar for the CCD (-) and CCD (+) models in both the central and peripheral areas (n = 6). N.S. indicates no statistical significance. (E) Intraocular pressure (IOP) was evaluated with a Tonovet® instrument, and no abnormal IOP elevation was observed in any of the groups (n = 6).

https://doi.org/10.1371/journal.pone.0191306.g005

damage by various intraocular surgery, or eye trauma, are included in this clinical research. Although we are currently collecting clinical data, we have preliminary evidence that confirms that injection of cultured human CECs, only the removal of the pathological corneal endothelium but not Descemet's membrane, results in regeneration of the corneal endothelium and restoration of a transparent cornea, regardless of the original diagnosis, including FECD (manuscript in preparation).

Descemet's membrane is the basement membrane of the corneal endothelium. Basement membranes are cell-adherent extracellular scaffolds located at the basal side of every epithelium and endothelium [30]. They are anchored to the cytoskeleton through receptors, and they also act as a signaling platform for various essential cell phenomena [30–33]. In various cell types, components of the basement membrane bind to their corresponding integrins to initiate signaling from the outside to the inside of the cells by recruiting cytoplasmic adaptor proteins, phosphorylating binding proteins, and binding adaptor proteins to the actin cytoskeleton [31–33]. Descemet's membrane is composed of type VI, VIII, XII, XVII collagens, glycoproteins (fibronectin, laminin, and osteonectin), and proteoglycans (versican and agrin) [20, 25, 34]. We have demonstrated that laminin-511 and 521 are expressed in Descemet's membrane and play an imporatant role in CEC adhesion and proliferation and in the maintenance of functions though binding to integrins α3β1 and α6β1 [35]. Accumulating evidence now indicates an essential role for the basement membrane in cell fate, leading to the assumption that Descemet's membrane will enhance engraftment of injected CECs in cell-based therapy.

Prior to initiating our clinical research, we performed numerous experiments using animal models to evaluate therapeutic effect and safety [16, 17, 24]. In terms of the method for removing the pathological corneal endothelium, we tried two methods: 1) remove only the corneal endothelium but not Descemet's membrane and 2) remove the corneal endothelium with Descemet's membrane by descemetorhexis. In rabbit and monkey corneal endothelial dysfunction models, we confirmed that the corneal endothelium was always restored when Descemet's membrane was not removed [16, 17, 24]. By contrast, the success rate of restoration of a transparent cornea was reduced, the healing time to exhibit a transparent cornea was lengthened, and the cell density of regenerated corneal endothelium was lower in the animal models with Descemet's membrane removal than in those without Descemet's membrane removal (data not shown).

In the current study, we evaluated the feasibility of performing a small descemetorhexis of the optical zone. Our thinking was that removal of Descemet's membrane in the optical zone is important for visual quality, while the remaining Descemet's membrane might improve the fate of injected CECs. We showed that the corneal endothelium is regenerated directly onto the corneal stroma (the area of Descemet's membrane removal) and corneal transparency was restored. However, recovery of central corneal thickness was slower when Descemet's membrane was removed. We speculated that removal of Descemet's membrane induced a greater severity of stromal edema than occurred when Descemet's membrane was not removed, if the

cell adhesion and the regeneration of corneal endothelium were similar in both the Descemet's membrane removal model and the Descemet's membrane non-removal model. Another possible explanation is that the corneal stroma is not an ideal substrate for adhesion of injected CECs or for recovery of CEC function when compared to the basement membrane. Even though the recovery time was longer, the final cell density and central corneal thickness, which are widely accepted as the most important clinical parameters of the corneal endothelium, were as good in the rabbit model with Descemet's membrane removal as in the model without Descemet's membrane removal at 14 days after surgery. Our study provides preclinical data showing that a small descemetorhexis of the optical zone may be a surgical option for cell based-therapy for the treatment of FECD.

In conclusion, we have demonstrated that a small descemetorhexis, in combination with cell-based therapy, is feasible to further improve visual quality after cultured CEC injection. Future randomized clinical trials of cell-based therapy for FECD, conducted with or without small descemetorhexisis, will be necessary to optimize the surgical protocol.

Supporting information

S1 File. Data set of Fig 5B–5E.
(XLSX)

Author Contributions

Conceptualization: Naoki Okumura, Shigeru Kinoshita, Noriko Koizumi.

Data curation: Naoki Okumura, Daiki Matsumoto, Yuya Fukui, Masataka Teramoto, Hirofumi Imai, Tomoki Shimada, Ursula Schlötzer-Schrehardt.

Formal analysis: Naoki Okumura, Daiki Matsumoto.

Funding acquisition: Naoki Okumura, Noriko Koizumi.

Investigation: Naoki Okumura, Daiki Matsumoto, Yuya Fukui, Masataka Teramoto, Hirofumi Imai, Tetta Kurosawa, Tomoki Shimada, Ursula Schlötzer-Schrehardt.

Methodology: Naoki Okumura.

Project administration: Naoki Okumura, Noriko Koizumi.

Resources: Friedrich Kruse, Ursula Schlötzer-Schrehardt.

Supervision: Noriko Koizumi.

Validation: Naoki Okumura, Noriko Koizumi.

Writing – original draft: Naoki Okumura.

Writing – review & editing: Naoki Okumura, Daiki Matsumoto, Yuya Fukui, Masataka Teramoto, Hirofumi Imai, Tetta Kurosawa, Tomoki Shimada, Friedrich Kruse, Ursula Schlötzer-Schrehardt, Shigeru Kinoshita, Noriko Koizumi.

References

1. Nishida T, Saika S. Cornea and sclera: Anatomy and physiology. In: Krachmer J, Mannis M, Holland E., editors. Cornea. 3rd ed. Maryland Heights MS: Mosby; 2011. pp. 3–24.
2. Tan DT, Dart JK, Holland EJ, Kinoshita S. Corneal transplantation. Lancet 2012; 379: 1749–1761. https://doi.org/10.1016/S0140-6736(12)60437-1 PMID: 22559901
3. Nijm LM, Mannis MJ, Holland EJ. The evolution of contemporary keratoplasty. In: Krachmer J, Mannis M, Holland E., editors. Cornea. 3rd ed. Maryland Heights MS: Mosby; 2011. pp. 1321–1325.

4. Gorovoy MS. Descemet-stripping automated endothelial keratoplasty. Cornea 2006; 25: 886–889. https://doi.org/10.1097/01.ico.0000214224.90743.01 PMID: 17102661
5. Melles GR, Ong TS, Ververs B, van der Wees J. Preliminary clinical results of Descemet membrane endothelial keratoplasty. Am J Ophthalmol 2008; 145: 222–227. https://doi.org/10.1016/j.ajo.2007.09.021 PMID: 18061137
6. Dapena I, Ham L, Melles GR. Endothelial keratoplasty: DSEK/DSAEK or DMEK–the thinner the better? Curr Opin Ophthalmol 2009; 20: 299–307. https://doi.org/10.1097/ICU.0b013e32832b8d18 PMID: 19417653
7. Price MO, Price FW Jr. Endothelial keratoplasty–a review. Clin Experiment Ophthalmol 2010; 38: 128–140. https://doi.org/10.1111/j.1442-9071.2010.02213.x PMID: 20398103
8. Guell JL, El Husseiny MA, Manero F, Gris O, Elies D. Historical review and update of surgical treatment for corneal endothelial diseases. Ophthalmol Ther 2014; 3: 1–15. https://doi.org/10.1007/s40123-014-0022-y PMID: 25134494
9. Patel SV. Graft survival and endothelial outcomes in the new era of endothelial keratoplasty. Exp Eye Res 2012; 95: 40–47. https://doi.org/10.1016/j.exer.2011.05.013 PMID: 21689649
10. Mimura T, Shimomura N, Usui T, Noda Y, Kaji Y, Yamgami S, et al. Magnetic attraction of iron-endocytosed corneal endothelial cells to Descemet's membrane. Exp Eye Res 2003; 76: 745–751. PMID: 12742357
11. Mimura T, Yamagami S, Yokoo S, Usui T, Tanaka K, Hattori S, et al. Cultured human corneal endothelial cell transplantation with a collagen sheet in a rabbit model. Invest Ophthalmol Vis Sci 2004; 45: 2992–2997. https://doi.org/10.1167/iovs.03-1174 PMID: 15326112
12. Ishino Y, Sano Y, Nakamura T, Connon CJ, Rigby H, Fullwood NJ, et al. Amniotic membrane as a carrier for cultivated human corneal endothelial cell transplantation. Invest Ophthalmol Vis Sci 2004; 45: 800–806. PMID: 14985293
13. Sumide T, Nishida K, Yamato M, Ide T, Hayashida Y, Watanabe K, et al. Functional human corneal endothelial cell sheets harvested from temperature-responsive culture surfaces. FASEB J 2006; 20: 392–394. https://doi.org/10.1096/fj.04-3035fje PMID: 16339916
14. Koizumi N, Sakamoto Y, Okumura N, Okahara N, Tsuchiya H, Torii R, et al. Cultivated corneal endothelial cell sheet transplantation in a primate model. Invest Ophthalmol Vis Sci 2007; 48: 4519–4526. https://doi.org/10.1167/iovs.07-0567 PMID: 17898273
15. Okumura N, Ueno M, Koizumi N, Sakamoto Y, Hirata K, Hamuro J, et al. Enhancement on primate corneal endothelial cell survival in vitro by a ROCK inhibitor. Invest Ophthalmol Vis Sci 2009; 50: 3680–3687. https://doi.org/10.1167/iovs.08-2634 PMID: 19387080
16. Okumura N, Koizumi N, Ueno M, Sakamoto Y, Takahashi H, Tsuchiya H, et al. ROCK inhibitor converts corneal endothelial cells into a phenotype capable of regenerating in vivo endothelial tissue. Am J Pathol 2012; 181: 268–277. https://doi.org/10.1016/j.ajpath.2012.03.033 PMID: 22704232
17. Okumura N, Sakamoto Y, Fujii K, Kitano J, Nakano S, Tsujimoto Y, et al. Rho kinase inhibitor enables cell-based therapy for corneal endothelial dysfunction. Sci Rep 2016; 6: 26113. https://doi.org/10.1038/srep26113 PMID: 27189516
18. Okumura N, Kinoshita S, Koizumi N. Application of Rho kinase inhibitors for the treatment of corneal endothelial diseases. J Ophthalmol 2017; 2017: 2646904. https://doi.org/10.1155/2017/2646904 PMID: 28751979
19. Hogan MJ, Wood I, Fine M. Fuchs' endothelial dystrophy of the cornea. 29th Sanford Gifford Memorial lecture. Am J Ophthalmol 1974; 78: 363–383. PMID: 4547212
20. Schlotzer-Schrehardt U, Bachmann BO, Laaser K, Cursiefen C, Kruse FE. Characterization of the cleavage plane in Descemet's membrane endothelial keratoplasty. Ophthalmology 2011; 118: 1950–1957. https://doi.org/10.1016/j.ophtha.2011.03.025 PMID: 21705086
21. Adamis AP, Filatov V, Tripathi BJ, Tripathi RC. Fuchs' endothelial dystrophy of the cornea. Surv Ophthalmol 1993; 38: 149–168. PMID: 8235998
22. Wacker K, McLaren JW, Amin SR, Baratz KH, Patel SV. Corneal high-order aberrations and backscatter in Fuchs' endothelial corneal dystrophy. Ophthalmology 2015; 122: 1645–1652. https://doi.org/10.1016/j.ophtha.2015.05.005 PMID: 26050543
23. Watanabe S, Oie Y, Fujimoto H, Soma T, Koh S, Tsujikawa M, et al. Relationship between corneal guttae and quality of vision in patients with mild Fuchs' endothelial corneal dystrophy. Ophthalmology 2015; 122: 2103–2109. https://doi.org/10.1016/j.ophtha.2015.06.019 PMID: 26189189
24. Okumura N, Kusakabe A, Hirano H, Inoue R, Okazaki Y, Nakano S, et al. Density-gradient centrifugation enables the purification of cultured corneal endothelial cells for cell therapy by eliminating senescent cells. Sci Rep 2015; 5: 15005. https://doi.org/10.1038/srep15005 PMID: 26443440

25. Weller JM, Zenkel M, Schlotzer-Schrehardt U, Bachmann BO, Tourtas T, Kruse FE. Extracellular matrix alterations in late-onset Fuchs' corneal dystrophy. Invest Ophthalmol Vis Sci 2014; 55: 3700–3708. https://doi.org/10.1167/iovs.14-14154 PMID: 24833739

26. Okumura N, Minamiyama R, Ho LT, Kay EP, Kawasaki S, Tourtas T, et al. Involvement of ZEB1 and Snail1 in excessive production of extracellular matrix in Fuchs endothelial corneal dystrophy. Lab Invest 2015; 95: 1291–1304. https://doi.org/10.1038/labinvest.2015.111 PMID: 26302187

27. Lorenzetti DW, Uotila MH, Parikh N, Kaufman HE. Central cornea guttata. Incidence in the general population. Am J Ophthalmol 1967; 64: 1155–1158. PMID: 6072991

28. Eye Bank Association of America. Eye Banking Statistical Report. Washington, DC 2016.

29. Gain P, Jullienne R, He Z, Aldossary M, Acquart S, Cognasse F, et al. Global survey of corneal transplantation and eye banking. JAMA Ophthalmol 2016; 134: 167–173. https://doi.org/10.1001/jamaophthalmol.2015.4776 PMID: 26633035

30. DiPersio CM, Zheng R, Kenney J, Van De Water L. Integrin-mediated regulation of epidermal wound functions. Cell Tissue Res 2016; 365: 467–482. https://doi.org/10.1007/s00441-016-2446-2 PMID: 27351421

31. Liu S, Calderwood DA, Ginsberg MH. Integrin cytoplasmic domain-binding proteins. J Cell Sci 2000; 113 (Pt 20): 3563–3571.

32. Hynes RO. Integrins: bidirectional, allosteric signaling machines. Cell 2002; 110: 673–687. PMID: 12297042

33. Delon I, Brown NH. Integrins and the actin cytoskeleton. Curr Opin Cell Biol 2007; 19: 43–50. https://doi.org/10.1016/j.ceb.2006.12.013 PMID: 17184985

34. Ljubimov AV, Atilano SR, Garner MH, Maguen E, Nesburn AB, Kenney MC. Extracellular matrix and Na^+,K^+-ATPase in human corneas following cataract surgery: comparison with bullous keratopathy and Fuchs' dystrophy corneas. Cornea 2002; 21: 74–80. PMID: 11805512

35. Okumura N, Kakutani K, Numata R, Nakahara M, Schlotzer-Schrehardt U, Kruse F, et al. Laminin-511 and -521 enable efficient in vitro expansion of human corneal endothelial cells. Invest Ophthalmol Vis Sci 2015; 56: 2933–2942. https://doi.org/10.1167/iovs.14-15163 PMID: 26024079

Graefe's Archive for Clinical and Experimental Ophthalmology
https://doi.org/10.1007/s00417-017-3889-1

CORNEA

Wide-field contact specular microscopy analysis of corneal endothelium post trabeculectomy

Naoki Okumura[1] · Daiki Matsumoto[1] · Yugo Okazaki[1] · Noriko Koizumi[1] · Chie Sotozono[2] · Shigeru Kinoshita[2,3] · Kazuhiko Mori[2]

Received: 25 October 2017 / Revised: 18 December 2017 / Accepted: 20 December 2017

Abstract

Purpose This study investigates the possible role of the filtration bleb in the continuous decrease in corneal endothelial cell (CEC) density observed following trabeculectomy.

Methods This study involved 51 eyes of 37 glaucoma patients who underwent trabeculectomy. The CEC density was determined by contact specular microscopy in three areas: (1) the cornea center, (2) near the trabeculectomy filtration bleb, and (3) the opposite side of the bleb. The eyes were grouped according to post-surgical follow-up years: 0–1 (Group 1), 1–2 (Group 2), 2–3 (Group 3), 3–4, (Group 4), and 4+ years (Group 5).

Results The mean CEC densities at the opposite side of the bleb, in the cornea center, and near the bleb were 2210 ± 487, 1930 ± 528, and 1519 ± 507 cells/mm^2, respectively, in all eyes. The CEC density was significantly lower near the bleb than at the other two sites. The coefficient of variation was significantly higher near the bleb than at the other two sites. The CEC densities at the cornea center and at the opposite side of the bleb showed no significant differences. However, the CEC densities near the bleb showed time-dependent decreases to 1790, 1601, 1407, 1339, and 1224 cells/mm^2 for Groups 1, 2, 3, 4, and 5, respectively.

Conclusions CEC density following trabeculectomy decreased near the bleb, but not at the cornea center, suggesting that the involvement of the filtration bleb in CEC density loss should be further examined to elucidate the pathology of CEC loss following trabeculectomy.

Keywords Trabeculectomy · Corneal endothelial cell · Specular microscopy

Introduction

The general aim of glaucoma treatment is to lower intraocular pressure (IOP) to a level that can suppress the progression of glaucomatous optic neuropathy. A frequent first-line treatment for IOP control is the topical administration of anti-glaucoma drugs. However, the insufficient control of IOP or the progression of perimetric damage, even with medical treatment and laser trabeculoplasty, sometimes requires that patients undergo surgical treatments.

Trabeculectomy is still the most commonly used glaucoma surgery in the world, even despite the introduction of glaucoma drainage implants (e.g., EX-PRESS filtration devices, Baerveldt glaucoma implants, and Ahmed valves) into clinical settings. However, the trabeculectomy procedure has associated problems, such as collapse of the anterior chamber, hypotony, choroidal detachment, and hypotony maculopathy [1]. A particularly devastating postoperative complication is corneal decompensation, a continuous loss of corneal endothelial cells (CECs) that occurs by an as yet unknown mechanism [2–5]. The aim of the present study was to use slit-scanning wide-field contact specular microscopy to

Electronic supplementary material The online version of this article (https://doi.org/10.1007/s00417-017-3889-1) contains supplementary material, which is available to authorized users.

✉ Kazuhiko Mori
kmori@koto.kpu-m.ac.jp

[1] Department of Biomedical Engineering, Faculty of Life and Medical Sciences, Doshisha University, Kyotanabe, Japan

[2] Department of Ophthalmology, Kyoto Prefectural University of Medicine, Kyoto, Japan

[3] Department of Frontier Medical Science and Technology for Ophthalmology, Kyoto Prefectural University of Medicine, Kyoto, Japan

investigate whether different areas of the cornea show differences in post-trabeculectomy CEC loss.

Materials and methods

This study was conducted in accordance with a protocol approved by the Institutional Review Board of Kyoto Prefectural University of Medicine, Kyoto, Japan. Clinical trial registration was obtained at UMIN UMIN000021264 (http://www.umin.ac.jp/english/). The study protocol followed the tenets set forth in the Declaration of Helsinki and written informed consent was obtained from all subjects prior to their involvement in the study.

We examined the corneal endothelium of consecutive trabeculectomy patients who had follow-up visits at the Kyoto Prefectural University of Medicine between July and August 2015. Patients who had undergone penetrating keratoplasty or shunt surgery and who were diagnosed with corneal endothelial dystrophies or active uveitis were excluded.

Contact specular microscopy examination

The corneal endothelium was evaluated with a prototype KSSP slit-scanning wide-field contact specular microscope (Konan Medical, Inc., Hyogo, Japan), as previously described [6]. Briefly, the wide-field contact specular microscope had a 1/2 in. camera including a 400,000-pixel charge-coupled-device sensor with 9.9× magnification, and a 40× magnification contact cone lens made from fluorite with numerous slits on both sides. Images of the corneal endothelium were obtained for three areas: (1) the cornea center, (2) the area near the trabeculectomy filtration bleb (approximately 5 mm from the corneal center), and (3) the opposite side of the bleb (5 mm from the corneal center). The images were obtained as movie files (MPEG-2 files) at the rate of 60 frames per second, and representative images were extracted from the MPEG-2 files.

Trabeculectomy surgical procedure

Sub-Tenon's capsule anesthesia was first performed. A fornix-based conjunctival flap and square 3 × 3 mm and 2.8 × 2.8 mm outer and inner scleral flaps of 1/2 and 4/5 thicknesses, respectively, were made. Mitomycin C (MMC, 0.4 mg/ml) was applied subconjunctivally around the scleral flap for 5 min using surgical sponges for all patients, and then was washed out with saline solution. The inner scleral flap was then dissected together with the trabecular meshwork. Peripheral iridectomy was performed, and the outer scleral flap was closed with interrupted 10–0 nylon sutures. The conjunctival flap was then tightly sutured with two interrupted 10–0 nylon wing sutures and a blocking mattress suture to form the filtration bleb, without leakage of aqueous humor. Patients with cataract underwent combined cataract surgery during the trabeculectomy. The phacoemulsification was performed through the scleral tunnel as a one-site procedure, and a foldable posterior chamber intraocular lens was inserted. All trabeculectomies were performed by the same surgeon (K.M.).

Statistical analysis

The data are presented as mean ± standard deviation (SD). The statistical significance (P-value) of differences between the mean values in two-sample comparisons was determined with Student's t-test. Multiple sample sets were analyzed using Dunnett's multiple-comparison test. The decrease in corneal endothelial cell density was analyzed with the Jonckheere-Terpstra trend test. $P < 0.05$ indicated statistical significance.

Results

Characteristics of trabeculectomy patients

Analysis of the CEC density in patients who had undergone trabeculectomy was conducted on 51 eyes of 37 glaucoma patients (17 males and 20 females; age range 47–86 years) who had undergone trabeculectomy at Kyoto Prefectural University of Medicine from 2004 to 2015. The eyes were divided into five groups based on the number of follow-up years after surgery: less than 1 year (Group 1: $n = 19$), at least 1 year but less than 2 years (Group 2: $n = 6$), at least 2 years but less than 3 years (Group 3: n = 6), at least 3 years but less than 4 years (Group 4: $n = 8$), and at least 4 years (Group 5: $n = 12$). The mean postoperative periods for Groups 1, 2, 3, 4, and 5 were 2.8 ± 1.6, 17.3 ± 3.1, 29.8 ± 1.3, 43.0 ± 3.0, 89.0 ± 23.3 months, respectively. The patient mean ages in the groups were similar, at 73.7 ± 9.0, 70.5 ± 10.2, 75.7 ± 5.9, 72.1 ± 9.2, and 69.2 ± 9.1 years, respectively (Table 1). Demographic data for glaucoma, such as duration of glaucoma, maximum intraocular pressure during observation time, and visual field loss (evaluated by Anderson's criteria) are shown in supplemental Table 1 [7].

CEC density of trabeculectomy patients

The mean CEC densities of all eyes at the opposite side of the bleb, at the cornea center, and near the bleb, as evaluated by slit-scanning wide-field contact specular microscopy (Fig. 1a), were 2210, 1930, and 1519 cells/mm^2, respectively, indicating a significantly lower CEC density near the bleb than at the other two sites (Fig. 1b). Consistently, the coefficient of variation (a value clinically used as an indicator of polymegathism) near the bleb was 0.38, and this value was significantly higher than at the center and at the opposite side

Table 1 Characteristics of the patients who underwent trabeculectomy

	Group 1 (0-1Y)	2 (1-2Y)	3 (2-3Y)	4 (3-4Y)	5 (4Y<)	Group 1–5
No. of eyes	19	6	6	8	12	51
Gender, no. (%)						
Male	9 (47.4)	1 (17.7)	3 (50.0)	4 (50.0)	5 (41.7)	22 (43.1)
Female	10 (52.6)	5 (83.3)	3 (50.0)	4 (50.0)	7 (58.3)	29 (56.9)
Age						
Mean ± SD, year	73.7 ± 9.0	70.5 ± 10.2	75.7 ± 5.9	72.1 ± 9.2	69.2 ± 9.1	71.7 ± 9.7
Range	47 to 86	54 to 85	71 to 84	57 to 80	51 to 80	40 to 86
Postoperative period						
Mean ± SD, month	2.8 ± 1.6	17.3 ± 3.1	29.8 ± 1.3	43.0 ± 3.0	89.0 ± 23.3	55.5 ± 68.8
Range	1 to 7	13 to 23	28 to 31	39 to 48	49 to 120	1 to 120
Cataract surgery, no. (%)						
Combined (one-site)	15 (78.9)	3 (50.0)	2 (33.3)	2 (25.0)	7 (58.3)	29 (56.9)
Trabeculectomy only	4 (21.1)	3 (50.0)	4 (66.7)	6 (75.0)	5 (41.7)	22 (43.1)

of the bleb sites (0.32 and 0.33, respectively) (Fig. 1c). The percentage of hexagonal cells (used clinically as an indicator of polymorphism) was significantly lower near the bleb than at the center (54.9 and 60.4%, respectively) (Fig. 1d). We provided baseline data of the clinical parameters of the corneal endothelium by evaluating 12 non-glaucoma subjects using slit-scanning wide-field contact specular microscopy; these results are shown in supplemental Fig. 1.

The CEC density of patients with trabeculectomy varied depending on follow-up duration. Representative slit-scanning wide-field contact specular microscopy images revealed a similar density and morphology for the CECs in all three areas in Group 1. By contrast, patients in Group 3 had similar CEC densities and morphology at the opposite side of the bleb and cornea center sites, but showed a decreased CEC density and a greater variation in cell size near the bleb. The decrease in density near the bleb area was even more evident in Group 5 and a density decrease was also observed in the cornea center in this group. Cell size was increased even at the opposite side of the bleb in Group 5 (Fig. 2).

The CEC densities at the cornea center were 2067, 2169, 1719, 2039, and 1626 cells/mm^2 in Groups 1, 2, 3, 4, and 5, respectively (Fig. 3a). Likewise, the CEC densities at the opposite side of the bleb were 2229, 2300, 1923, 2313, and 1995 cells/mm^2, respectively (Fig. 3b). We analyzed these data statistically using the Jonckheere-Terpstra test to evaluate whether a trend existed between the CEC density drop and the time after trabeculectomy. The CEC densities showed no significant decreases in the cornea center and the peripheral area at the opposite side of the bleb in any of the 5 groups ($p = 0.077$ and $p = 0.148$, respectively). However, the CEC densities near the bleb were 1790 ± 435, 1601 ± 184, 1407 ± 425, 1339 ± 572, and 1224 ± 543 cells/mm^2, respectively, indicating a time-dependent decrease in CEC density in this area only ($p = 0.001$) (Fig. 3c). We also evaluated the effect of combined one-site cataract surgery with trabeculectomy on the CEC densities. The mean CEC densities for eyes that underwent combined cataract surgery with trabeculectomy and eyes that underwent trabeculectomy alone were, respectively: 2125 ± 467 vs. 2204 ± 521 cells/mm^2 at the opposite side ($p = 0.57$), 1902 ± 577 vs. 1966 ± 467 cells/mm^2 at the center ($p = 0.67$), and 1545 ± 567 vs. 1483 ± 424 cells/mm^2 near the bleb area ($p = 0.70$), indicating that combined cataract surgery did not induce a significant CEC density drop (supplemental Table 2).

Discussion

CECs maintain corneal transparency by regulating the amount of water in the corneal stroma by pump-and-leak barrier functions [8]. Phenotypical features of CECs in the clinical setting include their limited proliferative ability [9, 10]. Damage to CECs for any reason, such as from Fuchs endothelial corneal dystrophy, cataract surgery, endotheliallitis, and trauma, triggers the remaining CECs to cover the damaged area by migration and cell enlargement, which results in a decrease in the overall CEC density. A critical CEC density decrease (usually to less than 500–1000 cells/mm^2) induces corneal decompensation [11].

Trabeculectomy is the most widely performed filtration surgery for glaucoma, but it has a high complication rate. For instance, one study of 1240 eyes with trabeculectomy revealed that 47% of the patients exhibited early postoperative complications, such as hyphema (24.6%), shallow anterior chamber (23.9%), hypotony (24.3%), and leakage from the bleb (17.6%). Although 4.4% of the patients had irreversible loss of visual acuity, most of these early complications were resolved within a few weeks [1]. By contrast, corneal endothelial damage is a devastating complication, which appears in both the early and late postoperative periods. For instance,

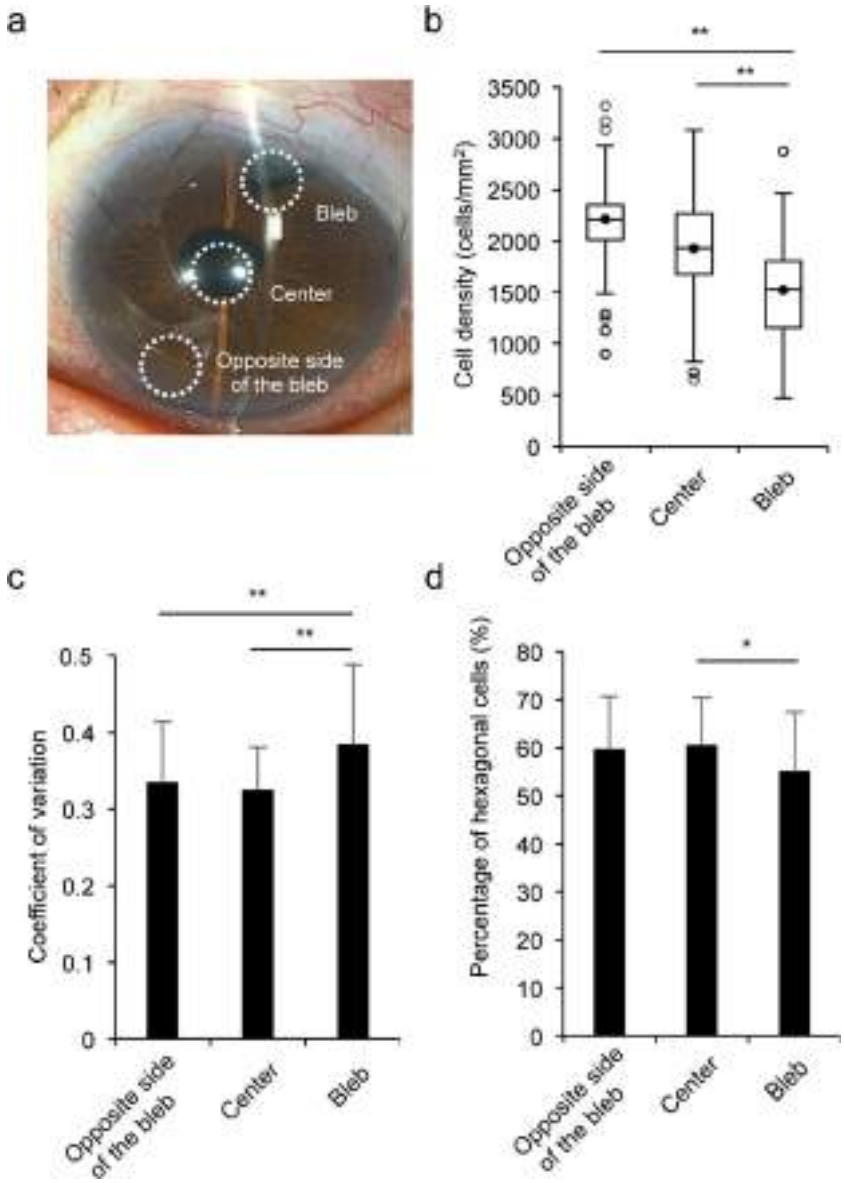

Fig. 1 Corneal endothelial cell (CEC) density of the patients who underwent trabeculectomy. **a** Images of the area where CEC was evaluated by slit-scanning wide-field contact specular microscopy. White dotted circles indicate the areas evaluated by contact specular microscopy. **b** Cell density at the opposite side of the bleb, at the cornea center, and near the bleb of all eyes of the patients who underwent trabeculectomy. The black symbols indicate the mean value, the horizontal lines in the boxes indicate medians, the bottom of each box indicates the 25th percentile, and the top of each box indicates the 75th percentile. The horizontal lines outside the boxes indicate the range of CEC density. Values beyond 1.5 times the interquartile range were considered outliers (circles). $^{**}p < 0.01$. **c** Comparison of the coefficients of variation of all eyes of the patients who underwent trabeculectomy, obtained from slit-scanning wide-field contact specular microscopy images taken at the opposite side of the bleb, at the cornea center, and near the bleb. $^{**}p < 0.01$. **d** Percentage of hexagonal cells of all eyes of the patients who underwent trabeculectomy, obtained from slit-scanning wide-field contact specular microscopy images taken at the opposite side of the bleb, at the cornea center, and near the bleb. $^{*}p < 0.05$

Arnavielle and colleagues reported a cell loss of 7.0% at 3 months and 9.6% at 12 months after trabeculectomy without antimetabolites [3]. In cases of MMC augmented trabeculectomy, Storr-Paulsen and colleagues reported cell losses of 9.5% at 3 months and 10.0% at 12 months, and suggested that active cellular enlargement and realignment occurred even at the chronic phase [4]. A recent prospective study on CEC loss after trabeculectomy and Ahmed glaucoma valve implantation showed a reduction in CEC density of 1.9% at 6 months and 3.2% at 12 months after trabeculectomy with the use of MMC [5].

Multiple studies have shown that CEC density drops after trabeculectomy, but the CECs in these studies were evaluated using noncontact specular microscopy, which only visualizes the corneal endothelium at the corneal center. Interestingly, Arnavielle and colleagues, who evaluated the central and superior cornea of patients after trabeculectomy using noncontact specular microscopy, showed CEC densities of 2096 cells/mm^2 centrally and 2369 cells/mm^2 superiorly at the preoperative stage, 1950 cells/mm^2 centrally and 2117 cells/mm^2 superiorly at 3 months, and 1894 cells/mm^2 centrally and 2087 cells/mm^2 superiorly at 12 months. Although the differences were not statistically significant, they suggested that the CEC density tended to decrease more slowly in the central cornea than in the upper cornea [3]. However, their evaluation of the upper cornea by noncontact specular microscopy (SP-2000P, TOPCON Corp., Tokyo, Japan) was thought to reflect the paracentral area, which is approximately 3 mm from the center, due to the features of noncontact specular microscopy.

In the current study, we utilized a prototype slit-scanning wide-field contact specular microscope that visualizes the corneal endothelium from the center to the periphery

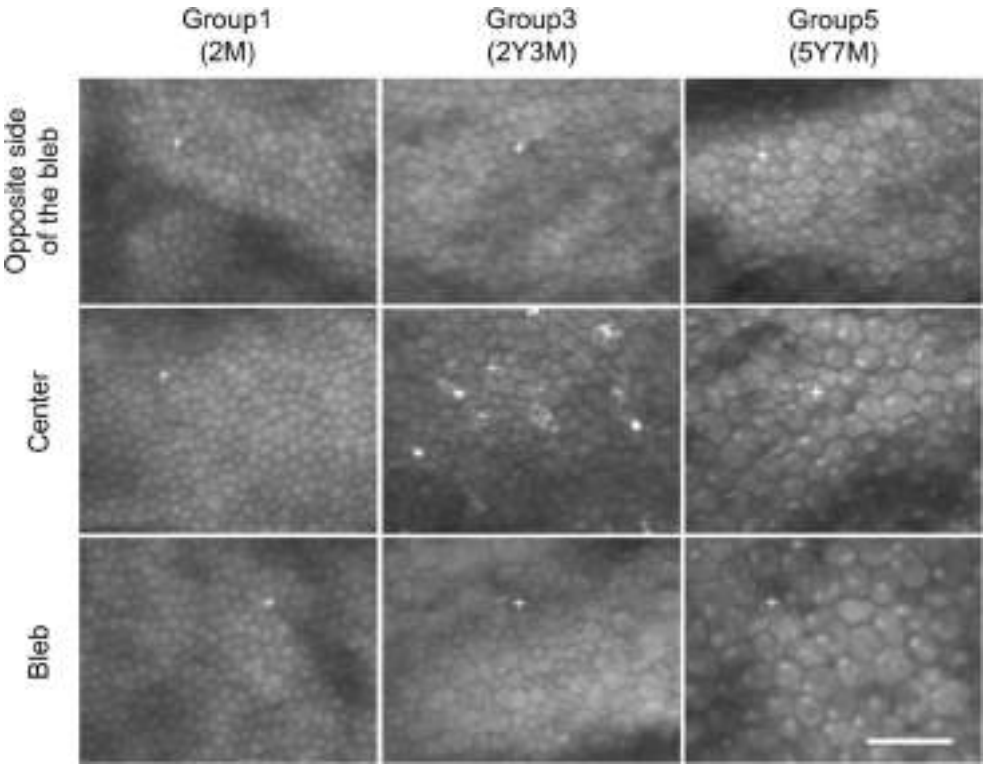

Fig. 2 Representative corneal endothelial cell (CEC) images obtained at different times in the postoperative period. Representative CEC images obtained by slit-scanning wide-field contact specular microscopy. The patients of group 1 had CECs of similar density and morphology in all areas. The patients of group 3 had CECs of similar density and morphology at the opposite side of the bleb and in the cornea center, but the CEC density was lower and the cell size was more variable. The patients of group 5 showed a more evident density decrease near the bleb area and the density also declined in the center, while the cell size increased at the opposite side of the bleb. Scale bar: 50μm

(approximately 5 mm from the center) [6]. Consistent with the suggestion by Arnavielle and colleagues [3], we demonstrated a significantly lower CEC density near the bleb than at the opposite side of the bleb and at the cornea center. The higher coefficient of variation and lower percentages of hexagonal cells at the area near the bleb than at the center also support impairment of the CECs in the area close to the filtration bleb. We showed that cell density significantly decreases throughout the 5 years of follow-up, but only in the area near the bleb and not in the center or at the opposite side of the bleb. Our results indicate that CEC loss continued over at least 5 years, that damage to the CECs was initiated in the bleb area, and that the damage might spread to the center and to the opposite side of the bleb by a compensating migration of residual CECs.

Several mechanisms of CEC loss after trabeculectomy have been postulated, such as direct damage to CECs by high IOP, cytotoxicity of glaucoma eye drops, intraoperative damage, hypoxic damage by impaired aqueous humor flow, and the intraoperative use of MMC [2, 12–14]. Among these proposed mechanisms, intraoperative use of MMC is consistent with our findings that CECs close to the bleb were continuously damaged over the long term, as MMC theoretically has the potential to damage CECs in both at short and long terms [15, 16]. Though the concentration and duration of intraoperative MMC varies from report to report [17], we applied 0.4 mg/ml MMC subconjunctivally for 5 min in the present study. If MMC is toxic to the corneal endothelium, analyzing the CEC density close to the bleb might be beneficial for optimization of MMC use during trabeculectomy (i.e., the concentration of MMC, duration of MMC treatment, and the positioning of the MMC soaked surgical sponge). Gagnon and colleagues showed that the corneal endothelial cell density is lower in the patients with glaucoma than in patients without glaucoma, and they proposed that high IOP, congenital alteration of corneal endothelium of glaucoma patients, and cytotoxicity of glaucoma eye drops are the mechanisms of cell loss [14]. However, other researchers have reported no cell density drop [18, 19]. Therefore, the involvement of these mechanisms in the cell loss after trabeculectomy cannot be discounted. Other possible explanations are that CECs were damaged by chronic inflammation induced by the bleb, jet flow of aqueous humor, and peripheral CEC migration from the cut edge of the cornea/trabeculum into the bleb, followed by subsequent cell death, but further study is needed.

The limitations of the current study include its cross-sectional study design, the inclusion of both eyes from some patients, and the potential for variation between the groups in the baseline characteristics of the patients. Another concern is the effect of combined cataract surgery conducted as one-site surgery on the density of superior CEC, although no significant difference was detected between patients who underwent trabeculectomy alone and patients who underwent trabeculectomy combined with cataract surgery. A prospective study is needed for a better evaluation of the role of the bleb in CEC loss after trabeculectomy.

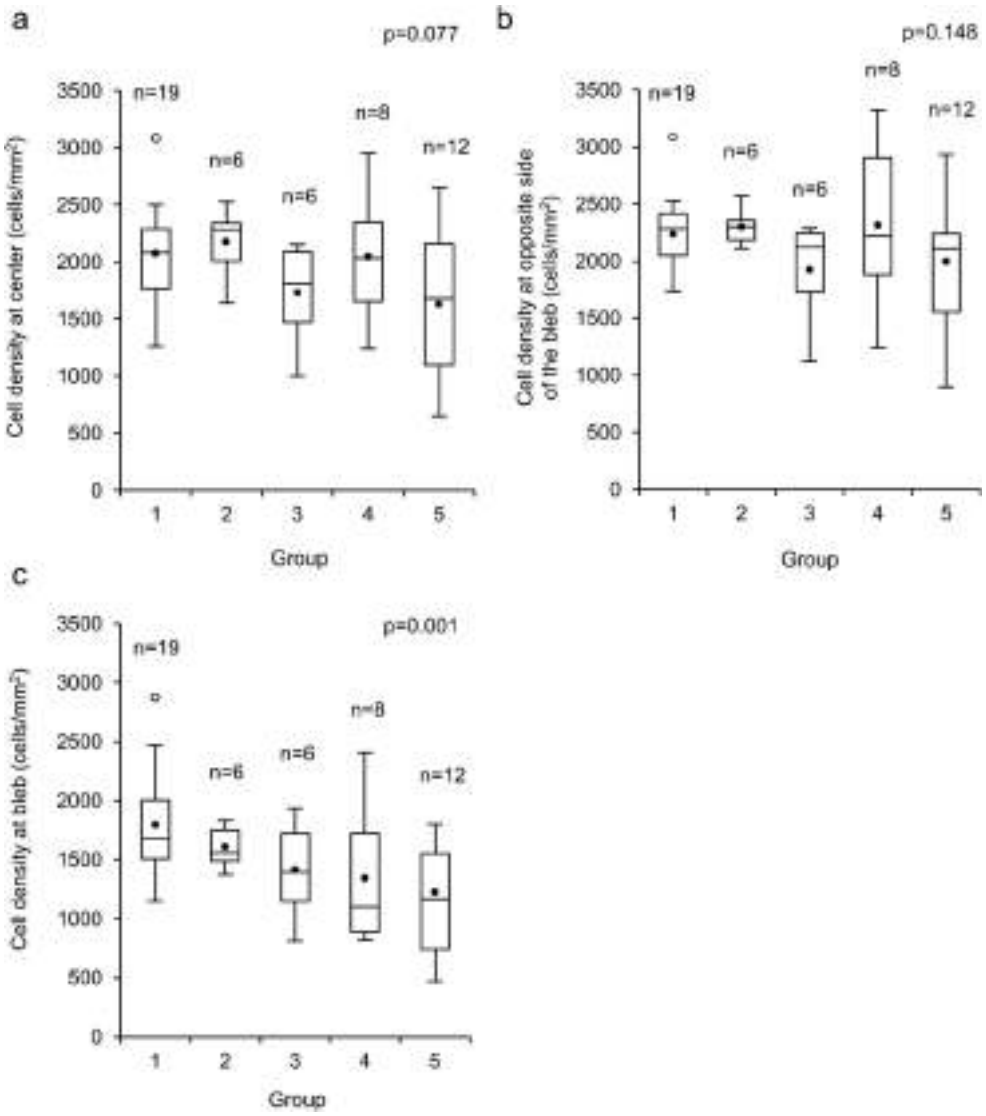

Fig. 3 Effect of the postoperative period on the corneal endothelial cell (CEC) density. **a** Effect of postoperative period on the CEC density at the corneal center. The black symbols indicate the mean value, the horizontal lines in the boxes indicate medians, the bottom of each box indicates the 25th percentile, and the top of each box indicates the 75th percentile. The horizontal lines outside the boxes indicate the range of CEC density. Values beyond 1.5 times the interquartile range were considered outliers (circles). **b** Effect of postoperative period on the CEC density at the opposite side of the bleb. **c** Effect of postoperative period on the CEC density in the bleb

In conclusion, we found that CEC density close to the filtration bleb decreased following trabeculectomy, even though the density at the cornea center did not decrease. Involvement of the filtration bleb in CEC density loss should be further examined to elucidate the pathology of CEC loss following trabeculectomy.

Funding No funding was received for this research.

Compliance with ethical standards

Conflict of interest All authors certify that they have no affiliations with or involvement in any organization or entity with any financial interest (such as honoraria; educational grants; participation in speakers' bureaus; membership, employment, consultancies, stock ownership, or other equity interest; and expert testimony or patent-licensing arrangements), or non-financial interest (such as personal or professional relationships, affiliations, knowledge or beliefs) in the subject matter or materials discussed in this manuscript.

Informed consent Informed consent was obtained from all individual participants included in the study.

Ethical approval All procedures performed in studies involving human participants were in accordance with the ethical standards of the institutional and/or national research committee and with the 1964 Helsinki Declaration and its later amendments or comparable ethical standards.

Financial interest The authors have no proprietary interest in this study.

References

1. Edmunds B, Thompson JR, Salmon JF, Wormald RP (2002) The National Survey of trabeculectomy. III. Early and late complications. Eye (Lond) 16:297–303. https://doi.org/10.1038/sj/eye/6700148
2. Sihota R, Sharma T, Agarwal HC (1998) Intraoperative mitomycin C and the corneal endothelium. Acta Ophthalmol Scand 76:80–82

3. Arnavielle S, Lafontaine PO, Bidot S, Creuzot-Garcher C, D'Athis P, Bron AM (2007) Corneal endothelial cell changes after trabeculectomy and deep sclerectomy. J Glaucoma 16:324–328. https://doi.org/10.1097/IJG.0b013e3180391a04
4. Storr-Paulsen T, Norregaard JC, Ahmed S, Storr-Paulsen A (2008) Corneal endothelial cell loss after mitomycin C-augmented trabeculectomy. J Glaucoma 17:654–657. https://doi.org/10.1097/IJG.0b013e3181659e56
5. Kim MS, Kim KN, Kim CS (2016) Changes in corneal endothelial cell after Ahmed glaucoma valve implantation and trabeculectomy: 1-year follow-up. Korean J Ophthalmol 30:416–425. https://doi.org/10.3341/kjo.2016.30.6.416
6. Tanaka H, Okumura N, Koizumi N, Sotozono C, Sumii Y, Kinoshita S (2016) Panoramic view of human corneal endothelial cell layer observed by a prototype slit-scanning wide-field contact specular microscope. Br J Ophthalmol DOI. https://doi.org/10.1136/bjophthalmol-2016-308893
7. Anderson D, Patella V (1999) Automated static Perimetry, 2nd edn. Mosby and Co, St Luis, pp 152–153
8. Mishima S (1982) Clinical investigations on the corneal endothelium. Ophthalmology 89:525–530
9. Joyce NC (2003) Proliferative capacity of the corneal endothelium. Prog Retin Eye Res 22:359–389
10. Bourne WM, McLaren JW (2004) Clinical responses of the corneal endothelium. Exp Eye Res 78:561–572
11. Tan DT, Dart JK, Holland EJ, Kinoshita S (2012) Corneal transplantation. Lancet 379:1749–1761. https://doi.org/10.1016/S0140-6736(12)60437-1
12. Setala K (1979) Corneal endothelial cell density after an attack of acute glaucoma. Acta Ophthalmol 57:1004–1013
13. Dreyer EB, Chaturvedi N, Zurakowski D (1995) Effect of mitomycin C and fluorouracil-supplemented trabeculectomies on the anterior segment. Arch Ophthalmol 113:578–580
14. Gagnon MM, Boisjoly HM, Brunette I, Charest M, Amyot M (1997) Corneal endothelial cell density in glaucoma. Cornea 16:314–318
15. Derick RJ, Pasquale L, Quigley HA, Jampel H (1991) Potential toxicity of mitomycin C. Arch Ophthalmol 109:1635
16. McDermott ML, Wang J, Shin DH (1994) Mitomycin and the human corneal endothelium. Arch Ophthalmol 112:533–537
17. Cabourne E, Clarke JC, Schlottmann PG, Evans JR (2015) Mitomycin C versus 5-fluorouracil for wound healing in glaucoma surgery. Cochrane database Syst rev: CD006259. https://doi.org/10.1002/14651858.CD006259.pub2
18. Korey M, Gieser D, Kass MA, Waltman SR, Gordon M, Becker B (1982) Central corneal endothelial cell density and central corneal thickness in ocular hypertension and primary open-angle glaucoma. Am J Ophthalmol 94:610–616
19. Kwon JW, Rand GM, Cho KJ, Gore PK, McCartney MD, Chuck RS (2016) Association between corneal endothelial cell density and topical glaucoma medication use in an eye Bank donor population. Cornea 35:1533–1536. https://doi.org/10.1097/ICO.0000000000000972

Involvement of Nectin–Afadin in the Adherens Junctions of the Corneal Endothelium

Naoki Okumura, MD, PhD, Takato Kagami, BS, Keita Fujii, BS, MS, Makiko Nakahara, PhD, and Noriko Koizumi, MD, PhD

Purpose: The cell–cell adhesion molecules, cadherins and nectins, are involved in the formation of adherens junctions. However, involvement of nectins in the corneal endothelium has not yet been established. This study investigated the involvement of nectins in adherens junctions of the corneal endothelium.

Methods: Nectin and cadherin expression in the corneal endothelium was evaluated by real-time polymerase chain reaction. Colocalization and direct binding of nectin-1 and N-cadherin to anchoring proteins (afadin and β-catenin, respectively) were determined by immunostaining and immunoprecipitation. The effect of afadin and N-cadherin knockdown on apical junctions was evaluated by immunostaining.

Results: Real-time polymerase chain reaction confirmed nectin-1, nectin-2, nectin-3, nectin-4, and afadin expression in the corneal endothelium. Immunofluorescence staining showed colocalization of nectin and afadin at the basal side of the tight junction (where adherens junctions typically locate) and immunoprecipitation confirmed direct binding of nectin to afadin. N-cadherin, P-cadherin, VE-cadherin, and OB-cadherin messenger RNAs were expressed in the corneal endothelium. N-cadherin and β-catenin colocalized at the cell–cell border, where they directly bound and formed a cell–cell adhesion complex. N-cadherin knockdown disrupted the normal expression pattern of zonula occludens protein-1 and afadin, but afadin knockdown had no effect on the expression pattern of zonula occludens protein-1 and N-cadherin.

Conclusions: We believe this to be the first report of conservation of the nectin–afadin system in the corneal endothelium and its involvement in the formation of adherens junctions. N-cadherin, as a member of the cadherin family, is also essential for the formation and maintenance of cell–cell adhesion mediated by nectins and tight junctions in the corneal endothelium.

Received for publication October 16, 2017; revision received December 3, 2017; accepted December 15, 2017. Published online ahead of print January 30, 2018.

From the Department of Biomedical Engineering, Faculty of Life and Medical Sciences, Doshisha University, Kyotanabe, Japan.

Supported by the Program for the Strategic Research Foundation at Private Universities from MEXT (N. Koizumi and N. Okumura).

The authors have no conflicts of interest to disclose.

Supplemental digital content is available for this article. Direct URL citations appear in the printed text and are provided in the HTML and PDF versions of this article on the journal's Web site (www.corneajrnl.com).

Correspondence: Noriko Koizumi, MD, PhD, Department of Biomedical Engineering, Faculty of Life and Medical Sciences, Doshisha University, Kyotanabe 610-0321, Japan (e-mail: nkoizumi@mail.doshisha.ac.jp).

Key Words: corneal endothelium, adherens junctions, nectin

(*Cornea* 2018;37:633–640)

The corneal endothelium regulates the amount of water in the corneal stroma, thereby maintaining corneal transparency. The cornea is an avascular tissue, so aqueous humor movement from the anterior chamber to the stroma, and from the stroma to the anterior chamber, is necessary for nutrition of the stroma. The essential roles of corneal endothelial cells (CECs) are their pump and "leaky barrier" functions, which balance the inflow of aqueous humor into the corneal stroma and its outflow to the anterior chamber.[1]

The apical junction, comprising adherens junctions and tight junctions, acts as a paracellular barrier, ensures cell polarity, and serves as a scaffold for signaling.[2] The tight junctions, located at the apical–lateral border, provide a barrier function for the epithelial cells by inhibiting the transport of large molecules. Adherens junctions are typically located on the basal side of tight junctions in mammalian epithelial cells.[3] They promote the formation of tight junctions and stabilize the barrier function.[4]

The formation of adherens junctions depends on cell–cell adhesion molecules, such as those of the cadherin superfamily, which includes over 70 proteins in mammals. Cadherins are Ca^{2+}-dependent molecules and exclusively regulate the intercellular junctions between cells that express the same types of cadherin.[2] Among the members of this superfamily, classical cadherins such as E-, N-, and P-cadherins have been extensively studied. N-cadherin is found in neurons and is detected in cells of neural and mesodermal origin. In the corneal epithelium, the nature of the cadherin members that regulate adherens junctions remains to be established, but N-cadherin is believed to play an important role.[5,6]

Another family of cell–cell adhesion molecules associated with adherens junctions is the nectins, which include 4 members: nectin-1, nectin-2, nectin-3, and nectin-4.[7,8] Unlike the cadherins, nectins are not dependent on Ca^{2+}, and they interact with both same and different nectin members.[7–9] Nectin is involved in cell–cell adhesion in various cell types, such as synapses in the hippocampus,[10] axons, and floor plate cells in the neural tube,[11] and Sertoli cells and germ cells in the testis.[12] However, to the best of our knowledge, involvement of nectin in the corneal endothelium has not been previously reported. In this study, we conducted

experiments to provide additional knowledge about apical junctions and especially to examine whether nectins and afadin (nectin-anchoring protein that bind to the actin cytoskeleton[8,13,14]) are involved in the formation of adherens junctions in the corneal endothelium.

MATERIALS AND METHODS

Ethics Statement

Human tissue used in this study was handled in accordance with the tenets set forth in the Declaration of Helsinki. Human donor corneas were obtained from SightLife (Seattle, WA). Informed written consent was obtained from the next of kin of all deceased donors for eye donation for research. All tissues were recovered under the tenets of the Uniform Anatomical Gift Act (UAGA) of the particular state in which the donor consent was obtained and the tissue was recovered. The cynomolgus monkey corneas used in this study were handled in accordance with the ARVO Statement for the Use of Animals in Ophthalmic and Vision Research. The protocols for general welfare of the monkeys and the procedures for isolation of the corneas were approved by the institutional animal care and use committee of Nissei Bilis Co, Ltd.

Reverse Transcription Polymerase Chain Reaction

Corneal endothelium and epithelium were scraped from 4 independent human donor corneas and 1 monkey donor cornea. Total RNA was extracted using the RNeasy Mini kit (Qiagen, Hilden, Germany) and the quality of the extracted RNA was measured with a NanoDrop spectrophotometer (Thermo Fisher Scientific Inc, Waltham, MA). First-strand complementary DNA was synthesized with 1 μg of total RNA using a ReverTra Ace reverse transcriptase kit (Toyobo Corporation, Osaka, Japan). The primers used for polymerase chain reaction (PCR) are listed in Supplemental Digital Content 1 (see Table, http://links.lww.com/ICO/A623). PCR reactions were performed with Extaq DNA polymerase (Takara Bio Inc, Otsu, Japan) under the following conditions: denaturation at 94°C for 30 seconds, 32 to 35 cycles of annealing at 54 to 60°C for 30 seconds, and elongation at 72°C for 30 seconds. The PCR products were separated by electrophoresis on 1.5% agarose gels in Tris-acetate buffer, stained with ethidium bromide, and analyzed with an LAS4000S luminescence imager (Fuji Film, Tokyo, Japan).

Immunofluorescence Staining

The monkey corneal endothelial cells (MCECs) were cultured as described previously.[15] Human corneal specimens and cultured MCECs were fixed in 0.5% formaldehyde and incubated in 2% bovine serum albumin for 30 minutes at room temperature to block nonspecific binding. Samples were incubated overnight at 4°C with antibodies against nectin-1 (1:300; Abcam, Cambridge, United Kingdom), afadin (1:300; Sigma-Aldrich Co, St. Louis, MO), N-cadherin (1:300; BD Biosciences, San Jose, CA), E-cadherin (1:200; BD Biosciences), β-catenin (1:200; Santa Cruz Biotechnology, Santa Cruz, CA), and zonula occludens (ZO) protein-1 (1:300; Life Technologies Corp, Carlsbad, CA). Alexa Fluor 488-conjugated goat anti-mouse (Life Technologies) was used as a secondary antibody at a 1:1000 dilution. Cell morphology was evaluated after actin staining with a 1:400 dilution of Alexa Fluor 594-conjugated phalloidin (Life Technologies). Nuclei were stained with 4′,6-diamidino-2-phenylindole (Dojindo Laboratories, Kumamoto, Japan). The samples were viewed with a fluorescence microscope (TCS SP2 AOBS; Leica Microsystems, Wetzlar, Germany). For confocal *z*-axis stacks, 40 images separated by 0.27 μm along the *z*-axis were acquired. The Manders colocalization coefficients were determined with ImageJ and the VolumeJ plugin for ImageJ.

Immunoblotting

The MCECs were washed with ice-cold phosphate-buffered saline, lysed with ice-cold radioimmunoprecipitation assay buffer containing phosphatase inhibitor cocktail 2 (Sigma-Aldrich Co) and protease inhibitor cocktail (Roche Applied Science, Penzberg, Germany), and then centrifuged. The supernatant containing the total protein was collected and an equal amount of protein was fractionated by sodium dodecyl sulfate-poly acrylamide gel electrophoresis and blotted onto polyvinylidene fluoride membranes. The polyvinylidene fluoride membranes were blocked with 3% nonfat dry milk, followed by an overnight incubation at 4°C with the following primary antibodies: afadin (1:1000; Sigma-Aldrich Co), nectin-1 (1:1000; Thermo Fisher Scientific Inc), N-cadherin (1:1000; BD Biosciences), β-catenin (1:1000; Santa Cruz Biotechnology), ZO-1 (1:500; Life Technologies Corp), rabbit IgG (1:1000; Cell Signaling Technology Inc, Danvers, MA), and GAPDH (1:3000; Medical & Biological Laboratories Co, Ltd, Nagoya, Japan). The blots were washed and incubated with horseradish peroxidase–conjugated secondary antibodies (1:5000; Cell Signaling Technology). The blots were developed with luminal for enhanced chemiluminescence using the Chemi-Lumi One Ultra (Nacalai Tesque, Kyoto, Japan), and documented using an LAS4000S luminescence imager (Fuji Film).

Immunoprecipitation Assays

The MCECs were washed with ice-cold phosphate-buffered saline, lysed with ice-cold radioimmunoprecipitation assay buffer containing protease inhibitor cocktail, centrifuged, and the supernatant representing total proteins was collected. The protein was incubated at 4°C for 1 hour with primary antibodies: 5 μg N-cadherin antibody (BD Biosciences), 5 μg nectin antibody (Life Technologies Corp), 5 μg afadin antibody (Sigma-Aldrich Co), and 1 μg normal rabbit IgG (Santa Cruz Biotechnology). The samples were then incubated at 4°C for 1 hour with 50% (vol/vol) ProteinG Sepharose (GE Healthcare, Piscataway, NJ). Samples were then used in immunoblotting assays.

Knockdown of Genes by Small Interfering RNA

The MCECs were seeded into a 24-well plate (Corning, NY) and cultured until they reached 50% to 70% confluence. The MCECs were then incubated with RNAi duplex (*CDH2*, *TJP1*, and *MLLT4*) and Lipofectamine RNAiMAX (Life Technologies Corp), according to the manufacturer's protocol. Random RNAi low guanine-cytosine (GC) was used as a control, and real-time polymerase chain reaction (RT-PCR) was performed to assess the knockdown of *CDH2*, *TJP1*, and *MLLT4*.

Statistical Analysis

Statistical analysis was performed with the Excel software program (Microsoft Corporation, Redmond, WA). Statistical significance (*P* value) of mean values of the 2-sample comparison was determined with the Student *t* test. $P < 0.05$ was considered statistically significant. Values shown represent mean ± SEM.

RESULTS

Expression of Nectins and Afadin in the Corneal Endothelium

Our evaluation of the expression of nectins and afadin in corneal endothelium by RT-PCR showed that *PVRL1*, *PVRL2*, *PVRL3*, *PVRL4*, and *MLLT4* (which encode nectin-1, nectin-2, necton-3, nectin-4, and afadin, respectively) were expressed in corneal endothelium derived from a human donor cornea (Fig. 1A). The corneal epithelium, which was used as a positive control, also expressed *PVRL1*, *PVRL2*, *PVRL3*, *PVRL4*, and *MLLT4*. We also confirmed the expression of *PVRL1*, *PVRL2*, *PVRL3*, *PVRL4*, and *MLLT4* in corneal endothelium obtained from 3 additional independent donors (Fig. 1B). Immunofluorescence staining showed that nectin-1 and afadin were colocalized at the cell–cell junction in both corneal endothelium and the corneal epithelium (Fig. 1C). Nectins are known to bind directly to afadin, which is an F-actin-binding protein in other kinds of cells. Our immunoprecipitation experiments showed that nectin-1 and afadin were coimmunoprecipitated in cultured MCECs (Fig. 1D).

Expression of Cadherins and Catenins in the Corneal Endothelium

RT-PCR showed that *CDH2*, *CDH3*, *CDH5*, and *CDH11* (which encode N-cadherin, P-cadherin, VE-cadherin, and OB-cadherin, respectively) were expressed in the corneal endothelium, whereas *CDH1*, *CDH4*, *CDH6*, and *CDH7* (which encode E-cadherin, R-cadherin, K-cadherin, and CDH7, respectively) were not expressed (Fig. 2A). The expression pattern of the cadherin types differed between the corneal epithelium and endothelium; notably, E-cadherin was expressed in the corneal epithelium but not in the corneal endothelium.

Catenins are a family of proteins found in cell–cell adhesion complexes, and adherens junctions typically include at least α-catenin and β-catenin. We confirmed the expression of catenin family proteins, and showed that *CTNNA1*, *CTNNB1*, *JUP*, and *CTNND1* (which encode α-catenin, β-catenin, γ-catenin, and p120-catenin, respectively) were

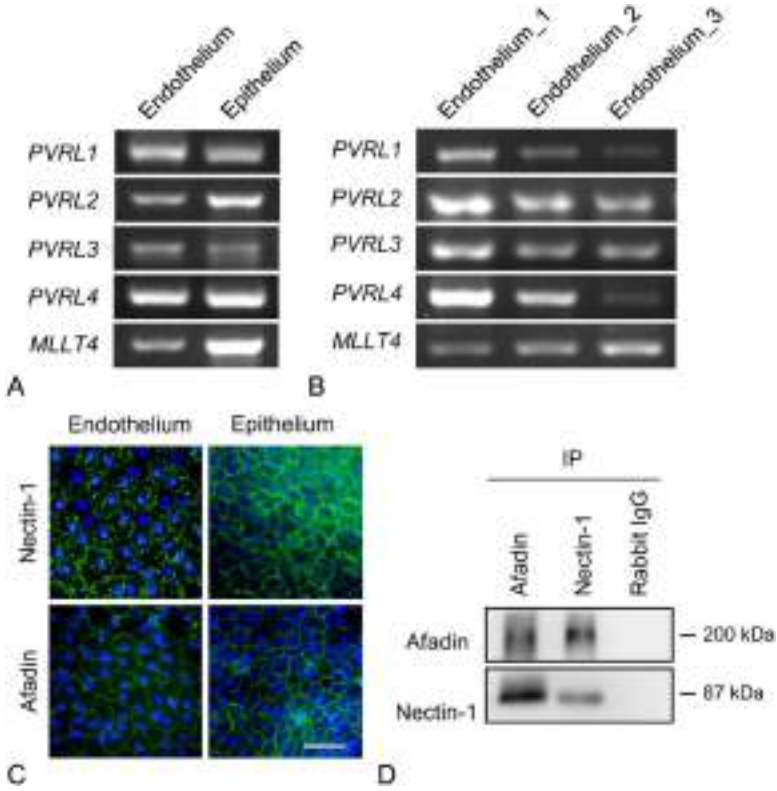

FIGURE 1. Expression of nectin and afadin in the corneal endothelium. A, Expression of 4 nectin members and afadin in the corneal endothelium obtained from human donor corneas was evaluated by RT-PCR. *PVRL1*, *PVRL2*, *PVRL3*, *PVRL4*, and *MLLT4*, which encode nectin-1, nectin-2, nectin-3, nectin-4, and afadin, respectively, were expressed at the mRNA level. *PVRL1*, *PVRL2*, *PVRL3*, *PVRL4*, and *MLLT4* were detected in corneal epithelium used as a positive control. B, Expression of *PVRL1*, *PVRL2*, *PVRL3*, *PVRL4*, and *MLLT4* was further confirmed in corneal endothelium obtained from 3 additional independent donors. C, Expression of nectin-1 and afadin in human donor corneas was evaluated by immunofluorescence staining. Expression of nectin and afadin was observed at the cell–cell border in both corneal endothelium and epithelium. Representative images from 3 independent donor corneas are shown. Scale bar: 50 μm. D, Direct binding of nectin and afadin was evaluated by immunoprecipitation assays by the use of cultured MCECs. Nectin-1 and afadin were coimmunoprecipitated, which suggests that nectin-1 and afadin were directly bound in the corneal endothelium. Experiments were performed in triplicate.

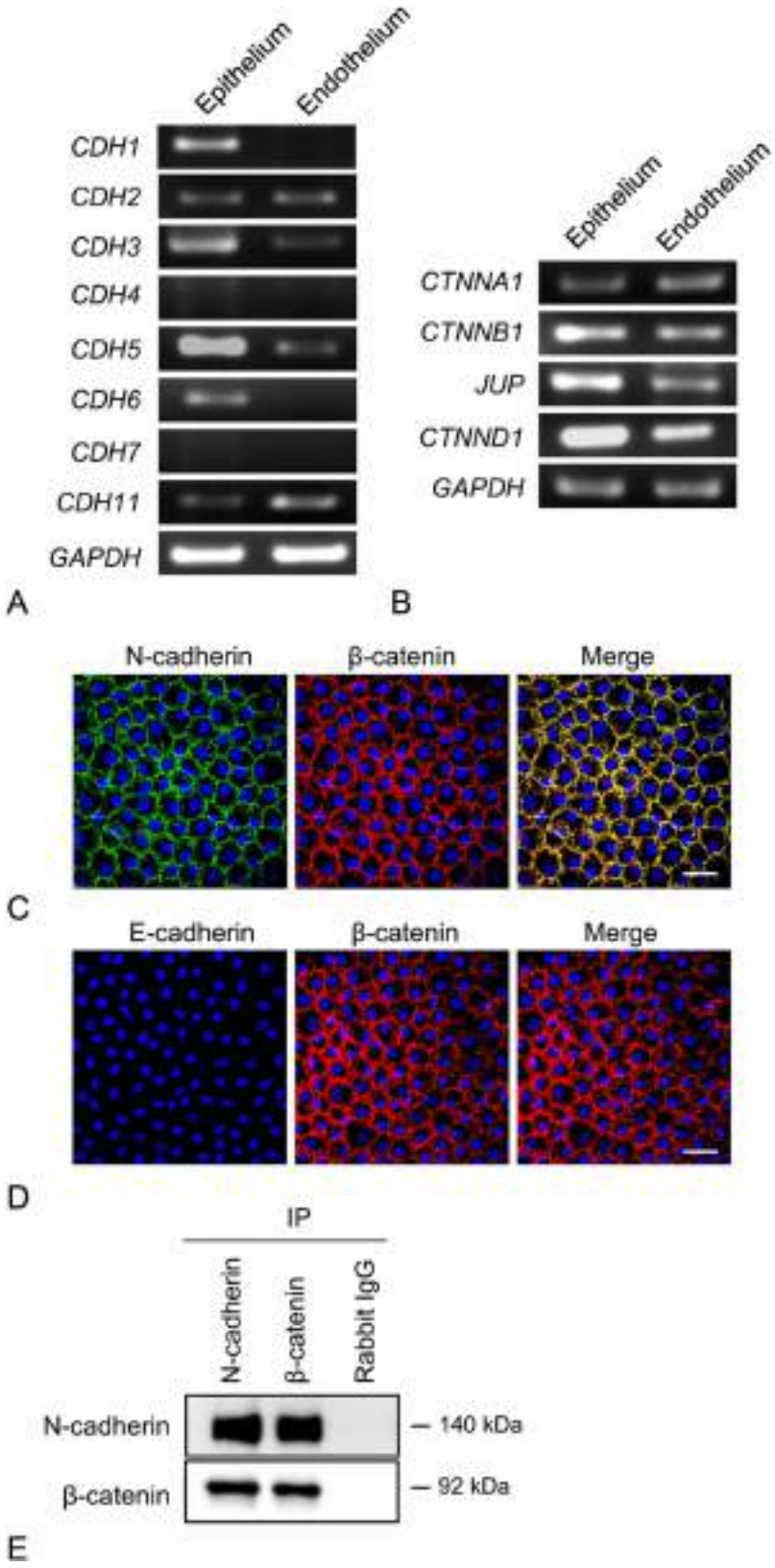

FIGURE 2. Expression of cadherins and catenins in the corneal endothelium. A, Expression of various types of cadherin and catenin in the human corneal endothelium obtained from donor corneas was evaluated by RT-PCR. *CDH2*, *CDH5*, and *CDH11* were expressed in the corneal endothelium, whereas *CDH1*, *CDH3*, *CDH4*, *CDH6*, and *CDH7* were not expressed at the mRNA level. B, Expression of various types of catenins was evaluated by RT-PCR. *CTNNA1*, *CTNNB1*, *JUP*, and *CTNND1* were expressed in the corneal endothelium, as well as in the corneal epithelium, which was used for the control. The experiment was performed in triplicate. C and D, Expression of N-cadherin and E-cadherin in human corneal endothelium was evaluated by immunofluorescence staining. N-cadherin and β-catenin were expressed at the cell–cell border and the merge image showed that they are colocalized, but E-cadherin was not detected. Scale bar: 100 μm. E, Direct binding between N-cadherin and β-catenin was evaluated by immunoprecipitation. N-cadherin and β-catenin were coimmunoprecipitated in cultured MCECs. The experiment was performed in triplicate.

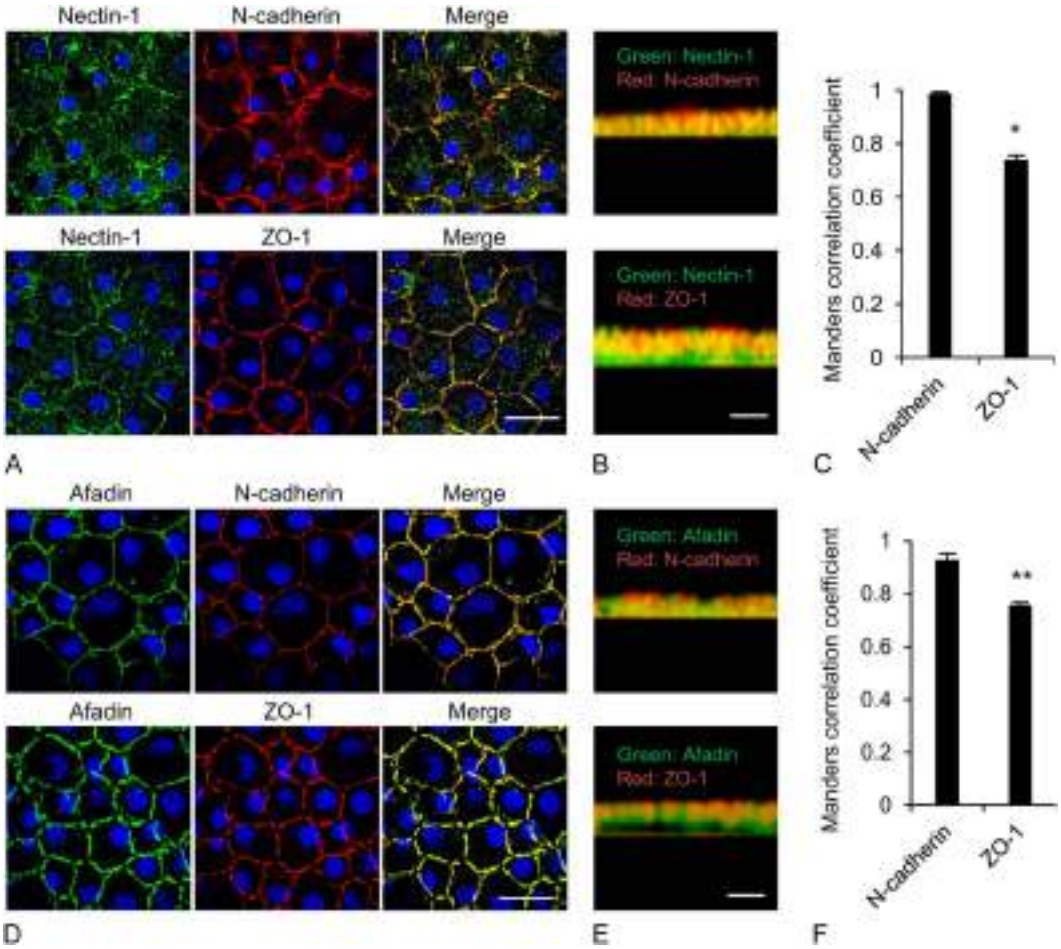

FIGURE 3. Localization of nectin and afadin in cell–cell adhesions. A, Human donor corneas were evaluated by immunofluorescence staining. Flat mount images showed that nectin-1 expression at the cell borders and colocalization with N-cadherin and ZO-1. Scale bar: 25 μm. B, For confocal *z*-axis stacks, 40 images separated by 0.27 μm along the *z*-axis were acquired. A sectional image obtained from confocal *z*-axis stacks showed that nectin-1 was widely costained with N-cadherin; however, nectin-1 was less costained with ZO-1 and tended to distribute beneath the ZO-1. C, Costaining of nectin-1/ZO-1 and nectin-1/N-cadherin was evaluated with ImageJ software. The Manders correlation coefficient was significantly lower for nectin-1 and ZO-1 than for nectin-1 and N-cadherin (0.74 and 0.99, respectively). Three images from 3 independent donor corneas were used for the analysis. The statistical analysis was performed using the Student *t* test. $*P < 0.01$. D, Flat mount images of human donor corneas showed that afadin expression at the cell borders and colocalization with N-cadherin and ZO-1. Scale bar: 25 μm. E, Sectional image obtained from confocal *z*-axis stack showed that afadin was widely costained with N-cadherin; however, afadin was less costained with ZO-1 and tended to distribute beneath the ZO-1. F, Costaining of afadin/ZO-1 and afadin/N-cadherin was evaluated by ImageJ software. The Manders correlation coefficient was significantly lower for afadin and ZO-1 than for afadin and N-cadherin (0.76 and 0.93, respectively). Three images from 3 independent donor corneas were used for the analysis. The statistical analysis was performed using the Student *t* test. $**P < 0.05$.

expressed in the corneal endothelium, as well as in the corneal epithelium (Fig. 2B).

Beta-catenin is a subunit of the cadherin protein complex, so we evaluated the distribution of N-cadherin and β-catenin in the human corneal endothelium. Immunofluorescence staining showed that N-cadherin and β-catenin were colocalized at the cell–cell junction, whereas E-cadherin was not expressed at either the messenger RNA (mRNA) or the protein level (Figs. 2C, D). The immunoprecipitation experiment with cultured MCECs then confirmed that N-cadherin and β-catenin were directly bound to form the cell–cell adhesion complex (Fig. 2E).

Localization of Nectin and Afadin in Apical Junctions

Immunofluorescence staining confirmed the expression of nectin-1 at cell–cell junctions and its colocalization with N-cadherin and ZO-1 in human donor corneas (Fig. 3A). Images obtained from confocal *z*-axis stacks showed that nectin-1 was widely costained with N-cadherin; however, nectin-1 was stained at the basal side of ZO-1 staining (Figs. 3B, C). Similarly, flat mount images showed that afadin was expressed at the cell–cell junction and colocalized with N-cadherin and ZO-1 (Fig. 3D). Confocal *z*-axis

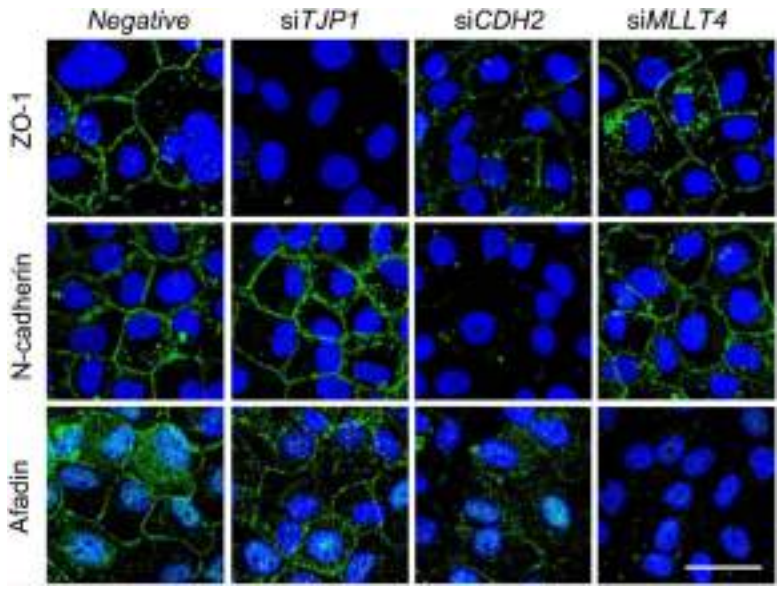

FIGURE 4. Effect of cellular stress on adherens junctions. Expression patterns and levels of ZO-1, N-cadherin, and afadin were evaluated in MCECs by immunofluorescence staining after knockdown of ZO-1, N-cadherin, and afadin. Knockdown of ZO-1 did not affect the formation of N-cadherin and afadin, and N-cadherin and afadin were expressed at the cell–cell border. The expression pattern of ZO-1 and N-cadherin was not altered in the afadin knockdown cells. However, knockdown of N-cadherin cause wide, but not complete, disruption of the normal expression pattern of ZO-1 and afadin. Representative images from 3 independent experiments are shown. Scale bar: 25 μm.

stacks showed that afadin was widely costained with N-cadherin, whereas afadin was observed at the basal side of ZO-1 (Figs. 3E, F).

Role of the Nectin–Afadin Complex in the Formation of Apical Junctions

We conducted experiments to evaluate the role of the nectin–afadin complex in the formation of adherens junctions and tight junctions using small interfering RNA (see Figure, Supplemental Digital Content 2, http://links.lww.com/ICO/A624). Immunofluorescence staining showed that knockdown of ZO-1 by small interfering RNA did not affect the formation of N-cadherin and afadin, because N-cadherin and afadin were expressed at the cell–cell junction. Likewise, the expression pattern of ZO-1 and N-cadherin was not altered in the afadin knockdown cells. Conversely, knockdown of N-cadherin caused a wide but not complete disruption of the normal expression pattern of ZO-1 and afadin (Fig. 4).

DISCUSSION

Nectins are members of adherens junction, but their involvement in corneal endothelium has not yet been

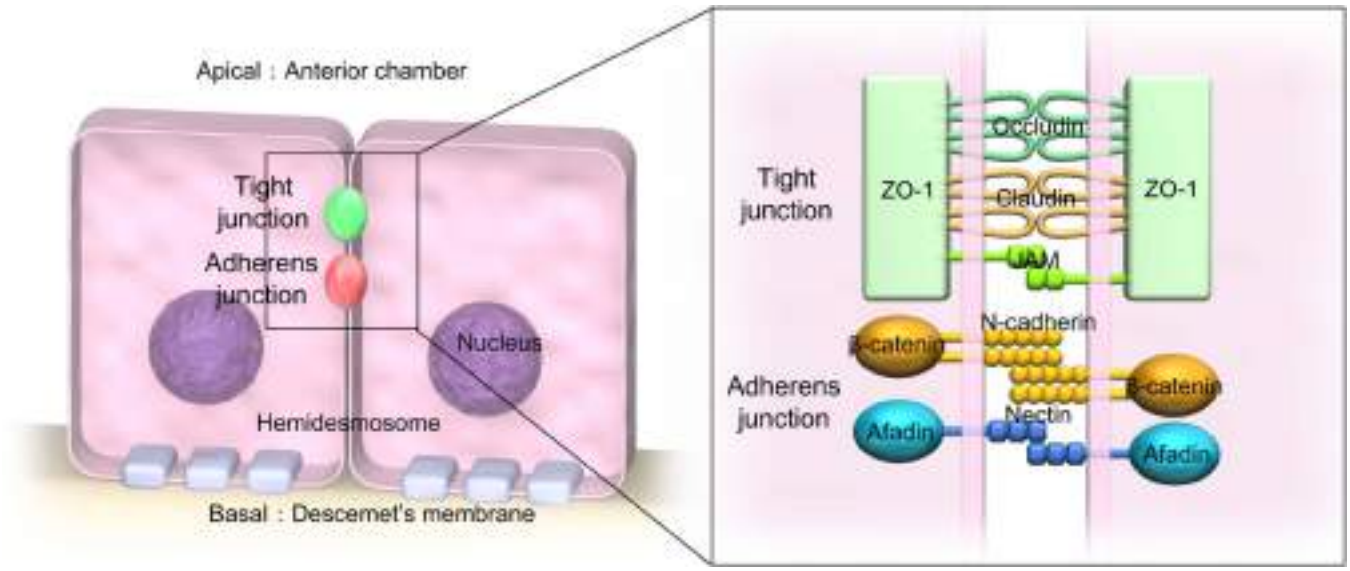

FIGURE 5. Schematic image of apical junction of corneal endothelium. A schematic image of the cell–cell adhesion in corneal endothelium taking into account the results of this study and previous studies by other researchers is shown. The nectin–afadin complex is involved in the formation of adherens junctions and N-cadherin-β-catenin complexes. The adherens junction is located at the basal side of a tight junction, as in other cell types. In tight junctions, adhesion molecules, such as claudins, occludin, and junctional adhesion molecules, bind to anchoring proteins, such as the ZO.

elucidated. In this study, we showed the expression of 4 types of nectins (*PVRL1*, *PVRL2*, *PVRL3*, and *PVRL4*, which encode nectin-1, nectin-2, nectin-3, and nectin-4, respectively) in human corneal endothelium. Adhesion molecules, such as cadherins and nectins, bind to anchoring proteins, such as catenins and afadin.[8,13,14] The functional modules comprising adhesion molecules and anchoring proteins then bind to the actin cytoskeleton.[16] We demonstrated that afadin (the anchoring protein for nectins) is expressed in CECs, and nectin binds directly to this afadin to form functional modules. Confocal *z*-axis stacks showed that nectin and afadin were distributed at the basal side of the tight junction, with N-cadherin. Taken together, our data suggest that the nectin–afadin system is conserved and is involved in the adherens junction of the corneal endothelium. Our schematic images showing the cell–cell adhesion in CECs take into account the results of this study, as well as previous studies by other researchers[17–19] (Fig. 5).

In addition to regulating cell–cell adhesion, nectins also regulate numerous other cellular functions, such as polarization, differentiation, proliferation, and cell movement in several cell types.[7–9] For example, the apicobasal cell polarity is initially decided by nectins. Cell–cell contact between Madin-Darby Canine Kidney cells is initiated by nectin at the protruding margin of the cells, followed by recruited clustering of E-cadherin to the nectin-based cell adhesion site.[20] Once the adherens junction has formed, tight junction modules are recruited and form tight junctions at the apical side of the adherens junction.[21] Nectins also play additional roles, apart from cell–cell adhesion, in cell differentiation. For example, nectin-1$^{-/-}$ mice show downregulated expression of the differentiation marker, loricrin, and have shiny and reddish skin, which suggests that nectin mediates differentiation during development.[22]

Nectin participation in broad and essential cell functions also extends to involvement in human diseases. For instance, Zlotogora-Ogur syndrome is induced by a mutation in *PVRL1*,[23,24] and an ectodermal dysplasia syndactyly syndrome is induced by a mutation in *PVRL4*.[25] Genome-wide association studies have revealed that a single-nucleotide polymorphism in *PVRL2* is associated with Alzheimer disease.[26,27] In the field of eye research, Lachke et al[28] have reported that nectin is connected to human ocular disease, as a mutation in *PVRL3* is associated with an disrupted mammalian lens and ciliary body development and induces severe bilateral congenital cataracts. In addition, nectins were originally identified as virus receptors, and they mediate virus entry.[7,8] Indeed, nectin-1 and nectin-2 can act as mediators of herpes simplex virus type 1 and 2 in ocular herpes.[29,30] At present, no diseases of the corneal endothelium have been linked to any abnormality in nectin, but involvement of nectins in maintaining homeostasis and their roles in pathological conditions or diseases are worthy of further investigation.

To the best of our knowledge, this is the first description of conservation of the nectin–afadin system in the corneal endothelium, and its involvement in the formation of the adherens junction. Because nectins cover broad and essential cell functions, further studies may be helpful for understanding the physiology and pathophysiology of the corneal endothelium.

ACKNOWLEDGMENTS

The authors thank Mr. Takashi Aiba for technical support.

REFERENCES

1. Dawson DG, Ubels LJ, Edelhauser FH. *Adler's Physiology of the Eye. 11th Edition*. Chapter 4 Cornea and Sclera. Amsterdam, Netherlands: Elsevier Inc; 2011:71–130.
2. Miyoshi J, Takai Y. Structural and functional associations of apical junctions with cytoskeleton. *Biochim Biophys Acta*. 2008;1778:670–691.
3. Farquhar MG, Palade GE. Junctional complexes in various epithelia. *J Cell Biol.* 1963;17:375–412.
4. Tsukita S, Furuse M. Occludin and claudins in tight-junction strands: leading or supporting players? *Trends Cell Biol*. 1999;9:268–273.
5. Reneker LW, Silversides DW, Xu L, et al. Formation of corneal endothelium is essential for anterior segment development—a transgenic mouse model of anterior segment dysgenesis. *Development*. 2000;127:533–542.
6. Vassilev VS, Mandai M, Yonemura S, et al. Loss of N-cadherin from the endothelium causes stromal edema and epithelial dysgenesis in the mouse cornea. *Invest Ophthalmol Vis Sci.* 2012;53:7183–7193.
7. Takai Y, Ikeda W, Ogita H, et al. The immunoglobulin-like cell adhesion molecule nectin and its associated protein afadin. *Annu Rev Cell Dev Biol.* 2008;24:309–342.
8. Takai Y, Miyoshi J, Ikeda W, et al. Nectins and nectin-like molecules: roles in contact inhibition of cell movement and proliferation. *Nat Rev Mol Cell Biol.* 2008;9:603–615.
9. Rikitake Y, Mandai K, Takai Y. The role of nectins in different types of cell-cell adhesion. *J Cell Sci.* 2012;125:3713–3722.
10. Mizoguchi A, Nakanishi H, Kimura K, et al. Nectin: an adhesion molecule involved in formation of synapses. *J Cell Biol.* 2002;156:555–565.
11. Okabe N, Shimizu K, Ozaki-Kuroda K, et al. Contacts between the commissural axons and the floor plate cells are mediated by nectins. *Dev Biol.* 2004;273:244–256.
12. Inagaki M, Irie K, Ishizaki H, et al. Role of cell adhesion molecule nectin-3 in spermatid development. *Genes Cells.* 2006;11:1125–1132.
13. Takai Y, Nakanishi H. Nectin and afadin: novel organizers of intercellular junctions. *J Cell Sci.* 2003;116:17–27.
14. Gumbiner BM. Regulation of cadherin-mediated adhesion in morphogenesis. *Nat Rev Mol Cell Biol.* 2005;6:622–634.
15. Koizumi N, Sakamoto Y, Okumura N, et al. Cultivated corneal endothelial cell sheet transplantation in a primate model. *Invest Ophthalmol Vis Sci.* 2007;48:4519–4526.
16. Tsukita S, Furuse M, Itoh M. Multifunctional strands in tight junctions. *Nat Rev Mol Cell Biol.* 2001;2:285–293.
17. Mandell KJ, Berglin L, Severson EA, et al. Expression of JAM-A in the human corneal endothelium and retinal pigment epithelium: localization and evidence for role in barrier function. *Invest Ophthalmol Vis Sci.* 2007;48:3928–3936.
18. Chen L, Ebihara N, Fujiki K, et al. Expression and distribution of junctional adhesion molecule-1 in the human cornea. *Jpn J Ophthalmol.* 2007;51:405–411.
19. Inagaki E, Hatou S, Yoshida S, et al. Expression and distribution of claudin subtypes in human corneal endothelium. *Invest Ophthalmol Vis Sci.* 2013;54:7258–7265.
20. Takai Y, Irie K, Shimizu K, et al. Nectins and nectin-like molecules: roles in cell adhesion, migration, and polarization. *Cancer Sci.* 2003;94:655–667.
21. Ohno S. Intercellular junctions and cellular polarity: the PAR-aPKC complex, a conserved core cassette playing fundamental roles in cell polarity. *Curr Opin Cell Biol.* 2001;13:641–648.
22. Wakamatsu K, Ogita H, Okabe N, et al. Up-regulation of loricrin expression by cell adhesion molecule nectin-1 through Rap1-ERK signaling in keratinocytes. *J Biol Chem.* 2007;282:18173–18181.

23. Suzuki K, Hu D, Bustos T, et al. Mutations of PVRL1, encoding a cell-cell adhesion molecule/herpesvirus receptor, in cleft lip/palate-ectodermal dysplasia. *Nat Genet.* 2000;25:427–430.
24. Yoshida K, Hayashi R, Fujita H, et al. Novel homozygous mutation, c.400C>T (p.Arg134*), in the PVRL1 gene underlies cleft lip/palate-ectodermal dysplasia syndrome in an Asian patient. *J Dermatol.* 2015;42: 715–719.
25. Brancati F, Fortugno P, Bottillo I, et al. Mutations in PVRL4, encoding cell adhesion molecule nectin-4, cause ectodermal dysplasia-syndactyly syndrome. *Am J Hum Genet.* 2010;87:265–273.
26. Harold D, Abraham R, Hollingworth P, et al. Genome-wide association study identifies variants at CLU and PICALM associated with Alzheimer's disease. *Nat Genet.* 2009;41:1088–1093.
27. Takei N, Miyashita A, Tsukie T, et al. Genetic association study on in and around the APOE in late-onset Alzheimer disease in Japanese. *Genomics*. 2009;93:441–448.
28. Lachke SA, Higgins AW, Inagaki M, et al. The cell adhesion gene PVRL3 is associated with congenital ocular defects. *Hum Genet.* 2012; 131:235–250.
29. Karaba AH, Kopp SJ, Longnecker R. Herpesvirus entry mediator is a serotype specific determinant of pathogenesis in ocular herpes. *Proc Natl Acad Sci U S A*. 2012;109:20649–20654.
30. Shukla ND, Tiwari V, Valyi-Nagy T. Nectin-1-specific entry of herpes simplex virus 1 is sufficient for infection of the cornea and viral spread to the trigeminal ganglia. *Mol Vis.* 2012;18:2711–2716.

ORIGINAL ARTICLE

Injection of Cultured Cells with a ROCK Inhibitor for Bullous Keratopathy

Shigeru Kinoshita, M.D., Ph.D., Noriko Koizumi, M.D., Ph.D., Morio Ueno, M.D., Ph.D., Naoki Okumura, M.D., Ph.D., Kojiro Imai, M.D., Ph.D., Hiroshi Tanaka, M.D., Ph.D., Yuji Yamamoto, M.D., Takahiro Nakamura, M.D., Ph.D., Tsutomu Inatomi, M.D., Ph.D., John Bush, B.A., Munetoyo Toda, Ph.D., Michio Hagiya, Ph.D., Isao Yokota, Ph.D., Satoshi Teramukai, Ph.D., Chie Sotozono, M.D., Ph.D., and Junji Hamuro, Ph.D.

ABSTRACT

BACKGROUND

Corneal endothelial cell (CEC) disorders, such as Fuchs's endothelial corneal dystrophy, induce abnormal corneal hydration and result in corneal haziness and vision loss known as bullous keratopathy. We investigated whether injection of cultured human CECs supplemented with a rho-associated protein kinase (ROCK) inhibitor into the anterior chamber could increase CEC density.

METHODS

We performed an uncontrolled, single-group study involving 11 persons who had received a diagnosis of bullous keratopathy and had no detectable CECs. Human CECs were cultured from a donor cornea; a total of 1×10^6 passaged cells were supplemented with a ROCK inhibitor (final volume, 300 μl) and injected into the anterior chamber of the eye that was selected for treatment. After the procedure, patients were placed in a prone position for 3 hours. The primary outcome was restoration of corneal transparency, with a CEC density of more than 500 cells per square millimeter at the central cornea at 24 weeks after cell injection. Secondary outcomes were a corneal thickness of less than 630 μm and an improvement in best corrected visual acuity equivalent to two lines or more on a Landolt C eye chart at 24 weeks after cell injection.

RESULTS

At 24 weeks after cell injection, we recorded a CEC density of more than 500 cells per square millimeter (range, 947 to 2833) in 11 of the 11 treated eyes (100%; 95% confidence interval [CI], 72 to 100), of which 10 had a CEC density exceeding 1000 cells per square millimeter. A corneal thickness of less than 630 μm (range, 489 to 640) was attained in 10 of the 11 treated eyes (91%; 95% CI, 59 to 100), and an improvement in best corrected visual acuity of two lines or more was recorded in 9 of the 11 treated eyes (82%; 95% CI, 48 to 98).

CONCLUSIONS

Injection of human CECs supplemented with a ROCK inhibitor was followed by an increase in CEC density after 24 weeks in 11 persons with bullous keratopathy. (Funded by the Japan Agency for Medical Research and Development and others; UMIN number, UMIN000012534.)

From the Departments of Frontier Medical Science and Technology for Ophthalmology (S.K., T.N., M.T., M.H.), Ophthalmology (M.U., K.I., H.T., Y.Y., T.I., J.B., C.S., J.H.), and Biostatistics (I.Y., S.T.), Kyoto Prefectural University of Medicine, and the Department of Biomedical Engineering, Doshisha University (N.K., N.O.) — both in Kyoto, Japan. Address reprint requests to Dr. Kinoshita at the Department of Frontier Medical Science and Technology for Ophthalmology, Kyoto Prefectural University of Medicine, 465 Kajii-cho, Hirokoji-agaru, Kawaramachi-dori, Kamigyo-ku, Kyoto 602-0841, Japan, or at shigeruk@koto.kpu-m.ac.jp.

Drs. Kinoshita, Koizumi, and Ueno contributed equally to this article.

N Engl J Med 2018;378:995-1003.
DOI: 10.1056/NEJMoa1712770

The corneal endothelium is a single layer of cells that line the posterior surface of the cornea. This cell layer maintains corneal transparency by regulating the flow of water from the aqueous humor into the cornea.[1] Corneal endothelial damage or disorder and subsequent loss of corneal endothelial cells (CECs) owing to pathologic conditions such as Fuchs's endothelial corneal dystrophy is compensated by the natural spread of the remaining CECs.[1] However, when CEC density, which typically exceeds 2000 cells per square millimeter in healthy persons, diminishes to fewer than 400 cells per square millimeter, corneal endothelial dysfunction and abnormal corneal hydration occur, resulting in corneal thickening and haziness known as bullous keratopathy[2]; this condition can ultimately lead to loss of vision.

The current treatments for bullous keratopathy include penetrating keratoplasty, Descemet's stripping automated endothelial keratoplasty, and Descemet's membrane endothelial keratoplasty, all of which involve the use of a donor cornea.[3-9] Although these surgical procedures are widely used, they are invasive, and their long-term clinical results remain unclear. Visual acuity after corneal transplantation is sometimes unsatisfactory because of a surgery-induced irregularity of the corneal structure. A surgical procedure that results in a healthy cornea with a normal shape and function that permit good visual acuity is therefore desired. Two procedures — one that involved the simple peeling of the Descemet's membrane from the central cornea[10] and one that involved the removal of localized corneal endothelium by freezing combined with the topical application of a rho-associated protein kinase (ROCK) inhibitor[11] — were reported to be effective in the treatment of early-stage corneal endothelial dysfunction but not in the treatment of advanced-stage diffuse corneal endothelial dysfunction.[11]

Successful procedures for culturing CECs have been reported in studies in humans and in nonhuman primates.[12-23] Taking into account this line of research, we developed an approach to treat severe corneal endothelial dysfunction through injection of cultured human CECs combined with a ROCK inhibitor into the anterior chamber. Although the ROCK inhibitor was used as an adjunctive drug to promote engraftment of CECs, we could not rule out the possibility that the ROCK inhibitor would have a therapeutic effect through its action on cells in situ.[23] In previous studies in rabbits and monkeys, we reported that CECs supplemented with a ROCK inhibitor, when injected into the anterior chamber, repopulated and self-organized[24,25] on the posterior surface of the cornea, had the functional properties of healthy corneal endothelium, and produced a normal cornea with no structural alteration.[26,27] Through this work, we determined that human CEC cultures comprise a plurality of subpopulations, some of which are unsuitable and unsafe for injection into human eyes.[28,29] We therefore devised a method[30] to consistently produce differentiated cultured functional human CECs. Here we report a case series of 11 consecutive patients with bullous keratopathy who were treated successfully by injection of human CECs supplemented with a ROCK inhibitor.

Methods

Study Design and Oversight

We conducted a nonrandomized, single-group study involving a small number of participants. The protocol and amendments (available with the full text of this article at NEJM.org) and other relevant study documentation of this clinical trial were reviewed for compliance with the guidelines on clinical research with human stem cells in Japan and were approved by the institutional review board at Kyoto Prefectural University of Medicine and by the Special Committee of the Japanese Ministry of Health, Labor, and Welfare. The authors vouch for the accuracy and completeness of the data and analyses and the reporting of adverse events and for the fidelity of the study to the protocol.

Patients

Eligible patients had received a diagnosis of bullous keratopathy; were between 20 and 90 years of age; and had an eye with no detectable CECs on specular microscopy (Fig. S1 in the Supplementary Appendix, available at NEJM.org), a corneal thickness greater than 630 μm and the presence of corneal epithelial edema, and a best corrected visual acuity below 0.5 (decimal visual acuity). Decimal visual acuity, which is widely used in Japan and Europe, is an alternative system to Snellen visual acuity and logMAR (logarithm of the minimum angle of resolution) visual acuity.[31] A decimal visual acuity of 0.5 corresponds to 20/40 (Snellen) and 0.30 (logMAR);

a decimal visual acuity of 0.1 corresponds to 20/200 (Snellen) and 1.00 (logMAR). All the patients provided written informed consent.

HUMAN CEC CULTURE AND QUALITY CONTROL

Corneas from deceased donors (range of age at death, 7 to 29 years) were used for the in vitro subculture material; the donor corneas were provided by SightLife. Human CECs were cultured at the Cell Processing Center of Kyoto Prefectural University of Medicine with the use of a standard operating procedure that conformed to the guidelines of Good Manufacturing Practices. Details of the culture procedure are described in the Supplementary Appendix. Cell lots for clinical application were examined to verify that they met criteria for surgical use (Table S1 in the Supplementary Appendix), and enzyme-linked immunosorbent assay or fluorescence-activated cell-sorting analysis (or both) was performed to elucidate the biologic characteristics of the cells. The cells were recovered by means of enzyme treatment with TrypLE Reagent (Thermo Fisher Scientific) and were washed with modified Opti-MEM I Reduced Serum Media (Thermo Fisher Scientific). The human CECs were then dispensed into a Proteosave container (Sumitomo Bakelite) to block nonspecific absorption of protein (1.5×10^6 cultured human CECs were distributed per 450 μl of modified Opti-MEM I supplemented with the ROCK inhibitor Y-27632 [Wako Pure Chemical Industries] at a final cell concentration of 100 μM).

SURGICAL PROCEDURE AND FOLLOW-UP

All surgical procedures were performed under local anesthesia. After a 1.6-mm incision was made at the corneal limbus, a silicone needle (Inami) was used to remove the abnormal extracellular matrix on the patient's Descemet's membrane or the degenerated CECs in an 8-mm-diameter area of the central cornea (or both). After this procedure, a 26-gauge needle was used to inject 1×10^6 (Patients 2 to 11) or 5×10^5 (Patient 1) cultured human CECs suspended in 300 μl of modified Opti-MEM I medium containing the ROCK inhibitor Y-27632 into the anterior chamber. The patients were then immediately placed in a prone position for 3 hours to enhance the adhesion of the injected cells (Fig. 1). After cell injection, all patients were administered systemic and topical glucocorticoids to inhibit acute inflammation or immunologic reaction, and antimicrobial agents were administered as prophylaxis against infection in accordance with the drug regimen we use in our regular corneal transplantation procedures (Table S2 in the Supplementary Appendix).

PRIMARY, SECONDARY, AND EXPLORATORY OUTCOMES

The primary outcome was restoration of corneal transparency with a CEC density of more than 500 cells per square millimeter at the central cornea at 24 weeks after cell injection. The secondary outcomes were a corneal thickness of less than 630 μm at 24 weeks after cell injection (with a decrease in corneal thickness from the preoperative [baseline] measurement) and an improvement in best corrected visual acuity of two lines or more on a Landolt C eye chart (a measure of decimal visual acuity) at 24 weeks after cell injection. We converted decimal visual acuity to logMAR visual acuity to facilitate statistical analysis. A decrease of at least 0.2 in logMAR visual acuity corresponds to an improvement of two lines or more on a Landolt C eye chart, and an increase of at least 0.2 in logMAR visual acuity corresponds to a deterioration of two lines or more. For decimal visual acuity, a higher value indicates better visual acuity, whereas for logMAR visual acuity, a lower value indicates better visual acuity. The primary and secondary outcomes were also assessed as exploratory outcomes at 2 years after cell injection. We assessed the safety of the treatment by monitoring the treated eyes and the patients for adverse events (Table S3 in the Supplementary Appendix).

STATISTICAL ANALYSIS

We calculated the percentage (with 95% confidence intervals) of treated eyes that met the primary and secondary outcomes. The exploratory outcomes were assessed as the change from the baseline measurement to 2 years (see the Supplementary Appendix). We also recorded intraocular pressure as a safety measure and assessed this outcome as the change from the baseline measurement to 2 years.

RESULTS

PATIENT CHARACTERISTICS

We enrolled patients between December 10, 2013, and December 16, 2014. We injected human CECs supplemented with the ROCK inhibitor into 11 eyes, in 11 consecutive patients, during the

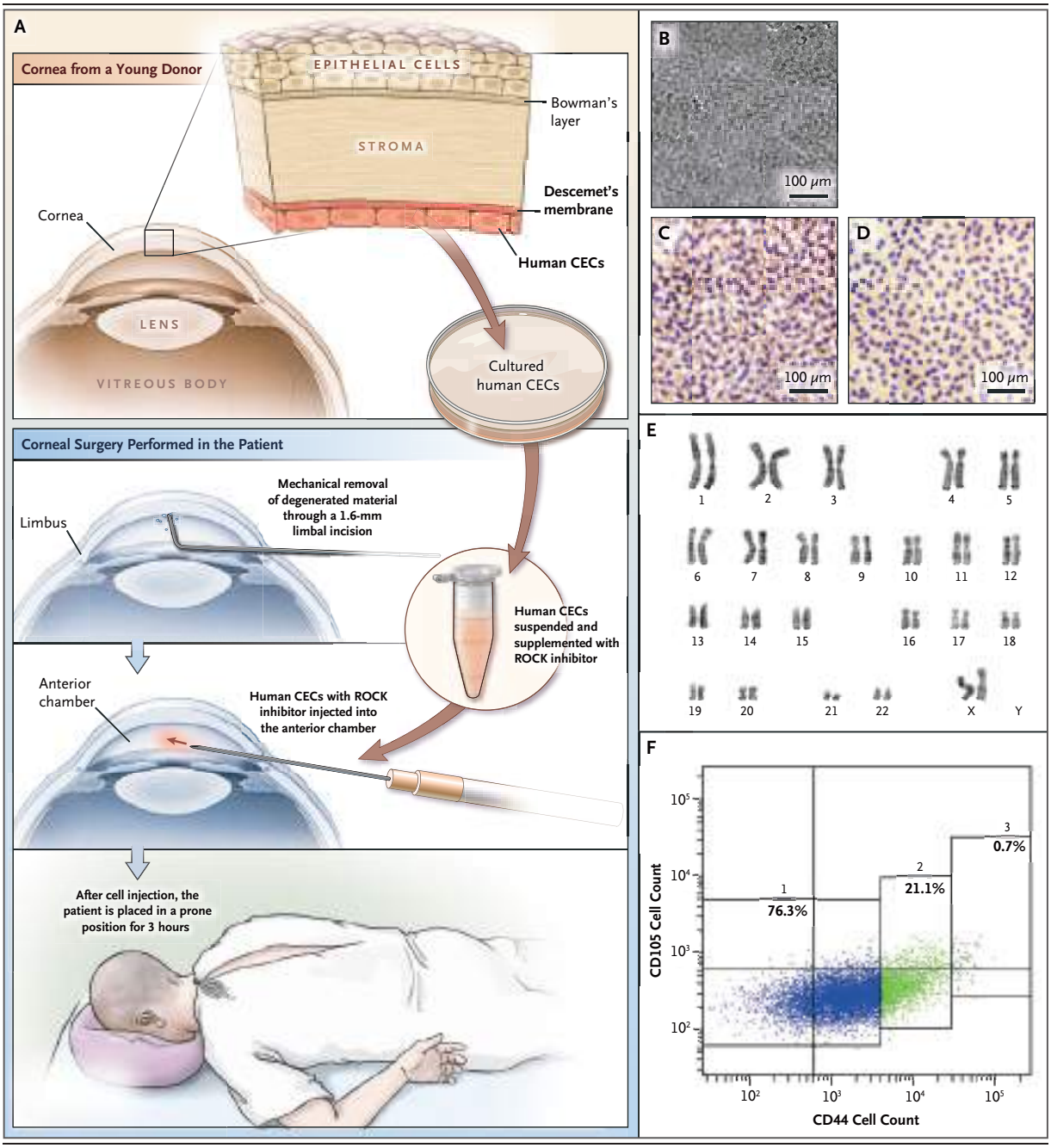

period from December 2013 through February 2014 (3 eyes) and September 2014 through December 2014 (8 eyes). The mean age of the patients was 64.4 years (range, 49 to 82), and 5 of the 11 patients (45%) were male. All the patients had pseudophakic bullous keratopathy (i.e., bullous keratopathy that develops after intraocular lens implantation in cataract surgery), with the following subtypes: Fuchs's endothelial corneal dystrophy (7 eyes), argon-laser iridotomy–induced bullous keratopathy (2 eyes), pseudoexfoliation syndrome–related bullous keratopathy (1 eye), and intraocular surgery–related bullous keratopathy (1 eye) (Table 1). The mean corneal thickness at baseline was 743 μm (range, 637 to 964). (Additional details are provided in the Supplementary Appendix.)

FEATURES OF THE CULTURED HUMAN CECS

We used seven lots of cultured human CECs (passaged two or three times). Each lot was derived from an independent donor. At the request of the Special Committee, for safety reasons we

Figure 1 (facing page). Preparation of Cultured Human Corneal Endothelial Cells.

Panel A shows the schema of cell-injection therapy, in which cultured human corneal endothelial cells (CECs) supplemented with a rho-associated protein kinase (ROCK) inhibitor are injected into the anterior chamber. After human CECs were removed from the Descemet's membrane of a cornea obtained from a young deceased donor, isolated human CECs free of any contamination were cultured and subcultured. A few hours before cell injection, the cells were recovered, suspended to obtain the appropriate number and density, and supplemented with the ROCK inhibitor. After mechanical removal of the abnormal extracellular matrix on the patient's Descemet's membrane or the degenerated CECs (or both), the cultured human CECs supplemented with the ROCK inhibitor were injected into the anterior chamber of one of the eyes of each participant. After the procedure, the patients were placed in a prone position for 3 hours. Panel B shows the cultured human CECs for clinical use. Panel C shows the expression of sodium–potassium ATPase by the cultured human CECs. Panel D shows the expression of ZO-1 by the cultured human CECs. Panel E shows the karyotype analysis of lot 5 of cultured human CECs. Panel F shows a representative result of the expression of CD44 and CD105 in the cultured human CECs using flow cytometry. The full vertical line indicates the boundary between the CD44-negative population and the CD44-positive population. The full horizontal line indicates the boundary between the CD105-negative population and the CD105-positive population. Rectangles 1, 2, and 3 indicate subpopulations of the cultured human CECs. The percentages of a negative to low level of CD44 expression (rectangle 1), a medium level of CD44 expression (rectangle 2), and a high level of CD44 expression (rectangle 3) were 76.3%, 21.1%, and 0.7%, respectively.

used one lot per patient in the first three patients (a total of three lots) and one lot for every two patients for the following eight patients (a total of four lots). All cultured human CECs were small, hexagonally shaped cells (no epithelial-to-mesenchymal transition–like cells) expressing ZO-1 and sodium–potassium ATPase. CEC density ranged from 1835 to 2530 cells per square millimeter. All seven lots used in this study met the prespecified quality-control requirements (Fig. 1, and Table S1 in the Supplementary Appendix), and no chromosomal abnormalities were observed. Enzyme-linked immunosorbent assay of the culture supernatant was performed at the final culture stage and revealed a type I collagen level lower than 15 ng per milliliter (lots 1 through 3) and an interleukin-8 level lower than 500 pg per milliliter and a platelet-derived growth factor BB level higher than 30 pg per milliliter (lots 4 through 7). In lots 2 through 7, the percentage of CECs with high levels of CD44 expression was below 10%. The viral antigens of herpes simplex virus type 1 and type 2, varicella–zoster virus, cytomegalovirus, Epstein–Barr virus, and parvovirus B19, as measured by polymerase-chain-reaction assay and standard bacterial testing, were found to be negative in the cultured cells and supernatant of all seven lots.

PRIMARY OUTCOME

At 24 weeks after cell injection, contact specular microscopic examination (Fig. S2 in the Supplementary Appendix) revealed that the primary outcome (i.e., restoration of corneal transparency with a CEC density of >500 cells per square millimeter) was met in 11 of the 11 treated eyes (100%; 95% confidence interval [CI], 72 to 100). CEC density ranged from 947 to 2833 cells per square millimeter in the 11 eyes (mean density, 1924 cells per square millimeter [95% CI, 1537 to 2312]) and exceeded 1000 cells per square millimeter in 10 eyes and 2000 cells per square millimeter in 6 eyes (Table 1, and Table S4 in the Supplementary Appendix).

SECONDARY OUTCOMES

At 24 weeks after cell injection, a corneal thickness of less than 630 μm was attained in 10 of the 11 treated eyes (91%; 95% CI, 59 to 100), with a mean corneal thickness of 549 μm (95% CI, 515 to 583). A significant improvement in best corrected visual acuity of two lines or more was attained at 24 weeks in 9 of the 11 treated eyes (82%; 95% CI, 48 to 98) (Table 1, and Table S5 in the Supplementary Appendix).

EXPLORATORY OUTCOMES

At 2 years after cell injection, corneal thickness was less than 600 μm in 10 eyes, and the cornea was thinner than the baseline measure in all 11 eyes (Table 1). There was a rapid decrease in corneal thickness within 4 weeks after cell injection, followed by a more gradual decrease over the next 5 months (Fig. 2A). The mean best corrected logMAR visual acuity decreased from 0.88 at baseline to 0.04, indicating an improvement (Fig. 2B). (Additional details are provided in Table S5 in the Supplementary Appendix.)

At 2 years after cell injection, each of the 11 eyes maintained corneal transparency (mean CEC density, 1534 cells per square millimeter [95% CI, 1213 to 1855]) (Fig. 3). The duration of corneal clearing (i.e., the amount of time that it took for the cornea to clear) differed slightly

Table 1. Patient Characteristics and Clinical Summary before and after Cell Injection.*

Patient No., Sex, and Age	Eye	Disease Subtype	Before Cell Injection†		24 Weeks after Cell Injection			2 Years after Cell Injection		
			Central Corneal Thickness	BCVA‡	CEC Density	Central Corneal Thickness	BCVA‡	CEC Density	Central Corneal Thickness	BCVA‡
			μm	*decimal visual acuity (logMAR)*	*cells/mm²*	*μm*	*decimal visual acuity (logMAR)*	*cells/mm²*	*μm*	*decimal visual acuity (logMAR)*
1, F, 68 yr	Right	Argon-laser iridotomy–induced BK	760	0.04 (1.40)	947	511	0.70 (0.15)	1029	532	1.00 (0.00)
2, M, 60 yr	Right	Fuchs's endothelial corneal dystrophy	964	0.05 (1.30)	1965	525	1.00 (0.00)	2193	538	1.00 (0.00)
3, M, 58 yr	Right	Fuchs's endothelial corneal dystrophy	727	0.20 (0.70)	2146	540	0.70 (0.15)	2115	546	1.50 (–0.18)
4, M, 71 yr	Right	Pseudoexfoliation syndrome–related BK	792	0.10 (1.00)	1271	640	0.40 (0.40)	871	710	0.40 (0.40)
5, M, 49 yr	Left	Fuchs's endothelial corneal dystrophy	637	0.40 (0.40)	1134	509	1.00 (0.00)	959	529	1.50 (–0.18)
6, F, 74 yr	Right	Argon-laser iridotomy–induced BK	775	0.10 (1.00)	2232	505	0.80 (0.10)	1447	525	1.00 (0.00)
7, F, 72 yr	Left	Fuchs's endothelial corneal dystrophy	750	0.30 (0.52)	2288	626	0.30 (0.52)	1316	550	0.80 (0.10)
8, F, 57 yr	Left	Fuchs's endothelial corneal dystrophy	657	0.20 (0.70)	2833	489	0.50 (0.30)	2188	503	0.70 (0.15)
9, M, 63 yr	Left	Intraocular surgery–related BK	649	0.40 (0.40)	1880	595	0.50 (0.30)	1546	543	0.80 (0.10)
10, F, 82 yr	Right	Fuchs's endothelial corneal dystrophy	741	0.20 (0.70)	2141	539	0.80 (0.10)	1600	523	0.90 (0.05)
11, F, 56 yr	Left	Fuchs's endothelial corneal dystrophy	725	0.03 (1.52)	2331	561	0.90 (0.05)	1610	572	1.00 (0.00)

* BK denotes bullous keratopathy, BCVA best corrected visual acuity, CEC corneal endothelial cell, and logMAR logarithm of the minimum angle of resolution.
† Before cell injection, CEC density was below the detection limit of the specular microscope in all 11 patients.
‡ Decimal visual acuity is widely used in Japan and Europe as an alternative system to Snellen visual acuity and logMAR visual acuity.[31] For decimal visual acuity, higher values indicate better visual acuity, whereas for logMAR visual acuity, lower numbers indicate better visual acuity: logMAR visual acuity=−log(decimal visual acuity).

Figure 2. Corneal Thickness, Best Corrected Visual Acuity, and Intraocular Pressure.

Measures of corneal thickness (Panel A), best corrected visual acuity (BCVA) (Panel B), and intraocular pressure (Panel C) are provided in box plots. The results with respect to the secondary outcomes of a corneal thickness of less than 630 μm and an improvement in BCVA of two lines or more on a Landolt C eye chart (a measure of decimal visual acuity) at 24 weeks, as compared with baseline, were significant (Table S5 in the Supplementary Appendix). BCVA is expressed as logMAR visual acuity, which was converted from decimal visual acuity to facilitate statistical analysis (a decrease of at least 0.2 in logMAR BCVA corresponds to an improvement of two lines or more on a Landolt C eye chart). There was no significant increase in intraocular pressure during each evaluation period. The horizontal line in the boxes represents the median, and the bottom and top of the boxes represent the lower and upper quartiles, respectively. I bars indicate 1.5 times the lower and upper quartiles, and the dots represent outliers.

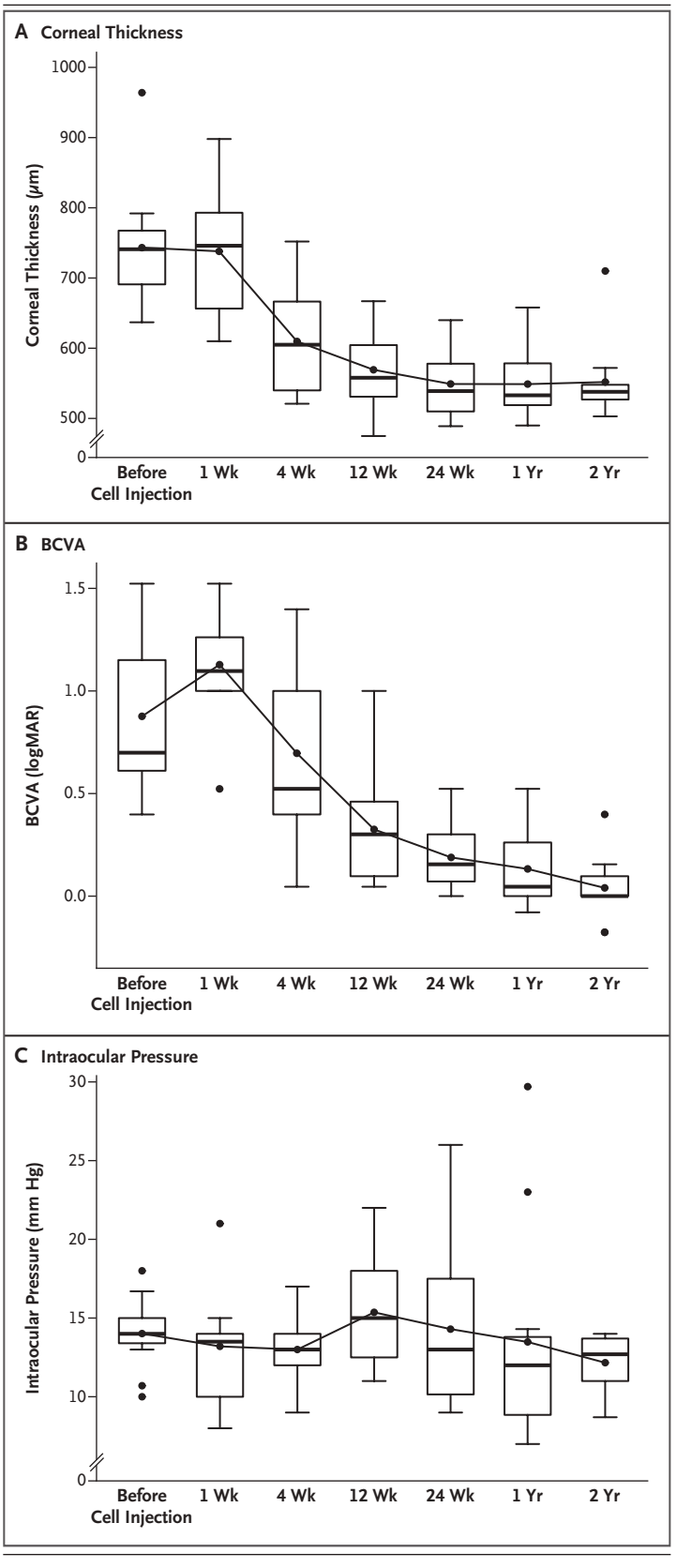

from patient to patient owing to variations in the quality of the injected cells and in the subtype of disease. (Additional details are provided in Table S4 and Figs. S3 through S5 in the Supplementary Appendix.)

SAFETY

We did not observe anterior uveitis, intraocular infection, or immunologic reaction in any of the patients after cell injection. The postoperative time course of intraocular pressure is shown in Figure 2C. In 10 of the 11 eyes, there was no increase in intraocular pressure during the 2-year period of evaluation. The treated eye in Patient 8 showed an increase in intraocular pressure (to 27 mm Hg) at 8 months after cell injection; the pressure resolved after trabeculotomy without the use of antiglaucoma eyedrop medication. At 2 years after cell injection, intraocular pressure was within the normal range in each of the 11 eyes. No abnormal findings from general health evaluations or blood tests were observed at 4, 12, and 24 weeks after cell injection. (Additional details are provided in Tables S5 and S6 in the Supplementary Appendix.)

DISCUSSION

Our findings showed that injection of human CECs supplemented with a ROCK inhibitor in patients with bullous keratopathy was followed by corneal restoration, with attainment of normal corneal thickness and resolution of corneal

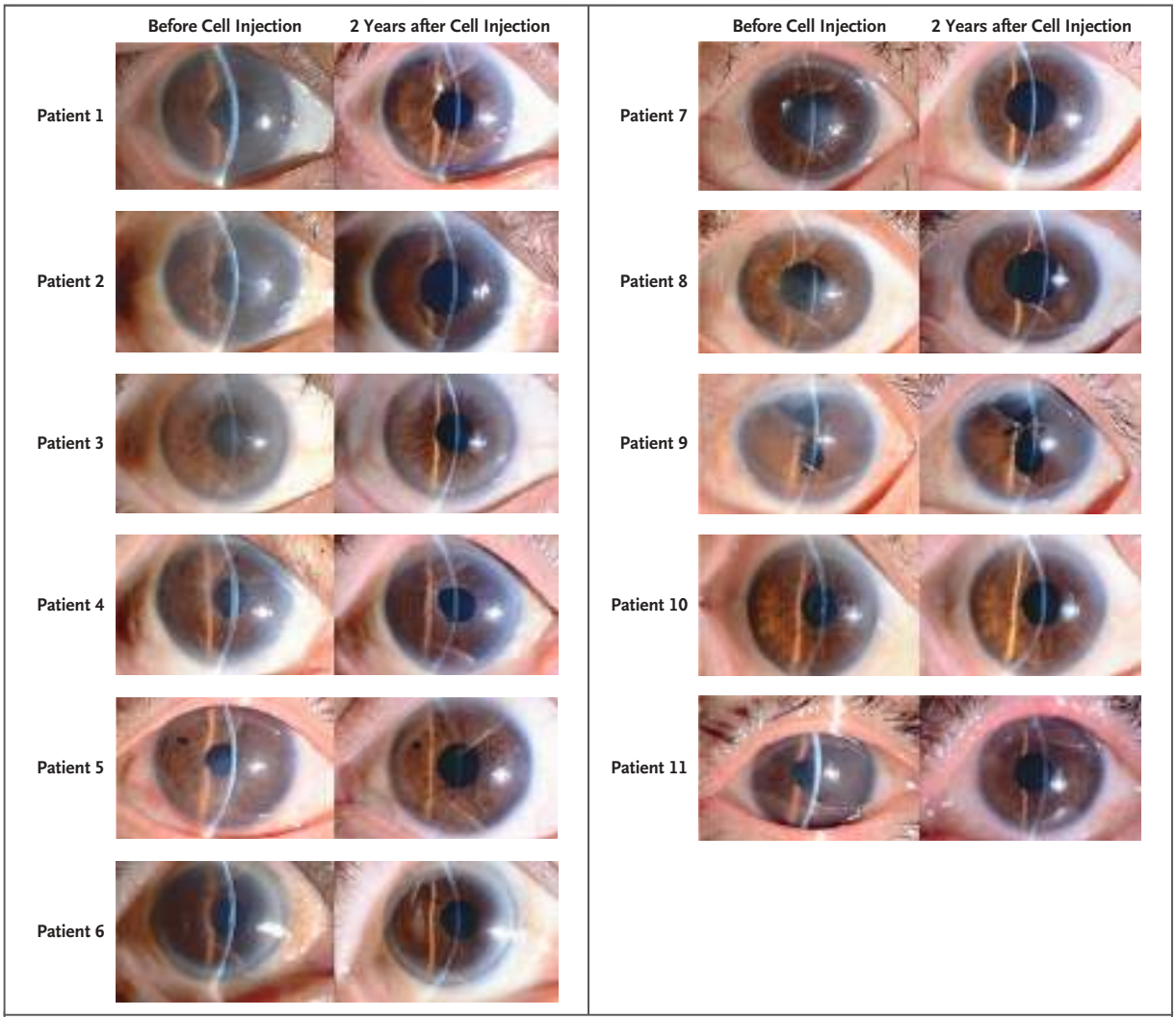

Figure 3. Slit-Lamp Microscopic Images of the Treated Eyes.

Slit-lamp microscopic photographs of all 11 treated eyes were obtained at baseline (before cell injection) and at 2 years after the injection of CECs supplemented with a ROCK inhibitor.

epithelial edema. Within the limits of this small, single-group study involving 11 patients who were followed for 2 years, the procedure was safe. We propose that injection of cultured human CECs supplemented with the ROCK inhibitor into the anterior chamber resulted in the repopulation of CECs on the Descemet's membrane and on the bare posterior surface of the corneal stroma. An alternative explanation is that the ROCK inhibitor or a factor released from the injected cells stimulated the CECs in the recipient to replicate; however, we consider this explanation to be unlikely because most of the eyes showed a high CEC density at 24 weeks after cell injection that mimics what would have been seen with ordinary corneal transplantation at 4 weeks.

We speculate that most of the injected CECs that did not attach to the cornea entered an adjacent vein through the trabecular meshwork and died or entered the systemic circulation. Because of the risk of ectopic tumor formation, we were particularly interested in the results of the blood tests and general health evaluations obtained from the participants after treatment; the normal findings were consistent with those from preclinical studies,[27] but we cannot rule out some potential for tumor formation over time or in future trials of this experimental intervention.

Elevated intraocular pressure occurred in one patient, in whom we diagnosed glucocorticoid-induced glaucoma, given the timing of presentation and the fact that there were no abnormal

findings associated with the trabecular meshwork. However, because of this observation, we plan to reevaluate the number and density of cells used in the injection in the event that further clinical trials are performed. Owing to the study design, we could not discern the extent to which the use of human CECs, the use of the ROCK inhibitor, and the decision to place patients in a prone position contributed to the clinical outcome. We observed no immune response to the human CECs during the follow-up period (the patients received topical glucocorticoids after the procedure), and previous studies have indicated induction of immune tolerance in the eye[32] and the anterior chamber–associated immune deviation of the eye.[33]

Supported by a grant from the Highway Program for Realization of Regenerative Medicine of the Japan Agency for Medical Research and Development (to Drs. Kinoshita and Koizumi), a grant from the Research Project for Practical Applications of Regenerative Medicine of the Japanese Ministry of Health, Labor, and Welfare (to Dr. Kinoshita), a grant from the Funding Program for Next-Generation World-Leading Researchers (NEXT Program) of the Japan Society for the Promotion of Science (to Dr. Koizumi), and a grant from the Program for the Strategic Research Foundation at Private Universities of the Ministry of Education, Culture, Sports, Science, and Technology (to Dr. Koizumi).

Disclosure forms provided by the authors are available with the full text of this article at NEJM.org.

We thank Drs. Hidenobu Tanihara and Kohei Sonoda for independent data monitoring; Dr. Hiroko Nakagawa (who passed away during the preparation of the manuscript); Satomi Sakabayashi, Kazuko Asada, Atsushi Mukai, Asako Hiraga, Yuki Hosoda, and Shunsuke Watanabe for technical assistance; and Drs. Shin-ichi Nishikawa, Ryosuke Takahashi, Akifumi Matsuyama, Kayo Takashima, Yoshitsugu Inoue, and Yoshiki Sasai for helpful comments.

REFERENCES

1. Dawson DG, Ubels JL, Edelhauser HF. Cornea and sclera. In: Levin LA, Nilsson SFE, Ver Hoeve J, Wu SM, eds. Adler's physiology of the eye. 11th ed. Edinburgh: Elsevier, 2011:71-130.
2. Bourne WM. Clinical estimation of corneal endothelial pump function. Trans Am Ophthalmol Soc 1998;96:229-42.
3. Tan DT, Dart JK, Holland EJ, Kinoshita S. Corneal transplantation. Lancet 2012; 379:1749-61.
4. 2015 Eye banking statistical report. Washington, DC: Eye Bank Association of America, 2016.
5. Gain P, Jullienne R, He Z, et al. Global survey of corneal transplantation and eye banking. JAMA Ophthalmol 2016;134:167-73.
6. Melles GR, Ong TS, Ververs B, van der Wees J. Preliminary clinical results of Descemet membrane endothelial keratoplasty. Am J Ophthalmol 2008;145:222-7.
7. Price MO, Giebel AW, Fairchild KM, Price FW Jr. Descemet's membrane endothelial keratoplasty: prospective multicenter study of visual and refractive outcomes and endothelial survival. Ophthalmology 2009;116:2361-8.
8. Schlögl A, Tourtas T, Kruse FE, Weller JM. Long-term clinical outcome after Descemet membrane endothelial keratoplasty. Am J Ophthalmol 2016;169:218-26.
9. Wacker K, Baratz KH, Maguire LJ, McLaren JW, Patel SV. Descemet stripping endothelial keratoplasty for Fuchs' endothelial corneal dystrophy: five-year results of a prospective study. Ophthalmology 2016;123:154-60.
10. Borkar DS, Veldman P, Colby KA. Treatment of Fuchs endothelial dystrophy by Descemet stripping without endothelial keratoplasty. Cornea 2016;35:1267-73.
11. Okumura N, Koizumi N, Kay EP, et al. The ROCK inhibitor eye drop accelerates corneal endothelium wound healing. Invest Ophthalmol Vis Sci 2013;54:2493-502.
12. Engelmann K, Friedl P. Optimization of culture conditions for human corneal endothelial cells. In Vitro Cell Dev Biol 1989;25:1065-72.
13. Zhu C, Joyce NC. Proliferative response of corneal endothelial cells from young and older donors. Invest Ophthalmol Vis Sci 2004;45:1743-51.
14. Joyce NC, Zhu CC. Human corneal endothelial cell proliferation: potential for use in regenerative medicine. Cornea 2004; 23:Suppl:S8-S19.
15. Mimura T, Yamagami S, Yokoo S, et al. Cultured human corneal endothelial cell transplantation with a collagen sheet in a rabbit model. Invest Ophthalmol Vis Sci 2004;45:2992-7.
16. Ishino Y, Sano Y, Nakamura T, et al. Amniotic membrane as a carrier for cultivated human corneal endothelial cell transplantation. Invest Ophthalmol Vis Sci 2004; 45:800-6.
17. Konomi K, Zhu C, Harris D, Joyce NC. Comparison of the proliferative capacity of human corneal endothelial cells from the central and peripheral areas. Invest Ophthalmol Vis Sci 2005;46:4086-91.
18. Mimura T, Yamagami S, Usui T, et al. Long-term outcome of iron-endocytosing cultured corneal endothelial cell transplantation with magnetic attraction. Exp Eye Res 2005;80:149-57.
19. Mimura T, Yamagami S, Yokoo S, et al. Sphere therapy for corneal endothelium deficiency in a rabbit model. Invest Ophthalmol Vis Sci 2005;46:3128-35.
20. Schmedt T, Chen Y, Nguyen TT, Li S, Bonanno JA, Jurkunas UV. Telomerase immortalization of human corneal endothelial cells yields functional hexagonal monolayers. PLoS One 2012;7(12):e51427.
21. Koizumi N, Sakamoto Y, Okumura N, et al. Cultivated corneal endothelial cell sheet transplantation in a primate model. Invest Ophthalmol Vis Sci 2007;48:4519-26.
22. Peh GSL, Toh KP, Wu FY, Tan DT, Mehta JS. Cultivation of human corneal endothelial cells isolated from paired donor corneas. PLoS One 2011;6(12):e28310.
23. Okumura N, Ueno M, Koizumi N, et al. Enhancement on primate corneal endothelial cell survival in vitro by a ROCK inhibitor. Invest Ophthalmol Vis Sci 2009;50:3680-7.
24. Sawai S, Thomason PA, Cox EC. An autoregulatory circuit for long-range self-organization in *Dictyostelium* cell populations. Nature 2005;433:323-6.
25. Chaffer CL, Thompson EW, Williams ED. Mesenchymal to epithelial transition in development and disease. Cells Tissues Organs 2007;185:7-19.
26. Okumura N, Koizumi N, Ueno M, et al. ROCK inhibitor converts corneal endothelial cells into a phenotype capable of regenerating in vivo endothelial tissue. Am J Pathol 2012;181:268-77.
27. Okumura N, Sakamoto Y, Fujii K, et al. Rho kinase inhibitor enables cell-based therapy for corneal endothelial dysfunction. Sci Rep 2016;6:26113.
28. Hongo A, Okumura N, Nakahara M, Kay EP, Koizumi N. The Effect of a p38 mitogen-activated protein kinase inhibitor on cellular senescence of cultivated human corneal endothelial cells. Invest Ophthalmol Vis Sci 2017;58:3325-34.
29. Hamuro J, Toda M, Asada K, et al. Cell homogeneity indispensable for regenerative medicine by cultured human corneal endothelial cells. Invest Ophthalmol Vis Sci 2016;57:4749-61.
30. Toda M, Ueno M, Hiraga A, et al. Production of homogeneous cultured human corneal endothelial cells indispensable for innovative cell therapy. Invest Ophthalmol Vis Sci 2017;58:2011-20.
31. Holladay JT. Visual acuity measurements. J Cataract Refract Surg 2004;30: 287-90.
32. Yamada J, Ueno M, Toda M, et al. Allogeneic sensitization and tolerance induction after corneal endothelial cell transplantation in mice. Invest Ophthalmol Vis Sci 2016;57:4572-80.
33. Streilein JW. Ocular immune privilege: therapeutic opportunities from an experiment of nature. Nat Rev Immunol 2003; 3:879-89.

Japanese Journal of Ophthalmology
https://doi.org/10.1007/s10384-018-0598-1

THE OFFICIAL INTERNATIONAL JOURNAL OF THE JAPANESE OPHTHALMOLOGICAL SOCIETY

CLINICAL INVESTIGATION

Endothelial cell loss and graft survival after penetrating keratoplasty for laser iridotomy-induced bullous keratopathy

Naoki Okumura[1] · Ayaka Kusakabe[1] · Noriko Koizumi[1] · Koichi Wakimasu[2] · Kanae Kayukawa[2] · Masami Kondo[1] · Kazuhiko Mori[3] · Chie Sotozono[3] · Shigeru Kinoshita[2,3,4]

Received: 27 June 2017 / Accepted: 2 April 2018

Abstract

Purpose To assess corneal endothelial cell loss after penetrating keratoplasty (PK) treatment for laser iridotomy (LI)-induced bullous keratopathy (BK).

Methods A retrospective study conducted on consecutive patients who underwent PK between March 2000 and December 2011. Patients who had undergone more than 24 months of follow-up were included. Patients who underwent PK were subcategorized into two groups based on their diagnosis of BK prior to PK; PK was performed to treat either LI-BK or non LI-BK. The cell density of the central corneal endothelium and the graft survival were evaluated during follow-up.

Results Corneal endothelial cell density decreased in a similar fashion in both the LI-BK and non LI-BK patients, though the cell density decreased significantly faster in the LI-BK group than in the non LI-BK group throughout the 108 months of the study ($p=0.026$). The mean cell loss at 36 months for the LI-BK group was 57.7% vs. 63.2% for the non LI-BK, 76.9% vs. 70.1% at 72 months, and 85.6% vs. 72.0% at 108 months. No eye among 21 eyes in the LI-BK group (0%) had failed grafts, whereas 4 of 25 eyes in the non LI-BK group (16.0%) had failed grafts at 60 months ($p=0.114$).

Conclusions The outcome of PK for BK secondary to LI was no worse than the outcome of PK for other types of BK. However, our long-term follow-up after PK showed that cell density decreased faster in the LI-BK group than in the non LI-BK, suggesting that cell loss might be involved in the existence of LI prior to PK.

Keywords Penetrating keratoplasty · Trabeculectomy · Corneal endothelial cell density

Introduction

Laser iridotomy (LI) is established as the first-line therapy for angle closure [1]. It is preferred over surgical iridectomy, as it requires no incisional invasion [2]. Some complications are reported, such as bleeding into the anterior chamber, unexpected laser burns to the cornea, cataract formation, and development of posterior synechiae, but LI has been confirmed as a relatively safe procedure that has no severe sight-threatening complications [3].

Despite the apparent safety of LI, several researchers report severe corneal endothelial cell loss and the induction of bullous keratopathy (BK) following LI, mainly in Asian populations (i.e., Japan, Singapore, and Korea) [3–8]. A nationwide questionnaire survey conducted in Japan revealed that 12.9% of the facilities reported the occurrence of BK caused by prophylactic LI, although the overall incidence was low [9]. Moreover, LI-induced BK is a frequent indication for corneal transplantation in Japan. A Japanese

Electronic supplementary material The online version of this article (https://doi.org/10.1007/s10384-018-0598-1) contains supplementary material, which is available to authorized users.

✉ Shigeru Kinoshita
shigeruk@koto.kpu-m.ac.jp

[1] Department of Biomedical Engineering, Faculty of Life and Medical Sciences, Doshisha University, Kyotanabe, Japan

[2] Baptist Eye Institute, Kyoto, Japan

[3] Department of Ophthalmology, Kyoto Prefectural University of Medicine, 465 Kajii-cho, Hirokoji-agaru, Kawaramachi-dori, Kamigyo-ku, Kyoto 602-0841, Japan

[4] Department of Frontier Medical Science and Technology for Ophthalmology, Kyoto Prefectural University of Medicine, Kyoto, Japan

national survey identified cataract surgery as the most common cause of BK (44.4%), with LI as the second most common cause (23.4%) between 1999 and 2001 [10]. This differs from the indication for corneal transplantation in Caucasian countries, where Fuchs endothelial corneal dystrophy is the leading cause [11].

The mechanisms by which LI causes corneal endothelial dysfunction are still unclear [2]. The currently proposed mechanisms include: (1) direct laser injury to the focal corneal endothelium, (2) mechanical shock waves generated by the laser, (3) thermal damage by a temperature rise of the aqueous humor, or (4) corneal endothelial burning by high temperature debris from the iris [3, 4, 6, 7]. These potential causes suggest the occurrence of acute damage to the corneal endothelium during or immediately after the LI procedure. A combination of mechanisms may also cause continuous damage to the corneal endothelium in the chronic phase [12–14].

These observations motivated the present evaluation of long-term outcomes of corneal transplantation performed to treat LI-induced BK. The aim of this study was to assess the extent of corneal endothelial cell loss following corneal transplantation for LI-induced BK.

Materials and methods

This study was performed according to a protocol approved by the Institutional Review Board of the Baptist Eye Institute, Kyoto, Japan and was conducted in accordance with the principles of the Declaration of Helsinki. The study was registered with UMIN (UMIN000021104) (http://www.umin.ac.jp/english/).

The medical records of consecutive patients who underwent penetrating keratoplasty (PK) at the Baptist Eye Institute between March 2000 and December 2011 were retrospectively investigated. Patients who had been followed up for more than 24 months were included. Patients who underwent trabeculectomy, pars plana vitrectomy, or goniosynechialysis, or who underwent PK for cosmetic purposes, were excluded. The patients with PK were subcategorized into two groups based on a diagnosis of BK prior to PK; PK was performed due to LI-BK or non LI-BK (Fig. 1). Anterior segments were evaluated by slit-lamp microscopy at the follow-up visit. The cell density of the corneal endothelium was analyzed with a non-contact specular microscope (EM-3000, Tomey Corporation).

PK was performed either under general anesthesia or retrobulbar anesthesia, according to each patient's status. Methylprednisolone was administered by an intravenous injection before PK for both LI-BK and non LI-BK patients who were preoperatively predicted to have a severe inflammatory response. The anterior chamber was replaced with

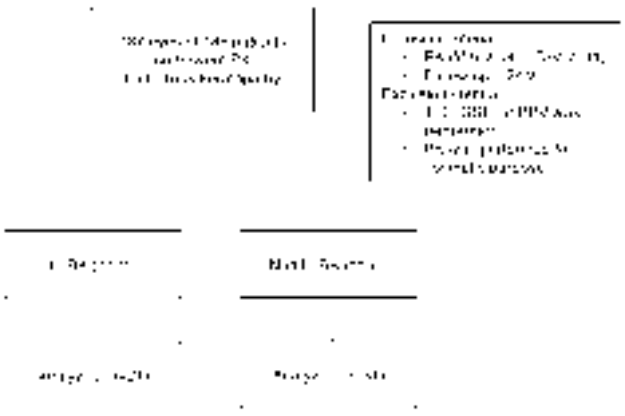

Fig. 1 Flow chart showing study participant inclusion. Abbreviations: PK, penetrating keratoplasty; LI-BK, argon laser iridotomy-induced bullous keratopathy; TLE, trabeculectomy; PPV, pars plana vitrectomy; and GSL, goniosynechialysis

Healon^{TM} ophthalmic viscoelastic substance (Abbott Laboratories), and the cornea was excised with curved corneal scissors. The donor corneas were trephined by the Barron^{TM} vacuum donor cornea punch (7.5 mm diameter). The corneal graft was sutured to the recipient with 4–8 interrupted and continuous running 10-0 nylon sutures. Topical antibiotics and corticosteroid drops were applied after PK and tapered down gradually. A single surgeon (S.K.) performed all PK procedures.

Statistical analysis was performed with R statistical package (version 3.4.1 for Windows). Student's t-test was applied to detect differences between two groups of donor age, donor size, and donor endothelial cell density data. The chi-square test was used to analyse the gender data and graft survival data. The slopes of cell loss of two groups were analyzed by a statistical test of the assumption of homogeneity of regression coefficients. To detect differences in cell density between the two groups, we applied Welch's t-test, and Bonferroni correction was used for a multiple-comparison correction. P-value of < 0.05 was considered statistically significant, but P-value of < 0.005 was considered statistically significant for the analyses to which Bonferroni correction was applied. Donor and recipient characteristics' data are presented as mean ± standard deviation (SD). The mean cell loss data are presented as mean ± standard error (SE).

Results

A total of 187 eyes of 186 patients underwent PK during the study period. Of these, 52 eyes of 52 patients were identified as meeting the inclusion criteria. Twenty-one eyes were included in the LI-BK group and 31 eyes were included in the non LI-BK group. The mean patient age was 60.4 ± 9.2

(range 33 to 75) years in the LI-BK group and 60.5 ± 12.0 (range 19 to 75) years in the non LI-BK group. In the 21 LI-BK patients, PK was combined with cataract surgery in 20 patients (IOL implantation in the capsular bag in 19 patients and IOL ciliary fixation in 1 patient) and PK alone was performed in one patient. In the 31 non LI-BK patients, PK was combined with cataract surgery in 14 patients (IOL implantation in the capsular bag in 10 patients and IOL ciliary fixation in 6 patients) and PK alone was performed in 17 patients. Baseline characteristics, such as age and gender, were similar between the groups, except for the indications for corneal transplantation. All LI-BK patients underwent LI prior to the diagnosis of BK, and other BK related pathological conditions, such as pseudophakic bullous keratopathy (PBK), aphakic bullous keratopathy (ABK), and Fuchs endothelial corneal dystrophy, were excluded. LI-BK patients who underwent pars plana vitrectomy before or after PK were also excluded. Donor characteristics between both groups were similar (Table 1).

Corneal endothelial cell density was determined from the patients whose corneal endothelial image was obtained by non-contact specular microscope. Though this density decreased in a similar fashion in both the LI-BK and non LI-BK groups, a statistical test of the assumption of homogeneity of regression coefficients revealed that cell density decreased significantly faster in the LI-BK group than in the non LI-BK group (p = 0.026) (Fig. 2). The mean cell loss in the LI-BK group increased from 25.6% at 12 months to 85.6% at 108 months (Supplementary Table 1). The mean cell loss in the non LI-BK group increased from 32.9% at 12 months to 72.0% at 108 months (Supplemental Table 1). The mean cell loss was not significantly higher for the LI-BK patients than for the non LI-BK patients throughout the observation time (Table 2). No graft failure (0%) occurred in any of the 21 eyes in the LI-BK group, while grafts failed in 4 of 25 eyes (16.0%) in the non LI-BK group during the 60 months after PK (p = 0.114).

Table 1 Characteristics of the donor and recipient eyes

	LI BK (n = 21)	Non LI BK (n = 31)	p value
Donor characteristics			
Age			0.98[a]
Mean ± SD, yrs	60.4 ± 9.2	60.5 ± 12.0	
Range	33 to 75	19 to 75	
Size			0.50[a]
Mean ± SD, mm	7.7 ± 0.1	7.7 ± 0.2	
Range	7.25 to 7.75	7.25 to 7.75	
Endothelial cell density			
Mean ± SD, cells/mm^2	2968 ± 445	2886 ± 333	0.46[a]
Recipient characteristics			
Age			0.11[a]
Mean ± SD, yrs	70.4 ± 6.2	65.4 ± 12.7	
Range	55 to 82	38 to 84	
Gender, no. (%)			0.21[b]
Male	7 (33.3%)	17 (54.8%)	
Female	14 (66.7%)	14 (45.2%)	
Diagnosis, no. (%)			
LI BK	21 (100.0%)	0 (0.0%)	
PBK	0 (0.0%)	10 (32.2%)	
Glaucoma related	0 (0.0%)	8 (25.8%)	
ABK	0 (0.0%)	6 (19.4%)	
Fuchs dystrophy	0 (0.0%)	4 (12.9%)	
Others	0 (0.0%)	3 (9.7%)	

[a] *P*-value of Student's t-test

[b] *P*-value of Chi-square test

Discussion

A national survey of BK in Japan revealed a mean interval from LI to the development of BK of 6.8 years, with a range between 2 months and 20 years [10]. Ang et al. similarly report a mean duration of 6.9 years and a range from 0.2 to 16 years in a Japanese population [7], whereas Lim et al. report a mean duration of 5.5 ± 2.8 years in a Chinese cohort in Singapore [6]. Thus, the mean duration for acute corneal endothelial damage is relatively long and some patients exhibit BK even 20 years after LI, which suggests the possibility of a combined mechanism that damages the corneal endothelium at the chronic phase.

Several potent causes of chronic corneal endothelial damage have been hypothesized. For example, Kaji and

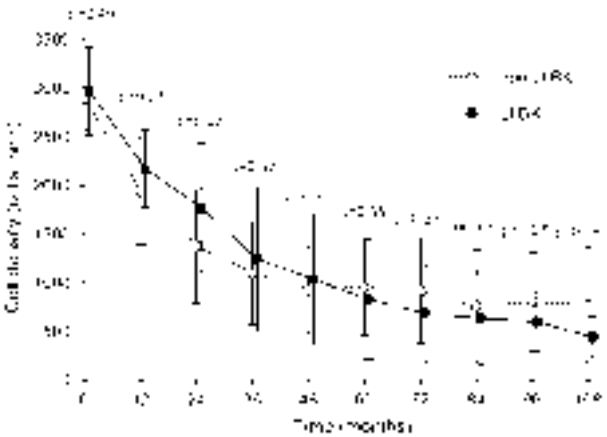

Fig. 2 Comparison of corneal endothelial cell loss after penetrating keratoplasty in the LI-BK and non LI-BK groups. The mean corneal endothelial cell densities of the patients who underwent penetrating keratoplasty for LI-BK and non LI-BK are plotted. Cell density continuously decreased in a similar fashion in both groups

Table 2 Numbers of graft failures in the LI BK and non LI BK groups

Time (month)	0	12	24	36	48	60	72	84	96	108
LI BK										
Total patient number (clear[1], clear without CE image[2], failed[3])	21 (21,0,0)	21 (21,0,0)	21 (21,0,0)	21 (21,0,0)	21 (21,0,0)	21 (21,0,0)	21 (19,2,0)	18 (17,1,0)	16 (14,2,0)	11 (9,2,0)
Non LI BK										
Total patient number (clear[1], clear without CE image[2], failed[3])	31 (31,0,0)	31 (31,0,0)	31 (29,2,0)	29 (27,1,1)	28 (25,2,1)	25 (21,0,4)	24 (15,4,5)	20 (14,0,6)	20 (12,1,7)	19 (12,0,7)
P-value[4]	1.00	1.00	1.00	1.00	1.00	0.114	0.051	0.021	0.011	0.012

1. Clear graft with corneal endothelium (CE) image was obtained by non-contact specular microscope
2. Clear graft, but CE image was not obtained by non-contact specular microscope
3. Accumulated numbers of patients with failed graft
4. *P*-value for Fisher's exact test (clear + clear without CE image vs. failed)

colleagues used a virtual model of LI to show that under certain conditions, such as a small diameter of the iris hole and a short distance between the iris hole and corneal endothelium, shear stress could cause time-dependent damage to the corneal endothelium [12]. Likewise, the monitoring of the aqueous flow by injection of silicone particles into the anterior chamber in rabbits revealed a faster aqueous humor stream (i.e., stronger shear) against the corneal endothelium following LI [13]. Higashihara and colleagues demonstrated a disruption of the blood-aqueous barrier in patients' eyes following prophylactic LI and suggest chronic postsurgical breakdown as a reason for corneal endothelial decompensation, possibly due to the humoral transport of substances such as prostaglandins and cytokines [14].

Recent developments in corneal endothelial transplantation have enabled the treatment of LI-induced BK with a success rate comparable to that for other types of BK [15–17]. Observations for 6 months and 3 years in independent facilities revealed that Descemet's stripping automated endothelial keratoplasty (DSAEK) for LI-induced BK showed equivalent corneal endothelial cell loss to that obtained for Fuchs endothelial corneal dystrophy and PBK [18, 19]. These data suggest that the existence of LI prior to corneal transplantation does not harm the donor corneal endothelium. In addition, these data may suggest that corneal endothelial damage by LI may arise predominantly due to acute injury occurring during or immediately following the procedure. In line with these findings, we showed that graft survival of PK was as good in the eyes with LI as in the eyes without LI. However, our study, which included 108 months long-term follow up, shows that the cell loss slope was significantly faster in the PK graft used to treat LI-induced BK than in grafts used to treat BK caused for other reasons. Since existence of LI prior to PK did not induce corneal endothelial decompensation after PK whereas it did induce corneal endothelial decompensation before PK, acute corneal endothelial injury by LI seems to plays an important role in inducing BK. However, our current results also support the existence of previously proposed chronic damage due to LI including shear stress or disruption of the blood-aqueous barrier [12–14].

LI has been performed using a few different laser types, including argon, neodymium-doped yttrium aluminum garnet (Nd:YAG), and argon Nd:YAG sequential lasers. Early research suggested that, in dark brown irises, the use of the Nd:YAG laser alone was less effective when compared to the argon laser [2]. In the 1990s, when researchers noticed the increasing incidence of LI-induced BK, procedures using argon lasers alone or argon Nd:YAG sequential procedures were preferred, perhaps due to their high effectiveness in dark Japanese irises [7, 9, 10]. However, the Nd:YAG laser enabled iridotomy under lower power than with the argon laser, because Nd:YAG has a high energy but a spot profile

with fewer and shorter duration laser flashes [7, 20]. One possible explanation why BK damage is more frequent in Asian countries could be the preference for argon lasers' use for dark irises [9, 10]. In line with this explanation, our data show that LI caused BK, but did not increase the graft failure after PK. As our study is a prospective study and many patients were referred to our hospital for the purpose of corneal transplantation, we were unable to obtain sufficient information about which laser was used for LI. Further study that will include information about the LI procedure will be beneficial for a better understanding of cell loss after PK for treating LI-BK.

In conclusion, we showed that the outcome of PK was no worse for BK secondary to LI than for other types of BK. However, our long-term observation showed that the corneal endothelial cell density exhibited a more rapid decrease in the LI-BK eyes than in the non LI-BK eyes after PK. These findings suggest that acute corneal endothelial injury by LI seems to be a necessary factor to induce BK, but the combined mechanisms of chronic injury cannot be excluded from the pathophysiology of corneal endothelial damage after LI.

Acknowledgements The authors wish to thank Dr. Hiroko Nakagawa for her valuable assistance with the collection of patient data, Dr. Kengo Yoshii and Mr. Ryousuke Hayashi for assistance with statistical analysis, and Mr. John Bush for editing the manuscript.

Conflicts of interest N. Okumura, None; A. Kusakabe, None; N. Koizumi, None; K. Wakimasu, None; K. Kayukawa, None; M. Kondo, None; K. Mori, None; C. Sotozono, None; S. Kinoshita, None.

References

1. Ramulu PY, Corcoran KJ, Corcoran SL, Robin AL. Utilization of various glaucoma surgeries and procedures in Medicare beneficiaries from 1995 to 2004. Ophthalmology. 2007;114:2265–70.
2. Wang PX, Koh VT, Loon SC. Laser iridotomy and the corneal endothelium: a systemic review. Acta Ophthalmol. 2014;92:604–16.
3. Pollack IP. Current concepts in laser iridotomy. Int Ophthalmol Clin. 1984;24:153–80.
4. Schwartz AL, Martin NF, Weber PA. Corneal decompensation after argon laser iridectomy. Arch Ophthalmol. 1988;106:1572–4.
5. Jeng S, Lee JS, Huang SC. Corneal decompensation after argon laser iridectomy—a delayed complication. Ophthalmic Surg. 1991;22:565–9.
6. Lim LS, Ho CL, Ang LP, Aung T, Tan DT. Inferior corneal decompensation following laser peripheral iridotomy in the superior iris. Am J Ophthalmol. 2006;142:166–8.
7. Ang LP, Higashihara H, Sotozono C, Shanmuganathan VA, Dua H, Tan DT, et al. Argon laser iridotomy-induced bullous keratopathy a growing problem in Japan. Br J Ophthalmol. 2007;91:1613–5.
8. Shimazaki J, Uchino Y, Tsubota K. Late irreversible corneal oedema after laser iridotomy. Br J Ophthalmol. 2009;93:125–6.
9. Kashiwagi K, Tsukahara S. Examination and treatment of patients with angle-closure glaucoma in Japan: results of a nationwide survey. Jpn J Ophthalmol. 2004;48:133–40.
10. Shimazaki J, Amano S, Uno T, Maeda N, Yokoi N, Japan Bullous Keratopathy Study G. National survey on bullous keratopathy in Japan. Cornea. 2007;26:274–8.
11. Eye Bank Association of America. Eye banking statistical report. Washington, DC. 2016.
12. Kaji Y, Oshika T, Usui T, Sakakibara J. Effect of shear stress on attachment of corneal endothelial cells in association with corneal endothelial cell loss after laser iridotomy. Cornea. 2005;24:S55–8.
13. Yamamoto Y, Uno T, Shisida K, Xue L, Shiraishi A, Zheng X, et al. Demonstration of aqueous streaming through a laser iridotomy window against the corneal endothelium. Arch Ophthalmol. 2006;124:387–93.
14. Higashihara H, Sotozono C, Yokoi N, Inatomi T, Kinoshita S. The blood-aqueous barrier breakdown in eyes with endothelial decompensation after argon laser iridotomy. Br J Ophthalmol. 2011;95:1032–4.
15. Kobayashi A, Yokogawa H, Sugiyama K. Descemet stripping with automated endothelial keratoplasty for bullous keratopathies secondary to argon laser iridotomy–preliminary results and usefulness of double-glide donor insertion technique. Cornea. 2008;27(Suppl 1):S62–9.
16. Kobayashi A, Yokogawa H, Sugiyama K. Non-descemet stripping automated endothelial keratoplasty for endothelial dysfunction secondary to argon laser iridotomy. Am J Ophthalmol. 2008;146:543–9.
17. Kobayashi A, Yokogawa H, Yamazaki N, Masaki T, Sugiyama K. The use of endoillumination probe-assisted Descemet membrane endothelial keratoplasty for bullous keratopathy secondary to argon laser iridotomy. Clin Ophthalmol. 2015;9:91–3.
18. Hirayama M, Yamaguchi T, Satake Y, Shimazaki J. Surgical outcome of Descemet's stripping automated endothelial keratoplasty for bullous keratopathy secondary to argon laser iridotomy. Graefes Arch Clin Exp Ophthalmol. 2012;7:1043–50.
19. Nakatani S, Murakami A. Three-year outcome of Descemet stripping automated endothelial keratoplasty for bullous keratopathy after argon laser iridotomy. Cornea. 2014;33:780–4.
20. Ho T, Fan R. Sequential argon-YAG laser iridotomies in dark irides. Br J Ophthalmol. 1992;76:329–31.

Immune Cells on the Donor Corneal Endothelium After Corneal Transplantation

Naoki Okumura, MD, PhD, Ryota Inoue, BS, MS,* Shinichiro Nakano, BS, MS,* Hirofumi Imai, BS,* Daiki Matsumoto, BS,* Kanae Kayukawa, MD,† Koichi Wakimasu, MD,† Koji Kitazawa, MD, PhD,† Noriko Koizumi, MD, PhD,* and Shigeru Kinoshita, MD, PhD†‡*

Purpose: The aim of this study was to investigate the existence of presumed immune cells observed by contact specular microscopy in patients who underwent penetrating keratoplasty (PK) and Descemet stripping automated endothelial keratoplasty (DSAEK).

Methods: This cross-sectional study was conducted on consecutive patients who underwent follow-up visits between January and March 2015 for previously performed PK or DSAEK. Presumed immune cell–suspected "cell-like white dots" were evaluated by scanning slit contact specular microscopy. The association between the grading of presumed immune cells with clinical parameters, such as corneal endothelial cell density, time after surgery, and the titer of steroid administration, was also investigated.

Results: A total of 54 eyes of 54 patients who underwent PK (32 eyes/32 patients) and DSAEK (22 eyes/22 patients) were evaluated, and suspected immune cells were observed in all patients. In the PK and DSAEK groups, the number of patients in the presumed immune cell grades 1, 2, 3, and 4 were 19, 10, 2, and 1 and 10, 8, 2, and 2, respectively (P = 0.663). No statistically significant association was found between the immune cell grades and the clinical parameters.

Conclusions: Immune cells were observed on the corneal endothelial grafts in all 54 patients who underwent PK or DSAEK. Although the number of immune cells varied between patients and showed no correlation with clinical parameters, it would be beneficial to conduct a future prospective study to analyze the effect of immune cells on postoperative corneal endothelial cell loss.

Received for publication February 8, 2018; revision received April 21, 2018; accepted May 15, 2018. Published online ahead of print June 26, 2018.
From the *Department of Biomedical Engineering, Faculty of Life and Medical Sciences, Doshisha University, Kyotanabe, Japan; †Baptist Eye Institute, Kyoto, Japan; and ‡Department of Frontier Medical Science and Technology for Ophthalmology, Kyoto Prefectural University of Medicine, Kyoto, Japan.
The authors have no funding or conflicts of interest to disclose.
Supplemental digital content is available for this article. Direct URL citations appear in the printed text and are provided in the HTML and PDF versions of this article on the journal's Web site (www.corneajrnl.com).
Correspondence: Shigeru Kinoshita, MD, PhD, Department of Frontier Medical Science and Technology for Ophthalmology, Kyoto Prefectural University of Medicine, 465 Kajii-cho, Hirokoji-agaru, Kawaramachi-dori, Kamigyo-ku, Kyoto 602-0841, Japan (e-mail: shigeruk@koto.kpu-m.ac.jp).

Key Words: penetrating keratoplasty, Descemet stripping endothelial keratoplasty, corneal endothelium

(*Cornea* 2018;37:1081–1086)

For more than a century, penetrating keratoplasty (PK) has been performed, and over the past decade, corneal endothelial transplantations such as Descemet stripping automated endothelial keratoplasty (DSAEK) and Descemet membrane endothelial keratoplasty (DMEK) have become widespread standard procedures for treatment of corneal endothelial decompensation.[1] Those corneal transplantation methods are now generally accepted as standard procedures; however, graft failure remains a long-term postoperative threat for patients who undergo surgery. Graft failure can be broken down into 3 main causes: 1) primary graft failure, 2) immunological rejection, and 3) late endothelial failure.[2] Although primary graft failure is mainly iatrogenic and the mechanism of immunological rejection has been intensively investigated, the primary mechanism of late endothelial failure has yet to be elucidated.

We recently reported the observance of "cell-like white dots" on the endothelium of the transplanted corneal graft via the use of scanning slit contact specular microscopy in patients who exhibited no characteristic features of graft rejection.[3] In addition, using rabbit models subjected to syngeneic or allogeneic corneal transplantation, we showed that "cell-like white dots" were evident only in the allogeneic corneal graft and that they were immune cells composed of, and at the least, T lymphocytes, B lymphocytes, macrophages, and neutrophils. We speculated that these immune cells observed on the corneal endothelium can play a role in the underlying pathophysiology of late endothelial failure and that these phenomena are worth investigation.[3]

In this current study, we used scanning slit contact specular microscopy to investigate the existence of "cell-like white dots" in patients who underwent PK and DSAEK. We also evaluated whether the numbers of the "cell-like white dots" (as presumed immune cells) were associated with clinical parameters such as corneal endothelial cell (CEC) density, the time at which they appeared after surgery, and the use of steroids.

MATERIALS AND METHODS

All clinical data were obtained in accordance with the tenets set forth in the Declaration of Helsinki. The study

TABLE 1. Characteristics of the Patients Who Underwent PK or DSAEK

	PK (n = 32)	DSAEK (n = 22)	Total (n = 54)
Age			
Mean ± SD, yrs	63.2 ± 20.0	73.5 ± 7.0	67.4 ± 16.7
Range	21–84	62–86	21–86
Sex, no. (%)			
Male	14 (43.8%)	7 (31.8%)	21 (38.9%)
Female	18 (56.2%)	15 (68.2%)	33 (61.1%)

protocol was approved by the Kyoto Ethics Review Committee, Kyoto, Japan (Approval #1604) (UMIN000024891).

In this study, we recruited consecutive patients who had undergone PK or DSAEK by a single surgeon (S.K.) and who underwent follow-up examination at the Baptist Eye Institute between January and March 2015. In the patients who underwent bilateral PK or DSAEK, the right eye data were used for the study. All patients were examined only once for this current research. Exclusion criteria included patients who had undergone DSAEK because of a failed PK graft and shunt surgery or who had been diagnosed with corneal endothelial dystrophies or active uveitis. The titer of steroid administration was scored as follows: 1) score 1: 0.1% betamethasone eye drops administered once daily and 2) score 0.1: 0.1% fluorometholone eye drops administered once daily. None of the patients in this study underwent systemic steroid treatment.

Anterior segments were evaluated by slit-lamp microscopy, and the corneal endothelium was analyzed with a prototype KSSP slit-scanning wide-field contact specular microscope (Konan Medical, Inc, Nishinomiya, Japan), as previously described.[4] The specular microscope had a ½-inch camera including a 400,000-pixel charge-coupled device sensor with ×9.9 magnification and a ×40 magnification contact cone lens. Corneal endothelial images were obtained as movie files (ie, MPEG-2 files) at the rate of 60 frames per second. The images, 5-mm in diameter, were obtained at the corneal center, and representative images were extracted from the MPEG-2 files. We graded the existence of presumed immune cells, represented as "white dots," as follows: grade 0 (no white dot observed in all images obtained by contact specular microscopy), grade 1 (white dot observed at the average number of 1 per field), grade 2 (white dots observed at the average number of 1–2 per field), grade 3 (white dots observed at the average number of 2–3 per field), and grade 4

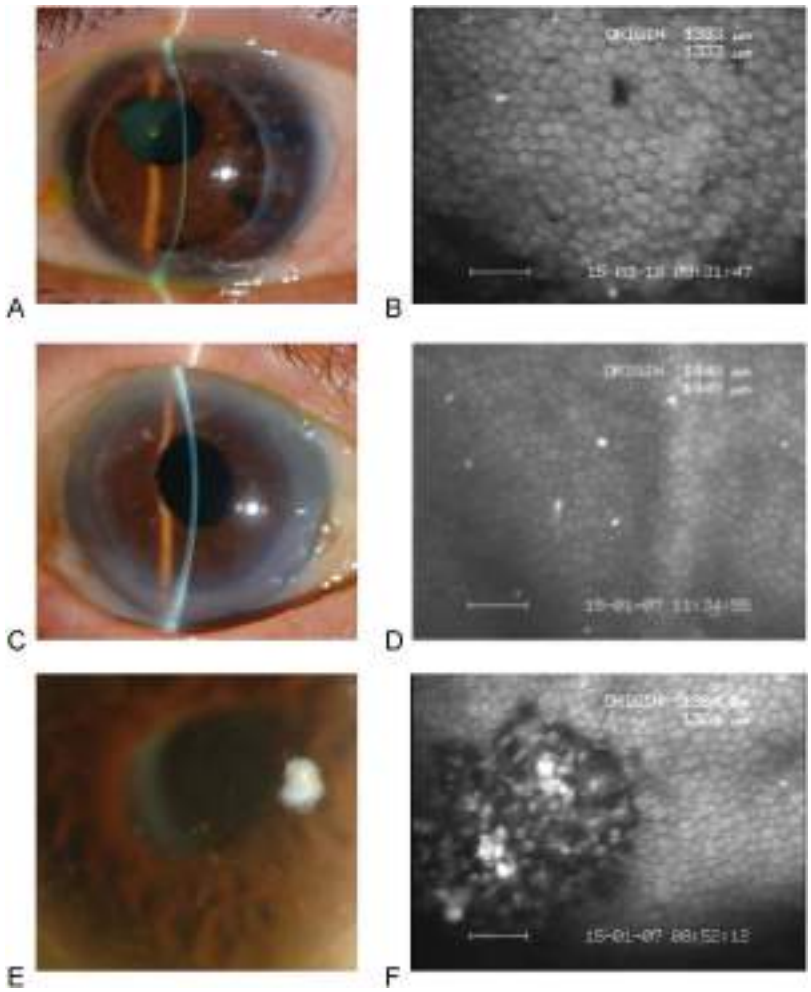

FIGURE 1. Slit-lamp and contact specular microscopy images of patients with immune cell–suspected "cell-like white dots" on their corneal endothelium. A, Slit-lamp microscopy image of a 44-year-old man who had undergone PK 6 years previously. No clinical features suggesting graft rejection were observed. B, Contact specular microscopy image showing the existence of "cell-like white dots" on the transplanted corneal endothelial graft. C, Slit-lamp microscopy image of an 86-year-old man who had undergone DSAEK 3 years previously. D, "Cell-like white dots" can be seen on the DSAEK corneal endothelial graft. E, Slit-lamp microscopy image of a 70-year-old man diagnosed with CMV corneal endotheliitis 2 months after undergoing DSAEK. F, "Cell-like white dots", which are suspected to be immune cells, were observed at the site of the damaged corneal endothelium by contact specular microscopy.

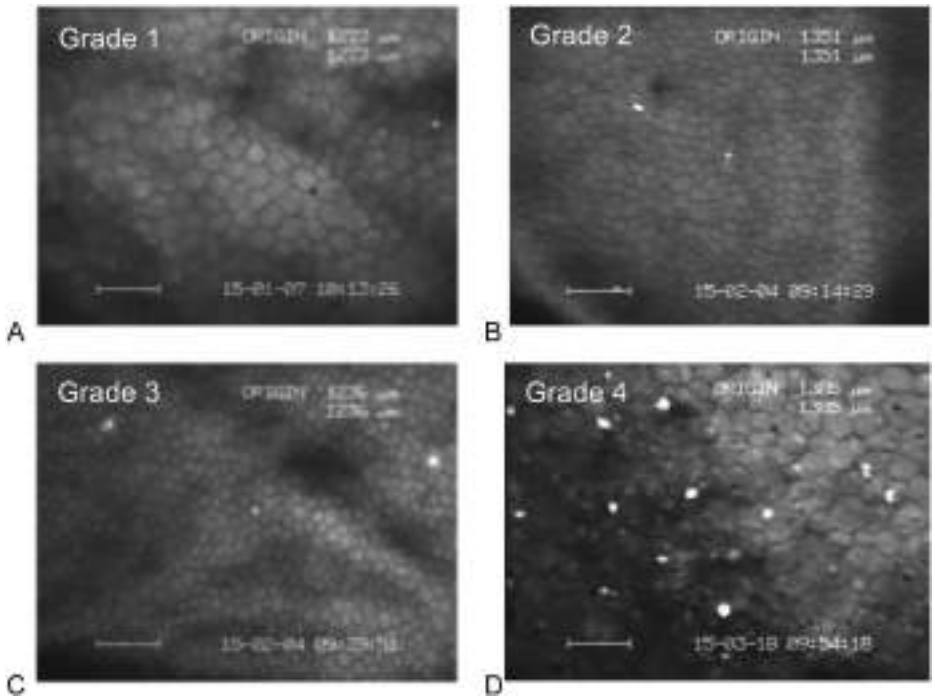

FIGURE 2. Grading of immune cell–suspected "cell-like white dots" evaluated by contact specular microscopy. A, Representative image of grade 1 (white dot observed at the average number of less than 1 per field). Note that although no white dot exists on the representative image, white dots were observed in the other areas in this patient. B, Representative image of grade 2 (white dot observed at the average number of 1–2 per field). C, Representative image of grade 3 (white dots observed at the average number of 2–3 per field). D, Representative image of grade 4 (white dots observed at the average number of more than 3 per field).

(white dots observed at the average number of more than 3 per field) (see Supplemental Table 1, Supplemental Digital Content 1, http://links.lww.com/ICO/A688).

Statistical analysis was performed with IBM SPSS Statistics version 24 (IBM Corp, Armonk, NY) software. The Fisher exact test was used to evaluate the differences of grade for the "cell-like white dots" between the 2 groups. The Spearman rank correlation coefficient was used to determine whether there were significant correlations between the grade of suspected immune cells and the other clinical factors including CEC density, time after surgery, and titer of steroid. $P < 0.05$ was considered statistically significant. Data were expressed as mean ± SD.

RESULTS

In the current study, a total of 54 eyes of 54 patients who underwent PK (32 eyes of 32 patients) and DSAEK (22 eyes of 22 patients) were evaluated at each follow-up visit during the study period. The mean patient age was 63.2 ± 20.0 years (range, 21–84 yrs) in the PK group and 73.5 ± 7.0 years (range, 62–86 yrs) in the DSAEK group (Table 1).

Representative slit-lamp microscopy images of a 44-year-old man who had undergone PK 6 years previously and of an 86-year-old man who had undergone DSAEK 3 years previously are shown in Figures 1A and 1C, respectively. No clinical signs of graft rejection, such as graft edema, Descemet folds, keratic precipitates, and conjunctival injection, were observed in both patients. In addition, no uveitis or other ocular inflammatory disorder was observed. However, the contact specular microscopy images demonstrated the presence of "cell-like white dots" on the grafted corneal endothelium (Figs. 1B, D). Representative slit-lamp microscopy images of a 70-year-old male patient who had been diagnosed with cytomegalovirus (CMV) corneal endotheliitis at 2 months post-DSAEK in whom the corneal endothelium is supposed to have immune cells are shown in Figure 1E. In that patient, keratic precipitates exhibiting coin-like lesions suggesting CMV corneal endotheliitis were observed,[5–7] and CMV was identified from the aqueous humor by polymerase chain reaction. Contact specular microscopy showed white dots, which we suspected to be immune cells, at the site of the damaged corneal endothelium (Fig. 1F). Those white dots showed a similarity to those observed in the patients who underwent PK or DSAEK (Figs. 1B, D).

Because the severity of presumed immune cells varied among the patients, we graded each patient according to the number of cell-like white dots (Figs. 2A–D) (see Supplemental Table 1, Supplemental Digital Content 1, http://links.lww.com/ICO/A688). The mean time after surgery was 55.0 ± 56.7 months (range, 4–186 mo) in the PK group and 31.1 ± 27.3 months (range, 2–94 mo) in the DSAEK group. In the PK group, the mean CEC densities in grades 1, 2, 3, and 4 were 1132 (n = 19), 1415 (n = 10), 763 (n = 2), and 549 (n = 1), respectively. In the DSAEK group, the mean CEC densities in grades 1, 2, 3, and 4 were 1008 (n = 10), 1316 (n = 8), 650 (n = 2), and 2211 (n = 2), respectively (Table 2). No grade 0 was observed in both groups. The Spearman rank correlation coefficient showed no statistically significant association between CEC density and the grade of immune cells in both PK and DSAEK groups ($P = 0.918$ and $P = 0.949$, respectively) (see Supplemental Figure 1, Supplemental Digital Content 2, http://links.lww.com/ICO/A689). No statistically significant difference between the keratoplasty techniques and the grade of immune cells was observed ($P = 0.671$).

Next, we evaluated the association between the presumed immune cells observed on the corneal endothelium of

TABLE 2. CEC Density in Each Grade of Immune Cells in Both PK and DSAEK Groups

	Grade 1	Grade 2	Grade 3	Grade 4	Total
	n = 19	n = 10	n = 2	n = 1	n = 32
PK					
Cell density (cells/mm^2)					
Mean ± SD	1132 ± 676	1415 ± 953	763 ± 370	549	1179 ± 759
Range	255–2506	329–2646	501–1024	549	255–2646
Time after surgery (mo)					
Mean ± SD	50.9 ± 49.5	34.9 ± 43.0	129.5 ± 79.9	185.0	55.0 ± 56.7
Range	6–171	4–112	73–186	185	4–186
	Grade 1	**Grade 2**	**Grade 3**	**Grade 4**	**Total**
	n = 10	**n = 8**	**n = 2**	**n = 2**	**n = 22**
DSAEK					
Cell density (cells/mm^2)					
Mean ± SD	1008 ± 396	1316 ± 586	650 ± 208	2211 ± 59	1197 ± 577
Range	363–1650	390–2083	503–797	2169–2252	363–2252
Time after surgery (mo)					
Mean ± SD	35.6 ± 30.2	25.4 ± 30.7	31.5 ± 17.7	31.5 ± 6.4	31.1 ± 27.3
Range	2–81	2–94	19–44	27–36	2–94

the graft and the clinical parameters. The Spearman rank correlation coefficient showed no statically significant association between the CEC density and the grade of immune cells in both PK (Fig. 3A) and DSAEK groups (Fig. 3B). In addition, no statically significant association was found between the time after surgery and the grading in both PK (Fig. 3C) and DSAEK groups (Fig. 3D). All patients were medicated with steroid eye drops (dexamethasone or fluorometholone), and none of the patients underwent systemic steroid treatment. Next, the association between the score of steroid use (as described above) and the grading of immune cells was evaluated. No statistically significant association was observed between the steroid score and the grade of immune cells in both PK (Fig. 3E) and DSAEK groups (Fig. 3F).

DISCUSSION

It has previously been reported that in patients who undergo PK, CEC density decreases 30% to 50% in the first postoperative year[8] and that the speed of CEC loss gradually declines during that period. Bourne et al,[9] Ing et al,[10] and Patel et al[11] showed in their prospective studies of a large PK series performed by a single surgeon that annual CEC loss was 7.8% from 3 to 5 years and 4.2% from 5 to 10 years and became similar to the level observed in normal corneas (0.6%)[12] from 10 to 15 years postoperatively. Likewise, multiple large cohort studies demonstrated that faster CEC loss was observed after PK in comparison with that of normal corneas.[13,14] Similar to PK, corneal endothelial transplantations such as DSAEK[15–19] and DMEK[20–22] reportedly exhibit faster CEC loss in comparison with that of normal corneas. However, although it is widely known that long-term postoperative results show faster CEC loss after corneal transplantation, the underlying mechanisms have yet to be fully elucidated.

It has been assumed that 1 possible explanation for long-term continuous CEC loss is the "chronic subclinical immune reaction to donor cells;" however, this assumption has yet to be proved. Birnbaum et al[23] reported that the annual loss of CECs was 1.1% in 6 patients who underwent autologous rotational keratoplasty, whereas the CEC loss in the histological control group (ie, 53 patients who underwent allogeneic PK) in that study was 16.7%. Although it was a retrospective study and included only 6 autologous rotational keratoplasty patients, they proposed that an immunological influence might be the primary cause of continuous CEC loss after corneal transplantation.

In this current study, we showed that "cell-like white dots," which based on the findings of rabbit model animal experiments are believed to be immune cells, were observed in all 54 patients (ie, the 32 PK patients and the 22 DSAEK patients) who do not exhibit any sign of corneal rejection. We theorized that if those suspected immune cells were induced by surgical intervention or simply by the wound healing process, a larger number of immune cells would be observed in the early period compared with the later period after corneal transplantation. However, our current results showed no correlation between the time after surgery and the grade of immune cells. In addition, our results showed no correlation between the titer of steroid administration and the grade of immune cells. Those findings might support the idea that immune cells were recruited by recognition of allogeneic CECs or corneal stromal cells.

It should be noted that one important question that remains is whether immune cells observed in the transplanted corneal graft induce CEC damage. Our current data showed no correlation between CEC density and the grade of immune cells. However, because this was a "cross-sectional" study, we were not able to evaluate the effect of the severity of immune cell grade on cell loss in the same patient by follow-up observation. As previously reported, CEC density during the early period post-PK is predictive of late-period endothelial graft failure, although overall CEC loss is not always predictive of corneal function.[2] For example, Nishimura et al[8]

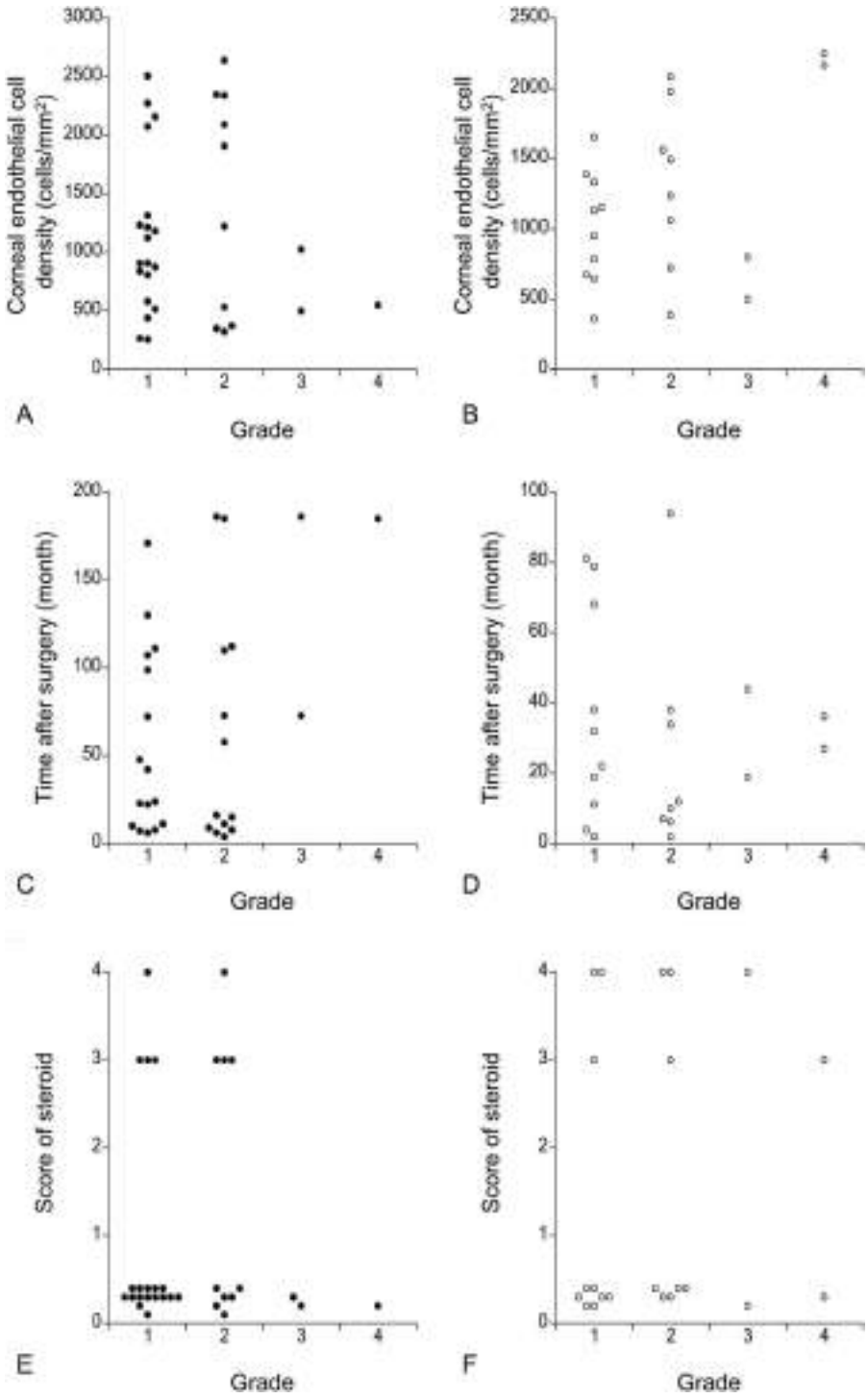

FIGURE 3. Association between the immune cells and the clinical parameters. A and B, No statistically significant association was observed between the CEC density and the grade of immune cells in both PK (P = 0.879) (A) and DSAEK groups (P = 0.166) (B). C and D, No statistically significant association was observed between the time after surgery and the grade of immune cells in both PK (P = 0.640) (C) and DSAEK groups (P = 0.966) (D). E and F, No statistically significant association was observed between the steroid titer and the grade of immune cells in both PK (P = 0.482) (E) and DSAEK groups (P = 0.599) (F).

reported that CEC loss at 2 months postoperatively was correlated with graft failure and that a Specular Microscopy Ancillary Study similarly showed that CEC density at 6 months postoperatively predicted corneal decompensation.[14] Therefore, it would be worth conducting a prospective study to evaluate the presence of immune cells in the earlier postoperative period and its correlation with future cell loss. In addition, we could not eliminate the possibility that not all "cell-like white dots" observed in our current study were alive immune cells and that certain numbers (or all) of the cells were not alive. From this aspect, a future prospective study in which the immune cells will be followed up in the same patients will reveal the cell fate; that is, whether the immune cells are recruited and then disappear or stay for a long period once they are recruited. Another interesting question is whether patients who undergo DMEK have immune cells

on the transplanted corneal graft. Because DMEK grafts include only CECs, and not stromal cells, it would be beneficial to understand how the immune cells were recruited; that is, allogeneic CECs recruited immune cells or allogeneic corneal stromal cells recruited immune cells.

In conclusion, the findings in this present study show that presumed immune cells exist on the grafted corneal endothelium in patients who undergo PK and DSAEK and that the number of those cells varies between patients. The findings in this cross-sectional study showed no correlation between the number of immune cells and CEC loss, the time after surgery, and the steroid titer. However, a future prospective study to analyze the effect of immune cells on future cell loss will hopefully provide beneficial information. Moreover, if immune cells are proven to be a causative factor for CEC loss, they might become a therapeutic target for preventing late-postoperative endothelial failure.

ACKNOWLEDGMENTS

The authors thank Dr. Hiroko Nakagawa for valuable discussion about this study and Mr. John Bush for editing the manuscript.

REFERENCES

1. Tan DT, Dart JK, Holland EJ, et al. Corneal transplantation. *Lancet*. 2012;379:1749–1761.
2. Patel SV. Graft survival and endothelial outcomes in the new era of endothelial keratoplasty. *Exp Eye Res*. 2012;95:40–47.
3. Koudouna E, Okumura N, Okazaki Y, et al. Immune cells on the corneal endothelium of an allogeneic corneal transplantation rabbit model. *Invest Ophthalmol Vis Sci*. 2017;58:242–251.
4. Tanaka H, Okumura N, Koizumi N, et al. Panoramic view of human corneal endothelial cell layer observed by a prototype slit-scanning wide-field contact specular microscope. *Br J Ophthalmol*. 2017;101:655–659.
5. Koizumi N, Yamasaki K, Kawasaki S, et al. Cytomegalovirus in aqueous humor from an eye with corneal endotheliitis. *Am J Ophthalmol*. 2006; 141:564–565.
6. Koizumi N, Suzuki T, Uno T, et al. Cytomegalovirus as an etiologic factor in corneal endotheliitis. *Ophthalmology*. 2008;115:292–297 e293.
7. Koizumi N, Inatomi T, Suzuki T, et al. Clinical features and management of cytomegalovirus corneal endotheliitis: analysis of 106 cases from the Japan corneal endotheliitis study. *Br J Ophthalmol*. 2015;99:54–58.
8. Nishimura JK, Hodge DO, Bourne WM. Initial endothelial cell density and chronic endothelial cell loss rate in corneal transplants with late endothelial failure. *Ophthalmology*. 1999;106:1962–1965.
9. Bourne WM, Hodge DO, Nelson LR. Corneal endothelium five years after transplantation. *Am J Ophthalmol*. 1994;118:185–196.
10. Ing JJ, Ing HH, Nelson LR, et al. Ten-year postoperative results of penetrating keratoplasty. *Ophthalmology*. 1998;105:1855–1865.
11. Patel SV, Diehl NN, Hodge DO, et al. Donor risk factors for graft failure in a 20-year study of penetrating keratoplasty. *Arch Ophthalmol*. 2010; 128:418–425.
12. Bourne WM, Nelson LR, Hodge DO. Central corneal endothelial cell changes over a ten-year period. *Invest Ophthalmol Vis Sci*. 1997;38:779–782.
13. Tan DT, Janardhanan P, Zhou H, et al. Penetrating keratoplasty in Asian eyes: the Singapore corneal transplant study. *Ophthalmology*. 2008;115: 975–982.e971.
14. Lass JH, Sugar A, Benetz BA, et al. Endothelial cell density to predict endothelial graft failure after penetrating keratoplasty. *Arch Ophthalmol*. 2010;128:63–69.
15. Terry MA, Wall JM, Hoar KL, et al. A prospective study of endothelial cell loss during the 2 years after deep lamellar endothelial keratoplasty. *Ophthalmology*. 2007;114:631–639.
16. Price MO, Price FW Jr. Endothelial cell loss after descemet stripping with endothelial keratoplasty influencing factors and 2-year trend. *Ophthalmology*. 2008;115:857–865.
17. Lee WB, Jacobs DS, Musch DC, et al. Descemet's stripping endothelial keratoplasty: safety and outcomes: a report by the American Academy of Ophthalmology. *Ophthalmology*. 2009;116:1818–1830.
18. Price MO, Price FW Jr. Endothelial keratoplasty: a review. *Clin Exp Ophthalmol*. 2010;38:128–140.
19. Price MO, Fairchild KM, Price DA, et al. Descemet's stripping endothelial keratoplasty five-year graft survival and endothelial cell loss. *Ophthalmology*. 2011;118:725–729.
20. Price MO, Giebel AW, Fairchild KM, et al. Descemet's membrane endothelial keratoplasty: prospective multicenter study of visual and refractive outcomes and endothelial survival. *Ophthalmology*. 2009;116:2361–2368.
21. Ham L, van Luijk C, Dapena I, et al. Endothelial cell density after descemet membrane endothelial keratoplasty: 1- to 2-year follow-up. *Am J Ophthalmol*. 2009;148:521–527.
22. Laaser K, Bachmann BO, Horn FK, et al. Donor tissue culture conditions and outcome after descemet membrane endothelial keratoplasty. *Am J Ophthalmol*. 2011;151:1007–1018 e1002.
23. Birnbaum F, Reinhard T, Bohringer D, et al. Endothelial cell loss after autologous rotational keratoplasty. *Graefes Arch Clin Exp Ophthalmol*. 2005;243:57–59.

Effect of a p38 Mitogen-Activated Protein Kinase Inhibitor on Corneal Endothelial Cell Proliferation

Makiko Nakahara, Naoki Okumura, Shinichiro Nakano, and Noriko Koizumi

Department of Biomedical Engineering, Faculty of Life and Medical Sciences, Doshisha University, Kyotanabe, Japan

Correspondence: Noriko Koizumi, Department of Biomedical Engineering, Faculty of Life and Medical Sciences, Doshisha University, Kyotanabe 610-0321, Japan; nkoizumi@mail.doshisha.ac.jp.

Submitted: March 20, 2018
Accepted: July 23, 2018

Citation: Nakahara M, Okumura N, Nakano S, Koizumi N. Effect of a p38 mitogen-activated protein kinase inhibitor on corneal endothelial cell proliferation. *Invest Ophthalmol Vis Sci*. 2018;59:4218–4227. https://doi.org/10.1167/iovs.18-24394

Purpose. We have performed clinical research on cell-based therapy for corneal endothelial decompensation since 2013. The purpose of this study was to investigate the usefulness of a p38 MAPK inhibitor for promoting proliferation of human corneal endothelial cells (HCECs).

Methods. HCECs were cultured in media supplemented with various low-molecular-weight compounds to screen for the effect of those compounds on cell proliferation. Activation of substrates of p38 MAPK and cell cycle regulatory proteins were evaluated by western blotting. Corneal endothelial wounds were created in a rabbit model, and p38 MAPK was applied in eye drop form, followed by evaluation of cell proliferation in the corneal endothelium by Ki67-immunostaining.

Results. HCECs cultured with SB203580 exhibited hexagonal morphology and similar size and morphology, whereas control HCECs cultured without inhibitor exhibited monolayer morphology and varied in size and morphology. Flow cytometry demonstrated that cell proliferation was significantly increased by SB203580. Western blotting showed activation of ATF2 and HSP27 (substrates of p38 MAPK), and upregulation of cyclin D and downregulation of p27 were induced by inhibiting p38 MAPK. In the rabbit model, promotion of wound healing of the corneal endothelium was associated with significant upregulation of Ki67-positive proliferating cells following topical administration of SB203580 when compared with untreated endothelium (50.9% and 36.1%, respectively).

Conclusions. Activation of p38 MAPK signaling due to culture stress might suppress the proliferation of HCECs, whereas a p38 MAPK inhibitor can counteract this activation and enable efficient in vitro HCEC expansion.

Keywords: corneal endothelium, p38 MAPK, tissue engineering

The pump and barrier function of the corneal endothelium regulates the amount of water in the corneal stroma and is essential for the maintenance of corneal transparency.[1] The corneal endothelium is located at the back of the cornea, where it forms a monolayer sheet-like structure composed of corneal endothelial cells (CECs). CECs have severely limited proliferative ability,[2,3] so severe damage to the corneal endothelium induces compensatory migration and spreading of the remaining cells to cover the damaged area. The result is a loss of CEC density, or corneal endothelial decompensation. A reduction in density below 500–1000 cells/mm^2 (cell density of the corneal endothelium in a normal subject is 2500–3000 cells/mm^2) renders the corneal endothelium unable to regulate the amount of water in the stroma, and the subsequent stromal swelling then results in vision loss.[1,4]

The only therapeutic option for treating this corneal endothelial decompensation has been corneal transplantation using donor corneas. The recent development of endothelial keratoplasties—such as Descemet's stripping endothelial keratoplasty (DSAEK)[5,6] and Descemet's membrane endothelial keratoplasty (DMEK)[7]—provide a less invasive and more efficient therapy than is obtained with conventional full thickness penetrating keratoplasty.[8] However, worldwide cornea donor shortages, chronic graft failure due to long-term continuous cell loss after transplantation, and difficulties in surgical procedures for endothelial keratoplasties are still problems that limit the effectiveness of these procedures in the clinical setting.[8,9] This has prompted efforts to develop tissue-engineering therapies that can overcome the problems associated with conventional corneal transplantation.

In 2013, we obtained approval from the Japanese Ministry of Health, Labour, and Welfare to initiate a first-in-man clinical trial at the Kyoto Prefectural University of Medicine (Clinical trial registration: UMIN000012534) to investigate co-injection of cultured CECs and a Rho kinase (ROCK) inhibitor as a treatment for corneal endothelial dysfunction.[10] Recently, we reported that corneal transparency was recovered with regeneration of corneal endothelium in the first 11 patients treated for corneal endothelial decompensation.[11] Although long-term studies are necessary to confirm the safety and efficacy in larger numbers of patients, the expectation is that human CECs (HCECs) will be introduced as a regenerative medical product. Therefore, at the time of this writing, we have been undertaking investigator-initiated clinical trials and preparing a company-initiated clinical trial to obtain approval for HCEC regenerative therapy by regulatory authorities.

Our HCECs are currently cultured at a Good Manufacturing Practice (GMP) grade cell-processing center and have been transplanted into patients in our clinical research. However, the in vitro expansion of HCECs with the required phenotype for clinical use is still surprisingly difficult.[10] Multiple problems arise when culturing HCECs, as these cells have limited

Table. Inhibitors for Screening the Effects on Proliferation of HCECs

Function	Reagent Name	Company	Concentration, μM
p38 MAPK inhibitor	SB203580	Cayman	10
ALK5 inhibitor	SB431542	Wako	1
MEK inhibitor	PD0325901	Wako	1
p53 inhibitor	Pifithrin-a	Calbiochem	1
NF-κB inhibitor	WithferinA	Wako	3
NF-kB inhibitor	BAY11-7082	Wako	1
PI3K inhibitor	LY2904002	Wako	1
MEK inhibitor	U-0126	Wako	1
Phosphodiesterase inhibitor	IBMX	Sigma-Aldrich	500
JNK inhibitor	SP600125	Calbiochem	1
HDAC inhibitor	SAHA	Sigma-Aldrich	1
ALK4, 5, 7 inhibitor	A-83-01	Wako	1
GSK3a/b inhibitor	BIO	Wako	1
Rho kinase inhibitor	Y-27632	Wako	10

proliferative ability, undergo transformation into a fibroblastic phenotype that will not regenerate corneal endothelium, and exhibit senescence that decreases the cell density.[12–16] These undesirable features of HCECs extend the duration required to obtain sufficient cell numbers, which will ultimately increase the final cost of a regenerative medical product.

In the current study, we screened the ability of multiple low-molecular-weight compounds to promote the efficiency of in vitro expansion of HCECs in culture. We found that a p38 MAPK inhibitor, SB203580, enhances HCEC proliferation, and we further evaluated the effect of inhibition of p38 MAPK on cell cycle regulatory molecules and on the changes in the function-related phenotypes of HCECs.

Materials and Methods

Ethics Statement

The human tissue used in this study was handled in accordance with the tenets set forth in the Declaration of Helsinki. Informed written consent was obtained from the next of kin of all deceased donors regarding eye donation for research. All tissue was recovered under the tenets of the Uniform Anatomical Gift Act (UAGA) of the particular state in which the donor consent was obtained and the tissue was recovered.

In animal experiments, rabbits were housed and treated in accordance with the ARVO Statement for the Use of Animals in Ophthalmic and Vision Research. The rabbit experiments were performed at Doshisha University (Kyoto, Japan) according to the protocol approved by the University's Animal Care and Use Committee (Approval No. A16036).

Cell Cultures

Human donor corneas were obtained from SightLife (Seattle, WA, USA). All corneas had been stored at 4°C in storage medium (Optisol; Chiron Vision, Irvine, CA, USA) for less than 14 days before use in experiments. Donors of the corneal tissues ranged in age from 53 to 69 years old. The culture medium was prepared according to published protocols.[17] Briefly, the Descemet's membrane including corneal endothelium was stripped from the donor corneas and digested with 1 mg/mL collagenase A (Roche Applied Science, Penzberg, Germany) at 37°C for 16 hours. HCECs were recovered and washed with OptiMEM-I (Thermo Fisher Scientific, Waltham, MA, USA), and then cultured in corneal endothelial growth medium.

Corneal endothelial growth medium was prepared by conditioning basal medium mix (OptiMEM-I, 8% fetal bovine serum [FBS], 5 ng/mL epidermal growth factor [EGF; Thermo Fisher Scientific], 20 μg/mL ascorbic acid [Sigma-Aldrich, St. Louis, MO, USA], 200 mg/L calcium chloride, 0.08% chondroitin sulfate [Sigma-Aldrich], and 50 μg/mL gentamicin [Thermo Fisher Scientific]) with NIH-3T3 cells according to published protocols.[14,16] Briefly, confluent 3T3 fibroblasts were incubated with 4 μg/mL mitomycin C (MMC) (Kyowa Hakkko Kirin Co., Ltd., Tokyo, Japan) for 2 hours, seeded on plastic dishes at a cell density of 2×10^4 cells/cm^2, and cultured with DMEM (Life Technologies Corp., Grand Island, NY, USA) supplemented with 10% FBS, 100 U/mL penicillin, and 100 μg/mL streptomycin (Nacalai Tesque, Inc., Kyoto, Japan). The 3T3 fibroblasts were washed 3 times with PBS and cultured with basal medium mix for an additional 24 hours. The medium was collected, filtered through a 0.22-μm filtration unit (EMD Millipore Corporation, Billerica, MA, USA), and used as corneal endothelial growth medium.

The HCECs were cultured in a humidified atmosphere at 37°C in 5% CO_2, and the corneal endothelial growth medium was replaced with fresh media every 2 days. When the cells reached confluency in 20 to 30 days, they were rinsed in Ca^{2+}- and Mg^{2+}-free phosphate buffered saline (PBS), trypsinized with 0.05% Trypsin-EDTA (Thermo Fisher Scientific) for 5 minutes at 37°C and passaged at a 1:2 ratio. The cell density was determined using ImageJ software (National Institutes of Health, Bethesda, MD, USA).

Inhibitors (SB203580 (Cayman Chemical, Ann Arbor, MI, USA), SB431542 (Wako Pure Chemical Industries, Ltd., Osaka, Japan), PD0325901 (Wako Pure Chemical Industries, Ltd.), Pifithrin-a (Calbiochem, San Diego, CA, USA), WithferinA (Wako Pure Chemical Industries, Ltd.), BAY11-7082 (Wako Pure Chemical Industries, Ltd.), LY2904002 (Wako Pure Chemical Industries, Ltd.), U-0126 (Wako Pure Chemical Industries, Ltd.), IBMX (Sigma-Aldrich), SP600125 (Calbiochem), SAHA (Sigma-Aldrich), A-83-01 (Wako Pure Chemical Industries, Ltd.), BIO (Wako Pure Chemical Industries, Ltd.), and Y-27632 (Wako Pure Chemical Industries, Ltd.) were added to evaluate the effect of inhibition of each signaling pathway on proliferation of HCECs (Table). In addition to SB203580, inhibitors of p38 MAPK signaling—including BIRB796 (Selleck Chemicals LLC, Houston, TX, USA), PH-797804 (Selleck Chemicals LLC), VX-702 (Selleck Chemicals LLC), and TAK-515 (Selleck Chemicals LLC), were also added to the culture medium, and their effect on proliferation of HCECs was evaluated.

Cell Proliferation Assay

HCECs were seeded at a density of 5000 cells/well in a 96-well plate, cultured for 24 hours, and then cultured for a further 24 hours in the presence or absence of inhibitors.

The number of viable cells was evaluated based on the amount of ATP by using a CellTiter-Glo Luminescent Cell Viability Assay using a Veritas Microplate Luminometer (Promega, Fitchburg, WI, USA) according to manufacturer's protocol. Six samples were prepared for each group.

DNA synthesis was detected as incorporation of 5-bromo-2-deoxyuridine (BrdU) using the Cell Proliferation Biotrak ELISA system, version 2 (GE Healthcare Life Sciences, Buckinghamshire, UK) according to the manufacturer's instructions. Briefly, HCECs were incubated with 10 μmol/L BrdU for 24 hours, further incubated with fixation solution (Amersham Biosciences, Freiburg, Germany) for 2 hours, and incubated with 100 μl of monoclonal antibody against BrdU for 30 minutes. The BrdU

absorbance was measured using a spectrophotometric microplate reader at a test wavelength of 450 nm.

Western Blotting

HCECs were lysed in ice-cold RIPA buffer (25 mM Tris-HCl, pH7.6, 150 mM NaCl, 1% Nonidet P-40, 1% sodium deoxycholate, and 0.1% SDS) with Phosphatase Inhibitor Cocktail 2 (Sigma-Aldrich) and Protease Inhibitor Cocktail (Nacalai Tesque). The supernatant containing the total proteins was collected by centrifugation and the protein concentrations were determined with the BCA protein assay kit (Pierce Biotechnology Rockford, IL, USA). Proteins were denatured with 5× sample buffer at 95°C for 5 minutes. An equal amount of protein was fractionated by SDS-PAGE and transferred to a PVDF membrane. The membrane was blocked with 3% non-fat dry milk (Cell Signaling Technology, Inc., Danvers, MA, USA) in TBS-T buffer (50 mM Tris, pH 7.5, 150 mM $NaCl_2$, and 0.1% Tween 20) for 1 hour at room temperature and then incubated overnight at 4°C with the following primary antibodies: ATF-2 (1:1000; Merck Millipore), phosphorylated ATF2 (1:1000; Santa Cruz Biotechnology), HSP27 (1:1000; Cell Signaling Technology), phosphorylated HSP27 (1:1000; Cell Signaling Technology), CyclinD1 (1: 1000; Cell Signaling Technology), CyclinD3 (1:1000; Cell Signaling Technology), p27 (1:1000; Santa Cruz Biotechnology, Santa Cruz, CA, USA), and GAPDH (1:3000; Medical & Biological Laboratories Co., Ltd., Nagoya, Japan). After washing with TBS-T buffer, the blots were incubated with horseradish peroxidase-conjugated secondary antibodies (1:5000: anti-rabbit, anti-mouse IgG; Cell Signaling Technology). The blots were developed with luminal for enhanced chemiluminescence (ECL) using the Chemi-Lumi One Ultra (Nacalai Tesque), documented by LAS4000S (Fuji Film, Tokyo, Japan), and analyzed with Image Gauge software (Fuji Film).

Immunofluorescent Staining

HCECs cultured on a 48-well cell culture plate and rabbit corneas were both fixed in 4% paraformaldehyde for 10 minutes, permeabilized with 0.2% Triton X-100 in PBS for 10 minutes and blocked with 1% bovine serum albumin (BSA) in PBS for 1 hour. HCECs were incubated with the following primary antibodies for 1 hour at room temperature: Ki67 (1:200, Agilent Technologies, Inc., Santa Clara, CA, USA), p27 (1:200, Sigma-Aldrich), Na^+/K^+-ATPase (1:200, Merck Millipore), and ZO-1 (1:200, Zymed Laboratories, South San Francisco, CA, USA). Either a 1:1000 dilution of Alexa Fluor 488-conjugated goat anti-rabbit IgG (Thermo Fisher Scientific) or Alexa Fluor 594-conjugated goat anti-mouse IgG (Thermo Fisher Scientific) was used for the secondary antibody. Nuclei were stained with 4′,6-diamidino-2-phenylindole dihydrochloride (DAPI) (Vector Laboratories, Burlingame, CA, USA). The HCECs were examined by fluorescence microscopy (BZ-9000; Keyence, Osaka, Japan), and rabbit corneas were examined by fluorescence microscopy (TCS SP2 AOBS; Leica Microsystems, Wetzlar, Germany).

Flow Cytometry Analysis

HCECs were seeded at a density of 100,000 cells/cm^2 onto 6-well plates and cultured overnight without FBS. The cells were cultured for 12 or 24 hours with or without supplementation with 10 μM SB203580. Cells were rinsed in PBS, dissociated to single cells using TrypLE Select (Thermo Fisher Scientific), collected by centrifugation, washed in PBS, resuspended in ice-cold 70% ethanol, and fixed at 4°C overnight. After incubation, cells were centrifuged and washed twice in PBS. Cells were incubated in 250 μg/mL RNase A (Promega, Fitchburg, WI, USA) in PBS at 37°C for 30 minutes, then suspended in a staining solution containing 50 μg/mL propidium iodide (Nacalai Tesque) at 4°C for 30 minutes. Flow-cytometry analyses were performed on an SH-800 instrument (Sony Corporation, Tokyo, Japan).

Rabbit Corneal Endothelial Damage Model

The central corneal endothelium of 12 eyes of 12 Japanese white rabbits was damaged by a protocol described previously.[18,19] Briefly, a 7-mm diameter stainless-steel probe was immersed in liquid nitrogen for 3 minutes, and the center of the rabbit cornea was frozen with the probe for 15 seconds while the rabbit was under general anesthesia. Fifty μl of 10 mM SB203580 in PBS was applied topically as an eye drop 4 times daily to the damaged six eyes of six rabbits; control rabbits received PBS applied 4 times daily to the damaged eyes ($n = 6$). Anterior segments were evaluated by slit-lamp microscopy. The rabbits were euthanized after 48 hours of treatment, and both Alizarin red staining and immunofluorescence staining were performed. The wound area was determined using the ImageJ software. Ki67 positive cells 3.5 mm distant from the center of the cornea were also evaluated.

Statistical Analysis

The statistical significance (*P* value) of the mean values of two-sample comparisons was determined with the Student's *t*-test. The statistical significance of the comparison of multiple sample sets was analyzed with Dunnett's multiple-comparisons test. Qualitative variables were analyzed with the chi-square test. Results were expressed as mean ± standard error of the mean (SEM). A *P* value less than 0.05 was considered statistically significant.

Results

Screening of Inhibitors for HCEC-Culture

We cultured HCECs in the presence of various low-molecular-weight compounds in the culture medium, which was conditioned with NIH3T3 cells, to screen the effect of potential inhibitors on cell culture (Table). Phase contrast images showed that HCECs cultured without inhibitors, shown as controls, exhibited a monolayer morphology but varied in cell size and morphology. By contrast, HCECs cultured with SB203580, SB431542, and Y-27632 exhibited hexagonal morphology and similar cell size and morphology, which is consistent with our previous reports.[13,16] HCECs cultured with some inhibitors, such as Withaferin A, LY2904002, SAHA, and IBMX, grew as monolayers but varied in cell size and morphology like the control cells (Fig. 1A, Supplementary Fig. 1). The cell numbers following culture with inhibitors were evaluated after 48 hours (30%–50% of confluency), and SB203580, BIO, and Y-27632 significantly increased the cell numbers (Fig. 1B). We further evaluated the effect of a combination of SB203580[16] and Y-27632[13] or SB431542,[15] which we previously reported to be beneficial for culturing HCECs. SB203580 and Y-27632 (but not SB431542) significantly increased the incorporation of BrdU. No synergetic effect on BrdU incorporation was observed for a combination of Y-27632 and/or SB431542 with SB203580 (Fig. 1C). The effect of SB203580 was evaluated on the proliferation of HCECs cultured with non-conditioned medium. Consistent with the findings in conditioned medium, BrdU absorbance was

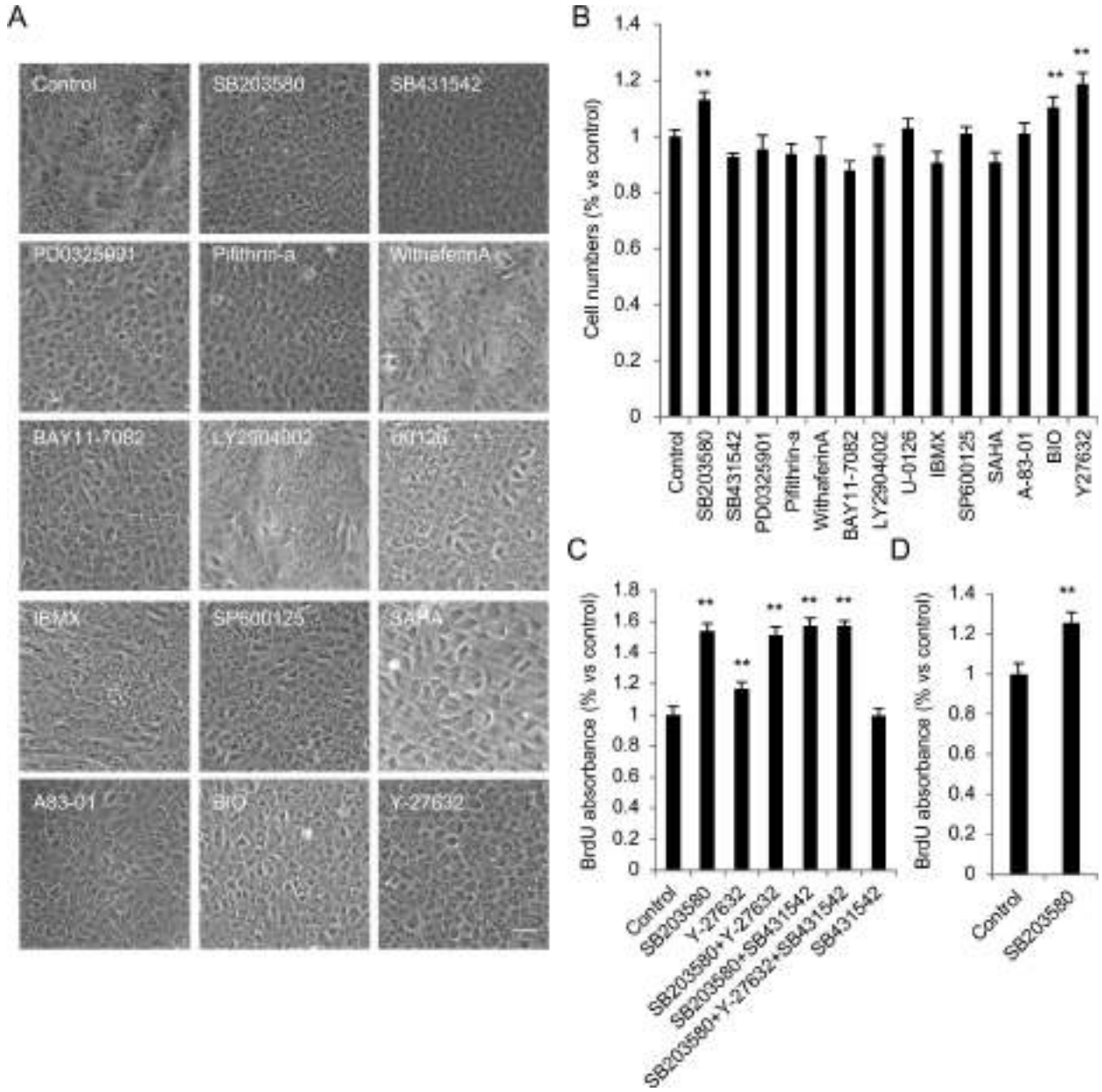

Figure 1. Screening of inhibitors for HCEC culture. (**A**) HCECs were seeded in culture medium supplemented with various inhibitors and then screened to determine the effect of inhibitors on cell morphology. Representative phase-contrast images show that HCECs cultured without inhibitor exhibit a monolayer morphology but vary in cell size and morphology. Conversely, HCECs cultured with the p38 MAPK inhibitors SB203580, SB431542, and Y-27632 exhibited hexagonal morphology in similar cell size and morphology. *Scale bar*: 100 µm. (**B**) HCECs were cultured with inhibitors for 48 hours and cell numbers were evaluated at 30%–50% of confluency. Treatment with the p38 MAPK inhibitors SB203580, BIO, and Y-27632 significantly increased the cell numbers. $n = 5$, $^{**}P < 0.01$. (**C**) The effect of combination of SB203580 with Y-27632 and SB431542 on cell proliferation was evaluated. SB203580 and Y-27632, but not SB431542, increased the incorporation of BrdU. Combination of Y-27632 or SB431542 with SB203580 showed no synergetic effect on BrdU incorporation. $n = 5$, $^{**}P < 0.01$. (**D**) HCECs were culture with non-conditioned culture medium, and the effect of supplementation of SB203580 on BrdU incorporation was evaluated. $n = 5$, $^{**}P < 0.01$.

significantly increased by SB203580 in non-conditioned medium (Fig. 1D).

Effect of p38 MAPK Inhibitor on Functional Property of HCECs

We evaluated the effect of SB203580 on cell density and functional properties, which are essential parameters for HCECs destined for clinical use in regenerative medicine. Phase contrast images showed that SB203580 enabled the cultivation of HCECs at a higher cell density and with smaller variations in cell morphology and cell size (Fig. 2A). Cell density measurements, evaluated by ImageJ, demonstrated that SB203580 significantly upregulated cell density in a dose-dependent manner (Fig. 2B). Na^+/K^+-ATPase, which represents the pump function, was weakly expressed in control HCECs, whereas HCECs cultured with 10 µM SB203580 expressed Na^+/K^+-ATPase at the cell-cell borders (Fig. 2C). Similarly, the expression of ZO-1, which represents the barrier function, was weak in the control HCECs, but ZO-1 was expressed at the cell-

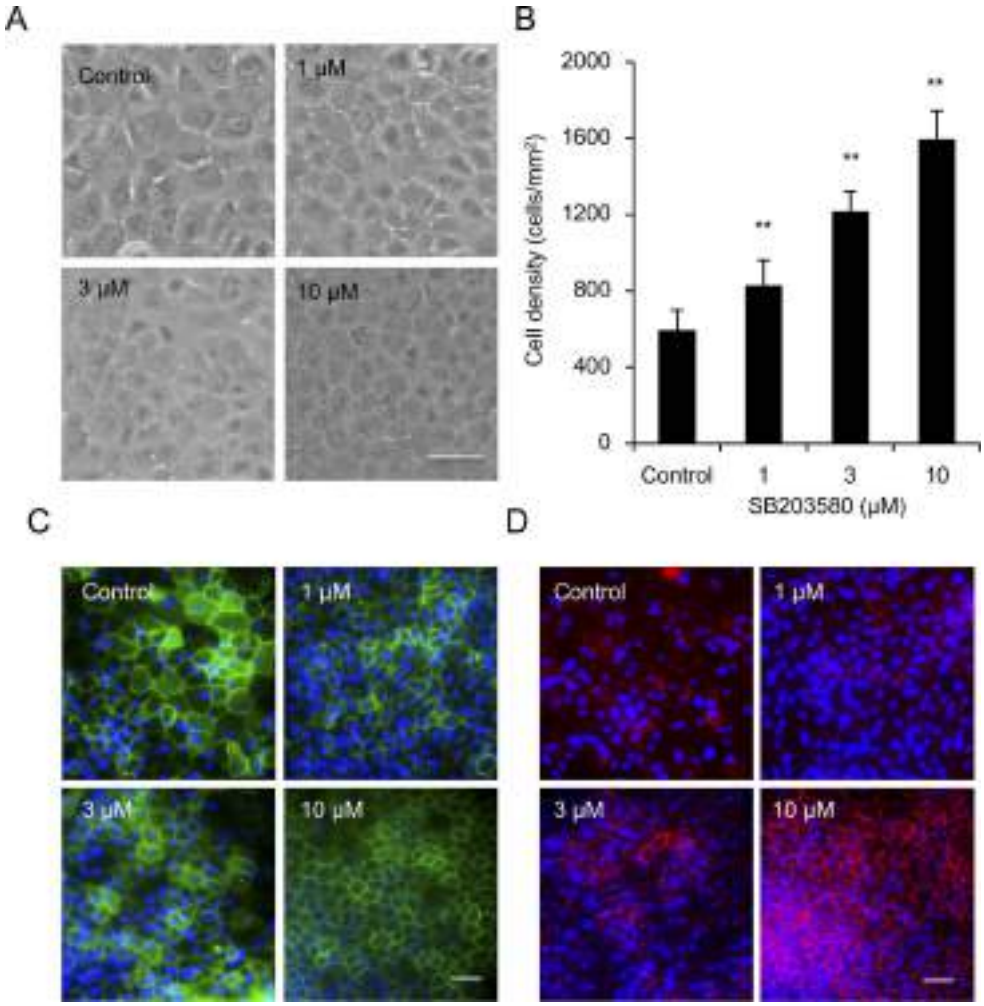

Figure 2. Effect of p38 MAPK inhibitor on functional property of HCECs. (**A**) HCECs were seeded on culture plates supplemented with various concentrations of SB203580 and maintained for 10–20 days after reaching confluence. Representative phase-contrast images show that 10 μM SB203580 enabled the cultivation of HCECs at a higher cell density and with smaller variations in cell morphology and cell size. *Scale bar*: 100 μm. (**B**) Cell density evaluated by ImageJ demonstrated that addition of SB203580 significantly upregulated cell density in a dose-dependent manner. $n = 4$, $^{**}P < 0.01$. (**C**) Immunostaining for Na^+/K^+-ATPase (marker of pump function) after HCEC culture for 10–20 days. Na^+/K^+-ATPase was weakly expressed in control HCECs, but HCECs cultured with 10 μM SB203580 expressed Na^+/K^+-ATPase at almost all cell-cell borders. Nuclei were stained with DAPI. *Scale bar*: 100 μm. (**D**) Immunostaining for ZO-1 (a marker of barrier function) after HCEC culture for 10–20 days. ZO-1 was weakly expressed in control HCECs, but HCECs cultured with 10 μM SB203580 expressed ZO-1 at almost all cell-cell junctions. Nuclei were stained with DAPI. *Scale bar*: 100 μm.

cell borders of all HCECs cultured with 10 μM SB203580 (Fig. 2D).

Effect of a p38 MAPK Inhibitor on Proliferation of HCECs

We evaluated the concentration dependence of SB203580 effects on cell numbers and showed that 1–10 μM was optimal for the cultivation of HCECs (Fig. 3A). Growth curves demonstrated that supplementation of the culture medium with SB203580 significantly increased the cell numbers for 14 days until the HCECs reached the confluent state (Fig. 3B). Immunofluorescence staining for Ki67 showed that the percentage of Ki67-positive proliferating cells was 7.4% in the control culture, but it was significantly increased to 14.7% by the addition of SB203580 for 24 hours ($P < 0.01$; Fig. 3C, 3D). Similarly, flow cytometry demonstrated that the numbers of PI-positive cells at the G2/M phase (shown in pink, Fig. 3E) and at the S phase (shown in orange, Fig. 3E) were significantly increased by addition of SB203580 after 24 hours of cultivation ($P < 0.01$; Fig. 3F).

As HCECs arrest at the G1 phase in vivo in response to cell cycle regulators, we investigated regulators that mediate the G1/S progression. Western blotting showed a more evident phosphorylation of pRb, the product of the *RB1* gene, following culture with SB203580 when compared to control cells (Fig. 4A). The levels of the D class of cyclins (D1 and D3), which are positive regulators of the G1/S progression, were higher in HCECs treated with SB203580 than in the control (Fig. 4A). Expression of cyclin-dependent kinase inhibitor p27Kip1, an important negative cell cycle regulator for HCECs, was down regulated by SB203580 (Fig. 4B). Consistently, immunofluorescence staining showed that the percentage of p27-positive cells was 55.1% in the control, but this value significantly decreased to 27.7% for HCECs treated with SB203580 for 24 hours (Fig. 4C, 4D).

We further evaluated whether the inhibition of HCEC proliferation by SB203580 (as an inhibitor of p38α and p38β) was a consequence of inhibiting p38 MAPK signaling or was

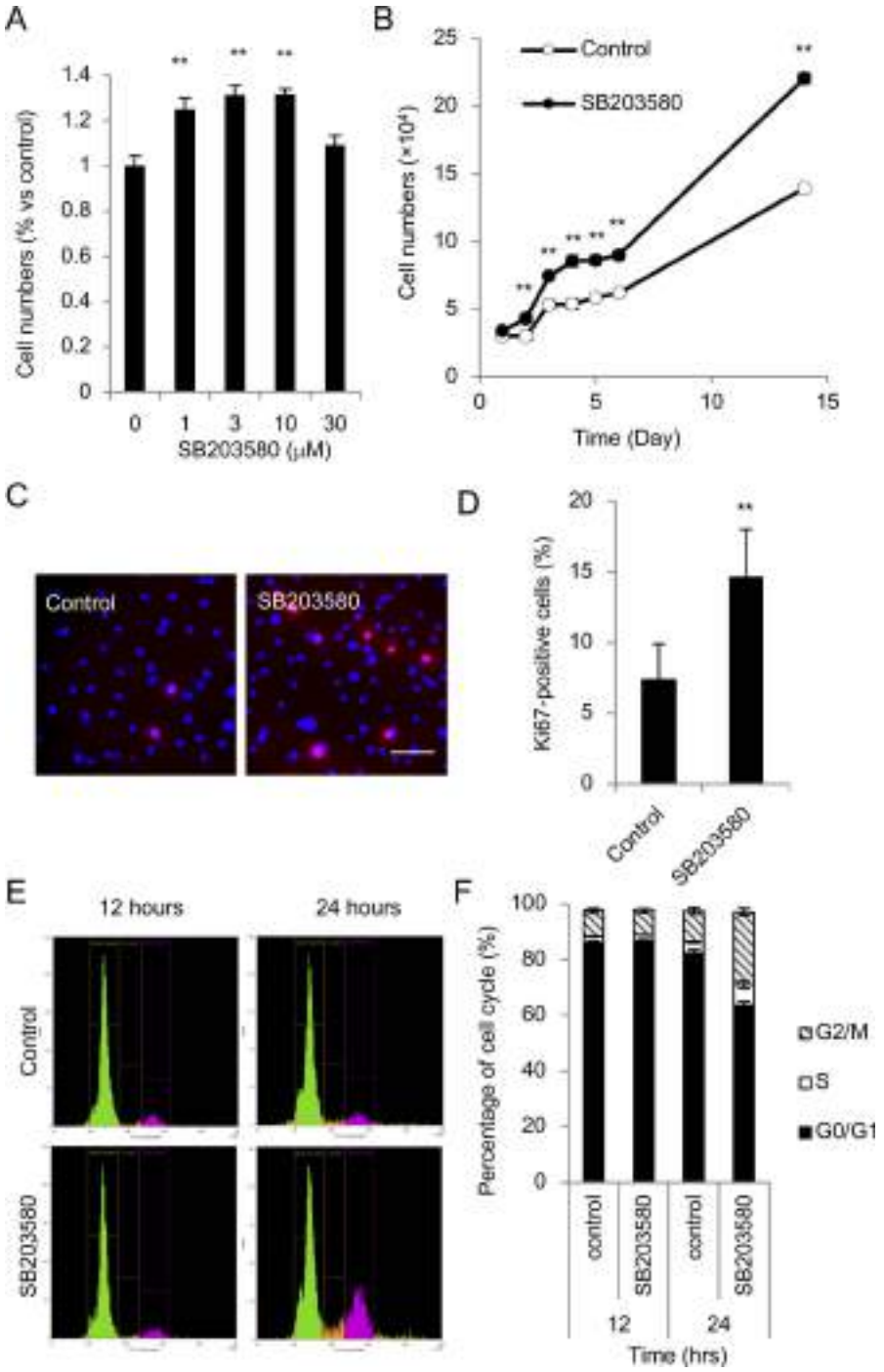

Figure 3. Effect of SB203580 on cell proliferation. (**A**) HCECs were cultured with various concentration of SB203580 for 48 hours and cell numbers were evaluated. CellTiter-Glo Luminescent Cell Viability Assay showed that 1–10 μM is the optimal concentration of SB203580 for the cultivation of HCECs. $n = 5$, $^{**}P < 0.01$. (**B**) Growth curve demonstrating that 10 μM SB203580 significantly increases the cell numbers for 14 days of culture until HCECs reach the confluent state. $n = 3$, $^{**}P < 0.01$. (**C**, **D**) Proliferating cells were evaluated by immunofluorescence staining of Ki67. The percentage of Ki67-positive proliferating cells was 7.4% in the control but was significantly increased to 14.7% by treatment with SB203580. $n = 5$, $^{**}P < 0.01$. (**E**, **F**) HCECs were seeded at a density of 5000 cells/well in a 6-well plate and cultured with or without supplementation of 10μM SB203580 for 12 or 24 hours. The cell cycle progression was evaluated by evaluating DNA-binding dyes, including propidium iodide (PI), using flow cytometry. *Green* indicates the G1 phase, *orange* indicates the S phase, and *pink* indicates the G2/M phase. $n = 3$.

instead an off-target effect of this molecule. Western blotting showed that phosphorylation of ATF2 and HSP27 were suppressed by SB203580 (Fig. 4E). As ATF2 and HSP27 are phosphorylated following the phosphorylation of p38 MAPK as downstream substrates, these results suggested that SB203580 inhibited the phosphorylation of p38 MAPK in HCECs.

We further evaluated the effect of p38 MAPK inhibition using several low-molecular-weight compounds known to inhibit the p38 MAPK signaling pathway. After cultivation of

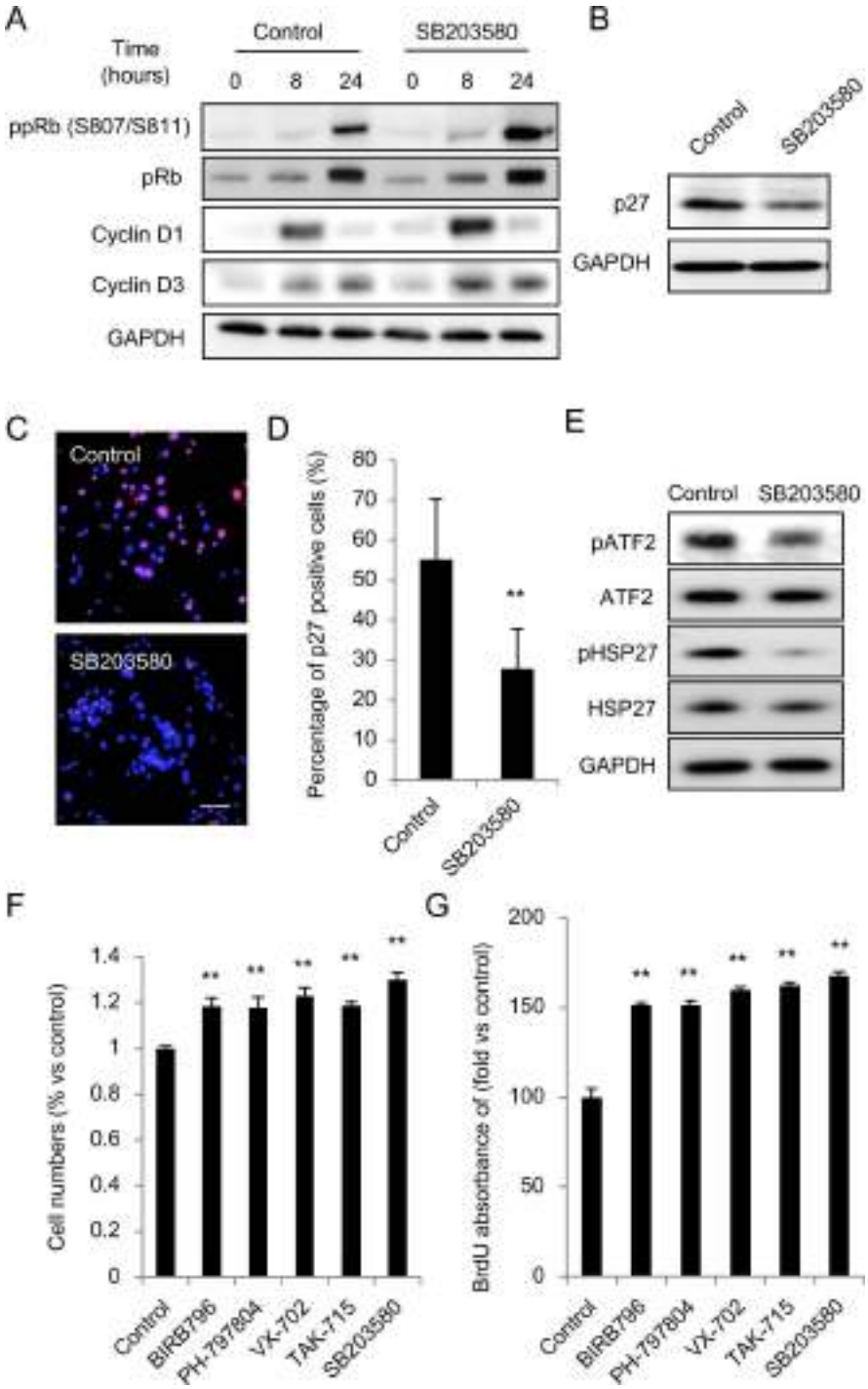

Figure 4. Effect of p38 MAPK inhibition on proliferation of HCECs. (**A**) HCECs were seeded with or without 10 μM SB203580 and the phosphorylation of pRb and expression level of cyclin D1 and D3 were evaluated by western blotting. Expression of phosphorylation of pRb was more evident by culturing with SB203580 comparison to control. Cyclin D1 was increased 8 hours after seeding HCECs, and the cyclin D3 was increased 8 and 24 hours after seeding HCECs. The expression level of cyclin D1 was higher after 8 hours and that of cyclin D3 was higher after 8 and 24 hours following treatment with SB203580 in comparison to the control. (**B**) HCECs were cultured with or without 10 μM SB203580 for 24 hours and the expression level of p27 was evaluated by western blotting. The expression level of p27 was lower in HCECs cultured with SB203580 when compared to the control. (**C**, **D**) HCECs were cultured with or without 10 μM SB203580 for 24 hours, followed by immunofluorescent staining for p27. Immunofluorescence staining showed that the percentage of p27 positive cells was 55.1% in control, but this value significantly decreased to 27.7% in HCECs treated with SB203580. *Scale bar*: 100 μm. $n = 5$, $^{**}P < 0.01$. (**E**) The effects of SB203580 on the phosphorylation of ATF2 and HSP27 were evaluated by western blotting. Phosphorylation of ATF2 and HSP27 was suppressed by SB203580. (**F**) The effect of p38 MAPK inhibition on cell numbers was evaluated by using several p38 MAPK inhibitors (BIRB796, PH-797804, VX-702, and TAK-515). After cultivation of HCECs with inhibitors for 48 hours, the inhibitors significantly increased cell numbers to levels similar to those achieved with SB203580. $n = 5$, $^{**}P < 0.01$. (**G**) HCECs were cultured with p38 MAPK inhibitors for 24 hours. Incorporation of BrdU was significantly increased by all inhibitors. $n = 3$, $^{**}P < 0.01$.

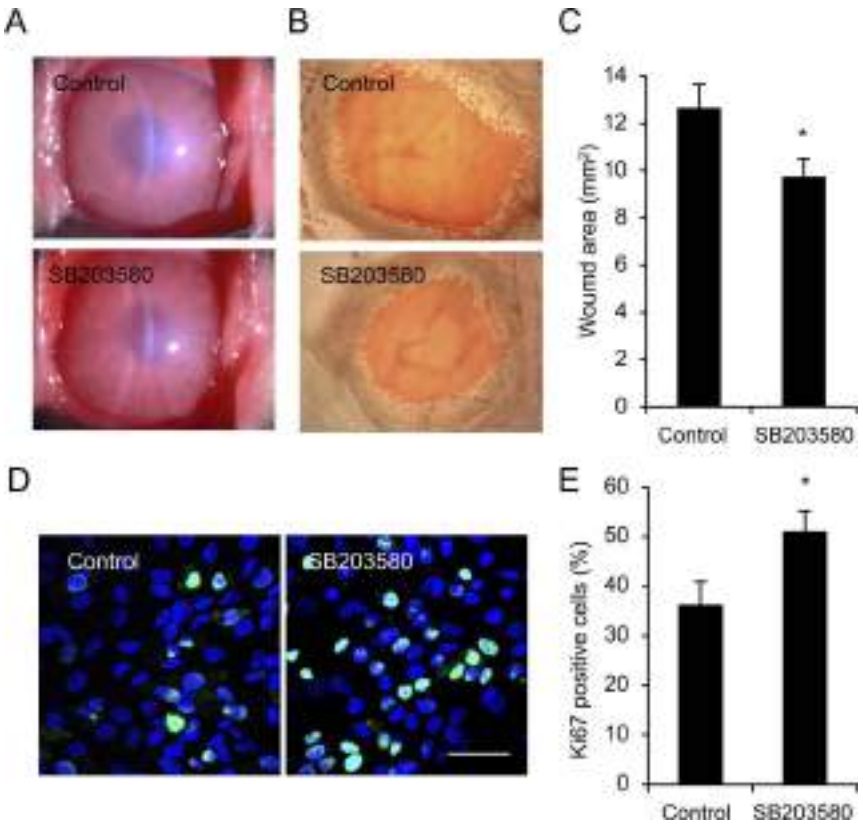

Figure 5. Effect of a p38 MAPK inhibitor on in vivo proliferation of corneal endothelium. (**A**) Rabbit corneal endothelial damage was created by transcorneal freezing (7-mm diameter) and 10 mM SB203580 in PBS were applied topically as an eye drop 4 times daily. Controls received PBS was applied 4 times daily ($n = 6$). Slit-lamp microscopy showed a tendency for the SB203580-treated corneas to be clearer than the untreated control eyes. (**B**, **C**) After 48 hours, wound areas were measured following Alizarin red staining. The wounded area of the corneal endothelium was significantly smaller after topical administration of SB203580 than after administration of vehicle. $n = 6$, $^*P < 0.05$. (**D**, **E**) Ki67 positive proliferation cells were evaluated by immunofluorescence staining. Ki67 positive cells 3.5 mm distant from the center of the cornea was significantly upregulated in the eyes treated with SB203580 than in the eyes treated with vehicle. $n = 6$, $^*P < 0.05$.

HCECs for 48 hours, the inhibitors BIRB796 (inhibitor of p38α), PH-797804 (inhibitor of p38α and p38β), VX-702 (inhibitor of p38α), and TAK-515 (inhibitor of p38α and p38β) significantly increased the HCEC numbers in a manner similar to that observed with SB203580 (Fig. 4F). Consistent with these results, the incorporation of BrdU was significantly increased by all the p38 MAPK inhibitors, indicating that inhibition of p38 MAPK signaling promotes proliferation of HCECs (Fig. 4G).

Effect of a p38 MAPK Inhibitor on the Proliferation of Corneal Endothelium in an In Vivo Model

Finally, we examined the effect of p38 MAPK inhibitor on proliferation of corneal endothelial cells using a rabbit wound model. Rabbit corneas were subjected to transcorneal freezing, and the wound areas were measured 48 hours after the topical administration of a drop of 10 mM SB203580. Slit-lamp microscopy showed a tendency for the SB203580-treated corneas to be clearer than the untreated control eyes (Fig. 5A). When the wound areas were measured following Alizarin red staining, the wounded area of the corneal endothelium was significantly smaller after topical administration of SB203580 (Fig. 5B, 5C). The numbers of cells expressing Ki67 3.5 mm distant from the center of the cornea were significantly increased in the eyes treated with SB203580 when compared with the eyes treated with vehicle (50.9% and 36.1%, respectively; Fig. 5D, 5E).

Discussion

One strategy for tissue engineering therapy aimed at treating corneal endothelial decompensation is the transplantation of a cultured corneal endothelial sheet, as in the DSAEK or DMEK procedures. We and several other researchers report that transplantation of corneal endothelial sheets regenerated transparent corneas in animal models,[20–22] but this strategy has yet to be introduced in human patients. A second strategy is to inject cultured CECs in the form of a cell suspension into the anterior chamber (cell-based therapy).[23–26] However, if the injected CECs do not spontaneously adhere to the posterior corneal surface of the recipient, the reconstruction of a corneal endothelium will fail. In 2009, we found that the selective ROCK inhibitor, Y-27632, promotes CEC adhesion to a substrate, enhances CEC proliferation, and suppresses CEC apoptosis,[13] and our subsequent reports confirm these findings and reveal the underlying mechanisms.[26–28] We therefore hypothesized that co-injection of a ROCK inhibitor would promote the adhesion of cultured CECs onto the natural substrate (posterior corneal surface), thereby supporting the regeneration of the corneal endothelium. Indeed, we have demonstrated that co-injection of cultured CECs and a ROCK inhibitor regenerate the corneal endothelium on the Descemet's membrane in rabbit and monkey corneal endothelial decompensation models.[25,26]

In addition to the development of surgical procedures for cell transplantation, cultivation of HCECs has been a problem that has stalled development of regenerative medicine. During

cell culture, HCECs spontaneously undergo fibroblastic changes, which are thought to be part of the epithelial mesenchymal transition. The result is the loss of functional properties, including the pump and barrier functions.[15] Even if cultured HCECs do not acquire these fibroblastic changes, they can undergo senescence, which decreases the cell density and again produces cells that are not applicable for clinical use.[16]

An additional complication is that the proliferative ability of HCECs is limited even under ideal culture conditions, so multiple procedures have been developed to promote cell proliferation.[29–32] For instance, we reported that the use of a ROCK inhibitor,[13] conditioned medium derived from mesenchymal stem cells,[14] and laminin 511 fragment as a culture substrate[17] enhances cell proliferation. In the current study, we screened several low-molecular-weight compounds and found that the p38 MAPK inhibitor, SB203580, promotes cell proliferation while maintaining cell density and functional properties. SB203580 is a commonly used inhibitor of p38 MAPK, but it also inhibits the phosphorylation and activation of protein kinase B.[33] Therefore, we used other p38 MAPK inhibitors (BIRB796, PH-797804, VX-702, and TAK-515) that were developed for clinical use, and we confirmed that all these p38 MAPK inhibitors enhance cell growth in a similar manner to that observed with SB203580. We further demonstrated that the p38 MAPK inhibitor induces cell proliferation in the rabbit corneal endothelial damage model. These results suggest that p38 MAPK signaling negatively regulates proliferation of CECs, and that this function is conserved in both in vivo and in vitro culture conditions.

The MAPK family includes enzymes that catalyze the phosphorylation of specific serines and threonines of target substrates and form a part of a cascade that converts extracellular signals to activate intracellular pathways.[34] The MAPK members include four main signaling modules: extracellular-signal-regulated kinase (ERK), ERK5, Jun-NH2-terminal kinases (JNK), and p38 MAPK.[35] The p38 MAPK group consists of four isoforms: p38α, p38β, p38γ, and p38δ, with p38α and p38β expressed universally in most tissues and p38γ and p38δ expressed in a tissue-specific manner (i.e., mainly expressed in skin, small intestine, and kidney).[36] The corneal endothelium expresses all four isoforms of p38 MAPK (data not shown).

MAPK kinase (MKK) 3 and MKK6 are the primary upstream activators of p38 MAPK, although MKK4 also activates p38 MAPK in specific situations.[33,37] Exposure to cellular stress and cytokines activates p38 MAPK by phosphorylation, which then regulates various cellular activities, such as differentiation, migration, cell death, and cellular senescence.[34,38] In addition, p38 MAPK also has known functions in cell proliferation.[33,39–43] Cell cycle regulating pathways, through which various cellular stresses are sensed and cell proliferation is suppressed by cell cycle checkpoints, are evolutionarily conserved in eukaryotic cells.[33] The p38 MAPK signaling pathway is involved in both the G1/S checkpoint[39,44,45] and the G2/M checkpoint.[46–49] In our current study, substrates of p38 MAPK, such as ATF2 and HSP27, were activated by phosphorylation, implicating an involvement of p38 MAPK signaling pathway activation during cell culture, probably due to culture stress. The complex that forms when cyclin D binds to and activates cyclin dependent kinase 4 and 6 is essential for the G1/S phase transition, and we showed that this complex is upregulated by inhibition of p38 MAPK. We also showed that inhibition of p38 MAPK suppresses the expression of p27Kip1, which negatively regulates the entry of corneal endothelial cells into the S phase.[50–52] Taken collectively, our data suggest that p38 MAPK signaling is involved in the G1/S phase transition through the regulation of G1/S phase cyclin and the CKI level. Future studies should elucidate whether p38 MAPK signaling regulates the cell cycle via the G2/M checkpoint as well as G1/S checkpoint to further our understanding of the regulation of cell proliferation in the corneal endothelium.

Recently, we reported that activation of p38 MAPK signaling due to culture stress induces senescence of HCECs in association with the hallmarks of cellular senescence, including SA-β-gal positivity, upregulation of cyclin dependent kinase inhibitors (CKI), and acquisition of a senescence-associated secretory phenotype (SASP).[16] We showed that inhibition of p38 MAPK signaling suppresses cellular senescence during cell culture.[16] In the current study, we demonstrated a second beneficial role of a p38 MAPK inhibitor. It might shorten the manufacturing time of HCECs by promoting cell proliferation.

In conclusion, activation of p38 MAPK signaling due to culture stress suppresses the proliferation of HCECs, whereas the use of a p38 MAPK inhibitor can counteract this activation and promote cell proliferation. One possible bottleneck of cell-based therapy is the cost of producing the cells as a regenerative medical product. Therefore, the use of a p38 MAPK inhibitor will potentially increase the efficiency of in vitro expansion, thereby resulting in a shorter manufacturing time and a lower cost for tissue engineering therapy for treating corneal endothelial decompensation.

Acknowledgments

The authors thank Fuyuki Ishikawa for valuable advice and Emi Ueda for technical assistance.

Supported by the Program for the Strategic Research Foundation at Private Universities from MEXT (NO, NK).

Disclosure: **M. Nakahara**, None; **N. Okumura**, P; **S. Nakano**, None; **N. Koizumi**, P

References

1. Nishida T, Saika S. Cornea and sclera: anatomy and physiology. In: Krachmer JH, Mannis MJ, Holland EJ, eds. *Cornea*. 3rd ed. St. Louis: Mosby; 2011:1:3–24.
2. Joyce NC. Proliferative capacity of the corneal endothelium. *Prog Retin Eye Res*. 2003;22:359–389.
3. Joyce NC. Proliferative capacity of corneal endothelial cells. *Exp Eye Res*. 2012;95:16–23.
4. Bourne WM. Clinical estimation of corneal endothelial pump function. *Trans Am Ophthalmol Soc*. 1998;96:229–239; discussion 239–242.
5. Price FW Jr, Price MO. Descemet's stripping with endothelial keratoplasty in 50 eyes: a refractive neutral corneal transplant. *J Refract Surg*. 2005;21:339–345.
6. Gorovoy MS. Descemet-stripping automated endothelial keratoplasty. *Cornea*. 2006;25:886–889.
7. Melles GR, Ong TS, Ververs B, van der Wees J. Descemet membrane endothelial keratoplasty (DMEK). *Cornea*. 2006; 25:987–990.
8. Tan DT, Dart JK, Holland EJ, Kinoshita S. Corneal transplantation. *Lancet*. 2012;379:1749–1761.
9. Patel SV. Graft survival and endothelial outcomes in the new era of endothelial keratoplasty. *Exp Eye Res*. 2012;95:40–47.
10. Okumura N, Kinoshita S, Koizumi N. Application of Rho kinase inhibitors for the treatment of corneal endothelial diseases. *J Ophthalmol*. 2017;2017:2646904.
11. Kinoshita S, Koizumi N, Ueno M, et al. Injection of cultured cells with a ROCK inhibitor for bullous keratopathy. *N Engl J Med*. 2018;378:995–1003.
12. Miyata K, Drake J, Osakabe Y, et al. Effect of donor age on morphologic variation of cultured human corneal endothelial cells. *Cornea*. 2001;20:59–63.

13. Okumura N, Ueno M, Koizumi N, et al. Enhancement on primate corneal endothelial cell survival in vitro by a ROCK inhibitor. *Invest Ophthalmol Vis Sci*. 2009;50:3680–3687.
14. Nakahara M, Okumura N, Kay EP, et al. Corneal endothelial expansion promoted by human bone marrow mesenchymal stem cell-derived conditioned medium. *PLoS One*. 2013;8: e69009.
15. Okumura N, Kay EP, Nakahara M, Hamuro J, Kinoshita S, Koizumi N. Inhibition of TGF-beta signaling enables human corneal endothelial cell expansion in vitro for use in regenerative medicine. *PLoS One*. 2013;8:e58000.
16. Hongo A, Okumura N, Nakahara M, Kay EP, Koizumi N. The effect of a p38 Mitogen-activated protein kinase inhibitor on cellular senescence of cultivated human corneal endothelial cells. *Invest Ophthalmol Vis Sci*. 2017;58:3325–3334.
17. Okumura N, Kakutani K, Numata R, et al. Laminin-511 and -521 enable efficient in vitro expansion of human corneal endothelial cells. *Invest Ophthalmol Vis Sci*. 2015;56:2933–2942.
18. Okumura N, Koizumi N, Ueno M, et al. Enhancement of corneal endothelium wound healing by Rho-associated kinase (ROCK) inhibitor eye drops. *Br J Ophthalmol*. 2011;95:1006–1009.
19. Okumura N, Koizumi N, Kay EP, et al. The ROCK inhibitor eye drop accelerates corneal endothelium wound healing. *Invest Ophthalmol Vis Sci*. 2013;54:2493–2502.
20. Ishino Y, Sano Y, Nakamura T, et al. Amniotic membrane as a carrier for cultivated human corneal endothelial cell transplantation. *Invest Ophthalmol Vis Sci*. 2004;45:800–806.
21. Mimura T, Yamagami S, Yokoo S, et al. Cultured human corneal endothelial cell transplantation with a collagen sheet in a rabbit model. *Invest Ophthalmol Vis Sci*. 2004;45:2992–2997.
22. Koizumi N, Sakamoto Y, Okumura N, et al. Cultivated corneal endothelial cell sheet transplantation in a primate model. *Invest Ophthalmol Vis Sci*. 2007;48:4519–4526.
23. Mimura T, Shimomura N, Usui T, et al. Magnetic attraction of iron-endocytosed corneal endothelial cells to Descemet's membrane. *Exp Eye Res*. 2003;76:745–751.
24. Mimura T, Yamagami S, Yokoo S, et al. Sphere therapy for corneal endothelium deficiency in a rabbit model. *Invest Ophthalmol Vis Sci*. 2005;46:3128–3135.
25. Okumura N, Koizumi N, Ueno M, et al. ROCK inhibitor converts corneal endothelial cells into a phenotype capable of regenerating in vivo endothelial tissue. *Am J Pathol*. 2012; 181:268–277.
26. Okumura N, Sakamoto Y, Fujii K, et al. Rho kinase inhibitor enables cell-based therapy for corneal endothelial dysfunction. *Sci Rep*. 2016;6:26113.
27. Okumura N, Nakano S, Kay EP, et al. Involvement of cyclin D and p27 in cell proliferation mediated by ROCK inhibitors Y-27632 and Y-39983 during corneal endothelium wound healing. *Invest Ophthalmol Vis Sci*. 2014;55:318–329.
28. Okumura N, Fujii K, Kagami T, et al. Activation of the Rho/Rho kinase signaling pathway is involved in cell death of corneal endothelium. *Invest Ophthalmol Vis Sci*. 2016;57: 6843–6851.
29. Shima N, Kimoto M, Yamaguchi M, Yamagami S. Increased proliferation and replicative lifespan of isolated human corneal endothelial cells with L-ascorbic acid 2-phosphate. *Invest Ophthalmol Vis Sci*. 2011;52:8711–8717.
30. Peh GS, Beuerman RW, Colman A, Tan DT, Mehta JS. Human corneal endothelial cell expansion for corneal endothelium transplantation: an overview. *Transplantation*. 2011;91:811–819.
31. Peh GS, Toh KP, Ang HP, Seah XY, George BL, Mehta JS. Optimization of human corneal endothelial cell culture: density dependency of successful cultures in vitro. *BMC Res Notes*. 2013;6:176.
32. Peh GS, Adnan K, George BL, et al. The effects of Rho-associated kinase inhibitor Y-27632 on primary human corneal endothelial cells propagated using a dual media approach. *Sci Rep*. 2015;5:9167.
33. Thornton TM, Rincon M. Non-classical p38 map kinase functions: cell cycle checkpoints and survival. *Int J Biol Sci*. 2009;5:44–51.
34. Chang L, Karin M. Mammalian MAP kinase signalling cascades. *Nature*. 2001;410:37–40.
35. Raman M, Chen W, Cobb MH. Differential regulation and properties of MAPKs. *Oncogene*. 2007;26:3100–3112.
36. Cuenda A, Rousseau S. p38 MAP-kinases pathway regulation, function and role in human diseases. *Biochim Biophys Acta*. 2007;1773:1358–1375.
37. Zarubin T, Han J. Activation and signaling of the p38 MAP kinase pathway. *Cell Res*. 2005;15:11–18.
38. Iwasa H, Han J, Ishikawa F. Mitogen-activated protein kinase p38 defines the common senescence-signalling pathway. *Genes Cells*. 2003;8:131–144.
39. Lavoie JN, L'Allemain G, Brunet A, Muller R, Pouyssegur J. Cyclin D1 expression is regulated positively by the p42/p44MAPK and negatively by the p38/HOGMAPK pathway. *J Biol Chem*. 1996;271:20608–20616.
40. Hui L, Bakiri L, Stepniak E, Wagner EF. p38alpha: a suppressor of cell proliferation and tumorigenesis. *Cell Cycle*. 2007;6: 2429–2433.
41. Davis T, Bachler MA, Wyllie FS, Bagley MC, Kipling D. Evaluating the role of p38 MAP kinase in growth of Werner syndrome fibroblasts. *Ann N Y Acad Sci*. 2010;1197:45–48.
42. Duch A, de Nadal E, Posas F. The p38 and Hog1 SAPKs control cell cycle progression in response to environmental stresses. *FEBS Lett*. 2012;586:2925–2931.
43. Lin DW, Chung BP, Kaiser P. S-adenosylmethionine limitation induces p38 mitogen-activated protein kinase and triggers cell cycle arrest in G1. *J Cell Sci*. 2014;127:50–59.
44. Casanovas O, Miro F, Estanyol JM, Itarte E, Agell N, Bachs O. Osmotic stress regulates the stability of cyclin D1 in a p38SAPK2-dependent manner. *J Biol Chem*. 2000;275:35091–35097.
45. Zhou BB, Elledge SJ. The DNA damage response: putting checkpoints in perspective. *Nature*. 2000;408:433–439.
46. Bulavin DV, Saito S, Hollander MC, et al. Phosphorylation of human p53 by p38 kinase coordinates N-terminal phosphorylation and apoptosis in response to UV radiation. *EMBO J*. 1999;18:6845–6854.
47. She QB, Chen N, Dong Z. ERKs and p38 kinase phosphorylate p53 protein at serine 15 in response to UV radiation. *J Biol Chem*. 2000;275:20444–20449.
48. She QB, Bode AM, Ma WY, Chen NY, Dong Z. Resveratrol-induced activation of p53 and apoptosis is mediated by extracellular-signal-regulated protein kinases and p38 kinase. *Cancer Res*. 2001;61:1604–1610.
49. Bulavin DV, Higashimoto Y, Popoff IJ, et al. Initiation of a G2/M checkpoint after ultraviolet radiation requires p38 kinase. *Nature*. 2001;411:102–107.
50. Kim TY, Kim WI, Smith RE, Kay ED. Role of p27(Kip1) in cAMP- and TGF-beta2-mediated antiproliferation in rabbit corneal endothelial cells. *Invest Ophthalmol Vis Sci*. 2001;42: 3142–3149.
51. Lee JG, Kay EP. Two populations of p27 use differential kinetics to phosphorylate Ser-10 and Thr-187 via phosphatidylinositol 3-Kinase in response to fibroblast growth factor-2 stimulation. *J Biol Chem*. 2007;282:6444–6454.
52. Lee JG, Kay EP. Involvement of two distinct ubiquitin E3 ligase systems for p27 degradation in corneal endothelial cells. *Invest Ophthalmol Vis Sci*. 2008;49:189–196.

Investigative Ophthalmology & Visual Science

Development of Cell Analysis Software to Evaluate Fibroblastic Changes in Cultivated Corneal Endothelial Cells for Quality Control

Naoki Okumura, MD, PhD, Keitaro Kobayashi, BS,† Naoya Ishida, BS,† Takato Kagami, BS,* Satoru Hiwa, PhD,† Tomoyuki Hiroyasu, PhD,† and Noriko Koizumi, MD, PhD**

Purpose: To develop software to evaluate the fibroblastic morphological changes in cultured human corneal endothelial cells (HCECs) as a quality control measure for use in tissue engineering therapy.

Methods: Software was designed to recognize cell borders, to approximate cell shape as an ellipse, and to calculate the aspect ratio of the ellipse as an indicator of severity of the fibroblastic morphological change. Using the designed software, 60 phase contrast images of polygonal HCECs and 60 phase contrast images of fibroblastic HCECs were analyzed. The correlations of the aspect ratio and other parameters (cell density, percentage of cells surrounded by 6 cells, and coefficient of variation) were evaluated.

Results: Cell shapes were recognized based on phase contrast images and were approximated as ellipses by software. The average aspect ratio was significantly higher (34.9% ± 6.1%) in fibroblastic HCECs than in polygonal HCECs (24.4% ± 2.3%) ($P < 0.01$). The aspect ratio showed a correlation with cell density, with the percentage of cells surrounded by 6 neighboring cells, and with the coefficient of variation (Pearson correlation coefficients, −0.84, −0.38, and 0.66, respectively).

Conclusions: We propose that fibroblastic alteration of HCECs can be evaluated by the cell morphology based on the aspect ratio. Software developed in this study, which can analyze the frequency and severity of fibroblastic alteration, will be useful for nondestructive assessment of cells destined for use in cell-based therapy for corneal endothelial decompensation.

Key Words: corneal endothelium, quality control, regenerative medicine, software

(*Cornea* 2018;37:1572–1578)

Received for publication March 15, 2018; revision received July 13, 2018; accepted July 31, 2018. Published online ahead of print September 18, 2018.

From the Departments of *Biomedical Engineering; and †Biomedical Information, Faculty of Life and Medical Sciences, Doshisha University, Kyotanabe, Japan.

Supported by the Program for the Strategic Research Foundation at Private Universities from MEXT (N.K. and N.O.).

The authors have no conflicts of interest to disclose.

Supplemental digital content is available for this article. Direct URL citations appear in the printed text and are provided in the HTML and PDF versions of this article on the journal's Web site (www.corneajrnl.com).

Correspondence: Noriko Koizumi, MD, PhD, Department of Biomedical Engineering, Faculty of Life and Medical Sciences, Doshisha University, Kyotanabe 610-0321, Japan (e-mail: nkoizumi@mail.doshisha.ac.jp).

Corneal transplantation is the only therapeutic choice for treating corneal endothelial decompensation, but it presents several challenges for both patients and physicians, including a shortage of donor corneas, late graft failure due to continuous cell loss, and graft rejection.[1] Therefore, numerous research groups, including our own, have devoted their efforts to the development of tissue engineering therapies that can overcome these problems.[2–8] In 2013, we obtained approval from the Japanese Ministry of Health, Labour and Welfare to initiate a first-in-human clinical trial of cell-based therapy to treat corneal endothelial dysfunction. Clinical data indicate that the procedure is safe and effective, suggesting that cell-based therapy has the potential for use as an alternative therapeutic choice for treating corneal endothelial decompensation.[9]

One bottleneck encountered in tissue engineering therapy for corneal endothelial decompensation has been the difficulty in cultivating human corneal endothelial cells (HCECs). Under culture conditions, HCECs typically undergo senescence[10] or show massive fibroblastic changes,[11,12] which precludes their use in treatment of corneal endothelial decompensation. Extensive research, including our own work, has now enabled successful in vitro expansion of HCECs,[10,11,13–21] but careful assessment of senescent or fibroblastic phenotypes is still an essential quality control requirement. We recently reported that senescent HCEC cultures are characterized by decreases in cell density, increases in the coefficient of variation for the mean cell area (standard deviation of mean cell area/mean cell area), and decreases in polygonality (the percentage of cells surrounded by 5, 6, or 7 neighbor cells).[22] We have previously created software that enables automatic analysis of these parameters from phase contrast images as a means of nondestructive quality assessment of cultured HCECs to exclude those displaying the senescent phenotype.[22] However, similar software remains to be developed for HCECs displaying the fibroblastic phenotype.

The aim of this study was to create software that can use phase contrast images to assess the severity of fibroblastic changes and the frequency of HCECs exhibiting fibroblastic

changes in cultured cell populations. Our software was designed to obtain a cell boundary from a phase contrast image, to approximate the cell boundary as an ellipse, and to evaluate the severity of fibroblastic morphological changes based on the aspect ratio of the ellipse.

MATERIALS AND METHODS

Cell Culture

Human donor corneas for research purposes were provided by SightLife (Seattle, WA). Ten human donor corneas (from persons >40 years of age) were used for the research. HCECs were isolated from donor corneas and cultured by the protocol described previously.[11,19,21] Briefly, Descemet membranes containing corneal endothelium were stripped from donor corneas and digested with collagenase A (Roche Applied Science, Penzberg, Germany). HCECs were recovered from digested Descemet membranes and were seeded on the culture plate.[21] The culture medium for HCECs was prepared by the protocol described previously.[19] Cell morphology was evaluated using phase contrast microscopy (DMI4000 B; Leica Microsystems, Wetzlar, Germany). Phase contrast images of confluent cultured HCECs (2–10 passages) were used for the study.

Actin Staining and Immunofluorescent Staining

HCECs were seeded in a 24-well cell culture plate and further cultured for 4 weeks after reaching confluence. Samples were fixed in 0.5% paraformaldehyde for 45 minutes at room temperature, washed with phosphate-buffered saline (PBS), and incubated for 30 minutes with 1% bovine serum albumin. The samples were incubated for 45 minutes at 37°C with antibodies against ZO-1 (1:200; ThermoFisher Scientific Inc, Waltham, MA). After washing with PBS, Alexa Fluor 488-conjugated goat anti-mouse (Life Technologies) was used as the secondary antibody at a 1:1000 dilution. F-actin was stained with a 1:400 dilution of Alexa Fluor 546-conjugated phalloidin (Life Technologies, Carlsbad, CA). Nuclei were stained with 4′, 6-diamidino-2-phenylindole (DAPI) (Dojindo Laboratories, Kumamoto, Japan). The samples were examined by fluorescence microscopy (BZ-9000; Keyence, Osaka, Japan).

Software

Software (hereafter referred to as Corneal Endothelial Cell Analyzer Version 2) was programmed to analyze fibroblastic changes in HCECs based on images obtained using phase contrast microscopy. Corneal Endothelial Cell Analyzer Version 2 was developed at Doshisha University with programming by Python (Python Software Foundation, https://www.python.org/, Beaverton, OR). Python was used in Eclipse (Eclipse Foundation, http://www.eclipse.org/, Ontario, Canada) with a PyDev (PyDev, http://www.pydev.org/) plug-in.

Cell–cell border images were obtained using Corneal Endothelial Cell Analyzer Version 2 by incubating HCECs in Ca^{2+}-free and Mg^{2+}-free PBS to weaken the apical junction and allow visualization of the cell–cell border. We previously reported that weakening of the apical junction is reversible and occurs without cell damage and that the treated HCECs could be further used for clinical purposes.[22] Phase contrast images were obtained with a phase contrast microscope, and the cell boundaries were defined with Corneal Endothelial Cell Analyzer Version 2 after the following processes: 1) denoising, 2) edge enhancement, 3) binarization, and 4) skeletonization. The cell shape was approximated to an ellipse from the obtained cell–cell border images. All cells except the cells that were on the edge of the phase contrast images were approximated. The aspect ratio was obtained as the ratio of the major axis and minor axis of the approximated ellipse by the following formula: (1 − minor axis)/major axis × 100. Clinical parameters, including the cell density, the numbers of surrounding cells, and the coefficient of variation, were defined using software that we previously reported.[22]

Statistical Analysis

The Student t test was applied to detect differences between 2 groups. The Pearson correlation coefficient was used to determine any significant correlations between the aspect ratio and other parameters, including corneal endothelial cell density, percentage of cells surrounded by 6 cells or 5, 6, or 7 cells, and the coefficient of variation. $P < 0.05$ was considered statistically significant.

RESULTS

Fibroblastic Morphological Changes of HCECs During In Vitro Expansion

Representative phase contrast images of HCECs exhibiting polygonal morphology and fibroblastic morphology are shown in Figure 1 (Fig. 1A, left). Actin staining revealed a cobblestone-like structure of the polygonal HCECs, which resembled that of the normal in vivo corneal endothelium, with actin distributed at the cell cortex of the HCECs. However, fibroblastic HCECs observed covering approximately 50% of the area showed actin-staining patterns similar to fibroblasts (Fig. 1A, middle). Immunofluorescent staining revealed a distribution of ZO-1 at the apical junction in polygonal HCECs, but this pattern was disrupted in fibroblastic HCECs (Fig. 1A, right).

Loss of the polygonal HCEC phenotype and acquisition of the fibroblastic phenotype during cultivation or passaging the cells showed a wide variation among the cells in the culture population. For example, the right-hand image in Figure 1B shows the polygonal morphology with no fibroblastic cells, the second image from the right shows approximately 20% of the area covered by fibroblastic cells, the third image from the right shows approximately 70% of the area covered with fibroblastic cells, and the left-hand image shows only fibroblastic cells. The cell boundaries of the phase contrast images of HCECs at the confluent state are indistinct, so the HCECs in Figure 1B were incubated in Ca^{2+}-free and Mg^{2+}-free PBS for 10 minutes to enhance the cell boundaries.[22]

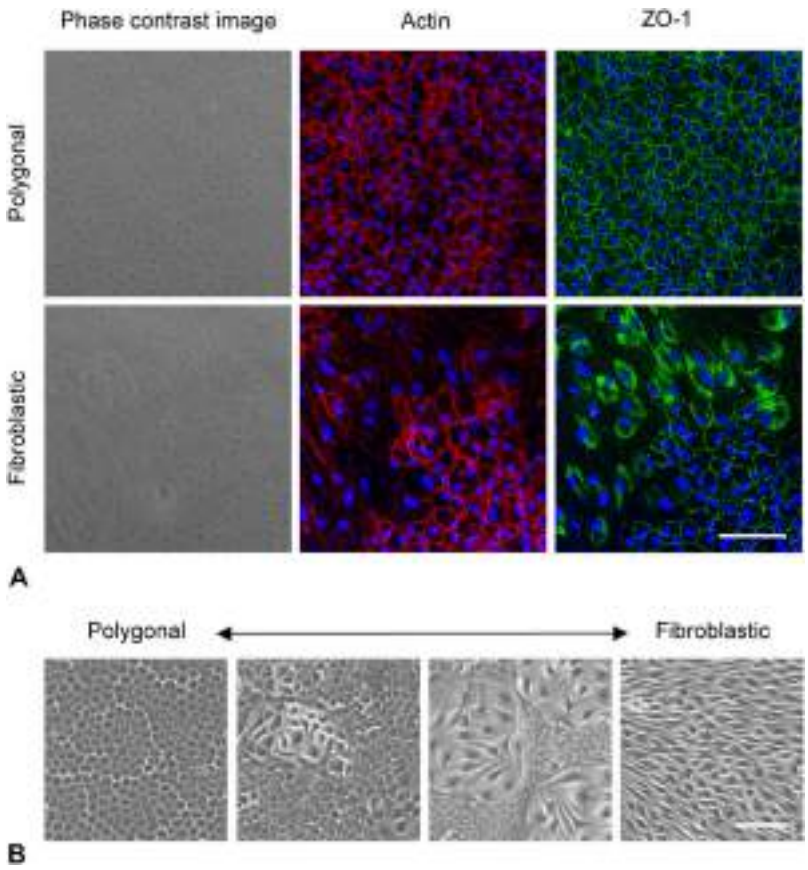

FIGURE 1. Fibroblastic morphological changes in human corneal endothelial cells (HCECs) during in vitro expansion. A, Representative phase contrast images of HCECs exhibiting polygonal morphology and fibroblastic morphology are shown (left). Actin staining shows actin distribution at the cell cortex in polygonal HCECs, but fibroblastic HCECs are observed in approximately 50% of the area, and the actin-staining patterns in the fibroblastic HCECs (middle) are similar to those of fibroblasts. Immunofluorescent staining shows a distribution of ZO-1 at the apical junction in polygonal HCECs, whereas those patterns are disrupted in fibroblastic HCECs (right). Scale bar: 100 μm. B, Representative phase contrast images with a varied degree of fibroblastic changes and the frequency of those cells among population are shown. The right-hand image shows polygonal morphology without fibroblastic cells, the image second from the right shows approximately 20% of the area covered with fibroblastic cells, the image third from the right shows approximately 70% of the area covered with fibroblastic cells, and the left-hand image shows only fibroblastic cells. Scale bar: 100 μm.

Evaluation of Fibroblastic Changes With the Designed Software

The phase contrast images were processed using the developed Corneal Endothelial Cell Analyzer Version 2 software through several steps: denoising, edge enhancement, binarization, and skeletonizing. HCECs were treated with PBS for 10 minutes to clarify the cell border (Figs. 2A-1). A denoised image was then obtained by extreme emphasis of the cell boundaries (Figs. 2A-2). An edge enhancement image was obtained to sharpen the cell boundaries (Figs. 2A-3). A binarization image was then obtained by binarizing the cell areas and the boundaries (Figs. 2A-4). Unnecessary lines that appeared after the edge enhancement process were removed, leaving the cell boundaries represented as black lines. A skeletonized image was obtained by thinning the black lines through the skeletonizing process (Figs. 2A-5).

We recently reported that the numbers of neighboring cells surrounding each cell are useful for evaluating the polymorphism of HCECs for quality control.[22] Phase contrast images showed that the usual number of neighbors of each polygonal HCEC was 6 (typically 5–7) (Fig. 2B, left). As with the polygonal HCECs, the number of neighboring cells for the fibroblastic HCECs was also 6 (also typically 5–7) (Fig. 2B, right), which suggests that the number of neighboring cells is not a useful parameter for determining fibroblastic changes. Therefore, we evaluated the feasibility of approximating each HCEC morphology as an ellipse and then using the aspect ratio of the ellipse to determine the severity of the fibroblastic changes. The representative images demonstrate that the approximated ellipse of a polygonal HCEC was almost a positive circle (Fig. 2C, left), whereas the approximated ellipse of a fibroblastic HCEC was a vertical ellipse (Fig. 2C, right). Approximation of the whole area of a phase contrast image of HCECs exhibiting both polygonal and fibroblastic morphology is shown in Supplemental Figure 1 (see Supplemental Digital Content 1, http://links.lww.com/ICO/A713).

The fibroblastic HCECs varied in the degree of fibroblastic severity and frequency, so our software was programmed to provide color maps and histograms of the aspect ratio. The representative color maps show a low aspect ratio, suggesting polygonal HCECs, as cold colors, and a high aspect ratio, suggesting fibroblastic HCECs, as warm colors (Fig. 3A). The histograms visually demonstrated the relative frequency of HCECs with various aspect ratios (Fig. 3B).

Correlation Between Indicators of Corneal Endothelium and the Aspect Ratio

Sixty phase contrast images of polygonal HCECs and 60 phase contrast images of fibroblastic HCECs, which were categorized by 2 independent researchers, were prepared to evaluate the feasibility of using Corneal Endothelial Cell Analyzer Version 2 to detect fibroblastic changes. The aspect

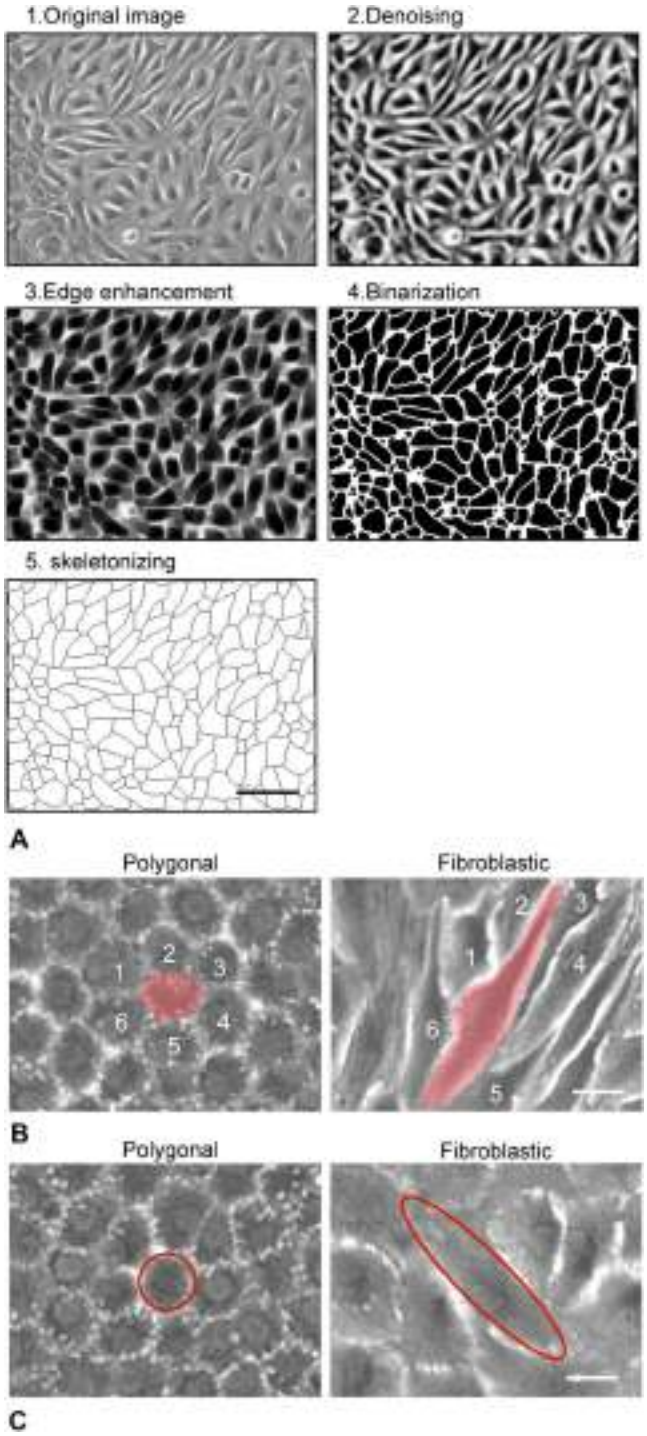

FIGURE 2. Approximation of the cell shape as an ellipse using the developed Corneal Endothelial Cell Analyzer Version 2 software. A, The phase contrast images were processed by software through several steps; that is, denoising, edge enhancement, binarization, and skeletonizing. Human corneal endothelial cells (HCECs) were treated with PBS for 10 minutes to enhance the cell border for further analysis by software (1). A denoising image was obtained by extreme emphasis of the cell boundaries (2). An edge enhancement image was obtained to sharpen the cell boundaries (3). A binarization image was obtained by binarizing the cell areas and the boundaries (4). Unnecessary lines that appeared after the edge enhancement process were removed, leaving the cell boundaries represented as black lines. A skeletonized image was obtained by thinning the black line through the skeletonizing process (5). Scale bar: 100 μm. B, Phase contrast images show that the number of neighboring cells of each polygonal HCEC was 6 (typically 5–7) (left). Similar to polygonal HCECs, the number of neighboring cells of fibroblastic HCECs was 6 (also typically 5–7) (right). Scale bar: 10 μm. C, Representative images show that the approximation ellipse of polygonal HCEC was almost a positive circle (left), whereas the approximation ellipse of a fibroblastic HCEC was a vertical ellipse (right). Scale bar: 10 μm.

ratios were analyzed in all images, and the mean of the average aspect ratio of each image was used for analysis. The mean of the average aspect ratios was significantly higher in fibroblastic HCECs (34.9% ± 6.1%) than in polygonal HCECs (24.4% ± 2.3%) ($P < 0.01$) (Fig. 4A).

In addition to the aspect ratio, we calculated the cell density, the percentage of cells surrounded by 6 cells, the percentage of cells surrounded by 5, 6, or 7 cells, and the coefficient of variation, and the means of each value were used for further analysis. The cell density showed a very strong correlation with the aspect ratio (Pearson correlation coefficient −0.84, $P < 0.01$, n = 120) (Fig. 4B). The percentage of cells surrounded by 6 neighboring cells, which is clinically used as an indicator of polymorphism, showed a weak correlation with the aspect ratio (Pearson correlation coefficient −0.38, $P < 0.01$, n = 120) (Fig. 4C). The percentage of cells surrounded by 5, 6, or 7 neighboring cells, which we previously reported as a feasible indicator of polymorphism for cultured HCECs, showed a very strong correlation with the aspect ratio (Pearson correlation coefficient −0.82, $P < 0.01$, n = 120) (Fig. 4D). The coefficient of variation, which is clinically used as an indicator of polymegathism, showed a strong correlation with the cell density (Pearson correlation coefficient 0.66, $P < 0.01$, n = 120) (Fig. 4E).

DISCUSSION

The use of HCECs in regenerative medicine for the corneal endothelium requires that the HCECs be expanded in vitro to obtain a sufficient number of cells for treatment of corneal decompensation. However, HCECs readily undergo fibroblastic morphological changes under culture conditions,[11,12] and HCECs with the fibroblastic morphology lose their pump and barrier functions and will not form an effective corneal endothelium. We previously screened 242 cell surface antigens of HCECs and showed that CD98, CD166, and CD340 are elevated in HCECs with the normal phenotype, whereas CD9, CD49e, CD44, and CD73 are elevated in HCECs with the fibroblastic morphology.[12] In addition, we demonstrated that HCECs sorted by flow cytometry as CD73 negative exhibited the normal polygonal morphology and expressed functional markers, whereas HCECs sorted as CD73 positive exhibited the fibroblastic phenotype.[12] This finding indicated that HCECs exhibiting

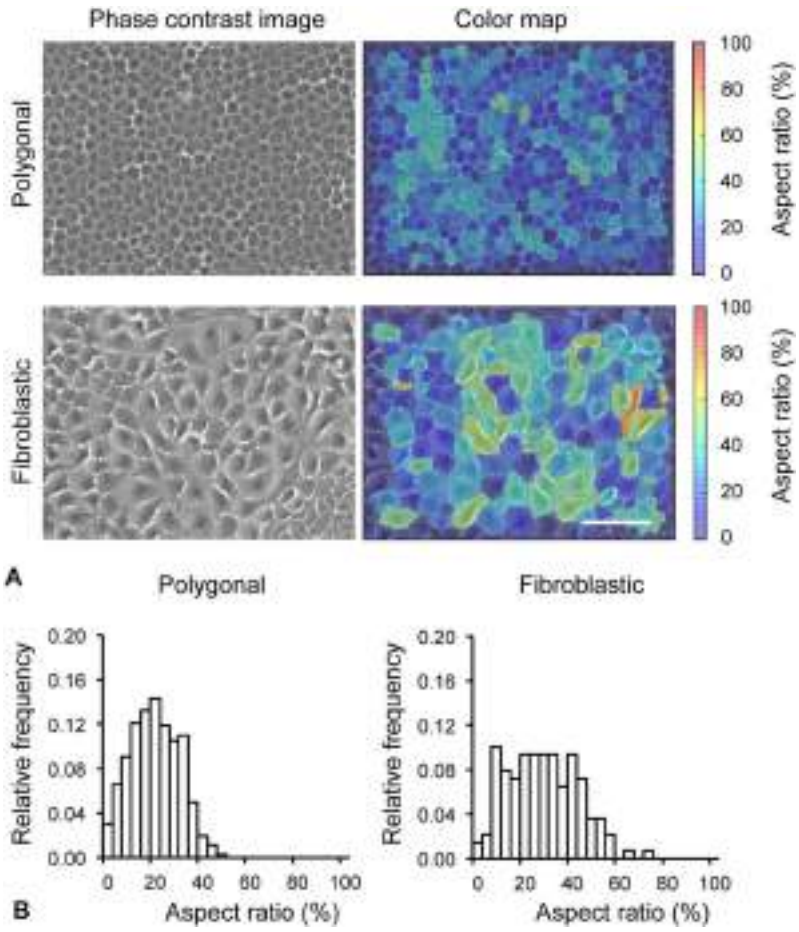

FIGURE 3. Color map and histogram of the aspect ratio of human corneal endothelial cells (HCECs). A, Software was programmed to provide color maps and histograms of the aspect ratio to visualize the variation in severity and frequency of fibroblastic changes in the culture population. Representative color maps show a low aspect ratio suggesting polygonal HCECs as cold colors and a high aspect ratio suggesting fibroblastic HCECs as warm colors. Scale bar: 100 μm. B, Histograms visually demonstrating the relative frequency of HCECs with various aspect ratios.

fibroblastic morphology lose their functional phenotype as HCECs and acquire a fibroblast-like phenotype. Fibroblastic HCECs should not be used for clinical purposes, so quality control that screens for fibroblastic changes is essential if HCECs are to be used for regenerative medicine.

As with the regulations imposed for drug development processes, regulatory authorities require pharmaceutical companies to perform quality control assessments on any cells or tissues that will be used in humans.[23,24] In 2013, we initiated clinical research into cell-based therapy that uses HCECs isolated and cultured from allogeneic donor corneas.[9] The HCECs are injected into the anterior chamber of the eye, in combination with a Rho kinase inhibitor,[7,8] as treatment for endothelial decompensation. For this clinical research, we assessed the quality of the injected HCECs by multiple screening steps, including cell viability (percentage of living cells >70%), visual inspection (percentage of cells exhibiting a non-HCEC phenotype <10%, no foreign bodies present, and no color changes), cell purity (concentration of collagen type 1 in the supernatant of culture medium <15 ng/mL), functional assurance (ZO-1 and Na^+/K^+-ATPase are detected by immunofluorescence staining), confirmation of no contamination of the culture medium (concentration of residual bovine serum albumin <125 ng/mL), bacterial testing (no detection of bacteria by culturing), mycoplasma testing (no detection by PCR), endotoxin test (<1.67 EU/mL), and parvovirus B19 testing (negative by a nucleic acid amplification technique [NAT]) (www.mhlw.go.jp/stf/shingi/2r9852000002wm7z-att/2r9852000002wmo5.pdf; this document is only written in Japanese, accessed on February 3, 2017, although the quality assessment items have been updated by official communication with Japanese Ministry of Health, Labour and Welfare). Our clinical research is now accumulating evidence that HCEC injection can regenerate a transparent cornea without severe adverse effects, although follow-up data are still required.[9] We have devoted our efforts to obtain approval for the use of HCECs as a cell-based product from authorities including Japanese Ministry of Health, Labour and Welfare and the Food and Drug Administration by conducting a clinical trial. For this reason, improvement and establishment of quality control for HCECs are urgent subjects.

In this study, our aim was to create a software program that would enable automatic evaluation of fibroblastic HCECs and that would provide subjective quality assessment. Software described in this study can obtain cell boundaries from phase contrast images and evaluate fibroblastic changes by approximating the cell morphology as an ellipse. The HCECs categorized as fibroblastic by trained researchers showed a higher aspect ratio compared with HCECs categorized as the normal polygonal phenotype. This finding suggested that

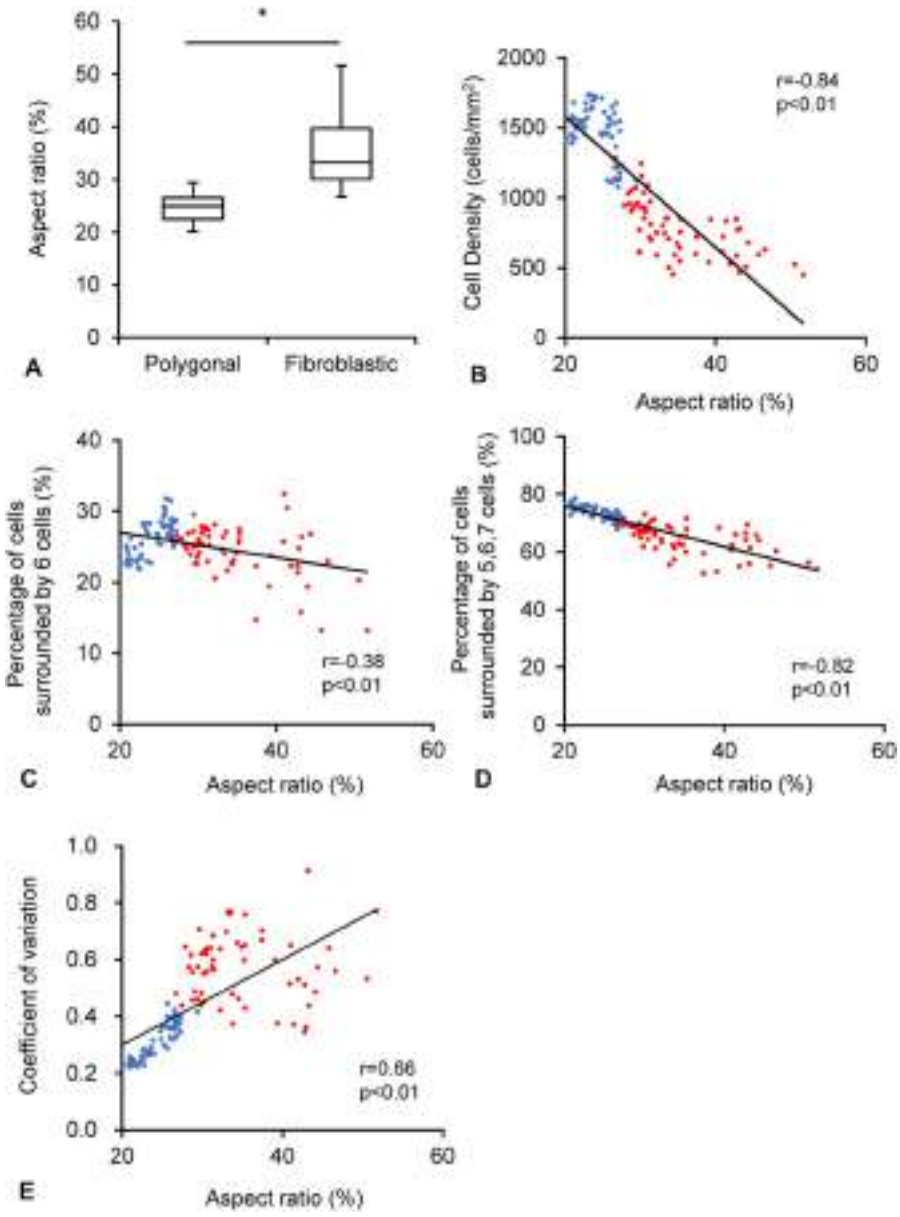

FIGURE 4. Correlation of the aspect ratio and other parameters: cell density, percentage of cells surrounded by 6 cells, and coefficient of variation. A, Sixty phase contrast images of polygonal human corneal endothelial cells (HCECs), and 60 phase contrast images of fibroblastic HCECs, were prepared and categorized by 2 independent researchers. The aspect ratio of HCECs in the images was analyzed, and the mean of the average aspect ratio of each image was used for analysis. The mean of the average aspect ratio was significantly higher (34.9% ± 6.1%) in fibroblastic HCECs than in polygonal HCECs (24.4% ± 2.3%) ($P <$ 0.01). The horizontal lines in the boxes indicate the medians, the bottom of each box indicates the 25th percentile, and the top of each box indicates the 75th percentile. The horizontal lines outside the boxes indicate the ranges of the aspect ratio. B, The cell density, percentage of cells surrounded by 6 cells, percentage of cells surrounded by 5, 6, or 7 cells, and the coefficient of variation were calculated based on the cell shape acquired by software, and the mean of each value was used for further analysis. The cell density showed a very strong correlation with the aspect ratio (Pearson correlation coefficient −0.84, $P <$ 0.01, n = 120). C, The percentage of cells surrounded by 6 neighboring cells, which is used clinically as an indicator of polymorphism, showed a weak correlation with the aspect ratio (Pearson correlation coefficient −0.38, $P <$ 0.01, n = 120). D, The percentage of cells surrounded by 5, 6, or 7 neighboring cells showed a very strong correlation with the aspect ratio (Pearson correlation coefficient −0.82, $P <$ 0.01, n = 120). E, The coefficient of variation, which is clinically used as an indicator of polymegathism, showed a strong correlation with the cell density (Pearson correlation coefficient 0.66, $P <$ 0.01, n = 120).

the aspect ratio calculated from approximated ellipses by our software is a practical and subjective index for evaluating fibroblastic changes. In addition, a higher aspect ratio strongly correlated with various indicators, including cell density, coefficient of variation, and polygonality,[25] which indicates that the aspect ratio is not a contradictory parameter to these other recognized indicators, and it therefore provides additional assessment of fibroblastic changes.

One drawback of this study is the lack of precise values for the aspect ratio and the frequency of fibroblastic cells necessary for conclusive determination that a population of HCECs is suitable for clinical purposes. Further validation of this software will also be required if the software is to be applied for quality assessment aimed at decisions on product release. Future studies should evaluate the effects of the aspect ratio value and the frequency of fibroblastic changes on clinical outcomes.

In summary, we propose that functional loss of HCECs associated with fibroblastic changes can be evaluated by cell morphology based on the cell's aspect ratio. We have created software that can analyze the frequency and severity of fibroblastic alteration that HCECs can potentially undergo during in vitro expansion. Automatic and subjective assessment is required for the production of cell-based products by pharmaceutical companies, so our proposed software will be useful in providing a nondestructive assessment of cells destined for use in cell-based therapy for corneal endothelial decompensation.

REFERENCES

1. Tan DT, Dart JK, Holland EJ, et al. Corneal transplantation. *Lancet.* 2012;379:1749–1761.
2. Mimura T, Shimomura N, Usui T, et al. Magnetic attraction of iron-endocytosed corneal endothelial cells to Descemet's membrane. *Exp Eye Res.* 2003;76:745–751.
3. Mimura T, Yamagami S, Yokoo S, et al. Cultured human corneal endothelial cell transplantation with a collagen sheet in a rabbit model. *Invest Ophthalmol Vis Sci.* 2004;45:2992–2997.
4. Ishino Y, Sano Y, Nakamura T, et al. Amniotic membrane as a Carrier for cultivated human corneal endothelial cell transplantation. *Invest Ophthalmol Vis Sci.* 2004;45:800–806.
5. Mimura T, Yokoo S, Araie M, et al. Treatment of rabbit bullous keratopathy with precursors derived from cultured human corneal endothelium. *Invest Ophthalmol Vis Sci.* 2005;46:3637–3644.
6. Koizumi N, Sakamoto Y, Okumura N, et al. Cultivated corneal endothelial cell sheet transplantation in a primate model. *Invest Ophthalmol Vis Sci.* 2007;48:4519–4526.
7. Okumura N, Koizumi N, Ueno M, et al. ROCK inhibitor converts corneal endothelial cells into a phenotype capable of regenerating in vivo endothelial tissue. *Am J Pathol.* 2012;181:268–277.
8. Okumura N, Sakamoto Y, Fujii K, et al. Rho kinase inhibitor enables cell-based therapy for corneal endothelial dysfunction. *Sci Rep.* 2016;6:26113.
9. Kinoshita S, Koizumi N, Ueno M, et al. Injection of cultured cells with a ROCK inhibitor for bullous keratopathy. *N Engl J Med.* 2018;378:995–1003.
10. Hongo A, Okumura N, Nakahara M, et al. The effect of a p38 mitogen-activated protein kinase inhibitor on cellular senescence of cultivated human corneal endothelial cells. *Invest Ophthalmol Vis Sci.* 2017;58:3325–3334.
11. Okumura N, Kay EP, Nakahara M, et al. Inhibition of TGF-beta signaling enables human corneal endothelial cell expansion in vitro for use in regenerative medicine. *PLoS One.* 2013;8:e58000.
12. Okumura N, Hirano H, Numata R, et al. Cell surface markers of functional phenotypic corneal endothelial cells. *Invest Ophthalmol Vis Sci.* 2014;55:7610–7618.
13. Miyata K, Drake J, Osakabe Y, et al. Effect of donor age on morphologic variation of cultured human corneal endothelial cells. *Cornea.* 2001;20:59–63.
14. Chen KH, Azar D, Joyce NC. Transplantation of adult human corneal endothelium ex vivo: a morphologic study. *Cornea.* 2001;20:731–737.
15. Zhu C, Joyce NC. Proliferative response of corneal endothelial cells from young and older donors. *Invest Ophthalmol Vis Sci.* 2004;45:1743–1751.
16. Okumura N, Ueno M, Koizumi N, et al. Enhancement on primate corneal endothelial cell survival in vitro by a ROCK inhibitor. *Invest Ophthalmol Vis Sci.* 2009;50:3680–3687.
17. Shima N, Kimoto M, Yamaguchi M, et al. Increased proliferation and replicative lifespan of isolated human corneal endothelial cells with L-ascorbic acid 2-phosphate. *Invest Ophthalmol Vis Sci.* 2011;52:8711–8717.
18. Peh GS, Toh KP, Wu FY, et al. Cultivation of human corneal endothelial cells isolated from paired donor corneas. *PLoS One.* 2011;6:e28310.
19. Nakahara M, Okumura N, Kay EP, et al. Corneal endothelial expansion promoted by human bone marrow mesenchymal stem cell-derived conditioned medium. *PLoS One.* 2013;8:e69009.
20. Peh GS, Toh KP, Ang HP, et al. Optimization of human corneal endothelial cell culture: density dependency of successful cultures in vitro. *BMC Res Notes.* 2013;6:176.
21. Okumura N, Kakutani K, Numata R, et al. Laminin-511 and -521 enable efficient in vitro expansion of human corneal endothelial cells. *Invest Ophthalmol Vis Sci.* 2015;56:2933–2942.
22. Okumura N, Ishida N, Kakutani K, et al. Development of cell analysis software for cultivated corneal endothelial cells. *Cornea.* 2017;36:1387–1394.
23. Sipp D. Hope alone is not an outcome: why regulations makes sense for the global stem cell industry. *Am J Bioeth.* 2010;10:33–34.
24. Lysaght T, Campbell AV. Regulating autologous adult stem cells: the FDA steps up. *Cell Stem Cell.* 2011;9:393–396.
25. Nishida T, Saika S. Cornea and sclera: anatomy and physiology. *Cornea.* 2011;1:3–24.

sistent vomiting is characteristic of diabetic ketoacidosis, so this mechanism seems unlikely.

White notes that our trial fluids were either hypotonic or somewhat hypertonic (taking into account potassium salts). We did not evaluate strictly isotonic fluids; however, our data indicate no association between fluid tonicity and neurologic outcome. Furthermore, in the Dallas study, the requirement for abnormal results on magnetic resonance imaging to diagnose cerebral injury or edema related to diabetic ketoacidosis differs from our study definition of this outcome and may account for the lower frequency reported. [3]

Russell and Kanthimathinathan note that, by random chance, the number of patients with a low pH in the slow-infusion groups was slightly higher than that in the fast-infusion groups. However, in our analyses, we compared proportions rather than absolute numbers of patients with the outcomes of interest. Therefore, the small difference in group numbers should not have had an effect on the results.

Nathan Kuppermann, M.D., M.P.H.
Nicole S. Glaser, M.D.

University of California Davis School of Medicine
Sacramento, CA
nkuppermann@ucdavis.edu

Since publication of their article, the authors report no further potential conflict of interest.

1. Glaser N, Barnett P, McCaslin I, et al. Risk factors for cerebral edema in children with diabetic ketoacidosis. N Engl J Med 2001;344:264-9.
2. Harris GD, Fiordalisi I, Harris WL, Mosovich LL, Finberg L. Minimizing the risk of brain herniation during treatment of diabetic ketoacidemia: a retrospective and prospective study. J Pediatr 1990;117:22-31.
3. Muir AB, Quisling RG, Yang MC, Rosenbloom AL. Cerebral edema in childhood diabetic ketoacidosis: natural history, radiographic findings, and early identification. Diabetes Care 2004;27:1541-6.

DOI: 10.1056/NEJMc1810064

Cultured Cells and ROCK Inhibitor for Bullous Keratopathy

TO THE EDITOR: The clinical trial on corneal endothelial cell (CEC)–injection therapy by Kinoshita et al. (March 15 issue)[1] is a landmark study in corneal transplantation. In the trial, seven patients had Fuchs's endothelial corneal dystrophy, characterized by extracellular matrix aggregates (guttae) that are known to inhibit CEC monolayer formation.[2,3] The authors noted that "a silicone needle . . . was used to remove the abnormal extracellular matrix," yet specular microscopic images showed guttae at 24 weeks after surgery. Do there exist data showing the elimination of guttae after scraping? Furthermore, guttae appear to have worsened from 24 weeks to 2 years (i.e., in Patients 3, 7, and 8). Do the authors believe this is due to new guttae formation or exposure of old guttae, resulting in toxic effects on overlying injected CECs? Have these patients worsened clinically during the past 3 years?

Stephen Wahlig, B.Sc.
Duke University Medical Center
Durham, NC

Viridiana Kocaba, M.D.
Edouard Herriot Hospital
Lyon, France

Jodhbir S. Mehta, M.B., B.S.
Singapore Eye Research Institute
Singapore, Singapore
jodmehta@gmail.com

No potential conflict of interest relevant to this letter was reported.

1. Kinoshita S, Koizumi N, Ueno M, et al. Injection of cultured cells with a ROCK inhibitor for bullous keratopathy. N Engl J Med 2018;378:995-1003.
2. Rizwan M, Peh GS, Adnan K, et al. In vitro topographical model of fuchs dystrophy for evaluation of corneal endothelial cell monolayer formation. Adv Healthc Mater 2016;5:2896-910.
3. Kocaba V, Katikireddy KR, Gipson I, Price MO, Price FW, Jurkunas UV. Association of the gutta-induced microenvironment with corneal endothelial cell behavior and demise in Fuchs endothelial corneal dystrophy. JAMA Ophthalmol 2018;136:886-92.

DOI: 10.1056/NEJMc1805808

TO THE EDITOR: In their article, Kinoshita et al. described a pioneering cell therapy for bullous keratopathy. Although this proof-of-concept study is promising, methodologic discrepancies complicate interpretation.

The study includes two culture protocols, two methods of removing damaged endothelium, two different injected suspensions, and five underlying pathologic conditions. Although these limitations are described, the limited cohort and hetero-

geneity are problematic. It is impossible to determine the origin of the reformed endothelium and whether it occurs through donor-cell integration, paracrine effects, the rho-associated protein kinase (ROCK) inhibitor, or a combination of these.[1]

We wonder whether the mechanism through which new endothelium is formed is allografting or cell regeneration, a matter with implications for immunosuppression and rejection. Negative controls (i.e., patients who undergo endothelial stripping without replacement) may be needed to unravel this process. We recently reported spontaneous reformation of the endothelium in 65% of patients who underwent endothelial stripping without transplantation, as early as 1 month postoperatively.[2] Kinoshita et al. report higher success rates at 2 years after surgery, but it would be interesting to simultaneously include negative controls, with salvage transplantations for patients who did not have a response.[2,3] Nevertheless, the work represents an important step forward.

Bert Van den Bogerd, M.Sc.
University of Antwerp
Wilrijk, Belgium
bert.vandenbogerd@uantwerpen.be

Sorcha Ní Dhubhghaill, M.D., Ph.D.
Antwerp University Hospital
Edegem, Belgium

Nadia Zakaria, M.D., Ph.D.
University of Antwerp
Wilrijk, Belgium

No potential conflict of interest relevant to this letter was reported.

1. Dana R. A new frontier in curing corneal blindness. N Engl J Med 2018;378:1057-8.
2. Van den Bogerd B, Dhubhghaill SN, Koppen C, Tassignon MJ, Zakaria N. A review of the evidence for in vivo corneal endothelial regeneration. Surv Ophthalmol 2018;63:149-65.
3. Bleyen I, Saelens IEY, van Dooren BTH, van Rij G. Spontaneous corneal clearing after Descemet's stripping. Ophthalmology 2013;120:215.

DOI: 10.1056/NEJMc1805808

THE AUTHORS REPLY: We appreciate the comments from Van den Bogerd et al. and Wahlig et al. regarding our article. In this study, we reported that the treated eyes had moderate-to-severe diffuse corneal edema and bullous keratopathy (Table 1, and Fig. S1 in the Supplementary Appendix of the article). There were no mild cases of Fuchs's endothelial corneal dystrophy with central corneal edema, a possible indication for endothelial stripping alone.[1] Severe bullous keratopathy cannot be cured by endothelial stripping alone. Although it is theoretically possible that a paracrine factor released from the injected cells or the ROCK inhibitor stimulated the reconstruction of corneal endothelium from endogenous CECs, we believe that it was the injected cultured CECs that directly contributed to the high postoperative CEC density mimicking conventional corneal transplantation. Our previous experiments in animals[2] produced identical results, although here, too, it is theoretically possible that the effect of the ROCK inhibitor or paracrine effects on endogenous CECs contributed to the reconstruction of corneal endothelium.

At surgery, we removed abnormal extracellular matrix, but not guttae, on the Descemet membrane by mechanical scraping. Specular microscopic images obtained 2 years postoperatively showed a slight decrease of guttae density, which suggests that the attachment of cultured CECs to the Descemet membrane was not accompanied by the formation of additional guttae.[3] The specular microscopic images of guttae at 24 weeks and 2 years after surgery were not in the same field (i.e., region). Thus, it was difficult to gauge the change in guttae density. The corneas of the seven patients with Fuchs's endothelial corneal dystrophy who have so far received our cell-injection therapy have remained transparent for more than 3 years after treatment.

Shigeru Kinoshita, M.D., Ph.D.
Kyoto Prefectural University of Medicine
Kyoto, Japan
shigeruk@koto.kpu-m.ac.jp

Noriko Koizumi, M.D., Ph.D.
Doshisha University
Kyoto, Japan

Morio Ueno, M.D., Ph.D.
Kyoto Prefectural University of Medicine
Kyoto, Japan

Since publication of their article, the authors report no further potential conflict of interest.

1. Borkar DS, Veldman P, Colby KA. Treatment of Fuchs endothelial dystrophy by Descemet stripping without endothelial keratoplasty. Cornea 2016;35:1267-73.
2. Okumura N, Koizumi N, Ueno M, et al. ROCK inhibitor converts corneal endothelial cells into a phenotype capable of regenerating in vivo endothelial tissue. Am J Pathol 2012;181:268-77.
3. Kinoshita S. The ongoing puzzle of the biological behavior of cornea guttae. JAMA Ophthalmol 2018;136:893-4.

DOI: 10.1056/NEJMc1805808